UNIVERSITEIT GENT

FACULTEIT WETENSCHAPPEN

Sediment concentrations, fluxes and source apportionment:

methodology assessment and application in Nete and Demer tributary basins (river Scheldt basin, Belgium)

Elin Vanlierde

Thesis submitted in fulfillment of the requirements for the degree of Doctor of Science, Geology

2013

Promotor: Em. Prof. Dr. Patric Jacobs

Promotor: Prof. Dr. Frank Mostaert

flanders HYDRAULICS RESEARCH

Faculty of Sciences

UNIVERSITEIT GENT

Ghent University
Faculty of Sciences
Department of Geology and Soil Science

Sediment concentrations, fluxes and source apportionment:

methodology assessment and application in Nete and Demer tributary basins (river Scheldt basin, Belgium)

Elin Vanlierde

2013

Thesis submitted in fulfillment of the requirements for the degree of Doctor of Science, Geology

Promotor: Em. Prof. Dr. Patric Jacobs

Promotor: Prof. Dr. Frank Mostaert

Vanlierde, E. (2013) Sediment concentrations, fluxes and source apportionment: methodology assessment and application in Nete and Demer tributary basins (river Scheldt basin, Belgium). PhD thesis. Flanders Hydraulics Research: Antwerp. ISBN 9789040303388. xli, 328 pp.

Author: Elin Vanlierde

Cover: Elin Vanlierde

Publisher: Flanders Hydraulics Research in association with Ghent University

ISBN 9789040303388

Wettelijk depot: D/2013/3241/129

Sediment concentrations, fluxes and source apportionment:

methodology assessment and application in Nete and Demer tributary basins (river Scheldt basin, Belgium)

Sedimentconcentraties, -fluxen en begroting van bronbijdragen:

beoordeling van methodologieën en toepassing ervan in Nete- en Demerbekken (Scheldebekken, België)

Elin Vanlierde

2013

Members of the Reading Committee

Prof. Dr. M. Chen (Vrije Universiteit Brussel, Belgium)

Prof. Dr. A. Collins (ADAS; University of Southampton, UK)

Prof. Dr. F. Mostaert (Flanders Hydraulics Research; Ghent University, Belgium)

Members of the Examination Committee

Prof. Dr. J. Verniers (Ghent University, Belgium)

Em. Prof. Dr. P. Jacobs (Ghent University, Belgium)

Prof. Dr. V. Dekov (University of Sofia, Bulgaria; IFREMER, France)

Prof. Dr. ir. G. Du Laing (Ghent University, Belgium)

Prof. Dr. ir. E. Smolders (Katholieke Universiteit Leuven, Belgium)

Em. Prof. Dr. ir. R. Verhoeven (Ghent University, Belgium)

Parent: person lovingly raising a child to the best of his capacity

Rock: solid mass that can be used as a stable foundation

Parent rock (geology): original rock from which something else is formed; the qualities of the parent rock will have a large influence on the nature of the resulting soil

This PhD thesis is dedicated to my parents,

parent rocks in every sense of the way.

Acknowledgements

First of all I would like to thank my two promotors, Prof. Dr. Patric Jacobs and Prof. Dr. Frank Mostaert. Without them, I would never have embarked on this journey. And their continuous support and belief in me have kept me going towards this end goal: a thesis and a doctors' degree.

I also would like to thank the members of my examination committee, who right at the end of the process, were still able to contribute greatly by interesting and thought-provoking comments. Thanks to you, this thesis is a better end product.

Furthermore, I have encountered people from all over the world, whom have selflessly accepted a sort of mentorship over me and whom have shared their insights and wisdom in various fields of science, but also their insights into life as a scientist and life in general.

Art Horowitz (and his wife Carolyn) have welcomed me in their home and gave me more than I could ever hope for and more than I can ever give back. I have decided to pay it forward and now spread the good cheer of Tom Lehrer to whomever wants to hear it.

Han Golterman (and his wife Nell) were kind enough to stop by regularly on their frequent trips between Holland and France. Every encounter taught me new things about iron chemistry and made me grow as a scientist. Now that you have settled in Holland indefinitely, I'll have to come visit you guys, instead of the other way around.

And finally Adrian Collins, whose enthusiasm about sediment fingerprinting is the best antidote against depression when yet another modelling result didn't turn out the expected results. It was a pleasure to see scientific hunger in action and to be ignited by it.

Additionally, I want to thank, I need to thank, ing. Jan De Schutter, without whom about 1/3 of this thesis would not have seen the light. MARS exists because of you. Your creative and continuously searching scientific mind is a treasure which is already being missed at FHR.

As institutes I would like to thank the Vlaamse Milieumaatschappij, the Department of Environment, Nature and Energy (Afdeling Land en Bodembescherming, Ondergrond, Natuurlijke Rijkdommen: Dienst Land en Bodembescherming) and Flanders Hydraulics Research for the use of their data.

I also have many people to thank in the academic and professional field, for helping me in a very practical way, by allowing me (and the students I supervised) to access their laboratories and play around with their equipment and helping me with some of my analyses. These people include Prof. Dr. Margaret Chen (VUB) for sharing her knowledge on flocs and for assisting in a sampling campaign, using her floc sampler; Prof. Dr. Peter Van de haute en Dr. Johan De Grave for making their microscopes available and Guido Uytersprot from the Laboratory of Environmental Toxicology of Ghent University for his assistance in the iron content analyses. Furthermore, I would also like to thank Prof. Dr. Louwye for providing me with sediment of the Diest Formation and ir. Ward De Cooman from the VMM, for the sampling campaigns in the Demer basin. Prof. Dr. Rene Van Grieken (Department of Chemistry, UA) I would like to thank for the XRF-analyses executed at his MiTAC research group. Additionally, I would like to thank Kurt Blom for keeping my computer virus-free and working.

I also want to thank the master and bachelor scription students whom I supervised. I invested a lot of energy in them, but they gave me so much more in return: Tom, Jozefien, Helena, Steven, Rindert, Bram, William and last but not least Patty, you were a delight to work with.

I also need to thank all the people who work at Flanders Hydraulics Research. They are at the moment my colleagues, but they have helped me all along the way: from the first day I started my master thesis until the day I finished the PhD, and they continue to be there for me. Some of these colleagues deserve a shout-out, so here it goes (in no particular order): Eric (for infecting me with love for the Scheldt, this will never go away); Steven (for his relentless search for the truth - or at least the journal articles in which this appears); Lia, Ellen, Rita, Mireille and the rest of the sedimentological lab team (for their excellent work and their good spirits, it was a joy to work alongside you); Hans, Jef, Ivo, Jean-Paul, Paul, Peter, Erwin, Guy and Leonid (for your devoted work on and around the field); Wouter, Erika and Stef (for your very much appreciated help with GIS-maps); Ricardo, Hans, Sam and Koen (for being my IT-life-lines, when a computer decided to crash once more, or a macro decided to do the complete opposite of what it was programmed to do); Stijn, Patrik and Joris (because it's good to have fellow PhD-writers who also work full time around), Fernando, Maarten, Leen, Peter, Niels, Yaïr, Gudrun, Ria, Thomas, Karen, Koen, Bram, Annelies and Ruben (a.k.a the rest of HIC in the present or the past) for being part of a great team, where I can feel at home. Also part of the team are the wonderful people of MOD. We couldn't do what we were doing without your support.

There are some people from FHR, whom I have not mentioned above, because they are more than colleagues. They were the shoulder I could cry on when things were just too hard to carry on my own and they were there to share a laughter. Lieve and Marc: I love you guys.

A special mention also goes to ir. Katrien Van Eerdenbrugh, who was, when she was still working at FHR, my supervisor. She gave me the room to learn one of the most important lessons in life: it is ok to fail. You learn from it and you get better at whatever it is you're doing. Look where I ended up…

And when I'm on the topic of special mentions, one person is absolutely deserved of a special mention: dr. Katleen Van Meel. We met through this PhD-work, we continued to work together at FHR, but what binds us is much more than chemistry, science or work. Because it takes a lion, to recognize one…

When it comes to the finalized product, my thanks goes out to Viki, David and Yvan. For fighting MS Word with me, and being just as perfectionistic as me. Also a big thank you to my TDT (typo detection team, consisting of Cristina, Marc, Rogier, Martijn, Laura, Leandro, Joris, Erik, Luc, Kevin and mental support from Menno). This group of friends (consisting of tango friends, soundtrack nuts, figure skaters and one statistical wonder, helped me out so much, finding typos where I could only see words and figures).

This PhD is much more than just 350+ pages. It represents a period of my life, a period in which I grew as a person. And therefore I cannot say that I could have finished this work, had it not been for this personal growth, which was enabled by so many people who were or still are part of my life.

My first big thank you goes to Ingridje, the best coach and friend anybody could want; Luis, who taught me not to judge myself, but to love myself instead; Els and Anneke, who both in their own way, have helped to lighten the load I was carrying, which made the trip that much easier.

But there are also so many people in my social network, who kept me sane, when I was going loopy, they kept me grounded, when I was ready to fly off, they helped me to be me. These people include my friends from my figure skating life, the tango scene and my fellow soundtrack geeks. A big shout-out goes to Bear McCreary, whose music became the soundtrack to my PhD, and whose encouragements on facebook brought a smile on my face.

And that brings me to facebook… Well, I'm not going to thank Mark Zuckerberg for creating it, but I am going to thank all my friends on there, whom have followed all of my PhD-related posts (and sometimes whining) and who found the time to keep posting sweet little nothings, and great humoristic quotes to keep my spirits up. You were essential to my good mood. Thank you guys so much.

We are nearing the end of this list, and so all who remain, are my nearest and dearest…

Alexander, Tine, Ywan and Marcel, you are all people who share a part of my soul and whom I love dearly. Distance doesn't mean anything when hearts are connected. You have always been there for me. Thank you so much.

My godfather and aunty, who have always believed in me, through thick and thin. I can only hope they realize how important they are to me.

My godmother and uncle, who have always been there for me, and are the best supporters a niece can ask for.

My cousin Rutger, whose cookery is legendary. He is also the first man to ever decorate my bathroom with candles and a computer playing meditation music, in an attempt to get me to relax and get my mind off this PhD. (Note to readers with a dirty mind: no he wasn't in the bathroom at the time I was taking the bath. He's my cousin…). In any case, Rutger, you rock!

My sister Kirstin and her husband Christophe, who have fed me when I was too tired to feed myself after another long day (and/or night) of PhD-work and who have pried me away from my books to take a walk along the Durme every now and again. Sis, you were always there to share anything that needed sharing, or draw a Tarot card to make sense of it all. You are my best friend, my closest family. De zusjes, die krijgt niemand uit elkaar…

And finally mom and dad. There is nothing left to say except: lover you ;-).

And to those I might forgot to mention by name, my gratitude is no less.

Abstract

The research executed within the framework of this PhD was aimed at determining the contributions of different sediment sources within the Nete and Demer tributary basins of the river Scheldt basin (Belgium).

This initial intent was then focussed into three focal points. First of all, the total suspended sediment flux was calculated at selected monitoring stations in rivers in the Nete and Demer basins. Secondly, the contribution of ferric authigenic sediment to the total suspended sediment transport in the Kleine Nete basin was determined, as this source of sediment is most often overlooked in sediment flux studies, even though its contribution can be quite substantial. And finally, the sediment fingerprinting approach for source apportionment was assessed for its applicability in the Demer basin.

Determining the total suspended sediment flux

The total sediment flux was determined for monitoring locations on the Kleine Nete (Grobbendonk), Demer (Aarschot), Gete (Halen) and Mangelbeek (Lummen), using both measurement data and rating curve estimates. The measurement data was obtained from water samples, automatically collected using an ISCO pumping sampler, programmed to take a sample every seven hours. Sediment concentrations of these samples were consequently gravimetrically determined (either by filtration or lyophilisation) in the sedimentological laboratory of Flanders Hydraulics Research.

However, data gaps were present in the time series, and therefore sediment concentrations needed to be estimated, using sediment rating curves. Which properties should be allowed into the rating curves and which transformation was needed, was investigated using one decade of Kleine Nete Grobbendonk discharge and sediment concentration data (1999-2009), complemented with two years (2008-2009) of physical parameter data (turbidity and conductivity data) obtained from monitoring the site with a YSI multi-parameter probe.

Different rating curves were compiled, using both untransformed and logarithmically transformed discharge data to estimate the sediment concentration as well as using discharge data and discharge-derived data (such as baseflow, interflow and runoff data, numerically filtered from the observed discharge) to estimate the sediment concentration and finally using all available data (i.e. adding turbidity and conductivity to above-mentioned parameters). Consequently, the data sets were also split into summer and winter data, and separate rating curves were established for each data set.

The results showed that regardless of which parameters were allowed to enter the rating curve, the non-logarithmically transformed data models, separating summer and winter curves performed the best. Furthermore, it is clear that allowing more properties, such as turbidity and conductivity, into the rating curve improves the predictive power. But even then, the uncertainty on the predictions remains quite high (about 50% of the average observed sediment concentration in the Grobbendonk sampling station for the period of record).

Nonetheless, if the objective is to calculate annual suspended sediment fluxes and more than 75% of the data is available (through measurement), then creating a sediment rating curve using non-logarithmically transformed discharge and suspended sediment concentration data (separated for summer and winter data) should suffice, and no strenuous effort should be put into finding a more suitable relationship, as the variance observed in the estimations for the remaining 25% provided

by the different rating curves, resulted in a spread of only 1 to 8% of the total observed suspended sediment flux.

However, if more detailed estimates are necessary, such as daily sediment concentrations (as needed for the authigenic sediment modelling or event-based studies) then the combination of discharge with discharge-derived parameters and physical parameters should be investigated to procure the most predictive relationship possible.

The annual suspended sediment fluxes determined at the Kleine Nete (Grobbendonk), showed significant variation, mostly caused by variation in annual discharge. The fluxes are higher in the first four years on record (11,500 – 15,800 tonnes) and then decline from 2003 onwards, stabilising around 6,000 tonnes per year, with a bump around 2007 where 7,900 tonnes was reported.

The suspended sediment fluxes determined at the Demer (Aarschot) for the period 2005-2007 show higher values than those observed in Grobbendonk. This is logical as the Demer catchment (upstream Aarschot) is not only many times larger than its Kleine Nete counterpart (2,163 km² versus 590 km²), it also drains areas more sensitive to physical erosion. However, a similar rise in annual sediment loads can be observed at the Aarschot station, in the year 2007, where the SSF values climb from +/- 25,000 tonnes up to 2006 and reaching 40,000 tonnes in 2007 (excluding the months of November and December 2007).

Additionally, a more detailed investigation into the sediment concentrations observed in the Demer at the Aarschot measurement location was executed for the period July 2003-May 2010, which showed that the river system underwent some significant changes in sediment supply during the period of record, transitioning from an originally slightly sediment-depleted system to a sediment-enriched system, caused by impactful maintenance works executed from November 2007 to March 2009. Subsequently, the river system has been gradually returning to its slightly sediment-depleted state. The timing of the different periods could be established by classifying the individual discharge events in the hysteresis classes defined in the pertinent literature, but also by investigating the lag-time between the arrival of the discharge peaks and corresponding sediment peaks. The latter proves to be as effective as and less time-consuming than the former.

During the period the river system was sediment-enriched, a special phenomenon could be observed at the Aarschot sampling location: a single discharge peak would generate a double sedimentary response; i.e. one sediment peak arrived more or less simultaneously with the discharge peak while a second sediment peak trailed behind the discharge peak. In the literature on this topic this phenomenon is rarely observed and discussed, and when observed, the trailing peak is attributed to slow processes such as river bank failure due to saturation of the bank. This is contrary to the observations in the Demer basin, where this phenomenon occurs frequently (from November 2007 to March 2009, almost half of the high-flow events observed in Aarschot produced such a double sediment peak). Additionally, most of the maintenance works took place close to the monitoring location and generated a sediment influx which was readily available in-stream for further transportation.

These observations lead to the hypothesis that bed load transport might be partly responsible for the observed double sedimentary responses and counter-clockwise hysteresis events. This hypothesis seems to be further confirmed by the similar shape of the discharge and trailing sediment peaks on the one hand and the fact that no significant increase in surface water sample values could be observed in the entire period of record on the other.

Budgeting authigenic sediment contributions

One sediment source was singled out for further investigation within the framework of this PhD research, i.e. authigenic sediment, as its contribution of authigenic sediment to the total suspended sediment load is usually neglected in modelling and apportionment studies. This type of sediment is created in fluvial systems when the groundwater, laden with solutes seeps into the surface water, where it is subjected to different reigning environmental conditions. Which compounds precipitate when groundwater interacts with the surface water depends on the ion composition in solution and therefore on the hydro-geological context of the region, as well as on the condition of the surface water. In the Nete and the northern part of the Demer basin ferric authigenic sediment is generated due to the significant influx of dissolved iron through seepage.

The authigenic sediment contribution to the total sediment flux in the Kleine Nete at the Grobbendonk location has both been determined through theoretical deduction as well as through modelling. For the latter the Model for Authigenic River Sediment (MARS) developed at Flanders Hydraulics Research was used, which further developed during the ongoing doctoral research (Vanlierde et al. 2005 a, 2005 b, 2006, 2007 a, 2007 b).

Both the theoretical deduction as well as the modelling approach used a variety of parameters, of which some were estimates. These parameters include groundwater seepage and the Fe(II)-concentration present in it. The former was obtained through numerical filtering of the total discharge while the latter was estimated to be 15 mg/l, using a variety of data sets and applying the median value of the Formation of Diest [0252]. By multiplying both parameters, the Fe(II) flux into the river can be calculated. Consequently, correction factors were created to convert the amount of Fe(II) entering the river system into the amount of authigenic sediment that was formed. The theoretical deductions using all these parameters, estimated the authigenic sediment to contribute in between 43 and 100% to the total sediment load at Grobbendonk. This shows that authigenic sediment should not be omitted from sediment transport modelling as this will lead to serious underestimations of the total sediment load of a river system.

To procure more precise estimates, the MARS model was constructed, which implements (besides the above mentioned input parameters and correction factors) erosion, resuspension and accumulation algorithms. MARS was consequently calibrated by comparing the modelled authigenic fluxes with the total suspended sediment fluxes observed at the Grobbendonk measurement location.

Further research into the nature and behaviour of the authigenic sediment was executed to gain insight into this material and to reduce some of the uncertainties still present in the MARS model. Sampling campaigns at Grobbendonk were executed at different locations in the cross-section to obtain insight into the distributional variability of particle size and shape, as well as iron concentrations present in solution and in solid phase. Filter papers, laden with flocculated material, were investigated using image analysis tools, which showed that close to the water surface and near the bottom the flocs are large, while in the middle of the vertical flocs are significantly smaller. Furthermore, the average observed floc size on a vertical seems inversely proportional to the average flow velocity present on that vertical. During these sampling campaigns sediment-water mixtures were sampled and acidified in the field, after which they were spectrophotometrically analysed to determine the iron content of the material and in solution. These analyses revealed most of the iron to be in the solid phase, confirming the hypothesis that the oxidation process of Fe(II) into Fe(III) is a fairly quick process, and will take place within the boundaries of the catchment in which the suspended sediment is sampled.

Consequently, a more detailed research into the iron content of the authigenic sediment was executed, sampling 'pure' authigenic sediment in the upper reaches of the Nete and northern part of the Demer basin and analysing the material using X-Ray Fluorescence (and Inductively coupled plasma mass spectrometry in the collaborative research with Dekov et al. (in prep.)) techniques. Average iron concentrations of 35% of the total sediment weight were observed in these samples. Furthermore, authigenic sediment contained high levels of organic matter (loss on ignition of +/- 30%).

Additionally, it could be established (in collaboration with Dekov et al. (in prep.)) that the ferric authigenic sediment in the Nete and Demer basins consists almost entirely of ferrihydrite, as a result of both microbial and inorganic precipitation.

Using this information to determine the stoichiometric correction factor, the MARS model was able to estimate the contribution of the authigenic sediment at Grobbendonk at 61% of the total load for the decade 1999-2009. As the Fe(II) concentration in groundwater is associated with large uncertainties, this will introduce the largest source of uncertainty to the model results.

Composite sediment fingerprinting

In the final part of this PhD research, the internationally applied composite sediment fingerprinting approach was assessed for its applicability in the Demer basin. The methodology was used to determine the contributions of eight principal tributaries to the total load observed in the Aarschot monitoring location on the Demer.

At the selected tributaries, time-integrated samplers were deployed upstream of their confluence with the Demer. They were emptied on a monthly basis, after which the material was lyophilized and consequently sieved to retain only the <63µm fraction. This fraction was then submitted to grain size analysis by laser diffraction, incineration to determine Loss on Ignition, density analysis by gas pycnometry and geochemical analysis by X-Ray Fluorescence.

Samples were also obtained from the outlet location (Aarschot), although not via a time-integrated sampler, but using flow-through centrifugation and also by compositing material from the automatically collected ISCO samples. These outlet samples underwent the same treatment as the tributary samples and the same properties were determined.

The sediment fingerprinting approach used to determine the contribution of the tributaries to the Aarschot load involves two main stages: source discrimination and source apportionment. The former entails the creation of a composite sediment fingerprint, by submitting the individual fingerprint properties to a Kruskal-Wallis H-test to confirm their ability to distinguish between the different tributaries and consequently putting the properties that passed the test into a stepwise multivariate Discriminant Function Analysis.

The second stage of sediment fingerprinting, the source apportionment, encompasses the application of a multivariate mixing model to provide quantitative estimates of the relative contributions of the individual tributaries to the sampled sediment load at the outlet station. The sediment mixing model itself is comprised of as many linear equations (also called objective functions) as there are properties selected in the composite fingerprint, and these linear equations relate the concentration of each property in the outlet sample to the mixture representing the sum of the contributions from the different sources.

The concentration of a source property, needed in this objective function, can either be the mean value of all observations, or Monte Carlo simulated property concentrations can be repeatedly entered into the objective function. In this thesis both methods were used.

Within the framework of this thesis, several composite fingerprints (Fingerprints A through E) were created, comprised of different combinations of properties. Each composite fingerprint was sufficiently capable of discriminating between the eight tributaries, to apportion their contributions. The models (objective functions) were also run using different combinations of correction factors (grain size, Loss on Ignition and discriminatory weighting correction factor or omitting all correction factors).

Disappointingly, the modelling results yielded source contributions with unacceptably high standard deviations and the models struggled to attribute the contributions to the correct tributaries, within regions with the same geological subsurface. Moreover, the Relative Mean Error (RME), suggested in the literature as a good estimator of the performance of the model, did not perform well. It failed to indicate the poor modelling results. Hence, a different estimator has been suggested in this thesis. RME_val is the relative mean error using only properties which were excluded from the composite fingerprint, but did pass the Kruskall-Wallis H-test.

In an attempt to obtain realistic modelling results with acceptable standard deviations, and low RME_val values, the spatial source set-up was simplified, by reducing the amount of sources (through combination of sources with similar chemical signatures), and new composite fingerprints (F through H) were created. The standard deviations became acceptable when the sources were grouped per geological setting (i.e. the northern tributaries were grouped and the southern tributaries were grouped) and the results proved realistic when compared to the total sediment fluxes at the Halen, Lummen and Aarschot sampling locations, i.e. the southern tributaries contribute between 75 and 95% of the observed load in Aarschot, while the northern tributaries contribute the remaining fraction.

The reasons behind the poor performance of the sediment fingerprinting approach can most likely be found either in the modelling set-up, in human intervention, causing un-sampled sources to enter the river system, distorting the sediment fingerprint, or in incorrect grain size and organic matter corrections, distorting the fingerprinting signals.

Therefore, the correction factors were investigated more closely. The Demer data set showed that when the grain size of the contributing sources significantly differ from one another, the grain size distribution observed in the outlet samples can most likely be attributed to sorting as well as mixing effects. In that case, the grain size corrections as applied in composite fingerprints A through H are oversimplified, which may explain the high standard deviations observed in the Monte Carlo simulated model runs.

Attempts to create a more complex grain size correction factor via natural water settling tests with Mangelbeek, Gete and Demer sediment, however, were not successful, as the highly flocculated material refused to fractionate properly, showing the impact of flocculation on the transport processes. Therefore, a different method to separate the flocculated sediment into separate fractions needs to be applied, if a more complex grain size correction factor is to be determined. Otherwise, spatial provenance fingerprinting cannot be executed with sufficient accuracy in the Demer basin (and by extension Flanders).

Organic matter corrections did not seem to aid the problem in spatial provenance fingerprinting, as the RME_val values were still not acceptable, and the results were often unrealistic. However, in source type fingerprinting in the Mangelbeek catchment, rich in authigenic sediment, it became

apparent that the simple organic matter correction might be performing acceptably. However, whether this can be applied to other catchments containing authigenic sediment still needs to be investigated.

To conclude, sediment fingerprinting in the Demer basin (and by extension in Flanders), using only the geochemical composition of the sediment, cannot be implemented as long as no applicable grain size correction factor is determined and its impact on the sediment fingerprinting results can be determined, allowing for the discrimination of uncertainty caused by the human impact and uncertainty caused by faulty correction factors.

Some of that uncertainty, however, can also be introduced by the mass balancing model set-up. Therefore, changing this set-up (by taking the statistical uncertainties even more into account) might have a beneficiary effect on the modelling results.

This is worth investigating.

Samenvatting

Het onderzoek uitgevoerd in het kader van dit doctoraatsonderzoek was gericht op het bepalen van de bijdragen van verschillende sedimentbronnen in de Nete- en Demer deelbekkens van het Scheldebekken (België).

Deze initiële doestelling werd omgezet in drie zwaartepunten. Ten eerste werd de totale flux van sediment in suspensie berekend ter hoogte van enkele geselecteerde monitoring locaties in het Nete- en Demerbekken. Ten tweede werd de bijdrage van ijzerrijk authigeen sediment aan het totale suspensietransport in het Kleine Nete bekken bepaald. Deze bron van sediment wordt vaak over het hoofd gezien in sedimentflux studies, terwijl de bijdrage ervan in bepaalde gevallen niet verwaarloosbaar klein is. Tot slot werd in dit doctoraatsonderzoek nagegaan in hoeverre de sediment fingerprinting aanpak gebruikt kan worden om de bijdrage van verschillende sedimentbronnen te begroten in het Demerbekken.

Bepalen van de totale flux van sediment in suspensie

De totale sediment flux werd bepaald ter hoogte van de monitoring locaties op de Kleine Nete (Grobbendonk), Demer (Aarschot), Gete (Halen) en Mangelbeek (Lummen). Hierbij werd gebruik gemaakt van zowel meetdata als schattingen gebaseerd op regressievergelijkingen. De meetdata werd verkregen uit watermonsters, elke zeven uur automatisch opgepompt door een ISCO sampler. Vervolgens werd van deze watermonsters, in het sedimentologisch laboratorium van het Waterbouwkundig Laboratorium (WL), de sedimentconcentratie gravimetrisch bepaald (door filtratie of lyofilisatie).

In de tijdreeksen waren echter onderbrekingen in de sedimentconcentraties aanwezig, die aan de hand van regressievergelijkingen moesten worden aangevuld. Om na te gaan welke parameters in deze regressievergelijkingen toegelaten mogen worden, werd gebruik gemaakt van een decennium aan debiet- en sedimentconcentratiegegevens te Grobbendonk (in de Kleine Nete), aangevuld met twee jaar (2008-2009) aan fysische parameter-data (turbiditeit en conductiviteit) verkregen via de YSI multi-parametersonde die ter plaatse hing.

Verschillende regressievergelijkingen werden opgesteld, waarbij de parameters zowel in niet-getransformeerde als logaritmisch getransformeerde vorm werden aangeboden en de data set eveneens in zomer- en winterdata werd opgesplitst. De parameters in kwestie kunnen in drie categorieën worden opgedeeld. Ten eerste werd sedimentconcentratie voorspeld gebruik makend van debietdata. Vervolgens werd nagegaan of het toevoegen van debiet-afgeleide parameters (zoals baseflow, interflow en oppervlakkige afstroming, verkregen aan de hand van numeriek gefilterde debietdata) de voorspelkracht van de regressievergelijkingen kon verhogen. Tot slot werden ook de fysische parameters conductiviteit en turbiditeit geïntroduceerd in de regressievergelijking en werd hun effect op de voorspelkracht nagegaan.

Uit de vergelijking van de resultaten bleek dat de seizoenale regressievergelijkingen die gebruik maakten van niet-logaritmisch getransformeerde data steeds het beste presteerden, ongeacht welke parameters aanwezig waren in de regressie curve. Verder kon vastgesteld worden dat het toelaten van meer parameters, zoals turbiditeit en conductiviteit, in de regressievergelijking de voorspelkracht laat toenemen. Toch blijft de onzekerheid op de voorspellingen relatief hoog (ongeveer 50% van de gemiddelde sedimentconcentratie waargenomen te Grobbendonk tijdens de onderzoeksperiode).

Indien de doelstelling zich echter beperkt tot het berekenen van jaarlijkse vrachten en daarbij 75% van de tijd, meetdata beschikbaar is, dan volstaat het om een winter- en een zomerregressievergelijking op te stellen, gebruik makend van niet-logaritmisch getransformeerde debiet en sedimentconcentratiedata. Er moeten geen verdere zware inspanningen geleverd worden om een betere relatie te vinden, aangezien de variantie aanwezig tussen de voorspellingen van de verschillende regressiemodellen voor de ontbrekende 25% van de data, slechts een spreiding van 1 tot 8% teweegbrachten in berekende jaarvrachten.

Indien echter meer gedetailleerde voorspellingen nodig zijn, zoals dagelijkse sedimentconcentraties (zoals gebruikt in de authigene sediment modellering, of in studies van een specifieke wasperiode) dan moet nagegaan worden welke combinatie van parameters, waaronder debiet en debiet-afgeleide parameters, alsook fysische parameters een regressiecurve vormt met de hoogste voorspelkracht.

De jaarlijkse sedimentvrachten bepaald in de Kleine Nete (Grobbendonk), vertoonden een significante variatie, vooral te wijten aan variatie in jaarlijkse afvoer. De vrachten zijn hoger in de eerste vier jaar van de meetperiode (11,500 – 15,800 ton) en nemen dan af vanaf 2003 om zich te stabiliseren rond de 6,000 ton per jaar, met een kleine toename rond 2007, waarbij 7,900 ton werd gerapporteerd.

De suspensievrachten bepaald voor de Demer (Aarschot) voor de periode 2005-2007 zijn hoger dan deze waargenomen te Grobbendonk. Dit is vanzelfsprekend, aangezien het Demerbekken (stroomopwaarts van Aarschot) niet alleen veel groter is dan het Netebekken (2,163 km² versus 590 km²), maar het tevens ook gebieden gevoeliger aan bodemerosie draineert. Ook in Aarschot werd een toename in sedimentvracht in het jaar 2007 vastgesteld. De jaarlijkse vracht klimt er van ongeveer 25,000 ton tot 2006 tot ongeveer 40,000 ton in 2007 (hierbij worden de maanden november en december 2007 buiten beschouwing gelaten).

Er werd eveneens een meer gedetailleerd onderzoek uitgevoerd naar de sedimentconcentraties waargenomen in de Demer te Aarschot tijdens de meetperiode Juli 2003-Mei 2010. Dit onderzoek wees uit dat het riviersysteem in deze periode significante veranderingen onderging in de aanvoer aan sediment. De rivier ging van een oorspronkelijk licht sediment-verarmd systeem naar een systeem sterk verrijkt aan sediment, veroorzaakt door impactvolle onderhoudswerkzaamheden die werden uitgevoerd van november 2007 tot maart 2009. Vervolgens bleek het riviersysteem zich weer te herstellen, en langzaam terug te keren naar een licht sediment-verarmd systeem.

De verschillende periodes konden afgebakend worden door de afzonderlijke wasgebeurtenissen in te delen in de verschillende hysteresis klassen gedefinieerd in de vakliteratuur. De afbakening kon echter ook gebeuren op basis van het tijdsverschil tussen de aankomst van de debietpiek en de daarbij horende sedimentpiek. Deze tweede methode bleek even effectief dan de eerste, maar nam minder tijd in beslag.

Wanneer het riviersysteem oververzadigd was aan sediment kon er een speciaal fenomeen waargenomen worden te Aarschot: één enkele debietpiek bleek in staat te zijn twee sedimentpieken te genereren, met name één sedimentpiek die min of meer gelijktijdig met de debietpiek aankomt en één sedimentpiek die met vertraging arriveert. In de literatuur wordt dit fenomeen zelden waargenomen en besproken. De enkele observaties spreken over een tweede sedimentpiek die het gevolg is van trage processen, zoals oeverafkalving door waterverzadiging van de oever. Dit is echter in tegenstelling tot de waarnemingen in het Demerbekken, waar dit fenomeen frequent voorkomt (van november 2007 tot maart 2009 werd bij bijna de helft van de wasgebeurtenissen een dubbele sedimentaire respons waargenomen). Daarenboven, de meeste

onderhoudswerkzaamheden vonden dicht bij het monitoringsstation te Aarschot plaats, en zorgden zo voor een influx aan sediment die meteen beschikbaar was voor verder transport.

Deze waarnemingen leiden tot de hypothese dat bodemtransport mogelijks mede verantwoordelijk is voor de dubbele sedimentaire reacties die in Aarschot geobserveerd werden alsook de hysteresis events die in tegenwijzerzin plotten tijdens deze periode. Deze hypothese lijkt verder bevestigd te worden door de gelijkaardige vorm van de debiet en de corresponderende achterophinkende sedimentpiek. Ook het feit dat geen significante toename in sedimentconcentratie kon worden opgemerkt in oppervlaktewater monsters gedurende de hele meetperiode.

Begroting van de bijdrage van authigeen sediment

Eén sedimentbron is in het kader van dit doctoraatsonderzoek verder uitgelicht, met name authigeen sediment. De bijdrage van deze bron aan de totale sedimentvracht wordt vaak genegeerd in modellerings- en sedimentbegrotingsstudies. Dit soort sediment wordt gevormd in riviersystemen wanneer opgeloste stoffen in het grondwater via kwel in het oppervlaktewater terecht komen waar ze vervolgens, blootgesteld aan meer zuurtstofrijke omgevingscondities, neerslaan als precipitaten. Welke verbindingen gevormd worden wanneer het grondwater in contact komt met het oppervlaktewater hangt af van de ionensamenstelling in oplossing en dus van de hydrogeologische context van het gebied. Natuurlijk spelen ook de heersende omstandigheden in het oppervlaktewater een belangrijke rol. In het Netebekken en het noordelijk deel van het Demerbekken wordt ijzerrijk authigeen sediment gevormd dankzij de belangrijke influx van opgelost ijzer via kwel.

De bijdrage van authigeen sediment aan de totale sedimentvracht in de Kleine Nete ter hoogte van het meetstation te Grobbendonk location is zowel theoretisch afgeleid als bepaald via modellering. Voor dit laatste werd het Model voor Authigeen Rivier Sediment (MARS) gebruikt dat ontwikkeld werd aan het Waterbouwkundig Laboratorium. MARS werd nog verder ontwikkeld tijdens het verdere doctoraatsonderzoek (Vanlierde et al. 2005 a, 2005 b, 2006, 2007 a, 2007 b).

Zowel de theoretische afleiding als de modelaanpak maken gebruik van een aantal parameters. Een van deze parameters is de grondwater influx (kwel), die begroot werd door middel van numerieke filtering. Verder wordt ook de Fe(II)-concentratie aanwezig in het grondwater als berekeningsparameter gebruikt. Een inschatting van deze concentratie is gemaakt aan de hand van een aantal verschillende datasets, waarbij uiteindelijk de mediaan van de observaties van de Formatie van Diest [0252] gebruikt werd, namelijk 15.7 mg/l. Door beide parameters te vermenigvuldigen met elkaar wordt de Fe(II)-flux naar de rivier toe berekend. Vervolgens werden correctie factoren bepaald die de hoeveelheid Fe(II) die in de rivier wordt geïntroduceerd omzetten naar hoeveelheid gevormd authigeen sediment.

De theoretische afleiding die gebruik maakt van al deze parameters, begroot de bijdrage van authigeen sediment aan de totale suspensievracht te Grobbendonk tussen 43 en 100%. Dit toont aan dat authigeen sediment niet mag achterwege gelaten worden in het modelleren van sediment transport, aangezien dit tot serieuze onderschattingen van de totale vracht van een riviersysteem kan leiden.

Om een nauwkeuriger inschatting te maken van de bijdrage werd het MARS-model ontwikkeld. Dit maakt, behalve van boven vermelde parameters en correctiefactoren ook gebruik van erosie, resuspensie en accumulatie algoritmes. MARS werd vervolgens gekalibreerd door de door MARS gemodelleerde authigene sedimentfluxen te vergelijken met de totale sedimentfluxen waargenomen te Grobbendonk.

Verder onderzoek naar de aard en het gedrag van het authigene sediment werd uitgevoerd om meer inzicht te verkrijgen in dit materiaal en om enkele van de onzekerheden, nog steeds aanwezig in MARS, te verkleinen. Bemonsteringscampagnes werden uitgevoerd te Grobbendonk op verschillende locaties in de dwarsdoorsnede, om inzicht te krijgen in de verdeling van deeltjesgrootte en -vorm, alsook in de concentraties van ijzer in oplossing en in precipitatie. Filters beladen met geflocculeerd materiaal werden onderzocht met behulp van beeldanalyse software. Hieruit bleek dat dicht bij het wateroppervlak en dicht bij de bodem de vlokken groter zijn dan in het midden van de verticale. Verder bleek een omgekeerd evenredige relatie te bestaan tussen de waargenomen vlokgrootte langsheen de verticale en de gemiddelde stroomsnelheid aanwezig op deze verticale. Tijdens deze bemonsteringscampagnes werden sediment-water mengsels bemonsterd en aangezuurd op het terrein, waarna ze spectrofotometrisch geanalyseerd werden om het ijzergehalte aanwezig in zowel het sediment als in het water te bepalen. Deze analyses toonden aan dat het meeste ijzer zich in de vaste fase bevond, wat de hypothese lijkt te bevestigen dat het oxidatie proces van Fe(II) naar Fe(III) inderdaad een vrij snel proces is, dat plaatsvindt binnen de grenzen van het bekken waarin het suspensiemateriaal verzameld is.

Vervolgens werd een gedetailleerder onderzoek uitgevoerd naar het ijzergehalte aanwezig in het authigene sediment. Hiervoor werd getracht 'puur' authigeen materiaal te bemonsteren in de bovenlopen van het Netebekken en het noordelijk deel van het Demerbekken. Dit materiaal werd geanalyseerd met behulp van X-straal Fluorescentie (en inductief gekoppeld plasma massaspectrometrie in het collaboratieve onderzoek met Dekov et al. (in prep.). De gemiddelde ijzerconcentratie in deze monsters bedroeg 35% van de totale sedimentmassa. Verder bleek het authigene sediment ook behoorlijk hoge gehaltes aan organisch materiaal te bevatten (met waarden van +/- 30% gloeiverlies).

Daarenboven kan vastgesteld worden (in samenwerking met Dekov et al. (in prep.)) dat het ijzerrijke authigene sediment in het Nete- en Demerbekken nagenoeg volledig uit ferrihydriet bestaat dat ontstaan is als een gevolg van zowel microbiële als anorganische precipitatie.

Gebruik makend van deze bijkomende informatie kon de stoichiometrische correctiefactor correct bepaald worden, en met een aanname over de sorptie correctiefactor kon het MARS model de gemiddelde jaarlijkse bijdrage van authigeen sediment aan de totale suspensievracht te Grobbendonk begroten op 61% voor het decennium 1999-2009. Vermits the onzekerheid op de Fe(II) concentratie in het grondwater het grootste is, zal dit de belangrijkste bijdrage leveren tot de onzekerheid op de modelresultaten.

Composiet sediment fingerprinting

In het laatste deel van dit doctoraal onderzoek werd de toepasbaarheid van de composiet sediment fingerprinting techniek nagegaan voor gebruik in het Demerbekken. Deze internationaal toegepaste methodologie werd gebruikt om de bijdragen van acht belangrijke bijrivieren aan de totale vracht van de Demer te Aarschot te begroten.

Stroomopwaarts van de mondingen van de acht geselecteerde bijrivieren in de Demer, werden tijdsintegrerende samplers geïnstalleerd. Deze werden maandelijks geleegd, waarna het materiaal gevriesdroogd werd en vervolgens gezeefd, zodat enkel de fractie <63µm wordt overgehouden. Van deze fractie werd vervolgens de deeltjesgrootte bepaald met behulp van laserdiffractie, alsook het gloeiverlies door verassing. Tevens werd de densiteit bepaald met behulp van gaspycnometrie en werd met behulp van X-straal fluorescentie de geochemische samenstelling onderzocht.

Ook werden monsters verzameld te Aarschot (het outlet-station). Hier kon echter geen tijdsintegrerende sampler geplaatst worden, en werd gebruik gemaakt van sediment verzameld door doorstroomcentrifuge alsook van mengmonsters gecreëerd door het samenvoegen van consecutief automatisch bemonsterde ISCO pompmonsters. Deze outlet monsters ondergingen dezelfde behandeling als de monsters verkregen in de bijrivieren en dezelfde parameters werden bepaald.

De sediment fingerprinting techniek die gebruikt werd om de bijdragen van de individuele bijrivieren na te gaan bestaat uit twee stappen: bron discriminatie en bron-bijdrage begroting. Bij bron discriminatie worden in eerste instantie alle gemeten parameters onderworpen aan een Kruskal-Wallis H-test, die hun mogelijkheid tot het onderscheiden van verschillende bijrivieren nagaat. Vervolgens worden de parameters die slagen in deze test, onderworpen aan een stapsgewijze Discriminant Function Analysis, die een uiteindelijke combinatie van parameters voorspelt die de beste discriminerende kracht heeft: de composiet fingerprint.

De tweede stap van het sediment fingerprinting proces, de bron-bijdrage begroting, omvat de toepassing van een multivariaat mengmodel dat kwantitatieve schattingen begroot van de relatieve bijdrage van de verschillende bijrivieren. Het sediment mengmodel zelf, bestaat uit een aantal lineaire vergelijkingen (ook wel 'objective functions' genoemd). Het aantal vergelijkingen stemt overeen met het aantal geselecteerde parameters in de composiet fingerprint en deze 'objective functions' vergelijken de concentraties van elke parameter in het outlet monster met de mengeling die de som van de bijdragen van de verschillende bronnen voorstelt.

De concentratie van een parameter van een bron, die nodig is in de 'objective function' kan ofwel de gemiddelde waarde van alle observaties van de bron zijn, of er kan gebruik gemaakt worden van Monte Carlo gesimuleerde parameter concentraties, die herhaaldelijk doorgerekend worden. In deze thesis zijn beide methodes gebruikt.

In het kader van deze thesis zijn meerdere composiet fingerprints opgesteld (Fingerprints A tot E), die elk bestonden uit verschillende combinaties van parameters. Elke composiet fingerprint was voldoende in staat om de acht bijrivieren van elkaar te onderscheiden. En de 'objective function' werden gevoed met verschillende combinaties aan correctiefactoren. Deze correctiefactoren corrigeerden voor deeltjesgrootte, voor gloeiverlies en voor de discriminatiekracht. Tevens werd een modelrun gedaan zonder dat correctiefactoren toegepast werden.

De modelresultaten waren echter teleurstellend, aangezien de gemodelleerde bronbijdragen onaanvaardbaar hoge standaardafwijkingen vertoonden en de modellen hadden moeilijkheden met het toekennen van bijdragen aan de juiste bijrivieren binnen een gebied met eenzelfde geologisch subtraat. Daarenboven bleek de relatieve gemiddelde fout (RME), die in de literatuur gesuggereerd wordt als een goede schatter voor de performantie van een model, niet goed te presteren. Deze parameter bleek niet in staat te zijn om de slechte resultaten als dusdanig te vlaggen. Daarom werd in deze theses een nieuwe schatter voorgesteld. RME_val is de relatieve gemiddelde fout van de parameters die wel slaagden voor de Kruskall-Wallis H-test, maar niet opgenomen zijn in de composiet fingerprint.

In een poging om meer realistische modelresultaten te verkrijgen, met aanvaardbare standaarddeviaties en lage RME_val waarden, werden de ruimtelijke bronnen gereduceerd in aantal, door een aantal bronnen (met gelijkaardige chemische samenstelling) samen te voegen. Hiervoor werden nieuwe composiet fingerprints opgesteld (F tot H). De standaard afwijkingen werden pas acceptabel wanneer de bronnen volledig via geologische setting werden gegroepeerd (m.a.w. de noordelijke en zuidelijke bijrivieren werden elk in één groep ondergebracht). De

resultaten van deze laatste groepering bleken ook realistisch wanneer ze vergeleken werden met de totale sedimentvrachten die te Halen, Lummen en Aarschot bemonsteringslocaties bepaald werden. Zo dichtte composiet fingerprint H de zuidelijke bijrivieren ongeveer 75 tot 95% van de totale vracht te Aarschot toe. De noordelijke bijrivieren dragen dus volgens het model de overige 5 tot 25% bij.

De oorzaken van de minder goede prestatie van de sediment fingerprinting techniek kunnen hoogstwaarschijnlijk gezocht worden ofwel in de modelopbouw, in menselijke impact (door onderhoudswerkzaamheden in de rivier) die ervoor gezorgd hebben dat niet-bemonsterd materiaal in de rivier terechtkwam waardoor de fingerprint verstoord werd, ofwel in het gebruik van onjuiste correctiefactoren voor deeltjesgrootte of organisch materiaal.

Daarom werden de correctiefactoren verder onderzocht. Aan de hand van de Demer dataset kon aangetoond worden dat wanneer de deeltjesgrootte van de bijdragende bronrivieren significant van elkaar verschillen, de deeltjesgrootteverdeling waargenomen in het outlet staal, waarschijnlijk kan toegeschreven worden aan effecten van sorteren en mengen. In dat geval blijken deeltjesgrootte correcties, zoals toegepast in composiet fingerprints A tot H, te gesimplificeerd te zijn, wat de hoge standaard afwijkingen in de modellen met Monte Carlo simulaties kan verklaren.

Pogingen om een complexere deeltjesgroottecorrectie te bepalen aan de hand van bezinkingstesten met materiaal en rivierwater van de Mangelbeek, Gete en Demer waren echter niet succesvol, aangezien het erg geflocculeerde materiaal niet gefractioneerd raakte. Daarom zal een andere methode ontwikkeld en gebruikt moeten worden om geflocculeerd sediment in verschillende fracties op te delen, zodat de relatie tussen deze fracties en de concentraties per parameter bepaald kan worden. Indien dit niet gebeurt, kan dit soort van fingerprinting (ruimtelijke bron fingerprinting) niet met voldoende nauwkeurigheid toegepast worden in het Demerbekken (en bij uitbreiding in Vlaanderen)

Organisch materiaal correcties leken het probleem in de ruimtelijke bron fingerprinting niet op te lossen, aangezien de RME_val waardes nog steeds onacceptabel hoog bleven en de resultaten waren onrealistisch. Echter, in het bron type sediment fingerprinting onderzoek in het Mangelbeekbekken (dat rijk is aan authigeen sediment) bleek dat een eenvoudige organisch materiaal correctie mogelijks wel goed werk levert. Of dit echter kan uitgebreid worden naar andere bekkens waar authigeen sediment significant aanwezig is, moet nog worden onderzocht.

Men kan dus besluiten dat sediment fingerprinting in het Demerbekken (en bij uitbreiding in Vlaanderen), waarbij uitsluitend gebruik gemaakt wordt van de geochemische samenstelling van het sediment niet kan gebruikt worden zolang er geen bruikbare deeltjesgrootte correctiefactor is vastgesteld en de impact hiervan op het sediment fingerprinting resultaat kan nagegaan worden. Hierdoor kan dan ook de onzekerheid op de modelresultaten door de impact van de menselijke ingrepen op de performantie van het model en de impact van de correctiefactoren uit elkaar gehaald worden.

Een gedeelte van deze onzekerheid echter, kan mogelijks geïntroduceerd worden door de opbouw van het sediment fingerprinting model. Daardoor kan een verandering in deze opbouw (waarbij nog meer rekening gehouden wordt met statistische onzekerheden) mogelijks een positieve invloed hebben op de modelresultaten.

Dit is het onderzoeken waard.

Content

List of tables

List of figures

Abbreviations

- A: Authigenic sediment; abbreviation used in fingerprinting samples
- ASF_{Resus}: Resuspended Authigenic Sediment Flux (used in PRE-MARS, MARS 1.0 and MARS 2.0)
- $ASF_{Resus,n}$: Resuspended Authigenic Sediment Flux originating from reservoir n (MARS 2.0)
- ASF_{Seep}: Authigenic Sediment Flux entering the river through groundwater seepage (used in PRE-MARS, MARS 1.0)
- ASF_{Set} : part of the ASF_{Seep} that settles on the riverbed (used in PRE-MARS, MARS 1.0)
- $ASF_{Set,Acc}$: settled authigenic material accumulated on the riverbed (used in PRE-MARS and MARS 1.0)
- $ASF_{Set,Acc,n}$: settled authigenic material accumulated on the riverbed in reservoir n (used in MARS 2.0)
- $ASF_{Set,Acc,n}^{\max}$: maximum of accumulated ASF that reservoir n can hold (used in MARS 2.0)
- ASF_{Sus}: part of the ASF_{Seep} that remains in suspension (used in PRE-MARS, MARS 1.0)
- ASSF: authigenic suspended sediment flux
- BCF: Bias Correction Factor
- BLKS: Brulandkrijtsysteem = Bruland Cretaceous System, groundwater system with phreatic aquifers in Nete and Demer basin
- C: Cultivate land; abbreviation used in fingerprinting samples
- CB: Channel Bank; abbreviation used in fingerprinting samples
- CKS: Centraal Kempisch Systeem = Central Campine System, groundwater system with phreatic aquifers in Nete and Demer basin
- DI water: deionised water
- DFA: Discriminant Function Analysis; statistical test used in sediment fingerprinting research to determine which properties are allowed to enter a composite fingerprint
- DQS: Documented Quality System of the Technical Supportive Services of the Department of Mobility and Public Works, location where Procedures, Instructions and Forms of (amongst others) FHR are stored
- EDI-method sampling: Equal-Discharge-Increment method sampling, sampling method to collect depth- and width integrated suspended sediment samples of a river cross-section.
- EDXRF: Energy Dispersive X-Ray Fluorenscence

- EIW: Emisson Inventory Water model, model used by VMM to calculate emissions into surface water originating from different sources.
- EWI-method sampling: Equal-Width-Increment method sampling, sampling method to collect depth- and width integrated suspended sediment samples of a river cross-section.
- F_s = general correction factor for source grouping (s); used in the objective function in the sediment fingerprinting research
- $Fe(II)_{Bf}$:Fe(II) concentrations present in the baseflow (used in PRE-MARS, MARS 1.0)
- $Fe(II)_{If}$: Fe(II) concentrations present in the interflow (used in PRE-MARS, MARS 1.0)
- F_{Cons}: correction factor that represents the fraction of accumulated authigenic sediment that can be resuspended (used in MARS 1.0)
- $F_{Cons,n}$: correction factor that represents the fraction of accumulated authigenic sediment that can be resuspended from reservoir n (used in MARS 2.0)
- F_{Er}: dimensionless fraction of authigenic settled sediment which is being resuspended due to the erodibility of the riverbed (used in MARS 1.0 and MARS 2.0)
- F_{Resus}: dimensionless fraction of accumulated ASSF that is being (eroded and) resuspended; combination of F_{Cons} and F_{Er} in MARS 1.0 (used in PRE-MARS and MARS 1.0)
- $F_{Resus,n}$: dimensionless fraction of accumulated ASSF that is being eroded and resuspended from reservoir n (used in MARS 2.0)
- F_{Set}: Settling Correction Factor (used in MARS 1.0)
- F_{So}: Sorption Correction Factor (used in MARS 1.0)
- F_{Sus}: Suspension Correction factor (used in PRE-MARS)
- F_{St}: Stoichiometric Correction Factor (used in MARS 1.0)
- F_T: Total Correction Factor; combination of F_{St} and F_{So} (used in PRE-MARS)
- FHR: Flanders Hydraulics Research
- GWL: Grondwaterlichaam = Groundwater body
- GS: grain size
- H: gauge height
- HCOV: Hydrogeologische Codering van de Ondergrond van Vlaanderen = Flemish hydrogeological codification system
- ISCO: automatic pumping sampler from Hach Company
- KW-test: Kruskal-Wallis H-Test; non-parametrical statistical test used in sediment fingerprinting research to confirm the ability of individual properties to distinguish between different sources

- LHS: Latin Hypercube Sampling; statistical method for sampling from a distribution in a stratified fashion
- LOI: loss of mass on ignition; laboratory analysis technique to estimate organic matter content
- MAD: Median absolute Deviate; a robust statistical scale estimator
- MARS: Model for Authigenic River Sediment
- MC: Monte Carlo simulations; computational algorithm that relies on random sampling to obtain numerical results
- OM: organic matter
- OMC: organic matter content
- P: Pastures; abbreviation used in fingerprinting samples
- Pdfs: probablility density functions
- PIDPA: Flemish Public water supply society for the Antwerp region
- PP: Predictive Power; used in sediment fingerprinting to indicate how well a single property or composite fingerprint is capable of correctly attributing sediment to its respective source
- PRESS: PRediction Error Sum of Squares; validation-type estimator of error
- Q: water discharge
- Q_{Bf}: Baseflow; Groundwater flow in the saturated zone, contributing to the total water discharge (used in PRE-MARS, MARS 1.0)
- Q_{Br}: breakpoint discharge above which physical remobilisation occurs (used in PRE-MARS)
- Q_{If}: Interflow; Groundwater flow in the unsaturated zone, contributing to the total water discharge (used in PRE-MARS, MARS 1.0)
- Q_{Of}: Overland flow; run-off, contributing to the total water discharge
- RME: relative mean error (of properties present in the composite fingerprint)
- RME_val: relative mean error of properties passing the KW-test, but not incorporated in the composite fingerprint
- RME_avg: relative mean error of all properties passing the KW-test, both included in and excluded from the composite fingerprint
- RMSE: Root Mean Square Error
- SSC: suspended sediment concentration
- SSC_{ISCO}: suspended sediment concentration from water samples obtained by an automatic pumping sampler

- SSC_{SW}: suspended sediment concentration from water samples obtained by superficial dip sampling
- SSF: suspended sediment flux
- TAW: Tweede Algemene Waterpassing; national reference level
- TIS: time-integrated sampler
- USGS: United States Geological Survey
- USLE: Universal Soil Loss Equation
- VMM: Vlaamse Milieu Maatschappij = Flemish Environment Agency
- WETSPRO: tool developed by Willems (2000) to seperate the total hydrograph in baseflow, interflow and overland flow contributions
- W_i = Discriminatory Weighting Correction Factor; used in the objective function in the sediment fingerprinting research
- W&Z: Waterwegen en Zeekanaal NV, water managers for the navigable rivers in Flanders
- XRF: X-Ray Fluorescence
- YSI-probe: Multi-parameter probe, measuring turbidity, conductivity, temperature, pH, redox-potential

Introduction

Objectives

Sediments in rivers are a natural part of the river system. The river is in a way a conveyer belt that transports material from the place of origin to the ocean, depositing some of its sediment along the way trying to find a state of equilibrium in a continuously changing environment.

These natural processes of erosion, deposition and transport of sediment in river systems, however, can pose problems for policy-makers and river managers, who need to address issues such as dredging, flood control, soil erosion and water quality. Therefore reliable measurement of sediment fluxes has always been of primordial importance as it allows the calculation of sediment budgets and gives indications on the changing nature of the river system. Also reliable information on sediment sources and their relative contribution to downstream sediment fluxes is of vital importance, if river management problems are to be addressed (Collins et al., 2001; Collins & Walling, 2004; Evans et al., 2006).

Therefore, the objective of this PhD thesis is to find answers to the following questions.

1. How much sediment is being transported in (selected) rivers within the river Scheldt basin?
2. Where does this sediment originate from?
3. And how much do specific sources contribute to the observed sediment fluxes?

To answer these questions a continuous collaboration with Flanders Hydraulics Research (FHR) was established, which allowed for a mutually enriching experience. FHR has a network of continuous measurement stations in the river Scheldt and its tributaries, where besides gauge height, discharge and stream velocity, also physical parameters and sediment concentrations are measured. However, for the sediment and physical parameter measurements, the applied methodologies had not been standardised or documented. Therefore, within the framework of this PhD, methodologies and procedures for executing terrain and laboratory measurements and analyses were either established or adjusted to meet international standards or site-specific needs and consequently formalised in instructions. These instructions can be found in the Documented Quality System of the Technical Supportive Services of the Department of Mobility and Public Works, and they were key to the sedimentological laboratory of FHR achieving an ISO 9001:2000 certification in 2009, and also contributed to FHR as an organisation achieving an ISO 9001:2008 certification in 2010.

After the methodologies and procedures were established, the data obtained from the continuous measurement stations of FHR could be used within the framework of this PhD research. However, attempting to answer these questions for the river Scheldt itself would be too ambitious (due to the complex nature of the tidally influenced and anthropogenically impacted river), therefore a smaller river system should be selected as study area within the framework of this thesis. Consequently, if the results of this PhD research prove promising, then this research can be extended to cover the entire river Scheldt basin. However, finding a sub-catchment representative of the variability present in the entire Scheldt basin is virtually impossible. Therefore, two separate sub-basins of the river Scheldt were selected.

The first selected sub-basin is the Nete basin, because of its presence of a specific sediment source: ferric authigenic sediment. This sediment source originates from precipitation of soluble iron due to changing environmental conditions. On an international level, very little is published about the contribution of this sediment source to the total sediment load of rivers. Generally,

publications addressing sediment sources (Collins et al., 1997 a, 1997 b, 1997 c; 2001; Walling et al., 1999; Collins & Walling, 2004; Alvarez-Guerra et al., 2009) and models calculating the amount of sediment entering the river (Morgan et al., 1998; Verstraeten et al., 2002; Van Rompaey et al., 2003; Collins et al., 2007), do not take authigenic sediment into account, but rather focus on other sources, such as physical erosion, biological sources (e.g. algae and diatoms) and anthropogenic sources (e.g. sewage treatment discharges and industrial discharges). This is most likely due to the fact that the regions of interest in these studies are often characterized by high land erosion, hence decreasing the relative contribution of authigenic sediments to the total sediment load transported by a river, or that in these regions, due to the lack of geological conditions favourable to the production of authigenic sediment, little is produced.

Nevertheless, when the conditions are favourable, authigenic sediment can significantly contribute to the total sediment load of a river system as is the case in the Nete basin where, due to its very specific geological and geographical setting, ferric authigenic sediment is produced in high quantities and contributes significantly to the total sediment load of the river system. Both theoretical calculations and numerical modelling were executed in the framework of this thesis to estimate the exact contribution of authigenic sediment source to the total sediment load (as is described in Chapter 8). However, to fully understand the impact of authigenic sediment on the sediment load it is necessary to gain a more detailed insight into the nature of this material, and therefore more exploratory research into the nature of the authigenic material was carried out (described in Chapter 9).

The second sub-basin was selected in order to attempt to apportion the contribution of different sources, including authigenic sediment. The Demer basin was selected because its northern half has a similar geological setting as the Nete basin, ensuring the generation of authigenic sediment, while the southern part is characterized by a completely different geological and topographical setting, ensuring erosion and therefore a greater detrital input in the sediment load of the Demer. Even though the Demer basin itself is not representative of the Scheldt basin, it does allow the study of mixing of sediment sources of a different geological nature.

To estimate the contributions of different sources some river basin managers make use of available models to predict soil erosion and resulting sediment delivery pressures (e.g. Morgan et al., 1998; Verstraeten et al., 2002; Van Rompaey et al., 2003; Collins et al., 2007). However, validation of the predictions by such models at catchment scale is frequently difficult, especially in situations where the model framework fails to represent the entire sediment budget (Strömqvist et al., 2008).

An approach often used to remedy this is composite sediment fingerprinting. This method, developed at the University of Exeter is widely used (Collins et al., 1996, 1997 a, 1997 b, 1997 c, 2003; Walling et al., 1999; Collins & Walling, 2002, 2004; Carter et al, 2003; Krause et al. 2003; Walling, 2000, 2003, 2005; Small et al., 2005; Minella et al., 2008 b; Juracek & Ziegler, 2009; Wilkinson et al., 2009; Stutter et al., 2009; Nosrati et al., 2011; Mukundan et al., 2011; Evrard et al., 2011; Navratil et al., 2012 amongst others) to identify the relative contribution of various watershed sources to the total suspended sediment load.

Therefore, within the framework of this PhD thesis, it is the objective to apply the sediment fingerprinting approach in the Demer basin and to, if necessary, adapt the methodology to suit the Flemish situation. Furthermore, the results of this research will allow for an estimation of the applicability of this methodology in other river systems in Flanders.

Overview of the structure of the thesis

This thesis is structured in five parts, preceded by this introduction and followed by a conclusion, as can be seen schematically in Figure 0.1.

The first part encompasses the more general information such as study area (Chapter 1), methodologies, and equipment used in the field (Chapter 2) and procedures, analyses and equipment used in the laboratory (Chapter 3). In these chapters the distinction will be clearly made between procedures and equipment used for the continuous monitoring at sediment measurement locations of FHR, and procedures and equipment used specifically for authigenic sediment research or sediment fingerprinting research.

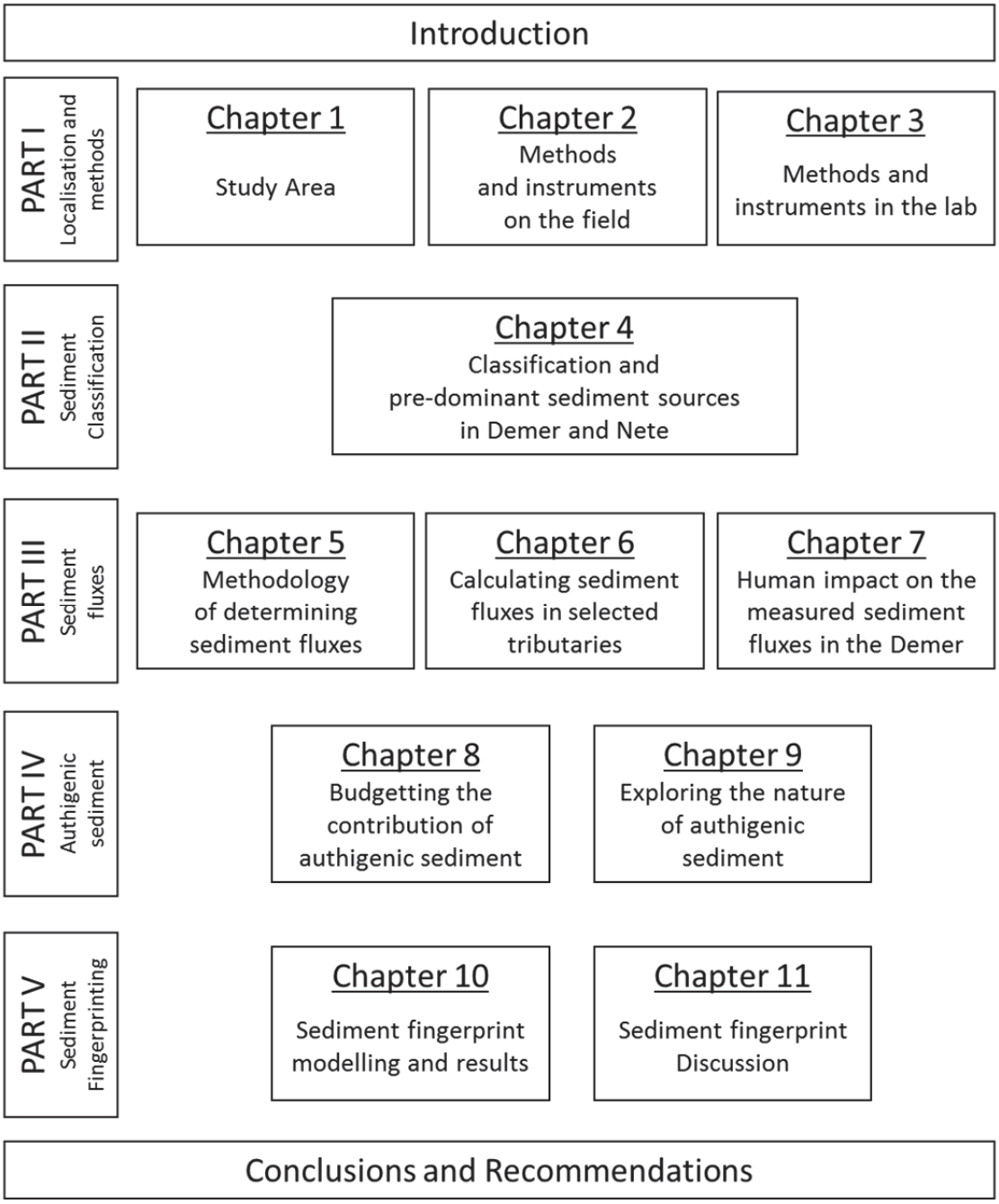

Figure 0.1: Overview of the structure of the thesis

As a significant portion of the research in this thesis concerns different sources of fluvial sediment, the different classifications of fluvial sediment as described in the literature are presented in Part II. This second part is only comprised of one chapter (Chapter 4) in which these classifications are summarised and the pre-dominant sources of fluvial sediment in the Demer and Nete basins are discussed.

Part III of this thesis addresses the issue of suspended sediment fluxes. If contributions are to be calculated, it is necessary to firstly establish the total suspended sediment load of a river system. Chapter 5 describes the methodology and challenges to obtain such suspended sediment fluxes and loads, while in Chapter 6 these methods are applied to calculate sediment fluxes for selected locations in the Demer and Nete basin, pivotal to the authigenic sediment and fingerprinting research. The final chapter in Part III, Chapter 7, addresses the impact of human intervention on the observed sediment fluxes in the measurement station of Aarschot on the Demer.

After the total sediment fluxes have been determined, the contributions of the authigenic sediment can be estimated using theoretical deduction and modelling. The MARS model (Model for Authigenic River Sediment) was developed at FHR for exactly that purpose, and it has undergone three different incarnations. They are all described in Chapter 8. However, the model used various assumptions, and to reduce the uncertainties on some of the estimates, research was done into the nature of the authigenic sediment and the suspended sediment present in these authigenic sediment-rich rivers. This research is discussed in Chapter 9, as are the final results of the MARS modelling for one decade of sediment transport in the Kleine Nete, using the insights obtained through this research.

The final part of this thesis, Part V, describes the sediment fingerprinting research. In Chapter 10, the methodology as established by Walling & Collins (2000) is explained in detail (and applied to the Demer basin) and consequently the modelling results are presented and discussed in detail. The suspended sediment fluxes as determined in Chapter 6 are consequently used as validation tools.

Some basin-specific conditions lead to insights into the useful and hindering effects of human impact in the river system. These are addressed in detail in a separate chapter (Chapter 11). Also discussed in this chapter is the use of specific correction factors, which are commonly introduced into the sediment fingerprinting modelling, but seem to be too simplistic or unnecessary in specific settings in the Demer basin.

To end this thesis, a final section (Conclusions and Recommendations) summarizes all the conclusions of the preceding chapters and presents suggestions for continuing research that might answer some of the questions that were raised through the research executed within the framework of this PhD.

Part I

Localisation and Methods

1. Study area

As explained in the introduction, two tributary basins of the river Scheldt have been selected (i.e. the Nete and Demer basins) as study areas within the framework of this thesis. If the results of this PhD research prove promising, then the same approach can be extended to cover the entire river Scheldt basin.

In this chapter, the geographic localisation, hydrography, relief, soil as well as soil use and geology of these two basins are discussed.

1.1 Geographic localisation and hydrography

The Nete basin and Demer basin neighbour each other. The Nete basin is situated in the northeastern part of Flanders, while the Demer basin situates itself just south of that, and even reaches partly into Wallonia (see Figure 1.1).

Figure 1.1: Localisation of the tributary basins within the river Scheldt basin
(raw GIS-data owned by VMM – Afdeling Operationeel Waterbeheer)

Hydrographically, the Nete basin is furthermore neighboured in the north and east by the Meuse basin, in the southwest by the Dijle basin and in the west by the Seascheldt basin. The entire Nete basin drains towards the latter. The Demer on the other hand, drains into the rivers Dijle and Zenne, whose basins borders the Demer's on the west. The Meuse basin borders the east and south sides of the Demer basin.

The total catchment area of the Nete basin is 1,673 km². 813 km² of these are drained by the Kleine Nete, while 736 km² are drained by the Grote Nete, and the remaining 124 km² are drained by the Beneden-Nete (Lower-Nete) as can be seen in Figure 1.2.

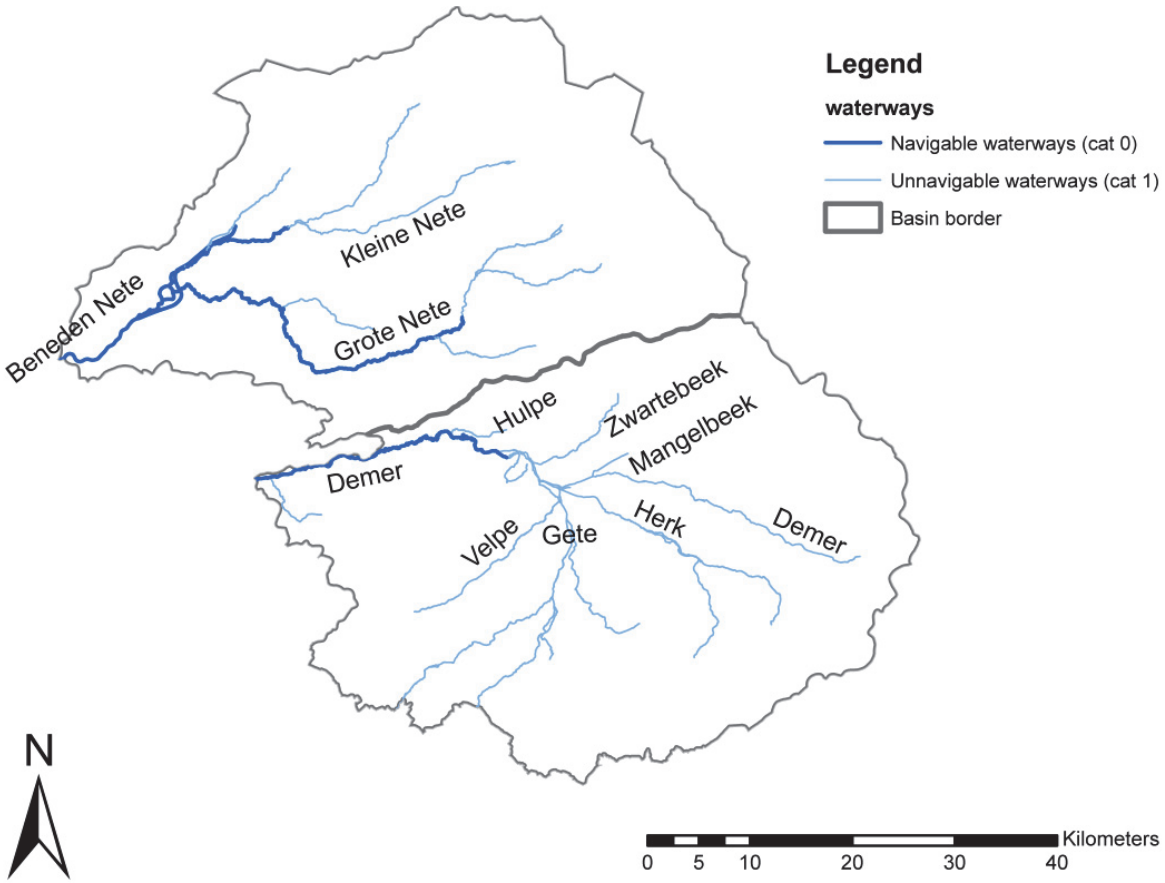

Figure 1.2: Demer and Nete basin with their principal tributaries
(raw GIS-data owned by VMM – Afdeling Operationeel Waterbeheer)

The Demer basin is somewhat larger than the Nete basin, with its total catchment area of 2,334 km², of which 1,919 km² are located in Flanders. Contrary to the Nete basin, with its two major tributaries, the Demer basin is divided into a northern and southern part, each with their proper set of tributaries, with the Demer itself flowing from east to west as the separator between the two parts, as can also been seen in Figure 1.2. The most significant tributaries entering from the north are (from source to mouth) the Mangelbeek, the Zwartebeek and the Winterbeek/Hulpe, while the southern most prominant tributaries are the Herk, the Gete and the Velpe. Figure 1.3 shows these two river basins and their most significant tributary catchments.

The Nete basin, unlike the Demer basin, is subjected to the tides present in the Scheldt. This influence can still be registered in the Lower-Nete, the Grote Nete up to Itegem and the Kleine Nete up to Grobbendonk. In the more upstream reaches of the basin where the influence is still measurable, it occurs in the form of backwater.

1.2 Relief

The Nete basin has a mostly flat topography, with heights varying from 0 to +/- 70 m TAW. The highest areas are situated in the eastern part of the basin, at the Kempens Plateau (Campine Plateau), near the border of the Meuse basin (see Figure 1.4).

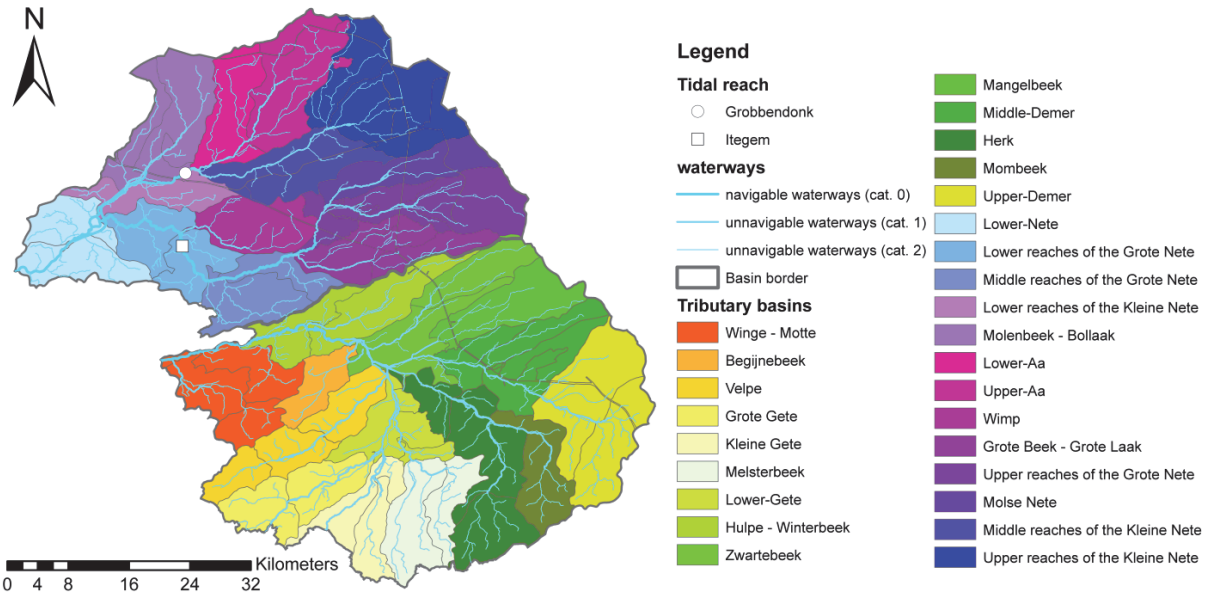

Figure 1.3: The Nete and Demer basins with their respective most significant tributary basins. The locations of Grobbendonk and Itegem show the penetration of the tide (raw GIS-data owned by VMM – Afdeling Operationeel Waterbeheer)

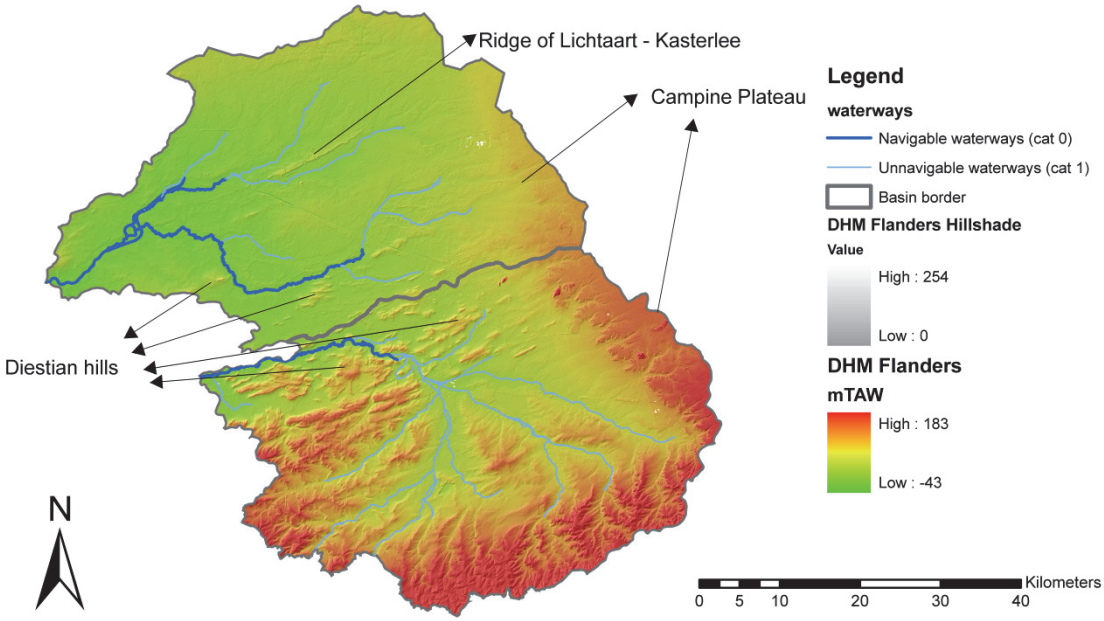

Figure 1.4: Relief of the Nete and Demer basin (raw GIS-data owned by FHR and VMM)

The relief in the northwest of the basin, determined by the Kleine Nete and the Aa differs from the relief in the southwest, which has the Grote Nete, the Molse Nete and the Grote Laak as major tributaries.

The north-western relief differentiates itself from the southern by the presence of SW-NE oriented poorly incised and wide river depressions, which are separated from one another by slightly

elevated sand ridges. The only exception in this northern Nete basin depression is the SW-NE oriented ridge of Lichtaart-Kasterlee, which consists of Pliocene sands covered by Quaternary cover sands, and in effect is the water divide between the Kleine Nete and the Aa.

The southwestern part of the Nete basin has a drainage pattern flowing from east to west, and the valleys of the streams are narrower than those of the north-western part, due to the southwest-northeast oriented Diestian hills, which have a much steeper slope than the Campine Plateau. The Diestian hills are fossilized shoals from the Late-Tertiary Diestian Sea, and as they are composed of iron-sandstones or limonite, they were able to withstand the weathering.

The Demer basin on the other hand is divided into three different regions, each characterized by a different relief. The three regions are called the Hageland region, the Campine Plateau and the Haspengouw region (see Figure 1.5). The latter can be divided into two sub-regions, Vochtig (humid) Haspengouw and Droog (dry) Haspengouw, based on the topography and the related variation in soil composition.

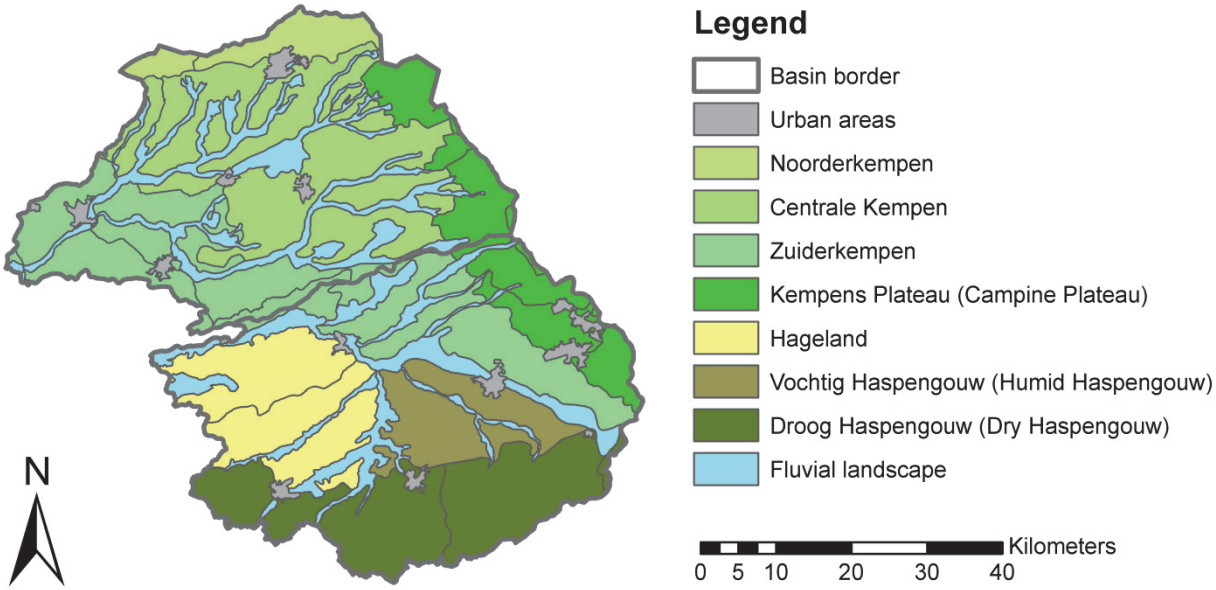

Figure 1.5: Flemish regions in the Nete and Demer basins (raw GIS-data owned by Afdeling Natuur en Bos)

The Hageland region's most dominant feature is a series of southwest-northeast oriented parallel hills, similar to those observed in the Nete basin. The Campine Plateau, is elevated but quite flat, with an average height of 80 m. Humid Haspengouw is characterized by a flat, only slightly wavy relief, varying from 30 m TAW in the north to 60 m TAW in the south while dry Haspengouw is a hilly relief, with level variations from 60 to 100 m, with in between locally elevated plateaus. The hills are remnants of the fluvial erosion taking place during the Quaternary.

1.3 Soil and soil use

The largest part of the Nete basin is located in the Sand Region. Hence, the Nete basin has mostly sandy soils, with the Campine podzol soil being a typical example. The southwestern part of the Nete basin however, is located in the sand-loam region, where mostly light sandy-loam soils appear. The transition between the two regions is formed by loamy sand soils.

In the past, the water system was a determining factor for land use in certain areas: valley soils were used as hay land while dryer parcels of lands were applicable for agriculture or housing.

However, over the last decennia this has changed drastically when large parts of the valley areas have been allocated to housing, infrastructure, industry, agriculture etc. This has significantly influenced the runoff and captation potential of the Nete valleys.

Currently, the surface of the Nete basin is occupied by 26.4% pastures and grass land, 23% by forrest (mostly located on the Campine Plateau and on the hill between Herentals and Kasterlee), and 20.5% by agri- and horticulture. The amount of impermeable surfaces has doubled in the last 20 years and represents now 25% of the Nete basin surface.

A not insignificant 2% of the surface of the Nete basin is covered with ponds, which are by-products of the excavation of white quartz-rich sands for the glass industry (Sands of Mol), or excavation of peat.

In the Demer basin the area north of the Demer (such as the Campine Plateau) is characterized by sandy soils. South of the Demer, the soils transition into sand-loam soils (Hageland and Humid Haspengouw) to end in loamy soils even further south (Dry Haspengouw).

In the Demer basin, soil use for agricultural purposes takes up about 40% of the available area. However, most of this is situated in the southern half of the basin (on the fertile loamy soils of the Hageland and Haspengouw regions). Pastures are good for about 20% of the soil use, and are concentrated on the wetter areas. Impermeable surfaces also take up around 20%. Forrest covers about 16% of the basin, mostly situated on the Campine Plateau (in the East of the Demer basin). About 1% of the surface of the Demer basin is used by ponds, some of which are used as active retention ponds during flood events.

1.4 Geology

The deep subsoil of Nete and Demer basins belong to two major tectonic units; the northern part of the Demer basin and the entire Nete basin are located in the Campine Basin, while the southern part of the Demer basin is located on the Brabant Massif. The latter is comprised of Caledonic (Cambrian-Silurian) rocks, which are covered by layers of Mesozoic, Tertiary and Quaternary age. As the Brabant Massif tilts towards the north, its Caledonic rocks occur deeper in the northern part of the Demer basin and deeper still in the Nete basin, where they form the basement for younger Variscan (Devonian-Carboniferous) rocks of the Campine Basin (a.o. coal), which are in turn covered by layers of Mesozoic, Tertiary and Quaternary age.

During the Cretaceous and the Tertiary the area was subjected to subsidence (which was more pronounced in the north than in the south). This lead to deposition of Mesozoic and Tertiary sediments sloping towards the north, with their thickness increasing from south to north. As a consequence of the sloping of the deposits, older Tertiary layers (Paleogene) crop out in the south of the Demer basin, while younger Tertiary (Neogene) deposits find their way to the surface in the Nete basin. The Neogene sands, which are directly deposited on the Formation of Boom (a clayey aquitard of Paleogenic age) and cover most of the Nete basin, reach a maximum thickness of about 200 m in the north-northeast of the Nete basin and winnow out along the Demer axis, where the Formation of Boom surfaces as can be seen on the geological map of the area (see Figure 1.6). A lithostratigraphic and chronostratigrafic description of all Tertiairy formations present in Flanders is presented in Table 1.1.

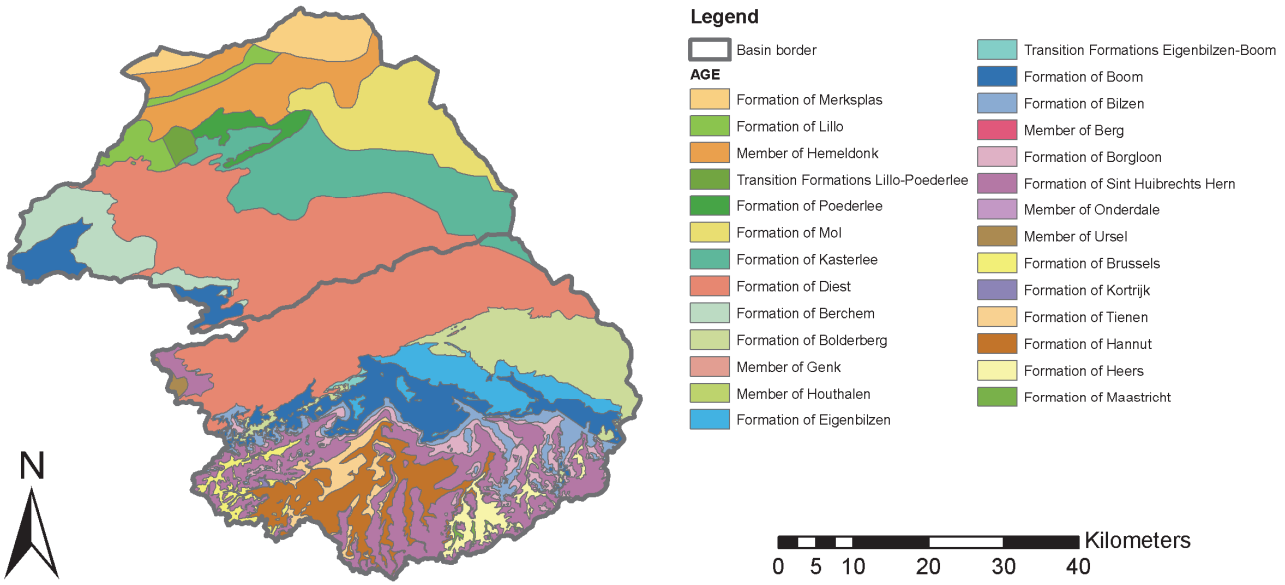

Figure 1.6: Geological map of the Nete and Demer basin
(raw GIS-data owned by Vlaamse Overheid-departement LNE – ALBON)

In the southern part of the Demer basin, the hilly relief is shaped by fluvial erosion taking place during the Quaternary. The rivers incised themselves in the younger Tertiary material of Eocene age (still present in the hills), allowing the Paleocene deposits to be exposed in the river valleys. The Tertiary deposits in this part of the Demer basin are covered by relatively thin Quaternary sandy-loam deposits, which are sensitive to erosion.

1.5 Hydrogeology

In the framework of studying the genesis of authigenic sediment, the contribution of groundwater seepage to the discharge of a river basin is of primordial importance. Therefore, for the Nete and Demer basins, only the phreatic groundwater bodies and the phreatic groundwater systems in which they sit are of interest within the framework of this PhD research and are therefore discussed in this section.

The terminology and names of formations, aquifers and aquitards used in this section are in Dutch as they are also based on the official HCOV-codification system[1] (the Hydrogeologische Codering van de Ondergrond van Vlaanderen). This is a codification system, based on the geological formations, naming the successive aquifers and aquitards, defined in VLAREM I (Order of the Flemish Government of 6 February 1991 concerning Environmental Licences). However, where possible, an English translation will be provided between ( ) and in italic. The complete HCOV codes are presented in Addendum A, and in this thesis these codes are noted in between [ ].

Groundwater systems are comprised of different grondwaterlichamen (GWL) (*groundwater bodies*). Such a groundwater body is defined by the Water Framework Directive as a distinct volume of water. The codification of these groundwater bodies is based on the HCOV-code of the most significant aquifer.

[1] The Hydrogeologische Codering van de Ondergrond van Vlaanderen (HCOV) is a four-digit code in which the first two numbers group a succession of geological layers that have similar hydrological properties and therefore form one unit. The third number in the HCOV-code, shows the detailed division between aquifers and aquitards. Finally, the fourth number identifies hydrogeological basic units. For more information, consult Databank Ondergrond Vlaanderen (DOV, 2011).

Table 1.1: Lithostratigraphic and chronostratigrafic description of all Tertiairy formations present in Flanders. Table based on (DOV, 2011), which based the Paleogene on Maréchal and Laga (1988) and the Neogene on De Meuter & Laga (1976)

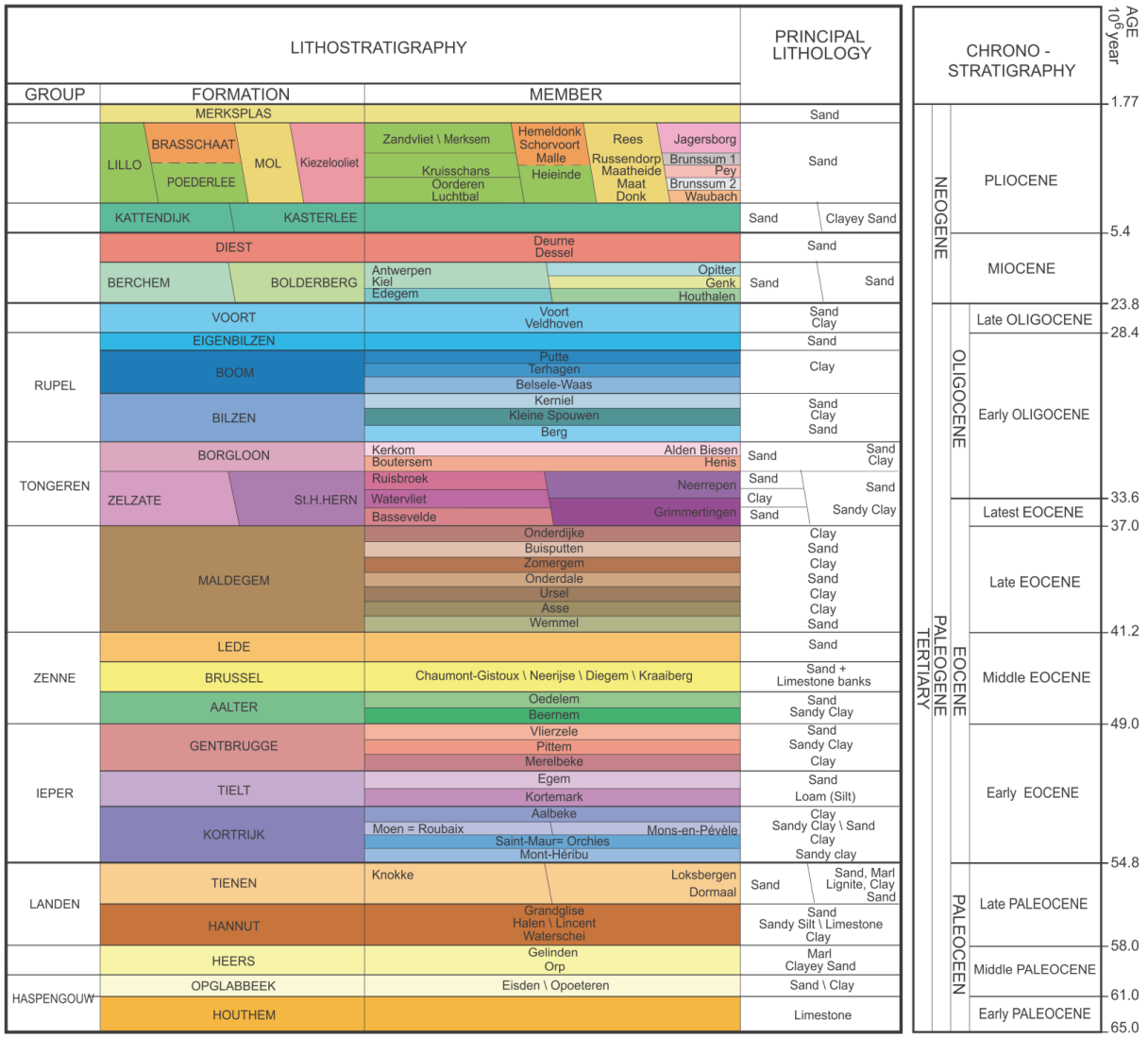

There are two groundwater systems with phreatic aquifers in the Demer and Nete basins: the Centraal Kempisch Systeem (CKS), (*Central Campine System*) overlays the Brulandkrijtsysteem (BLKS) (*Bruland Cretaceous System*) and both are separated from one another by the Boom Aquitard [0300]. Both are present in the Demer and Nete basins but the BLKS system is of more importance in the (southern) part of the Demer basin than it is in the Nete basin as can be seen in Figure 1.7 which shows the localisation of the six groundwater systems present in Flanders and can be seen on a NE-SW cross-section through the Nete and Demer basin as presented in Figure 1.8.

Within the **Centraal Kempisch Systeem (CKS)** only two water bodies are phreatic in the Nete and the Demer basin and are therefore of interest in the framework of this thesis:

- The most significant one is the Centrale zanden van de Kempen (Central Campine sands) water body (CKS_0200_GWL_1), which is comprised of sediments from the Quartaire Aquifersystemen [0100] (*Quaternary aquifer system*) and sediments from the Kempens Aquifersysteem [0200] (*Campine Aquifer system*). The groundwater flow in this groundwater body is varied.

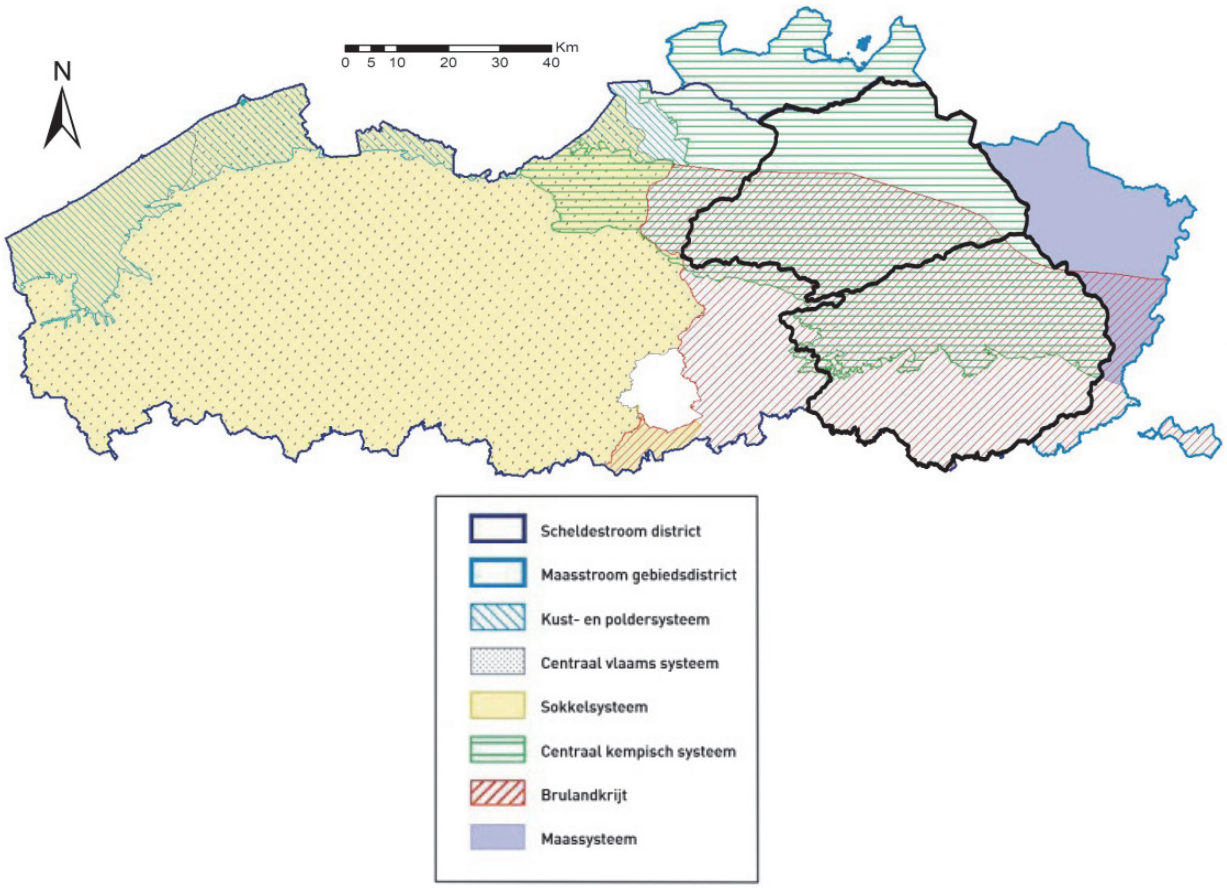

Figure 1.7: The six groundwater systems in Flanders (based on VMM (2008 a, 2008 b))

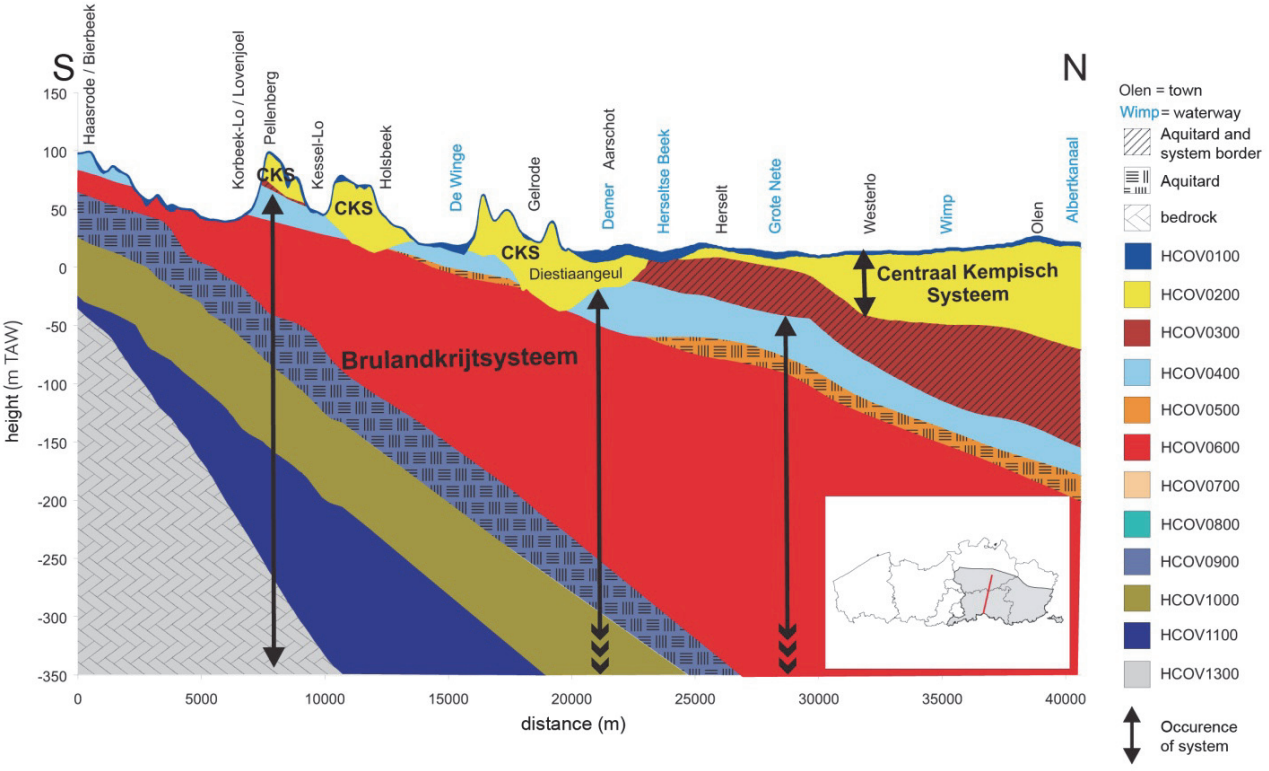

Figure 1.8: Northeast-southwest cross-section through the Nete and Demer basin (based on VMM, 2008 a)

- The second water body is the Diestiaangeul: contact Brusseliaan (*Diestian gully: contact with Brusselian*) (CKS_0250_GWL_1). The Diestiaangeul was formed during the Miocene, which was then filled in with Zand van Diest [0252] (*Diestian Sands*). The Boom Aquitard [0300], the system-dividing aquitard, has been eroded away by the gully and the Zand van Diest is directly deposited onto the Zand van Brussel [0620] (*Brusselian sands*). The groundwater in the Neogene sands flows, guided by the topography, in northern direction.

- Most of the Neogene aquifers in CKS (zandige top van de Formatie van Lillo [0233], Zand van Poederlee en/of zandige top van Kasterlee [0234], Zand van Diest [0252] and Zand van Berchem [0254]) contain relatively high to high quantities of glauconite.

Within the **Brulandkrijtsysteem (BLKS)** only three water bodies are phreatic or partially phreatic in the Nete and/or Demer basins and are therefore of importance in the framework of this thesis:

- The Brusseliaanvenster contact Diestiaan (*Brusselian window contact with Diestian*) water body BLKS_0600_GWL_3 is comprised of the Eocene Zand van Brussel [0620] (*sands of Brussels*) and it is the only groundwater body of the BLKS that is phreatically present in the Nete basin. In the Demer basin this groundwater body is only partly phreatic.

- The other BLKS groundwater body is the Brusseliaan Aquifer (BLKS_0600_GWL_1), which is comprised of the Zand van Brussel [0620] and the Zand van Mons-en-Pévèle [0923] (*sands of Mons-en-Pévèle*) but also contains sands from the Ieperiaan Aquifer [0800] (Ypresian aquifer). This ground water body is only (phreatically) present in the Demer basin.

- Finally, the last groundwater body of interest in the Demer basin is the phreatic part of the Oligoceen Aquifer Systeem (*Oligocene Aquifer System*) (BLKS_0400_GWL_1S). This groundwater body is comprised of deposits from the Oligoceen Aquifer systeem [0400], and on certain isolated hills in the area of Kortemberg–Bertem-Herent, this groundwater body is in direct contact with the Zand van Diest [0252], which is also considered part of BLKS_0400_GWL_1S.

The streams in the Nete basin and the northern part of the Demer basin, are mostly fed by groundwater originating from the CKS. And the aquifer that contributes most to the seepage is the Zand van Diest [0252], due to its thickness and high permeability (respectively maximal 150 m thick and K_h = 6-14 m/day (Lebbe, 1999)). These sands have been deposited, during the Miocene, in a gully, previously eroded into the Boom Aquitard [0300]. Because of the genesis, this formation is quite heterogeneous in composition. Lithologically, this formation is mostly comprised of green and brown glauconite-rich coarse sands. But locally zones rich in clay and mica are present as well as iron sandstone banks. Locally the formation has a base gravel of flattened flint nodules. This heterogeneous character leads to extremely variable concentrations of Fe(II) present in the formation, as will be discussed in more detail in Chapter 8. Nonetheless, a high influx of soluble iron into the Nete basin and the northern part of the Demer basin is ensured.

1.6 Conclusion

The neighbouring Nete and Demer basins have been selected as study areas within the framework of this thesis. The northern part of the Demer basin and the Nete basin have similar settings

(geological, relief, and soil and soil use), while the southern part of the Demer basin differs from that.

The northern part of the Demer basin and the Nete basin are characterized by a flat topography and sandy soils (apart from the Campine Plateau, which due to its gravel deposits is quite erosion resistant). About 20% of the soils are covered by impermeable surfaces, while 20% (mostly located on the Campine plateau) is covered in forrest. The rest is used for agri- and horticulture or pastures and grass land. (Hydro-)geologically, this region is characterized by Neogene iron-rich sands, which are directly deposited on the Formation of Boom (of Paleogene age). They reach a maximum thickness of about 200m in the north-northeast of the Nete basin and winnow out along the Demer axis. Due to the high iron-content of most of the aquifers in the Neogene sands (in particular the Zand van Diest [0252]) this will be the engine for the authigenic sediment production discussed in Chapters 8 and 9.

The southern part of the Demer basin, is characterized by a more hilly relief, and soil use more directed at agriculture. Geologically, older Tertiary layers surface (Paleogene age) and are covered with relatively thin Quaternary sandy-loam deposits (up to 20 m thick in the southern part of the Demer basin), which are sensitive to erosion. This will ensure a larger contribution of detrital sediment sources in the southern tributaries of the river Demer than were present in the northern tributaries and in the Nete basin.

2. Materials and methods applied on the field

This chapter describes the techniques and equipment used within the framework of this PhD. As mentioned in the introduction, this research was executed in close collaboration with Flanders Hydraulics Research. However, at the beginning of the PhD research, the methodology for monitoring sediment concentrations and/or physical parameters as deployed at FHR, even though based on international methodologies, lacked standardisation. Additionally, the methodology was not well-documented. Therefore, within the framework of this PhD thesis, and in collaboration with FHR field and laboratory personnel, a set of standardized methodologies, based on international standards and on site-specific conditions, was composed for the continuous sediment monitoring efforts of FHR. The methods were translated into instructions and forms, which are stored in the Documented Quality System (DQS) of the Technical Supportive Services of the Department of Mobility and Public Works and have been kept up to date since.

Therefore, the monitoring methods and equipment used in the routine monitoring of sediment and physical parameters by FHR, as far as applicable to the research of this PhD, are mentioned in Section 2.1. Furthermore, the methods and materials of the field work specifically executed for this PhD research are discussed in Section 2.2.1 (when related to the authigenic sediment research, addressed in Part IV) and in Section 2.2.2 (when related to the sediment fingerprinting research, addressed in Part V).

2.1 Instrumentation and monitoring methods as used at routine sediment monitoring locations of FHR

2.1.1 Suspended sediment sampling

From 1992 onwards, FHR has been monitoring suspended sediment concentrations (SSC) in tributaries of the river Scheldt basin, including the Nete and Demer, and on the Scheldt itself. At these locations, suspended sediment is being sampled on a regular base, using different sampling techniques. Figure 2.1 gives an overview of the locations where FHR routinely monitors sediment concentrations, using grab sampling, automatic sampling and EWI-method sampling (techniques which are all discussed in detail in the consequent sections).

2.1.1.1 Grab sampling

On every sediment monitoring location (both in the tidal as in the non-tidal part of the Scheldt basin location where sediment measurements have been executed) water samples have been collected on a weekly basis, either by bucket sampling or weighted-bottle grab sampling.

When collecting a grab sample by bucket, the bucket is lowered into the river after which a part of the content is transferred into a recipient (a 1 or 0.5 litre bottle). This technique is also applied by the Flemish Environment Agency (VMM, 2012) when sampling the rivers for physico-chemical water analysis, in which one of the parameters reported is the suspended sediment concentration.

However, this technique has some disadvantages. It is a superficially collected point sample, which will lead to an underprediction of the sediment concentration present throughout the entire cross-section, if the water in the river is not well-mixed. Furthermore, taking of a subsample from the bucket by pouring water into another recipient, or by lowering a bottle into the bucket will introduce additional uncertainty into the analysis.

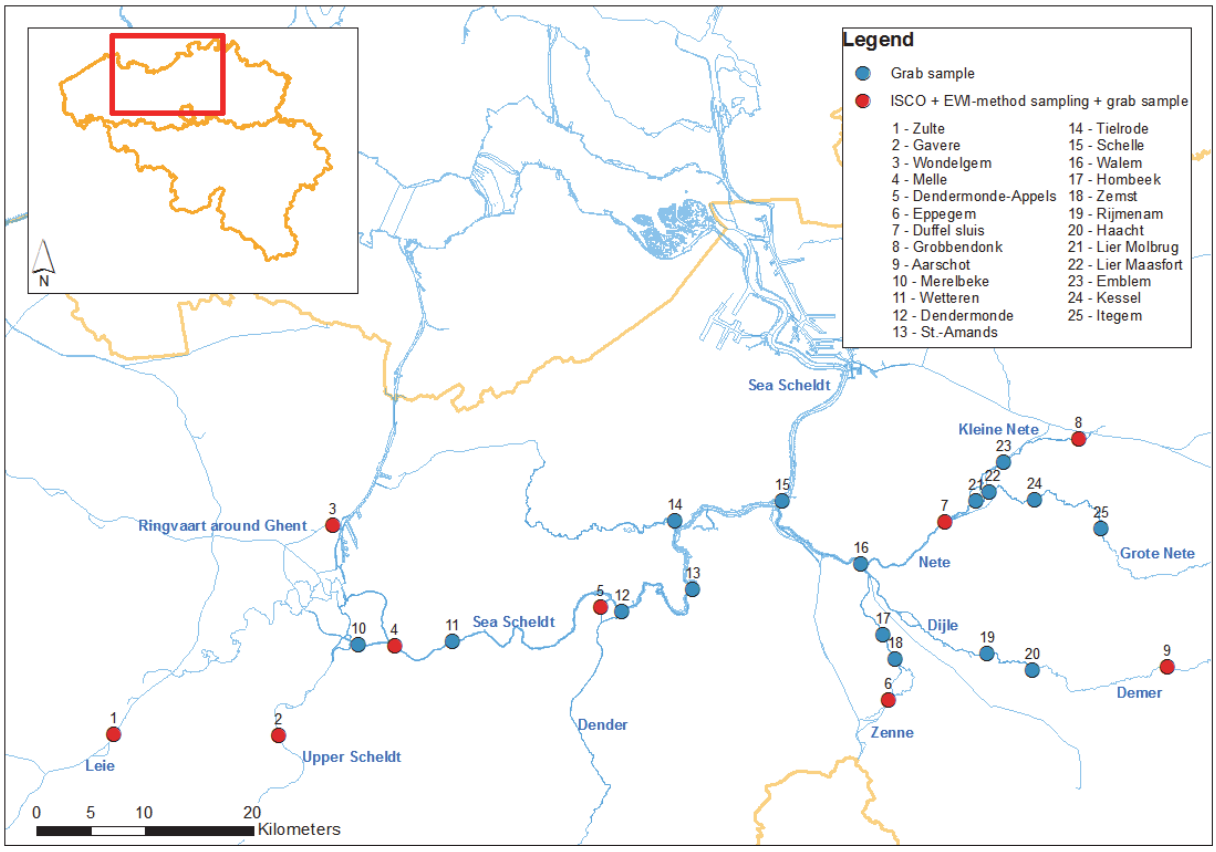

Figure 2.1: Sediment monitoring locations maintained by FHR (situation 2012)

Therefore, FHR designed and constructed a weighted-bottle sampler, shown in Figure 2.2, that eliminates some of these issues. Due to its weight it will lower more easily into the river, hence allowing for sampling more deeply than the most superficial water layers.

Figure 2.2: Weighted-bottle sampler as constructed by FHR

Figure 2.3: Unrefrigerated SIGMA 900 automatic pumping sampler, with 24 bottles

Whether this yields a sediment concentration representative of the entire cross-section, however, can only be determined by cross-sectional calibration sampling efforts as discussed in Paragraph 2.1.2.3, but it does yield higher sediment concentrations than the superficial bucket sampling.

Another advantage of the weighted-bottle sample, is that the recipient is filled while sampling, and no further subdividing of the sampled water-sediment mixture is required, eliminating the extra source of potential inaccuracy. The bottle is taken out of the sampler and transported to the sedimentological lab of FHR for analysis.

To conclude, for the sampling locations of FHR, the choice has been made to unify the sampling methodology from 2011 onwards, and since then sampling has only been executed using a weighted-bottle sampler on every one of their sampling locations. The methodology is described in detail in Instruction I-WL-PP33-8 (Vereecken & Mostaert, 2013 a).

2.1.1.2 Automatic sampling

The easiest way to collect water samples with a high frequency is using an automated device. Since the start of the monitoring on the non-tidal locations, FHR has installed automatic pumping samplers. Initially, FHR installed SIGMA 900 Standard Portable Sampler equipment (Hach company, Loveland, Colorado, USA). These samplers contained 24 1L bottles, and had been programmed to sample every 7 hours, as to fill their entire bottle set in one week (see Figure 2.3).

However, these samplers had a limited suction lift, which sometimes caused problems (samplers being flooded during high-flow conditions; see Figure 2.4 for an illustration). Also, they lacked refrigeration capabilities, which could cause problems during summer periods when elevated temperatures would increase biological growth in the sampled water samples, prior to them being transported to the sedimentological lab of FHR for analysis.

Figure 2.4: Aarschot sediment monitoring location during a) low-flow conditions (5-6-2008) and b) high-flow conditions (2-3-2004) leading to the inundation of the construction containing the SIGMA 900 sampler.

Therefore, from 2006 onwards, on the FHR sediment monitoring locations, the SIGMA samplers have been replaced with ISCO 6712FR samplers (Teledyne Isco, Inc., Lincoln, New England, USA), which have a greater suction lift and store the samples refrigerated on site (see Figure 2.5). The sampling frequency has remained unchanged (water samples collection takes place every seven hours). The methodology of maintenance (timely replacing of tubing, check of internal clocks, entering sampling programmes, …) is explained in Instruction I-WL-P34-1 (Vereecken & Mostaert, 2013 b).

Figure 2.5: Refrigerated ISCO 6712FR automatic pumping sampler, with 24 bottles (Teledyne Technologies Inc.; 2012)

2.1.1.3 Cross-sectional sampling

The purpose of collecting sediment samples is to determine the instantaneous sediment concentration at a cross-section. However, the grab sampling and automatically sampling described above happens in only one point of the cross-section, and the sediment concentration in that single point is not necessarily representative of the sediment concentration present in the entire cross-section.

Therefore, it is necessary to sample the cross-section in such a way that the end result will be a sample representative of the mean discharge-weighted sediment concentration present in the river at that moment. A method to obtain such representative samples, is to collect isokinetic depth-integrated samples at multiple verticals, which produce a discharge-weighted (velocity-weighted) sample. The US Geological Survey (USGS) uses two basic methods to define the location or spacing of these verticals. One is based on Equal Increments of water Discharge (EDI-method sampling); the second is based on Equal Increments of stream or channel Width (EWI-method sampling).

Both of these techniques have been extensively described in Edwards & Glysson (1999) and in Wilde (2006) and have previously been addressed in relation to FHR's early sampling strategy in Vanlierde (2003). Both methods have advantages and disadvantages, though when executed correctly, should give identical results. In the end, at the FHR's sediment measurement locations where ISCO samplers are installed, the EWI-method sampling was selected.

This method entails dividing the cross-section at the sampling location into a number (in between 10 and 20) of equal-width increments (see Figure 2.6). Samples are collected by lowering and raising a collapsible-bag depth-integrating suspended-sediment sampler US D-96 A1 (FISP, USGS Hydrologic Instrumentation Facility, Mississippi, USA) see Figure 2.7) through the water

column at the centre of each increment; this sampling location is referred to as the vertical. The combination of the same constant transit rate used to sample at each vertical and the isokinetic property of the sampler results in discharge-weighted subsamples for each increment.

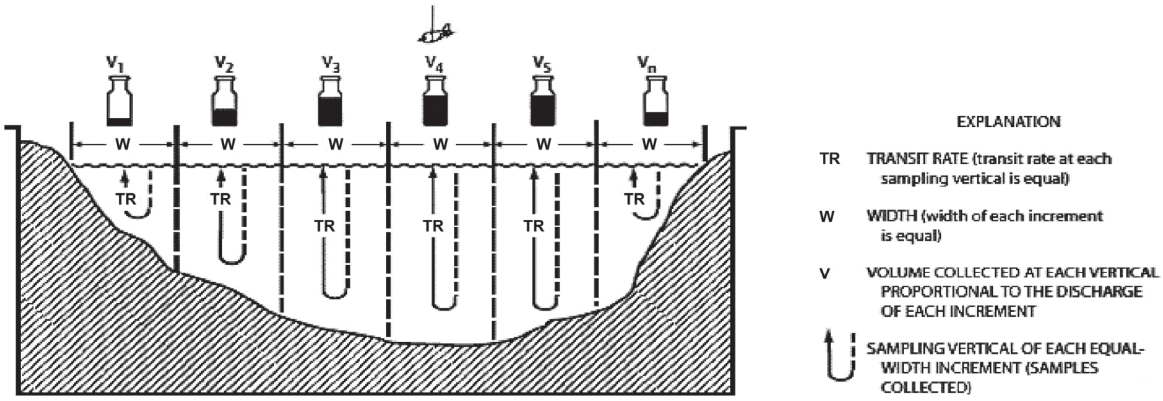

Figure 2.6: Equal-width-increment method for collection of water samples (modified from Edwards & Glysson, 1999)

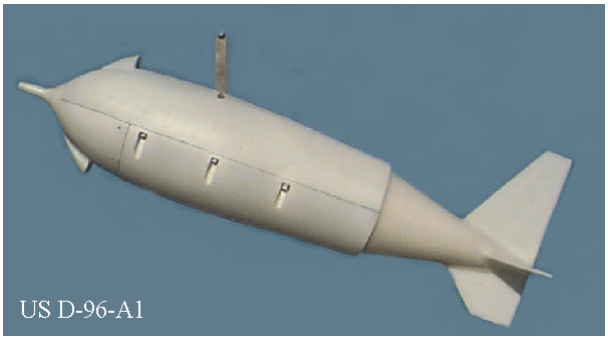

Figure 2.7: Collapsible bag depth-integrating sampler of the type US D-96-A1 (Davis, 2005)

Figure 2.8: Churn sample splitter (FISP, 2011)

Finally, all the subsamples of the individual verticals are composited into one sample which is proportional to total stream flow. The compiling takes place in a churn sample splitter (see Figure 2.8). This composite sample is then transported to the laboratory for representative subsampling and consequent analysis (see Chapter 3).

Consequently, a relation between point sediment concentrations (i.e. the automatically collected samples) and cross-sectional sediment concentrations (obtained through EWI-method sampling) can be constructed, allowing the point samples to be transformed into values representative of the entire cross-section. However, to create an accurate rating curve it is necessary to execute the EWI-method sampling over the entire range of discharge conditions present at the sampling location. In practice, a rule of thumb is used that every 10% of the observed hydrograph at least three EWI-method samplings should be executed (pers. com. A. Horowitz, USGS Atlanta, GA). Or in other words, a rating curve that can be applied to correct point sampled sediment concentrations, should have at least 30 sampling points, evenly spread out over the entire range of discharge conditions. This presents some challenges, as extremely high and low discharge conditions do not always present themselves within business hours, and field personnel is not always available for sediment sampling in these periods as Q/H and Q/Q calibration measurements need to be executed as well.

Additionally, the Flemish rivers present some extra challenges. First of all, quite a few of the rivers are subjected to hysteresis. This process, which is discussed in detail in Part III, causes the lack of coinciding of the sediment peak with the corresponding discharge peak. Therefore it is of importance to not sample during different discharge conditions, but rather to sample when different suspended sediment concentrations are present in the river.

Secondly, presence of navigation in waterways can potentially have a significant impact on the suspended sediment flux transported in the river as well as on the EWI-method sampling process. The sailing of a ship can bring sediment in resuspension, which would otherwise remain on the riverbed given the reigning flow conditions. As such, navigation can increase the sediment flux transported. Furthermore, in busy waterways, such as the Leie, the Upper-Scheldt and the Ringvaart, it is impossible to execute an EWI-method sampling without being interrupted by navigation.

Therefore, in the FHR procedure for the EWI-method sampling, described in Instruction I-W-PP33-5 (Vereecken & Mostaert, 2012), a distinction in EWI-method sampling was made for locations hindered by and unhindered by navigation. In the latter the standard USGS methodology as described above is used. When the navigation is a hindering factor, adjustments to the procedures have been implemented to regain insight into the impact of the navigation on SSC of the cross-section as well as the SSC of the ISCO samples.

The differences entail:

- Samples obtained from the individual verticals are no longer compiled into one sample in the churn sample splitter, but are rather analysed separately for SSC and grain size.
- When a ship passes, the timing is recorded and the next vertical is sampled after the waves made by the ship have passed.
- This same vertical is sampled again, more than 10 minutes after the ship passed, to allow for studying the influence of the ship's passing on the observed SSC.
- The automatic sampler is programmed to sample every five minutes, to get a more detailed view of the variations in the SSCs observed during the time it takes to execute an EWI-method sampling.

As the Demer, the Nete and their tributaries have little to no navigation on them, the standard USGS EWI-method sampling was applied at the sampling locations in these basins.

2.1.2 Physical parameters monitoring

More detailed insight into sediment transport can be obtained by continuous monitoring of other parameters such as turbidity and conductivity as they can be used as proxies in predictions of suspended sediment concentrations. Therefore, from 2005 onwards, FHR has equipped its routine sediment measurement locations on the river Scheldt tributaries with YSI multi-parameter probes, initially with YSI 6920 series afterwards also using YSI 6600 series probes (YSI inc., Yellow Springs, Ohio, USA) (see Figure 2.9).

Even if the optical probes (turbidity, dissolved oxygen, chlorophyll and blue-green algae probes) are equipped with a wiper system, as can be seen in Figure 2.9, it is still necessary to have a rigorous maintenance schedule for these probes.

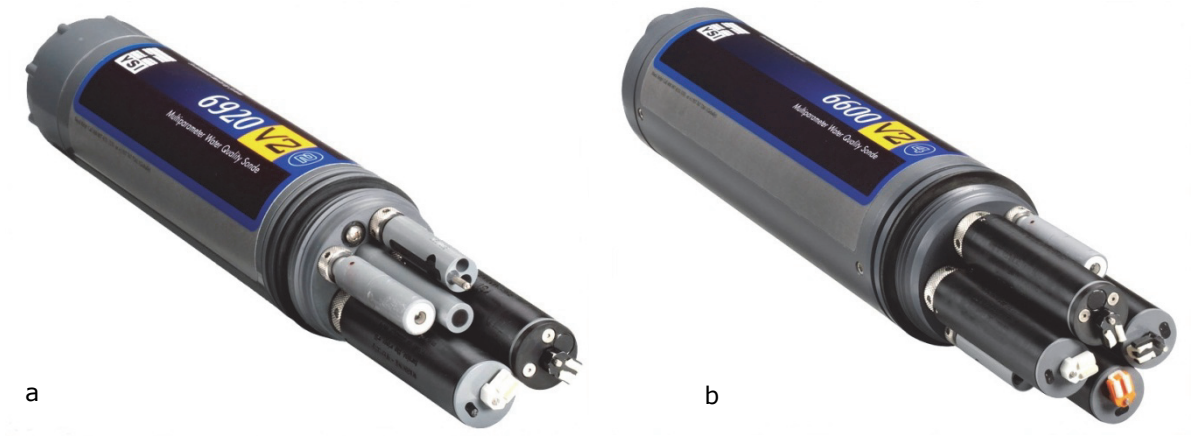

Figure 2.9: YSI multiparameter probes: a) YSI type 6920 equiped to measure temperature, pH, conductivity, redox potential and turbidity and b) YSI type 6600 equiped to measure temperature, pH, conductivity, redox potential, turbidity, dissolved oxygen, chlorophyll, and blue-green algae (YSI, 2012 a; 2012 b)).

Therefore, routinely the probes are cleaned on-site on a weekly basis, and brought into the sedimentological laboratory for calibration on a monthly basis, as is documented in Instruction I-WL-PP31-12 (De Schutter & Mostaert, 2010). This ensures a valid comparison of turbidity data over time, between sites, and among projects.

Some of these parameters (such as temperature) are monitored to be directly reported in annual or decennial reports. Others, like conductivity, can be used as input to produce derived parameters such as salinity. Turbidity is a parameter which falls in the latter category and is internationally used as a proxy to derive sediment concentrations (Truhlar, 1978; Gippel, 1995; Foster et al. 1992; Riley 1998;Pfannkuche & Schmidt 2003; Minella et al., 2008 a; Rasmussen et al., 2009). Sometimes, more than one proxy is used to establish a good sediment concentration prediction (as will be discussed in Chapter 5 along with the challenges this presents).

The question can be raised why proxies should be used to predict requested parameters such as suspended sediment concentration. First of all, multi-parameter probes are capable of monitoring at a much higher frequency than sediment samples can be sampled and analysed. Therefore, in order to study short-lived fluvial sedimentary processes, like the arrival of a sediment peak, monitoring of turbidity offers one of the only feasible and affordable solutions.

Additionally, it is possible to deploy multi-parameter probes on locations where it is impossible to install automatic samplers (for example in the middle of the River Scheldt, where intense navigational traffic hinders the sampling). Furthermore, the automatic sampling process does not always run flawlessly (pumping issues such as bottles overfilling or water being pumped next to instead of into the bottle, battery problems, samplers being flooded, tubing being frozen, etc.), which can lead to big gaps in the data. These missing data can be complemented by sediment concentrations derived from proxy-measurements (which will be addressed in detail in Section 5.2).

Furthermore, when measuring multiple parameters some of them can be used to validate another parameter. Conductivity and turbidity for instance often have opposite responses to a high-water event. Influx of fresh (rainfall) water will dilute the solutes in the surface water, hence lowering the conductivity, while the increased stream flow and the possible erosion will lead to an increase in sediment concentration and therefore turbidity.

Finally, one of the most significant advantages of multi-parameter measurements is that the data can be transmitted telemetrically, and can therefore be followed in real-time, allowing for a much quicker intervention in case of equipment failure on-site, but also allows for fast response if interesting phenomena are observed on site. Either by launching a detailed sampling campaign (such as EWI-method cross-sectional sampling as previously discussed in Section 2.1.2.3), or by going on site and programming the sampler to sample more frequently. In the framework of this PhD, some detailed sampling campaigns were executed at the Aarschot sampling location, during and after several discharge peaks. Results of these are discussed in detail in Chapters 7, 10 and 11. The process of extra sampling during high-flow conditions can be automated (by coupling the start of the automatic sampling to a rise in turbidity or gauge height above a certain threshold (Lewis, 1996; Van Hoestenberghe et al., 2006).

2.2 PhD-specific instrumentation and monitoring methods

2.2.1 Instrumentation and monitoring methods as used in the authigenic sediment research

To obtain a better insight into the iron content in the river, the nature of the ferric sediment and its distribution throughout the cross-section, a set of detailed sampling campaigns was launched in 2006 (on 6 & 8 March, on 9 May and on 11 & 19 October), of which the first three sampling campaigns were executed within the framework of the dissertation of Helena Belien, and the latter two sampling campaigns took place during the bachelor internships of Rindert Janssens and Bram van Eetvelt, all of which were executed and written under the supervision of Elin Vanlierde.

As such, the sampling strategy, sample preparation and analyses of these campaigns are only briefly discussed in this thesis. For the detailed description of these campaigns the reader is referred to the dissertation Belien (2006) and internship reports (Janssens (2007) and Van Eetvelt (2007) in question.

Finally, an extra sampling campaign was executed on 7 June 2010, which was part of an investigation in collaboration with the Universities of Sofia, Kiel, Antwerp, Eötvös and Ottawa as well as the Swedish Museum of Natural History, the Imperial College London and the USGS. Within the framework of this study, which focussed on ferric precipitations in groundwater-fed river systems, the collected samples were investigated for chemical, mineralogical and isotope composition. The results are in preparation of publication (Dekov et al., in prep.) and will also be shortly discussed in Section 9.2.3.

2.2.1.1 Extra sampling equipment

To obtain a point water sample which has a sediment concentration representative of the SSC present in that point in the cross-section, it is necessary to sample isokinetically. This will ensure no enrichment or depletion of particles larger than 63µm as would be the case with non-isokinetic sampling (Edwards & Glysson, 1999)).

Even though the US-D96 A1 mentioned above in Section 2.1.1.3 samples isokinetically, it also is a depth-integrating sampler, which prohibits the isokinetic sampling at a certain point in the cross-section. Therefore, another device was used, i.e. a 'watertrap' sampler (Eijkelkamp Agrisearch Equipment, Giebeek, the Netherlands) (see Figure 2.10).

Figure 2.10: Watertrap sampler (Eijkelkamp, 2012)

Because of the way this sampler is constructed, the water can flow unhindered through the sampler, which prevents the shape of flocs being altered when flowing through the device.

In the framework of the authigenic research, this sampler was deployed and its content (+/- 1.1 litre) was emptied into a beaker. The samples were consequently analysed for iron content, sediment concentration and floc size (see Section 3.2.1). For the latter, it is important to note that during the recovery of the sampler, the flocs present in the water might scavenge smaller flocs and thus increase in size. However, due to the fact that the sediment (and floc) concentrations were fairly low during the sampling campaigns, this effect will be minimal.

Also, when transferring its content (+/- 1.1 litre) into a beaker the particles will be subjected to turbulence, which might cause the flocs to disagragate again. Therefore, the emptying of the sampler into the beaker was executed very carefully to minimize the turbulence, in an attempt to minimize the alteration of the shapes of the flocs. Once in the beaker, subsamples could be taken.

It should be noted that for floc size analyses, more appropriate sampling equipment exists, such as the in-situ floc sampler, patent pending, apparatus invented and built by Prof. Dr. ir. Margaret Chen. As this type of sampler was not available and as larger volumes were needed (as multiple analyses needed to be executed on the samples), the water trap sampler was used.

2.2.1.2 Sampling campaigns 7 and 8 March and 9 May 2006

During the first three campaigns different points in the cross-section of the Kleine Nete at the Grobbendonk monitoring station were sampled with the Eijkelkamp watertrap sampler. On March 7 2006 water samples were taken on three different depths of two selected verticals, while on 8 March 2006 samples were collected at one depth on five different verticals (see Figure 2.11 for the exact localisation in the cross-section).

At each sampling point three replicate samples were collected. Furthermore, an EWI-method sampling (see Section 2.1.1.3) was executed and three representative subsamples were obtained by churning the composite sample in the churn sample splitter (discussed in Section 2.1.1.3).

On 9 May 2006, like on 7 March, samples were taken on three different depths of two selected verticals (as can also be seen in Figure 2.11). However, no EWI-method sampling was executed during that sampling campaign

2.2.1.3 Sampling campaign 11 October 2006

During the sampling campaign of 11 October 2006, at the Grobbendonk monitoring site, three replicate water samples were taken with the Eijkelkamp watertrap sampler at different depths along four verticals in the cross-section (the exact localisation is once more depicted in Figure 2.11). Also, three replicate automatic samples were collected with the SIGMA 900 sampler, which was standard equipment on this site.

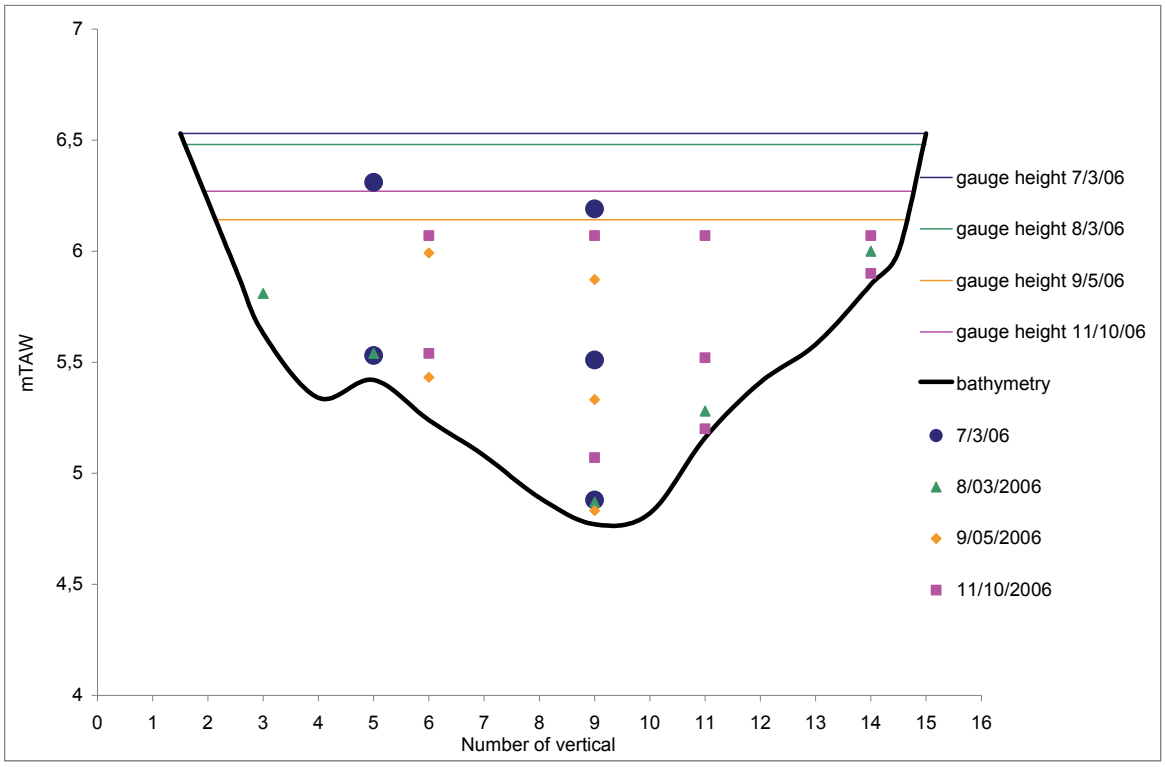

Figure 2.11: Schematic overview of the sampling locations at the Grobbendonk monitoring site during the sampling campaigns on 7 & 8 March 2006, 9 May 2006 and 11 October 2006

2.2.1.4 Sampling campaign 19 October 2006

Analogue to the sampling campaign of 11 October 2006, three replicate water samples were taken on every sampling location during the sampling campaign of 19 October 2006. But instead of sampling different locations in one cross-section at Grobbendonk monitoring station, grab samples were collected by bucket (of which subsamples were carefully obtained for further analysis) in different streams within the Nete and Mangelbeek catchment areas, of which was presumed they had high levels of authigenic sediment present in their sediment. Figure 2.12 shows the locations that have been sampled during this campaign.

2.2.1.5 Sampling campaign collaborative research 7 June 2010 (Dekov et al., in preparation)

This final sampling campaign was executed on sampling points in the Nete and the Mangelbeek catchments of which previous sampling campaigns had indicated that the iron content in the samples was elevated. These previous sampling campaigns were the one on 19 October 2006 (mentioned in Section 2.2.1.4) as well as sampling executed within the framework of the sediment fingerprinting research (which will be addressed below in Section 2.2.2 and in Chapter 10).

At these selected sampling locations (see Figure 2.13) suspended flocculated material and deposited sediment/flocs were studied. The suspended sediment was sampled by grab sampling with 10 litre plastic buckets, while the bed sediment samples were collected with plastic spoons in 200-ml plastic bottles. One of the riverbed samples was light-grey sediment supposed to represent background sedimentation devoid of Fe-rich suspended flux.

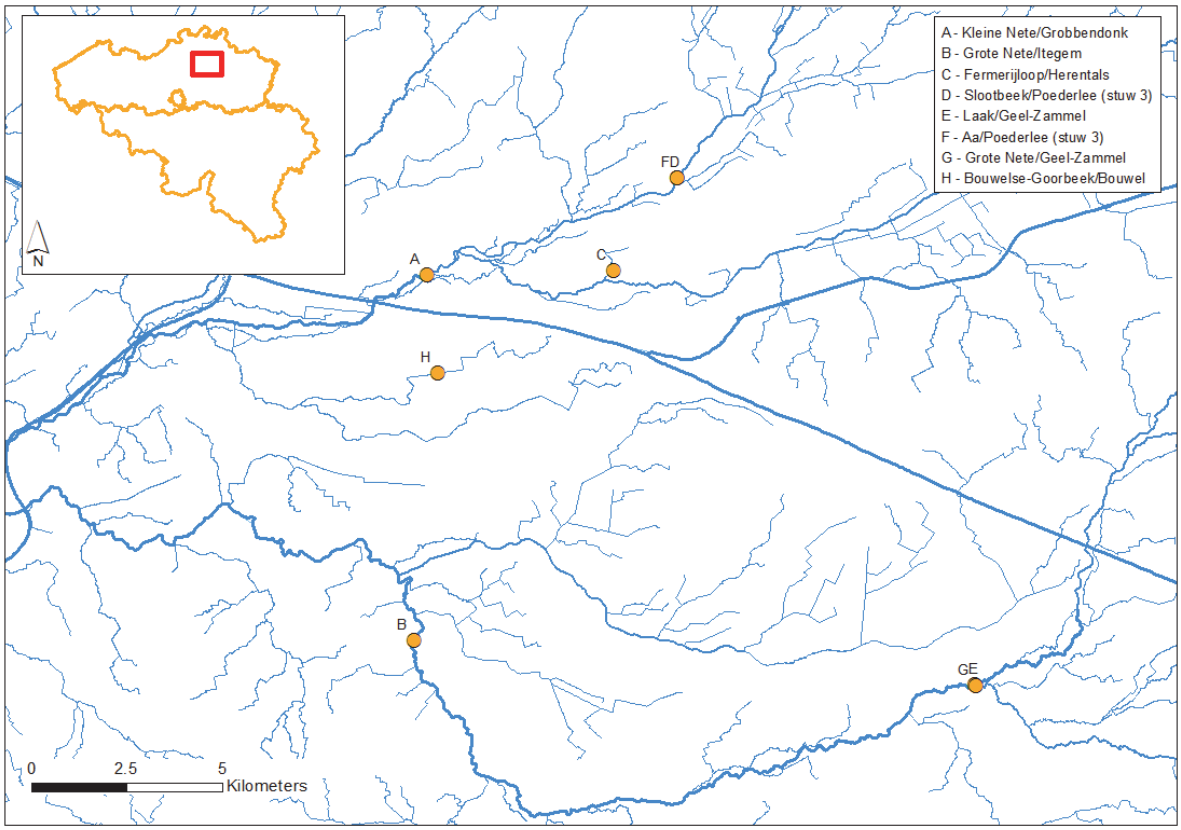

Figure 2.12: Localisation of sampling points of the 19 October 2006 sampling campaign

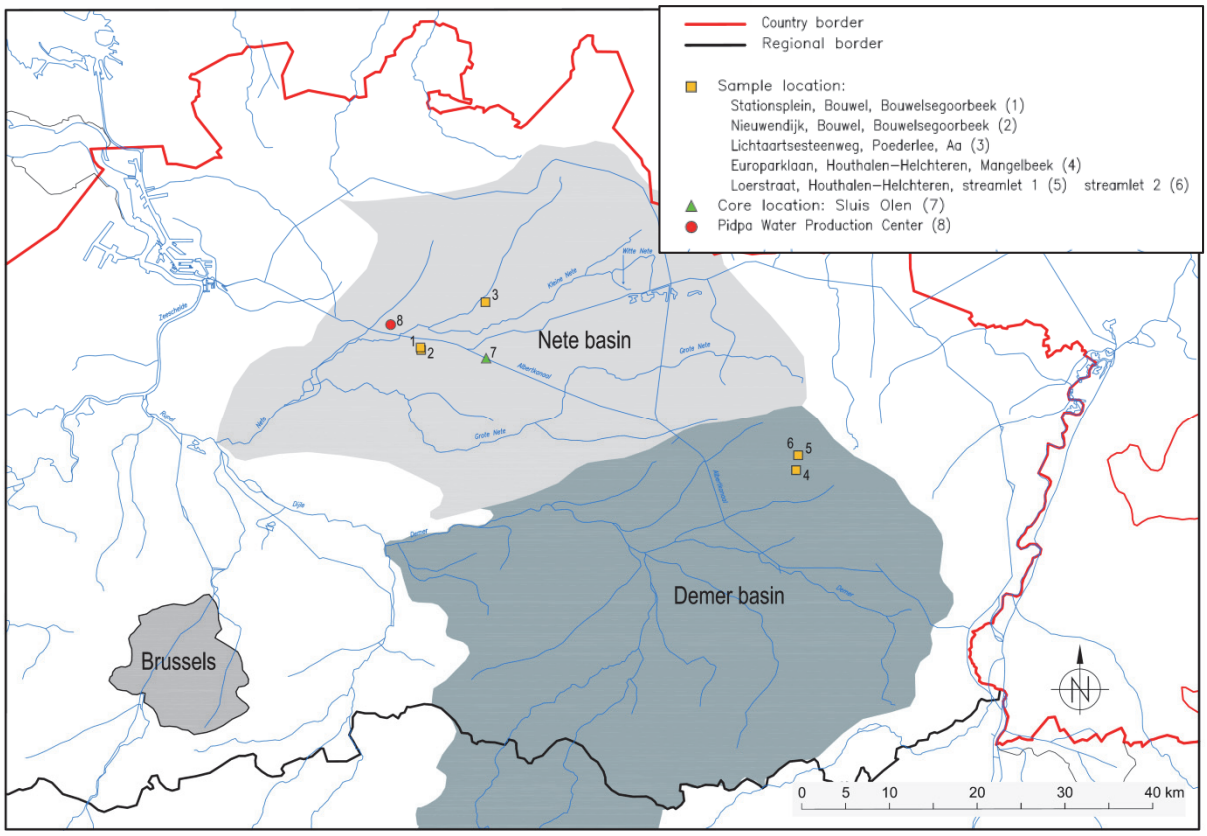

Figure 2.13: Localisation of sampling points of the 7 June 2010 sampling campaign

Additionally, one sand sample from the Diest Formation (i.e., the aquifer supplying most of the dissolved Fe to the river systems in the region) was provided by Prof. Louwye (Department of Geology, Ghent University), as well as one sample of red precipitate obtained from the Pidpa groundwater pumping system (Grobbendonk).

2.2.2 Instrumentation and monitoring methods as used in the sediment fingerprinting research

Besides discharge (Q) and sediment fluxes (two parameters which FHR routinely monitors in Flemish rivers), the sediment fingerprinting research, as executed in the framework of this thesis, requires specific sediment sampling techniques both in-stream as well as on-land (which are not routinely executed at FHR). Therefore the methodologies had to be based on international literature taking into account site-specific constraints. Both in-stream as well as on-land methods and instruments are described in detail in the sections below.

As FHR and/or the Flemish Environment Agency (Vlaamse Milieumaatschappij-VMM) already have discharge monitoring locations (or gauge height (H) monitoring locations with a calibrated Q/H relationship) in the Demer and on the tributaries of the Demer, those sites were preferentially selected to sample suspended sediment as required within the framework of the sediment fingerprinting research, which will also be addressed in detail in the sections below.

2.2.2.1 In-stream sampling methods and instrumentation

The Demer basin consists of multiple sub-catchments, which are shown in Figure 1.3. Of those sub-catchments eight were selected for time-integrated sediment fingerprinting monitoring, based on their size and the availability of a discharge monitoring location (see Figure 2.14). In two of those, the outlet locations were additionally equipped with automatic pumping samplers (ISCO's) and YSI multi-parameter probes (as described in Sections 2.1.1.2 and 2.1.2) alongside the existing gauge height monitoring devices, in order to obtain insight into the sediment transport at these sites. Of these two selected sites, one was located in the northern part of the Demer basin (Lummen in the Mangelbeek catchment) and one was located in the south (Halen in the Gete catchment).

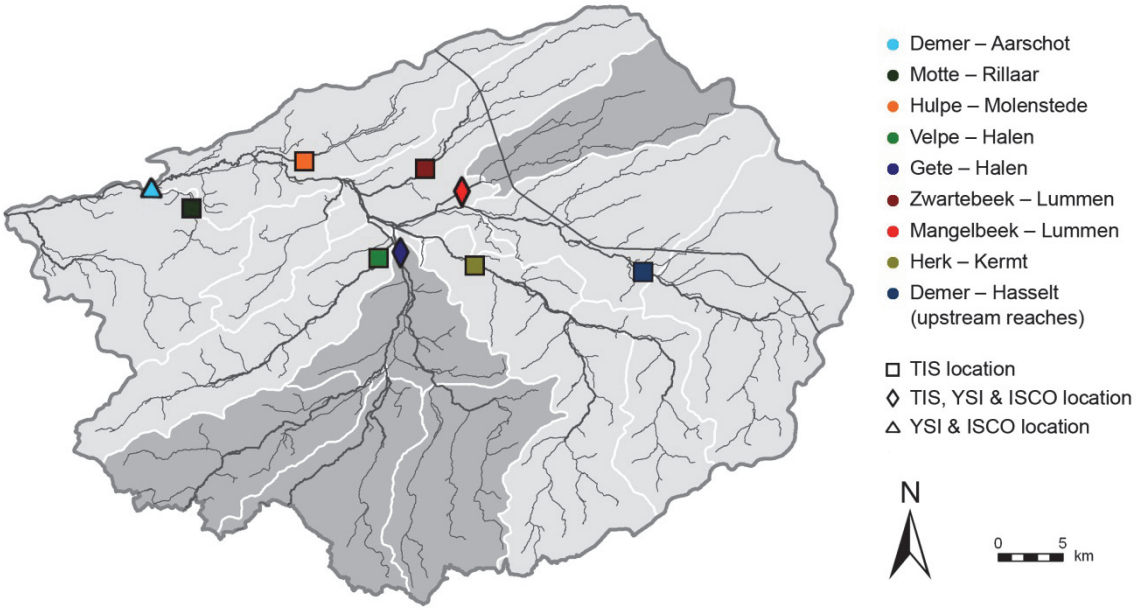

Figure 2.14: Locations of time-integrated samplers and ISCO samplers in the Demer basin

The sampling and monitoring equipment was provided and maintained by FHR in the same way as its other (routine) measurement locations for the duration of the research.

However, sediment fingerprinting research requires monitoring and sampling methods that differ from automatic sampling and parameter monitoring, and it has a number of constraints:

- Enough material should be sampled to complete geochemical and sedimentological analyses
- The material collected should be representative of the entire time period the sampling occurred.
- The material should be representative of the suspended sediment transported by the stream.
- When collecting bed sediment, one should take into account to only sample material that could possibly be resuspended.

A very cheap and efficient way to sample suspended sediment in-stream in a time-integrated fashion is by using a time-integrated sampler (TIS) as developed by Philips et al. (2000). This simple sampler utilizes ambient flow to induce sedimentation by settling and can be deployed unattended in small streams.

The design has been slightly adjusted since and applied as a time-integrated sediment sampler in other international studies (Collins et al., 2001; Gruszowski et al., 2003; Collins & Walling, 2004, 2006; McDowell & Wilcock, 2004; Walling, 2005; Martínez-Carreras et al., 2010).

FHR has implemented this adapted design and constructed TISes mounted on I-profiles (see Figure 2.15) to weigh them down to withstand moderate stream flows. They have been deployed in the eight selected tributaries (as can be seen in Figure 2.14), which were still wadable but with more difficulty (such as is the case at the monitoring locations on the Zwartebeek in Lummen or on the Gete in Halen).

Figure 2.15: Time-integrated sampler (TIS) as constructed and deployed by FHR

Consequently, the samplers were emptied once every month, during low-flow conditions, and the timings were recorded in detail in a logbook, which has been reported in Vanlierde et al. (2008). The content of the TISes, about 10 litre of sediment-rich water was transported in an air-tight plastic bucket to the sedimentological laboratory of FHR, where it was stored at 4°C to allow the sediment to settle, without giving the organic material present a chance to increase significantly.

A TIS as constructed by FHR, however, could not be deployed at the main outlet station selected for this sediment fingerprinting research, namely the sediment monitoring location at Aarschot on the Demer. Stream velocities were too high to properly install the sampler. The average stream velocities at the Aarschot sampling location during high-flow

conditions range around 1.3 m/s (reaching 2 m/s at the surface). Furthermore, as the river is not wadable difficulties in emptying the TIS also presented itself. However, an attempt to install a TIS and leave it attached with cables to the bridge was launched but turned out unsuccessful, as drift-debris being stuck on these cables pulled the sampler from its place.

Therefore, alternative sampling approaches were considered. First of all, suspended sediment samples have been collected using a flow-through centrifuge (some samples were collected with the AS16-2Y-IJY Alfa Laval centrifuge (Alfa Laval Corporate AB, Lund, Sweden) from the VMM, while others were collected with the Emmie (Alfa Laval) centrifuge (Alfa Laval Corporate AB, Lund, Sweden) from FHR and a submersible pump (type SQ/SQE, Grundfos, Bjerringbro, Denmark) from FHR, a sediment collecting technique also used in international fingerprinting research (Ongley & Blachford, 1982; Ongley & Thomas, 1989; Rees et al., 1991; Walling & Collins, 2000; Stutter et al., 2009; Wilkinson et al., 2012). The methodology for sampling sediment with the Emmie centrifuge has been documented in Instruction I-WL-PP33-9 (Vereecken & Mostaert, 2013 c). Due to the elevated stream flows the weighted intake nozzle of the pump remained in the upper water layers while sampling.

Even though this method of sampling suspended sediment does yield sufficient material to do a complete geochemical analysis, it is only a point sample, both in time (sampling enough material for one analysis takes less than an hour) as in place (the sample was taken in superficial water layers). As it was difficult to predict when the sediment peaks would arrive due to hysteresis effects (which will be discussed in detail in Part III), another approach was sought for collecting more time-integrated suspended sediment samples at the Aarschot outlet station.

This new approach was found in using the ISCO automatic pumping sampler, which was already on location at the Aarschot sampling site. The ISCO collects water samples every seven hours. Therefore, for a longer period of time (such as the monthly sampling period used for TISes) a significant 'bulk' water sample was potentially available through compiling these individual water samples together.

However, SSC was also a parameter of interest in these samples as well, and this is generally determined by filtration (see section 3.1.2), which has a higher accuracy for water samples low concentrations. However, this analysis method renders the sediment unavailable for further geochemical and grain size analyses. Therefore, a balance was struck and SSC was only determined by lyophilisation (see section 3.1.3) when sufficient solids were available in the 1L recipients.

In practice, the content of all ISCO bottles with high sediment concentrations (i.e. the samples taken during the sediment peak) and a few 1L ISCO bottles preceding and succeeding this sediment peak were lyophilized. This approach allowed for the construction of a (set of) composite sediment samples, each of sufficient mass to geochemically analyse, which represent the sediment passing by the ISCO during that period of the event.

Besides sampling of suspended sediment, bed material was also collected in an attempt to investigate if it could be discriminated from the on-land sediment sources contributing to the total sediment load. The riverbed material was sampled by VMM using their sampling protocol (VITO, 2012). Afterwards, a subsample of this well-mixed riverbed material was made available to the sedimentological laboratory of FHR for further analysis.

A special mention should be made about the sampling of the authigenic material in the headwater of the Mangelbeek catchment. This took place, either by sampling superficial flocs by grab sampling, or by collecting deposited sediment on the riverbed with plastic spoons.

2.2.2.2 On-land sampling techniques

When sampling source material from the field for sediment fingerprinting research, the guidelines as indicated by Collins (1995) and Walling & Collins (2000) were followed.

Samples of different types of sources (+/- 500 g) were collected with a stainless steel spade or spoon, which was repeatedly cleaned to avoid inter-sample contamination. Also, special care was given to ensure that only material likely to be eroded was sampled. This means in the case of sampling of source material from different land uses, only the top layer (0-2 cm) of surface soil was collected, whilst in the case of channel bank sampling, material from reaches where the banks are characterised by erosion scars on-land was collected.

The exact location of the samples will be shown in Chapter 10, where the different sources selected for fingerprinting are addressed.

3. Sample preparation and laboratory analysis techniques

Analogue to the structure in Chapter 2, Chapter 3 first discusses the sample preparation and laboratory analysis techniques routinely used in the sediment laboratory of FHR. In the second part of this chapter the PhD-specific techniques are discussed, first within the framework of the authigenic sediment research (Section 3.2.1), then within the framework of the sediment fingerprinting research (Section 3.2.2).

3.1 FHR's routine sample preparation and laboratory analysis techniques

In the framework of routine operational sediment monitoring, automatically pumped water samples, manually collected grab samples and cross-sectional water samples are delivered to the sedimentological laboratory of Flanders Hydraulics Research. In this lab these water samples are routinely analysed for SSC, and on selected samples grain size is also routinely determined. Furthermore, organic matter content can also be estimated based on the loss of mass on ignition. The applied techniques are concisely described below with attention to details that are important in the framework of this PhD research for the further interpretation of these acquired data. The entire procedures, which have been finalised in collaboration with the lab-technicians of FHR, are documented in specific laboratory instructions which are available on the DQS of the Technical Support Services of the department of Mobility and Public Works.

3.1.1 Representative subsampling with a churn sampler splitter

When a water sample is too large to be analyzed as such, or when multiple samples are necessary to analyze different parameters, the original sample needs to be divided into subsamples. Each of these subsamples should contain suspended and dissolved concentrations that are virtually equal to those in every other subsample. This problem is encountered for instance in samples obtained from cross-sectional sampling with the EWI-method on rivers without frequent navigation, as this entails a composite sample which is comprised of samples of individually sampled verticals and the total volume can mount up to 13 litres.

The subsampling method selected is to use a churn sample splitter (Scienceware, Bel-Art Products, Pequannock, New Jersey, USA) (see Figure 2.6), a device recommended by the USGS (Lane et al., 2003) as a sample splitter to procure representative subsamples. To do so, the composite sample is transferred into the churn sample splitter (or is preferably collected in the churn sample splitter) and the churn is moved up and down at a constant velocity. After at least 10 churns, the sample is sufficiently homogenised to start taking subsamples. The applied procedure is documented in instruction I-WL-PP33-5 (Vereecken & Mostaert, 2012).

Importantly, the churn sample splitter is only capable of producing representative subsamples when certain conditions are met, such as particle size of the suspended sediment is ≤ 250 µm, the suspended concentrations remain under 1,000 mg/l and the sampled volume is no greater than 13 litres. Depending on which churn sample splitter is used (4 litres or 14 litres size) the respective final 1 or 4 litres in these sample splitters cannot be used to reliably produce representative subsamples and should therefore be discarded. If these conditions are not met, the splitting accuracy becomes unacceptable.

3.1.2 Determining suspended sediment concentration by filtration

Suspended sediment concentration is per definition the amount of sediment in a volume of water or written as an equation (Eq. 3.1):

$$SSC(mg/l) = \frac{m_{SS}(mg)}{V_{water}(l)} \quad \text{Eq. 3.1}$$

in which: - m_{SS} is the mass of suspended sediment present in the water sample
- V_{water} is the volume of water of the sample

The standard way of determining the mass of suspended sediment is gravimetrically, based on NBN EN 872 norm, using filtration to determine the mass of the sediment. During the period of 1999-2011 different brands of cellulose nitrate filters, such as Millipore and Sartorius have been used at FHR, but all filter papers had a pore size of 0.45µm. After the filtration, the filter papers are left to dry in an oven (Heraeus T20 Function line, Hanau, Duitsland) at 105°C for 3 hours, after which they are allowed to cool down in an electronic desicator (Boekel Dricycler 1344412, Boekel Scientific, Feasterville, Pennsylvania, USA). Finally, their weight is determined on an analytical scale (either Sartorius AC201S, Sartorius, Vilvoorde, Belgium or the Mettler AT200 and Mettler-Toledo XP204, Mettler-Toledo, Lot, Belgium) with an accuracy of 0.0001 g.

The volume of water (V_{water}) is also gravimetrically determined, by weighing the water samples prior to filtration and determining the weight of the empty sampling recipient afterwards. For this weighing either a Sartorius LA6200 (Sartorius, Vilvoorde, Belgium) or a Mettler-Toledo MS6002SDR/01 (Mettler-Toledo, Lot, Belgium) scale is used with an accuracy of 0.01 g.

The entire procedure is registered in the laboratory instruction I-WL-PP31-5 (De Schutter & Mostaert, 2009 a).

3.1.3 Determining suspended sediment concentration by lyophilisation

When the collected water samples contain a sediment concentration which is too high to allow for a speedy and accurate filtration, the SSC determination is still executed in a gravimetrical way, but the separation of liquid and solids is not based on filtration (and drying), but on freezing and sublimation.

The lyophilisation process, however, is a much more time-consuming process than filtration, and is therefore only rarely used. The process requires some preparatory steps, such as the resting of the recipients in a cold storage room to allow the suspended sediment present to settle. After weighing the water-filled recipients to determine V_{water}, as described in Section 3.1.2, the clear supernatant water can either be decanted or minutely removed with a vacuum pump to minimize disturbance of the deposited sediment. The sediment is then transferred into aluminium trays or plastic petri dishes, depending on the volume that needs to be dried, and is put into the freezer at -35°C to solidify prior to being put into the lyophilisator (Gamma 1-16 LSD, Martin Christ, Osterode am Harz, Germany) where they are dried in 10 to 15 hours. The entire procedure and different drying programmes are described in the laboratory instruction I-WL-PP31-3 (De Schutter & Mostaert, 2009 b).

Next, the dry sediment is weighed and m_{SS} is determined after which Equation 3.1 is applied to gravimetrically determine SSC.

3.1.4 Determining organic matter content

In the sedimentological laboratory of FHR, organic matter content (OMC) is not determined directly, rather the loss on ignition (LOI) is determined through incineration of the sediment. The material that needs to be incinerated is put into a crucible and weighed prior to incineration with one of the above-mentioned analytical scales with an accuracy of 0.0001 g. Next, the crucibles are put into the muffle furnace (type Nabertherm L15/11 B170, Nabertherm, Lilienthal, Germany) during 6 hours. The first three hours the furnace is programmed to climb to 550°C, the next 3 hours it is programmed to remain at this temperature. Consequently, the crucibles are put into the electronic desicator to cool down before determining their weight on the analytical scales with an accuracy of 0.0001 g. The entire procedure is described in detail in laboratory instruction I-WL-PP31-6 (De Schutter & Mostaert, 2009 c).

3.1.5 Determining grain size distribution

For certain water samples, such as cross-sectional EWI-method samples or selected automatically pumped samples, grain size is routinely determined. The selected method is laser diffraction, with a Mastersizer 2000 (Malvern Instruments Ltd., Great Malvern, UK). The measuring principle of laser diffraction is based on the measurement of the scattering pattern that particles cause when they are radiated with a laser beam. From the detected diffraction pattern, based on the Mie scattering theory, the size of the particles can be calculated. The Mastersizer can measure the size of particles in between 0.02 and 2000µm. Also for an accurate measurement the length-width ratio of the particles cannot exceed 3/1 (Malvern Instruments Ltd., 2007).

At FHR, the water samples that need to be recuperated (for further analysis such as determination of SSC) are manually measured by using the Hydro 2000 M/MU module, while grain size of sediment samples that can be discarded afterwards can be determined by the Hydro 2000S and Autosampler 2000 in a automated way; the detailed procedure is described in I-WL-PP31-4 (De Schutter & Mostaert, 2009 d). Both techniques allow the water/sediment mixture to circulate in a continuous way through the detection cell, allowing particles to be aligned in respect to the laser beam in all possible angles. Therefore, the grain size of a particle is reported as the diameter of a sphere which has the same volume as the measured particle. This inherently leads to different results than other grain size measurement techniques such as sieving, sedigraphy or pipet settling methods would yield.

The different grain size analyseis techniques were compared in ring tests in which FHR participated along with other Flemish and Dutch laboratories to compare grain size measurement results (Spronk & Bakker, 2012). This exercise took place within the framework of a joined monitoring campaign to study the physical and ecological situation in the Scheldt estuary (MONEOS), and the aim was to create a standardized methodology for the different instruments used in the various laboratories, to obtain comparable results. The final conclusion and recommendations of that test were that laser diffraction can indeed be used to determine the <63µm fraction, but that the determination is quite unstable and sensitive to physical forces exerted on the particles during the analysis. Therefore to obtain reproducible and repeatable results, the analysis needs to be executed following a strict, regulated protocol. The protocol suggested in Spronk & Bakker (2012), resembled closely the protocol already in use at FHR, and has been incorporated in instruction used in FHR I-WL-PP31-4.

Additionally, the ring tests showed that freezing and defrosting of sediment samples, do not have a significant influence on the grain size distribution.

Therefore it can be concluded that the Mastersizer data can be used to compare the grain size distribution data of the different samples obtained and analysed within the framework of this PhD, as the same protocol was used to analyse all. However, it is more difficult to compare this data set with data from other authors, using different grain size measurement techniques, equipment and protocols.

3.2 PhD-specific sample preparation and laboratory analysis techniques

3.2.1 Sample preparation and laboratory analysis techniques as used in the authigenic sediment research

Researching ferric authigenic sediment, which is prone to flocculation, demanded extra analyses (of which the results are discussed in Chapter 9). Therefore, extra sampling campaigns were executed in the Nete and northern part of the Demer basin in 2006 as mentioned in Section 2.2.1. During these campaigns, samples were collected to gravimetrically determine SSC and LOI, microscopically determine the shape and size of the flocs as well as to spectrophotometrically analyse the soluble iron content present in river water (Fe(II)) and the iron content present in the solid phase (Fe(III)).

The gravimetric analysis of SSC and LOI was executed on EWI-method samplings executed on the sampling campaigns of 11 and 19 October 2006, analogue to the routine sampling (as discussed in Sections 3.1.2 and 3.1.4 (respectively according to the Instruction I-WL-PP31-5 (De Schutter & Mostaert, 2009 a) and I-WL-PP31-6 (De Schutter & Mostaert, 2009 c). However, on 11 October 2006, a 1 litre subsample was collected from the churn sample splitter, while on 19 October 2006, the volume was reduced to 250 ml, due to clogging problems with the filter papers experienced in the laboratory with the samples of the previous campaign. The additional (non-routinely executed) sample preparation and analysis techniques are discussed below.

The sample preparations and analysis techniques of the extra sampling campaign executed on 7 June 2010 used in the collaborative research reported in Dekov et al. (in prep.), will not be addressed in this chapter as they are described in detail in said article. Only the results will be used in Section 9.2.3 and applied in Section 9.4.

3.2.1.1 Determining Fe(II) and Fe(III)-content

During the first two campaigns (7 and 8 March 2006) where different points in the cross-section of the Kleine Nete at the Grobbendonk monitoring station were sampled (see Section 2.2.1.2), total iron concentrations were only indicatively estimated by analysis using method 8008 with a portable Hach DR/890 Portable Datalogging Colorimeter (Hach company, Loveland, Colorado, USA) three weeks after sampling and after grain size analysis. Due to the limited range in Fe concentration detection of this instrument (0 to 3 mg/l), it could only be established that the concentrations in most samples were higher than this detection limit (Belien, 2006).

To obtain more quantitative insight into the Fe(II) and Fe(III) concentrations at the different sampling points, the sampling campaign on 9 May was executed, again at the Grobbendonk monitoring location. This time two spectrophotometrical methods were applied: on the one hand was the Merck SQ 118 spectrophotometer (Merck KGaA, Darmstadt, Germany) used on site, applying the 00796 Reagent Test, method number 204 with10-mm cells, while on the other hand the same device was used under laboratory conditions when applying the Merck 14896 Cel Test. The differences between the two tests are described in detail in Belien (2006). However, even

though great care was taken not to contaminate the samples on the field, an apparent contamination of the deionised (DI) water, which was used to dilute the samples on-site, rendered some of the results less accurate, as was reported in Belien (2006).

Therefore, a third set of sampling campaigns was launched on 11 and 19 October 2006. The first campaign focused once more on the Grobbendonk monitoring site, while the latter campaign included other sampling locations in the Nete basin (as is discussed in Sections 2.2.1.3 and 2.2.1.4). The spectrophotometrical approach was maintained, however instead of using pre-prepared chemical tests, the analysis described in Golterman (2004) and Golterman pers. com. was applied. Below, this method has been briefly described, but the reader is referred to the bachelor internship reports of Janssens (2007) and Van Eetvelt (2007) where this methodology is discussed in great detail.

During the 11-10-2006 campaign, for every location in the cross-section three samples were obtained using the water trap, and from each a 30 ml subsample was filtered (hence three filter papers were available for microscopic analysis afterwards). The filtrate was combined and acidified, using 1 drop of 10M HCl to keep the Fe(II) in soluble condition, and transported to the laboratory (in this case the Laboratory of Environmental Toxicology and Aquatic Ecology of Department of Applied Ecology and Environmental Biology, UGent), where the acidity of the solution was neutralized using NaOH, after which o-phenantroline solution was added, 30 minutes prior to analysis with the Merck SQ 118 spectrophotometer. This procedure allowed for the determination of the Fe(II) concentration in the water.

The Fe(III) concentration present in the sediment-water mixture could be determined by subtracting the Fe(II) from the total iron concentrations present in the water. To determine the latter, what remained of the water trap samples sampled at one and the same location, was first of all combined in a churn sample splitter, and consequently a representative subsample was collected, acidified with ascorbic acid and also transported to the Laboratory of Environmental Toxicology and Aquatic Ecology. There, once again, o-phenantroline solution was added 30 minutes prior to analysis with the Merck SQ 118 spectrophotometer.

An identical sample preparation and laboratory analysis approach was used for the samples obtained on 19-10-2006. The only difference between the two campaigns was that the material was sampled by bucket and not with a water trap.

It should be remarked that for each sampling day (i.e. 11 and 19 October 2006) a set of calibration standards was generated, using Mohr's salt, which were used to establish calibration curves. The standards were measured prior to and subsequent the analysis of the samples. The curves are presented in Janssens (2007) and Van Eetvelt (2007).

3.2.1.2 Particle size analyses

3.2.1.2.1 Primary particle size analysis by laser diffraction

Of the composite sample present in the churn sample splitter, representative 1 litre subsamples were collected, during the sampling campaigns of 11 and 19 October 2006. These were used to determine the primary grain size distribution by laser diffraction with the Malvern Mastersizer (see Section 3.1.5). To ensure the sediment was broken down to its primary particles, the sample was treated with ultrasonic dispersion for 2 minutes.

3.2.1.2.2 Microscopic photography and image analysis of flocs

The shape and size of flocs, however, cannot be studied by laser diffraction, as this process will destroy them. Therefore, the filter papers obtained during the above-mentioned sampling

campaigns in 2006 were used for microscopic analysis. Filtrations, using a Millipore filtration system with 0.45µm Millipore cellulose nitrate filters, were executed on 30 ml (March 7 and 8) or on 10 ml (May 9) subsamples of the point samples collected with the watertrap, as well as on churned subsamples of these point samples (to study the impact of churn sample splitting on floc size) and on 20 ml subsamples of automatically collected samples (using the SIGMA 900 automatic pumping sampler). The filter papers were consequently dried at FHR and microscopically photographed in the labs of the Mineralogy and Petrology Research Unit of the Department of Geology at UGent.

From the first sampling campaigns in March 2006, over the campaign in May 2006 to the final campaigns in October 2006 different microscopes, lighting techniques and magnifications have been tested and applied. For the first three campaigns an Olympus BH2 (Olympus America Inc. Center valley, Pennsylvania, USA) and a SteREO Discovery.V12 microscope (Carl Zeiss, Oberkochen, Germany), both equipped with a ColorView Soft Imaging System digital camera, were used, and variable magnifications were tested, as extensively described in Belien (2006). This approach however, did not yield undivided success, and Belien made recommendations concerning to improve the data quality obtained from the images. These included ensuring a good noise-signal ratio is of primordial importance and therefore the lighting of the filter papers should be adequate. Furthermore, Belien concluded that the amount of flocs present in the microscopic image also had an impact on the statistical difference she observed in the results of the March 7 and May 9 2006 sampling campaigns. The difference in floc count was the direct result of lowering the volume of river water that was filtered (from 30 ml per filter paper on 7 March down to 10 ml per filter paper on 9 May). Due to the low floc count on the 9 May campaign, the statistical data set was too small to render good results.

Belien (2006) consequently used UTHSCSA Image Tool (an image processing software developed by C. Donald Wilcox, S. Brent Dove, W. Doss McDavid and David B. Greer in the Department of Dental Diagnostic Science at The University of Texas Health Science Center, San Antonio, Texas) to gain data from the microscopic imagery and consequently statistically analyzed these data in SPSS, a software package used for statistical analysis. She concluded that the parameters 'Roundness', 'Compactness' and 'Elongation' should be excluded from the statistical analyses as they are too sensitive to noise.

Learning from these experiences, during the two sampling campaigns in October 2006, 30 ml river water was filtered on site and afterwards photographed under a Olympus BH2 microscope, with both an ocular and an objective magnification of 10 and transparent lighting. Of each filter paper ten photographs were taken according to a set pattern (see Figure 3.1), to have a representative sampling of the flocs present on the entire filter paper. The microscopic photographs were then processed with the UTHSCSA Image Tool (an image processing software).

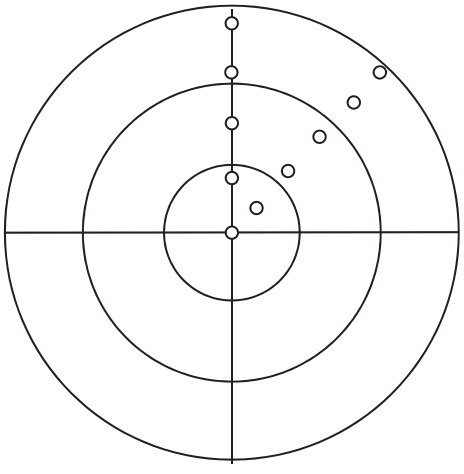

Figure 3.1: Schematic overview of a filter paper and the localisation of the ten microscopic photographs.

In this image-analysis software the pictures were changed from colour to grey scale prior to setting the threshold to allow the software to identify the particles as objects. Due to the colour of the filter, which can change depending on the colour of the finest fraction on the filter, this threshold needs to be set manually.

After setting the threshold, the software measures and calculates a series of indicative parameters such as area, perimeter, major and minor axis length, Ferret diameter, elongation, roundness and compactness for each identified particle visible in the image. All but the last three parameters were then consequently exported and statistically analysed as is described in Belien (2006) and Vanlierde et al. (2007 a) and will be addressed in Section 9.1.

3.2.1.3 Collaborative research (Dekov et al., in preperation)

From the river water samples, collected on 7 june 2010, the suspended matter was extracted through centrifugation (8,000 rpm for 30 minutes at 18°C air temperature). All samples (both suspended matter and material deposited on the river bed) were lyophilsed (at -32°C for 8 hours) prior to any further treatment. After drying, the samples were grained to fine powder in agate mortar.

At the Chemistry Department of the University of Antwerp the chemical composition of the samples was determined by X-ray fluorescence (XRF) by Katleen Van Meel using the procedure described in Section 3.2.2.3. Furthermore, mineralogical characterisation was obtained at this department, using scanning Electron Microscopy (SEM) (JSM-6300, V=10 kV, I=12 nA, electron beam diameter of 1 µm) by Giuliana Gatto Rotondo and micro-Raman molecular spectroscopy (MRS) by Larysa Darchuk using a Renishaw InVia micro-Raman spectrometer with a laser excitation at 785 and 514 nm equipped with a Peltier air-cooled CCD detector. More details about the SEM and MRS technique and procedure can be found in the publication by Darchuk et al. (2010).

The mineralogy has further been characterised by Vesselin Dekov at the Department of Geology and Paleontology of the University of Sofia, using X-ray Diffraction (a Philips X-ray diffractometer PW 1710 with an automatic divergence slit and a monochromatic Cu Kα radiation at 40 kV and 35 mA). Random powder mounts were scanned from 5 to 80 °2θ, with a 0.01 °2θ step, at 2 s/step. Additional information on the experimental set-up can be found in De Maeyer-Worobiec et al. (2011).

Transmission electron microscopy (TEM) was executed at the Department of Earth Sciences, University of Ottawa by Danielle Fortin, using a Philips CM-10 operated at 80kV. Energy dispersive spectroscopy was performed with an EDDAX Sapphire detector that collects spectra over 100 s (live time) with a beam diameter of approximately 200 nm. More information can be found in Langey et al. (2009).

Mössbauer spectrometry was executed by Erno Kuzmann at the Laboratory of Nuclear Chemistry, of the Eötvös University. The 57Fe Mössbauer spectra of the powder samples were recorded in transmission geometry by a conventional constant acceleration type Mössbauer spectrometer (WISSEL) at room and liquid nitrogen temperatures. A 57Co(Rh) source of a 1*109 Bq activity was used and the spectrometer was calibrated with α-Fe at room temperature. More detail on the procedure is explained in Kamnev et al. (2013).

Trace and rare earth element composition of the samples was determined by Inductively Coupled Plasma Mass Spectrometry (ICP-MS) using an AGILENT 7500cs instrument. This was executed by Dieter Garbe at the Institut fuer Geowissenschaften, Abt. Geologie, Universitaet Kiel. Details on the optimisation of this procedure are given by Garbe-Schönberg (1993).

At the Laboratory for Isotope Geology of the Swedish Museum of Natural History, Kjell Billstrom analysed the radiogenic isotopes of Sr, Nd, Pb of the samples. The chemical preparation was performed according to standard routines (De Ignacio et al., 2006). A Thermo-Finnigan Triton thermal ionization mass spectrometry (TIMS) instrument was used for the Sr and Nd isotope

analyses. Pb isotopic analyses were performed on a Micromass Isoprobe multi-collector ICP-MS. The isotope measurements were conducted on a HR Nu-Plasma MC-ICP-MS (Nu Instruments). Additional information on the isotope analysis of Sr, Nd and Pb are provided by Dekov et al. (2009).

To conclude, Wayne Shanks of the U.S. Geological Survey analysed the oxygen isotopes (δ18O) in two red suspension samples using a CO2 laser fluorination system similar to those described by Sharp (1990) and Spicuzza et al. (1998). Oxygen isotopic analyses were performed using a Finnigan MAT 252 mass spectrometer, more information can be found in the work by Balci et al (2012).

3.2.2 Sample preparation and laboratory analysis techniques as used in sediment fingerprinting research

Some analyses in the framework of the sediment fingerprinting research were very similar to analyses routinely executed in the sedimentological laboratory of FHR such as the determination of SSC by filtration (see Section 3.1.2), the organic matter content (Sections 3.1.4) and the determination of grain size (see Section 3.1.5). However, they differ in the way that the initial product was dried material instead of sediment present in water samples (grain size analysis), or on filter papers (LOI analysis). This difference, however, does not affect the analyses techniques in any other way then having to add the dry material in a beaker of water prior to analysing the grain size, or having to put the sediment directly into the crucible for incineration, rather than having to use a filter paper as transport medium in the case of LOI analysis.

Also, some of the SSC determination of the Aarschot, Mangelbeek and Gete outlet stations happened through lyophilisation rather than by filtration, to leave the sediment accessible for further analysis.

However, some other laboratory analyses in the framework of sediment fingerprinting demanded specific sample preparation and were not routinely executed in the sedimentological laboratory of FHR, or needed to be out-sourced to a different laboratory. These techniques are described below.

3.2.2.1 Sample preparation prior to analysis

3.2.2.1.1 Oven drying and lyophilisation

Sediment samples collected within the framework of the sediment fingerprinting research are either rather 'wet' samples such as the material collected from the TISes, the sampled bed material or individual ISCO sample bottles (as described in Section 2.2.2.1), or the samples are relatively 'dry' such as the sampled soil and river bank material (as described in Section 2.2.2.2).

Both sets of sediment need to be dried further to a state that allows dry sieving, but the approach for each differs. On the one hand the already air-dry or slightly humid sediments are put in an oven at a temperature of 50°C until all the humidity has been evaporated. Drying at higher temperatures is avoided to minimise the likelihood of chemical changes in the samples (Peart, 1984; Grimshaw et al., 1974). On the other hand, the wet sediments need to be lyophilised. As described above in Section 3.1.3, the recipients are left to rest in a cold storage room to allow the suspended sediment present to settle. However in case of the buckets containing the content of the TISes, it proved necessary sometimes to accelerate the deposition of suspended sediment by centrifugation using an Avanti J-26XPI centrifuge (Beckman Coulter, Brea, California, USA). The remaining sediment is then transferred into aluminium trays. All rinsing of the buckets and

centrifuge recipients is done with the clear river water, to prevent a change in the chemical equilibrium of the sediment-water balance.

3.2.2.1.2 Sieving

Once the sediments are dry, the samples are gently disaggregated using a pestle and mortar. Consequently, the sediment is dry-sieved using a two-part sieve (constructed from PVC) with a disposable nylon mesh with pore diameter of 63 µm in between (see Figure 3.2). The sieve is deconstructed and cleaned in between two sievings, and the mesh is changed to minimize cross-contamination between samples.

3.2.2.1.3 Preparation for XRF analysis

The chemical composition of the sediment samples has been determined by X-Ray Fluorescence (XRF) which is addressed in Section 3.2.2.3. In the framework of this thesis, this analysis technique has been applied on both filter papers, laden with sediment particles (thin film XRF) and on a pelletized sediment-wax mixture.

Initially, it was attempted to analyse the filter papers readily available from the previous gravimetrical determination of SSC (as described in Section 3.1.2) for the Aarschot, Mangelbeek and Gete sampling locations, and to filter material collected with the TISes from the other locations, as was discussed in Berckmans (2005). However, this approach could not be applied for the fingerprinting research for two reasons:

- The sediment-laden filters curled during the drying process (see Figure 3.3). When left drying under a PVC ring to prevent this curling up, the filters remained straight but the sediment from the iron-rich rivers showed desiccation cracks (see Figure 3.4). This, however, is unacceptable for XRF analysis.
- To have a high degree of accuracy with XRF measurements, the sediment film on the filters should be as thin as possible. The readily available filtration papers, with material obtained from the ISCO bottles for SSC-determination, are usually laden with too much sediment for accurate thin-film XRF analyses.

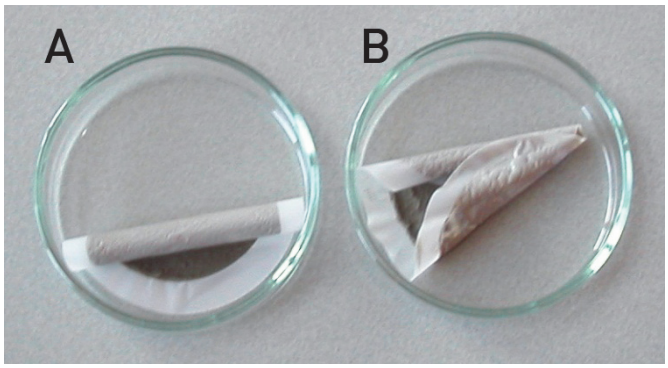

Figure 3.2: Rolled-up filter papers laden with sediment of the Velpe in Halen (A) and of the Mangelbeek in Lummen (B)

Figure 3.3: 63µm two-part sieve

Therefore, this approach was only used to estimate the ratios of elements present in the different subsamples produced by the settling test (discussed in Section 3.2.2.4), as those tests yielded insufficient material for pellet analyses.

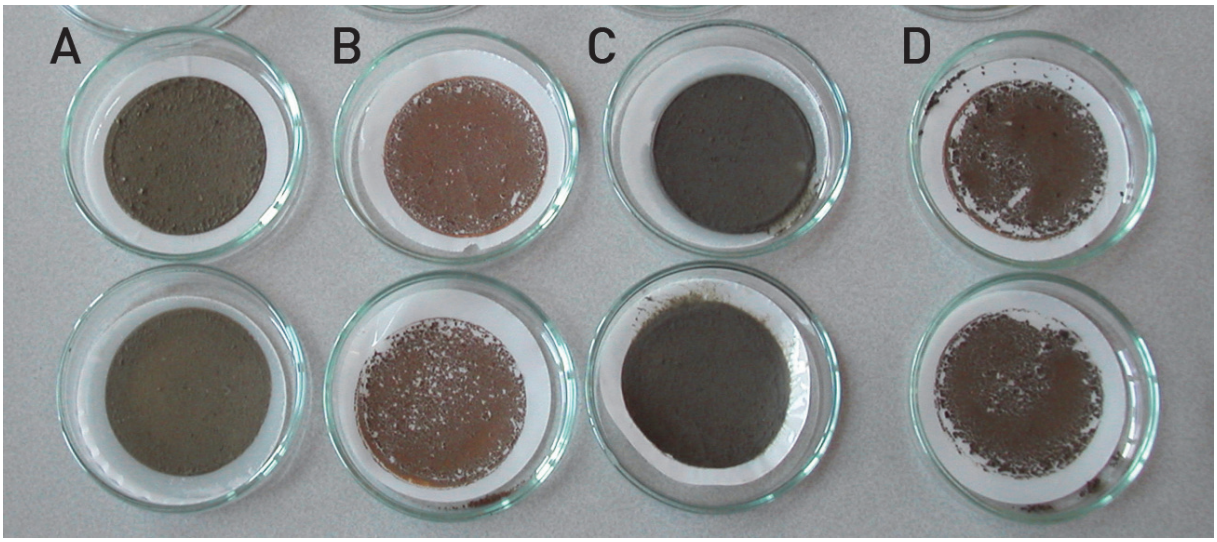

Figure 3.4: Sediment filters laden with sediment from the Demer in Aarschot (A), the Zwartebeek in Lummen (B), the Velpe in Halen (C) and the Mangelbeek in Lummen (D). Filter papers B and C show desiccation cracks.

For the rest of the sediment fingerprinting research, sediment-wax pellets were created which could consequently be analysed with XRF. To create these pellets, the dried and sieved (see Sections 3.2.2.1.1 and 3.2.2.1.2) typically 6 g of sediment was mixed with 1.2 g of wax, which would allow the pellets to have a minimum thickness of 6 mm. However, when less than 6 g of sediment was available, a smaller quantity of sediment (minimum 5 g) was used, but the 5:1 sample to wax ratio was maintained.

Consequently, the sediment-wax mixture was homogenized in a MM301 Retsch mixing mill (Retsch, Haan, Germany) prior to being pressed into pellets in the Air-EZ™ 40 Ton Air Powered Automated Lab Press (International Crystal Laboratories, New Jersey, United States) using pressurized air (ca. 2 minute duration) and 25 mm diameter stainless steel dies. These procedures have been documented in the FHR instructions I-WL-PP31-8 (De Schutter & Mostaert, 2009 e) and I-WL-PP31-9 (De Schutter & Mostaert, 2009 f).

Consequently, the pellets were transported to the Department of Chemistry, Environmental Analysis Group of the University of Antwerp (Belgium) for EDXRF analysis (see Section 3.2.2.3).

3.2.2.2 Determining density of dry sediment

After incineration and consequent removal of the organic matter from the sediment, the density of the remaining mineral fraction was determined by gas-pycnometer (AccuPycII 1340, Micromeritics Instrument Corporation, Norcross, Georgia, USA). The measuring principle of this device is based on determining the volume of the sediment sample by pressure change of a gas (helium) between the calibration chamber and the measuring chamber. The density of the measured sample is then derived from the determined volume and the mass of the sediment (which was determined prior to analysis).

One measurement of density with the gas pycnometer entails eight volume measurements, which yield an averaged density (with an accuracy of 0.0001 g/cm³) and a standard deviation. If this standard deviation was greater than 0.0050 g/cm³ the measurement was repeated. The methodology is described in detail in Instruction I-WL-PP31-10 (De Schutter & Mostaert, 2009 g).

3.2.2.3 Chemical composition analysis by XRF

XRF stands for X-ray fluorescence, which means that samples are excited by X-rays and the emission of characteristic "secondary" (or fluorescent) X-rays that are generated this way are recorded and used for quantification. The X-rays are typically generated by bombarding the anode in the X-ray tube with electrons of a predetermined current and voltage, but other X-ray sources like a radioactive source are also possible. The XRF phenomenon is widely used for elemental analysis for a vast number of elements with atomic numbers between 11 (Na) and 92 (U), also in aquatic sedimentary research (such as Eisma et al., 1984; Hinrichs et al., 2002; Davide et al., 2003; Vanhoof et al., 2004; Osán et al., 2007; Collins and Walling, 2007; Van Meel, 2009).

All XRF analyses in the framework of the sediment fingerprinting research of this thesis, have been executed at the Department of Chemistry, Environmental Analysis Group of the University of Antwerp (Belgium), under the supervision of dr. Katleen Van Meel (Van Meel et al., 2008; 2010).

This research group makes use of an Epsilon 5 (PANalytical, Almelo) high-energy EDXRF machine, using a polarizing beam. This instrument has a 600 W Gd-anode with exciting voltages of 25-100 kV and 0.5-24 mA current. The High Purity Ge-detector (HPGe) has an energy range of 0.7-200 keV and a resolution at Mn K_α of <165 eV. For this particular machine, elements ranging from Al till U can be analysed quantitatively. Excitation conditions were chosen based on a previous application with soil and sediment samples. Van Meel (2009) was able to show a Compton correction was appropriate to provide a simple and reliable method of matrix correction for the heavy elements. Furthermore, Van Meel (2009) constructed calibration curves for the EDXRF, using Standard Reference Materials as well as spiked secondary standards. This method proved successful by comparing it with ICP atomic emission spectroscopy, as was also reported in Van Meel (2009).

3.2.3 Determining geochemistry and grain size distribution on sediment fractionated by settling

The settling velocity of suspended sediment will be impacted by the presence of authigenic material. This material has an effect on the shape and size and therefore settling and resuspension behaviour of the sediment. This is of importance in both the authigenic sediment research (as is addressed in Chapter 9) as well as in the sediment fingerprinting research (discussed in Chapter 11).

Therefore, settling tests have been executed within the framework of the master dissertation of Patty Cant. This dissertation was executed and written under the supervision of Elin Vanlierde. The methodology is briefly described below, however the reader is referred to Cant (2010), where the methodology and procedures are described in great detail.

The settling tube used for these tests was constructed at FHR and consists of a cylindrical tube of 2m length constructed in transparent PVC, which has an inside diameter of 19 cm (see Figure 3.5). This width is sufficient to minimise the disturbance in settling behaviour due to wall-sediment interaction. At the bottom of the cylinder a funnel with a tap is attached, to be able to sample settled sediment for further analysis. Each time the funnel, which has an exact content of 2.2 litres is emptied, the water in the settling tube will lower with 7.8 cm. This has been taken into account in the sampling strategy of the settling tests.

Suspended sediment was collected in bulk at Lummen (Mangelbeek), Halen (Gete) and Aarschot (Demer). And the settling tests were executed for all three locations, using the river water (previously centrifuged to remove any sediment). The site-specific material was entered at the top of the two meter long tube and on the bottom subsamples were collected at seven pre-determined timings. The timings of the sampling (to obtain sedimentologically interesting fractions) were based on theoretical calculations using Stokes' Law, using assumptions about the density of the material used.

Figure 3.5: Settling tube constructed in FHR's sedimentological laboratory

Table 3.1: Timing of collection of subsamples at the bottom of the settling tube for the material of the Gete (Halen), Mangelbeek (Lummen) and Demer(Aarschot)

	Gete	Mangelbeek	Demer
subsample 1	0:01:15	0:01:11	0:01:45
subsample 2	0:02:20	0:02:20	0:02:36
subsample 3	0:03:30	0:03:14	0:03:30
subsample 4	0:07:48	0:07:48	0:07:48
subsample 5	0:11:24	0:11:24	0:11:24
subsample 6	0:28:00	0:28:00	0:28:00
subsample 7	1:06:00	1:06:00	1:06:00
subsample 8	20:47:30	20:46:12	20:46:00

Subsequently, the collected fractionated samples were wet-sieved through a 63µm mesh and both the coarse and fine material per sub-fraction were subjected to particle size analysis using the Malvern Mastersizer 2000 (as described in Section 3.1.5) and SSC determination using both filtration and lyophilisation techniques (as described in Sections 3.1.2 and 3.1.3). The fines were consequently also subjected to geochemical analysis by XRF (see Section 3.2.2.3). However, in the settling test research, thin film XRF analysis was performed, using material deposited on filter papers.

Great care went into ensuring those filter papers were not overladen. Results, as far as they are applicable to the sediment fingerprinting research are discussed in Section 11.1.3. The results could also be applied in the MARS-modelling research, which is discussed in Section 9.1.3.

Part II

Sediment classification

4. Classification of fluvial sediment and an overview of pre-dominant sediment sources in the Nete and Demer basin

Historically, fluvial sediment has been classified in three different ways, and terminology such as wash load and suspended sediment or bed load and bed-material load have often been used interchangeably in the literature. To avoid confusion, the different historical classifications of fluvial sediment, i.e. based on measurement methodology, transport mode and origin (Simons & Sentürk, 1977) are discussed in the subsequent sections. The classification based on the sediment origin is more elaborately discussed (in Section 4.3), as it not only includes the classification based on the source within the river (riverbed versus wash load) but also described the classification based on the origin of the sediment before it reached the river. This latter classification is particularly important in the sediment load calculations discussed in Part III, as well as in the authigenic sediment research (reported in Part IV) and the sediment fingerprinting research (as addressed in Part V of this thesis). In this section the different sediment sources and their prevalence in Flanders is dicussed as well.

4.1 Classification of fluvial sediment based on measurement method

The first of the three classification methods is based on the measurement method and it is visualized alongside the other two methods in Figure 4.1. It is noteworthy that the size of the boxes are not indicative of the absolute amounts of the various loads; they solely illustrate that the various loads are not necessarily equal.

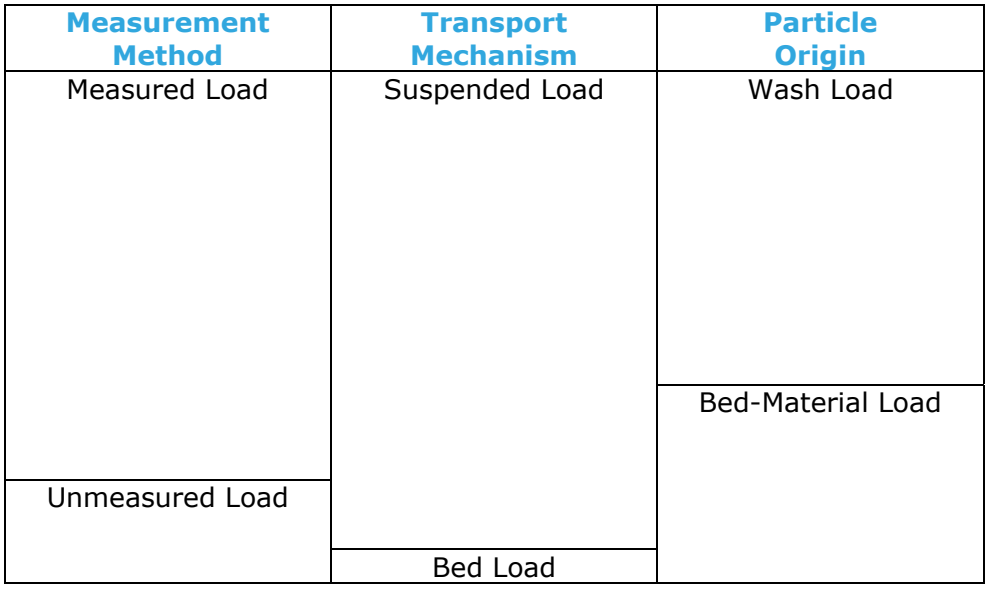

Figure 4.1: Classification of fluvial sediment transport based on measurement method, transport mode and (intra-river) origin (adapted from Biederharn et al., 2006)

The measurement method divides the fluvial sediment into two categories: measured and unmeasured zone. When sampling a vertical using a depth-integrating nozzle sampler, as reported by Meade et al. (1985); Taylor et al. (1990); Martin et al. (1992) and applied by the USGS (Edwards & Glysson, 1999; Horowitz et al., 1990), and by FHR, as described in Section 2.1.1.3, the

division between the two zones is due to the design of the sampler. As the physical location of the sampler nozzle relative to the bottom of the sampler prevents the nozzle from passing through the zone close to the bed, it is impossible to sample the entire depth.

The unmeasured zone characteristically carries the higher concentration and coarser particles and may or may not account for a large part of the total suspended sediment, depending upon the depth, velocity, and turbulence of the flow through the vertical. The measured sediment discharge is nearly equal to the total sediment discharge if the velocity and turbulence conditions within the sampled vertical overcome the tractive force transporting the bed load in the unmeasured zone and effectively disperse all of the sediment being transported into suspension throughout the total depth (Edwards & Glysson, 1999).

When using other types of samplers (such as automatic pumping samplers, watertrap samplers, buckets or weighted-bottles) the unmeasured zone is much larger, as the sampled zone includes only the point location from which the sample is obtained. This will be discussed further when addressing cross-sectional variability in sediment concentrations (see Section 5.1.2)

4.2 Classification of fluvial sediment based on transport mechanism

The second method of classifying fluvial sediment is according to its transport mechanism. In this way, fluvial sediment is divided as being either bed load or suspended load (see Figure 4.1). Suspended sediment moves in the water column above the bed and is rarely in contact with it. Bed load, on the other hand, is made up of particles that are rolling, sliding or saltating and which are therefore, either continuously or intermittently in contact with the bed. The distinction between bed and suspended loads is not obvious in the field, but it is physically significant (Biedenharn et al., 2006). In this technical note they cite Bagnold (1966) who demonstrated that the submerged weight of grains moving as bed load is supported solely by solid-to-solid contact at the bed, while that of suspended load is supported entirely by anisotropic turbulence due to fluid shear flow.

In case of classification by transport mechanism, the total sediment load is the sum of the suspended load and bed load. Generally, the depth-integrating sampler used to measure sediment in transport collects the majority of the suspended sediment, while leaving a portion of the sediment (the suspended sediment close to the bed and the bed load sediment) unsampled. When automatic pumping samplers are deployed, they are usually mounted sufficiently high above the riverbed, allowing them to sample the suspended load.

4.3 Classification of fluvial sediment based on sediment origin

The third basis for classification of the sediment load is based on the source of the sediment. As multiple interpretations of 'sediment source' are present in the literature, they will be separately addressed in the sections below.

4.3.1 Bed-material versus wash-load

One possible subdivision that for the classification of fluvial sediment based on the origin of the sediment, is the one between bed-material load and wash-load. There is a great variety in how these terms have been defined in the literature.

On one side, Biedenharn et al. (2006) define bed-material load as the sediment in transport that is comprised of particles found in 'appreciable quantities' in the channel bed, while defining wash load

as sediment in transport that is derived from sources other than the bed. As such, wash load is finer than the bed-material load and is not found in 'appreciable quantities' in the bed, e.g. banks, gullies, and runoff. The total load consists of the sum of the bed-material load and the wash load. Biedenharn et al. (2006), however indicate that the precise definition of what constitutes an 'appreciable quantity' is unclear, meaning that the threshold grain size separating bed-material load and wash load may be defined in several ways.

Einstein (1950) defines wash load as the grain size of which 10 percent of the bed mixture is finer. The principle that is accepted here is that wash load may be defined on the basis of its absence from the bed material and that the size criterion used to define it (in this case D10) must, therefore, be expressed in relative rather than absolute terms.

Using a D5 or D15, would therefore also be applicable. Howerver, Biedenharn et al. (2006) do warn that applying such a relative size criterion, leads to defining silt and clay in a sand-bed channel as wash load and sand as bed load, while sand would be considered the wash load in a gravel-bed channel (provided that the D10 of the bed was 2 mm or coarser).

Other definitions of wash load can be found such as:

- "consisting of particles smaller than 0.063 mm" (hence, corresponding to the division between sand and silt in the Wentworth scale) as used by Yang & Simões (2005), Knighton (1998) and Richards (1982);
- "… sediment that moves in suspension in the flow but is not represented in the bed of the channel. It is generally assumed that the transport of the wash load is supply dependent and is independent of the local flow conditions.", as reported by Bettess (1994)
- Graf (1984) agrees with Einstein, as he indicates that the wash load is made up of sizes finer than the bulk of the bed-material load, and states: "The wash load rate can be related to the available supply of solid particles within the watershed; it enters the watercourse by sheet wash, bank caving, etc., but is merely washed through the sections."

4.3.2 Sediment sources within the catchment

Up until this point (and as visualized in Figure 4.1) the classification of fluvial sediment based on the origin of the sediment has been reduced to the binary division between wash load and bed-material load. However, other subdivisions are possible. This is confirmed by the definition the USGS applies for fluvial sediment: fluvial sediment is fragmentary material that originates mostly from weathering of rocks and is transported by, suspended in, or deposited from water (FISP, 1963); it includes chemical and biological precipitates and decomposed organic material, such as humus (Edwards & Glysson, 1999).

This definition highlights some of the most prevalent sources of fluvial sediment, i.e. sediment derived from physical erosion (from fields, from the riverbed, …), biogenically formed sediment (diatomic silica, …) and chemically precipitated sediment (such as authigenic sediment). These sources, as well as sediment derived from antropogenic sources (industrial discharges, sewage discharges, road runoff, … left unmentioned in the USGS definition) are discussed below, as well as their prevalence in Flanders.

4.3.2.1 Physical erosion

Erosion is the result of the acquisition or plucking of loose fragments by the erosional agent, the wearing away of resistant surfaces by impact from materials in transit, and the mutual wear of particles in transit through contact with each other (Thornbury, 1954).

Traditional forms of physical erosion are water erosion, wind erosion and mass transport, all of which are present in Flanders (Van Kerckhoven et al., 2009; Van Den Eeckhaut et al., 2007). Other soil loss processes are also recognised, such as tillage erosions (Govers et al., 1994; Van Muysen et al., 2000) or soil loss through harvesting of crops such as potatoes and beetroot (Poesen et al., 2001). Of these soil loss processes, only water erosion is significantly responsible for transport of sediment to rivers. The spatial distribution of the potential soil loss by this type of erosion in Flanders is visualized in Figure 4.2. Because the spatial pattern of soil loss due to water erosion in Flanders is mainly constricted by topography, a significant difference between northern and southern Flanders is visible. Additionally, the loamy and sand-loamy soils of the southern part of Flanders are also more sensitive for soil loss by water erosion than the sandy soils of the north.

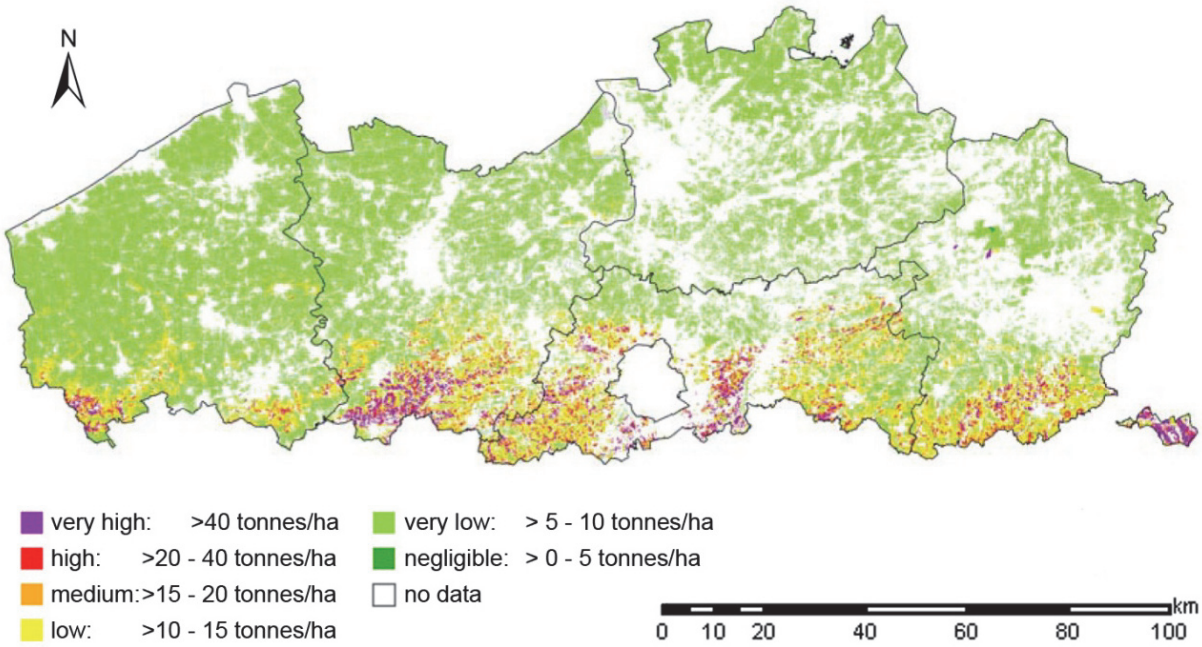

Figure 4.2: Spatial distribution of the average annual potential soil loss by water erosion, aggregated by plot in Flanders for the year 2011 (adapted from Overloop et al., 2011)

This division is also present in the study area for this thesis: the Nete basin and the northern part of the Demer basin both have average annual soil losses by water erosion that are very low (<0,5 tonnes per hectare per year), while some of the highest erosion potential in Flanders is present in the Demer basin, with values reaching 51 tonnes per hectare per year.

However, not all of the eroded material will be delivered to the river and different methods are applied in the literature to determine the sediment yield. Current tools include various forms of sediment rating curves that may account for changes in land management and temporal variability in sediment yield (USEPA, 1999), as well as geographic information system (GIS)-based models such as SWAT (Neitsch et al., 2005), HSPF (Bicknell et al., 1993), AGNPS (Young et al., 1989) or WATEM/SEDEM (Desmet & Govers, 1996; Van Oost et al., 2000). These models use various forms of the Universal Soil Loss Equation (USLE) for soil loss and sediment yield estimates.

The WATEM/SEDEM model has yielded estimates for Flanders for the annual sediment delivery to rivers, as well as estimates for sediment export by rivers, which are presented in Table 4.1 (Overloop et al., 2011). The river basins of interest for this thesis, i.e. the Nete and the Demer basin, have a modelled sediment delivery to the river of respectively around 6,500 and 145,000 tonnes per year; while the sediment export by the river (once again, modelled by WATEM/SEDEM) only mounts to respectively 4,500 and 108,000 tonnes per year. The decrease between sediment delivered to the river and sediment exported can be explained by sedimentation processes. When navigation becomes hindered, or inundation risks become increased, this surplus can be removed from the river system by dredging.

Table 4.1: Reference scenario (for the year 2005) for sediment delivery and export by water erosion in Flemish River basins, using the WATEM/SEDEM model, implementing a standardized rainfall erosivity of 880 mm/ha/year (adapted from Overloop et al., 2011).

Basin	Total sediment production (tonnes)	Total sediment deposition (tonnes)	Total sediment delivery to rivers (tonnes)	Total sediment export by rivers (tonnes)
Demer	634,369	489,557	144,813	107,824
Dender	238,854	178,664	60,190	51,705
Yser	127,866	91,605	36,261	30,085
Leie	144,635	111,728	32,907	27,682
Meuse	140,545	89,233	51,312	15,730
Nete	20,188	13,838	6,349	4,536
Polders and Bruges' canals	23,258	14,558	8,700	4,490
Scheldt upstream Ghent	263,185	195,138	68,047	63,092
Zenne	167,820	121,031	46,789	31,228
Tributary basins Scheldt	75 ,690	56,732	18,958	15,964
Flanders	**1,839,276**	**1,363,828**	**475,448**	**352,923**

In addition to creating point source fluvial sediment contribution, physical erosion can also be a diffuse source of contaminants in the river system. Therefore, besides the quantity, the quality of the sediment delivered into the river system is of importance, which is why VMM has modelled the diffuse input of sources using the Emisson Inventory Water model (EIW). This resulted in an emission inventory, which summarizes the influxes of heavy metals, polyaromatic hydrocarbons, oxygen-binding substances and nutrients, for all potential sources in Flanders. Table 4.2 shows the results of this modelling for the heavy metals emissions, which indicates that the Demer basin has the highest influx of all of the heavy metals reported.

Table 4.2: Annual heavy metal emissions originating from soil erosion (Syncera Water, 2005).

	As (kg/y)	Cd (kg/y)	Cr (kg/y)	Cu (kg/y)	Hg (kg/y)	Pb (kg/y)	Ni (kg/y)	Zn (kg/y)
Yser basin	243	10	474	218	7	512	115	794
Basin of the Bruges canals	41	2	79	36	1	85	19	132
Basin of the Ghent canals	35	1	69	32	1	75	17	116
Lower Scheldt basin	71	3	139	64	2	150	34	233
Leie basin	248	10	482	222	7	522	117	808
Upper Scheldt basin	409	17	797	366	12	862	194	1,336
Dender basin	288	12	562	258	8	607	137	941
Dijle and Zenne basin	364	15	709	326	11	766	172	1.188
Demer basin	765	32	1,490	684	22	1,611	362	2,496
Nete basin	35	1	67	31	1	73	16	113
Meuse basin	201	8	392	180	6	424	95	657
Flanders	**2,701**	**114**	**5,260**	**2,417**	**78**	**5,686**	**1,279**	**8,814**

4.3.2.2 Anthropogenic sources

4.3.2.2.1 Indirect anthropogenic impact on sediment generation and transport

Humans have always made adjustments to the environment they live in; be it through utilising the land through agriculture or by constructing roads, houses or even through canalisation of rivers or building dikes in combination with controlled flooding areas. These adjustments increase or reduce the amount of runoff water, concentrate its flow, and/or alter the natural resistance to flow and sediment movement. Such changes in the amount of natural flow and in the conveyance systems are the key to sediment problems.

In Flanders, the human impact on soil erosion through soil use change has been significant. Forrest or even pastures know little to no soil erosion, but the introduction of agricultural lands has increased the erosivity of the soils greatly.

This indirect anthropogenic impact, however, will not be regarded in this PhD thesis as a separate source of sediment. It plays a significant role in the creation and transport potential of detrital sediment sources, which is part of the physical erosion described in the previous section (Section 4.3.2.1).

4.3.2.2.2 Industrial and domestic discharges

Flanders is a densely populated region, and quite intensely industrialized. This has its repercussions on the production of waste water. Both industrial and sewage discharges (treated or non-treated by sewage treatment plants) are superfluously present in Flanders.

Even though strongly regulated in Flanders, these discharges can still impact sediment transport significantly. For one, these discharges add to the total dissolved load in the river systems, which can already be quite substantial under natural conditions, as is well-documented in the literature (Walling & Webb, 1983).

Furthermore, it should be taken into account that the dissolved load being discharged is not necessarily in chemical equilibrium with the river water it is discharged in. Therefore, the dissolved phase can be sorbed onto existing natural sediment or it can precipitate, thus forming authigenic sediment.

Finally, besides increasing the dissolved load, the industrial and domestic discharges will also add directly to the suspended sediment load, as also non-dissolved material is being discharged.

As stated above, VMM is responsible for monitoring the emissions of pollutants and nutrients. Their measuring network is quite extensive and incorporates both sewage treatment facilities as well as individual industrial sites. In the Demer and Nete basins the points of wastewater discharge by both sewage treatment facilities and individual industries are densely implanted, as can be seen in Figure 4.3. Each of these locations has a different quantity and composition of effluents. Raw data for the year 2007 of both discharge and property concentration of these effluents, were obtained from VMM.

Consequently, using this data, the wastewater discharge that entered the river system directly or after treatment in a sewage treatment centre in the year 2007 could be calculated for the major tributaries of the Demer and Nete basins.

This has been reported in Table 4.3, in combination with the total measured annual discharge for each of these tributaries (raw data provided by FHR and VMM), allowing for the calculation of the contribution of the waste water discharge to the total discharge. It should be remarked that only the effluents that were discharged upstream of the respective discharge measuring station have been taken into account. This is to allow for a correct calculation of these contributions.

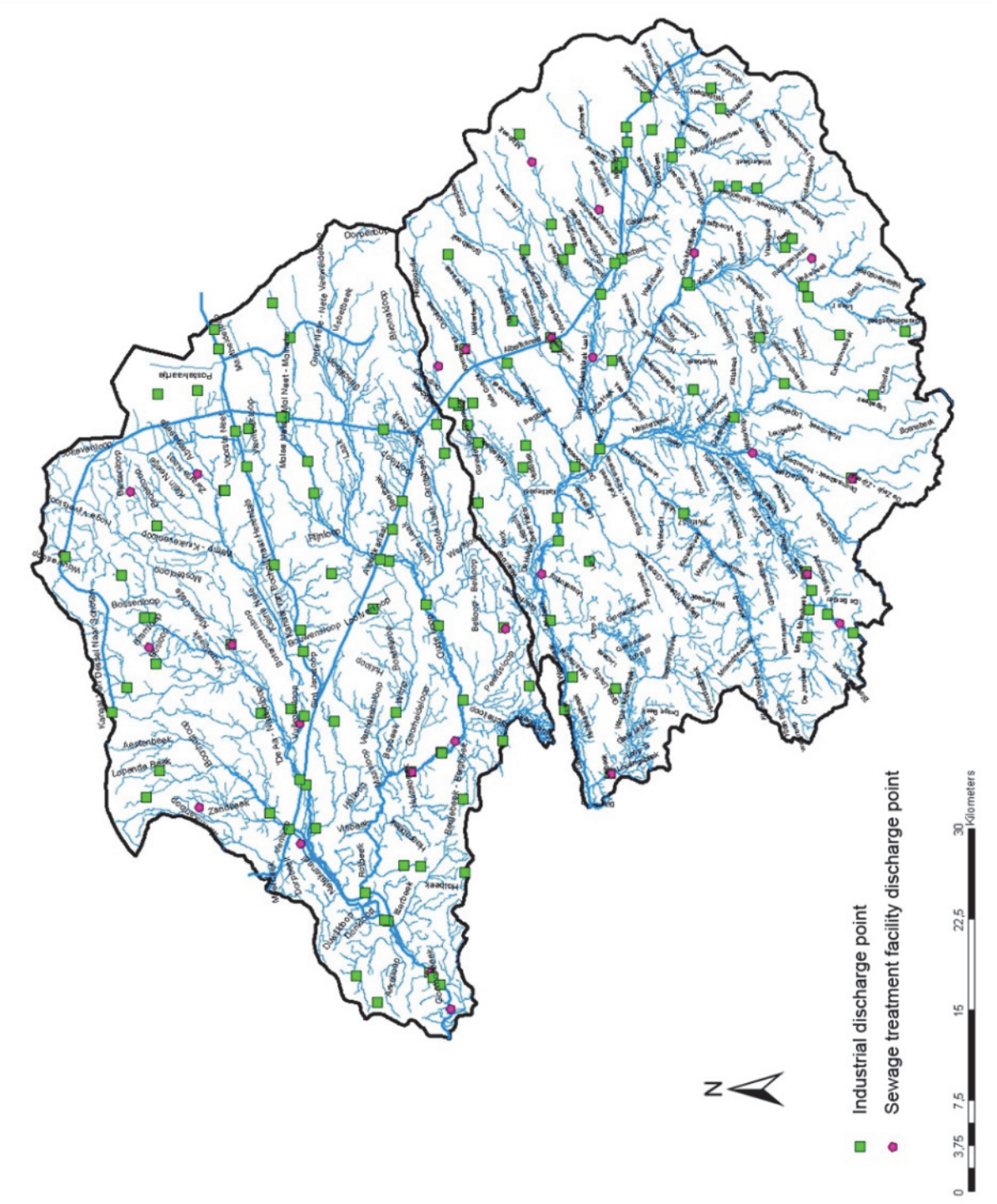

Figure 4.3: Locations of wastewater discharge in the Demer and Nete basins by sewage treatment facilities and individual factories for the year 2007, data obtained from VMM)

Table 4.3: Contribution of industrial and sewage treatment facility effluents (Q_{Eff}) to the total surface water discharge of tributaries in the Demer and Nete basin (Q_{SW}) for the year 2007; (raw data: VMM and FHR)

	Tributary	Q_{SW} (10^3 m³/y)	Q_{Eff} (10^3 m³/y)	Contribution (%)
Nete	Grote Nete (upstream Hulshout)	162410	33064	20
	Wimp	58279	7363	13
	Kleine Nete (without Aa)	116982	10339	9
	Aa	103407	21678	21
Demer	Motte	13214	117	1
	Hulpe	39650	13298	34
	Zwartebeek	29263	3605	12
	Mangelbeek	38028	7543	20
	Gete	133608	23924	18
	Herk	51363	4470	9
	Velpe	27205	2	0
	Demer upstream Hasselt	74123	24056	32

These calculations show that in the Demer basin, the upper-Demer (upstream Hasselt) and the Hulpe received the highest contribution of effluent discharges (around 33%), while in the Nete basin, the Grote Nete (upstream the discharge measuring station of Hulshout) and the Aa received up to one fifth of their surface water discharge through industrial and sewage treatment effluents. However, this does not readily imply that these tributaries have the highest contributions of anthropogenic sediment, as the concentration of pollutants and substances in these effluents differ per individual discharge. This is illustrated in Tables 4.4 and 4.5 (for the year 2007) for the Nete and Demer basins respectively. In these tables, the total anthropogenic load per tributary of each contaminant is reported, as well as the concentrations this represents (by dividing the total anthropogenic load by the total annual discharge of the tributary). The discharge data was obtained from VMM and FHR. Once again, the concentrations and loads were calculated by only taking effluents into account that enter the river upstream of the discharge measurement location.

From Table 4.4 it is clear that the Grote Nete is the tributary which carries the biggest load in the Nete basin. For 14 out of the total 22 measured elements the maximal load was observed in this tributary. However, when looking at the concentrations these loads represent in the different tributaries, the Grote Nete has only nine elements left for which its concentrations are the maximal ones throughout the Nete basin.

Furthermore, it is noteworthy that some maximal loads (6 elements), and even more maximal concentrations (9 elements) are registered in the Kleine Nete (excluding the tributary Aa). Also, the Wimp, which is a relatively small tributary of the Grote Nete, does not transport for any element the maximal load observed in the Nete basin, however it does drain the highest concentrations of Zn and B measured in the Nete basin.

From Table 4.5, it can be concluded the Hulpe transports the biggest load for most of the measured elements (16) and does this by carrying the highest concentrations. Even though the Hulpe also clocks off on 16 elements whose concentrations are the maximal ones throughout the Demer basin, these are not all the same elements as those whose maximal loads were observed in the Hulpe.

Also clear from the data presented in Table 4.5 is that the Motte, Zwartebeek, Gete, Velpe and Herk never transport any maximal loads or concentrations.

Table 4.4: Loads and concentrations of industrial and sewage treatment effluents for the year 2007 for selected tributaries in the Nete basin. Numbers in blue represent the maximum load registered in the Nete basin, numbers in red represent the highest effluent concentration measured in the Nete basin. Numbers in bold represent the highest value for both Demer and Nete basin (original data VMM and FHR)

		Grote Nete (upstream Hulshout)	Wimp	Kleine Nete (without Aa)	Aa
Ag_{Tot}	kg/y	0.5	24.1	**51.7**	0.2
	µg/l	0.0	3.3	**5.0**	0.0
Al_{Tot}	kg/y	3388.2	58.5	239.6	452.7
	µg/l	102.5	7.9	23.2	20.9
As_{Tot}	kg/y	**156.8**	0.2	74.3	0.9
	µg/l	4.7	0.0	7.2	0.0
B_{Tot}	kg/y	6749.8	2073.1	960.8	1244.7
	µg/l	204.1	281.6	92.9	57.4
Ba_{Tot}	kg/y	**20739.6**	47.4	68.9	25.0
	µg/l	627.2	6.4	6.7	1.2
Cd_{Tot}	kg/y	23.3	0.7	11.2	2.4
	µg/l	0.7	0.1	1.1	0.1
Co_{Tot}	kg/y	**1995.5**	0.1	240.6	1.6
	µg/l	**60.4**	0.0	23.3	0.1
Cr_{Tot}	kg/y	37.8	11.1	62.9	5.5
	µg/l	1.1	1.5	**6.1**	0.3
Cu_{Tot}	kg/y	84.4	22.9	466.6	98.8
	µg/l	2.6	3.1	**45.1**	4.6
Fe_{Tot}	kg/y	**16953.8**	1107.4	2207.2	1496.1
	µg/l	512.8	150.4	213.5	69.0
Hg_{Tot}	kg/y	**7.6**	0.1	0.2	0.1
	µg/l	**0.2**	0.0	0.0	0.0
Mn_{Tot}	kg/y	**2029.6**	25.9	103.9	56.3
	µg/l	61.4	3.5	10.1	2.6
Mo_{Tot}	kg/y	653.7	29.6	51.1	2096.1
	µg/l	19.8	4.0	4.9	96.7
Ni_{Tot}	kg/y	390.3	66.8	**821.1**	166.6
	µg/l	11.8	9.1	**79.4**	7.7
Pb_{Tot}	kg/y	12.1	6.9	27.1	9.4
	µg/l	0.4	0.9	2.6	0.4
Sb_{Tot}	kg/y	9.6	0.0	**36.6**	17.0
	µg/l	0.3	0.0	**3.5**	0.8
Se_{Tot}	kg/y	**114.7**	0.3	92.3	5.5
	µg/l	3.5	0.0	**8.9**	0.3
Sn_{Tot}	kg/y	**1345.1**	8.1	39.5	33.0
	µg/l	40.7	1.1	3.8	1.5
Te_{Tot}	kg/y	0.000	0.000	0.000	0.019
	µg/l	0.000	0.000	0.000	0.001
Ti_{Tot}	kg/y	361.8	2.9	5.6	4.6
	µg/l	10.9	0.4	0.5	0.2
V_{Tot}	kg/y	**72.2**	0.6	6.8	1.8
	µg/l	2.2	0.1	0.7	0.1
Zn_{Tot}	kg/y	**3410.0**	810.1	912.4	1696.4
	µg/l	103.1	**110.0**	88.2	78.3

Table 4.5: Loads and concentrations of industrial and sewage treatment effluents for the year 2007 for selected tributaries in the Demer basin. Numbers in blue represent the maximum load registered in the Demer basin, numbers in red represent the highest effluent concentration measured in the Demer basin. Numbers in bold represent the highest value for both Demer and Nete basin (original data VMM and FHR)

		Motte	Hulpe	Velpe	Gete	Zwartebeek	Mangelbeek	Herk	Demer (upstream Hasselt)
Ag_{Tot}	kg/y	0.0	0.1	0.0	0.0	0.0	0.6	0.0	0.0
	µg/l	0.0	0.0	0.0	0.0	0.0	0.1	0.0	0.0
Al_{Tot}	kg/y	0.0	3730.9	0.0	**6160.6**	2.8	154.4	0.0	2899.9
	µg/l	0.0	**280.6**	0.0	257.5	0.8	20.5	0.0	120.6
As_{Tot}	kg/y	0.5	129.6	0.0	2.7	0.0	0.3	1.1	25.0
	µg/l	3.8	**9.7**	0.0	0.1	0.0	0.0	0.2	1.0
B_{Tot}	kg/y	0.0	6602.1	0.0	**7492.9**	360.0	58.8	0.0	5840.0
	µg/l	0.0	496.5	0.0	313.2	99.9	7.8	0.0	242.8
Ba_{Tot}	kg/y	0.0	20550.2	0.0	319.3	0.2	0.9	0.0	215.3
	µg/l	0.0	**1545.4**	0.0	13.3	0.0	0.1	0.0	9.0
Cd_{Tot}	kg/y	0.0	**29.1**	0.0	0.1	0.0	0.6	0.0	0.9
	µg/l	0.0	**2.2**	0.0	0.0	0.0	0.1	0.0	0.0
Co_{Tot}	kg/y	0.0	9.9	0.0	5.2	0.0	0.1	0.0	13.8
	µg/l	0.0	0.7	0.0	0.2	0.0	0.0	0.0	0.6
Cr_{Tot}	kg/y	0.0	23.7	0.0	47.7	0.2	4.7	2.3	**115.3**
	µg/l	0.0	1.8	3.3	2.0	0.1	0.6	0.5	4.8
Cu_{Tot}	kg/y	0.0	**472.5**	0.1	36.9	0.0	18.9	9.2	78.2
	µg/l	0.0	35.5	32.0	1.5	0.0	2.5	2.1	3.3
Fe_{Tot}	kg/y	0.0	11450.0	0.0	5261.8	10.2	43.2	0.0	8802.9
	µg/l	0.0	**861.0**	0.0	219.9	2.8	5.7	0.0	365.9
Hg_{Tot}	kg/y	0.0	0.1	0.0	0.5	0.0	0.6	0.0	0.1
	µg/l	0.0	0.0	0.0	0.0	0.0	0.1	0.0	0.0
Mn_{Tot}	kg/y	0.0	1493.0	0.0	1429.6	0.1	5.0	0.0	594.7
	µg/l	0.0	**112.3**	0.0	59.8	0.0	0.7	0.0	24.7
Mo_{Tot}	kg/y	0.0	74.2	0.0	36.5	0.1	0.7	0.0	**2331.8**
	µg/l	0.0	5.6	0.0	1.5	0.0	0.1	0.0	**96.9**
Ni_{Tot}	kg/y	0.0	245.3	0.0	556.7	0.5	111.5	1.1	576.0
	µg/l	0.0	18.4	8.3	23.3	0.1	14.8	0.3	23.9
Pb_{Tot}	kg/y	0.0	**50.0**	0.0	5.3	0.0	15.4	0.0	25.4
	µg/l	0.0	**3.8**	0.0	0.2	0.0	2.0	0.0	1.1
Sb_{Tot}	kg/y	0.0	15.0	0.0	0.2	0.0	0.3	0.0	2.5
	µg/l	0.0	1.1	0.0	0.0	0.0	0.0	0.0	0.1
Se_{Tot}	kg/y	0.0	88.3	0.0	13.0	0.0	0.2	0.0	1.3
	µg/l	0.0	6.6	0.0	0.5	0.0	0.0	0.0	0.1
Sn_{Tot}	kg/y	0.0	1237.9	0.0	220.5	0.0	0.8	0.0	101.7
	µg/l	0.0	**93.1**	0.0	9.2	0.0	0.1	0.0	4.2
Te_{Tot}	kg/y	0.0	**5.6**	0.0	0.1	0.0	0.1	0.0	0.3
	µg/l	0.0	**0.4**	0.0	0.0	0.0	0.0	0.0	0.0
Ti_{Tot}	kg/y	0.0	**451.3**	0.0	39.8	0.1	0.5	0.0	32.2
	µg/l	0.0	**33.9**	0.0	1.7	0.0	0.1	0.0	1.3
V_{Tot}	kg/y	0.0	53.6	0.0	18.2	0.0	0.1	0.0	22.8
	µg/l	0.0	**4.0**	0.0	0.8	0.0	0.0	0.0	0.9
Zn_{Tot}	kg/y	0.0	812.7	0.1	967.5	156.3	531.6	227.3	1205.7
	µg/l	0.0	61.1	71.3	40.4	43.4	70.5	50.9	50.1

When combining the data from Tables 4.3, 4.4 and 4.5, it is clear that the highly-concentrated big effluent volumes of the Hulpe result in high concentrations of effluents in the surface water. But the contribution of the Demer upstream Hasselt, while nearly identical in its effluent/surface water discharge ratio as the Hulpe's, does not reach equally high concentrations of pollutants in the surface water.

The same conclusion can be drawn for the tributaries in the Nete basin, where both the Grote Nete and the Aa had 1/5 of their surface water volume originating from industrial and sewage treatment effluents, but only the Grote Nete will transform that into the highest concentrations of some specific contaminants.

Finally, it should be remarked that in the discussion above, only maximum values of loads and concentrations have been addressed. This does however not signify that rivers that do not transport maximal loads or concentrations are unpolluted. They can still transport significant amounts of pollutants as can be seen in Tables 4.4 and 4.5.

Some considerations should be taken into account when interpreting the date in Tables 4.3, 4.4 and 4.5. First of all, it should be remarked that all of the data presented in these tables is of the year 2007, and that effluent discharges might differ from year to year. However, the year 2007 was selected for close investigation because the sediment fingerprinting sampling in the tributary catchments took place during this year.

Secondly, all the pollutants in these effluents are entering the river system in a dissolved phase. Whether they remain in solution depends on the environmental conditions of the surface water they are discharged in. In other words, the chemical equilibrium of the surface water these effluents are discharged into, will define whether these discharges will contribute to the soluble or suspended load of the rivers. This aspect will also be addressed in Section 4.3.2.3, where groundwater contributions are discussed.

4.3.2.2.3 Diffuse anthropogenic pollution

Not all anthropogenic pollution enters the river system through sewage treatment plants or industrial discharges. These are all point sources which can be monitored at the specific locations where they enter the river system. However, certain types of anthropogenic pollution are diffuse, and enter the river system as such. Examples of diffuse sources are road dust, shipping and corrosion of building materials. VMM has also used EIW (Syncera Water, 2005) to estimate the contributions of the most prevalent heavy metals per tributary obtained through these sources.

4.3.2.2.4 Maintenance works

Flemish rivers undergo a variety of human interventions, which might impact the sediment load they transport. Some of these interventions can be temporary in nature, such as the building of a bridge, construction works along river banks or dike maintenance works which may temporarily increase the influx of sediment into the river. Other human interventions may affect the sediment transport regime for a medium to very long time (dredging or de-meandering of rivers).

The impacts of such works have already become quite apparent in the case study at Aarschot sampling station which will be discussed in Chapter 7.

4.3.2.3 Authigenic sediment

4.3.2.3.1 Definition

Authigenic sediment is defined as sediment occurring in the place where it was originally formed (McGraw-Hill, 2003). Authigenic sediment is often discussed in deep-sea settings where it is defined as deep-sea sediment that has been formed in place on the seafloor, of which metal-rich sediments and manganese nodules are considered the most significant authigenic sediments in modern ocean basins (Luyendyk, 2012).

However, in a fluvial context, as is the focus of this PhD thesis, the term authigenic sediment should rather be applied to sediment particles formed in the river course due to interaction between waters with different origin and/or composition.

The broadest definition of the term 'authigenic sediment' would also include fluvial biogenic sediment as it is also generated in streams. However, in the framework of this thesis, authigenic sediment is restricted to the generation of chemical precipitates.

4.3.2.3.2 Creation of ferric authigenic sediment

Authigenic sediment is generated in rivers when dissolved compounds encounter changes in reigning chemical, physical and biological conditions, forcing them to precipitate. Such changes in environmental conditions can for instance be observed in estuarine systems where saline-fresh water interactions cause flocculation and sediment creation.

In fluvial systems, authigenic sediment is created when groundwater, laden with solutes, seeps into the surface water, where it is subjected to different reigning environmental conditions. Which compounds precipitate when groundwater interacts with the surface water depends on the ion composition in solution and therefore on the hydro-geological context of the region, as well as on the condition of the surface water.

VMM has tried to estimate the emissions of heavy metals contributed to the surface water by the groundwater, using the EIW model (Syncera Water, 2005). This model requires emission factors on the one hand and the groundwater discharge on the other hand. However, basin-specific data on the latter was not at the disposal of VMM, so they only published the emission factors (see Table 4.6). These emission factors are substance specific and are expressed as gross emission per m³ per year.

In the framework of this thesis, only the creation and contribution of ferric authigenic sediment to fresh water fluvial systems in Flanders (i.e. in the Nete and Demer basins) is studied. The creation and contribution of other forms of authigenic sediment fall outside of the scope of this thesis. Groundwater discharges for the Kleine Nete and Mangelbeek catchments have been calculated and have consequently been used to determine the influx of solute iron into the river, as described in Chapter 8.

Table 4.6: Emission factors for different metals (Syncera Water, 2005)

As	5 $\frac{mg}{[Q_{GW}]\cdot y}$
Cd	1 $\frac{mg}{[Q_{GW}]\cdot y}$
Cr	10 $\frac{mg}{[Q_{GW}]\cdot y}$
Cu	20 $\frac{mg}{[Q_{GW}]\cdot y}$
Hg	0.05 $\frac{mg}{[Q_{GW}]\cdot y}$
Pb	5 $\frac{mg}{[Q_{GW}]\cdot y}$
Ni	10 $\frac{mg}{[Q_{GW}]\cdot y}$
Zn	60 $\frac{mg}{[Q_{GW}]\cdot y}$

Figure 4.4 schematically depicts the processes involved in the generation of ferric authigenic sediment through groundwater seepage. The process starts when rainfall percolates through the sub-soil, of which only the upper meters have a weak pH buffering capacity. Further down, thick layers of iron-rich sands possess a low pH-buffering capacity, which, in combination with the reigning redox-conditions, creates a reducing environment. This ensures the presence of substantial amounts of Fe(II) in the groundwater.

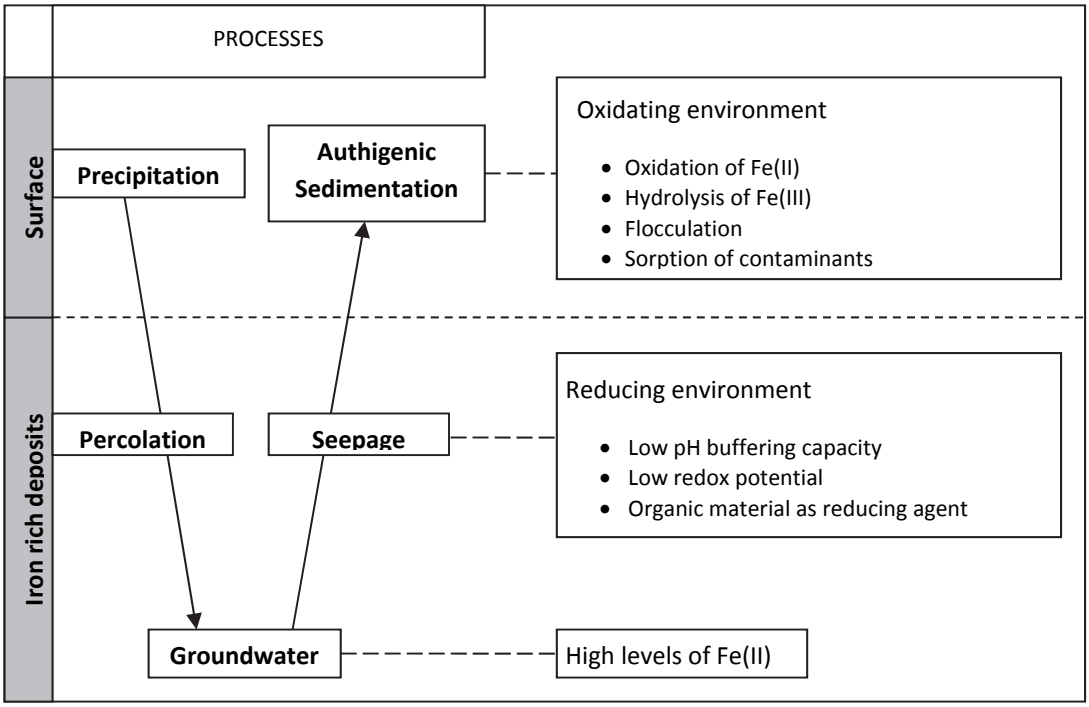

Figure 4.4: Schematic view of the production processes of ferric authigenic sediment

Once the groundwater seeps into the river, it encounters more oxidising environmental conditions, which will lead to the oxidation of the Fe(II), followed by the hydrolysis to hydro-ferric oxide as indicated by Stumm & Morgan (1996). These authors also indicate that the attachment of a hydroxy group to ferric ions is a relatively slow process in aerated surface waters with low pH-values, but the process picks up the pace at more neutral pH-values.

Additionally, it should be remarked that amorphous hydro-ferric oxide is an insoluble compound, which can sorb amongst others contaminants and nutrients onto its surface and which can easily flocculate, thus adding to the weight of the newly created authigenic sediment.

4.3.2.3.3 Occurrences of significant/elevated ferric authigenic sediment creation in Flanders

As described above, authigenic sediment is created when previously soluble ions (transported by groundwater) are forced to precipitate in order to be chemically in equilibrium with their new surrounding environmental conditions in the surface water.

This process takes place in nearly every river system around the world that is fed through groundwater seepage with a high solute content. However, the significance of the contributions of authigenic sediment to the total sediment load can be quite low, rendering them negligible in comparison to other sediment sources in the basin.

Specific geological settings of a region, however, can ensure a significant contribution of authigenic sediment to the total sediment load of the river system. In this study, such a region is located in the northeastern part of Flanders, in the Nete basin and the northern part of the Demer basin.

Its flat topography (see Figure 1.4) ensures a low run-off erosion rate, as can be observed in the erosion map of Flanders (see Figure 4.2). These low erosion rates, combined with the presence of ditches and trenches adjacent to the fields, minimizes input of detrital sediment sources into the river.

Furthermore, the geological settings of this region ensure a high production of authigenic sediment. As mentioned in Section 1.5 the clayey Boom Formation, because of its very low permeability, serves as an aquitard that divides the groundwater into two separate ground water systems: the Centraal Kempisch Systeem (CKS) and the Brulandkrijtsysteem (BLKS). The streams in the Nete basin and the northern part of the Demer basin are therefore mostly fed by groundwater seepage from the CKS. Within the two phreatic groundwater bodies present the Neogene, sandy aquifers can be grouped into three sets: (1) the Sands of Brasschaat and/or Merksplas [0231], and the Sands of Mol [0232]; (2) the sandy top of the Formation of Lillo [0233] and the Sands of Poederlee and/or Sandy top of Kasterlee [0234]; and (3) the Sands of Diest [0252] and the Sands of Berchem [0254]. Aquifers 2 and 3 contain high quantities of iron minerals (e.g. glauconite). This leads to an elevated content of Fe(II) in the groundwater, as discussed above in Section 4.3.2.3.2. As aquifer 3 (the Formation of Diest) is responsible for most of the groundwater seepage into the Nete and northern part of the Demer basin, due to its thickness and high permeability (respectively maximal 150 m thick and K_h = 6-14 m/day (Lebbe,1999)), a high influx of soluble iron into these basins is ensured.

The significant impact this authigenic sediment can have on the total load can be visually verified by the colour of the water. Figure 4.5 shows the confluence of the Laak with the Grote Nete, where the high iron content of the Laak is clearly visible.

Possibly, other Flemish regions have the potential to contribute ferric authigenic sediment to the total suspended sediment load. However, to obtain insight in this, data on water quality and water fluxes of all Flemish phreatic groundwater systems and surface waters are needed, and this falls outside of the scope of this PhD-research.

Figure 4.5: Confluence of the Laak with the Grote Nete at Geel Zammel

4.3.3 Sediment sources as defined in the sediment fingerprint research

The objective in sediment fingerprinting research is to determine the individual contributions of different sediment sources to the fluvial sediment flux in a sampling location. Within the framework of this research, sources are differentiated based on their spatial provenance as well as on their source type. Walling & Collins (2000) defined the spatial provenance of suspended sediment as either tributary sub-catchments or the different geologies comprising the study area, whereas differentiating the sediment sources based on source types, according to these authors, is based on either surface and subsurface sources or land use and channel banks. This is graphically presented in Figure 4.6.

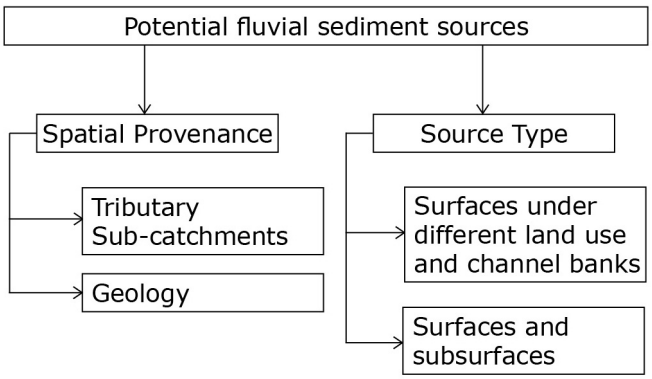

Figure 4.6: Classification of potential sources of fluvial sediment as applied in sediment fingerprinting (adapted from Walling & Collins (2000))

As Walling and Collins are the pioneers of the composite sediment fingerprinting, their methodology and therefore their classification of sources is widely applied in the literature. Successful spatial source discrimination and consequent source apportionment has been reported by amongst others Collins et al. (1996, 1997 a), Evrard et al. (2011) and Navratil et al. (2012), while successful source type discrimination has been published by Peart & Walling (1986, 1988), Collins et al. (1997 b), Collins & Walling (2002, 2004, 2007), Carter et al. (2003), Kraus et al. (2003), Walling (2003), Small et al. (2005), Minella et al. (2008 b), Juracek & Ziegler (2009), Wilkinson et al. (2009), Stutter et al. (2009), Nosrati et al. (2011) and Mukundan et al. (2011). Some research successfully combined both spatial provenance and source type fingerprinting (e.g. Walling et al., 1999; Walling, 2000; Collins et al., 1997 c, 2003 and Walling, 2005). This list is absolutely not exhaustive, but merely illustrates the worldwide use of this technique.

4.4 Conclusions

Within the framework of this PhD, the above-mentioned classification systems will be used as follows:

- When determining the sediment loads at selected sampling locations (as reported in Part III), the only sediment concentration obtainable is the 'measured load'. However, this can potentially be converted into a total suspended load through site-specific (and possibly discharge-specific) correction factors, which will be discussed in Section 5.1.
- The authigenic sediment research, as addressed in Part IV, focuses on one particular sediment source only, i.e. the chemical precipitation of authigenic sediment.
- In Part V, which focuses on the sediment fingerprinting research in the Demer basin, the classification system as mentioned in Section 4.3.3 (and shown in Figure 4.6) is applied. Spatial source apportionment modelling has been executed and is discussed in Chapter 10, while the impact of the different origins of the sediment (as described in Section 4.3.2) on source type and spatial source fingerprinting is addressed in Chapter 11.

Part III

Sediment fluxes

5. Methodology and challenges in the determination of fluvial sediment fluxes

One of the objectives within the framework of this PhD thesis, is to budget the relative contributions of different sources to the total transported suspended sediment load in the Nete and Demer basins. Therefore, it is necessary to determine the total suspended sediment loads passing at selected locations in these basins.

However, depending on both the sampling strategy and the homogeneity of the sediment concentration throughout the cross-section, the determined sediment load can deviate from the actually transported sediment load. Therefore, in Section 5.1, the challenges of measuring sediment fluxes are addressed and solutions for the FHR sediment monitoring locations to deal with temporal and spatial variability of sediment concentrations in the cross-section are presented.

Finally, no matter how good the sampling strategy and the laboratory analyses schemes are defined, Murphy's Law will always intervene, leaving the data-analyst with data gaps. Section 5.2 deals with how to statistically correct for these data gaps, and how to ensure a good estimate of annual sediment fluxes.

5.1 Sampling strategies

A great deal of variation can be expected in the (suspended) sediment concentration at any given location in the stream's cross-section. First of all because sediment sources contributing to the suspended load, are located at different distances from the observation point, but secondly also because the different ways fine and coarse sediments are transported in stream channels.

Only when the water has enough turbulence (for example at small streams with high-flow velocities during high-flow events) will the entire sediment load be homogeneously dispersed throughout the corss-section. In Flanders, this sort of turbulence can be present in more upstream river sections, allowing for point sampling to give a good insight into the transported sediment load, as demonstrated by Van Hoestenberghe (2008) for the upper reaches of the Demer and Bovenschelde basins. However, in the more downstream sections of the Flemish waterways the sediment is not homogeously distributed throughout the cross-section, causing concentration gradients to be present.

These variations in sediment concentration do not only manifest themselves spatially (two points in the cross-section will have different sediment concentrations), but also temporally (the sediment concentration at one point in the cross-section will change through time). This has been reported extensively on an international scale (Walling & Webb, 1981, 1985; Edwards & Glysson, 1999; Horowitz et al., 1989, 1990; Olive & Rieger, 1992; Walling et al., 1992; Horowitz, 1995) Therefore, to estimate the sediment transport at a gauging station for a specific period (be it annual, seasonal or per event), it is necessary to have a good understanding of both the spatial and temporal sediment variation at the specific sampling site.

5.1.1 Taking temporal variability into account

The problem of temporal variability can only be addressed by adjusting the sampling frequency (as has been reported by Edwards & Glysson (1999), Horowitz (1995), Horowitz et al. (2001) and Coynel et al. (2004) amongst others. Depending on which time scale and for what sort of river

system one wishes to report representative sediment loads, sampling frequency needs to be increased. It is self-explanatory that when one is interested in observing the variations in sediment concentration occurring within a single event more frequent sampling is needed then when annual sediment fluxes are to be determined.

Within the framework of this PhD, both annual sediment fluxes need to be determined (for selected locations in the Nete and Demer basin) as well as there is a need to understand sediment dynamics and the processes taking place, at selected locations in these rivers. For the latter, it is necessary to determine sediment fluxes on a shorter time frame, hence more frequent sediment sampling is required.

Typically, the larger the river and the basin it drains, the longer a particular event has to continue for it to have a significant impact on the annual fluxes of suspended sediment and most certainly on the associated trace elements (Ongley, 1992; de Vries & Klavers, 1994). For large river basins (such as the Rhine and the Meuse) weekly sampling should be sufficient for the determination of annual fluxes (de Vries & Klavers, 1994). Horowitz et al. (2001) used daily measurements to estimate suspended sediment fluxes in the rivers of the NASQUAN (National stream Quality Accounting Network) programme. This programme includes rivers such as the Mississippi, Columbia, Colorado and Rio Grande.

The observations of Coynel et al. (2004) confirm that the larger the river basin, the lower the sampling frequency can be to still obtain good estimates of the annual suspended sediment fluxes. Coynel et al. compared the necessary sampling frequency in two very different river basins. The Garonne River is a typical large plain river with a drainage basin of 53,100 km², while the Nivelle River drains a typical Pyrenean mountainous watershed. Of the total drainage area of the latter, only the 165 km² (not-tidally influenced) was monitored in Coynel et al.'s study. This study showed that the Nivelle River needed to be sampled every 7 hours to obtain a lower than 20% deviation of simulated flux estimates from reference fluxes. The Garonne River only needed to be sampled every 3 days to obtain a similar accuracy.

When comparing the size of the drainage basins of the Garonne and the Nivelle with those of the Kleine Nete (590 km² upstream FHR's sediment monitoring location in Grobbendonk), the Mangelbeek (190 km² upstream FHR's sediment monitoring location in Lummen), the Gete (811 km² upstream FHR's sediment monitoring location in Halen) and finally the entire Demer basin (2,163 km² upstream FHR's sediment monitoring location in Aarschot) it is clear they will require more frequent sampling than once every three days. The automatic sampling, as is used at FHR, samples every 7 hours. This should be sufficient to observe the events that have an impact on the annual sediment fluxes.

Continuous sampling might be eliminated by programming an automatic sampler to start sampling (more frequently) when the gauge height surpasses a location specific, pre-determined level. However, sediment peaks do not always coincide with their corresponding discharge peaks. This phenomenon is called hysteresis and it is well-documented in the literature (e.g. Heidel, 1956; Klein, 1984; Williams, 1989; Kleinhans, 2005; Lefrançois et al., 2007; Salant et al., 2008). It can potentially leave the sediment peak (partially) un-sampled if it precedes the discharge peak, or if it lags too far behind its discharge peak.

Williams (1989) was able to divide his observations into five classes (single-valued line, clockwise hysteresis, counter-clockwise hysteresis, single valued line plus loop and figure eight). This classification, or a simplified variant using only the first three classes, has since been used by many authors (Klein, 1984; Lenzi & Marchi, 2000; Lefrançois et al., 2007, Salant et al., 2008; Rodriguez-

Blanco et al., 2010 and others). In Table 5.1 the observations of temporal occurrence of the SSC and Q peaks are listed for each of the hysteresis classes as well as the interpretations of these river system responses as reported by various authors. Figure 5.1 illustrates these phenomena with data taken from the Aarschot sampling location (for its exact location see Figure 2.1).

Table 5.1: Overview of observations of relative temporal occurrence of the suspended sediment (SSC) peaks and discharge (Q) peaks per hysteresis class as well as the interpretations of these river system responses as reported by various authors

	Observation	Interpretation
Class I Single-valued line	- Sediment and discharge peaks arrive simultaneously and the SSC/Q ratio of the rising and the descending limb remains constant (Williams, 1989)	- Unrestricted mobilisation and transport of particles during the flood for the concerned range of discharge (Wood, 1977; Jansson, 2002) - Sources at low discharge can be fine deposited sediment (Hudson, 2003) or pre-destructed bank materials (Lenzi & Marchi, 2000) - Sources at high discharge can be coarser deposited sediment and/or bank and channel hydrological erosion (Lefrançois et al., 2007) - When discharge is linked to surface runoff sources can also be more remote (Lefrançois et al., 2007)
Class II Clockwise loop	- Sediment peak arrives prior to discharge peak (Williams, 1989) - Sediment and discharge peaks arrive simultaneously but the skewness of the sediment peak is smaller than that of the discharge peak (Williams, 1989)	- Mobilisation of particles whose availability is restricted during the flood for the concerned range of discharge (Williams, 1989) - Depletion of available sediment before the water discharge has peaked (Arnborg et al., 1967; Walling, 1974; Wood, 1977; VanSickle & Beschta, 1983; Salant at al., 2008) - Formation of an armoured layer prior to the occurrence of the discharge peak (e.g. Arnborg et al., 1967) - Sources of sediment are removal of sediment deposited in the channel with a decreasing availability during the event - (e.g. Lenzi & Marchi, 2000; Steegen et al., 2000; Jansson, 2002)
Class III Counter-clockwise loop	- Sediment peak arrives later than the discharge peak (Williams, 1989) - Sediment and discharge peaks arrive simultaneously but the skewness of the sediment peak is smaller than that of the discharge peak (Williams, 1989)	- Sediment is transported at mean flow velocity which is generally lower than the velocity of the flood wave (Heidel, 1956; Klein, 1984) - High soil erodibility in conjunction with prolonged erosion during the flood (Kung & Chiang, 1977) - More distant sediment sources such as hill slope soil erosion or the upstream channel (Brasington & Richards, 2000; Lenzi & Marchi, 2000; Goodwin et al., 2003; Orwin & Smart, 2004) - Sediments can also come from processes with slow dynamics (slower than the discharge rise), e.g. bank collapse may happen when bank material is sufficiently saturated (Lefrançois et al., 2007)
Class IV Single-valued line plus loop	- Sediment/discharge relation for a single hydrological event can plot as a single-valued relation in one range of discharges and a sequential loop in the adjoining range of discharges. (Williams, 1989)	- Combination of Class I and II or III - Possible causes are similar to the ones described above
Class V Figure eight	- Sediment/discharge ratios are larger for one range of Q on the rising limb of the hydrograph and smaller for another range of Q on that limb, compared to the same values of Q on the falling limb (Williams, 1989)	- Combination of Classes II and II - Possible causes are similar to the ones described above

This phenomenon will be addressed in more detail and illustrated with data from the Kleine Nete (Grobbendonk) and Demer (Aarschot) measurement locations in Chapters 6 and 7.

Some events can cause such a big change in the behaviour of a river system, that a specific discharge condition occurring after this event will trigger a completely different sediment response than similar discharge conditions would have triggered prior to this event. In the Mississippi for instance the sediment supply was depleted in such a way after a major rainfall event, that the sedimentary response of the river was significantly lowered for the subsequent years (Horowitz, 2003, 2006). This would ensure the necessity to develop at least two separate SSC-Q rating curves, one prior of the event and one that can be applied after the event.

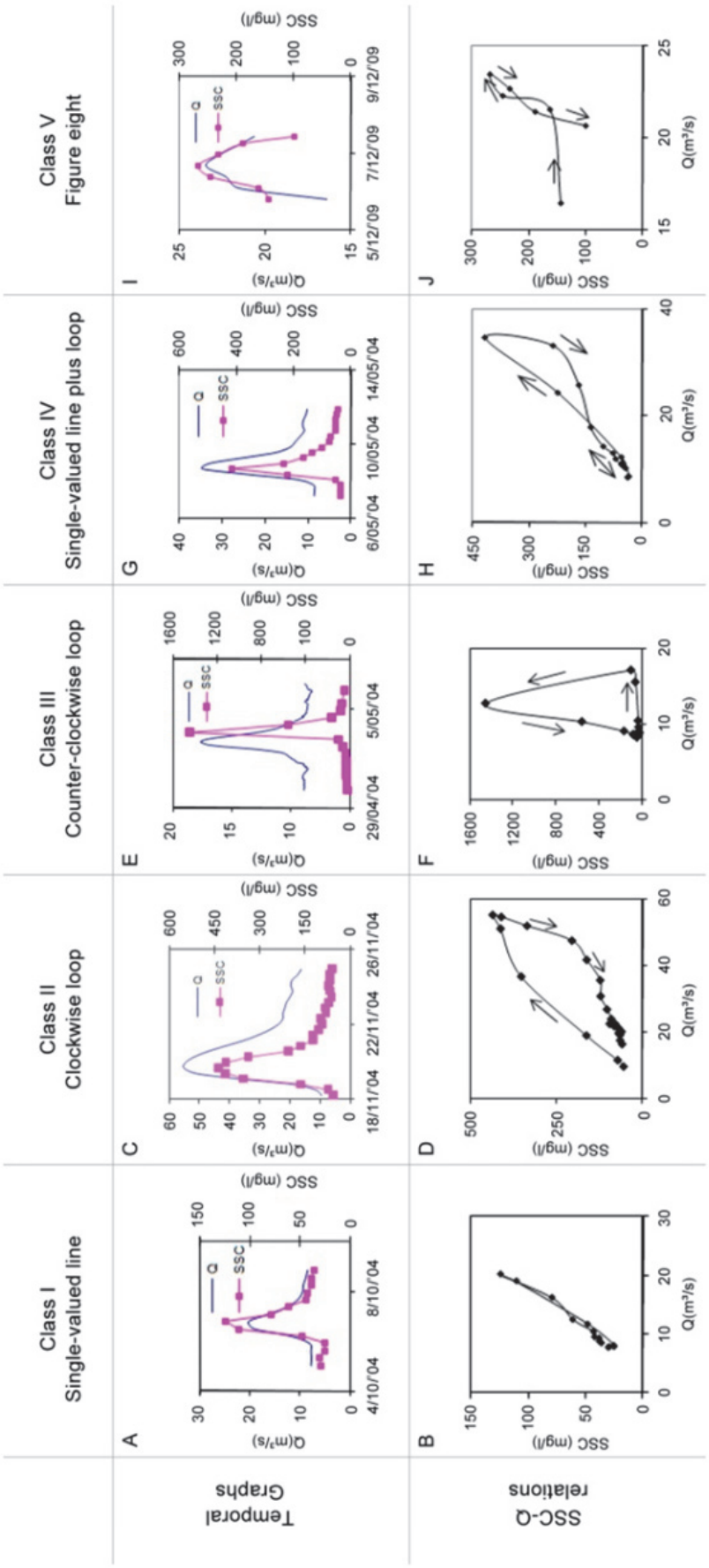

Figure 5.1: Illustrating the five hysteresis classes: temporal graphs and SSC-Q relations with data from the Aarschot sediment monitoring location on the Demer

For the above-mentioned reasons, all of FHR's continuous sediment monitoring locations have been equipped with automatic pumping samplers (see Section 2.1.1.2) for frequent sampling. Standard, the samplers are programmed to sample every seven hours, which is sufficient to determine annual sediment loads. However, for covering the temporal variability during individual events this sampling frequency is insufficient. Therefore, within the framework of this PhD research the sampling interval has occasionally been increased to one sample every hour.

The temporal resolution of sediment data can also be increased through rating curves based on a proxy (such as discharge, turbidity, conductivity etc.) or a combination of proxies. This approach is discussed below in Section 5.2 and is consequently applied to selected locations in Chapter 6. To obtain proxies, multi-parameter probes have been installed at specific sediment monitoring locations. These probes register a variety of parameters amongst which turbidity, as has been discussed in Section 2.1.2.

Through these site-specific rating curves suspended sediment concentrations can be estimated for the smallest time resolution the proxy data is available for. However, this only provides sediment concentration information on a specific point in the cross-section, so the issue of cross-sectional non-homogeneity remains .

5.1.2 Taking cross-sectional variability into account

Sampling consistently at the same point in a cross-section is very likely to introduce bias in the calculation of the sediment load. In general, the resulting time series is unlikely to give a representative estimate of the average sediment concentration present throughout the cross-section.

This is illustrated by comparing three different types of grab samples obtained at the Eppegem sediment monitoring location, located on the river Zenne. This location has been sampled by FHR both with a weighted-bottle sampler as well as with a bucket sampler, while VMM applied only bucket sampling as a means of determining SSC (amongst other parameters). Figure 5.2 shows the results of these three different sampling techniques, along with the measured discharge for the period 1999-2009.

Visually, two trends can clearly be observed. On the one hand, from 2007 onwards, the sediment concentrations dropped significantly, regardless of which sampling technique was used (T-test, Assuming Unequal Variances; $\alpha < 0.05$; see Table 5.2). This change in transported sediment concentrations can be attributed to the activation of the Brussels North sewage treatment facility upwards the sampling location.

On the other hand, differences between the different sampling techniques can also be observed in Figure 5.2. FHR's weighted-bottle samples are on average higher in SSC content than VMM's bucket samples, which are in turn higher in SSC than FHR's bucket samples. This trend is observed both before and after the activation of the sewage treatment facility. The overall effect of sampling methods is tested using one-way ANOVA, followed by the Tukey's Honest Significant Difference post-hoc test to compare the means of the individual methods with each other. Table 5.3 shows the test results for the 2000-2006 time span, while Table 5.4 shows these for the period 2007-2009. Overall, sampling technique had a significantly effect both before and after 2007. However, the difference between bucket samples obtained by VMM and obtained by FHR show no significance difference after 2007.

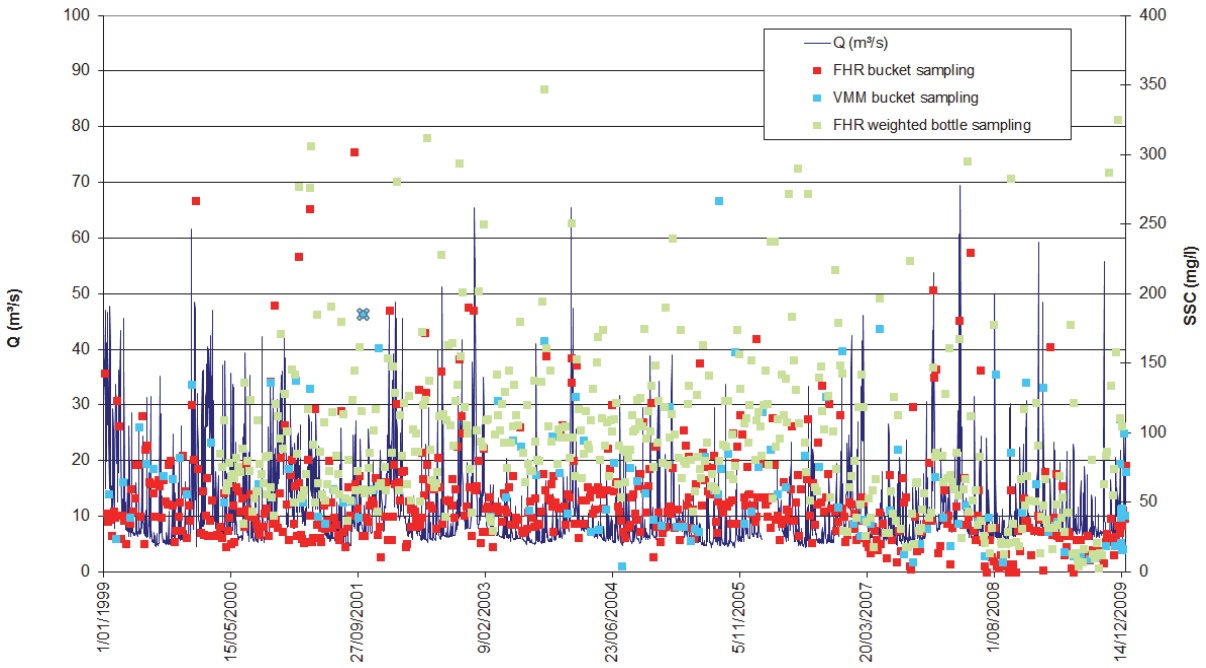

Figure 5.2: Discharge (m³/s) and SSC obtained through three different types of grab sampling (mg/l) as observed at the Eppegem sediment monitoring location on the river Zenne; (data obtained from FHR and VMM)

Table 5.2: T-test, Assuming Unequal Variances, on SSC-values after 1-1-2007 for three different grab sampling methods (weighted-bottle sampling and bucket sampling by FHR and bucket sampling by VMM) at the sediment monitoring station of Eppegem on the river Zenne, for the periods 2000-2006 and 2007-2009.

	FHR weighted-bottle samples		FHR bucket samples		VMM bucket samples	
	2000-2006	2007-2009	2000-2006	2007-2009	2000-2006	2007-2009
Mean	114.50	66.72	57.05	36.55	86.39	47.01
Variance	9329.58	3653.81	1338.44	1358.06	8170.93	1488.52
Observations	329	129	381	145	67	50
Hypothesized Mean Difference	0		0		0	
Df	368		259		95	
t Stat	6.35		5.71		3.20	
P(T<=t) two-sided	<0.001		<0.001		0.0019	
t Critical two-sided	1.97		1.97		1.99	

Table 5.3: Results of the One-way ANOVA (a) and Tukey's Honest Significant Difference post-hoc test (b) on samples obtained using three different sampling techniques (FHR weighted-bottle samples, FHR buchet samples and VMM buchet samples), at Eppegem sampling location from 2000 to 2006.

a)

		F	df	P
Sampling method	AOV	54.94	2 774	<0.001

b)

	Difference of means	95%CI	p
FHR bucket samples-FHR weighted-bottle samples	-57.5	-70.3/-44.6	<0.001
VMM bucket samples-FHR weighted-bucket samples	-28.1	-51.0/-5.2	0.011
VMM bucket samples-FHR bucket samples	29.3	6.7/52.0	0.0069

Table 5.4: Results of the One-way ANOVA (a) and Tukey's Honest Significant Difference post-hoc test (b) on samples obtained using three different sampling techniques (FHR weighted-bottle samples, FHR buchet samples and VMM buchet samples), at Eppegem sampling location from 2007 to 2009.

a)

		F	df	P
Sampling method	AOV	13.68	2 321	<0.001

b)

	Difference of means	95%CI	p
FHR bucket samples-FHR weighted-bottle samples	-30.2	-43.8/-16.6	<0.001
VMM bucket samples-FHR weighted bucket samples	-19.7	-38.5/-0.9	0.037
VMM bucket samples-FHR bucket samples	10.5	-8.0/28.9	0.38

That a difference is observed between the two types of bucket sampling in the first place is remarkable, and shows that next to the sampling equipment, other factors influence the measurements. These include the procedure for subsampling from the bucket and the exact location in the cross-section from which the sample is taken.

The spatial variability, as discussed above, can be addressed by collecting depth- and width integrated samples covering a wide range of discharge conditions (Edwards & Glysson, 1999; Wilde, 2006). The different sampling methods to obtain depth- and width integrated samples (i.e. the Equal Width Increment (EWI) method and the Equal Discharge Increment (EDI) method) in the framework of sediment measurements at FHR was also discussed in Vanlierde (2003).

As already discussed in Section 2.1.1.3, at the FHR sampling locations EWI-method sampling was selected as a means of correcting the spatial variability and the methodology was adjusted to be applicable on rivers with active navigation. The samplings have been executed from 2004 onwards, albeit infrequently.

Obtaining a complete data set, that covers the full range of discharges, has proven difficult, partly because the presence of hysteresis complicates the successful timing of the sampling campaigns.

Correctly predicting the arrival time of the discharge peak at a specific location is far easier than predicting the arrival time of the sediment peak. Consequently, no complete cross-sectional correction coefficients have been established, for the sampling locations in the Nete and Demer basins. Therefore, all subsequent budgeting has been executed on the sediment concentrations determined at the sampling points in the river sections and the results should be interpreted as such.

5.2 Statistical approach to obtain estimates for missing values

When the data set contains significant gaps (due to technical difficulties on site or in the laboratory), these gaps need to be filled in by estimated sediment concentrations in order to be able to calculate sediment fluxes. A method often applied to predict sediment concentrations is the use of rating curves (based on a variety of parameters). This methodology is described below.

5.2.1 Linear Regression – model development

Hydrological and sedimentological parameters such as discharge, turbidity, sediment concentrations, pH, conductivity, etc. are often related to one another, and in many cases, linear regression models can be used to describe the relation. Hence, regression analysis can be used to develop relations between discrete laboratory analyses of manually collected water samples

(response variables) and continuously measured hydrological data (explanatory variables). This approach is widely recognized and used in various scientific publications (Walling, 1977 a, 1977 b; Walling & Webb, 1988; Fenn et al., 1985; Crawford, 1991; Asselman, 2000; Christensen et al., 2000, 2001; Lenzi & Marchi, 2000; Lenzi et al., 2003; Horowitz et al., 2001; Horowitz, 2003; Uhrich & Bragg, 2003; Lietz & Debiak, 2005; Rasmussen et al., 2008) to name but a few.

In this study, the methodology for developing regression models as suggested by Rasmussen et al. (2010*)* is applied. In Chapter 6 this is illustrated by a detailed study on the data sets of the Grobbendonk measurement station, addressing some of the site-specific problems as well as problems associated with the monitoring scheme. Additionally, sediment flux calculations for the Aarschot, Halen and Lummen measurement stations have also been calculated and reported in Chapter 6, so they can be applied in Parts IV and V.

There are many explanatory variables that can be used in a regression model, including: continuous real-time measurements of conductance, pH, water temperature, turbidity, dissolved oxygen, redox potential and discharge. Hence, it is not always easy to determine which of these are to be included in a regression model. This makes the selection of an appropriate model a somewhat subjective process that relies on the best professional judgement of the modeller.

Only if there is some physical basis or explanation for their inclusion, a variable should be allowed into the model; furthermore, the addition of a variable to a model must make a significant improvement in model performance.

Scatter plots and correlation coefficients of explanatory variables (such as discharge and turbidity) to response variables (suspended sediment concentration) are a simple way to identify which of the variables are possible candidates for prediction, and which data transformation might improve the relation between explanatory and response variables. Generally, the closer the correlation coefficient is to 1 (perfect positive correlation), the stronger the association between variables.

A regression model can be created that relates the explanatory variables to the response variable (in this case SSC). The regression model will in that case take the shape of Equation 5.1. Optimal values for β coefficients can be calculated using n simultaneous measurements of both the explanatory and response variables. The least squares method is then used to calculate optimal coefficient values.

$$SSC_i = \beta_0 + \beta_1 V_{1,i} + \beta_2 V_{2,i} + \beta_j V_{j,i} + \varepsilon_i \qquad \text{Eq. 5.1}$$

in which:
- SSC_i is the response variable, the suspended sediment concentration
- i is 1, 2, ...n measurements of variables,
- j is the number of explanatory variables entered in the regression
- V_1, V_2, V_j are the measured variables
- $\beta_0, \beta_1, \beta_2, \beta_j$ are constant coefficients calculated by regression analysis
- ε_i is the random error of the regression, which has a mean value of zero

When the relationship between two parameters on a scatter plot shows curvature, it is common to log transform the explanatory and response variables of hydrologic data in order to reduce this curvature and simplify the analysis (Ott, 1993). Log transformation can help meet linear regression assumptions that residuals are normally distributed and of constant variance.

Consequently, the regression model will take the shape of Equation 5.2.

$$\log_{10} SSC_i = \beta_0 + \beta_1 \log_{10} V_{1,i} + \beta_2 \log_{10} V_{2,i} + \beta_j \log_{10} V_{j,i} \quad \text{Eq. 5.2}$$

in which: - SSC_i are the computed values of the response variable, i.e. suspended sediment concentration

Both Equations 5.1 and 5.2 make mention of multiple explanatory variables. Stepwise-regression analysis is one possible way to select explanatory variables in an objective manner. Pearson's correlation coefficient is used to evaluate which variables can be used together in the model. If the correlation between two explanatory variables is too strong, at most one of these variables can be included in the model. To add value to a model, adding a variable should substantially increase the R^2, decrease the Root Mean Square Error (RMSE) and minimize the PRESS-statistic while decreasing the residual standard deviation (Helsel & Hirsch, 2002). This will be further addressed in Section 5.2.3.

When no usable interrelation can be found between SSC and another parameter (such as Q) for a particular calibration set for a particular site (based on a low R^2), then the mean suspended sediment concentration should be used to obtain at least an estimation of the instantaneous daily fluxes (Horowitz et al., 2001).

5.2.2 Bias Correction Factor

Log_{10} transformation of the response variable (SSC), however, has a consequence that must be considered when computing suspended sediment concentrations. The computed values must be transformed back to the original units, and this step introduces a (typically negative) bias in the computed SSC-values (Miller, 1951; Walling, 1977 b; Koch & Smillie, 1986) unless the data are perfectly and positively correlated, which is rarely the case. The bias arises because regression predicts the mean of a normal distribution in log units, and the retransformed values result in the geometric mean in linear space, which is almost always smaller than the arithmetic mean.

To correct for retransformation bias, some authors (Duan, 1983; Helsel & Hirsch, 2002; Rasmussen et al., 2008, 2010 amongst others), suggest multiplying the retransformed SSC by a bias correction factor (see Equation 5.3).

$$SSC_i = 10 \cdot \left[\beta_0 + \beta_1 \log_{10} V_{1,i} + \beta_2 \log_{10} V_{2,i} + \beta_j \log_{10} V_{j,i}\right] \cdot BCF \quad \text{Eq. 5.3}$$

in which: BCF is the bias correction factor

Duan (1983) introduced a nonparametric bias-correction factor, which is called the "smearing" estimator. The smearing factor is calculated from the mean of the residual values (Equation 5.4)

$$BCF = \frac{\sum_{i=1}^{n} 10^{\log SSC_i - \log \hat{SSC}_i}}{n} \quad \text{Eq. 5.4}$$

in which: - SSC_i is the i^{th} measured suspended sediment concentration

- $\hat{SSC}_i$ is the i^{th} regression-computed suspended sediment concentration
- n is the number of measured suspended sediment concentrations in the model-calibration data set

However, other studies have indicated that applying such a correction factor does not always improve the predictive power of the model (Walling & Webb, 1988), which lead Horowitz et al. (2001) to only apply the smearing factor when it reduced the difference between the predicted and the actual flux estimates.

5.2.3 Linear Regression: model evaluation

The linear regression models are evaluated both visually and statistically in order to compare their predictive value, following basically the approach outlined in Helsel & Hirsch (2002). First, the data is visually examined by plotting the respons variable in function of the different predictor variables. In case non-linear trends can be observed, an appropriate transformation (e.g. the log transformation) is applied. Next to that, the different plots together with the correlation statistics form the basis for the selection of possible predictor variables in the model.

After building the model and estimating the different coefficients, these coefficients are examined in sign and magnitude, in order to assure they have scientifically possible values. Next, a T-test is applied in order to test whether the coefficients differ significantly from zero. When so, the related predictor variable is assumed to contribute significantly to the prediction of the SSC-values.

The validity of the models is evaluated by checking for any violation of the assumptions made by using the linear regression approach. More specifically, residual plots are used to control whether the assumptions of homoscedasticity, linearity and independence of the prediction data are violated. A histogram is constructed to check whether the residuals are normally distributed. However, mild violations of the assumptions are unlikely to influence the predictive power of the model, so models are not excluded based only on these checks.

To test the predictive power of the models the "PRESS" statistic, or the "PRediction Error Sum of Squares" is calculated (see Equation 5.5).

$$\text{PRESS} = \sum_{i=1}^{n} e_{(i)}^{\ 2} \qquad \text{Eq. 5.5}$$

in which: n = number of observations

$e_{(i)}$ = Prediction residual $= y_i - \hat{y}_{(i)}$

in which: $\hat{y}_{(i)}$ is the regression estimate of y_i based on a regression equation computed leaving out the i^{th} observation. The (i) symbolizes that the i^{th} observation is left out of the computation.

PRESS is a validation-type estimator of error. Instead of splitting the data set in half, one-half to develop the equation and the second to validate it, PRESS uses n-1 observations to develop the equation, then estimates the value of the one left out. It then changes the observation left out, and repeats the process for each observation. The prediction errors are squared and summed. Minimising PRESS means that the equation produces the least error when making new predictions. In multiple regression it is a very useful estimate of the quality of possible regression models.

5.3 Conclusion

At the sediment monitoring locations of FHR, automatic samplers are installed and programmed to sample every seven hours. This sampling frequency is sufficient to calculate annual sediment fluxes. However, when gaps are present in the sediment concentration data, these need to be filled

in using linear regression rating curves and/or multivariate rating curves, using a variety of hydrological and/or physical parameters, which should be site-specifically selected.

Furthermore, when sediment fluxes are required for shorter time periods (such as per event) these rating curves are required.

The sediment concentrations obtained from automatic sampling and/or grab sampling should still be corrected to be representative of the concentrations present in the cross-section. Insufficient sampling was executed at FHR to this date to be able to execute this correction for the calculations.

6. Calculating suspended sediment fluxes at selected locations

In the framework of this PhD thesis, daily average SSCs, and derived suspended sediment flux (SSF) data from Grobbendonk measurement station are required for application in MARS modelling (addressed in Part IV), while similar information was needed from the Aarschot, Halen and Lummen locations for the sediment fingerprinting research (as is addressed in Part V).

Even though these locations were equipped with automatic samplers (as explained in Section 2. 1.1.2) for the duration of the respective periods of interest, some daily average SSC data are not readily available due to mechanical failure on site, laboratory error or other unforeseen events.

Therefore, to obtain predictions of daily average sediment concentration values for days where no actual SSC-data were available, linear regression models were created based on the methodology as explained in Section 5.2.

In the first section of this chapter this methodology is applied to the Grobbendonk data set and multiple models are developed and evaluated, allowing for detailed investigation of hysteresis and seasonal variability as well as aiding in the data validation of physical parameters such as turbidity and conductivity.

In the second section of this chapter the overall conclusions drawn from this exercise are applied to the calculation of the SSCs and SSFes on the other locations of interest.

Finally some conclusions about the determined sediment fluxes are drawn in the third section.

6.1 Determining sediment concentrations and fluxes at the Grobbendonk measurement location

The Grobbendonk measurement location on the Kleine Nete has had an automatic sampling device installed from February 1999 onwards. The device was removed for almost over a year (from February 2000 up until July 2002) after which it was reinstalled and it has never left the site since. Hence, sediment concentration data is available for the better part of the period of interest (1999-2009).

As a multi-parameter probe (YSI) has only been installed at Grobbendonk measurement station from 2005 onwards, at least two sets of regression models need to be constructed, if the entire period of interest wants to be covered. The first one, covering the entire period of interest (1999-2009), is fed only by discharge and discharge-derived parameters (such as baseflow, interflow and discharge values of the previous and subsequent day) which are available as daily averages for every location for the entire period of interest. The second set of regression models is based on as many explanatory variables as are available (including validated YSI parameters) and which are only available from 2005 onwards.

To compare the effectiveness of the different models, statistical tests have been executed and graphs have been plotted, all of which have been included in Addendum B.

6.1.1 Prediction of SSC based on mean observed SSC-value

As stated in Section 5.2.1, when no usable interrelation can be found between SSC and another parameter for a particular calibration set at a particular sampling site, then the mean suspended sediment concentration should be used to obtain at least an estimation of the instantaneous daily fluxes (Horowitz et al., 2001). Therefore, the RMSE and PRESS statistics using this approach have been calculated for the period of 1999-2009 and presented in Table 6.1, as model nr 1. This table gives a résumé of the most important test-statistics of all predictive models that are discussed in this chapter. The test statistics of this $\overline{SSC}$-model will be used to compare the predictive power of the other models. The latter should perform significantly better as to be used in favour of this simple model. The RMSE of the $\overline{SSC}$-model is quite elevated (26.40 mg/l) which is higher than the average observed SSC (25.18 mg/l), which leaves room for improvement by other models.

Table 6.1: Overview of main test parameters for all discharge and discharge-derived parameter driven models for Grobbendonk measurement station (1999-2009)

model	Model	R^2	RMSE (mg/l)	PRESS	RMSE/mean SSC
1	SSC = SSC(mean)	/	26.40	1863074	104.9
Models based on discharge					
2	SSC = f(Q)	0.49	18.84	948757	74.8
3	SSCwinter = f(Q)	0.41	18.41	908587	73.1
	SSCsummer = f(Q)	0.30			
4	log SSC = f(logQ) without BCF	0.54	19.23	985623	76.4
5	log SSC = f(logQ) with BCF		19.04	963635	75.6
6	log SSCwinter = f(logQ) without BCF	0.58	18.83	946871	74.8
	log SSCsummer = f(logQ) without BCF	0.26			
7	log SSCwinter = f(logQ) with BCF	0.58	19.02	961856	75.5
	log SSCsummer = f(logQ) with BCF	0.26			
Models based on discharge and discharge-derived parameters					
8	SSC = f(Q, QIFp, QOFn, QOF, QBFn, Qn, Qp)	0.54	17.85	868907	70.9
9	SSCwinter = f(Q, Qp, QOFn, QIFp)	0.46	17.58	840068	69.8
	SSCsummer = f(Q, QIFp)	0.32			
10	log SSC = f(logQ, logQIFp, logQOFn, logQBFn, logQIF) without BCF	0.56	18.86	953149	74.9
11	log SSC = f(logQ, logQIFp, logQOFn, logQBFn, logQIF) with BCF		19.00	968757	75.4
12	log SSCwinter = f(logQ, logQIFp, logQn) without BCF	0.62	17.93	862120	71.2
	log SSCsummer = f(logQOF, logQBFn) without BCF	0.28			
13	log SSCwinter = f(logQ, logQIFp, logQn) with BCF	0.62	17.98	860186	71.4
	log SSCsummer = f(logQOF, logQBFn) with BCF	0.28			
Models based on discharge, discharge-derived parameters and physical parameters					
14	SSC = f(Qn, QIF, Cond, QIFn, Turb)	0.69	12.95	69003	51.4
15	SSCwinter = f(QIF, Cond, QIFp)	0.57	11.94	54662	47.4
	SSCsummer = f(Qn, Turb, QIFp, QOFp)	0.86			
16	logSSC = f(logQn, logTurb, logQIF', logCond, logQBFn') without BCF	0.81	13.63	68147	54.1
17	logSSC = f(logQn, logTurb, logQIF', logCond, logQBFn') with BCF		13.73	70301	54.5
18	logSSCwinter without BCF = f(log Qn, QIFn, Turb, QBFn)	0.75	15.47	58901	61.4
	logSSCsummer = f(Turb, Qn)	0.68			
19	logSSCwinter with BCF = f(log Qn, QIFn, Turb, QBFn)	0.75	15.36	59816	61.0
	logSSCsummer = f(Turb, Qn)	0.68			

6.1.2 Regression models based on discharge

As discussed in Chapter 5, stream flow (or discharge) is widely recognized as a potential explanatory variable for suspended sediment concentration. If a simple linear regression between SSC and Q yields fairly accurate predictions of SSC-values, researchers often opt to use this. After all, discharge is a reasonably easy measurable parameter and it is readily available on most sediment monitoring sites.

Figure 6.1 shows the scatter plot of SSC data, which was obtained from plotting automatically 7 hourly-collected pump samples at the Grobbendonk measurement station, against the corresponding 15 minute-averaged discharge data (Q) for the period 1999-2009.

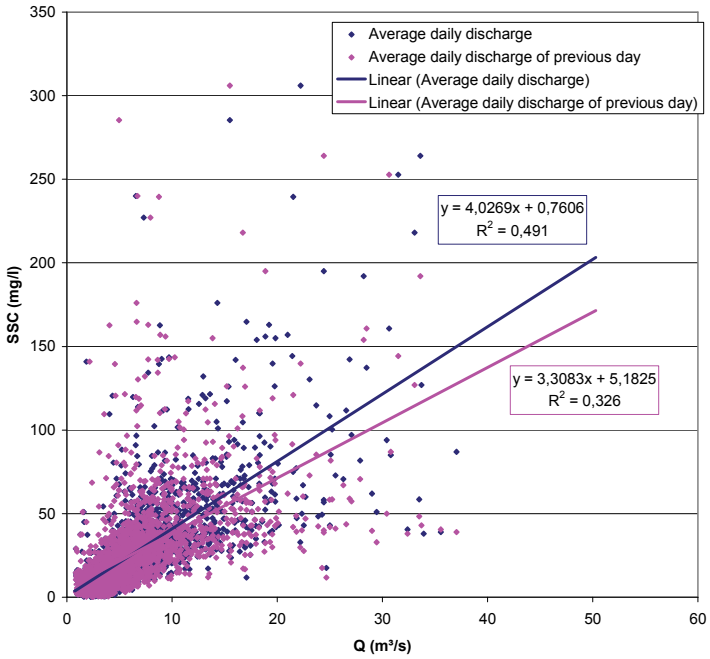

Figure 6.1: Scatter plots of SSC versus Q data obtained from Grobbendonk measurement station (from 1999-2009), plotting both instantaneous samples as well as calculated daily averages

Figure 6.1 also shows the scatter plot of the daily averaged values of both parameters. It is clear that both sets of parameters have a positive correlation, although the variability observed in SSC-values can only be partly described by Q (as is demonstrated by the relatively low R^2-values). Also, no significant differences could be observed between the SSC/Q ratios obtained from instantaneous values and the one obtained from daily averages (see Table 6.2). Therefore, daily average values will be used in the further analysis of this chapter, as not always instantaneous values are present for all potential explanatory variables, and daily average SSC-values are necessary input values for the modelling of authigenic sediment contributions as will be addressed in Part IV.

Table 6.2: T-test; Two sample assuming equal variance, between the ratios of daily values of SSC and Q on the one hand and ratios of instantaneous SSC- and Q-values on the other hand

	ratio SSC/Q_{day}	ratio SSC/Q_{15}
Mean	4.17	4.14
Variance	9.70	9.78
Observations	2659	7717
Pooled Variance	9.76	
Hypothesized Mean Difference	0	
df	10374	
t Stat	0.452	
P(T<=t) two-sided	0.651	
t Critical two-sided	1.960	

6.1.2.1 Constructing and evaluating linear regression models of the form: SSC = f(Q)

The regression model (model nr 2) predicting SSC-values based on daily average Q-values, as shown in Figure 6.1, follows Equation 5.1 and took the shape of:

$$SSC_i = 4.027 \cdot Q_i + 0.761 + \varepsilon_i \qquad \text{Eq. 6.1}$$

Using the suggestions by Helsel & Hirsch (2002) for model evaluation as cited in Section 5.2, the regression model stated in Equation 6.1 (model nr 2) performs relatively poorly. First of all, the heteroscedasticity seems to indicate that the data needs to be transformed. Nonetheless, the model was produced and steps 2 to 8 from the model evaluation were executed. These tests show that the R^2 value is relatively low (0.49). Furthermore, the residuals, even though fairly normally distributed, show heteroscedasticity when plotted in function of predicted values. Nonetheless, RMSE and PRESS-values were calculated and they are presented as model nr 2 in Table 6.1, where they can be compared to their respective counterpart values of the $S\bar{S}C$ -model.

Even though the RMSE of linear model nr 2 dropped down to 18.85 mg/l, it was still over 75% of the mean observed SSC-value, which is still quite elevated. Nevertheless, a significant drop in PRESS statistics can be observed: using the regression model reduces the PRESS statistic to half of the PRESS statistic obtained by the $S\bar{S}C$-model. As it is the purpose of this study to make predictions, the PRESS statistic is the deciding parameter.

Next, the long term and/or seasonal variability within the model should be checked by plotting the residuals versus time. Figures 6.2 and 6.3 show the residuals being plotted against respectively the years and months they were observed in. Using boxplots allows for comparison of the median (solid line), interquartile range (box), range of non-outlier values (whiskers) and the outliers (dots and stars) between the different groups of values. The former figure shows no distinct trends in between the different years, giving no reason to make separate rating curves for individual years.

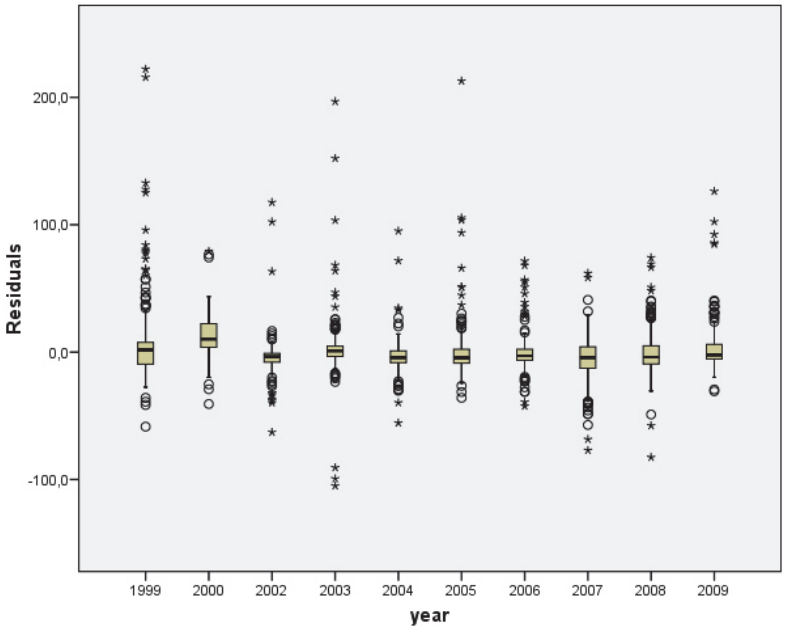

Figure 6.2: Residuals versus time (in years) of model nr 2 for data from Grobbendonk measurement station (1999-2009)

From Figure 6.3 it is clear that a greater variance can be observed during the winter months, while the means of the residuals do seem to remain fluctuating around zero for every month of the year.

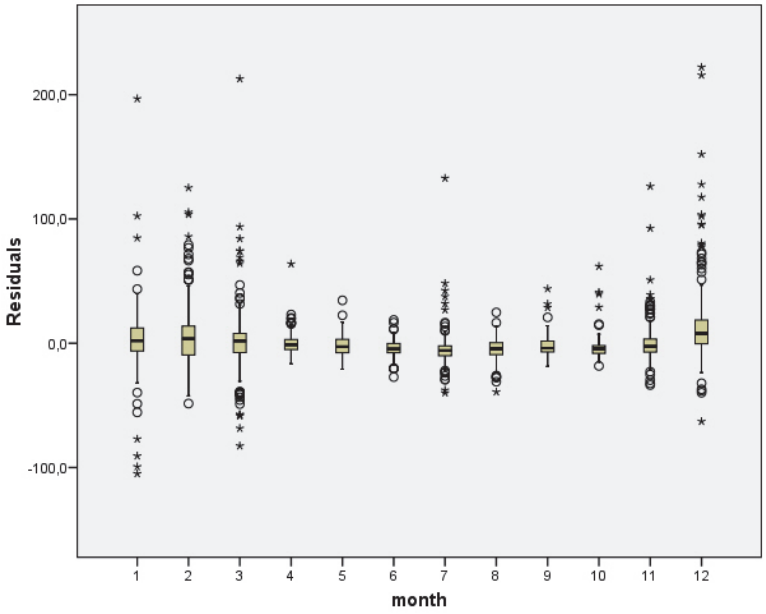

Figure 6.3: Residuals versus time (in months) of model nr 2 for data from Grobbendonk measurement station (1999-2009)

This is visualized in Figure 6.4, which shows that at the Grobbendonk location the summer (April untill September) and winter (October untill March) data mostly overlap, but that the summer is not characterized by as many high discharges as the winter months.

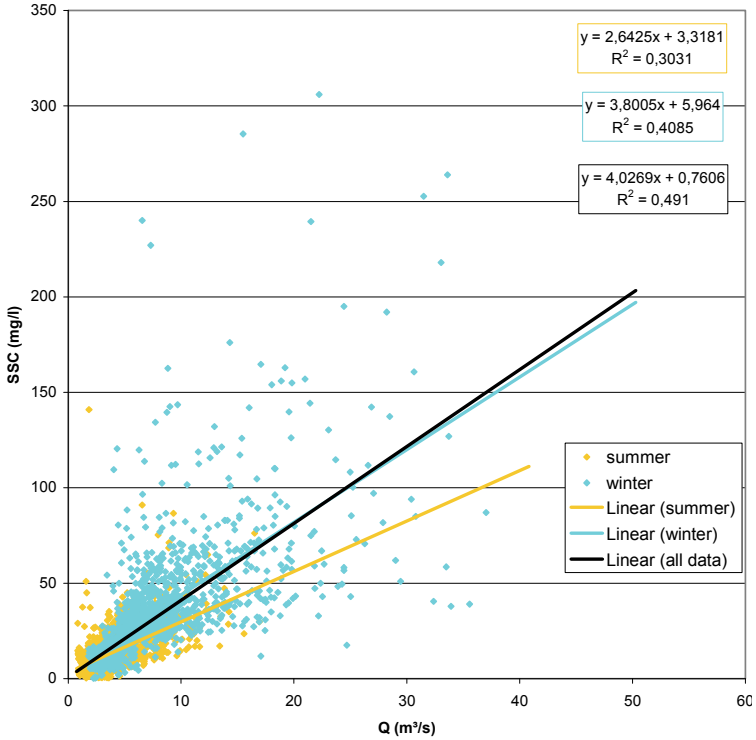

Figure 6.4: Residuals versus time (in months) of model nr 2 for data from Grobbendonk measurement station (1999-2009)

Hence, a new model was developed, consisting of two separate rating curves: one for winter and one for summer data. These respectively took the shape of:

$$SSC_{i,winter} = 3.800 \cdot Q_i + 5.964 + \varepsilon_i \quad \text{Eq. 6.2}$$

$$SSC_{i,summer} = 2.643 \cdot Q_i + 3.318 + \varepsilon_i \quad \text{Eq. 6.3}$$

When evaluating this model (model nr 3) by looking at its RMSE and PRESS statistics, as presented in Table 6.1, it is clear that it performs similarly to model nr 2 (Equation 6.1) that does not discriminate between the seasons.

6.1.2.1.1 Understanding the reason behind the variance

If long term or seasonal variability cannot adequately explain the variance observed between SSC and Q, often the phenomenon called hysteresis, which has been extensively addressed in Section 5.1.1, is the main instigator. Figure 6.5 shows the time series of sediment and discharge data from the Grobbendonk measurement station for a period of ten days, in which three subsequent events took place. It can clearly be seen that in event 1 the sediment concentration and discharge peak at the same moment, but that the sediment concentration descends more rapidly than its discharge counterpart.

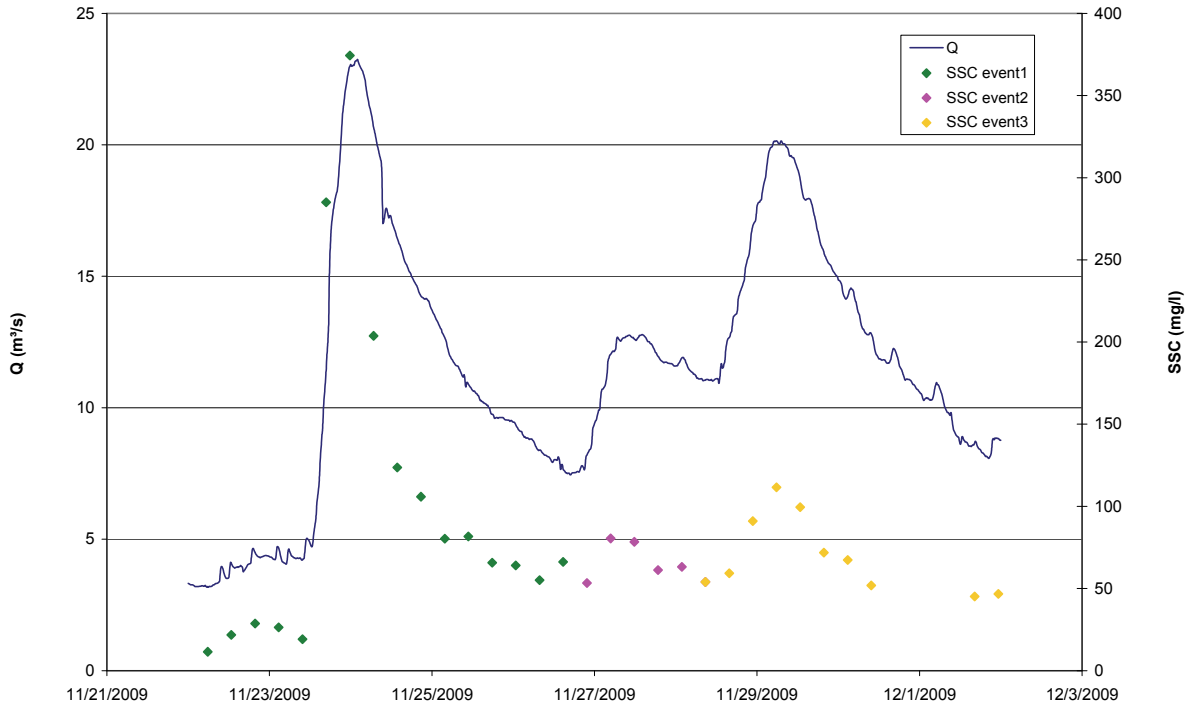

Figure 6.5: SSC and Q data from Grobbendonk measurement station from 22 November until 2 December 2009 in which three separate events are indicated

Therefore, when a scatter plot is created from Q and SSC data, (see Figure 6.6), this first event clearly describes a very large clockwise hysteresis loop. The second event on the other hand forms only a small clockwise hysteresis loop that subsequently leads into the third event which plots as a single line. This trend can be explained by sediment deprivation of the river: most of the sediment is mobilised and transported during the rising limb of the first event, causing a much lower sediment concentration during the descending limb of the first event. The second event repeats this on a smaller scale (with a smaller loop, with lower sediment concentrations) to end with the third event, where the system has found a sort of balance (SSC-values remain constant on the rising and descending limb). However, the SSC-concentrations are much lower in the second and

third event, than those observed during the first event during similar discharge conditions, indicating that in comparison to before event 1, the system is sediment-depleted.

In certain river systems the hysteresis effect could possibly be diminished by using daily average values instead of instantaneous values as this would reduce the variance caused by the time shift

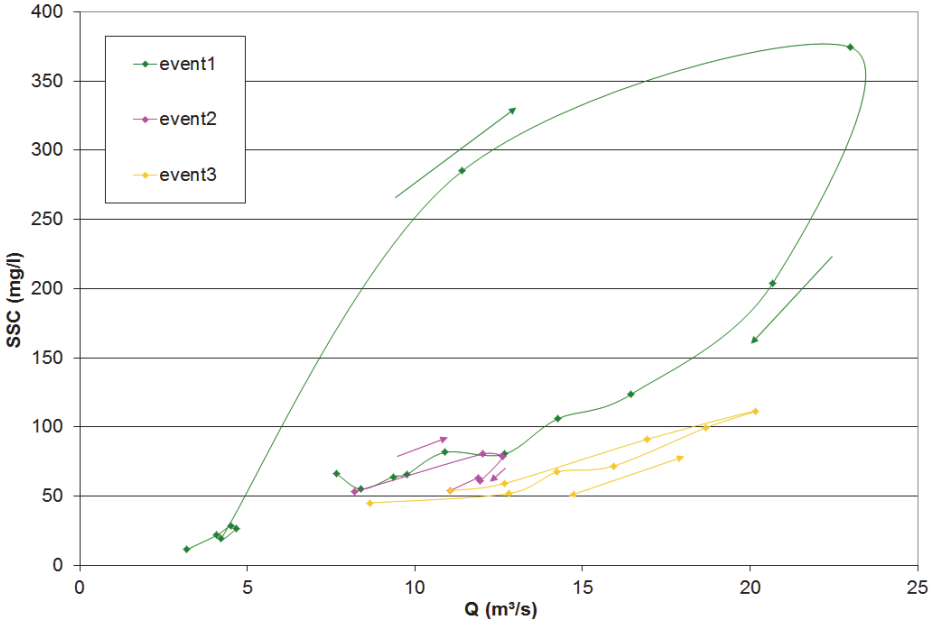

Figure 6.6: Scatter plot for SSC and Q Grobbendonk data for the period 22 November–2 December 2009, showing clockwise hysteresis for events 1 and 2 and a single line for event 3

between SSC and discharge peaks. However, when the variance is not limited to a shift in arrival time between SSC and discharge peaks, but also entails a change in sediment concentration in consequent peaks (due to sediment depletion of upstream reaches of the catchment), these daily average values will do little to lower the overall variance, as can be confirmed by the lack of significant increase in R^2-values (R^2 increases from 0.4895 to 0.491) as can be seen in Figure 6.1.

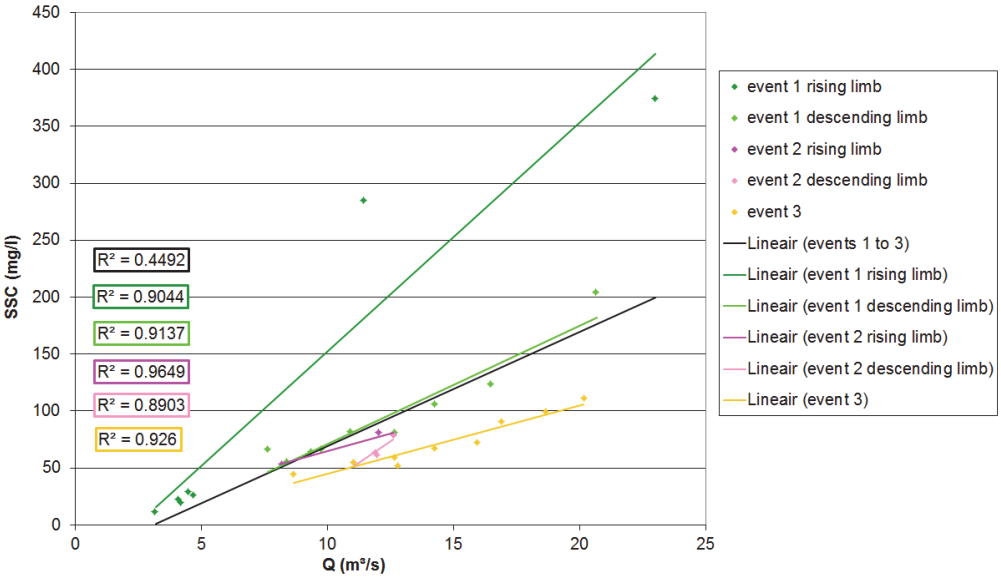

Figure 6.7: Scatter plot for SSC and Q Grobbendonk data for the period 22 November–2 December 2009. Both the overall rating curve for the entire data set is indicated as well as the individual rating curves for rising and descending limbs of events 1 and 2 and the rating curve for event 3

Even though the overall descriptive power of a single rating curve for the 22 November until 2 December time period is rather low (R^2 = 0.45), as can be seen in Figure 6.7, the predictive power of Q for separate parts of this hydrograph are much higher, but these individual linear relationships between SSC and Q differ substantially from one another. In the case of the Grobbendonk location, as seen in Figure 6.7, separate rating curves are established for the rising limb and descending limbs of event 1 and 2 and a separate curve is established for the subsequent linear relationship in event 3. They each have significantly higher R^2's (ranging from 0.89 up to 0.96).

The fact that multiple well-fitted relationships can be found between Q and SSC, gives weight to the choice to look for a regression model using or based on discharge data. However, due to the hysteresis (caused by the sediment depletion of the upstream reaches), this relationship is changing so rapidly throughout time that the overall relationship will have a lower predictive power than if one would be able to use the myriad of different consequent Q-SSC relationships.

It is noteworthy, that one direct approach to lower the variance of a data set, i.e. to exclude outliers from the analysis, should not be applied in this case. Figure 6.8 shows seasonally split and un-split Grobbendonk data, both with and without outliers (any value which deviates from the mean, more than three times the value of standard deviation). It can be observed that indeed the R^2 increases significantly by eliminating certain outliers, but it can also be seen that the removal of the outliers has an impact on the slope of the rating curves; they all decreased. This is logic, as the outliers function as leverage points, and hence have a far higher impact on the slope compared to the other points. As most of the data points that have been considered outliers are actually data points generated by the hysteresis process, and are therefore legitimate data points, this artificial way of increasing the R^2 should not be applied and other means should be attempted, such as data transformation.

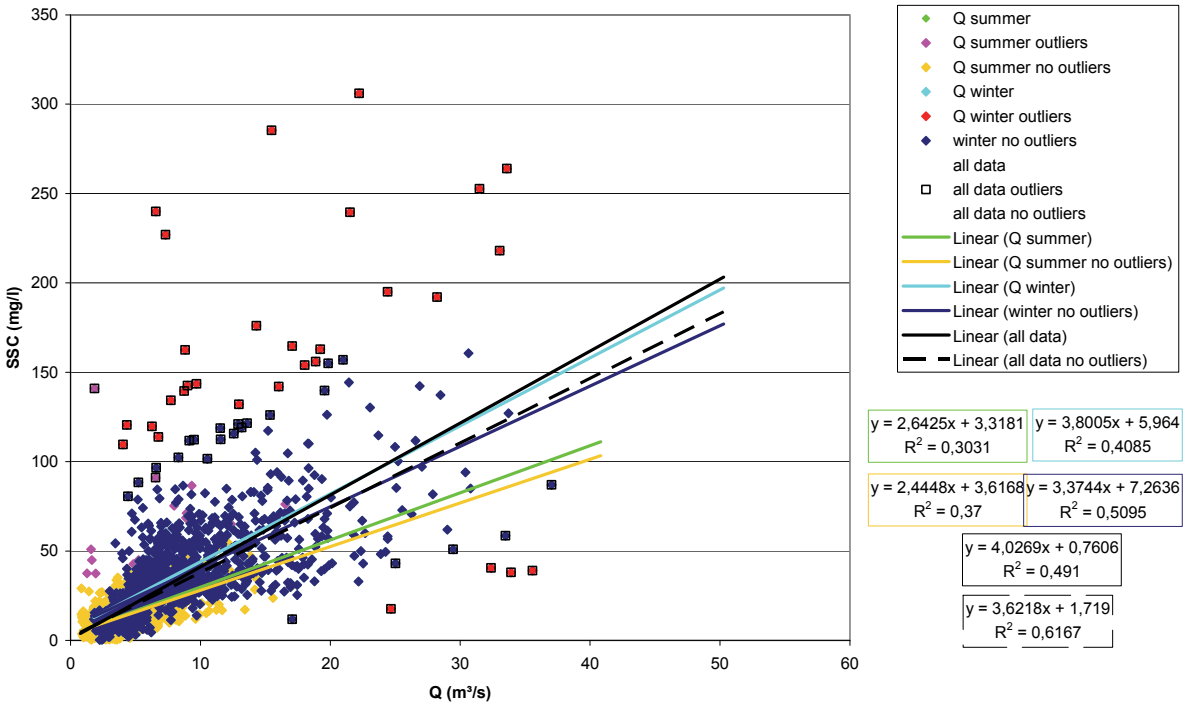

Figure 6.8: Seasonal scatter plots of SSC versus Q data obtained from Grobbendonk measurement station for the period 1999-2009, with rating curves for data sets both with and without outliers.

6.1.2.2 Data transformation

Even though a directly proportional relationship between SSC and Q can be established for the Grobbendonk measurement station, data transformation does seem to be in order, as heteroscedasticity is present.

The most commonly used data transformation for SSC-Q rating curves is log transformation, as this helps to spread the data more equally along the estimated regression line. Log-transformation can help meet the linear regression assumptions of normally distributed residuals and constant variance.

The graphical plot presented in Figure 6.9, shows the same data as was presented in Figure 6.8 but log_{10}-transformed. It can clearly be seen that the variability of y in the log transformed data of Figure 6.9 is much more uniform for different levels of x than it was for the non-transformed data. The higher variability in the lower regions of x-values, can partly be contributed to limitations of the balance at very low concentrations. The improved correlation (higher R^2) suggests that log_{10}-transformation may indeed improve the regression model. This is tested in the next section.

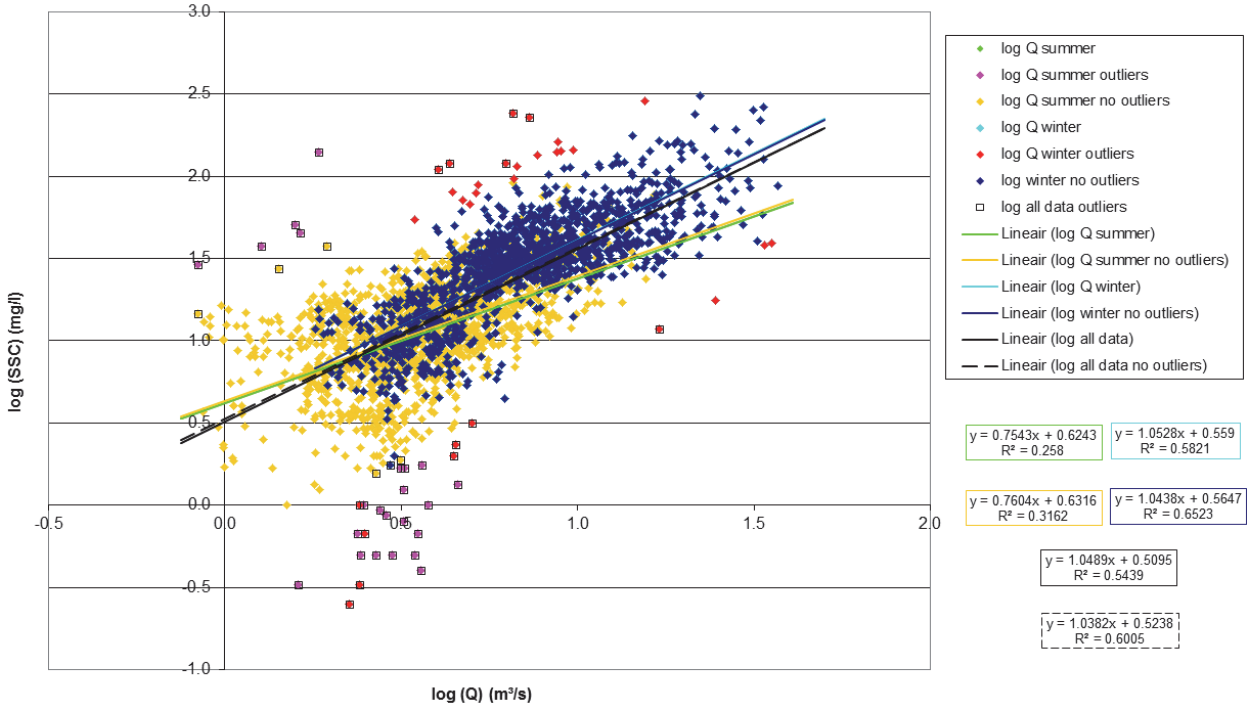

Figure 6.9: Log_{10}-transformed seasonal scatter plots of SSC versus Q data obtained from Grobbendonk measurement station for the period 1999-2009, with rating curves for data sets both with and without outliers.

Furthermore, when comparing Figures 6.8 and 6.9 it can clearly be seen that log_{10}-transformation will leave the data less sensitive to outliers. Even though eliminating these would of course increase the R^2 (one might say artificially) it will not significantly change the resulting rating curve. Hence, outliers are left in this data set and are taken into account in the analysis.

6.1.2.3 Constructing and evaluating linear regression models of the form: log SSC = f(logQ)

When solely the log_{10}-transformed discharge data is used as a potential explanatory variable for log-transformed SSC-values, the regression model could then be expressed in the form of Equation 5.2 and will look like this:

$$\log SSC_i = 1.049 \cdot \log Q_i + 0.509$$ Eq. 6.4

As stated in Section 5.2.2, retransforming $\log_{10}$-transformed data back to the original units, introduces a bias in the computed average suspended-sediment concentration values (Miller, 1951; Koch & Smillie, 1986). For the $\log_{10}$-transformed data, the SSC can therefore be calculated (derived from Eq. 5.3) as:

$$SSC_i = 10^{(1.049 \cdot \log_{10} Q_i + 0.509)} \times BCF$$ Eq. 6.5

in which: BCF is the bias correction factor

The linear regression model stated in Equation 6.5 can have two shapes, one (model 4) in which no BCF has been applied (BCF equals 1 in this case) and one (model 5) in which the BCF equals 1.196 and was calculated as indicated by Equation 5.4. Both models have consequently been evaluated using the same methodology as applied in Section 6.1.2.1 and the main test-statistics are presented Table 6.1. These statistics show an increase in R^2 value (from 0,49 up to 0,54 after $\log_{10}$-transformation). Also the heteroscedasticity observed in the residuals plotted versus the predictions has disappeared, although, it is clear that there are more observations for low x-values than for higher valued x-measurements.

However, the calculated RMSE and PRESS statistics of model nr 4 show a slight deterioration in comparison to the models created from non-$\log_{10}$-transformed data (models nr 2 and 3) and even though applying the BCF (model nr 5) does lower the PRESS-statistic it is still higher than the non-$\log_{10}$-transformed models.

When investigating long term and seasonal variability, box plots of the residuals are once more created, grouped per year (see Figure 6.10) and per month (see Figure 6.11). In these plots the trends are more pronounced than in the plots of the non-log-transformed data set (see Figures 6.2 and 6.3).The seasonal variability is more readily visible, with median values dipping under zero for summer and staying above zero for winter months, while still no significant trends can be spotted in the yearly grouped data set, showing no need to create individual annual rating curves.

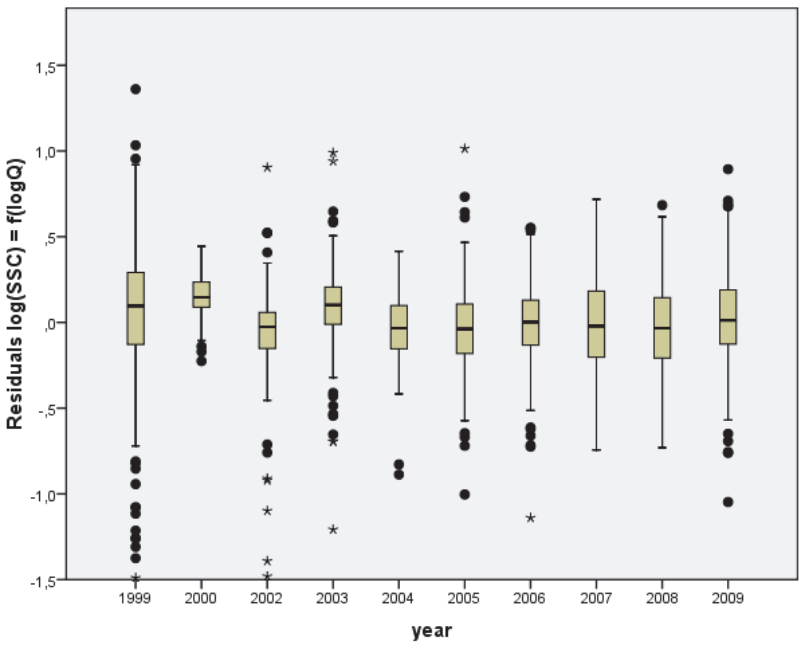

Figure 6.10: Residuals versus time (in years) of models nr 4 and 5 for data from Grobbendonk measurement station (1999-2009)

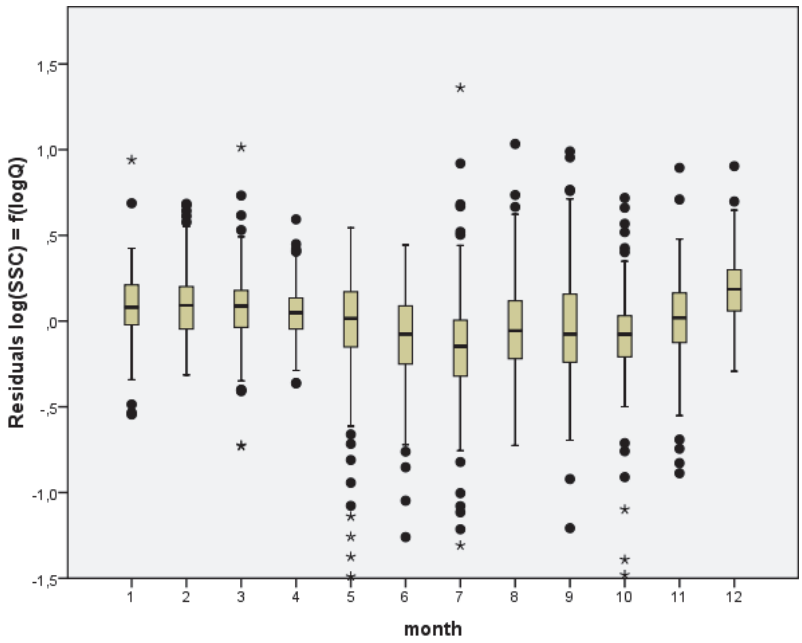

Figure 6.11: Residuals versus time (in months) of models nr 4 and 5 for data from Grobbendonk measurement station (1999-2009)

This different seasonal sedimentary response of the river can also be seen in Figure 6.9, where summer and winter data rating curves have different slopes. Therefore, just like in Section 6.1.2.1 two models have been developed, each consisting of two rating curves, one for each season (see Equations 6.6 and 6.7).

$$\log SSC_{i,winter} = 1.053 \cdot \log Q_i + 0.559 \quad \text{Eq. 6.6}$$

$$\log SSC_{i,summer} = 0.754 \cdot \log Q_i + 0.624 \quad \text{Eq. 6.7}$$

In the first model (model nr 6) no BCF was applied (the BCF equalled one), while in the second model (model nr 7) two (seasonal rating curve-specific) BCF's were calculated based on Equation 5.4. The winter-specific BCF equals 1.144 while the summer BCF is slightly higher (1.207). The test-results as presented in Table 6.1 show that the R^2 value of the $\log_{10}$-transformed winter data is higher than the R^2 values of the previous models, while the summer data R^2 value is quite low (which can be explained by the significant variability observed during low discharge conditions). This is also visible in the plot of residuals versus predicted data as seen in Addendum B. When looking at RMSE and PRESS statistics, one can state that the $\log_{10}$-transformed data reacts similarly as the non-transformed data did to the seasonal approach: applying two separate rating curves for summer and winter data does not significantly improve the predictive power of the model.

6.1.3 Regression models based on discharge and discharge-derived parameters

6.1.3.1 Constructing and evaluating linear regression models of the form: SSC = f(Q&Q-derived parameters)

The total hydrograph can be separated into different contributions using WETSPRO. This tool, developed by Willems (2000) applies the numeric filtering procedure developed by Nathan & McMahon (1992) to divide the measured discharge into a contribution of baseflow, interflow and

run-off. Baseflow (Q_{BF}) is herein defined as the groundwater flow in the saturated zone, while interflow (Q_{IF}) represents the groundwater flow in the unsaturated zone and overland flow (Q_{OF}) is the run-off (DHI, 2000). WETSPRO has been calibrated for the Nete basin, using data up to the year 2002, as part of the project 'Actualisation of the Sigmaplan' (IMDC et al., 2003). These settings have consequently been used to divide the total hydrograph of the subsequent years up to the year 2009 into its contributing partial flows. These results will also be applied in the modelling of genesis of authigenic sediment as discussed in Part IV.

It is possible that the discharge-derived parameters baseflow, interflow and overland flow will help to improve the regression analysis, as Grobbendonk is situated in a catchment that has a high occurrence of ferric authigenic sediment, therefore, groundwater-associated parameters could potentially be useful explanatory variables. In other catchments the run-off component could be very indicative. It is therefore useful to investigate all of these parameters. Figure 6.12 shows the scatter plots of daily averaged Q, Q_{BF}, Q_{IF} and Q_{OF} against the measured SSC.

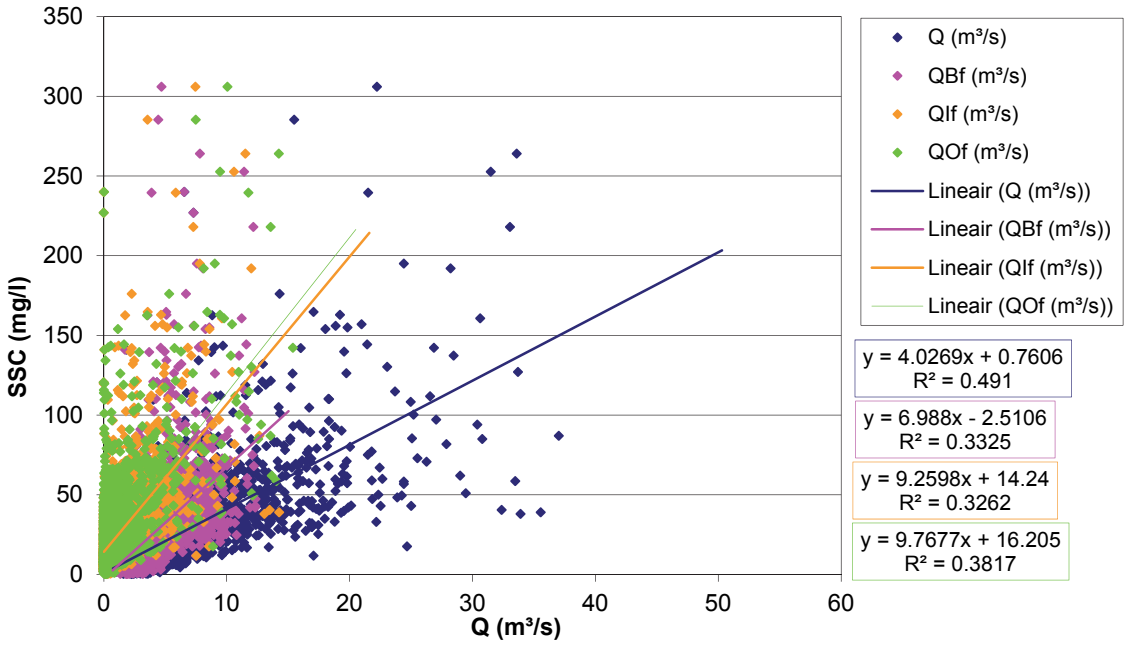

Figure 6.12: Scatter plots of SSC versus Q and Q-derived data (Baseflow (QBF), Interflow (QIF) and Overland flow (QOF)) obtained from Grobbendonk measurement station for the period 1999-2009

Due to the present hysteresis issues, the discharge-derived parameters of previous (suffix p) and consequent days (suffix n) might be predictive of the sedimentary response and will also be considered as potential predictive variables for the non-$\log_{10}$-transformed regression model.

Which parameters are finally allowed into the model, is based on the instructions specified in Section 5.2.3. Firstly, two-tailed Pearson's r correlation coefficients have been determined for all parameters (see Addendum B), which revealed all discharge-derived parameters correlated significantly with SSC at a level of α=0.05. However, the three baseflow parameter (Q_{BF}, Q_{BF_p} & Q_{BF_n}) have correlation coefficients that were greater than 0.95, indicating unacceptable multicollinearity. In this case only the variable which correlated the strongest with SSC (Q_{BF_n}) was allowed into the regression analysis. This analysis was executed in stepwise fashion and the final form of the model (model nr 8) is stated in Equation 6.8.

$$SSC_i = -8.986 \cdot Q_i + 3.441 \cdot Q_{IF_p i} + 14.737 \cdot Q_{OF_n i} + 21.447 \cdot Q_{OF,i} + 18.844 \cdot Q_{BF_n i} - 8.370 \cdot Q_{n,i} + 3.296 \cdot Q_{p,i} - 1.444 + \varepsilon_i \quad \text{Eq. 6.8}$$

In Table 6.1 it can be seen that even though the R^2 value does not significantly increase, the RMSE and PRESS statistics of this model are slightly lower than the models nr 2 and 3 (the non-$\log_{10}$-transformed Q-based models).

Even though, the seasonal variation is once again only slightly visible in the residuals grouped per month and plotted against time (see Figure 6.13), another model (model nr 9) was created. This model consisted of two seasonal rating curves, as model 3 had also a slightly better predictive power than model nr 2, without their residual plots having indicated such an improvement. Figure 6.14, which showed the residuals grouped per year and plotted against time, still gives no indication to construct annual rating curves.

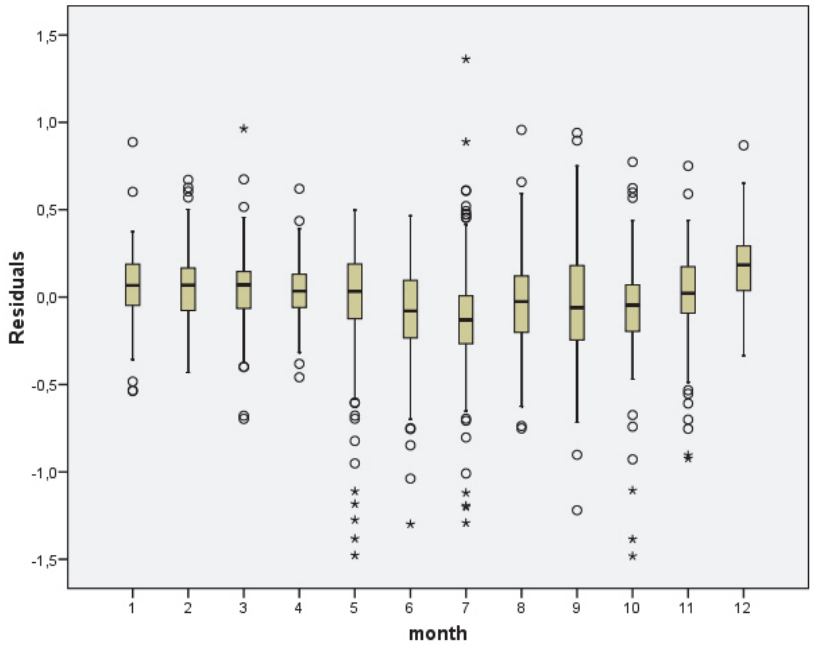

Figure 6.13: Residuals versus time (in months) of model nr 8 for data from Grobbendonk measurement station (1999-2009)

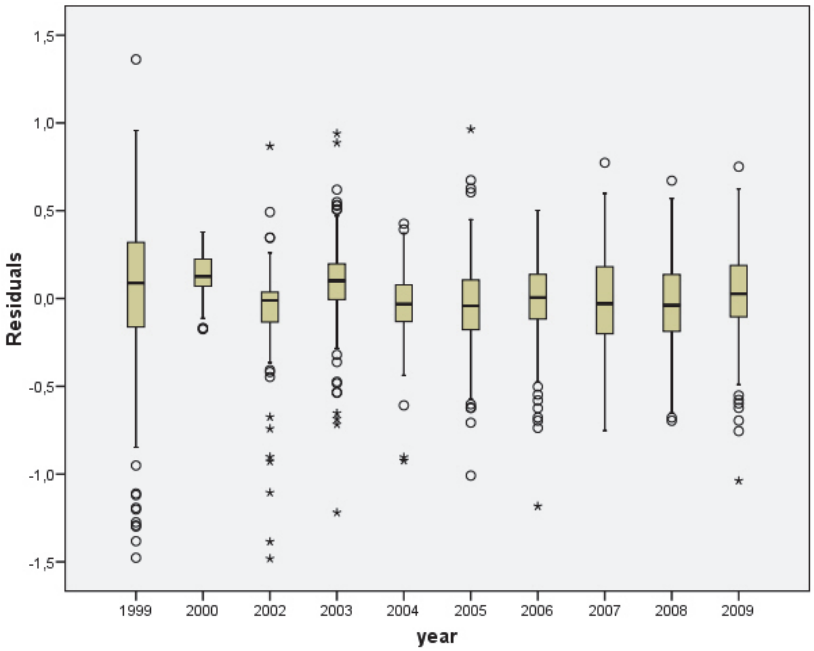

Figure 6.14: Residuals versus time (in years) of model nr 8 for data from Grobbendonk measurement station (1999-2009)

The winter and summer data were separately investigated for multicollinearity (see Addendum B) but yielded the same result as the combined data set, hence the same parameters were allowed to enter the stepwise linear regression. The seasonal rating curves took their final shapes as stated in Equations 6.9 and 6.10.

$$SSC_{i,winter} = 4.613 \cdot Q_i + 0.777 \cdot Q_{p,i} + 2.563 \cdot Q_{OF_n i} + 3.441 \cdot Q_{IF_p i} + 6.282 + \varepsilon_i \quad \text{Eq. 6.9}$$

$$SSC_{i,summer} = 3.302 \cdot Q_i + 2.374 \cdot Q_{IF_p i} + 2.318 + \varepsilon_i \quad \text{Eq. 6.10}$$

It is noteworthy that both separate rating curves contain less predictive parameters than the overall rating curve, stated in Equation 6.6. Furthermore, their statistical test-results (see Table 6.1 model 9) show that the RMSE and PRESS statistics declined a little bit (in comparison to the single rating curve for discharge-derived parameters (model 8)).

6.1.3.2 Constructing and evaluating linear regression models of the form: log SSC = f(logQ & logQ-derived parameters)

Figure 6.12 showed the non-$\log_{10}$-transformed discharge-derived data, and the obvious heteroscedasticity seems to indicate a need of data transformation, although the graph showing the residuals plotted versus the predicted values of model 8 (see Addendum B) does not show this as clearly. Nevertheless, like in Section 6.1.2.2 the discharge-derived data was $\log_{10}$-transformed. As some of the discharge-derived parameters not always contribute to the total measured discharge, and therefore sometimes descend to zero, the $\log_{10}$-transformation was performed on the actual data value increased with 1, as is written down in Equations 6.11, 6.12 and 6.13.

$$\log_{10} Q'_{BF} = \log_{10}(Q_{BF} + 1) \quad \text{Eq. 6.11}$$

$$\log_{10} Q'_{IF} = \log_{10}(Q_{IF} + 1) \quad \text{Eq. 6.12}$$

$$\log_{10} Q'_{OF} = \log_{10}(Q_{OF} + 1) \quad \text{Eq. 6.13}$$

Consequently, two-tailed Pearson's r correlation coefficients were determined which showed all discharge-derived parameters to still correlate significantly (α=0.01.) with SSC-data. However, the $\log_{10}$-transformed data showed more parameters to exhibit an unacceptable level of multicollinearity (see Addendum B) than the non-transformed data did in Section 6.1.3.1. Besides the three baseflow parameters (Q_{BF}, Q_{BF_p} & Q_{BF_n}), the discharge parameters (Q, Q_p & Q_n) also showed correlation coefficients that were greater than 0.95. In this case respectively Q_{BF_n} and Q were allowed into the regression analysis, along with the other parameters which had passed the collinearity test, as they correlated the strongest with SSC. In the end the final rating curve of the $\log_{10}$-transformed data took the shape of:

$$\log SSC_i = 0.520 \cdot \log Q_i - 0.489 \cdot \log Q'_{IF_p i} + 0.96 \cdot \log Q'_{OF_n i} + 0.723 \cdot \log Q'_{BF_n i} + 0.551 \cdot \log Q'_{IF,i} + 0.361 \quad \text{Eq. 6.14}$$

Retransforming the $\log_{10}$-transformed data back to the original units, will introduce a bias. Therefore, like in Section 6.1.2.3, from Equation 6.12 two models were created, one (model nr 10) without a BCF and one with it (model nr 11). The BCF was calculated using Equation 5.3 and yielded a value of 1.184, which was then implemented in model nr 11.

In Table 6.1 it can be seen that the R^2 value of this set of $\log_{10}$-transformed models, is not significantly higher than the non-$\log_{10}$-transformed model (model nr 8) and again the absolute values of the t-statistics were higher than 2. However, similar to what was observed and reported in Section 6.1, the predictive power of the non-$\log_{10}$-transformed discharge-derived model was stronger than model based on $\log_{10}$-transformed data.

As taking the seasonal variability into account strengthened the predictive power of the non-$\log_{10}$-transformed model (model 9), this was also investigated for the $\log_{10}$-transformed data. Figure 6.15 shows the slight seasonal variation as presented in the plotting of the residuals grouped per month and plotted against time, while Figure 6.16 shows that no significant difference can be observed between individual years.

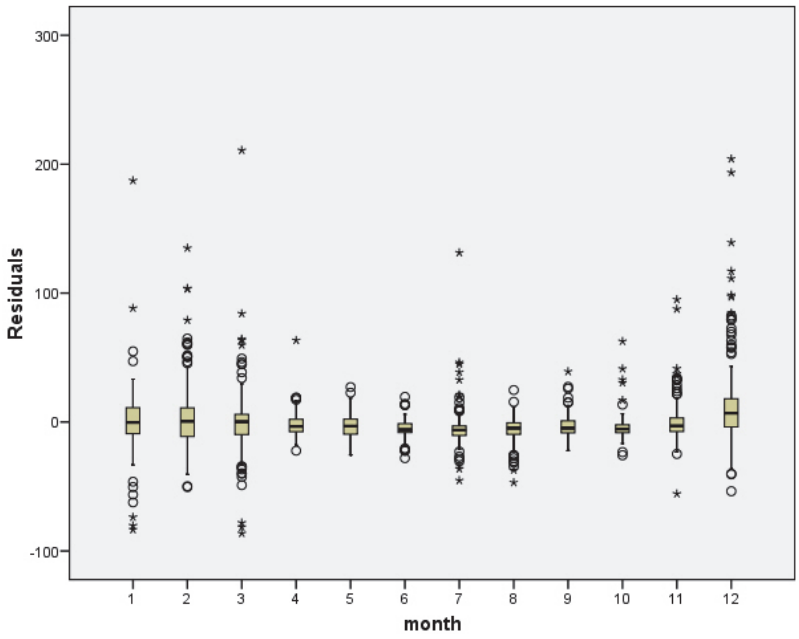

Figure 6.15: Residuals versus time (in months) of models nr 10 & 11 for data from Grobbendonk measurement station (1999-2009)

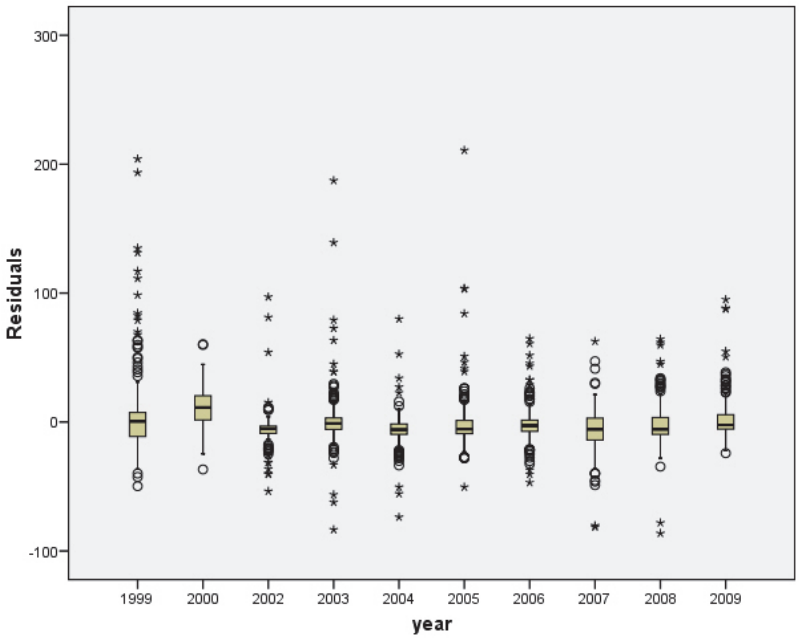

Figure 6.16: Residuals versus time (in years) of models nr 10 & 11 for data from Grobbendonk measurement station (1999-2009)

The winter and summer data were separately investigated for multicollinearity, as described above, but both showed only the baseflow parameters to be multicollinear. From those Q_{BF_n} was selected to be entered into the stepwise linear regression because of its strongest correlation with SSC, along with the other parameters that passed the test. The seasonal rating curves took their final shapes as stated in Equations 6.15 and 6.16.

$$\log SSC_{i,winter} = 0.908 \cdot \log Q_i - 0.274 \cdot \log Q'_{IF_p i} + 0.367 \cdot \log Q'_n + 0.465 \quad \text{Eq. 6.15}$$

$$\log SSC_{i,summer} = 0.663 \cdot \log Q'_{OF,i} + 0.899 \cdot \log Q_{BF_n i} + 0.435 \quad \text{Eq. 6.16}$$

Again, the model statistics were reported in Table 6.1, where it can be seen that the R^2-values are slightly elevated when comparing them to the non-$\log_{10}$-transformed model (model nr 9). Furthermore, as observed with the non-$\log_{10}$-transformed data models, the seasonal rating curves contain each less predictive parameters than the overall rating curve, stated in Equation 6.12.

Next, from this set of rating curves, two models were derived to investigate the impact of applying a BCF. Model nr 12 does not apply a BCF while model nr 13 applies seasonal BCF's . The winter BCF was calculated, once again using Equation 5.3, to be 1.129, while the summer BCF equalled 1.198.

As was observed for non-$\log_{10}$-transformed-data, splitting the data set in two seasonal rating curves, lowers the RMSE and PRESS-values and therefore increases the predictive power of the model (see Table 6.1 model 9).

6.1.4 Comparing the performance of the discharge and discharge-derived prediction models

Before investigating the predictive power of models based on a combination of YSI-data and discharge-derived data, the models described above in Sections 6.1.1, 6.1.2 and 6.1.3 are compared based on their RMSE and PRESS statistics as well as on their predictive results.

From the models 1 through 11, model number 9 (summer and winter separated, non-logarithmically transformed data, allowing discharge-derived parameters to enter) has the lowest RMSE and PRESS statistics. However, model number 9 performs only slightly better than the other models. The only exception is model nr 1 which was based solely on the mean sediment concentration value. This model performance the worst.

Next, the annual SSFes predicted by the different models are compared to the fluxes obtained from the measurements. As these latter contained some gaps, the fluxes summarised per year, are actually only partial fluxes. Hence, Figure 6.17 shows both the measured SSFes summarised per year as well as the prediction results of the models for the same time period (therefore excluding the model results from dates when measurements were missing). The percentage of the time data was missing per year is presented in Table 6.4.

From Figure 6.17 it is clear that a significant spread in predictions can be observed, and that a particular model can predict the observed data of one year very well, while under or over predicting the SSF significantly the next year.

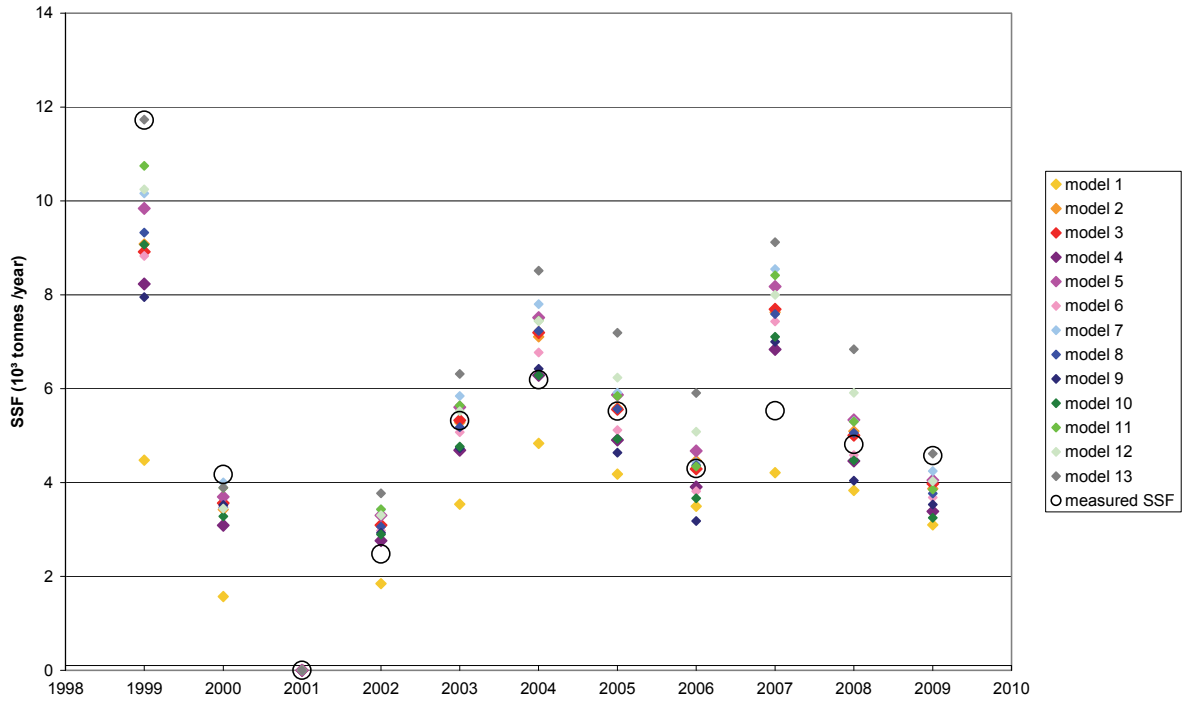

Figure 6.17: Measured SSFes and model results for data from Grobbendonk measurement station (1999-2009)

Table 6.3: Percentage of time no SSF-data were available in the measurements of Grobbendonk station, and the percentage of annual sediment flux the various models calculated to fill in these blanks.

		Model nr												
	Data gaps	1	2	3	4	5	6	7	8	9	10	11	12	13
	% time	% flux	% flux	% flux	% flux	% flux	% flux	% flux	% flux	% flux	% flux	% flux	% flux	% flux
1999	13	9	20	21	19	22	21	23	21	21	21	24	21	23
2000	83	54	64	62	61	65	60	63	64	54	61	65	67	70
2001	100	100	100	100	100	100	100	100	100	100	100	100	100	100
2002	61	64	83	83	82	84	84	85	84	82	84	86	84	86
2003	16	12	20	21	19	22	21	23	18	18	17	20	18	19
2004	2	1	2	2	2	2	2	2	1	1	1	2	2	2
2005	10	6	5	5	4	5	4	5	5	5	4	5	5	6
2006	20	19	26	27	24	27	26	29	26	27	24	27	26	29
2007	26	20	30	29	28	31	29	32	30	26	27	31	31	34
2008	21	17	17	18	15	17	16	18	16	17	14	16	16	18
2009	19	19	28	29	26	29	28	31	28	30	26	29	28	30

However, one model (model nr 1, which uses the mean observed SSC value for SSF calculations) constantly underpredicts the observed measurements, and should therefore be excluded for further use.

Furthermore, all models seem to underpredict the monitored SSF in 2000 while they overpredict the values in 2002. This is a fringe effect of the modelling hiatus that started and ended in those years. In 2000 only the winter months January and February were monitored, and therefore the predictions of the models underestimate. The models based on $\log_{10}$-transformed data with BCF (models nr 5, 7, 11 & 13) however, perform reasonably well under these conditions. The

monitoring in 2002 only started up again in July, hence foregoing the winter months of January through March for further analysis, causing most models to have a slight overprediction.

Also, in wetter years, with more high discharge registrations, the results of the different models will be more variable than in years with less high-flow events, as the associated SSC predictions are more uncertain during high-flows. This is illustrated in Figure 6.18 which shows a positive correlation between the standard deviation observed between all model predictions made for a specific year and the total measured discharge that year. Furthermore, the 90th percentile of discharge observed in the different years, correlates nicely with the standard deviation measured that year. The mean discharge and the 10th percentile of the discharge measured that year, correlate little to not at all with the standard deviation of the modelled results, showing that the modelled low-flow conditions contribute less to the annual SSF. This conforms to observations (Huygens et al., 2001; De Sutter, 2000) that the largest contributions to the total sediment flux happen in only a small percentage of the time (during high-flow conditions).

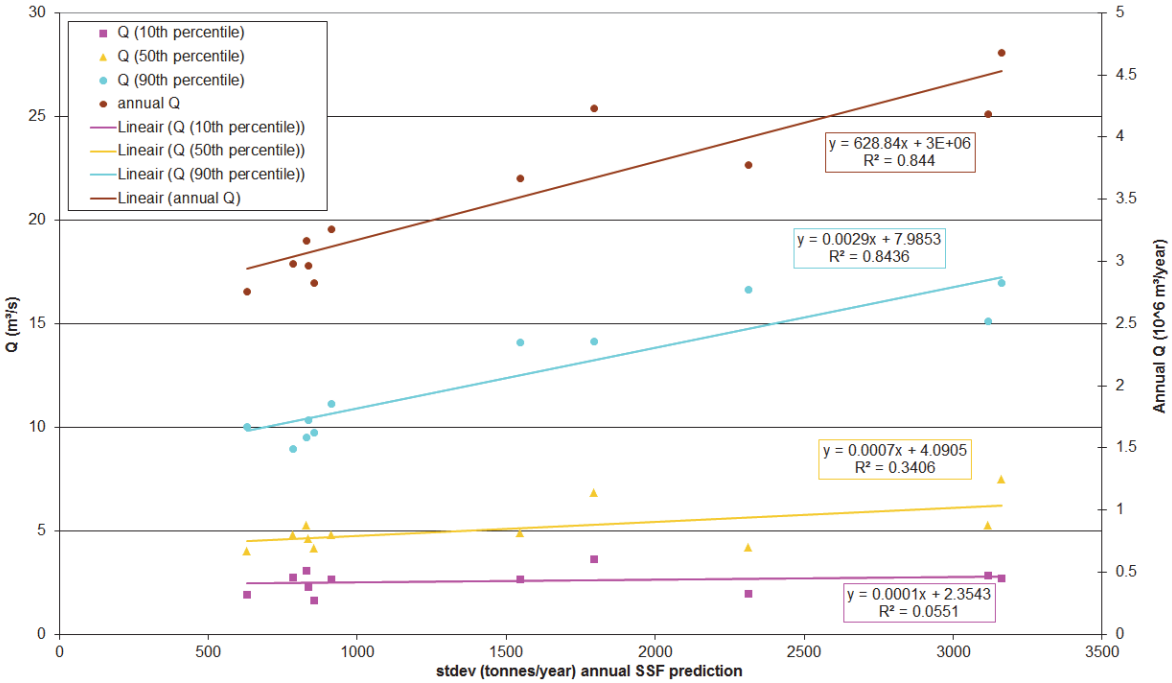

Figure 6.18: Correlation plot of total annual measured discharge at Grobbendonk measurement station (1999-2009) as well as 10th, 50th and 90th percentile of discharge measured those years plotted against the standard deviation of all model predictions made for that specific year.

In the framework of this PhD thesis, these models were not developed to predict entire years' worth of SSFes, but only to fill in missing daily values in existing data sets. Table 6.3 shows, besides the percentage of data gaps, the percentages of the total annual flux the modelled partial fluxes represent. If the distribution of the discharges present during the periods of missing data were identical to the distribution of the discharges used to create the model, the percentage of modelled partial SSFes would be identical to the percentage of time they needed to cover. This is of course not the case. If more high-water conditions had missing data-points, the modelled flux would represent a higher percentage of the annual total flux, while if more low-flow conditions were to be completed through modelling, these modelled results would represent a lower percentage of the total annual SSF. This again can clearly be observed in the years 2000 and 2002. In the year 2000 only the first two (winter) months were monitored, but the remaining 80% of the time relatively only counts for around 60% of the annual SSF, as predominantly summer months remain to be predicted. The reverse is the case for 2002, where the first six months (including the

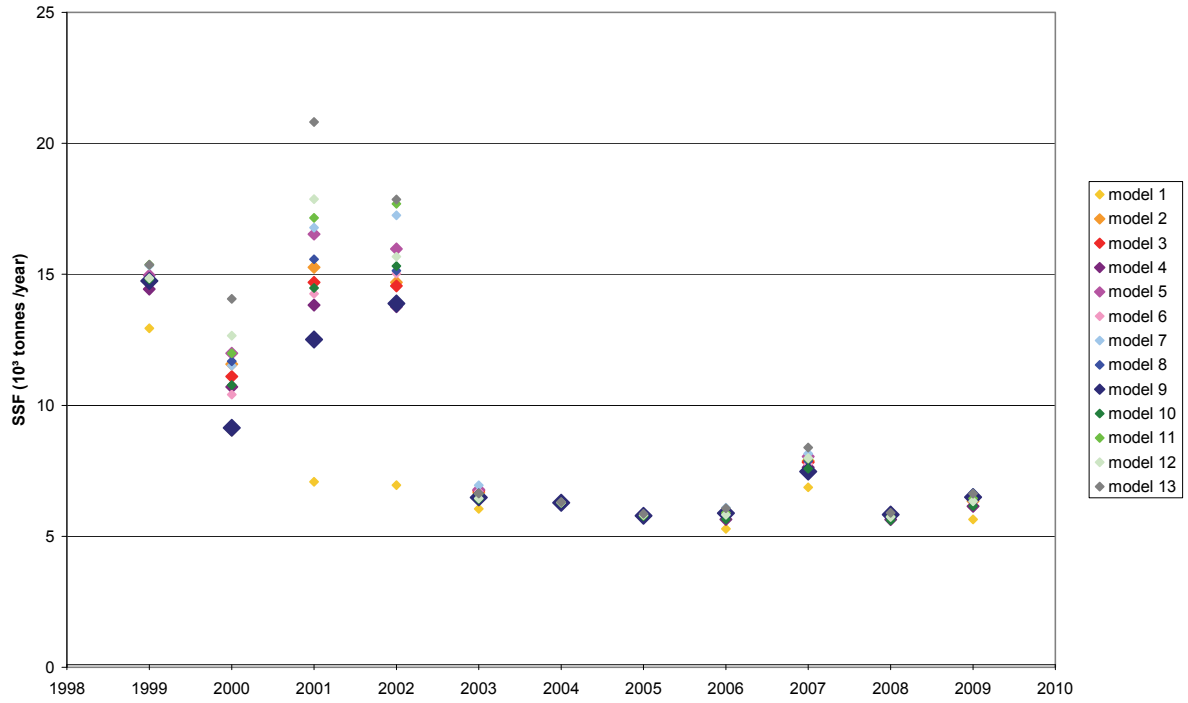

Figure 6.19: Annual SSFes at Grobbendonk monitoring station as obtained through complementing daily averages of SSF measurements with model predictions

important first two winter months) are missing from the monitoring, causing the model-predicted 60% of the time, to weigh in for more than 80% of the total calculated transport.

Finally, when SSFes are calculated based on measurements complemented with modelling, all results fall within acceptable ranges for years where more than 75% of the time SSC-values were available as can be seen in Figure 6.19.

This is also tabulated in Table 6.4, where can be observed that the spread between minimal and maximal predicted annual SSFes (based on calculations of all models save for model nr 1) constitutes only 1-8% of the mean total SSF for years with more than 75% observations. When more data is missing, the different models tend to give a wider range of predictions, which can go up to more than 50% for the completely unmonitored year of 2001.

To conclude, as all models (except model nr 1) perform similarly, the model with the lowest RMSE and PRESS statistics is used for comparison with the model based on a combination of physical parameter and discharge-derived data.

Table 6.4: Mean annual SSFes based on the results of measurements complemented with the modelling results of models 2-13 as well as the spread between the maximal and minimal predicted SSF. This spread is also expressed as a percentage of the mean SSF.

	mean SSF (tonnes/year)	spread (tonnes/year)	Spread / mean SSF (%)
1999	14899	943	6
2000	11457	4888	43
2001	15766	8064	51
2002	15507	3932	25
2003	6616	487	7
2004	6296	36	1
2005	5797	100	2
2006	5855	398	7
2007	7873	870	11
2008	5773	283	5
2009	6394	461	7

6.1.5 Regression models based on discharge, discharge-derived and other physical parameters

As FHR has only sparsely executed the time-consuming process of data validation on its measurement stations, turbidity and conductivity data from Grobbendonk measurement station have been validated in the framework of this PhD for the period 2008-2009. These two parameters were selected as they are considered to have the most predictive power for predicting SSC-values. Turbidity is directly influenced by the amount of sediment in the water, which makes the water more turbid. Conductivity is linked to the dilution of the river water caused by the influx of fresh (rain) water. During such an event, sediment will be entering the river system, which will lead to increased SSCs. Even though the YSI-probe was installed at Grobbendonk measurement station during this time period, data was not recorded during the entire period due to technical failure of the probe, and during the validation process, some extra data needed to be removed. Hence correlations with SSC were evaluated using a more limited dataset. Figure 6.20 shows the available daily average turbidity, conductivity and SSC-values at Grobbendonk measurement station for the period 2008-2009. Therefore, to calculate an annual SSF, the data points that are missing due to lack of YSI-data, will still need to be filled in with one of the previously determined discharge and discharge-derived regression models, as based on the test-statistics presented in Table 6.1.

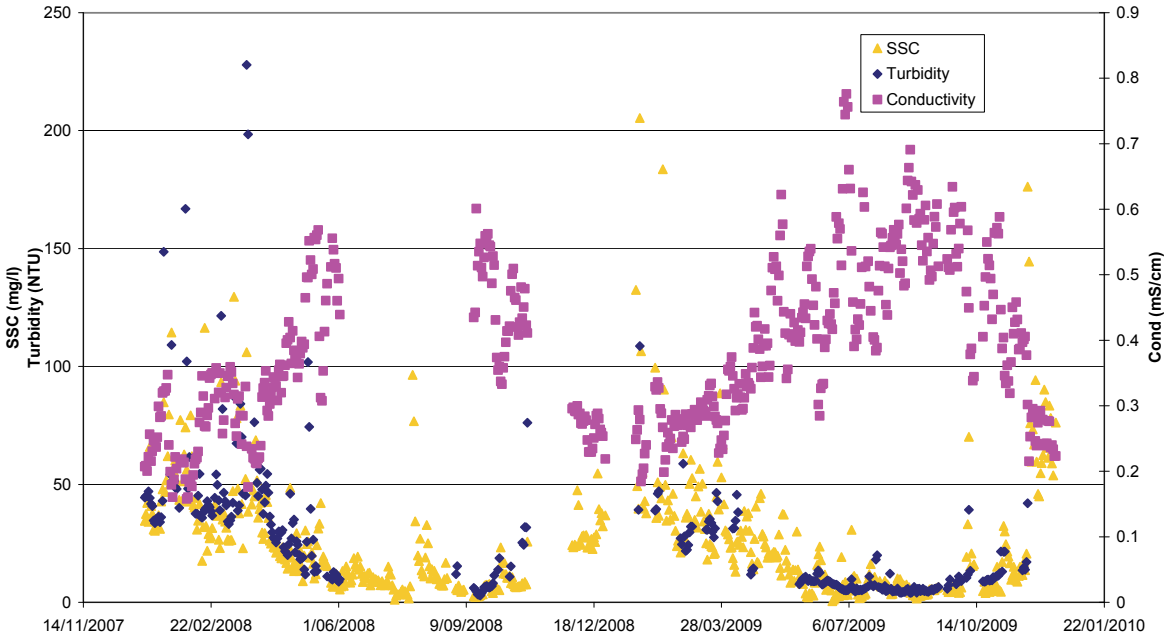

Figure 6.20: Availability of average daily conductivity, turbidity and SSC-values, after data validation

Like in the previous sections of this chapter, the linear regression models under investigation are tested statistically, as described in Section 5.2, and the tables and graphs have once more been included in Addendum B.

Figure 6.21 shows the scatter plot of turbidity and conductivity versus SSC. It can be seen that turbidity has a positive (linear) correlation with SSC, while conductivity has a negative (logarithmic) one. However, both show a significant difference in variability of conductivity and turbidity values for different SSC-values, indicating data transformation might help to build a better prediction model.

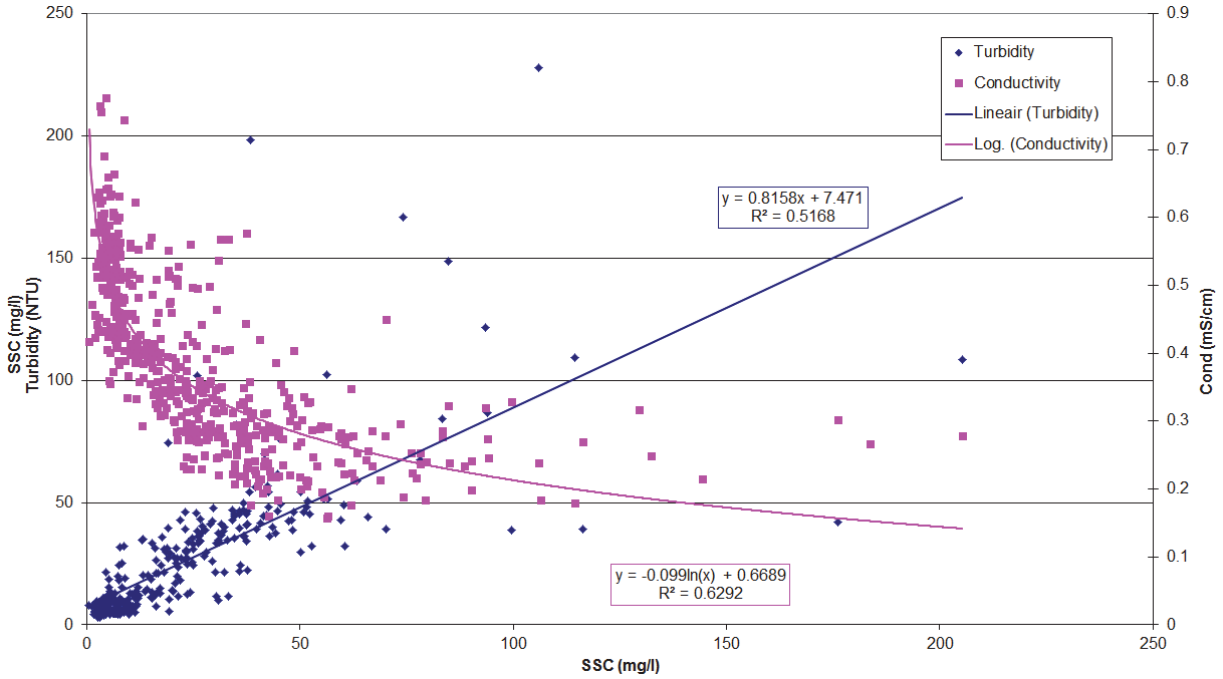

Figure 6.21: Scatter plot of turbidity and conductivity data in function of measured SSC at Grobbendonk monitoring station (2008-2009)

Therefore both $\log_{10}$-transformed and untransformed turbidity and conductivity data as well as all the parameters already tested in Section 6.1.3, were tested using Pearson's r correlation coefficients to determine correlation with SSC and possible multicollinearity between the different parameters (see Addendum B).

Of the non-$\log_{10}$-transformed data turbidity and conductivity both proved to correlate with SSC at a level of 0.05 α, while no other multicollinearity appeared than the previously determined one between baseflow parameters. Hence, all but Q_{BF} and Q_{BF_p} were entered into a stepwise linear regression analysis, which yielded following rating curve (Equation 6.17) as optimum predictor.

$$SSC_i = 3.435 \cdot Q_{n,i} - 13.155 \cdot Q_{IF,i} - 54.047 \cdot Cond + 9.166 \cdot Q_{IF_n i} + 0.093 \cdot Turb + 27.223 \qquad \text{Eq. 6.17}$$

The R²-value of this model (presented in Table 6.1 as model nr 14) is the highest observed yet. The RMSE dropped down to 13 mg/l, what is 59% of the mean SSC-value observed for the period 2008-2009.

As conductivity is a parameter which is readily influenced by the seasons, two separate rating curves (one for summer months and one for winter months) were constructed. Pearson's r (see Addendum B) analysis showed besides the multicollinearity of the baseflow parameters, that Q_{OF_p} was not correlating to SSC for the winter data, hence this parameter was removed from the stepwise linear regression. For the summer data the baseflow parameters also showed multicollinearity as did the discharge parameters. Hence, Q_{BF}, Q_{BF_p}, Q and Q_n were prohibited from entering the stepwise linear regression analysis.

The final seasonal rating curves took following form:

$$SSC_{winter,i} = -19.962 \cdot Q_{IF,i} - 130.542 \cdot Cond + 21.306 \cdot Q_{IF_n i} + 75.783 \quad \text{Eq. 6.18}$$

$$SSC_{summer,i} = 10.358 \cdot Q_{OF,i} + 0.141 \cdot Turb_i + 11.183 \cdot Q_{OF_n i} - 18.226 \cdot Q_{IF_n i} + 3.288 \cdot Q_p - 2.313 \quad \text{Eq. 6.19}$$

The test-statistics are summarized in Table 6.1 (as model nr 15) and show reasonably elevated R^2-values and yet another slight decrease in RMSE and PRESS-values.

As stated above, also $\log_{10}$-transformed turbidity and conductivity data was tested for correlation with log SSC and multicollinearity. There was a significant correlation (α=0.05) between these parameters and $\log_{10}$SSC and no extra multicollinearity was observed in the data set that was not reported above in Section 6.1.3. However, the parameters omitted from entering the stepwise linear regression in this data set were Q_{BF}, Q_{BFp}, Q and Q_p. The final regression analysis rendered following rating curve:

$$\log SSC_i = 1.241 \cdot \log Q_{n,i} + 0.437 \cdot \log Turb - 0.615 \cdot \log Q'_{IF,i} - 0.625 Cond - 0.605 \cdot \log Q'_{Bf_n i} + 0.80 \quad \text{Eq. 6.20}$$

The R^2-values rose to a very acceptable 0.81. Once more, as the data was $\log_{10}$-transformed, two models were once again developed from this rating curve; one (model nr 16) without the use of a BCF, and model nr 17 applying a BCF with value 1.093 (calculated using Equation 5.3). Table 6.5 shows that the RMSE and PRESS statistics of these models react to being log transformed much like the discharge-derived parameters: they rise slightly in comparison to the non-$\log_{10}$ transformed data.

Table 6.5: Comparison between models 1-19 for the data set 2008-2009

	PRESS	RMSE
1	300,830	23.40
2	99,615	17.51
3	90,091	16.64
4	108,040	18.26
5	99,637	17.52
6	101,028	17.64
7	95,472	17.17
8	83,159	15.84
9	74,295	15.00
10	98,834	17.41
11	91,748	16.74
12	85,368	16.15
13	79,005	15.61
14	69,003	12.95
15	54,662	11.94
16	68,147	13.63
17	70,301	13.73
18	58,901	15.47
19	59,816	15.36

Finally, once again the seasonal variability is taken into account and investigated to see if it can strengthen the predictive power of the model. The winter and summer data were separately investigated for multicollinearity as described above. Both showed multicollinearity for the baseflow parameters (and Q_{BF_n} was selected to be entered into the stepwise linear regression because of its strongest correlation with SSC). Furthermore, for summer data, the discharge parameters were collinear, and Q_n was allowed to enter the analysis, along with the other parameters that passed the test. The seasonal rating curves took their final shapes as stated in Equations 6.20 and 6.21.

$$\log SSC_{i,winter} = 3.229 \cdot \log Q_{n,i} - 1.308 \cdot \log Q'_{IF_n i} + 0.352 \cdot \log Turb_i - 1.687 \cdot \log Q_{BF_n,i} - 0.481 \cdot \log Q_{OF_n,i} + 0.87 \quad \text{Eq. 6.21}$$

$$\log SSC_{i,summer} = 0.459 \cdot \log Turb_i + 0.731 \cdot \log Q_{n,i} + 0.086 \quad \text{Eq. 6.22}$$

Once more, these rating curves are tested. Model nr 18 does not apply a BCF while model nr 19 uses a winter-BCF that equals 1.084, and a nearly identical summer-BCF of 1.089. As can be seen in Table 6.1, the R^2-values are acceptable. However, the RMSE and PRESS statistics have increased in comparison to their non-logarithmically transformed counterparts.

For comparative reasons, the RMSE and PRESS statistics of models nr 1-13 have also been recalculated for the same reduced temporal data set of 2008 and 2009, by which models 14-19 have been produced. These statistics are shown in Table 6.5 and show that model 15 (with summer and winter rating curves, using non-logarithmically transformed turbidity, conductivity and discharge-derived data) is able to predict the SSC concentrations the best. The RMSE equals 12mg/l which represents 47% of the average measured SSC.

6.1.6 Conclusion

Within each of the three analysed sub-groups (using only discharge, using discharge and discharge-derived parameters or using all available parameters), the non-logarithmically transformed data models, separating summer and winter curves performed the best.

Furthermore, it is clear that allowing discharge-derived parameters to enter the model yields a slight improvement of the predictive power, while allowing other hydrological parameters to enter, improves the modelling result more. Even then, the uncertainty as estimated by the RMSE is still quite high (about 50% of the average observed sediment concentration in the Grobbendonk sampling station for the period of record).

Applying the mean observed sediment concentration to fill in gaps, should only be allowed when no relationship between discharge and transported sediment can be established, as using the mean values tends to underestimate the transport flux significantly.

When daily automatically collected samples are present, sediment concentration values need to be estimated only for those days that equipment malfunctioned (either on the field or in the laboratory). Therefore, if the objective is to calculate annual suspended sediment fluxes and more than 75% of the data is available, then applying a non-logarithmically transformed relationship between Q and SSC (separated for summer and winter data) to fill in the remaining 25% should suffice. The spread between minimal and maximal predicted annual SSFes for those years (based on calculations of the different models) constituted only 1-8% of the mean total SSF. When more data is missing, the different models tend to give a wider range of predictions. In those cases, a different approach should be selected.

This is also the case more detailed estimates are required, such as daily sediment concentrations (as needed for the MARS modelling in Part IV, or event-based studies), then the combination of discharge with discharge-derived parameters and physical parameters should be investigated to procure the most predictive relationship possible. If these relationships are still not satisfactory, it might be useful to abandon linear regression techniques and replace the missing data using other methods, such as for instance imputation.

6.2 Determining sediment concentrations and fluxes for the Demer, Gete and Mangelbeek

In the framework of validating the sediment fingerprinting studies, SSF data is required for the Aarschot measurement location (located on the Demer) which is used as outlet for the fingerprint studies, as well as for two selected tributaries. The first tributary is the Gete, and is selected to be

representative for the southern tributaries. Its measurement location is situated just upstream of the confluence of the Gete with the Velpe in Halen. The second selected tributary is the Mangelbeek, which represents the northern tributaries. Its measurement location is situated in Lummen. All exact location are presented in Figure 2.14 in Chapter 2.

For all locations, daily SSFes were either obtained through measurement or through the use of a set of rating curves (non-logarithmically transformed winter and summer rating curves, based on discharge data).

These sets of rating curves took the following shape:

- Demer at Aarschot (for the period 01-01-2005 up to 31-10-2007)

$$SSC_{i,winter} = 3.9368 \cdot Q_i + 1.9422 + \varepsilon_i \quad \text{Eq. 6.23}$$

$$SSC_{i,summer} = 3.9419 \cdot Q_i - 0.6778 + \varepsilon_i \quad \text{Eq. 6.24}$$

- Gete at Halen (for the period 01-05-2007 up to 31-10-2007)

$$SSC_{i,winter} = 70.947 \cdot Q_i - 95.094 + \varepsilon_i \quad \text{Eq. 6.25}$$

$$SSC_{i,summer} = 8.533 \cdot Q_i + 36.219 + \varepsilon_i \quad \text{Eq. 6.26}$$

- Mangelbeek Lummen (for the period 01-05-2007 up to 31-10-2007)

$$SSC_{i,winter} = 14.938 \cdot Q_i + 22.388 + \varepsilon_i \quad \text{Eq. 6.27}$$

$$SSC_{i,summer} = 14.294 \cdot Q_i + 24.889 + \varepsilon_i \quad \text{Eq. 6.28}$$

At the Aarschot sampling location, SSC-data is available from 2000 to 2012. However, in the framework of the sediment fingerprinting studies data from 2007-2009 is of most interest. Furthermore, in order to enable comparison with the WATEM-SEDEM determined sediment export fluxes (as mentioned in Chapter 4), the year 2005 has to be taken up in the analysis as well. Therefore, SSFes of the years 2005 up to 2009 need to be determined within the framework of this PhD.

However, from 13 November 2007 to the end of 2009 seriously elevated SSC-values (up to values higher than 200g/l) were measured at the location, which pushed the calculations for the SSF for those years to unrealistic heights (see Table 6.6). The potential reasons behind these high values observed in the sediment concentrations, are discussed in detail in Chapter 7.

Table 6.6: Annual suspended sediment fluxes at Aarschot (Demer), Halen (Gete), Lummen (Mangelbeek) sampling locations, based on measurement data (FHR) complemented with rating curve estimates

		% of time data available	partim SSF measured (tonnes)	SSF gap modelled (tonnes)	SSF_total (tonnes)
Aarschot	2005	86	25521	3032	28553
	2006	75	20624	3716	24340
	2007 (including elevated SSC data)	76	700363	8361	708724
	2007 (excluding elevated SSC data)	69	24245	16406	40651
	1-5-2007 to 31-10-2007	79	7406	1255	8661
Halen	1-5-2007 to 31-10-2007	86	4957	668	5624
Lummen	1-5-2007 to 31-10-2007	83	473	133	606

As these extremely high sediment concentrations prove hindering in the validation exercise for the sediment fingerprinting modelling, suspended flux calculations for the Gete, Mangelbeek and Demer were limited to the period May 2007 (the first month the ISCO samplers were fully operational in Halen and Lummen) to October 2007 (data also reported in Table 6.5).

Besides this limited period, annual fluxes for the years 2005, 2006 and 2007 were determined for Aarschot as well. For the year 2007, calculations were executed both including and excluding the elevated November and December 2007 data, showing the serious impact of those few data points.

6.3 Conclusions about determined suspended sediment fluxes and comparison to model results

The suspended sediment fluxes determined at the Grobbendonk location (combining measurement and rating curve estimated data) range from 5,800 to around 15,800 tonnes per year in the period 1999-2009. However, the SSFes are higher in the first four years of record (11,500 – 15,800 tonnes) and then decline from 2003 onwards, stabilising around 6,000 tonnes per year, with a bump around 2007 where 7,900 tonnes was reported.

As expected, the suspended sediment fluxes determined in Aarschot for the period 2005-2007 show higher values than those observed in Grobbendonk, as the Demer catchment (upstream Aarschot) is not only many times larger than its Kleine Nete counterpart (2,163 km² versus 590 km²), it also drains areas more sensitive to physical erosion.

However, a similar rise in SSF can be observed at the Aarschot station, in the year 2007, where the SSF values climb from +/- 25,000 tonnes before 2007 and reaching 40,000 tonnes in 2007 (excluding the unrealistically elevated sediment concentrations observed in November and December 2007).

For the period May-October 2007, the Demer transported almost 8,600 tonnes of sediment of which 65% can be attributed to the Gete. Only 600 tonnes can be attributed to the Mangelbeek, showing clearly that the southern tributaries in the Demer basin (which are draining the erosive hillsides of the Hageland and Haspengouw) contribute much more sediment to the sediment load observed in Aarschot than the northern tributaries (like the Mangelbeek) do.

In Chapter 4 (see Table 4.1), the sediment delivery by water erosion to the Flemish rivers is reported, alongside the total sediment export by the rivers, as modelled by a spatially distributed soil erosion and sediment delivery model (WATEM/SEDEM) for the year 2005 (Overloop et al., 2011). It can clearly be seen that the values reported there differ from the suspended sediment fluxes calculated in this chapter.

Not only are the SSFes of the Demer overestimated by a factor 4, the Nete is highly underestimated. According to the WATEM/SEDEM model the entire Nete only exported 4,500 tonnes in 2005, while the measurements in Grobbendonk (Kleine Nete) already summed up to 5,800 tonnes in that year. The export of the Grote Nete would most likely double that number.

The overestimation of the Demer fluxes cannot be explained by the enlargement of the geographic catchment area from Aarschot to the mouth of the Demer (which would only account for 8%, not 400%), nor can it be explained by the fact that the SSF data obtained through measurements are not yet corrected for cross-sectional variability (as explained in Section 5.1.2), as the samples in Aarschot are taken relatively closely to the riverbed. This would most likely lead to an overestimation of the SSF rather than to underestimation. These differences illustrate the need for

quality sediment concentration and sediment flux data in the Flemish rivers, as modelling is not always capable of producing acceptable estimate values.

7. Impact of human intervention on sediment fluxes and transport regime in the Demer

7.1 Introduction

As already discussed in Chapter 5, discharge peaks do not always coincide with their corresponding sediment concentration peaks; this process is called hysteresis. Clockwise hysteresis generally occurs when the SSC peak precedes the Q peak, while counter-clockwise hysteresis occurs when the SSC peak trails behind the Q peak. Therefore, the time interval (also known as lag-time) between these peaks can be indicative of changes in the transport regime of the river or of new sources contributing to the sediment supply.

Therefore, these temporal relationships between sediment concentration and discharge values as well as sediment concentration variations themselves, are interesting to investigate to regain insight into the river response to change. Hence, this is investigated at the Aarschot sampling location for a seven year period and links with human interventions in the Demer and its tributaries were sought.

The type of human intervention this chapter focuses on is maintenance works such as dredging of the riverbed, or river bank maintenance, as have been briefly addressed in Section 4.3.2.2.4. It is shear impossible to obtain a complete overview of all possible impactful events for a basin heavily subjected to anthropogenic activity, as multiple parties are responsible for the maintenance in different parts of the river system, and communication between the different parties can be spurious.

However, an attempt was made to gather as much information as possible for the Demer basin for the period July 2003 until May 2010. For this period, all maintenance works performed in the Demer basin have been obtained from the river basin manager 'Waterwegen en Zeekanaal NV' (W&Z). The timing and nature of these maintenance works as well as the distance to Aarschot monitoring station is reported in Table 7.1. These works could range from damming of a river arm to work on foundations of an old mill, to cleaning out of drainage pipes to dredging activities. Some of these interventions created an immediate impact on the sediment availability in the river channel. This is also reported in Table 7.1.

7.2 Observations

7.2.1 Dividing of period of record based on variance in sediment concentrations

Discharges and the suspended sediment concentrations obtained from both automatically collected samples (SSC_{ISCO}) and weekly collected surface water grab samples (SSC_{SW}) at the Aarschot sampling location are depicted in Figure 7.1 for the entire period of record. The timing of the most impactful maintenance works is also indicated and each individual sediment peak (SSC_{ISCO}) higher than 3 g/L can be attributed to one of the maintenance works listed in the overview presented in Table 7.1. Furthermore, it is important to note that the automatically collected sediment samples have a very large variability, therefore the SSCs have been plotted on a logarithmic scale.

Table 7.1: Overview of the location, timing, nature and impact on the sediment transport monitored at Aarschot for the different maintenance works (data obtained from W&Z)

nr	Distance upstream from Aarschot sampling station	Period	Time	Nature of maintenance works	Impact
1	13 km	1	17/11/2003-25/11/2003	removal of bridge	Low
2	13 km	1	26/11/2003-30/04/2004	construction of bridge	Low
3	13 km	1	09/12/2003-17/12/2003	work on pillar foundations	Low
4	16 km	1	January 2004	renewal FHR measuring station	Low
5	<1 km	1	November 2004	construction of a wall	Low
6	13 km	1	June 2005	dike reinforcements	Low
7	<1 km	1	July 2005	damming of Demer for mill foundation research	Low
8	<1 km	1	November 2006	pipe placement and removal of valves	Low
9	3.5 km	1	April 2007	bridge restoration	Low
10	<1 km	1	15/06/2007-15/12/2007	construction of pumping station	Low
11	<1 km	1	02/05/2007-04/05/2007	dam construction Demer for restoration of mill foundations	Low
12	<1 km	2	10/11/2007	removal of dam on Demer	High
13	20 km	2	03/03/2008-05/03/2008	sludge removal	Low
14	<1 km	2	07/03/2008-14/03/2008	structural dike works and widening of the river	High
15	<1 km	2	03/04/2008-08/04/2008	structural dike works and widening of the river	High
16	<1 km	2	11/06/2008	cleaning of discharge canals	Low
17	13 km	2	03/11/2008-19/12/2008	repairing water control structure	Low
18	0-15 km	2	26/01/2009-28/01/2009	river bank maintenance	High
19	0-15 km	2	17/02/2009-31/03/2009	river bank maintenance	High
20	0-15 km	2	28/03/2009-30/03/2009	river bank maintenance	High
21	<1 km	3	08/10/2009-09/10/2009	maintenance of shutter weirs	Low
22	<1 km	3	20/03/2010-24/03/2010	maintenance of shutter weirs	Low
23	<1 km	3	09/05/2010-10/05/2010	maintenance of shutter weirs	Low
24	<1 km	3	21/05/2010-27/05/2010	works at lock	Low
25	<1 km	3	August 2009-December 2010	construction of a walkway with remodelling of the winter bed profile of the river	Low-medium
25.1			August 2009-October 2009	deconstruction of old quay – construction of new quay	Medium
25.2			05/01/2010	deconstruction of old quay – construction of new quay	Medium
25.3			09/02/2010-10/02/2010	removal gabions	Low
25.4			March 2010-April 2010	cementing the river bank	Low
25.5			May 2010	removal gabions	Medium

Based on the change in variability of SSC_{ISCO}, a tentative division of the entire measurement period in three separate periods is suggested. During Period 1, which runs from the beginning of the period of record until 9 November 2007, the highest SSC_{ISCO} values observed range around 1-1.5 g/L. This is up to two orders of magnitude smaller than the highest SSC_{ISCO} values observed in Period 2 (from 10 November 2007 until 31 March 2009), which range from 11 to 270 g/L. However, from April 2009 onwards (Period 3), these extremely high sediment loads are no longer observed and in this period the highest SSC_{ISCO} values drop to ca. 1-3.5 g/L. The periods have also been indicated on Figure 7.1.

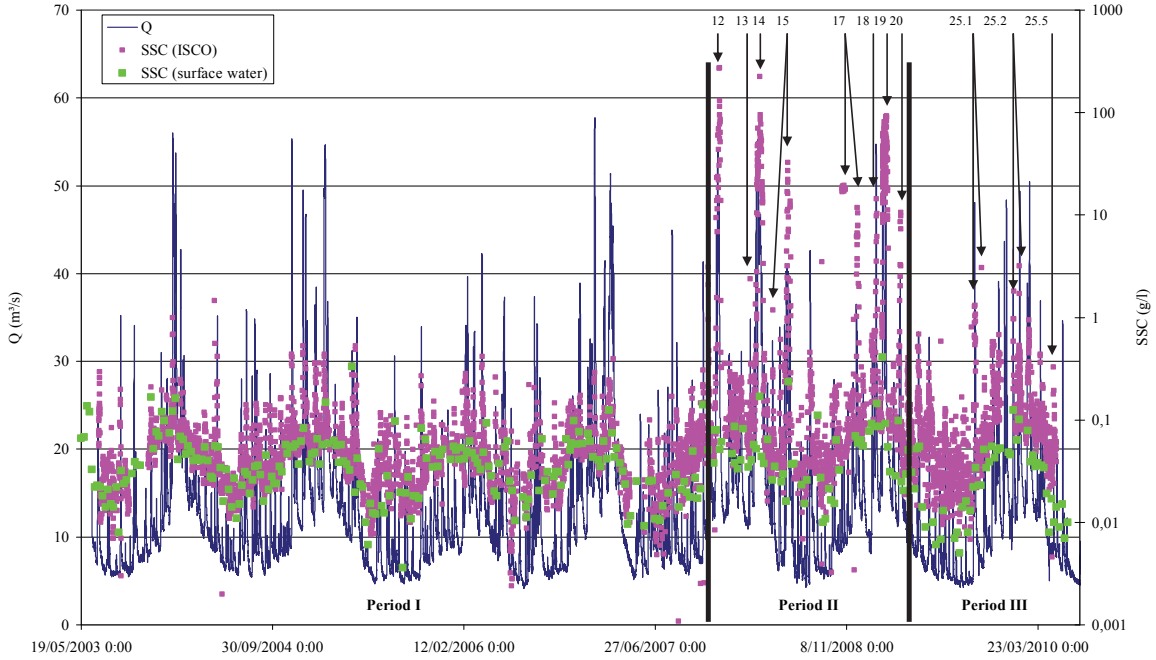

Figure 7.1: Q, SSCs from the automatically collected samples (SSC_{ISCO}) and SSCs from the weekly collected surface water dip samples (SSC_{SW}) from July 2003 until May 2010. Also indicated is the timing of the most impactful maintenance works (see Table 7.1 for the codification of the timing).

It is important to note that the SSC_{SW} samples do not show the same changes in variance between the three periods as could be observed in the automatically collected water samples. Hence, the subsequent study of the relationships between SSC and Q focuses mainly on the SSC_{ISCO} values.

7.2.2 Lag-time and hysteresis effects for SSC_{ISCO}

In the Demer at the Aarschot monitoring station, hysteresis and other phenomena can be observed. To get a first indication of what type of hysteresis is prevalent in the Demer basin, the lag-time between SSC and Q peaks is investigated. Figure 7.2 shows the lag-time (measured in hours) observed in the automatically collected ISCO-samples. Negative values observed in this graph indicate that the SSC peak actually preceded the Q peak. When interpreting this data however, one has to take into account that discharge measurements are available every 15 minutes, whereas sediment samples have only been automatically collected every seven hours. Therefore, the exact timing of the sediment peak is subjected to a larger uncertainty than the timing of the Q peak. This is presented in Figure 7.2 by the error bars. The length of the lower and upper whiskers is determined by the amount of hours between the moment of the highest sediment concentration measured and the respectively preceding or subsequent sampling time. In most cases both whiskers have a length of 7 hours.

Some descriptive statistics concerning the lag-time recorded in the three periods proposed in Section 7.2.1 are reported in Table 7.2, which shows the lag-time values present in Period 1 have a smaller variance than those in Period 2, and that the lag-times in Period 3 plot in between the variances of Periods 1 and 2. Furthermore, the three periods differ significantly from one another (T-test assuming unequal variances with a significance level α of 0.05). The statistical data are represented in Table 7.3.

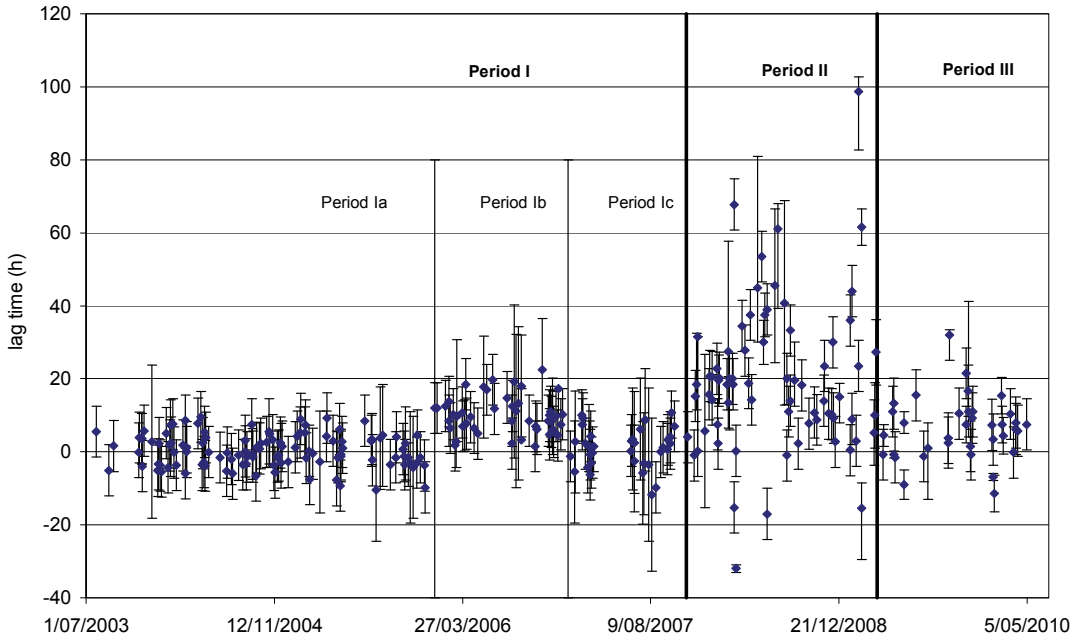

Figure 7.2: Time (in hours) that the sediment peak (observed in the automatically collected ISCO-samples) lags behind its corresponding discharge peak

Table 7.2: Descriptive statistics of the lag-time observed between Q and SSC_{ISCO} peaks observed in the three periods (and sub-periods)

Period	Mean (h)	Variance (h)	Min (h)	Max (h)
1	2.9	39.4	-11.8	22.5
2	23.2	341.5	-32.0	98.8
3	6.9	67.5	-11.3	32.0
1a	0.4	19.7	-10.5	9.6
1b	10.0	25.3	1.5	22.5
1c	1.0	27.9	-11.8	10.7

Table 7.3: Results of various t-Tests (Two-Sample Assuming Unequal Variances) between lag-time data from the different periods and sub-periods

	t Stat	P(T<=t) two-sided	t Critical two-sided
Periods 1-2	8.49	<0.001	2.00
Periods 1-3	2.65	0.012	2.02
Periods 2-3	5.94	<0.001	1.99
Periods 1a-1b	11.59	<0.001	1.99
Periods 1a-1c	0.67	0.51	2.01
Periods 1b-1c	7.92	<0.001	1.99

Looking more closely at Period 1, it can clearly be observed that the lag-times of the year 2006, indicated as Period 1b in Figure 7.2 and Tables 7.2 and 7.3, differ significantly from the other lag-times within that period. The period preceding 2006 and the period following 2006 (respectively called Period 1a and 1c) do not significantly differ from one another.

Additionally, it can be observed that in Periods 1a and 1c the moments of maximal discharge and sediment concentration tend to coincide (see Table 7.2), whereas in Period 1b, sediment peaks lagged on average 10 hours behind their corresponding discharge peaks.

Period 2 on the other hand is characterized by elevated lag-times (averaging around 20 hours) and a very high variance. The sediment peaks in this period lag up to 99 hours behind their respective discharge peaks, but can also precede them up to 32 hours.

Finally, Period 3 resembles a mixture of the two previous periods, with a considerable variance and an average lag-time of 7 hours.

However, even when the exact peak moments of respectively discharge and sediment concentration coincide, hysteresis can still be present due to a difference in skewness in the sediment and discharge peaks, as explained in Chapter 5 (see Table 5.1) and illustrated in Figure 5.1. Therefore, for each period, the monitored hydrologic events were plotted and their hysteresis classes were determined according to the guidelines presented in Table 5.1. These data, presented in Table 7.4 show that in Periods 1b, 2 and 3 counter-clockwise hysteresis prevails, whereas in Periods 1a and 1c clockwise hysteresis is present in more than 50% of the cases, but other classes are also represented.

Table 7.4: Number of observations of monitored hydrologic events in specific hysteresis classes and their respective percentages (at Aarschot monitoring location for the three different periods)

	Period 1a		Period 1b		Period 1c		Period 2		Period 3	
	observations	%	observations	%	observations	%	observations	%	observations	%
single-line value	10	24	0	0	1	6	0	0	1	5
clockwise	27	66	3	10	10	56	5	9	2	10
counterclockwise	13	32	28	90	6	33	51	91	17	85
single line + loop	1	2	0	0	0	0	0	0	0	0
Figure Eight	0	0	0	0	2	11	0	0	1	5
Sum	41	100	31	100	18	100	56	100	20	100

7.2.3 Double sedimentary response for SSC_{ISCO}

During Periods 2 and 3, it could be observed that under certain conditions, a discharge event has two sediment concentration peaks in its close vicinity: the first one coincides with the discharge peak itself, or with its rising limb (the coinciding sediment peak), while the second one lags behind the discharge peak (the trailing sediment peak).

An example of such a double sedimentary response is presented in Figure 7.3 that displays the data from the detailed sampling campaign of February-March 2009, when the ISCO-sampler was programmed to sample every hour. In that period two discharge events were observed; the first (Q_1) peaked on 11 February 2009 at 54.9 m³/s and the second (Q_2) peaked seven days later at 50.2 m³/s. Both of these discharge values belong to the highest 1% percentile of discharges recorded at the Aarschot measuring station since the beginning of the recording (1975). On the one hand, each discharge event has a sediment peak coinciding with it, while on the other hand, each Q event is also characterized by a trailing sediment peak, which lags 99 hours (first event) and 61.5 hours (second event) behind their respective discharge peaks.

In Periods 2 and 3, this phenomenon of double sediment peaks can almost exclusively be observed during high discharge conditions (above 30 m³/s). In about 40% of the situations where the discharge peak is higher than 30 m³/s the river system reacts with a double sedimentary response. Furthermore, the river system produces such a double sedimentary response in about 70% of the cases where high discharge conditions are combined with significant (more than 20 hours lag-time) counter-clockwise hysteresis. In discharge events without significant lag-time difference logically only one sediment peak can be observed, coinciding with its discharge peak.

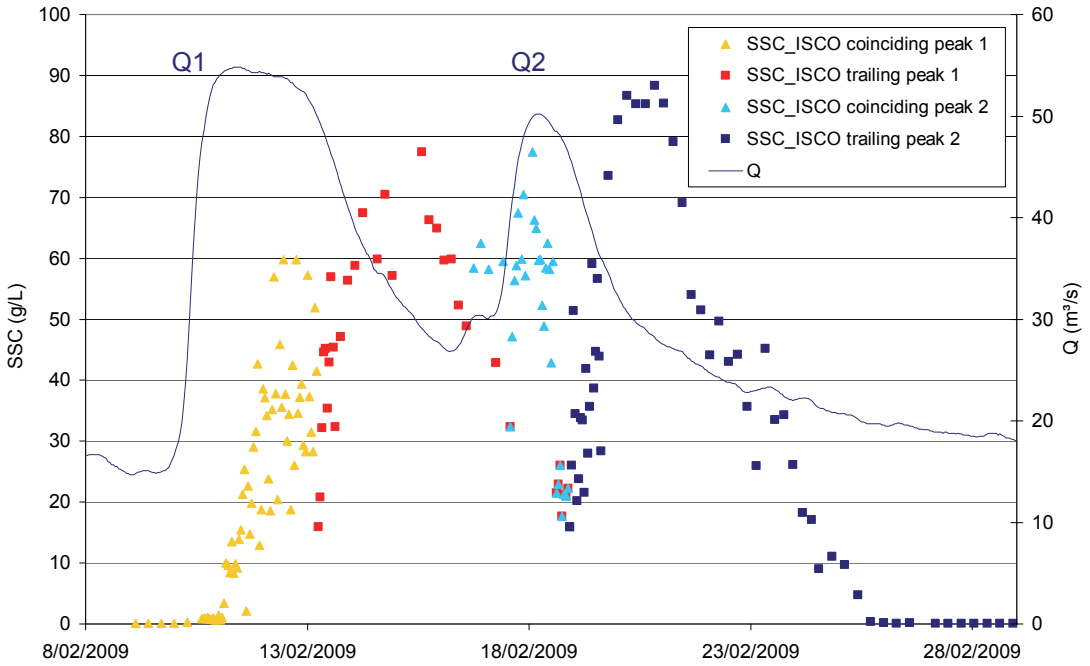

Figure 7.3: Q and SSCs from the automatically collected samples (SSC_{ISCO}) from the detailed sampling campaign from 8/2/2009 until 3/3/2009. Each of the two discharge peaks (Q1 and Q2) have a coinciding and a trailing sediment peak associated with them

Figure 7.4 shows the maximal SSCs plotted in function of the maximal measured Qs for each event. The data points have been divided in summer data (from 1 May until 31 October) and winter data (from 1 November until 30 April). Confidence intervals of 90% have been plotted for both data sets. Importantly, when medium to high discharge peaks (>30 m³/s) were preceded by another elevated discharge peak less than a week prior, some of the sediment peaks of the second event appear as outliers. Therefore these 'secondary peaks' have been separately plotted.

For Period 1, presented in Figure 7.4a, it can be seen that during summer similar discharge values lead to slightly lower sediment concentration responses, but that the 90% confidence bands of summer and winter data overlap mostly. Furthermore it can be observed that secondary peaks plot in the lower half or below the 90% confidence bands.

In Period 2, a significant different relation between sediment concentration peak values and discharge values between summer and winter data can be observed, as can be seen in Figure 7.4b. This is most apparent for higher discharge values and secondary peak data. The latter values plot for both summer and winter clearly above their respective 90% confidence bands.

In Period 3, the summer and winter relations between peak sediment concentrations and discharges coincide again (see Figure 7.4c). During the summer period, however, the data points are significantly more scattered, as can be seen in the width of the 90% confidence bands. As the conditions during Period 3 were not very favourable for creating secondary peaks, only one was observed, during winter conditions which plotted below the 90% confidence bands.

To conclude, the data of Period 3 are presented in comparison to their respective counterparts of Periods 1 and 2 in Figure 7.5a (winter) and 7.5b (summer). In those figures it can clearly be observed that the winter data of Period 3 plot in between the relations of Period 1 and 2 and that the summer data of Period 3 plot above those of Periods 1 and 2.

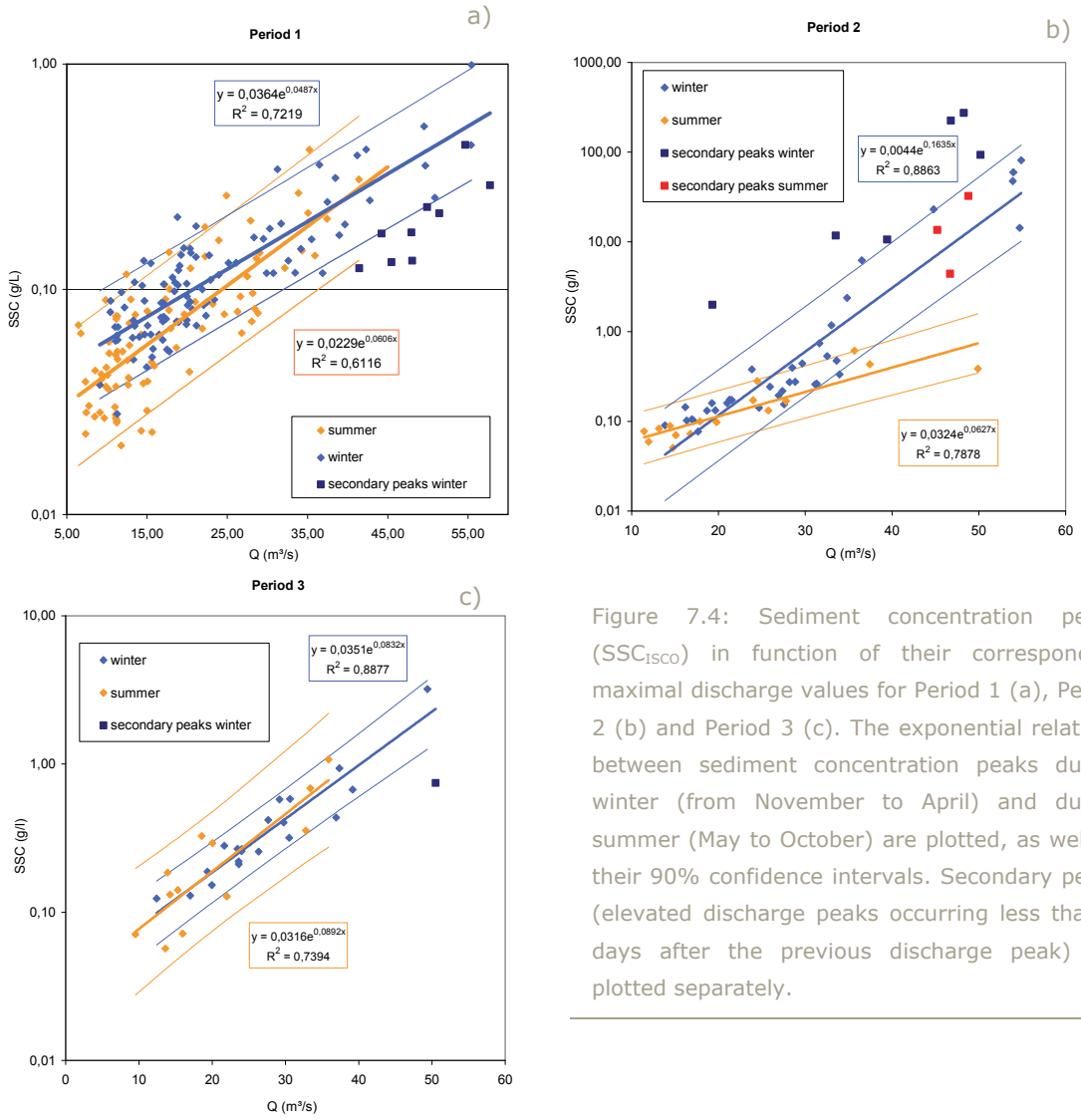

Figure 7.4: Sediment concentration peaks (SSC_{ISCO}) in function of their corresponding maximal discharge values for Period 1 (a), Period 2 (b) and Period 3 (c). The exponential relations between sediment concentration peaks during winter (from November to April) and during summer (May to October) are plotted, as well as their 90% confidence intervals. Secondary peaks (elevated discharge peaks occurring less than 7 days after the previous discharge peak) are plotted separately.

7.3 Interpretations and discussion

7.3.1 Period 1 (May 2003 – November 2007)

Peak sediment concentration values from the automatically collected samples (SSC_{ISCO}) varied in between 30 mg/l and 1.5 g/l. Although, as can be seen in Figure 7.4a, the river system seemed to react with slightly lower sediment concentrations during summer in low-flow conditions, the confidence intervals of the summer and winter data mostly overlap. Therefore, it is reasonable to conclude that only one (exponential) relationship exists between sediment concentrations and discharge during Period 1.

Furthermore, it can also be observed in Figure 7.4a that secondary peaks would not always follow the regression established for the primary peaks. This suggests that a 'history effect' takes place, where the antecedent event has an effect on the subsequent event. Kleinhans et al. (2007) discuss such a 'history effect', where sediment sorting created in antecedent discharge waves may be preserved to some extent and may thus influence sediment transport in the next discharge wave, causing hysteresis. In this study however, an impact on the actual sediment concentration transported is observed. During Period 1, the sediment concentration of secondary peaks either fell in the lower regions of the 90% confidence interval of the regression curve or plotted below it (as

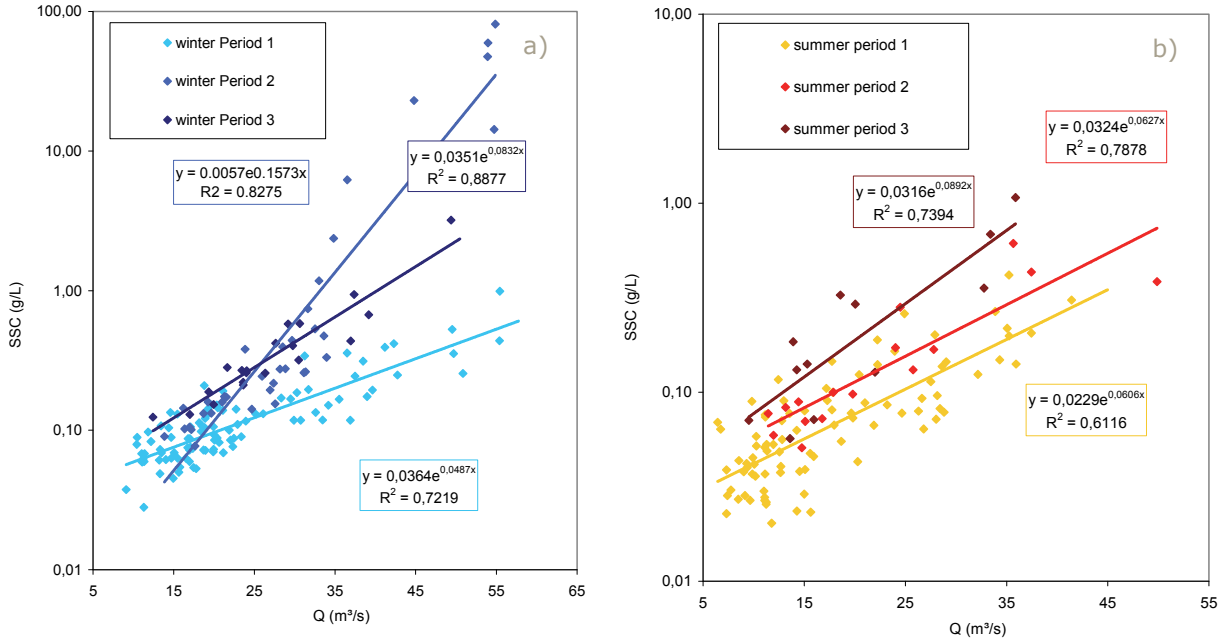

Figure 7.5: The relations between sediment concentration peaks (SSCISCO) and their corresponding maximal discharge values for Periods 1, 2 and 3, during summer (a) and during winter (b). secondary peaks have been omitted.

can be seen in Figure 7.4a), which leads to the hypothesis that the Demer basin during Period 1 had a somewhat restricted sediment supply. Consequently, during high-flow events most of the available sediment would be washed away, causing a drop in sediment load during the subsequent discharge event.

This hypothesis is confirmed by the sense of hysteresis loops. During Periods 1a and 1c more than half of the discharge events fall within the hysteresis class 2 (i.e. clockwise hysteresis), which is generally interpreted as caused by a river system in which sediment deposited in the channel will be brought into transport with a decreasing availability during the event (e.g. Lenzi & Marchi, 2000; Steegen et al., 2000; Jansson, 2002). Also single-valued line events are observed in these two periods, indicating unrestricted sediment supply in the river system.

Period 1b, however, is characterized by counter-clockwise hysteresis loops. This, according to the literature should indicate that more distant sediment sources such as hill slope soil erosion or the upstream channel are contributing sediment (Brasington & Richards, 2000; Lenzi & Marchi, 2000; Goodwin et al., 2003; Orwin & Smart, 2004; Salant et al., 2008), or that the sediments come from processes with slow dynamics such as bank collapsing after sufficient saturation of the bank material (Williams, 1989; Lefrançois et al., 2007). As no information concerning maintenance works or land use changes were available for the upstream sections of the tributaries of the Demer basin, these hypotheses cannot be confirmed, but it is reasonable to assume either maintenance works or a temporary additional sediment supply in a tributary of the Demer were responsible for the delay in the arrival of sediment peaks, while not increasing the total SSC-values observed.

7.3.2 Period 2 (November 2007 – March 2009)

During Period 2 the sediment dynamics of the river system changed significantly. This can be derived not only by the significant increase in maximal SSC_{ISCO} values observed in Period 2 compared to Period 1 (indicating the introduction of new sediment sources into the river system), but can also be noticed in the ratio between peak SSC_{ISCO} and peak Q values. Not only do the slopes of the relationships of winter and summer data differ (see Figure 7.4b), unlike the single relationship observed during Period 1, but both relationships plot higher than their counterparts

from Period 1 (see Figures 7.5a and b), albeit more clearly during high discharges appearing under winter conditions.

The river system also reacts differently during secondary peak events. SSC_{ISCO} values were remarkably higher than the regression predictions (see Figure 7.5), contrary to the observations during Period 1. This seems to suggest that the Demer basin has been replenished and moved from a somewhat sediment-depleted river system in Period 1 to a sediment-enriched river system in Period 2. When in such an enriched system two high-discharge events occur with little time in between, the first event will cause sediment to be stirred up of which part would be transported and part would be readily available for transport by the next event, causing a higher sediment peak, even though the actual second discharge peak might be lower. An example of this river system behaviour can be observed in Figure 7.3. This sort of 'replenishment' behaviour was also observed by Salant et al. (2008) and they suggested rapid input of sediment supply such as bank destabilisation and bank failure as an explanation.

The cause of the replenishment of the river system in the Demer basin can be found in the impactful maintenance works taking place in Period 2. These interventions are responsible for a rapid input of sediment supply, and some of these works include river bank maintenance, which could lead to bank failure. However, as most of these works were located relatively close to the measuring station and the sediment was readily available in the channel, hysteresis loops of the single-valued line class would be expected to appear, as in the literature (Williams, 1989; Wood, 1977; Jansson, 2002) this hysteresis class is associated with unrestricted mobilisation and transport of particles. However, during Period 2 mainly counter-clockwise hysteresis was observed (see Table 7.4). In the literature (Klein, 1984; Williams, 1989; Lenzi & Marchi, 2000; Fang et al., 2008) the counter-clockwise class is explained as the result of any of at least four causes: 1) particles originate from distant sources and reach the channel by the effect of soil erosion on hillsides or in the headwater of the catchment; 2) seasonal variability of rainfall distribution and sediment production; 3) sediment input is caused by processes with slow dynamics such as bank collapse; and 4) relative travel times of the flood wave and the sediment flux.

In case of the Demer basin the first two explanations are not applicable as the sediments made available by the maintenance works are located in the river channel, relatively close to the sampling station and the counter-clockwise hysteresis is found throughout winter and summer periods alike. A slow process such as river bank failure after river bank saturation could potentially explain the double sedimentary responses observed at the beginning of 2009, as river bank maintenance was executed in the Demer basin (from close to the Aarschot measurement location to 15 km upstream of it). However, the material was readily available on these river banks and for the other maintenance works, which also produced double sedimentary responses, the dynamics of sediment input should be considered fast as those types of maintenance works left the sediment readily available in the river channel at a close distance to the measurement location. Therefore only one possible explanation for the counter-clockwise hysteresis remains: the sediment is being transported at a velocity slower than the travel velocity of the discharge wave.

In general (Heidel, 1956; Williams, 1989; Brasington & Richards, 2000; Eder et al., 2010) it is considered that the bulk of the suspended sediment is transported at mean flow velocity, which is significantly lower than the flood wave celerity. The further away the source is located from the sampling station, the more this effect will become apparent. In the Demer basin, however, the sources of sediment originating from the maintenance works are located close by, yet the amount of time the sediment peak lags behind the discharge peaks can be considerable (up to 96 hours).

Therefore, it is proposed here that the sediment observed in the ISCO-samples is travelling at a velocity lower than the mean stream velocity and is therefore being transported through saltation or bed transport processes rather than through suspension.

This interpretation can be further underpinned by the fact that the nozzle of the automatic ISCO-sampler was located relatively close to the bottom (+/- 15 cm above the riverbed) on a river bank which was stabilized with rock rubble for bridge stability, through which the cross-section remains stable. Also giving weight to the interpretation is the fact that no increase in sediment concentration could be observed in the superficial water samples (see Figure 7.1).

The fact that the sediment observed in the ISCO-samples is indeed bed load material, rather than suspended sediment could also explain why a single discharge event can result in two observed sediment responses. Such a double sedimentary response is rarely reported in the literature. Only Salant et al. (2008) reported such an occurrence. They observed a sediment and discharge peak, which coincided, followed by a sudden increase in SSC during low discharges on the falling limb of a hydrograph. Their interpretation of this rare phenomena was that a rapid input of sediment supply occurred, such as bank destabilisation and failure as an explanation. In the Aarschot measuring station however, during Periods 2 and 3 these double sedimentary responses are not rare, but are observed during almost half of the high-flow events, indicating that a simple bank collapse cannot be the root cause of these observations.

Possibly, the theory that bed load material is being observed could help explain these observed double sedimentary responses. As the transport velocity of bed load is significantly lower than the average stream velocity, this might explain the late arrival of the second sediment peak. The coinciding sediment peak, might simply be caused by the arrival of resuspended material, which originated from the maintenance work locations close-by, and which reached the measuring station during the rising limb or the peak moment of the hydrograph, while the trailing sediment peak was constituted of bed sediment which arrived through saltation, rolling and other bed load transport processes.

The hypothesis that bed load might play a significant part in the sediment concentrations observed at the Aarschot sampling location seems to be further confirmed by the similar shape of the discharge and trailing sediment peak. The secondary peak (caused by bank failure) reported by Salant et al. (2008) had a distinctly different shape, with a long tail of elevated sediment concentrations. At the Aarschot location however, when these trailing peaks, which have a counter-clockwise hysteresis due to their late arrival because of their slow saltation velocity, are plotted on top of their corresponding Q peaks, the hysteresis disappears and a single-valued line appears, which shows the resemblance in shape of the peaks and is in effect the expected river system reaction if the sediment would have been transport at average stream velocity. This is illustrated in Figure 7.6, where the SSC_{ISCO}-values of the trailing sediment peak of events Q1 and Q2 (previously shown in Figure 7.3) are plotted against Q-values both without and with a time shift. This seems to confirm that only a lowered sediment transport velocity is in play, but that in effect the river system is reacting as described in the literature (Wood, 1977; Williams, 1989; Lenzi & Marchi, 2000; Jansson, 2002; Hudson, 2003; Lefrançois et al. 2007).

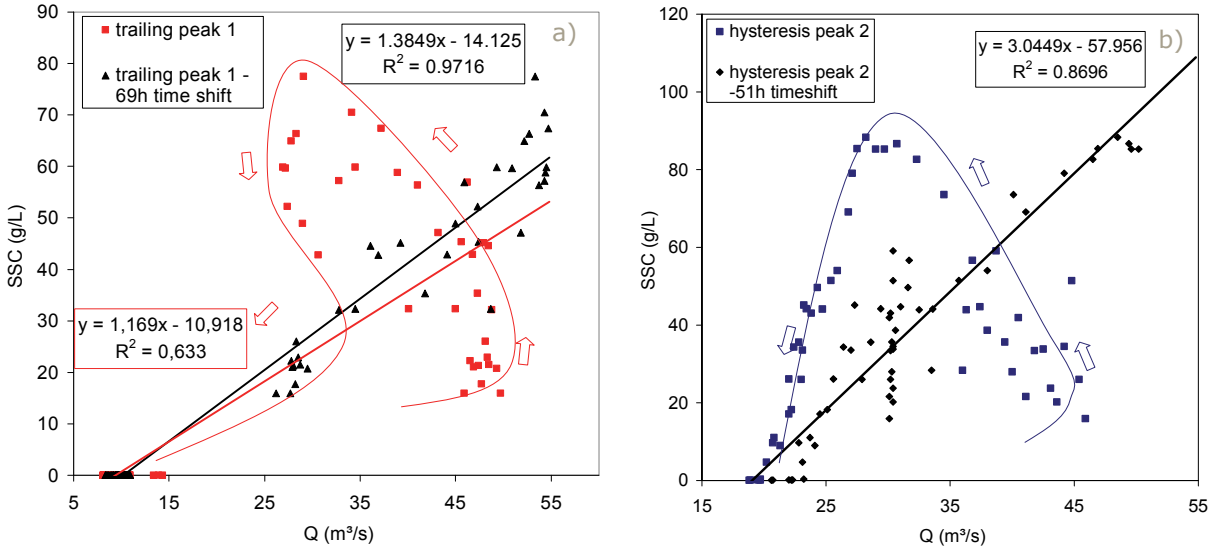

Figure 7.6: SSC_{ISCO} plotted in function of Q: counter-clockwise hysteresis loop and time-shifted relationship for trailing sediment peak for event Q1 (a) and event Q2 (b) (as defined in Figure 7.3)

7.3.3 Period 3 (April 2009 – May 2010)

Period 3 is characterized by some minor maintenance works and one big construction work, entailing the remodelling of the winter bed profile of the Demer only 250 m upstream of the Aarschot sampling station, that took place during most of Period 3 in different intervals. As the winter of 2009-2010 was quite severe, the works had to be halted then, and most work was performed during the summer months.

Therefore, the interpretation of Period 3 is that the river system is trying to return to its original, slightly sediment-depleted state, but is being resupplied on and off, mostly during summer periods.

This hypothesis is confirmed by the observations of SSC_{ISCO} values. The peak SSC_{ISCO} values are distinctly lower than those observed in Period 2 but still slightly elevated in comparison to Period 1. Also, the relationship between peak sediment concentrations and peak discharge values during winter, as can be observed in Figure 7.5a, plots in between these of Period 1 and 2. During the summer months of Period 3 however, the observed peak sediment concentrations were more elevated than those observed under similar discharge conditions in Period 1 and 2 (Figure 7.5b). This indicates that during these months, when flow conditions are generally not very favourable for transporting high concentrations of sediment, some of the sediment made readily available by the construction works, was transported downstream.

During Period 3, the system returned to a single relationship between peak SSC and peak Q values, which is still slightly elevated in comparison to the levels of Period 1 as can be seen in Figure 7.4c. This seems to confirm that the river system is in the process of returning to its initial (sediment-deprived) state. Furthermore, the sole secondary peak observed in Period 3 plotted below the 90% confidence bands, which indicates that at that moment, during winter conditions, the river system was sediment-depleted.

The hysteresis patterns observed during Period 3 are clearly still counter-clockwise dominated (see Table 7.4). This proves that even though the river system is starting to become sediment-deprived again, sediments provided by the construction works seem to have been transported via bed load, hence their relatively late arrival at the measuring station only 250 m downstream.

7.4 Conclusions

During the period of record, the Demer basin was observed at the Aarschot sampling station while the river system underwent some significant changes concerning sediment supply. The basin went from an originally slightly sediment-depleted system (Period 1) to a sediment-enriched system (Period 2) and is from Period 3 onwards gradually returning to its original state. The cause of the changes could be identified as the implementation of individual maintenance works, although not all alterations have the same impact. Additionally, gathering all the information concerning maintenance works is not an easy feat, and information concerning maintenance works in non-navigable rivers was more difficult to obtain than information concerning the navigable part of the Demer. This is due to the fact that these sections of the rivers are managed by different river basin managers.

Maintenance works involving disturbance of the riverbed or river bank material relatively close to the sampling station in Aarschot caused a significant increase in the sediment concentrations measured in the Aarschot sampling station, while maintenance works further upstream, and with less perturbation of soil and riverbed seemed to influence the sediment load far less.

As a result of these works, sediment became readily available in the channel and was transported at the time of the works or at the time of the next elevated discharge event. The differences between SSC_{ISCO} and SSC_{SW}, on the one hand and the shape of the hysteresis on the other hand, lead to the hypothesis that the excess sediment is transported as bed load, rather than as suspended load.

This could potentially explain why during Periods 2 and 3, frequently two sediment peaks arrived induced by a single discharge peak. This phenomenon, rarely observed in the literature, was quite common during the periods of sediment enrichment in the Demer basin. The initial peak could be the suspension transport of sediment readily available on the riverbed, leading to clockwise hysteresis or single line responses. The second peak (the trailing peak) on the other hand could be the sediment being transported as bed load and arriving later as this material is being transported at a lower velocity than the suspended material.

While maintenance works seem to have a clear influence on the river dynamics, it becomes evident that not the whole cross-section is affected equally. The surface water samples do not seem to be affected as much as samples taken closer to the riverbed. A full determination of the cross-section at the time of a particularly high SSC_{ISCO}-value would be needed to determine the full implications on the total sediment flux. However, due to the large lag-times it is difficult to predict when such a trailing peak would arrive.

When studying the alterations of the river dynamics, which appear to be reversible, as in time and with fewer disturbances the system seems to return to its original state, generally accepted approaches such as investigating variances of sediment concentrations and classifying the temporal relations between sediment and discharge peaks in their respective hysteresis classes were used. However, another easy and simple indicator for changes in the river system is the lag-time between the moment of discharge peaks and their corresponding sediment peaks. This technique is as effective and less complex than using the hysteresis classes to help separate periods with different river system dynamics.

Furthermore, secondary sediment peaks, defined as sediment peaks associated with medium to high discharge peaks (>30m³/s in case of the measurement station in Aarschot) preceded by another elevated discharge peak less than a week prior, can be used to assess the state of sediment depletion or sediment enrichment of a river system.

Part IV

Authigenic sediment

8. Budgeting the contribution of authigenic sediment to the total suspended sediment load

In this chapter an attempt is made to determine the contribution of authigenic sediment to the total sediment load of the Kleine Nete catchment, upstream the Grobbendonk monitoring station (see Figure 1.3 for the exact location). In Section 8.1, the contribution of the authigenic sediment to the total load is theoretically deduced, while in Section 8.2 the contribution is being modelled. Part of the research described in the sections below has already been presented at multiple symposia, and reported in Vanlierde et al. (2005 a, 2005 b, 2006, 2007 a and 2007 b).

8.1 Calculating the contribution of authigenic sediment fluxes to the total sediment load by theoretical deduction

Determining the contribution of groundwater-derived authigenic material to the total suspended sediment flux requires a variety of hydrological, mineralogical, and chemical data (shown schematically in Figure 8.1). The SSF has been already determined in Chapter 6. However, in order to estimate the authigenic suspended sediment flux (ASSF), the following additional parameters also need to be estimated: (1) groundwater discharge; (2) groundwater Fe(II) concentrations; (3) the mineralogical composition of the authigenic precipitates (a stoichiometric factor), and (4) the mass of sorbed chemical constituents to the authigenic precipitates (a sorption factor).

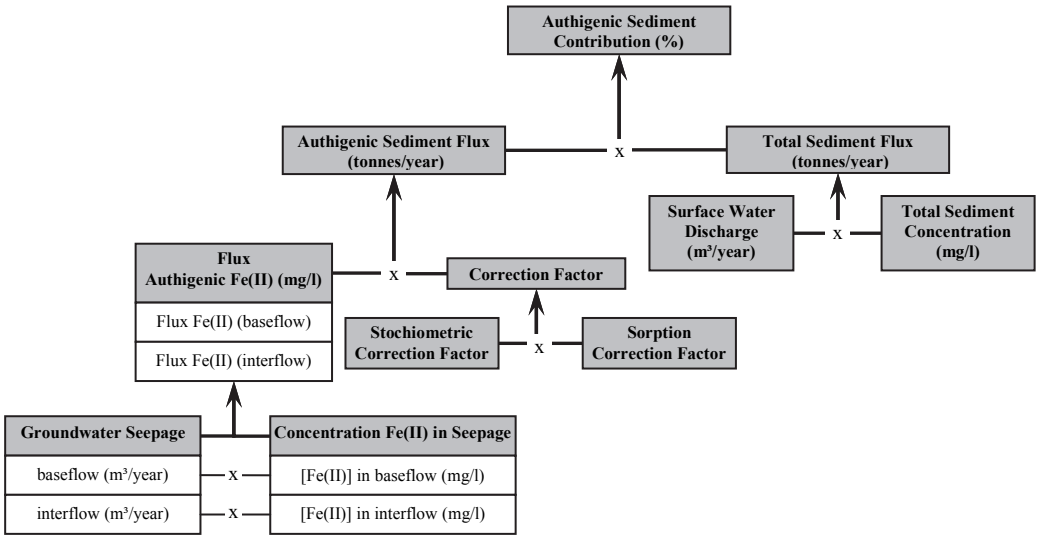

Figure 8.1: Schematic overview of the methodology and correction factors used to calculate the theoretical contribution of authigenic material to the suspended sediment load.

The need for the first two types of data is self-evident, as once they are multiplied, they yield a ferric flux. Mineralogical composition is important because the same amount of Fe(II) can generate different masses of authigenic material, depending on the final mineralogical composition. The sorption factor is impactful because authigenic Fe-oxides have extremely high surface areas capable of concentrating a number of different trace elements (e.g. Cu, Zn, Cd, Pb, Ni) that could increase the mass of the authigenic contribution (Stumm & Morgan, 1970; Horowitz; 1991; Tessier, 1992). The next sections explain in detail how estimates of each of these parameters were obtained.

8.1.1 Determining annual groundwater contribution

The exact contribution of groundwater seepage to the total water discharge is not easy to estimate. For the Kleine Nete, several approaches have yielded a variety of results. Van Der Beken & Huybrechts (1990) estimated that between 1901 and 1986, groundwater contributed on average 62% to surface-water discharge of the Nete basin. Batelaan (2006) compared Sloto & Crouse's (1996) baseflow separation method with Wittenberg's (1999) for different sites, including some in the Nete basin. The method by Sloto & Crouse (1996) yielded baseflow contributions in the Nete basin between 72 and 81% of the total discharge, whereas Wittenberg (1999) placed the contribution of the baseflow between 73 and 84%.

Groundwater contributions can also be separated from the total hydrograph using the WETSPRO tool (Willems, 2000), which divides the measured discharge into a contribution of baseflow, interflow and run-off (as already discussed in Section 6.1.3.1). This procedure was previously calibrated for the Nete basin as part of the project 'Actualisation of the Sigmaplan' (IMDC et al., 2003), where the authors found that during the period 1 February 1999–31 January 2000, the groundwater accounted for about 88% of the total discharge.

In the framework of this PhD thesis, the calibrated WETSPRO procedure was used to expand the existing time series of daily base- and interflow data to include data up to 2009. The average groundwater contributions estimated in this way, surmounted to 85% of the surface water discharge for the period 1999 to 2009. The individual annual contributions of baseflow and interflow, as determined by WETSPRO, are reported in Table 8.1.

Table 8.1: Overview of annual discharge data and discharge-derived data for the period 1999 up to 2005, as well as contribution of groundwater to the total flow

Year	1999	2000	2001	2002	2003	2004	2005	2006	2007	2008	2009	average 1999-2009
Discharge (Mm³)	227	254	281	251	170	196	179	178	220	190	166	210
Baseflow (Mm³)	147	168	180	163	112	127	121	116	143	127	107	137
Interflow (Mm³)	45	49	57	48	32	38	33	35	44	36	33	41
Groundwater contribution (%)	84	85	84	84	85	85	86	85	85	86	85	85

The variability found in the different approaches described above can be explained not only by the different periods considered but also by the fact that the flexibility of the non-linear baseflow separation techniques yields a computed baseflow closer to the total discharge hydrograph than can be achieved with classical linear approaches, as noted by Wittenberg (1999). Nonetheless a consistent result among different analyses is that the contribution of seepage in the Kleine Nete catchment is substantial in relation to the total water discharge, which in turn will lead to a high production of authigenic sediment.

8.1.2 Determining concentrations of Fe(II) in baseflow and interflow

The second parameter that needs to be determined to estimate the contribution of groundwater-derived authigenic material to the total suspended sediment flux, is the average Fe(II)-concentrations entering the river through groundwater seepage. These need to be determined for both baseflow and interflow. As mentioned in Section 4.3.2.3.2., VMM modelled gross emission of specific heavy metals into the surface water, using the EIW model (see Table 4.6). However, VMM did not model the contribution of iron. Therefore, another approach needed to be developed in order to obtain insight into the Fe(II) concentrations in the groundwater feeding the Nete basin. Examination of a number of sources (the Belgian Nuclear Research Centre (Blommaert et al.,

1988)) and databases (Flemish Public water supply society for the Antwerp region (PIDPA), VMM and the Institute of Nature Conservation (INBO)) provided information on the iron content in the groundwater bodies CKS_0200_GWL_1 and CKS_0250_GWL_1 and their respective aquifers (see Section 1.5). These data indicated that concentrations of iron vary over a wide range throughout the region, and even vary quite locally. As a result of this large variation, the input of the Fe(II) concentration will be the largest origin of uncertainty in the calculation of the authigenic contribution to the total sediment flux. Furthermore, it should be remarked that values of total Fe concentration can be used to estimate Fe(II) concentrations because at the reigning pH and redox conditions, all iron present will be in its reduced state. Table 8.2 gives an overview of the observed variability as well as values for pH and redox observed in the individual aquifers.

Table 8.2: Values for redox potential (Eh), pH and concentrations of Fe_{Tot}, (raw data obtained from VMM) in the different groundwater systems present in the Kleine Nete basin (raw data obtained from VMM) as well as values for redox potential (Eh) (raw data obtained from FHR) , pH, concentrations of Fe_{Tot}, and the percentages of Fe_{Tot} and P_{Tot} present in the total suspended sediment (raw data obtained from VMM).

		Surface water	Groundwater					
			CKS_0200_GWL_1				CKS_0250_GWL_	
		Kleine Nete Grobbendonk	Merksplas Brasschaat [0231]	Mol [0232]	Lillo [0233]	Poederlee Kasterlee [0234]	Diest [0252]	Berchem [0254]
Eh (mV)	Min	81	-36	97	121	-2	101	-64
	Max	562	690	580	420	551	280	240
	Median	329	174	354	256.5	260.5	148.5	113
pH	Min	6.30	4.69	5.05	6.37	4.46	5.28	5.48
	Max	8.21	6.21	6.97	7.53	7.39	8.04	7.44
	Median	7.30	5.96	6.54	7.09	5.83	6.26	6.89
$[Fe_{tot}]$ (mg/l)	Min	0.70	0.20	0.00	0.03	0.05	0.05	0.07
	Max	11.40	68.10	10.46	26.04	98.73	148.01	42.80
	Median	4.29	4.77	0.43	2.36	9.10	15.68	1.56
$\frac{[Fe_{Tot}]}{[SSC]}(\%)$	Min	6.45						
	Max	75.20						
	Median	27.07						
$\frac{[P_{Tot}]}{[SSC]}(\%)$	Min	0.81						
	Max	43.33						
	Median	3.60						

To be able to link these aquifer data to baseflow and interflow concentrations, the following approach was used: as the Kleine Nete directly overlies the highly permeable Diest Formation and actually incises it, it is plausible to conclude that groundwater from this formation largely outweighs contributions from other aquifers. Therefore, the Fe(II) concentrations of the Diest Formation [0252] are used as an estimate of the groundwater baseflow contribution. However, as the Fe(II)-concentration data from the formation are highly skewed, the median concentration of the largest data set (obtained from VMM) of 15.7 mg/l was used. Values for Fe(II) concentrations in the interflow were initially estimated to be higher than those in the baseflow due to rainwater infiltration into the phreatic layer. As the overlying soil has little buffering capacity, pHs as low as 4 have been observed; median Fe(II) concentrations ranging from 15 to 25 mg/l have been estimated using data from VLM (1997). In modelling efforts later undertaken (and addressed in Sections 8.2 and 9.4) Fe concentrations equalling those in the baseflow (15 mg/l), or even lower than those present in the baseflow (10 mg/l) were assumed.

8.1.3 Determining the stoichiometric and sorption correction factors

As explained in Section 4.3.2.3.2, the Fe(II) entering the river will become chemically unstable and will oxidize due to changing environmental conditions (pH and redox conditions). However, the mass of authigenic iron compounds generated by the same amount of dissolved Fe(II) can vary significantly, depending on the wide variety of mineralogical forms that can occur in freshwater (Stumm & Morgan, 1970) and the sorption of the precipitate formed. For example, stoichiometrically, 1 g of Fe(II) can form 1.51g of hematite, 1.59 g of lepidocrocite, 1.90 g of ferrihydrite, 3.35 g of strengite, or 3.79 g of mitridatite. Hence, theoretically, the stoichiometric factor (F_{St}) could maximally range from 1.51 to 3.8.

In later stages of this PhD study, more insight was regained into which stoichiometric forms of iron are present in the authigenic sediment (see Chapter 9), but initially a theoretical approach was used. In theory (Stumm & Morgan, 1970) ferric hydroxide ($Fe(OH)_3$) is the direct result of ferrous iron oxidation and precipitation and in time, ferric hydroxide will be mineralized. The principal forms of mineralized ferric iron found in soils are amorphous hydrous ferrihydryte ($Fe(OH)_3$), ferric oxide ($Fe_2O_3 \bullet XH_2O$), maghemite (γ-Fe_2O_3), lepidocrocite (γ-FeOOH), hematite (α-Fe_2O_3), and goethite (α-FeOOH).

Possibly also abundantly present in the Kleine Nete catchment are iron phosphates. Measurements by VMM in the Kleine Nete at Grobbendonk for the period 1999-2004 indicated elevated phosphorus contents in sediments (see Table 8.2). These high phosphate content values measured are caused by intensive agricultural activity as well as by the high population density in the basin. However, Fe concentrations were even more abundantly present, suggesting that the available phosphate is bound to the iron, thus explaining the relative low concentrations of soluble ortho-phosphates in the surface water (respectively <0.3 mg P/l for Kleine Nete as mentioned in AMINAL (2003)). This could lead to an increase of the stoichiometric correction factor toward the upper end of the determined range (around 3.3 to 3.5).

Besides the stoichiometric factor, another correction is needed to calculate the ASSF: the sorption correction factor (F_{So}). Colloidal and flocculated iron compounds will sorb cations, which will add to the mass of the authigenic precipitates. It should be noted that the addition in mass is likely to be substantially smaller than the increase due to stoichiometric factors. As a rule of thumb, Vance (1994) indicates that amorphous hydro-ferric oxide is capable of adsorbing 0.5 mmol of ionic material per gram hydro-ferric oxide. Clarck (2009), however, states that the cation exchange capacity of ferric iron oxyhydroxides (ferrihydrite) is even greater than that of smectite clays, with values often exceeding 5 to 7 mmol/g, in case of neutral to high pH conditions. These pH conditions are actually met in the surface water of the Kleine Nete (see Table 8.2) and therefore substantial sorption could take place. Depending on which ions are being adsorbed and which compound is being formed, the weight of the sediment will increase in mass respectively by 0.1 up to 1 gram per gram sediment. These respective increases correspond with a sorption correction factor (F_{So}) ranging between 1.05 and 2.

To obtain a total correction factor (F_T), both correction factors (F_{So} and F_{St}) must be multiplied. However, to obtain the theoretical interval of F_T, one should take notice that high sorption capability is mostly confined to hydrous ferric oxide, and much less to compounds with higher stoichiometric values, as the former is usually present in colloidal form and therefore has greater specific surface area, leading to a higher sorption coefficient (Stumm & Morgan, 1970; Lijklema, 1979). Therefore, the upper boundary F_T-value of 4.00 is obtained by multiplying the highest F_{St}-value (3.8) with the lowest F_{So}-value (1.05), while the lower boundary value of F_T, 1.57, is obtained by multiplying the lowest F_{St}-value (1.5) also with the lowest F_{So}-value (1.05). It should be noted

that this total correction factor, however, does not include any increase in mass due to microbiological activity.

8.1.4 Calculating the theoretical range of generated authigenic sediment

To procure the broadest theoretical range in annually produced authigenic sediment, the lowest value of total Fe(II) flux (determined in Section 8.1.2) is multiplied with the lowest value of F_T, (as described in Section 8.1.3) and the highest value of total Fe(II) flux is multiplied with the highest value of F_T. Results of this exercise were reported in Vanlierde et al. (2007 a) and are presented in Table 8.3.

Table 8.3: Overview of the measured total SSFes, at Grobbendonk on the Kleine Nete, as well as the theoretically deduced ASSFes and their relative contribution to the total SSF. * The maximum values of authigenic sediment fluxes are higher than the measured SSFes, which leads to values of contribution over 100%. As this is physically impossible, the maximum authigenic contribution is considered to be 100%.

	Measured SSF	ASSF by theoretical deduction			
	Total SSF (ton)	Potential range of ASSF (tonnes)		Potential contribution of ASSF to the total SSF (%)	
		Min	max	min	max
1999	14,775	4,774	13,922	36	100*
2000	11,220	5,440	15,777	46	100*
2001	15,624	5,882	17,223	45	100*
2002	15,482	5,358	15,544	41	100*
2003	7,274	3,643	10,561	41	100*
2004	6,314	4,109	11,968	52	100*
Average	**11,782**	**4,868**	**14,166**	**43**	**100***

Consequently, these ranges in ASSFes have been compared to the actual sediment transport effectively measured on site (for the period 1999-2004) to obtain the widest possible range authigenic material can contribute to the total sediment transport in the Kleine Nete at the Grobbendonk measurement station. These results are also presented in Table 8.3.

It should be noted that the ranges of contribution reported in this table, are calculated based on median values of Fe concentrations in the groundwater. As stated above, a large degree of uncertainty is associated with these values. Therefore, the actual range of potential authigenic contributions to the total sediment load might be even wider than the 43-100% stated above.

8.2 Modelling the contribution of authigenic sediment

8.2.1 MARS model

In the previous section, the contribution of the authigenic sediment to the total load was deduced in a theoretical way. A more refined estimate of the total authigenic contributions to the suspended sediment flux can be obtained using a numerical model. An initial 0D-model was developed by Jan de Schutter (FHR) in a Microsoft Excel environment in which the output is also generated. The model predicts the flux of authigenic sediment, produced by groundwater seepage, while taking into account settling, erosion and accumulation processes, using algorithms to approximate the observed complexity in hydraulic, physical, chemical and biological processes in the river. These

algorithms are empirically derived and optimized by fitting the modelled ASSFes onto the total SSFes.

The first attempt at modelling the contribution of the ASSF to the total load in the Kleine Nete was reported in Vanlierde et al. (2005 a), where it was featured without a name. In the subsequent publications (Vanlierde et al., 2005 b, 2006, 2007 a, 2007 b), the model in its various incarnations, all developed at FHR, would be named Model for Authigenic River Sediment (MARS from now onwards). Below, the different incarnations of the model are described.

8.2.1.1 Initial model (PRE-MARS)

The initial model, developed by Jan De Schutter, which will be called PRE-MARS from now onwards in this thesis, makes use of all the parameters mentioned in Section 8.1. It starts by calculating the daily authigenic sediment flux entering the river through groundwater seepage (ASF_{Seep}) by multiplying the daily flux of Fe^{2+} entering the river with factors accounting for stoichiometric and sorption corrections, as explained in Section 8.1. Mathematically this is expressed in Equation 8.1.

$$ASF_{Seep} = \left[\left(Q_{Bf} \cdot Fe(II)_{Bf}\right) + \left(Q_{If} \cdot Fe(II)_{If}\right)\right] \cdot F_T \qquad \text{Eq. 8.1}$$

in which:
- ASF_{Seep} is the authigenic sediment flux entering the river through groundwater seepage
- Q_{Bf} is the Baseflow; that is the groundwater flow in the saturated zone, contributing to the total water discharge
- Q_{If} is the Interflow; that is the groundwater flow in the unsaturated zone, contributing to the total water discharge
- $Fe(II)_{Bf}$ is the Fe(II) concentration present in the baseflow
- $Fe(II)_{If}$ is the Fe(II) concentration present in the interflow
- F_T is the total correction factor

The model uses two additional separate algorithms to approximate the observed sediment transport patterns in the river. A first algorithm, the suspension algorithm, determines the percentage of authigenic suspended sediment delivered by groundwater (ASF_{Seep}) that will remain in suspension during low-flow conditions (ASF_{Sus}), as flocculation, presence of rooted water plants and other factors will influence the settling behaviour of the freshly-formed authigenic sediment. It also determines how much of the ASF_{Seep} will settle (ASF_{Set}). These fluxes (ASF_{Sus} and ASF_{Set}) are calculated as stated in Equations 8.2 and 8.3. In PRE-MARS a specific breakpoint discharge (Q_{Br}) is defined above which physical remobilisation appears to occur. The actual value was determined by examining the SSFes as a function of the discharge at the Grobbendonk monitoring site (see Figure 8.2). The sediment fluxes start to increase from discharge values higher than 10.6 m^3/s, which is consequently used as Q_{Br}.

It is clear from these mathematical notations that no sediment will settle on the riverbed when the reigning discharge surpasses the Q_{Br}-value.

$$ASF_{Sus} = ASF_{Seep} \cdot F_{Sus} \qquad \text{Eq. 8.2}$$

$$with: \quad F_{Sus} = a \cdot e^{kQ} \quad for \quad Q \le Q_{Br}$$
$$F_{Sus} = 1 \quad for \quad Q > Q_{Br}$$

and

$$ASF_{Set} = ASF_{Seep} - ASF_{Sus}$$ Eq. 8.3

in which:
- ASF_{Sus} is the part of the ASF_{Seep} that remains in suspension
- ASF_{Set} is part of the ASF_{Seep} that will settle on the riverbed
- F_{Sus} is the suspension correction factor
- Q_{Br} is the breakpoint discharge above which physical remobilisation occurs
- Coefficients a and k are dimensionless constants

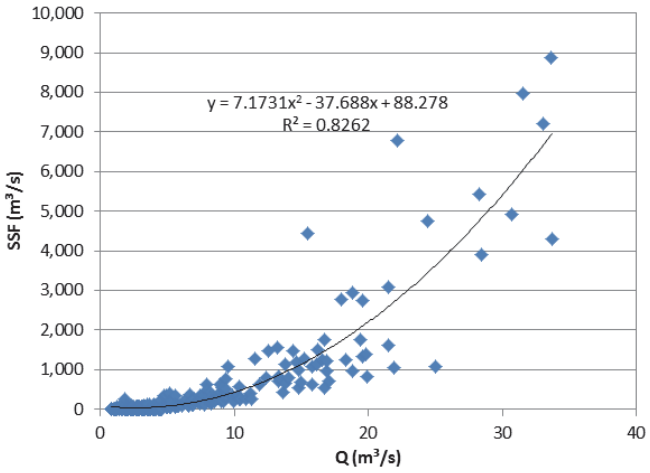

Figure 8.2: The break point for physical remobilisation of suspended sediment determined by examining the SSC as a function of discharge at Grobbendonk (Kleine Nete)

The second algorithm models the resuspension of already settled sediment. This resuspension algorithm determines how much of the accumulated settled authigenic material ($ASF_{Set,Acc}$) can be resuspended, given sufficient flow conditions, based on the amount of accumulated sediment, as expressed in Equation 8.4. Obviously, during low-flow conditions, when discharge values are below the Q_{Br}, no resuspension will take place.

The total accumulated authigenic sediment available ($ASF_{Set,acc}$) tallies the amount of sediment which accumulates during low-flow conditions and resuspends during high-flow conditions. This is mathematically written in Equation 8.5.

$$ASF_{Resus} = F_{Resus} \cdot ASF_{Set,Acc}$$ Eq. 8.4

$$with: \quad F_{Resus} = b \cdot e^{lQ} \quad for \quad Q > Q_{Br}$$
$$F_{Resus} = 0 \quad for \quad Q \le Q_{Br}$$

in which:
- ASF_{Resus} is the part of the accumulated settled sediment that will resuspend
- F_{Resus} is the dimensionless fraction of authigenic settled sediment which is being (eroded and) resuspended
- $ASF_{Set,Acc}$ is the settled authigenic material accumulated on the riverbed
- Coefficients b and l are dimensionless constants

$$ASF_{Set,Acc} = \sum_{i=0}^{t-1} ASF_{Set} - \sum_{i=0}^{t-1} ASF_{Resus} + ASF_{Set}$$ Eq. 8.5

in which: t = time stap for which $ASF_{Set,Acc}$ is calculated

Finally, the PRE-MARS model calculates the total authigenic suspended sediment flux (ASSF) as a sum of what remains in suspension during low-flow conditions and what will be remobilized during high-flow conditions, as expressed in Equation 8.6.

$$ASSF = ASF_{Sus} + ASF_{Resus}$$ Eq. 8.6

In both algorithms the coefficients and the constants were obtained by fitting the ASSF to the observed total SSF. Table 8.4 shows the final input values as they were used in Vanlierde et al. (2005 a), while Table 8.5 shows the modelled authigenic contribution to the total suspended sediment flux observed at Grobbendonk measurement station. As such, Table 8.5 gathers the summarized data of the model results presented in the published articles by Vanlierde et al. (2005 a, 2007 a, 2007 b).

Table 8.4: Overview of the values of the different parameters used in the various incarnations of the MARS-models and as (*) published in Vanlierde et al. (2005 a); (•) published in Vanlierde et al. (2007 a); (◇) published in Vanlierde et al. (2007 b); (Δ) model run using F_T 2.85 (see Section 9.4)

Parameter name	Values PRE-MARS (*)	Values MARS 1.0 (•)	Values MARS 2.0 (◊)	Values MARS 2.0 (Δ)
Fe_{Bf} (mg/l)	15.68	15	15.68	15.68
Fe_{If} (mg/l)	25	15	10	10
F_{St} (-)	/	2.99	2.05	1.90
F_{So} (-)	/	1.34	1.07	1.50
F_T (-)	3.6	4.00	2.19	2.85
a (-)	0.1229	1.0569	2.6741	2.6741
k (-)	0.1824	0.0729	0.1093	0.1093
b (-)	0.0002	0.5683	1.0162	1.0162
l (-)	0.4162	0.0006	0.0014	0.0014
c (-)	/	0.3638	0.0151	0.0151
m (-)	/	0.0006	0.1733	0.1733
$ASF^{max}_{Set,Acc,1}$ (Mtonne)	/	/	20	20
$ASF^{max}_{Set,Acc,2}$ (Mtonne)	/	/	224	224

Table 8.5: The contribution of the authigenic suspended sediment flux to the total SSF observed at Grobbendonk measurement station as modelled by PRE-MARS (Vanlierde et al. (2005 a), MARS 1.0 (Vanlierde et al. (2007 a) and MARS 2.0 Vanlierde et al. (2007 b) for various time periods.

		PRE-MARS	MARS 1.0	MARS 2.0
	SSF	$\frac{ASSF}{SSF}\cdot 100$ (%)	$\frac{ASSF}{SSF}\cdot 100$ (%)	$\frac{ASSF}{SSF}\cdot 100$ (%)
Feb 1999-Jan 2000	13,400	70	/	/
1999	14,775	/	68	57
2000	11,220	/	96	58
2001	15,624	/	91	64
2002	15,482	/	75	58
2003	7,274	/	58	66
2004	6,314	/	62	76
2005	5,748	/	/	68
Average	**10,829**	**70**	**75**	**64**

8.2.1.2 MARS 1.0

MARS 1.0 was developed to take the consolidation process, which influences the resuspension of deposited sediment into account. Additionally, the correction factors were extended as well.

As MARS 1.0 was developed from the PRE-MARS model, it shares some algorithms with its predecessor. MARS 1.0 also starts by calculating the daily authigenic sediment flux entering the river through groundwater seepage (ASF_{Seep}) by multiplying the daily flux of Fe^{2+} entering the river with factors accounting for stoichiometric and sorption corrections, as explained in Section 8.1. The correction factors could be separately put into MARS 1.0. Mathematically, this is expressed in Equation 8.7, which closely resembles Equation 8.1:

$$ASF_{Seep} = \left[\left(Q_{Bf}\cdot Fe(II)_{Bf}\right)+\left(Q_{If}\cdot Fe(II)_{If}\right)\right]\cdot F_{St}\cdot F_{So} \qquad \text{Eq. 8.7}$$

Next, MARS 1.0 uses three separate algorithms to approximate the observed sediment transport patterns in the river, instead of the two used in PRE-MARS. The first algorithm, the settling algorithm, is the counterpart of the suspension algorithm used in PRE-MARS. Instead of determining the percentage of ASF_{Seep} that will remain in suspension, this algorithm calculates the fraction that will settle on the riverbed due to several factors influencing the settling behaviour of sediment, mainly discharge, as is expressed in Equation 8.8. Derived from it in Equation 8.9 is the percentage of ASF_{Seep} which will remain in suspension.

$$ASF_{Sus} = ASF_{Seep} \cdot \left[1 - F_{Set}\right] \qquad \text{Eq. 8.8}$$

$$with: \quad F_{Set} = a \cdot e^{-kQ}$$

and

$$ASF_{Sus} = ASF_{Seep} - ASF_{Set} \qquad \text{Eq. 8.9}$$

in which:
- F_{Set} is the settling correction factor
- coefficients a and k are dimensionless constants

It should be noted that MARS 1.0 no longer uses a breakpoint discharge to determine if material will settle rather than resuspend. However, in the MARS 1.0 algorithms that govern settling and suspension, Q remains a determining factor.

The second algorithm models the effect of consolidation processes and the residence time on the settled sediment. The longer sediment remains on the riverbed, the more it will consolidate, which will, in turn, demand higher flow conditions for remobilisation. The consolidation algorithm expressed in Equation 8.10 has an exponential form, which is derived from the exponential functions describing the consolidation process (De Smedt et al., 1989). It determines how much of the settled authigenic material can be resuspended, based on the amount of accumulated sediment, given the presence of sufficient flow conditions (as addressed in Equation 8.11).

$$F_{Cons} = b \cdot e^{-l \cdot ASF_{Set}} \qquad \text{Eq. 8.10}$$

in which:
- F_{Cons} is the correction factor that represents the fraction of accumulated authigenic sediment that can be resuspended
- coefficients b and l are dimensionless constants

The third algorithm is expressed in Equation 8.11 and models the discharge-dependent erodibility of the river. Again, it takes the form of an exponential function of the measured discharge, which is consistent with the observed exponential relation between water discharge and sediment flux at the Grobbendonk site.

$$F_{Er} = c \cdot e^{mQ} \qquad \text{Eq. 8.11}$$

$$with: \quad if \quad F_{Er} > 1 \quad then \quad F_{Er} = 1$$

in which:
- F_{Er} is the dimensionless fraction of authigenic settled sediment which is being resuspended due to the erodibility of the riverbed
- coefficients c and m are dimensionless constants

The overall 'resuspension algorithm', which is a combination of the two previous algorithms (as can be seen in Equation 8.12), provides the fraction of available settled and accumulated authigenic sediment that could be eroded and resuspended.

$$F_{Resus} = F_{Er} \cdot F_{Cons}$$ Eq. 8.12

The actual flux of resuspended authigenic sediment (ASF_{Resus}) is obtained in the same way as in PRE-MARS, (Equation 8.4), by multiplying the resuspended fraction (F_{Resus}) by the total accumulated authigenic sediment available ($ASF_{Set,acc}$). However, there are no discharge restrictions in the calculation of F_{Resus} as were present in PRE-MARS. $ASF_{Set,Acc}$ is also modelled in a similar fashion as in PRE-MARS, but instead of using sums of accumulated and resuspended material, MARS 1.0 is programmed to 'remember' the storage content, and therefore the formula takes the expression in Equation 8.13.

$$ASF_{Set,Acc} = ASF_{Set,Acc,t-1} - ASF_{Resus,t-1} + ASF_{Set}$$ Eq. 8.13

in which: t = timestap for which $ASF_{Set,Acc}$ is modelled

Finally, MARS 1.0 calculates the total ASSF identically to PRE-MARS as stated in Equation 8.6, i.e. by addition of ASF_{Sus} and ASF_{Resus}.

In all three algorithms the coefficients and constants were obtained by fitting the ASSF to the observed total suspended sediment flux. Table 8.4 reports the final input values as they were used in Vanlierde et al. (2007 a), while Table 8.5 presents the modelled authigenic contribution to the total suspended sediment flux observed at Grobbendonk measurement station.

8.2.1.3 MARS 2.0

MARS 2.0 was a further development from the MARS 1.0 model and shares its main basic structure, but it incorporates in addition the idea that not all settled material has the same erodibility. Freshly settled material, for example, is easily resuspendable. However, it will cause the previously deposited material to become more consolidated, and therefore less easy to resuspend. Hence, a set of three separate 'reservoirs' dividing the available $ASF_{Set,Acc}$ was introduced in MARS 2.0. When the first reservoir, which contains the easiest resuspendable material, is completely filled, reaching its maximum value at $ASF^{max}_{Set,Acc,1}$, the $ASF_{Set,Acc}$ in excess will overflow into the second reservoir, and when this one is filled as well (reaching its maximum value $ASF^{max}_{Set,Acc,2}$), the amount of settling material in excess will start to fill the third and last reservoir. This least resuspendable reservoir does not have a specified maximum.

Due to the presence of the reservoirs, ASF_{Resus} in MARS 2.0 is calculated differently from MARS 1.0. First of all ASF_{Resus} is now the sum of the three fluxes, each originating in their own reservoir ($ASF_{Resus,n}$) as shown in Equation 8.14. And while the calculation of each respective $ASF_{Resus,n}$ still resembles Equation 8.4 in MARS 1.0, as the multiplication of the total accumulated authigenic sediment available in the respective reservoir ($ASF_{Set,acc,n}$) by the respective resuspension factor ($F_{Resus,n}$), both parameters are calculated slightly differently.

$$ASF_{Resus} = \sum_{n=1}^{3} ASF_{Resus,n} = \sum_{n=1}^{3} \left(F_{Resus,n} \cdot ASF_{Set,Acc,n} \right)$$ Eq. 8.14

in which:
- $ASF_{Resus,n}$ is the resuspended ASSF originating from reservoir n
- $F_{Resus,n}$ is the fraction of accumumlated ASSF that is being resuspended from reservoir n
- $ASF_{Set,Acc,n}$ is the settled authigenic material accumulated on the riverbed in reservoir n
- n is the number of the settling reservoir, which can be 1, 2 or3

The available sediment in each reservoir $ASF_{Set,Acc,n}$ depends on the available total accumulated material $ASF_{Set,Acc}$ (which is still calculated as in MARS 1.0, as can be seen in Equation 8.13).

Equations 8.15, 8.16 and 8.17 show how the $ASF_{Set,Acc,n}$ will depend, for each respective reservoir, on the available $ASF_{Set,Acc}$.

$$If \quad ASF_{Set,Acc} > ASF^{max}_{Set,Acc,2} \quad then \quad \begin{aligned} ASF_{Set,Acc,1} &= ASF^{max}_{Set,Acc,1} \\ ASF_{Set,Acc,2} &= ASF^{max}_{Set,Acc,2} \\ ASF_{Set,Acc,3} &= ASF_{Set,Acc} - ASF^{max}_{Set,Acc,1} - ASF^{max}_{Set,Acc,2} \end{aligned} \qquad \text{Eq. 8.15}$$

$$If \quad ASF^{max}_{Set,Acc,1} < ASF_{Set,Acc} < ASF^{max}_{Set,Acc,2} \quad then \quad \begin{aligned} ASF_{Set,Acc,1} &= ASF^{max}_{Set,Acc,1} \\ ASF_{Set,Acc,2} &= ASF_{Set,Acc} - ASF^{max}_{Set,Acc,1} \\ ASF_{Set,Acc,3} &= 0 \end{aligned} \qquad \text{Eq. 8.16}$$

$$If \quad ASF_{Set,Acc} < ASF^{max}_{Set,Acc,1} \quad then \quad \begin{aligned} ASF_{Set,Acc,1} &= ASF_{Set,Acc,1} - ASF_{Set,Acc} \\ ASF_{Set,Acc,2} &= 0 \\ ASF_{Set,Acc,3} &= 0 \end{aligned} \qquad \text{Eq. 8.17}$$

in which: $ASF^{max}_{Set,Acc,n}$ is the maximum of accumulated ASF that reservoir n can hold

However, MARS 2.0 allows for an initial input value for $ASF_{Set,Acc}$, allowing reservoir 3 to never be emptied. This ensures that in practice MARS 2.0 always runs under the constraints provided by Equation 8.15.

The resuspension factor for each individual reservoir ($F_{Resus,n}$) is calculated in MARS 2.0 based on MARS 1.0's Equation 8.12, but the consolidation factor is different for each reservoir ($F_{Cons,n}$) as is noted in Equation 8.18.

$$F_{Resus,n} = F_{Er} \cdot F_{Cons,n} \qquad \text{Eq. 8.18}$$

in which: $F_{Cons,n}$ is the fraction accumulated ASSF that is being resuspended from reservoir n

$F_{Cons,n}$ is calculated the same way as its counterpart F_{Cons} in Equation 8.10 in MARS 1.0, using an exponential function, but the calculation of the available settled flux differs due to the division of $ASF_{Set,Acc}$ in three different reservoirs. Therefore the calculation of $F_{Cons,n}$ is expressed as stated in Equation 8.19.

$$F_{Cons,n} = b \cdot e^{l \cdot \sum_{i=1}^{n} ASF_{Set,Acc,n}} \qquad with: \quad F_{Cons,n} = 0 \quad for \quad \sum_{i=1}^{n} ASF_{Set,Acc,n} = 0 \qquad \text{Eq. 8.19}$$

Finally, MARS 2.0, as both PRE-MARS and MARS 1.0, calculates the total authigenic suspended sediment flux (ASSF) as stated in Equation 8.6, i.e. by addition of ASF_{Sus} (Equation 8.8) and ASF_{Resus} (Equation 8.14).

In all algorithms the coefficients and constants were obtained by fitting the ASSF to the observed total suspended sediment flux. Table 8.4 shows the final input values as they were used in Vanlierde et al. (2007 b), while Table 8.5 shows the modelled authigenic contribution to the total suspended sediment flux observed at Grobbendonk measurement station.

Additionally, one more observation can be made. In Table 8.5 it can be seen that the total SSF drops significantly: from 11,000 to 15,000 tonnes per year from 1999 up to 2002, to around half of that (+/- 6,000 tonnes/year) and decreases even further in the consequent years. This can be explained by the fact that during relative dry summers (such as the summer of 2003), the sediment is left to accumulate (and consolidate) on the riverbed, and moreover, it gives water plants a chance to grow and to retain some of the sediment as well. Normally, during high discharge events, the following winter this material will be brought back in suspension. This process is visualized in Figure 8.3, which shows the total mass of authigenic material accumulated on the riverbed for the period 1999 – 2005 at Grobbendonk measurement station, modeled by MARS 2.0. The year 2001 for instance was a very wet year, with some elevated winter events, causing a significant resuspension of sediment (giving rise to an annual SSF of 15,000 tonnes) and leaving a net loss in the accumulated sediment in the system.

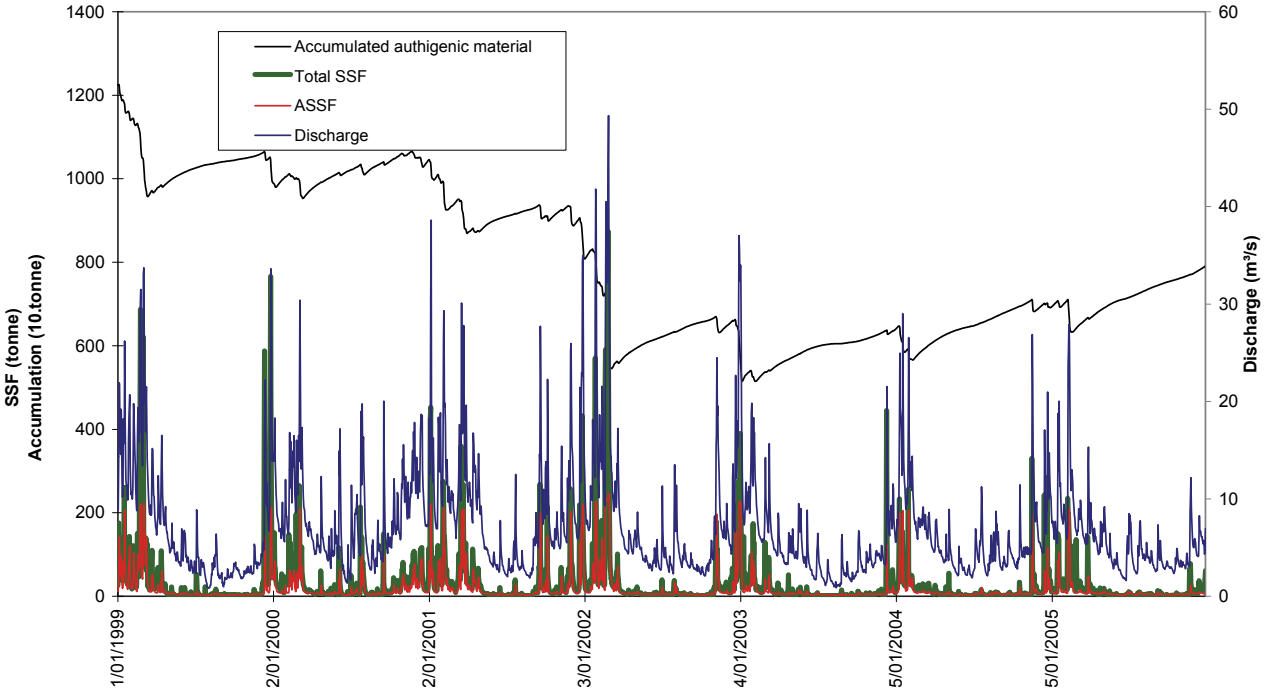

Figure 8.3: Q, ASSF, total SSF and total mass of authigenic material accumulated on the riverbed for the period 1999 – 2005 at Grobbendonk measurement station

The year 2003, on the other hand, was a much drier year, leading to a net accumulation on the riverbed, even after the winter's events have passed. Figure 8.3 also shows that even though discharges increased once more in the subsequent years, the net annual accumulation continues. This seems to suggest that the consolidation and retention processes demand higher discharge events to resuspend material which has been deposited for longer time periods.

8.3 Conclusion

Theoretical deductions of how much the authigenic sediment can potentially contribute to the total sediment fluxes observed at Grobbendonk measurement station provide estimates between between 43 and 100% contribution. This quite large range is caused by the uncertainty of some of the input parameters used, like noted before (in section 8.1.2) the largest uncertainty is associated with the input value for the Fe(II) concentration in groundwater.

However, the MARS model can give a more precise estimate. This model, in its different incarnations, places the average annual contribution of authigenic sediment to the total sediment flux at Grobbendonk between 65 and 75%.

To obtain these results, various factors had to be estimated and assumptions had to be made and put into the MARS-model:

- Groundwater contributions was obtained through WETSPRO numerical filtering. On average the groundwater contributed 85% for the decade 1999-2009;
- Fe(II) concentration present in the groundwater was estimated using a variety of groundwater data. Because of the large variability in the data, the median value of the Formation of Diest [0252] (15.7 mg/l) was entered into the modelling;
- Assumptions about the erosion and resuspension algorithms.

The MARS-model gives also an explanation for the decrease of total suspended sediment flux observed from 2003 onwards. This decrease is most likely due to consolidation and sediment retention on the riverbed, caused by relative drier years (years with lower total annual discharge). Since 2003, the flow conditions have not been sufficiently high to resuspend all of the previously accumulated bed material. Even for years with higher annual discharges than 2003 (such as 2004 and 2005) this did not lead to an increase in total observed SSFes, suggesting that the discharge peaks required to resuspend material which has been deposited longer, need to be more elevated. This aspect will be further explored in Chapter 9.

A model such as MARS cannot readily be validated, as it is necessary to determine the contributions of authigenic sediment during different flow conditions and it is difficult to differentiate between authigenic and non-authigenic material in a sample at the Grobbendonk location.

It is not without challenge to obtain insight into the composition and shape of the flocculated sediment, partly authigenic in nature. The additional research into this authigenic material, present in the Nete and northern part of Demer basin, is addressed in detail in Chapter 9.

9. Exploring the nature of authigenic sediment

The MARS-model was created to calculate the contributions of authigenic sediment to the total suspended sediment flux observed in the river system. However, some assumptions about the composition and nature of the authigenic sediment were made in Chapter 8. To reduce the uncertainties associated with those assumptions, some more research into the shape and size of the authigenic material as well as into the composition was executed.

In Section 9.1 the shape and size of the material is discussed. These will have an impact on the settling velocity and hence, settling tests were executed, which are addressed in Section 9.2. Additionally, the chemical composition of the suspended sediment is more elaborately investigated in Section 9.3.

To conclude, the insights obtained from this research are implemented in the MARS-model and in this form the model was used to calculate one decade's worth of authigenic contribution to the total suspended sediment flux in the Kleine Nete in Grobbendonk.

9.1 Investigating shape and size of the authigenic material and the impact on the settling velocity

The ferric authigenic material, due to the way it is generated and its composition, is prone to flocculation. This process is defined by Guy (1970) as the attraction between primary particles upon collision in a water suspension with a low electrokinetic potential. Most such floccules are unstable and break up in other suspensions that lack the required flocculating agent.

Furthermore, flocculation is a function of biological agents (e.g. bacteria and polysaccharides etc.), organic material, clay minerals, meteorological factors (e.g. rainfall related water discharge), hydrological conditions (e.g. turbulence, tide) and chemical components (e.g. complex iron-oxides and -hydroxides) (Van Leussen, 1994; Droppo et al., 1997; Droppo et al., 2000; Mikes et al., 2004; Govoreanu, 2004; Nopens, 2005; Chen et al., 2005).

Therefore, to gain a better insight into the structure and shape of the ferric flocs and how they are distributed in the cross-section, a detailed set of extra sampling campaigns was launched in 2006 (as was discussed in Sections 2.2 and 3.2.1). The results will be discussed in Sections 9.1.1 and 9.1.2.

Additionally, one of the driving factors behind the MARS-model is the assumption that the authigenically created sediment will remain in suspension as long as the stream flow is sufficiently elevated. MARS 2.0 also takes into account that the sediment will resuspend after deposition, and this is put into the model as a function of the available stream flow and the time the sediment has been left on the riverbed. However, as the authigenic material created in the Nete basin is highly flocculated, this will have a direct effect on the settling velocity (Li & Ganczarczyk, 1987; Droppo et al., 2005) and the resuspension potential.

Therefore, natural water settling tests have been executed and discussed in Section 9.1.3 to gain some insight into the behaviour of suspended sediment enriched in authigenic material.

9.1.1 Particle size analysis at Grobbendonk monitoring location

The initial sampling campaigns in March and May 2006 (as reported in Belien (2006) and Belien et al. (2006) focused on the vertical variability of floc size in the cross-section of the Grobbendonk sampling site (for the exact locations of the sampling points in the cross-section see Figure 2.9). As the sample preparation and microscopic analysis procedures were still being researched at the time, the results that could be drawn from the statistical analysis of the microscopic images were preliminary and held many recommendations for the following sample campaigns.

One of these recommendations was that the signal-noise ratio needed to be as high as possible, so that afterwards, all particles smaller than a certain cut-off boundary size could be eliminated prior to statistical analysis.

Belien (2006) eliminated all records that had a major ax length shorter than 13.97 µm or a minor ax length shorter than 8.90 µm. These lower boundaries for cut-off originated from a previous (unpublished) sample campaign at FHR's Grobbendonk measurement location, executed in collaboration with Prof. Dr. ir. Margaret Chen (VUB) using an in-situ floc sampler[2].

Even though the results of the image analyses of the March 2006 campaigns were preliminary, they confirmed that the material transported in suspension in the Kleine Nete is highly flocculated in nature.

Furthermore, the flocs have dimensions that significantly vary (T-test assuming equal variances with a significance level of α=0.05) in function of water depth. Close to the water surface, the flocs are large, while at around 60% of the total water depth, flocs are significantly smaller, the largest flocs were observed close to the riverbed (see Tables 9.1 and 9.2). This variability in floc sizes is most readily visible in the maximal floc sizes, but can also visually be observed as is shown in Figure 9.1.

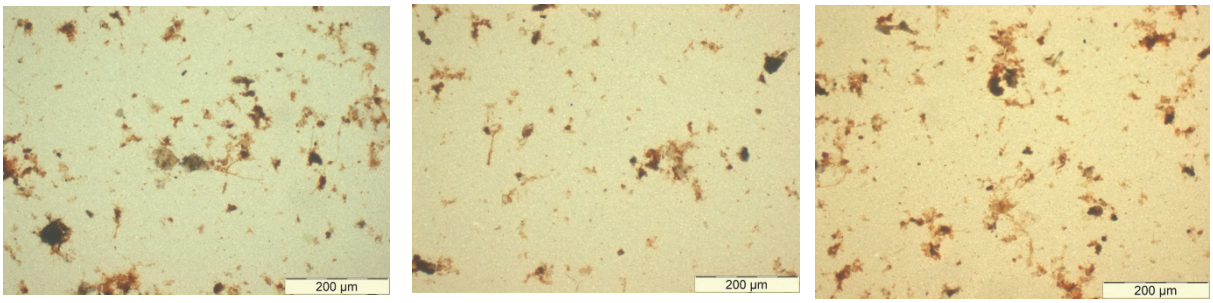

V9 034 V9 102 V9 165

Figure 9.1: Microscopic images of flocs on different depths of vertical 9 sampled on 7 March 2006 at Grobbendonk sampling location. (V9 034) 19% water depth; (V9 102) 58% water depth; (V9 165) 94% water depth.

Additionally, the largest average floc sizes observed on 9 May 2006 at vertical 9, which was the vertical with the highest average flow velocity) have more than twice the area of those observed on 7 March 2006 at the same vertical. This could be linked to the flow velocity on these verticals at the time: on 9 May the average velocity on vertical 9 was 0.535 m/s, while on 7 March it reached 0.652 m/s. Hence the average observed floc size on a vertical seems to be inversely proportional to the present average flow velocity of that vertical.

[2] patent pending, apparatus invented and built by Prof. Dr. ir. Margaret Chen

Table 9.1: Shape and size characteristics of three sample locations on vertical 9 at the Grobbendonk sampling location, respectively sampled 34 cm (V9 034), 102 cm (V9 102) and 165 cm (V9 165) under the water surface on 7 March 2006. Average, minimum and maximum values have been calculated using the noise cut-off boundary applied in Belien (2006)

	V9 034		V9 102		V9 165	
	average	max	average	max	average	max
Area (µm²)	152	6,759	117	5,430	159	9,358
Perimeter (µm)	69	1,349	64	1,069	69	1,199
Major Axis Length (µm)	17	214	16	139	17	163
Minor Axis Length (µm)	9	68	8	92	9	95
Feret Diameter (µm)	10	93	9	83	10	109
Elongation	2.5	3.1	2.6	1.5	2.6	1.7
Roundness	0.4	0.1	0.4	0.1	0.4	0.1
Compactness	0.7	0.4	0.7	0.6	0.7	0.7

Table 9.2: Shape and size characteristics of four sample locations on vertical 9 at the Grobbendonk sampling, respectively sampled 7 cm (V9 007), 27 cm (V9 027), 81 cm (V9 081) and 131 cm (V9 131) cm under the water surface on 9 May 2006. Average, minimum and maximum values have been calculated using the noise cut-off boundary applied in Belien (2006)

	V9 007		V9 027		V9 081		V9 131	
	average	max	average	max	average	max	average	max
Area (µm²)	500	36,700	529	27,300	371	14,100	533	27,300
Perimeter (µm)	116	1,545	117	958	88	791	117	1,806
Major Axis Length (µm)	31	363	30	250	27	177	31	426
Minor Axis Length (µm)	15	196	16	171	15	140	16	143
Feret Diameter (µm)	19	216	19	186	18	134	19	187
Elongation	2.1	1.9	2.0	1.5	1.8	1.3	2.2	3.0
Roundness	0.4	0.2	0.4	0.4	0.6	0.3	0.4	0.1
Compactness	0.7	0.6	0.7	0.7	0.8	0.8	0.7	0.4

On 7 October 2006 a similar campaign was executed on the Kleine Nete at the Grobbendonk measurement location (see Figure 2.9 for the exact localisation of the samples in the cross-section). The recommendations that were formulated after the previous campaigns were taken into consideration, and data from two sample locations on two different depths on a vertical 5 m from the left bank were analysed and similar conclusions could be drawn.

Again it could be observed that the dimensions of the flocs significantly vary (T-test assuming equal variances with a significance level of $\alpha=0.05$) as a function of water depth. Due to fine clayey and colloidal material colouring the background of the microscopic pictures, it was important to filter out background noise, a necessary step, as was indicated by Belien (2006).

This time, two different approaches were used to eliminate the noise. On the one hand the same approach, used by Belien (2006) and described above was applied (eliminating all records with a major axis length shorter than 13.97 µm or a minor axis length shorter than 8.90 µm). However, this cut-off boundary was considered to be potentially too arbitrary, being based on the observations of only one sampling campaign, and therefore possibly excluding significant data. Hence, another cut-off boundary was selected: all particles with a Feret diameter smaller than or equal to 2 µm were eliminated as noise.

The Feret diameter represents the longest dimension of a particle independent of its angular rotation at the time the image was captured. As such, using this parameter as cut-off boundary

would ensure that only noise generated by the filter paper as well as clayey particles that form no part of a floc would be eliminated. Nevertheless, to make sure mostly noise was eliminated and no significant data was lost, grain size analysis by laser diffraction was executed on the subsamples obtained from the churn sample splitter containing the residual volume of the three replicate samples taken at each sampling location after the 30 ml was filtered. This analysis showed that the <2µm fraction barely represented respectively 0 and 6.33 volume percentage of sample V6.020 and V6.073, ensuring that indeed little to no significant data was lost.

When comparing the results of the parameter analyses with both cut-off boundaries (as is reported in Table 9.3) it is clear that the maximal values remain unchanged. The average values, however, drop significantly when the Feret >2µm is used as the cut-off boundary. This is logical, as many smaller particles are left in the data analysis. Nonetheless, the same trends remain visible: big flocs are present near the surface and near the riverbed. Even though the biggest flocs are observed near the surface, on average the flocs near the riverbed are larger.

Table 9.3: Shape and size characteristics of two sample locations, respectively sampled 20 cm (V6 020) and 73 cm (V6 073) under the water surface on 11 October 2006. Average, minimum and maximum values have been calculated using the noise cut-off boundary (a) applied in Belien (2006) and (b) Feret diameter >2µm.

	V6 020						V6 073					
	average		max		min		average		max		min	
	A	b	a	b	a	b	a	b	a	b	a	b
Area (µm²)	780	75	20,439	20,439	66	3	927	147	11,628	11,628	62	3
Perimeter (µm)	166	28	1,973	1,973	40	5	172	39	1,310	1,310	42	5
Major Axis Length (µm)	40	8	486	486	14	2	43	11	260	260	14	2
Minor Axis Length (µm)	23	4	170	170	9	0	25	6	131	131	9	1
Feret Diameter (µm)	2	6	13	161	1	2	2	8	7	122	1	2
Elongation	0.4	1.9	0.9	62.0	0.0	1.0	0.4	1.8	0.9	51.2	0.1	1.0
Roundness	25.7	0.6	161.3	1.5	9.2	0.0	28.3	0.7	121.7	1.5	8.9	0.0
Compactness	0.7	0.8	0.9	1.3	0.1	0.1	0.7	0.8	1.0	1.2	0.2	0.1

Also when comparing the results from the October 2006 campaign (Table 9.3) with the previous campaigns (Tables 9.1 and 9.2) the hypothesis that the average observed floc size on a vertical is inversely proportional to the present average flow velocity of that vertical seems to be confirmed. The average stream velocity present on vertical 6 on 11 October was 0.25 m/s, which is significantly lower than the average velocities observed during the previous campaigns. The average floc area was once again significantly higher (1.5 times the average floc area of the May 9 2006 sampling and up to 5 times the average floc area observed during the 11 March 06 campaign).

The most likely explanation for these observations is a physical phenomenon. It can be theorised that higher flow velocities lead to larger forces on the flocs, causing them to break up in smaller pieces thus reducing their individual floc size.

9.1.2 Particle size analysis in different streams in the Nete basin

Even though it was the intent to research the variety of floc sizes at different streams in the Nete basin (at the sampling locations described in Section 2.2.1.4 and localized in Figure 2.10) and filter papers were produced, no actual image analysis was executed. After quick inspection of the filter papers the variability was enormous. Some of the sampling locations (like the Slootbeek shown in Figure 9.2a) had interwoven flocs, making it impossible to use the image analysis procedure that was described in the previous section. Other locations, like the Aa (presented in Figure 9.2b) had

little or no flocs present at the time of sampling. Hence, it was decided to only use the chemical data from the sampling campaign executed on 19 March 2006, and to forego on particle size analysis at these locations.

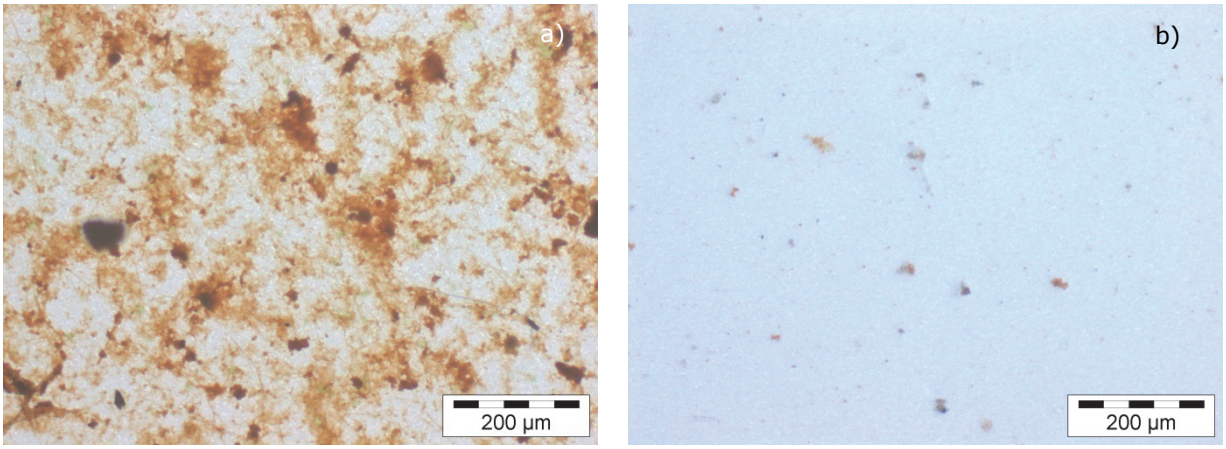

Figure 9.2: Microscopic images of flocs on a filter paper sampled at the Slootbeek (a) and the Aa (b), showing the significant difference in floc appearance.

9.1.3 Settling tests

One of the driving factors behind the MARS-model is the assumption that the authigenically created sediment will remain in suspension as long as the stream flow is sufficiently elevated. MARS 2.0 also takes into account that the sediment will resuspend after deposition, and this is put into the model as a function of the available stream flow and the time the sediment has been left on the riverbed. However, as the authigenic material created in the Nete basin is highly flocculated (as is illustrated in the previous section), this will have a direct effect on the settling velocity (Li & Ganczarczyk, 1987; Droppo et al., 2005) and the resuspension potential.

Therefore, natural water settling tests have been executed to gain some insight into the behaviour of suspended sediment enriched in authigenic material. These settling tests were intended to foremost answer questions linked to the sediment fingerprinting research, addressed in Part V. Therefore, these tests were executed using the settling tube and methodology described in Section 3.2.3 with suspended sediment and natural water collected at Lummen (Mangelbeek), Halen (Gete) and Aarschot (Demer). Of these three locations, the Mangelbeek most closely resembles the conditions encountered in the Kleine Nete, as authigenic sediment is also abundantly present in the Mangelbeek's sediment load.

The fractionation procedure entailed the settling out of sediment particles (or flocs in this case), at different time intervals (reported in Table 3.1). These intervals were selected to differentiate the sediment in subfractions of different particle size, and on the bottom at nine different timings, subsamples were collected and consequently analysed for particle size and composition as described in Section 3.2.3.

Table 9.4: Theoretical grain size ranges of the subsamples determined using Stokes' Law and sample-specific densities

	Mangelbeek		Gete (µm)		Demer (µm)	
	max	min	max	min	max	min
1		165		170		134
2	165	115	170	124	134	108
3	115	96	124	99	108	94
4	96	60	99	62	94	63
5	60	49	62	49	63	54
6	49	30	49	35	54	39
7	30	19	35	19	39	23
8	19	4	19	4	23	5
9	4		4		5	

After these analyses the expected grain size fractionation was re-calculated for each sampling location, still using Stokes' Law, but taking into account the exact sampling time, the density of the material present in the individual subsamples (obtained by analysing the dried material in the pycnometer) and the height of the water column containing the concentrated sediment. Therefore each subsample contains a potential range of grain sizes, reported in Table 9.4.

The settling procedure, however, did not yield the expected separated grain size fractions, as can be seen in Figure 9.3, which shows for the Demer, Gete and Mangelbeek sediment, the percentages of material coarser and finer than 63 µm, as well as the OM percentages associated with these fractions, present in the different subfractions.

According to Stokes' Law, the coarse material (>63 µm) should have settled in the first four subfractions, while the fine material should have arrived from subfraction 5 onwards. These figures clearly show that coarse material is present until the final fractioning and moreover, the fine material is already abundantly present in the first subfractions of the Demer and Gete samples. Even though the dimensional effects of the settling tube and the sampling strategy of the settling tests might partially explain the results deviating from Stokes' Law, these reasons do not explain the arrival of fines in the first fractions. This can only be attributed to flocculation effects.

9.1.4 Conclusion

The different sampling campaigns gave some insight into the shape, size and distributional variability of flocculated sediment present in the Kleine Nete at the Grobbendonk measurement station. Close to the water surface and near the bottom the flocs are large, while in the middle of the vertical flocs are significantly smaller.

Furthermore, the hypothesis that the average observed floc size on a vertical is inversely proportional to the average flow velocity present on that vertical is confirmed by the samples analysed.

The natural water settling tests executed on material of the Demer basin show the significant impact flocculation has on the settling velocity of suspended material. Fine material will deposit more quickly on the riverbed when it is part of a floccule, while coarser particles will remain in suspension longer if they are part of a floccule, due to the buoyancy effect of the floc structure.

Even though these insights into the structure and settling velocity did not yield any practical changes in the input variables and coefficients of the MARS model, it did show that the settling and resuspension algorithms in MARS should be location specific and possibly even time specific. This has not yet been implemented into the MARS model but it is a recommendation to do so in future research.

9.2 Chemical composition of authigenic sediment and its residing water

Besides determining site-specific coefficients for the settling and resuspension algorithms in MARS, the most important variables still under discussion are the stoichiometric and sorption correction factors. Even though theoretical assumptions were incorporated into the models, a better estimation of the mineralogical condition of the iron precipitates and their sorptive power would allow for a smaller uncertainty concerning the quantity of authigenic ferric sediment generated from the influx of Fe(II) from seepage. Below several approaches to gain insight into the chemical composition and into the contribution of the groundwater-delivered iron to the total mass of the sediment are discussed.

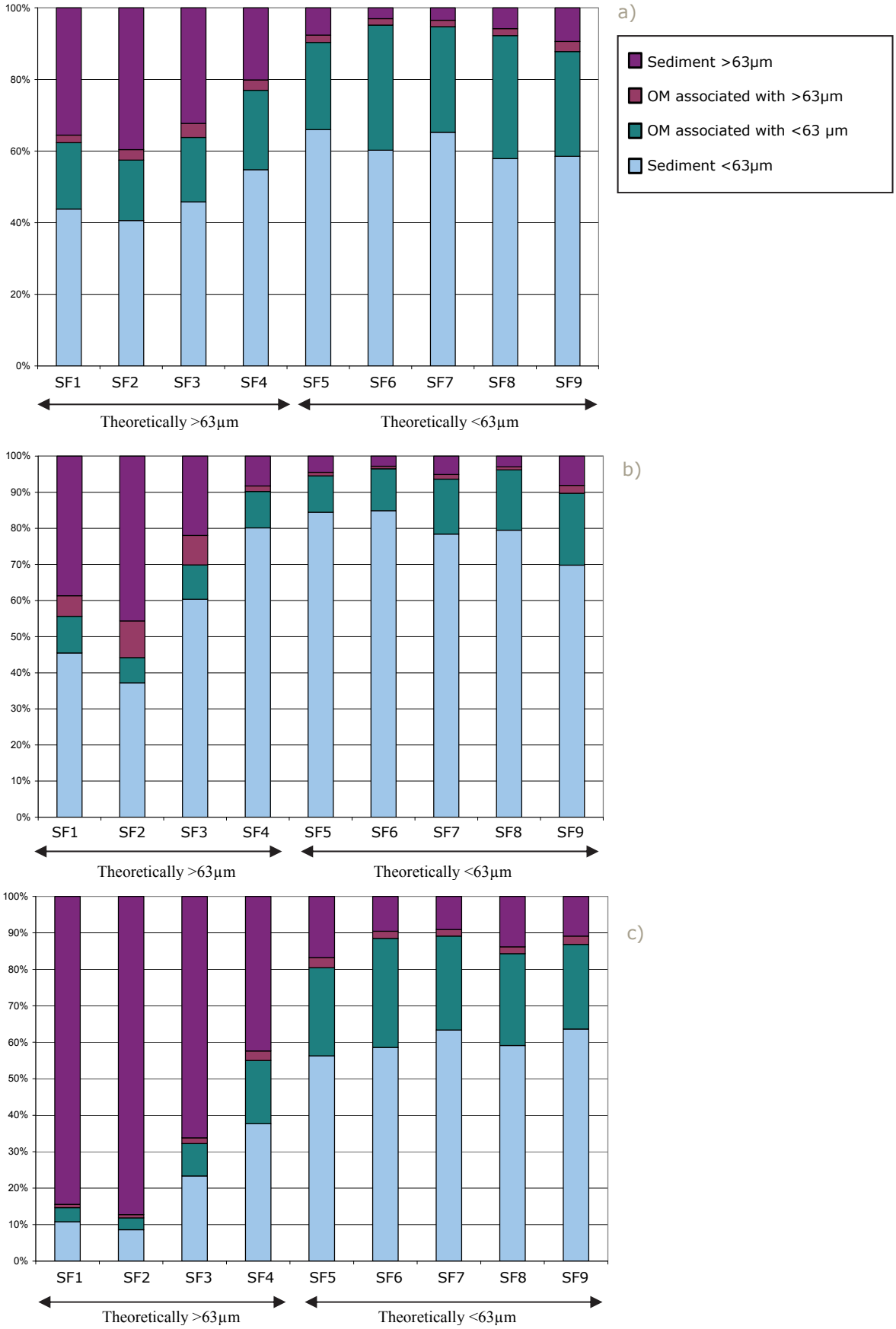

Figure 9.3: Percentages of material both coarser and finer than 63µm, as well as the associated OM percentages, present in different subfractions of the settling experiment using material from Aarschot (Demer) (a), Halen Gete (b) Lummen Mangelbeek (c), adapted from Cant (2010).

9.2.1 Spectrophotometric and gravimetrical analysis

Initially, attempts were made to gain insight into the contribution of iron to the total mass of suspended sediment present in a water sample. The sampling campaigns executed in 2006 (already described in Sections 2.2.1 and 3.2.1.1) were also tailored to gather information about the iron content in soluble condition in the river water and the iron content in the flocs.

During the first three campaigns in 2006 (7 and 8 March and 9 May 2006), no reliable data concerning iron concentrations could be obtained due to problems in sampling strategy, contaminated DI water and constrictions in analytical detection limits as mentioned in Section 3.2.1.1. During the sampling campaigns of October 2006 however, these problems were addressed and the obtained results are discussed below.

For each location sampled, after the sample preparation and laboratory analyses, following parameters are available: Fe(II) concentration in the river water, Fe_{Tot} for the water-sediment mixture, SSC and LOI. Furthermore, from these measured parameters Fe(III) concentration in the sediment and Fe(III) and LOI weight percentages in the sediment could be derived. Table 9.5 presents the summarized data obtained from the 11 October 2006 campaign at the Grobbendonk sampling site (the complete analytical data can be consulted in Janssens (2007) and in Van Eetvelt (2007). The samples were collected at 4 verticals (see Figure 2.9 for the exact localisation in the cross-section) at different depths (noted in cm below the water surface in the naming of the sample).

Table 9.5: Summary of the spectro-photometrically determined Fe(II) and Fe_{Tot} concentrations and gravimetrically determined SSC and LOI data and derived parameters for the 11 October 2006 campaign

Sample Code	Fe(II) (mg/l)	Fe_{Tot} (mg/l)	Fe_{Tot} stdev (mg/l)	Fe_{Tot} stdev (%)	Fe(III) (mg/l)	SSC (mg/l)	LOI (mg/l)	Fe(III) (%)	LOI (%)
V6 020	0.01	2.01	0.07	3.5	2.01	12.3	5.5	16.3	44.4
V6 073	0.18	2.23	0.11	4.8	2.05	27.0	20.7	7.6	76.8
V9 020	0.15	2.10	0.05	2.4	1.96	15.2	9.8	12.9	64.8
V9 120	0.08	3.05	0.03	0.9	2.98	30.1	21.8	9.9	72.4
V11 020	0.00	1.80	0.04	2.0	1.80	11.0	6.6	16.3	60.2
V11 075	0.14	1.77	0.05	2.8	1.63	13.2	5.1	12.3	38.8
V11 113	0.14	1.70	0.04	2.3	1.56	11.4	5.4	13.7	47.7
V14 020	0.11	1.74	0.05	2.6	1.63	10.9	5.6	14.9	51.3
V14 045	0.00	1.69	0.04	2.3	1.69	10.3	6.6	16.5	64.8
AS	0.20	2.10	0.05	2,4	1.90	12.9	8.3	14.8	64.6

Table 9.6 on the other hand presents the summarized data obtained from the sampling campaign executed on 19 October 2006 at different locations in the Nete basin (see Figure 2.10 for the exact localisation). The complete analytical data can be consulted once more in Janssens (2007) and in Van Eetvelt (2007).

During the sampling campaign of 19 October 2006, SSC was determined on a subsample of only 250 ml, instead of on 1 litre subsamples as was the case for the 11 October 2006 sampling campaign. Due to low concentrations present in certain samples, it was impossible to deduce correct gravimetric contributions of Fe(III) and LOI in these samples. The cause of these low concentrations is that the sampling activities occurred during low-flow conditions as can be seen in Figure 9.4, which shows the hydrograph and sediment concentrations measured at the Grobbendonk monitoring site during 2006 as well as the timing of the sampling campaigns. The gauge height during the campaign on 19 October 2006 was even lower than the one observed during 11 October 2006, explaining the higher relative error for this campaign in comparison with the first.

Table 9.6: Summary of the spectrophotometrically determined Fe(II) and Fe_{Tot} concentrations and gravimetrically determined SSC and LOI data and derived parameters for the 19 October 2006 campaign.

	Fe(II) (mg/l)	Fe(tot) (mg/l)	$Fe_{(tot)}$ stdev (mg/l)	$Fe_{(tot)}$ stdev (%)	Fe(III) (mg/l)	SSC (mg/l)	LOI (mg/l)	Fe(III) (%)	LOI (%)
Kleine Nete (Grobbendonk)	0.11	1.95	0.33	17.02	1.84	*<20*	*<25*	-	-
Grote Nete (Itegem)	0.00	3.84	0.27	7.13	3.84	*<25*	*<10*	-	-
Fermerijloop (Herentals)	0.05	8.22	1.05	12.75	8.17	167.3	88.7	4.9	53.0
Slootbeek (Poederlee stuw 3)	0.00	20.72	1.13	5.47	20.72	195.3	141.3	10.6	72.4
Laak (Geel-Zammel)	0.01	0.31	0.00	1.38	0.31	*<5*	*<1*	-	-
Aa (Poederlee Stuw 3)	0.10	1.43	0.34	23.96	1.33	*<5*	*<1*	-	-
Grote Nete (Geel-Zammel)	0.05	4.46	0.01	0.29	4.41	91.1	28.9	4.8	31.8
Bouwelse Goorbeek (Bouwel)	0.15	19.65	0.05	0.27	19.50	*<20*	*<1*	-	-

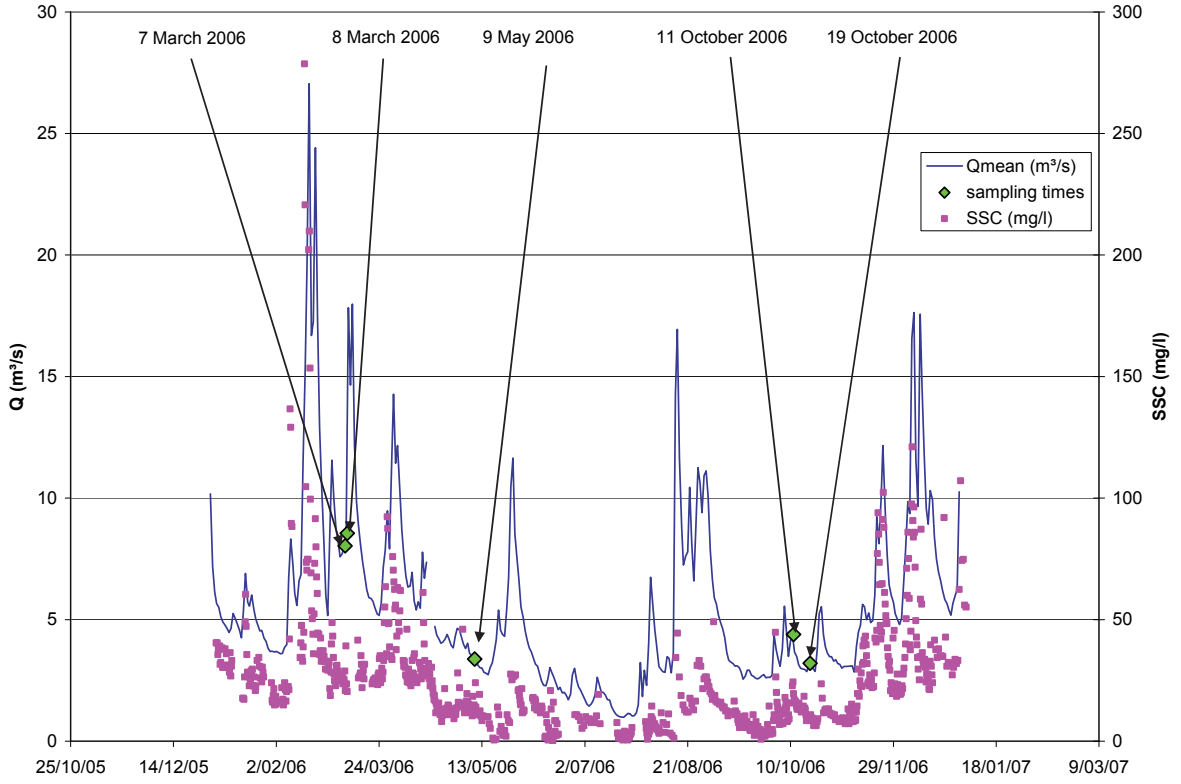

Figure 9.4: Daily mean Q and SSCISCO-values, observed at Kleine Nete (Grobbendonk) monitoring site during 2006. The timing of the authigenic sediment sampling campaigns is also indicated.

The low suspended sediment concentrations did however, in combination with the absence of any particles larger than 2,000 µm allow the churn sample splitter to subsample accurately (as has been discussed in Section 2.1.1.3). This is confirmed by the low standard deviations observed for the Fe_{Tot} analysis executed on the replicate (churn sample splitted) samples during the first campaign. During the second campaign, the standard deviations were slightly more elevated but were still acceptably low.

A significant positive correlation could be found between the LOI(%) and the SSC (Pearson's r correlation significant to a level of 0.01), indicating that the more solid material is present in the sample, the higher the organic matter content (see Table 9.7).

Table 9.7: Pearson correlation matrix for variable LOI, SSC and Fe(II).
** Correlation is significant at 0.01 level, * Correlation is significant at 0.05 level

		SSC (mg/l)	Fe(III) (%)	LOI (%)
SSC (mg/l)	Pearson Correlation	1	-.879(**)	.655(*)
	Sig. (2-tailed)		0.001	0.040
	N	10	10	10
Fe(III) (%)	Pearson Correlation	-.879(**)	1	-0.483
	Sig. (2-tailed)	0.001		0.158
	N	10	10	10
LOI (%)	Pearson Correlation	.655(*)	-0.483	1
	Sig. (2-tailed)	0.040	0.158	
	N	10	10	10

No significant correlation could be established between Fe(III)-content and LOI, which seems to indicate that for the Kleine Nete at the Grobbendonk site, organic matter is not only linked to the authigenic sediment.

As stated above, due to smaller subsample volumes and lower SScs during the sampling campaign of 19 October 2006, some parameters fell below detection limits, allowing for them only to be used indicatively.

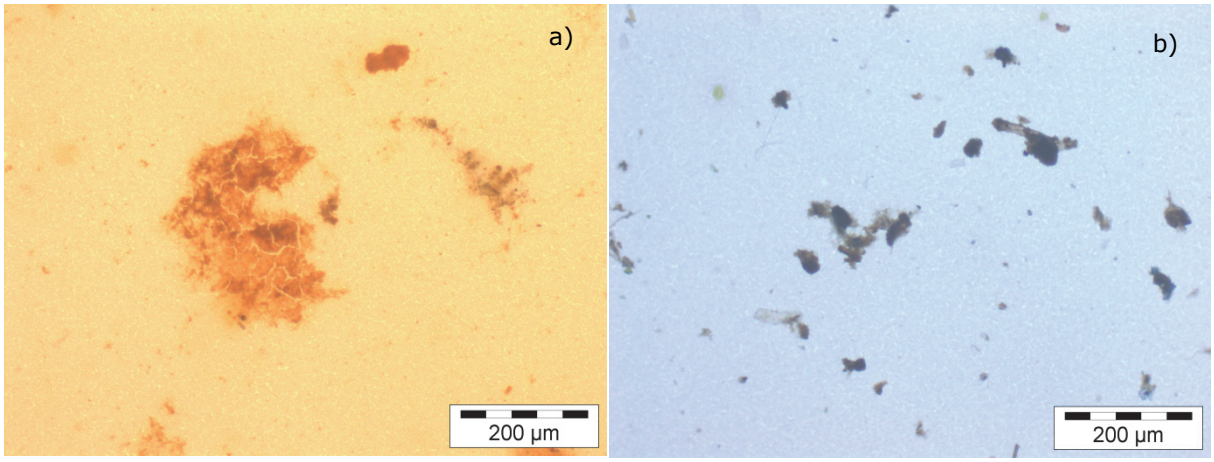

Figure 9.5: Microscopic images of the Bouwelse Goorbeek (Bouwel) (a) and the Fermerijloop (Herentals) (b) in which the difference in iron content can be observed through difference in colour of the flocs and small particles colouring the background of the filter

Despite these uncertainties, it is still clear that the differences in contribution of Fe(III) to the solid phase are quite substantial.

They range from a mere 5% to comprising the entire solid load. This is even visually perceivable in the difference in colour of the background and of the particles in the microscopic images of the iron-rich Bouwelse Goorbeek (see Figure 9.5a) and the almost iron-free Fermerijloop (see Figure 9.5b).

Due to the variability observed in Fe(III) and organic matter content in the different samples it is difficult to narrow down the stoichiometric and/or sorption correction factors. Hence, other techniques needed to be applied.

9.2.2 XRF-analysis

In the framework of the sediment fingerprinting research (discussed in Part V) samples of authigenic material were collected in the headwaters of the Mangelbeek catchment. Furthermore, suspended sediment was time-integratedly collected upstream of the confluence of the Mangelbeek and Zwartebeek streams into the river Demer.

Comparing these data sets gives an insight into the differentiation the suspended sediment encounters during its travel from source to outlet. The authigenic sediment was sampled to be representative of its 'purest' form (so that little to no other sediment sources were present and would interfere with the analysis). It was sampled in relatively pristine headwaters (very small creeks and streams) in which no industrial discharges were present. Emissions by diffuse sources (such as road run-off) and some household effluents however might already have been present in the water and sorbed onto the sediment. Where possible and enough suspended material was present, authigenic material was sampled using only the suspended material. However, in clear water streams the need arose to sample deposited flocculated material as well, to obtain sufficient material for XRF analysis.

After sample preparations, these sediments were analysed for a variety of parameters including LOI and geochemistry by XRF (as described in Section 3.2.2). Table 9.8 shows the relevant data collected at these locations while Figure 9.6 visualizes this data.

Even though no data was available from the Kleine Nete catchment, insights into the composition of the authigenic sediment in the Mangelbeek, and suspended sediment in the Mangelbeek and Zwartebeek catchments can still be used for investigation into the MARS correction factors to be applied in the Kleine Nete, as the Mangelbeek and Zwartebeek catchments are underlain by the same geological formations as the Nete basin, and the generation of authigenic sediment happens in the same way. The variability between the Mangelbeek and Zwartebeek outlet samples shows the impact of different emissions in the various tributaries.

When comparing the data sets, it is clear that the authigenic sediment is depleted of detrital sediment in comparison to the sediment collected at the outlet stations, as can be seen in Figure 9.6a. This figure shows the average, minimal and maximal weight percentages of Si, Al, Ca, K and Ti, elements associated with the mineral fraction of aluminosilicates, quartz, etc. This confirms on the one hand that the authigenic sediment was in fact relatively 'pure' at the headwater locations where it was sampled, and it indicates that this sediment source is diluted further downstream with other sediment sources, such as soil erosion. This is also confirmed by the slight drop in iron content (as can be seen in Figure 9.6b) as well as by the increase in the outlet stations in Zr and Rb (see Figures 9.6f) which are also usually associated with the mineral phase.

Figure 9.6b also shows that the LOI (and therefore the organic matter content) is high (ranging around 30%) and it remains high in the outlet samples. For comparative measures, in catchments with far less iron content (authigenic material) in its sediment transport, the organic matter content is much lower (organic matter contents from the southern tributaries of the Demer, void from ferric authigenic sediment only report +/- 10% LOI as is reported in Chapter 10 (see Addendum C).

The average P-values (see Figure 9.6c) more than doubled from headwaters to the outlet, which can be explained by household effluents and agricultural activity. Moreover, as authigenic sediment sorbed trace elements from the river water, and the amount of sorbed elements is a function of the residence time of the sorbent (iron oxyhydroxites) in the medium (river water), most trace elements concentrations (Zn, Mn, B, Pb, Cu, Cr and V) were elevated in the outlet stations

Table 9.8: Average, minimal and maximal observed geochemistry results obtained by XRF-analysis of authigenic sediment collected in the headwaters of the Mangelbeek, as well as from suspended sediment collected at the Mangelbeek and Zwartebeek sampling outlet sampling locations. <dl indicates below detection limit.

		LOI	Al	Ca	Fe	K	Si	P	S	Ti	Ba	Cr	Cu	Pb	Mn	Ni	Sr	V	Zn	Ce	Rb	Zr
		%	%	%	%	%	%	ppm	ppm	ppm	ppm	ppm	ppm	ppm	ppm	ppm	ppm	Ppm	ppm	ppm	ppm	Ppm
authigenic sediment Mangelbeek	1	N.A.	0.7	<dl	29.0	<dl	<dl	4490	7000	<dl	<dl	39	10	46	527	52	76	<dl	645	<dl	<dl	<dl
	2	N.A.	0.2	<dl	24.1	<dl	<dl	2860	17300	<dl	<dl	18	20	20	299	28	106	<dl	333	<dl	<dl	<dl
	3	N.A.	0.4	<dl	28.7	<dl	<dl	2010	5250	<dl	<dl	21	8	28	267	25	43	<dl	209	<dl	<dl	<dl
	4	28.1	0.7	0.1	26.8	<dl	<dl	3454	2528	843	156	1	27	149	193	24	19	<dl	166	33	19	16
	5	N.A.	0.1	<dl	28.4	<dl	<dl	5150	17800	<dl	<dl	<dl	8	12	598	17	251	<dl	141	<dl	<dl	<dl
	6	31.3	1.1	<dl	25.8	<dl	<dl	10054	4288	1272	138	13	71	148	163	24	3	<dl	268	100	16	83
	7	35.3	0.7	0.6	25.7	<dl	<dl	3904	2983	978	179	0	40	132	273	24	26	<dl	245	35	18	35
	8	31.1	0.7	0.2	26.7	<dl	<dl	3465	4493	864	173	<dl	25	154	182	24	21	<dl	196	34	20	18
Mangelbeek - Lummen	1	35.2	1.4	0.5	22.4	<dl	3.9	7847	2706	1788	218	30	50	127	478	28	46	<dl	1011	50	31	185
	2	N.A.	1.5	0.3	22.5	<dl	6.5	9366	5241	1785	236	31	66	138	429	23	40	<dl	1436	49	30	104
	3	29.8	1.3	0.7	22.7	<dl	3.4	11857	3871	1507	227	16	57	134	623	23	41	<dl	1014	44	31	102
	4	30.9	1.7	0.5	20.8	<dl	9.1	7902	3584	2063	242	40	72	125	469	24	47	10	1552	50	32	81
	5	28.6	2.0	0.4	18.8	0.3	14.5	7421	6500	2421	275	57	107	142	397	29	47	31	1608	55	37	124
	6	29.3	1.6	0.4	20.2	0.1	10.0	6947	5560	2197	238	54	81	154	447	33	44	26	1703	52	40	122
	7	33.1	1.5	0.3	22.1	<dl	6.5	8131	3228	1855	225	35	61	134	582	31	41	<dl	1411	47	32	91
	8	38.1	1.7	0.5	19.4	<dl	13.7	8262	5183	2155	250	40	75	121	493	39	43	19	1352	52	29	103
	9	29.5	1.8	0.3	18.9	0.3	15.5	7545	6711	2292	259	48	84	124	438	35	41	28	1301	55	37	148
	10	34.2	1.7	0.5	19.4	0.1	10.6	7336	5015	2364	253	47	90	132	453	31	46	16	1121	58	35	153
	11	31.8	1.5	0.5	20.8	<dl	7.1	8077	4357	2050	239	37	77	128	439	32	47	<dl	1150	53	30	152
Zwartebeek - Lummen	1	31.1	1.3	0.7	23.9	<dl	0.7	10438	2440	1392	227	16	58	140	507	23	38	<dl	648	45	32	61
	2	<dl	1.3	0.4	24.0	<dl	2.6	9440	1768	1401	241	17	42	138	778	23	35	<dl	618	43	37	83
	3	30.1	1.3	0.4	24.0	<dl	2.6	9440	1768	1401	241	17	42	138	778	23	35	<dl	618	43	37	83
	4	30.5	1.2	1.0	23.9	<dl	0.1	7913	2165	1293	235	17	49	137	940	25	42	<dl	559	41	34	78
	5	29.8	1.6	0.9	20.8	<dl	8.6	12137	2534	1771	313	94	126	177	456	46	54	5	753	46	35	95
	6	25.1	1.4	0.5	21.5	<dl	8.6	12058	2731	1785	288	29	29	110	506	25	44	<dl	486	47	35	282
	7	28.4	1.0	0.4	24.2	<dl	1.0	8760	1668	1342	229	15	45	141	440	24	33	<dl	540	41	33	70
	8	31.5	1.1	0.6	23.8	<dl	<dl	8976	2592	1399	222	18	43	127	276	24	37	<dl	608	55	32	68
	9	28.1	1.1	0.3	23.2	<dl	1.9	9702	2737	1529	236	23	42	125	323	29	33	<dl	605	46	29	143
	10	31.7	1.2	0.5	23.2	<dl	0.7	10072	2962	1557	235	21	44	127	298	24	36	<dl	564	46	30	86
	11	31.2	1.1	0.3	23.6	<dl	0.2	9851	4231	1499	229	17	52	129	372	24	30	<dl	632	43	28	67

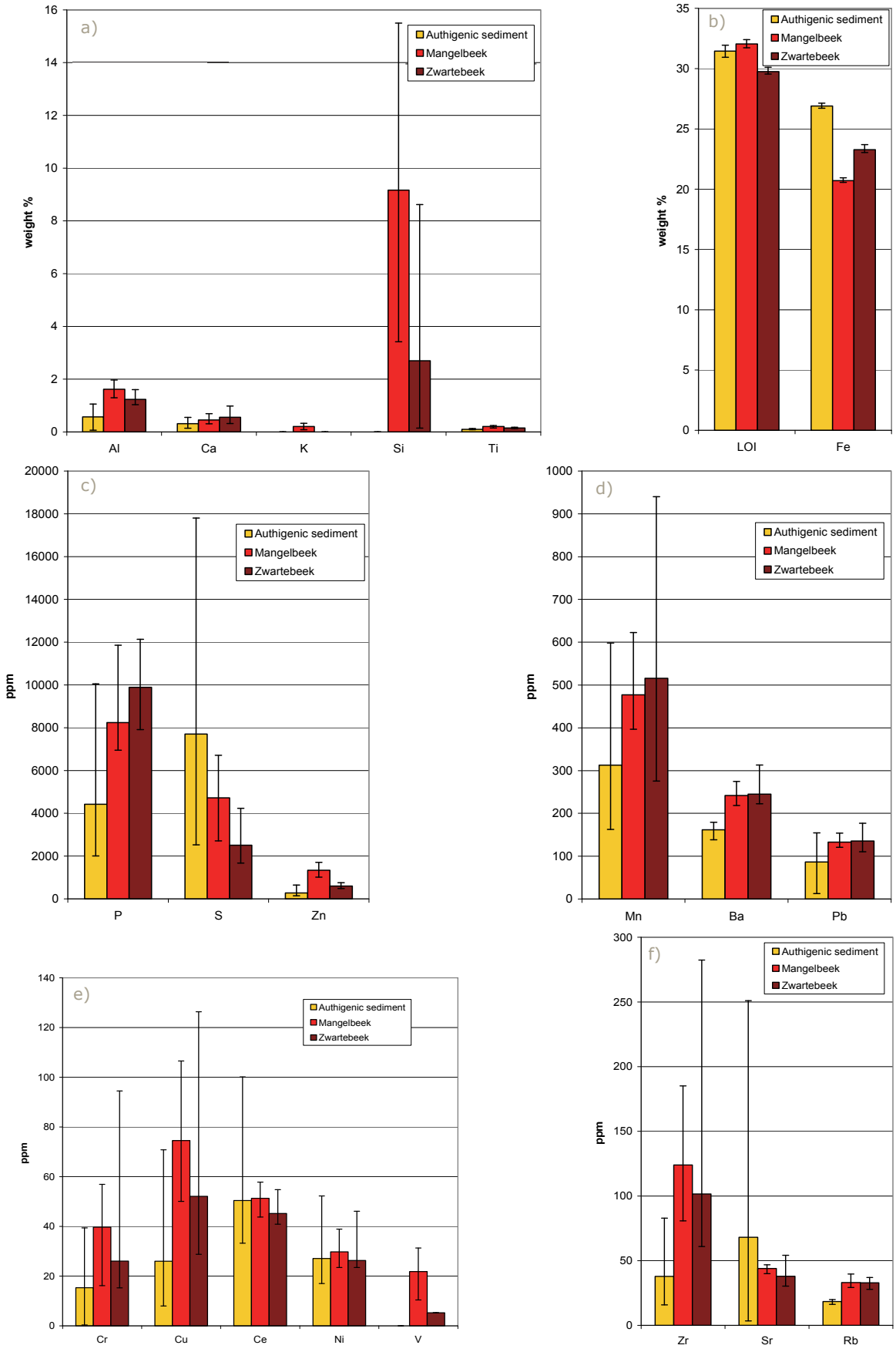

Figure 9.6: Summary of the geochemical XRF-analyses of the authigenic sediment sampled in the Mangelbeek headwaters, as well to the suspended sediment sampled at the Mangelbeek and Zwartebeek outlets. The columns represent the average values observed, while the whiskers show the maximal and minimal values observed

compared to the authigenic sediment (see Figures 9.6c, d, e). Of all chemical elements analyzed only S, Sr and Fe drop in concentration when moving downstream, while Ni and Ce remain stable.

9.2.3 Collaborative research (Dekov et al., in preparation)

After above mentioned previous attempts, it became clear that further investigation of the mineralogical, physical chemical and biological structure of the authigenically formed flocs would be too time consuming to execute within the framework of this PhD, and falls outside the technical expertise required in this PhD resrearch. Nevertheless, a collaborative research about these ferric precipitates in the Nete and Demer river basins was set up (as previously mentioned in Section 2.2.1.5).

The detailed description of methods and sampling strategies used in this study, as well as the final results will be submitted to the journal 'Chemical Geology' in the near future (Dekov et al. (in prep.)), however the results of this research, as far as they shed insight into the nature of the authigenic sediment and the stoichiometric and sorption factors, will be shortly addressed below.

The sampling locations (as shown in Figure 2.11) were selected based on the terrain knowledge gathered from the previous authigenic sediment research campaigns as well as from the sediment fingerprinting research. Like in the previous campaign, great care was taken to ensure authigenic sediment was sampled in its purest form, at headwater locations in the Nete and Mangelbeek catchments) where little to no other sediment sources were present and would interfere with the analysis. In this study, however, the suspended and deposited authigenic sediment was studied separately. The samples collected included three suspended sediment samples and six deposited (superficial riverbed) red sediment samples as well as one light-grey riverbed sample that was representative of the background sedimentation devoid of Fe-rich suspended flux. Also, one sand sample from the Diest Formation [0252] and one sample of red precipitate collected at the Pidpa water production centre (Grobbendonk) were analysed.

Dekov et al. (in prep.) were able to establish through Scanning Electron Microscope observations that the authigenic material is a result of both microbial and inorganic precipitation. Furthermore, they proved through Mössbauer, micro-Raman and XRD analysis that both the red suspended sediment as well as the riverbed material was entirely composed of ferrihydrite.

The geochemistry part of this study revealed that the suspended authigenic material was slightly richer in Fe than the deposited authigenic sediments (mean ~35% and ~31%, respectively, with maximal values of 38% and 32% respectively). These values are significantly higher than some of the values observed in the 2006 sampling campaigns (see Section 9.2.1), but are closer to the observed Fe-concentrations in the XRF data obtained for the fingerprinting research (Section 9.2.2).

Moreover, the authigenic sediment scavenges a number of trace elements from the river water, and as stated above the amount of sorbed elements is a function of the residence time of the sorbent (ferrihydrite) in the medium (river water). Hence, the deposited authigenic sediment contained higher trace element (As, Li, Sc, V, Co, Ni, Zn, Rb, Y, Zr, Cd, Sb, Cs, Ba, ΣREE, Hf, Tl, Pb, Th and U) concentrations than its suspended counterpart. The deposited authigenic sediment was also enriched compared to the suspended material in elements that originate from the detrital component (Si, Al, Ti and K). Both types of samples had similar concentrations of W, Sr and Mo. Table 9.9 gives an overview of the geochemistry results.

Table 9.9: Average geochemical results for the three suspended and six deposited authigenic sediment samples and one background sample collected in the headwaters of the Mangelbeek and Nete catchment, as reported in Dekov et al. (in prep.)

	suspended authigenic sediment	deposited authigenic sediment	background sediment
Si (%)	1.88	4.13	79.80
Al (%)	0.14	0.32	1.24
Fe (%)	35.10	31.43	0.00
Mn (%)	0.03	0.03	0.01
P (%)	1.24	0.38	0.00
S (%)	0.44	0.54	0.24
Ca (%)	1.40	1.22	0.00
K (%)	0.01	0.10	0.27
Ti (%)	0.07	0.08	0.14
Cl (%)	0.17	0.17	0.08
As (ppm)	19.03	24.80	2.50
Nb (ppm)	1.67	1.53	6.32
W (ppm)	2.65	2.98	2.95
Li (ppm)	1.33	2.52	5.79
Sc (ppm)	0.53	1.00	0.84
V (ppm)	16.87	34.85	10.70
Cr (ppm)	40.00	28.42	14.90
Co (ppm)	2.08	4.27	0.62
Ni (ppm)	5.45	9.73	2.27
Cu (ppm)	17.37	11.70	3.47
Zn (ppm)	86.83	112.32	52.10
Rb (ppm)	3.68	9.76	16.10
Sr (ppm)	87.00	58.82	21.00
Y (ppm)	5.13	8.31	3.64
Zr (ppm)	0.50	12.12	37.90

	suspended authigenic sediment	deposited authigenic sediment	background sediment
Mo (ppm)	2.09	2.23	0.14
Cd (ppm)	0.60	1.03	0.34
Sn (ppm)	1.28	0.95	0.56
Sb (ppm)	1.02	1.36	0.35
Cs (ppm)	0.16	0.29	0.44
Ba (ppm)	62.93	117.53	141.00
La (ppm)	5.72	8.41	6.64
Ce (ppm)	14.45	20.07	14.10
Pr (ppm)	1.54	2.23	1.63
Nd (ppm)	6.42	9.10	6.10
Sm (ppm)	1.26	1.81	1.15
Eu (ppm)	0.28	0.39	0.20
Gd (ppm)	1.19	1.76	0.97
Tb (ppm)	0.16	0.24	0.13
Dy (ppm)	0.85	1.29	0.69
Ho (ppm)	0.16	0.25	0.13
Er (ppm)	0.41	0.66	0.34
Tm (ppm)	0.05	0.09	0.05
Yb (ppm)	0.35	0.58	0.36
Lu (ppm)	0.05	0.09	0.05
Hf (ppm)	0.13	0.40	1.04
Tl (ppm)	0.04	0.06	0.11
Pb (ppm)	10.18	14.87	8.70
Th (ppm)	0.46	1.02	1.68
U (ppm)	0.28	0.34	0.44

The background sediments contained less Fe, Mn, Ca, S, Cl and P, and more Si, Al and Ti than the authigenic sediment. They were also depleted in V, Co, Ni, Cu, Sn, Mo, As and Sb, and enriched in Li, Nb, Rb, Zr, Hf and Tl when compared to the authigenic material.

The geochemical and isotopic research also yields insight into the origin of the authigenic sediment. The red suspension, red sediments, background sediments have similar REE patterns with weak positive Ce anomaly, weak negative Eu anomaly and enrichment in light REE as those observed in the Diest aquifer sands, suggesting that the red suspension and sediment have inherited their REE patterns from the aquifer.

Futhermore, the red riverine suspension and sediment contain Sr derived from three sources: geogenic (local rocks), anthropogenic and, presumably seawater, while the Pb isotope data fit with a binary mixing involving a geogenic and an anthropogenic (dominant) source. The anthropogenic input of Sr and Pb to the studied river systems is totally sequestrated by the natural precipitation of ferrihydrite and the background sediment does not show any anthropogenic influence. Also, the Nd budget of the red suspension and sediment is controlled by the geogenic (aquifer) source and shows little anthropogenic impact.

Furthermore, O-isotope data suggest that ferrihydrite precipitation occurs at low temperatures (T<20°C) and it is a result of precipitation from different source waters. Therefore, even though groundwater is quantitatively the main contributor to the river discharge, other sources probably also contribute significantly to the chemistry of the precipitates as well. As discussed in Section 4.3.2.2.2 industrial discharges and sewage treatment contribute varyingly to the different tributaries of the Nete and Demer tributary basins (ranging from 0 up to 34% of their total discharge measured in 2007, as is presented in Table 4.3). However finding these results in such upstream locations, where no industrial and sewage treatment facilities discharge into the streams, seems to indicate that the anthropogenic input comes from household discharges, not yet collected by sewage drainage and by road runoff. It also indicates that the sampled sediment is not 100% pure authigenic sediment, as was intended when sampling.

9.2.4 Conclusion

The geochemical research of surface water and suspended sediment provided some insight into the composition of the authigenic sediment. This material exists almost entirely out of ferrihydrite, which is a result of both microbial and inorganic precipitation. The low levels of Fe(II) present in the surface water at the different location tested in the Nete basin confirm the hypothesis that the oxidation process of Fe(II) into Fe(III) is a fairly quick process, and will take place within the boundaries of the catchment in which the suspended sediment is sampled.

The authigenic material is characterised by very high iron concentrations (mean Fe concentrations of 35% were observed in the samples collected at the head waters and maximal value of 38.1% was even observed) and also has significantly high levels of organic matter content (LOI of +/- 30%).

9.3 Discussion: Re-evaluating the correction factors

9.3.1 The Total Correction Factor (F_T)

MARS has been developed to model the contribution of authigenic sediment to the total sediment flux, based on a known influx of Fe(II) entering the river through groundwater seepage. As such, one total correction factor (F_T) as applied in PRE-MARS suffices to model this.

If the premise is accepted that the authigenic sediment sampled at the headwaters of the Mangelbeek and Nete basin is indeed 'pure' authigenic sediment, than the inversed iron concentration (in weight percentage divided by 100) observed in these samples equals F_T.

It should be remarked that this hypothesis entails that all organic matter present in the sample is linked to the authigenic sediment. As Dekov et al. (in prep.) has shown, a significant part of the authigenic material is a result of microbial precipitation. As such, certainly a part of the organic material is directly linked to the presence of authigenic sediment in the system. Furthermore, besides the bacterial presence, other organic material will use the ferrihydrites sorptive power as a source of nutrients, ensuring higher production of organic material. Therefore, authigenic sediment is likely to be responsible for at least a significant portion of the organic material present in the samples. This hypothesis seems to be supported by the observation of significantly higher LOI in the iron-rich tributaries (+/- 30%) in comparison to non-iron-rich tributaries of the Demer basin, which only have a LOI of +/- 10% (as is determined in the framework of the sediment fingerprinting research and reported in Addendum C).

However, whether or not the authigenic sediment is a direct or indirect source of organic material might be considered an unnecessary discussion, as most of the organic material sampled (which was attached to the suspended sediment) will have originated in the river itself and can therefore be considered authigenic in nature.

Because of this reasoning, and because of the significant impact the iron ferric oxides have on the presence of organic matter, it has been opted to go ahead and use the inversed Fe-concentration as an estimator for the F_T. However, one should take into account that applying such a F_T, will lead to a slight overestimation of the authigenic sediment contribution.

Furthermore, it should be pointed out that F_T can only be calculated using the Fe-concentration data obtained from the authigenic sediment sampling in the headwaters of the iron-rich catchments. If the iron concentrations obtained from more downstream locations would be used, the dilution with other sediment sources would increase the F_T artificially, causing an unacceptable overestimation of the authigenic contribution to the total SSF.

This effect is presented in Table 9.10, which shows an overview of the F_T values calculated based on the data reported by Dekov et al. (in prep.) and the fingerprinting XRF analyses. In this table the 'purest' form of authigenic sediment is represented by the suspended authigenic sediment sampled by Dekov et al. (in prep.), which also reports the lowest SSC/Fe ratio (2.85). The deposited sediment (of which Dekov et al. (in prep.) reported it contained more traces of detrital sources) has an average ratio of 3.18. The authigenic sediment sampled during the fingerprinting campaign (and which contained a mixture of suspended and deposited material from the headwaters) had a higher ratio (3.72), indicating that probably somewhat more detrital material was sampled with the deposited material.

Nonetheless, when comparing these values with the ratios obtained from the outlet sampling at the Mangelbeek and Zwartebeek outlet stations (in the framework of the sediment fingerprinting campaign) it can clearly be seen that the latter are more elevated (respectively 4.83 and 4.30). At these outlet locations the authigenic sediment has been diluted with other sources.

Table 9.10: Overview of the F_T values calculated based on the data reported by Dekov et al. (in prep.) and the fingerprinting XRF analyses

Datasource	Location	Average F_T	Max F_T	Min F_T
Dekov et al. (in prep.)	suspended authigenic sediment	2.85	2.93	2.76
Dekov et al. (in prep.)	deposited authigenic sediment	3.18	5.05	2.62
Sediment fingerprinting	Authigenic sediment (Mangelbeek headwaters)	3.72	4.15	3.45
Sediment fingerprinting	Outlet Mangelbeek	4.83	5.33	4.40
Sediment fingerprinting	Outlet Zwartebeek	4.30	4.80	4.12

This conclusion is confirmed by observations of VMM in the Mangelbeek catchment. VMM has been taking superficial water samples by grab sampling, and consequently the samples are analysed for a myriad of parameters. Only a few of those (such as total Fe and total P content and suspended sediment concentration) are of interest to this research. Plotting the SSC/Fe_{Tot} ratio of this data is comparable to the F_T factor calculated using the Dekov et al. (in prep.) and fingerprinting data.

However, some considerations should be taken into account. Due to using the Fe_{Tot} concentration and not the iron concentration in the solids, an underestimation of the F_T factor will take place, especially in areas of the catchment with high Fe(II) influx from the groundwater seepage. Furthermore, due to the low sediment concentrations present in these samples (maximal observed SSC for all locations in the Mangelbeek catchment was 151 mg/l) the relative error on the

SSC/Fe_{Tot} ratio might be considerably high, creating scatter when SSC is plotted as a function of Fe_{Tot} (as can be seen in Figure 9.7).

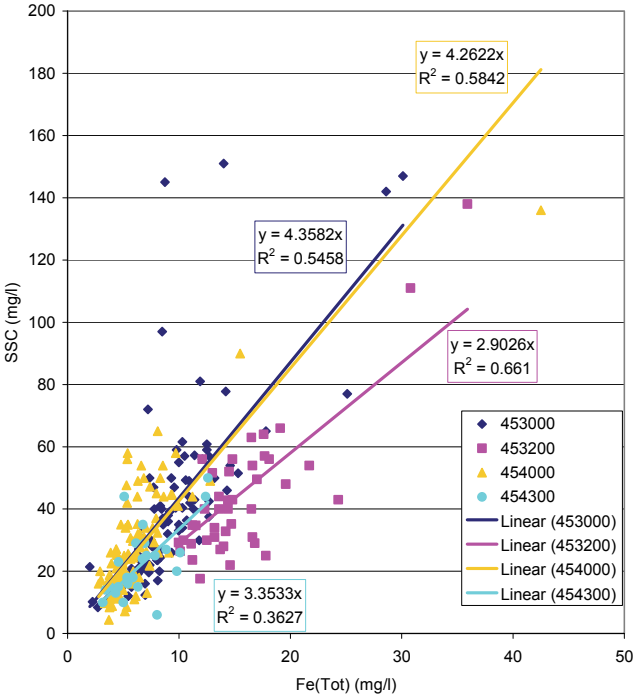

Figure 9.7: The relation between total iron (Fe_{Tot}) and suspended sediment concentrations (SSC) at different locations in the Mangelbeek catchment (data and codification from VMM)

Hence, the data obtained from VMM should only be used indicatively. Of the locations sampled in the Mangelbeek catchment, see Figure 9.8 for localisation, the more upstream locations (453200 and 454300) have lower FT-values (respectively 2.90 and 3.35) than the downstream locations (453000 with FT equalling 4.36 and 454000 with FT equalling 4.26). The FT values seem in accordance with those derived from the XRF data reported in Section 9.2.2 and the FT-values derived from the Dekov et al. (in prep.) data.

To conclude, applying the lowest F_T value (2.85) seems the best estimate. However, one should take the possible sorption into account that will take place while the sediment moves downstream and encounters pollution, which will cause a slight increase in the F_T. The impact of this extra sorption will be discussed in Section 9.3.3.

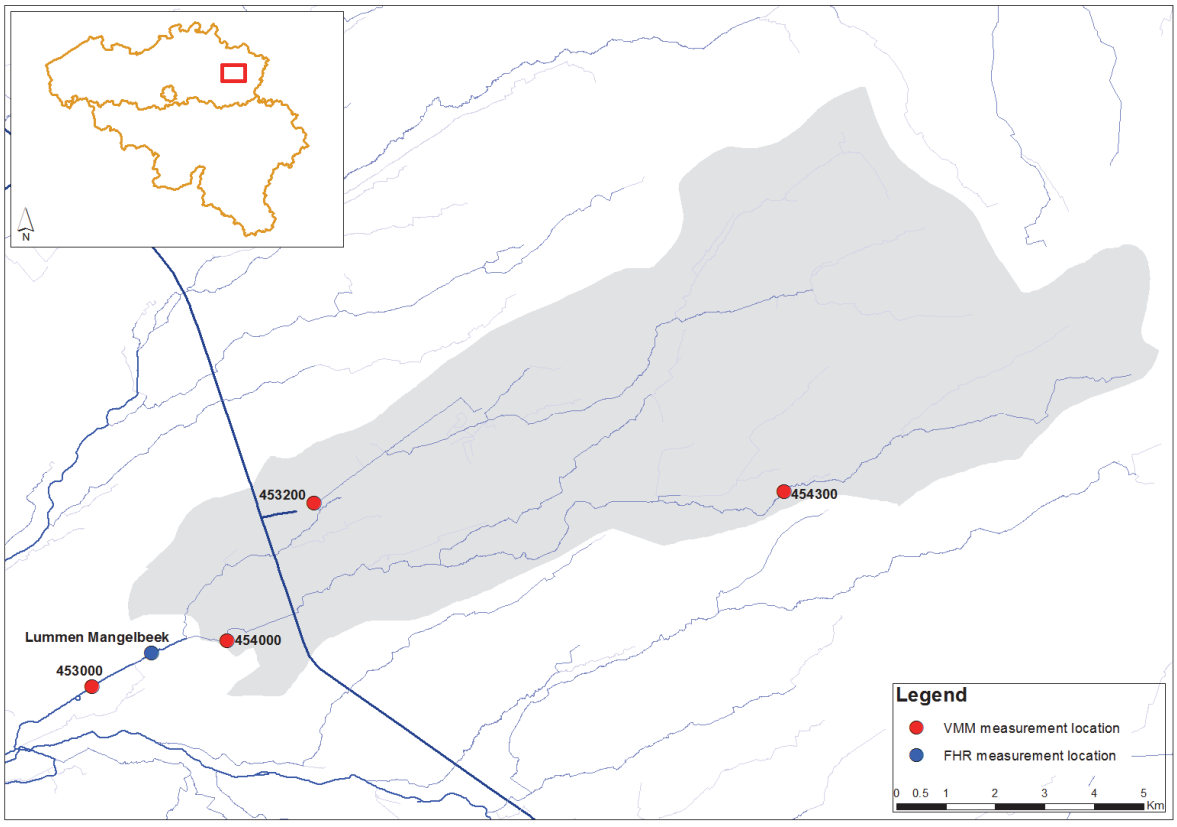

Figure 9.8: Localisation of four measurement locations of VMM located in the Mangelbeek catchment

9.3.2 The Stoichiometric Correction Factor (F_{St})

As pointed out in Section 9.2.3 Dekov et al. (in prep.) were able to determine that the authigenic sediment sampled in the headwaters of the Mangelbeek and the Nete basins was entirely composed of ferrihydrite. Hence, the Stoichiometric Correction factor should equal 1.90.

However, considerable amounts of phosphor (ranging around 1%) were found in the suspended sediment samples of the Mangelbeek and Zwartebeek (see Table 9.8 and Figure 9.6). This phosphor most likely originates from agricultural influx and household effluents. As such, it might interact with the available iron present in the river to form iron phosphates. If this is the case, then the Stoichiometric Correction Factor will be higher than 1.90 (as various ferric phosphates have significantly higher molecular masses. Strengite for instance would require a F_{St} of 3.35).

Determining if the P is located in the sediment in the vicinity of the Fe observations of more downstream (and P-enriched) sediments, could be done by using Scanning Electron Microscope analyses. This would already give insight whether the P-fraction is associated with the authigenic sediment, if not in the mineral phase, than at least through sorption.

Further analyses with Mössbauer, micro-Raman and XRD should allow insight into the mineral structure of the phosphates, allowing for contributing the impact of the P to the F_{St} or the F_{So}. However, these analyses fall outside the scope of this PhD.

9.3.3 The Sorption Correction Factor (F_{So})

Using the geochemical data obtained in the XRF analyses within the framework of sediment fingerprinting and the geochemical data obtained from the Dekov et al. (in prep.) research, different estimates of the F_{So} can be established.

A first approach is to simply summarize the weight of all elements that could possibly be sorbed onto the ferrihydrite and compare them to the Fe-content in the samples. In case of the fingerprinting data set the selected elements were: Ba, Cr, Cu, Pb, Mn, Ni, V, Zn, Ce and Zr. For the Mangelbeek samples, the Zwartebeek samples and the authigenic samples, the average weights were determined and consequently summarized.

Next, these sums were divided by the average Fe-concentrations present in the samples of the respective rivers, in order to calculate the amount of weight 1 g of Fe could potentially sorb. To conclude the respective F_{So} factors can be derived by adding 1 to these ratios. These F_{So} factors are presented as F_{So} (1) in Table 9.11.

Table 9.11: Sorption correction factors calculated based on the addition of weight of Ba, Cr, Cu, Pb, Mn, Ni, V, Zn, Ce and Zr ($F_{So}(1)$) and based on the addition of Ba, Cr, Cu, Pb, Mn, Ni, V, Zn, Ce, Zr, As, Nb, W, Co, Y, Mo, Cd, Sn, Sb, Cs, La, Pr, Nd, Sm, Eu, Gd, Tb, Dy, Ho, Er, Tm, Yb, Lu, Hf, Tl, Th, U ($F_{So}(2)$)

Data set	Location	$F_{So}(1)$	$F_{So}(2)$
sediment fingerprinting data	Zwartebeek	1.0074	1.0083
	Mangelbeek	1.0122	1.0135
	Authigenic	1.0094	1.0104
Dekov et al. (in prep.) data	Suspended sediment		1.0016
	Riverbed sediment		1.0025

Next, the same methodology was used to estimate F_{So} factors for the suspended and riverbed material collected by Dekov et al. (in prep.), using their data set. As the chemical analysis was more extensive, besides the above mentioned elements, the following elements were also included into the calculation of the weight of the sorbed elements: As, Nb, W, Co, Y, Mo, Cd, Sn, Sb, Cs, La, Pr, Nd, Sm, Eu, Gd, Tb, Dy, Ho, Er, Tm, Yb, Lu, Hf, Tl, Th, U. The F_{So} factors obtained using these elements are also reported in Table 9.11 (as F_{So} (2)).

As the total weight contribution of these extra elements constantly amounted to 10% of the total mass of all potentially sorbed elements in the Dekov et al. (in prep.) data set, the F_{So} factors based on the fingerprinting data set could be increased (by multiplying the weight by 1.11) to take the elements into account that were not analysed. These are also tabulated as $F_{So}(2)$ in Table 9.11.

Even though this method presumes that all elements found in the material were sorbed onto the ferrous flocs, which might not be the case, the obtained F_{So} factors are clearly underestimations. First of all, because the elements sorbed, will not (always) be sorbed in their elemental form, but rather in oxygenated or hydrated form. As their stoichiometric configuration is not known, it is difficult to estimate how much the total weight of these elements represents.

Furthermore, the F_{So} factors calculated for the authigenic sediment sampled in the headwaters, will not have had the chance to come in contact with some of the chemicals entering the river downstream. Hence, the potential sorption is higher than the sorption observed in the headwaters. This seems to be confirmed by the higher F_{So} factors observed at the Mangelbeek and Zwartebeek outlet station in comparison to the F_{So} factors observed in the authigenic samples (of the Dekov data set). However, the authigenic samples of the fingerprinting campaign did yield sorption levels equal to those of the outlet station.

Therefore another approach was used to estimate F_{So} factors: an approach based on the average sorption capacity reported in the literature. As stated above, it is indicated in the literature that amorphous hydro-ferric oxide has very high sorption capabilities. Numbers vary from 0.5 mmol of ionic material per gram hydro-ferric oxide (Vance, 1994) to 7 mmol/g in case of neutral to high pH conditions (Clarck, 2009). As the sorption capacity of hydro-ferric oxides varies from 0.5 up to 5-7 mmol of ionic material per gram hydro-ferric oxide, this again leaves quite a big spread. Nevertheless, F_{So}'s for both 0.5 and 7 mmol were estimated, using an 'average' atomic mass of the elements sorbed onto the authigenic material in the headwaters of the Mangelbeek, and Nete catchments (as available in the sediment fingerprinting and Dekov data sets).

To obtain such an 'average' atomic mass of the elements, the atomic weight of each potentially sorbed element was weighted based on the contribution to the total sorbed weight observed per sample. The obtained atomic weights per sampling location are reported in Table 9.12 and all fall within a range of 75-88 g/mol.

Table 9.12: Average molecular weight of the sorbed elements, based on the sediment fingerprinting data set and Dekov et al. (in prep.) data set as well as sorption correction factors calculated based on the sorption of 0.5 mmol of weighted elements per g ferrihydrite ($F_{So}(3)$) and based on the sorption of 7 mmol of weighted elements per g ferrihydrite ($F_{So}(4)$)

Data set	Location	avg mol weight (g/mol)	$F_{So}(3)$	$F_{So}(4)$
Sediment fingerprinting data	Zwartebeek	86.7838	1.0824	2.1542
	Mangelbeek	80.0524	1.0760	2.0647
	Authigenic sediment	80.0524	1.0760	2.0647
Dekov et al. (in prep.) data	Suspended sediment	75.4270	1.0717	2.0032
	Riverbed sediment	77.7028	1.0738	2.0334
average		80.0037	1.0760	2.0640

Consequently, these 'average' atomic weights were used to calculate the F_{So} factors of the different location, applying 0.5 and 7 mmol sorption per g ferryhydrite as guidelines. These F_{So} factors are respectively reported in Table 9.12 as F_{So} (3) and F_{So} (4).

Notably, even the 0.5 mmol estimate yields significantly higher F_{So} than the summed totals using the elemental summarisation. F_{So} factors based on using averaged atomic weights vary from 1.08 (for 0.5 mmol sorption) up to 2.06 (for 7 mmol sorption). Further investigation with sorption tests can reveal how much is effectively sorbed onto the authigenic material. However, these tests fall outside the scope of this PhD research.

However, a quick calculation shows that the 7 mmol sorption is an overestimation. If the average iron content obtained from the samples collected at the outlet location of the Mangelbeek (20.7%) is multiplied with both the F_{St} observed for ferrihydrite (1.9) and the average F_{So} factor calculated based on sorption of 7 mmol (2.06), the authigenic material would contribute around 80% of the total mass of the sediment. However, already 30% was accounted by organic matter content. Hence, the 7 mmol is an overestimation of the sorption capacity. Using the 0.5 mmol sorption F_{So} (1.08) the contribution of the authigenic sediment drops down to 42%, leaving room for the organic matter as well as for more than 25% allochtoneous sediment. Therefore, most likely, the 0.5mmol is an underestimation. The actual F_{So} will therefore be somewhere in between 1.08 and 2.06.

Similar calculations can be executed using the Zwartebeek samples (which had an average iron content of 23.3%). The theoretically calculated authigenic contribution climbs to 91.4 and 47.6% using 2.06 and 1.08 F_{So}s respectively. These values also indicate that ferrihydrite most likely sorps in between 0.5 mmol and 7 mmol. The difference in the ranges of authigenic contribution calculated shows the significant impact the sorption can have on the total authigenic sediment contribution.

When multiplying F_{St} of ferrihydrite (1.9) with the two F_{So}-values determined above, the F_T will vary in between 2.51 and 3.91.

9.3.4 Conclusion

Through geochemical and mineralogical analyses it has been shown that the authigenic sediment collected at the headwaters of the Mangelbeek and Kleine Nete catchments consists mostly of ferrihydrite, of microbial and inorganic precipitation.

Whether iron phosphates are present is yet to be determined. This uncertainty leaves room for interpretation for the stoichiometric and sorption factors that should be used in the MARS models.

However, as the correction factors F_{St} and F_{So} are separately entered into MARS, but multiplied within the model, it suffices to enter one F_T correction factor. F_T-values can either be estimated using a SSC/Fe ratio (as explained in Section 9.3.1) or by multiplying a F_{St} with a F_{So}. The former yielded a F_T-value of 2.85, while the latter yields different estimates based on which correction factors are used. If a F_{St} of 1.9 is used (assuming all authigenic sediment remains in the form of ferrihydrite, and does not increase due to the presence of P), than the F_T can only vary with the degree of sorption. Using the different sorption estimates (mentioned in Section 9.3.3) the F_T can vary from 2.51 (using the 0.5mmol sorption rule) to 3.91 (using the 7mmol sorption rule).

With all of these new insights, it was opted for the final run with the MARS 2.0 model, to use an F_T value of 2.85 to calculate the authigenic contribution of one decade of Grobbendonk sampling data (1999-2009).

9.4 Modelling one decade of authigenic contribution

With all of these new insights, it was opted for the final run with the MARS 2.0 model, to use an F_T value of 2.85 to calculate the authigenic contribution of one decade of Grobbendonk sampling data (1999-2009).

The discharge data was obtained from FHR and put into the WETSPRO module to calculate baseflow, interflow and runoff components, the summarized results of which have already been presented in Table 8.1.

The annual suspended sediment fluxes were calculated based on daily average SSC measurement data procured from the automatic sampling. Gaps in this data set were completed using estimates from the set of rating curves determined in Chapter 6 (Equations 6.9 and 6.10).

All input parameters used in this final run are identical (besides the correction factors F_{So}, F_{St} and F_T) and all are presented next to the previously implemented parameter data in Table 8.4, while Table 9.13 shows the model results of this final model run. On average, this model run places the authigenic contribution to the total observed suspended sediment flux at the Grobbendonk measurement site for the decade 1999-2009 at 61%.

Table 9.13: Authigenic sediment contribution to the total suspended sediment flux for the years 1999 to 2009, obtained by MARS 2.0 modelling, using an F_T-value of 2.85.

Year	Discharge (Mm^3/year)	total SSF (tonne/year)	number of daily SSC-values measured	ASSF (tonne/year)	ASSF/SSF*100 (%)
1998	227	14739	324	9001	61
1999	254	11038	62	6828	62
2000	281	14725	0	10517	71
2001	251	14487	142	9493	66
2002	170	6489	306	4504	69
2003	196	6287	360	4926	78
2004	179	5822	328	4036	69
2005	178	5914	293	4027	68
2006	220	7803	270	7223	93
2007	190	5879	288	3925	67
2008	166	6503	294	4052	62
2009	210	9062	242	6230	70
Average 1999-2009	**227**	**14739**	**324**	**9001**	**61**

It should be noted that this modelling result does not take the uncertainty associated with the Fe(II) concentration in groundwater into account. The median value of the observed range of Fe(II) concentrations was used as input in order to have the most robust and therefore more realistic value. The actual contribution, however, can still significantly vary and more monitoring of the groundwater concentration would therefore be helpful.

Figure 9.9 visualizes the two final annual ASSF model results alongside the observed annual discharge and total SSF values. It is clearly visible that the total SSF as well as the ASSF vary in function of the total annual discharge observed. The contribution that the authigenic sediment represents stays more or less constant. This implies that during dry years, less authigenic sediment is created (because of less Fe(II) entering the river system) but also other sources contribute less to the total sediment flux. During years with higher annual discharge, the authigenic sediment generation is increased, but other sources will proportionally increase as well (because for instance more detrital sediment reaches the river through increased soil loss erosion).

In Section 8.2.1.3 it was observed that the total SSF kept decreasing after 2003 even though the discharge rose again in 2004 and 2005. This trend is indeed overturned in the year 2007, where higher discharges once more generated higher total SSFes. This suggests that the total annual discharge in 2007, and the stream velocities present during individual events within that year, were sufficiently high to cause resuspension of the deposited material, and overcome the consolidation and sediment retention which prohibited resuspension in the year 2004 and 2005.

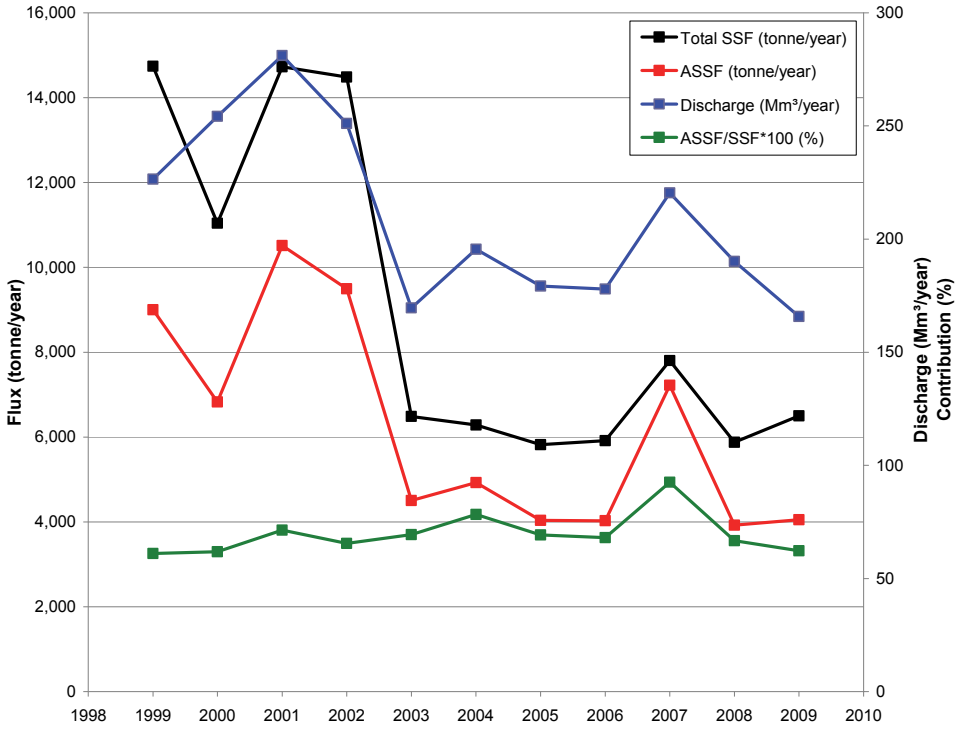

Figure 9.9: Annual Q and SSF-values measured at Grobbendonk monitoring station in the Kleine Nete, as well as modelled annual authigenic sediment fluxes (ASSF), obtained with MARS 2.0, using a F_T = 2.85, and the contributions these ASSFes represent to the total SSF

To conclude, it can also be hypothesized that the sizable contribution of authigenic sediment to the total suspended sediment transport in the Kleine Nete basin, could potentially explain the significant underestimation of sediment transport as reported by the soil erosion and sediment delivery model (WATEM/SEDEM), as previously discussed in Section 6.3. According to the WATEM/SEDEM model the entire Nete only exported 4,500 tonnes in 2005, while the measurements in Grobbendonk (Kleine Nete) already summed up to over 5,800 tonnes in that year. However, of those 5,800 tonnes, 56 to 70% was authigenically generated, and would therefore not be included in the soil erosion part of the WATEM/SEDEM model.

This shows that authigenic sediment should be taken into account in sediment apportionment and transport models.

Part V

Sediment fingerprinting

10. Budgeting sediment sources in the Demer basin using the sediment fingerprinting approach

10.1 Introduction and objectives

River basin managers often find themselves confronted with sediment-related issues, such as soil erosion, deposition and storage of sediment as well as associated nutrients and contaminants on riverbeds. And they try to find the appropriate mitigation strategies (Alvarez-Guerra et al., 2009). In relation to the targeting of management options, reliable information on sediment sources and their relative contribution to downstream sediment fluxes is of vital importance (Collins et al., 2001; Collins & Walling, 2004; Evans et al., 2006).

Some river basin managers make use of available models to predict soil erosion and resulting sediment delivery pressures (e.g. Morgan et al., 1998; Verstraeten et al., 2002; Van Rompaey et al., 2003; Collins et al., 2007). However, validation of the predictions by such models at catchment scale is frequently difficult, especially in situations where the model framework fails to represent the entire sediment budget (Strömqvist et al., 2008). An approach often used to remedy this is sediment fingerprinting. This method is widely used to identify the relative contribution of various watershed sources to the total suspended sediment load.

Sediment fingerprinting is founded on two main assumptions: first, that potential sediment sources can be discriminated on the basis of measurements of physical or chemical properties (otherwise known as fingerprints); and secondly, that comparison of the properties or fingerprints of suspended sediment with those of source material samples allows for determining the relative importance of individual sources.

A myriad of properties has been used for sediment source tracking such as sediment colour (Grimshaw & Lewin, 1980), plant pollen (Brown, 1985), mineral magnetic properties (Caitcheon, 1993; Walden et al., 1997; Dearing, 2000; Hatfield & Maher, 2008), rare earth elements (Kimoto et al., 2006), fallout and/or environmental radionuclides (Olley et al., 1993; Collins & Walling, 2002; Walling, 2003, 2005; Wilkinson et al., 2009), stable isotopes (Douglas et al., 1995; Fox & Papanicolaou, 2007), soil enzyme activity (Nosrati et al., 2011) and the geochemical composition of the sediment (Lewin & Wolfenden, 1978; Collins et al., 1996, 1997 a, 1997 b, 1997 c, 1998, 2001, 2003; Collins & Walling, 2002, 2004, 2007; Walling et al., 1993, 1999; Minella et al., 2008 b; Juracek & Ziegler, 2009; Evrard et al., 2011; Navratil et al., 2012).

Within the framework of this PhD thesis the objectives are:

- To apply the sediment fingerprinting approach (as has been developed and expanded by Prof. dr. Des Walling and Prof. dr. Adrian Collins) in a Flemish river basin (i.e. the Demer basin) using the geochemical composition of the sediment as fingerprints;
- To adapt the methodology if necessary to suit the Flemish situation;
- To compare the sediment fingerprint model results with the sediment fluxes measured at selected tributaries;
- To evaluate the possibility of sediment fingerprinting to apportion authigenic sediment;
- To estimate the applicability of the methodology in other river systems in Flanders.

10.2 Selection of study area in Flanders

The selection of the Demer basin as study area for the sediment fingerprinting research in Flanders was based on the fact that this basin contains some interesting characteristics and represents unique challenges. One of these challenges is the presence of authigenic sediment as a sediment source in the northern tributaries (due to its geological substrate), while this source is lacking in the southern tributaries, as was addressed in Section 4.3.2.3. The geological differences in the subsoil lend themselves to apply a sediment fingerprint based on spatial provenance (as was explained in Section 4.3.3), and therefore at a minimum the northern tributaries should be easily distinguishable from the southern ones, based on geochemical composition of the respective sediment.

Furthermore, the Demer basin (as is the rest of Flanders) is submitted to a significant anthropogenic input (through discharges from sewage treatment facilities and industrial discharges as addressed in Section 4.3.2.2.2). Depending on the nature of the discharges, this might allow further discrimination between tributaries.

10.3 Defining sources in Demer catchment

When defining sources (within the framework of sediment fingerprinting) a common distinction is made between spatial provenance and source type as discussed in Section 4.3.3. Sampling of both types of sources has been executed in the framework of this PhD. The exact localisation and sampling strategy is discussed below.

10.3.1 Spatial provenance

In 2004-2005 a reconnaissance study concerning sediment fingerprinting in the Demer basin was executed in the framework of the master thesis of Jozefien Berckmans, under supervision of Elin Vanlierde (Berckmans, 2005). The intent of this research was to test the methodology of spatial source fingerprinting in the Demer basin, and to investigate if the geologically different substrates observed in the north and the south of the basin would show up in the fingerprint.

As such, the main eight tributary subcatchments of the Demer basin were selected as spatial sediment sources, of which three (the Mangelbeek, Zwartebeek and the Hulpe) drain the northern part of the basin and three (the Gete, the Velpe and the Herk) the southern portion. Geologically, the northern and southern part of the Demer basin differ significantly: the southern part is characterized by loess deposits, and the northern part characterized by iron-rich Tertiary sands producing authigenic iron. The final two subcatchments (the upper reaches of the Demer and the Motte) drain areas underlain by both of the principal geological formations.

Each selected tributary was equipped with a time-integrated sampler (TIS) at a downstream location (as described in Section 2.2.2.1), and the exact location was shown in Figure 2.14. The TISes each collected one sample (from 9 March to 4 May 2005).

The outlet sampling location for the spatial provenance research was selected on the Demer itself at Aarschot, where FHR has a continuous sediment and discharge monitoring station. However, during this preliminary research, no actual sampling could be executed at the Aarschot location, as the attempt to lower a TIS into the river at this location failed. The flow velocity of the river was too high to lower the TIS from the bridge, and the section was too deep to retrieve a deposited TIS. Furthermore, attempts to construct a set-up with ropes to collect it afterwards attracted driftwood, leading to the tipping over of the sampler. In the end, no attempt was made in this

preliminary research to calculate the contributions of the tributaries to the total sediment flux observed in Aarschot.

The TIS samples were wet-sieved, separating the <63µm fraction, which was consequently semi-quantitatively analysed at VITO, using XRF analysis. The preliminary results indicated, based on the one set of samples collected, that the eight tributaries of the Demer could all be discriminated from one another.

To confirm these preliminary findings, a more elaborate sampling campaign was initiated. From 14 March 2007 up until 22 May 2008, the TISes were deployed once more in the tributaries at the exact same locations, and this time they were emptied on a monthly basis. The logbook of these samplings has been reported in Vanlierde et al. (2008). Again, as outlet location FHR's Aarschot sampling location was selected. Even though no TIS samples could be recovered from this location, it was deemed that the insight into the sediment budget at Aarschot sampling location during and prior to the sediment fingerprinting sampling was invaluable.

Therefore, as explained in Section 2.2.1, to obtain mixed sediment samples at the outlet station of Aarschot, approaches other than TIS-sampling had to be attempted. Outlet samples were collected by flow-through centrifugation in addition to automatically collected composite samples. Figure 10.1 shows the sampling periods of the TISes at the tributaries as well as the sampling moments at the Aarschot outlet station. These numberings are from now on used throughout the thesis to name the different outlet samples. Also presented in this figure are the Q and SSC-values obtained through the continuous monitoring efforts.

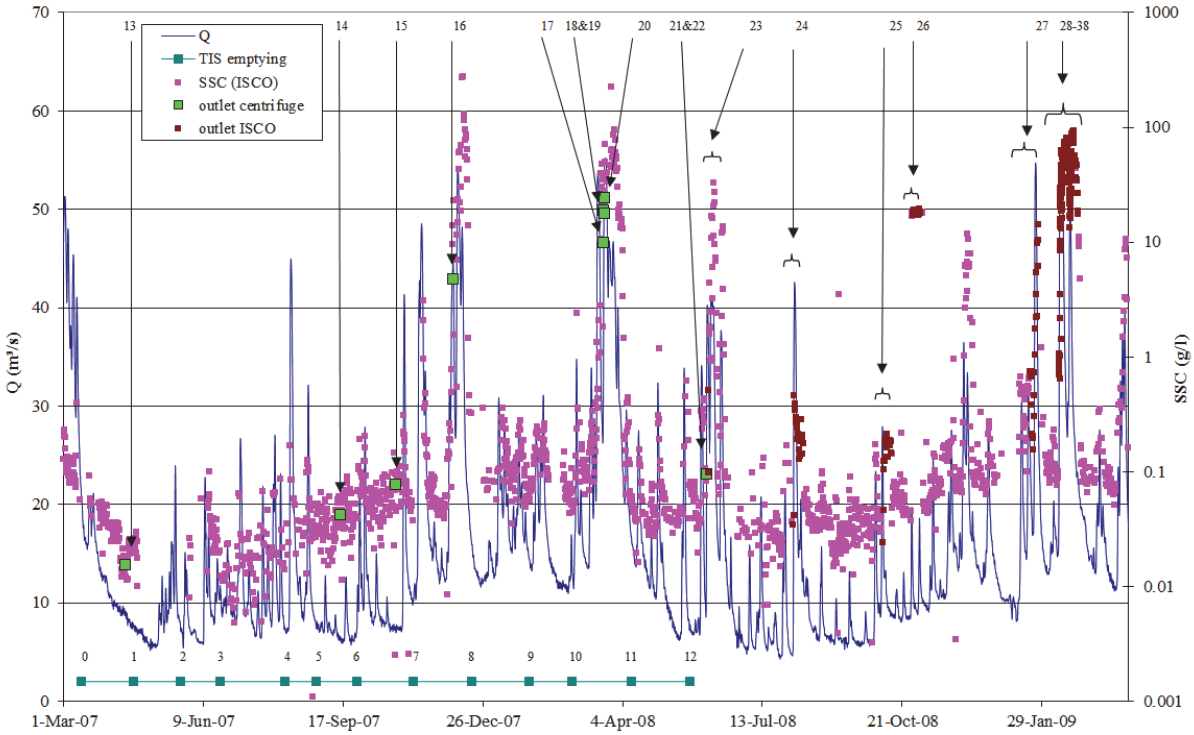

Figure 10.1: Timing of placing (0) and emptying (1-12) of TISes as well as timing of sampling of outlet samples with flow-through centrifuge (13-22) and compositing of automatically collected ISCO samples (23-38). Also represented are the measured Q and SSC_{ISCO}-values.

Samples prepared from the ISCO sampler (samples 23 to 26) did not contain sufficient material to analyse for all properties, and were hence excluded from further research. The complete data set of analysis is reported in Addendum C.

10.3.2 Source types

Besides determining sediment contributions of tributaries to the Demer, it was also opted to sample soil material from different source types (i.e. different soil use types, riverbed material and river banks). Because sampling the entire Demer basin would demand an analysis effort too elaborate within the framework of this PhD, two subcatchments in different geological settings were selected to test the efficacy of the technique.

As southern tributary, the Gete was selected. This largest tributary of all Demer tributaries is constituted of four subcatchments: the Kleine Gete, Grote Gete and Melsterbeek subcatchments, which merge into the Lower-Gete. The outlet location was selected at the discharge measurement location of FHR in Halen, which covers 811 km² of catchment area.

Within this catchment area and along all four subcatchments soil samples were collected of three different soil types, those being: cultivated land (C), Pasture (P) and channel bank (CB). The exact sample locations are shown in Figure 10.2, while the sampling technique used has already been described in Section 2.2.2.2.

Furthermore, riverbed samples were collected by the VMM at selected sampling locations (also indicated in Figure 10.2). The material was transported to the sedimentological laboratory at FHR, where it was processed identically to the other samples collected.

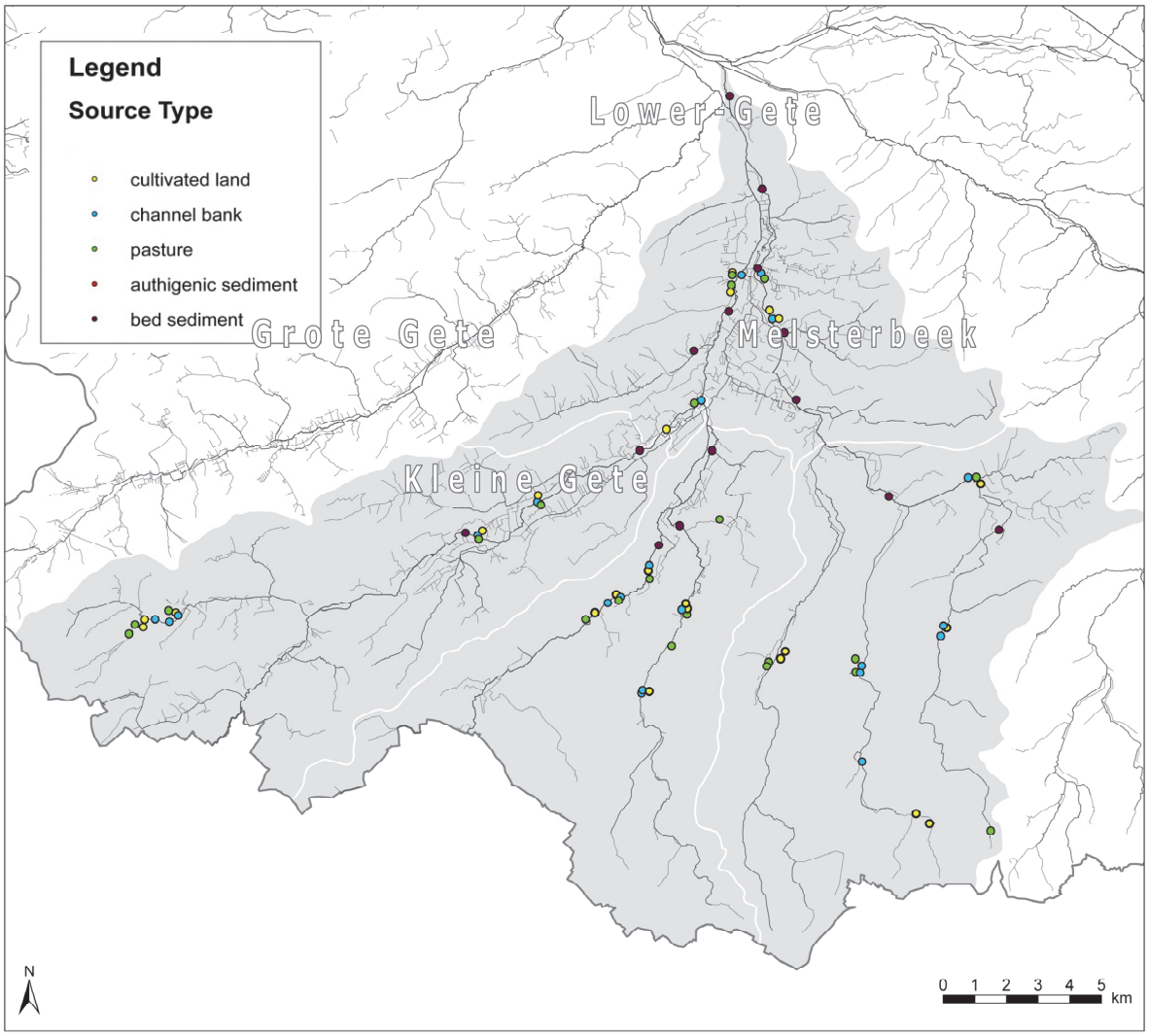

Figure 10.2: Localisation of sediment source sampling in the Gete catchment.

As northern tributary, the Mangelbeek was selected. This smaller tributary is constituted by two subcatchments (the Mangelbeek and the Laambeek). As outlet the FHR/VMM discharge monitoring station of Lummen was selected, which covers 100 km² of catchment area. This entire catchment area was sampled for the same soil types as were investigated in the Gete basin: cultivated land (C), Pasture (P) and channel bank (CB). In addition, in the upstream reaches of the Mangelbeek, authigenic samples (A) were collected (as already addressed in Chapter 9). Again, riverbed samples were collected at selected sampling locations by VMM and analysed in the sedimentary laboratory of FHR and at the University of Antwerp. All sample locations for the Mangelbeek catchment are presented in Figure 10.3.

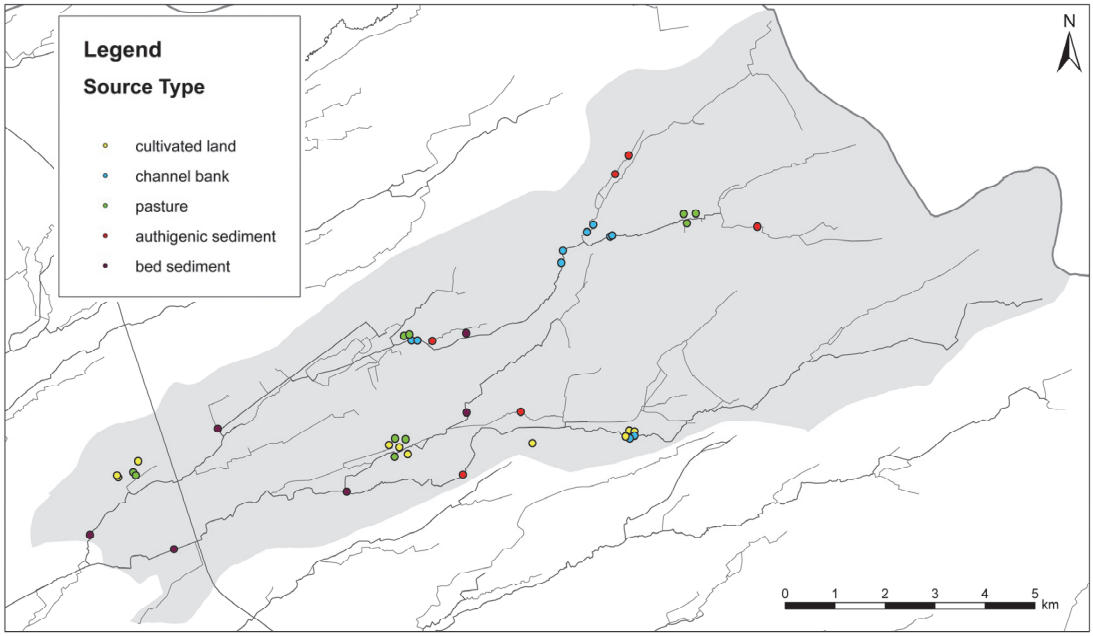

Figure 10.3: Localisation of sediment source sampling in the Mangelbeek catchment.

Analogue to the spatial source samples, these source type samples were consequently prepared for and underwent analysis to obtain a myriad of geochemical and physical parameters as described Section 3.2.2. The complete data set of analysis for the Gete and Mangelbeek catchments are reported in respectively Addendum D and E.

As in the Mangelbeek basin authigenic sediment is a major contributor, results obtained through sediment fingerprinting could potentially confirm the modelling results provided by the MARS 2.0 modelling.

10.4 Methodology of sediment fingerprinting as applied to spatial provenance modelling in the Demer basin

The sediment fingerprinting methodology as applied in this thesis is based on the approach developed at the University of Exeter, by Prof. dr. Des Walling and Prof. dr. Adrian Collins. The methodology section of this chapter uses 'Integrated Assessment of Catchment Sediment Budgets: a technical manual' (Walling & Collins, 2000) as main reference work. Additional literature sources will be mentioned in the text itself.

The sediment fingerprinting procedure involves two main stages, namely: source discrimination and source apportionment.

Source discrimination, which entails the creation of a composite sediment fingerprint, is comprised of a two-step statistical procedure:

a) Employment of a non-parametric statistical test (Kruskal-Wallis H-test) to confirm the power of individual fingerprint properties to distinguish between different sources in an unequivocal manner. Those properties providing greater contrasts between the individual sources generate larger test statistics, and where these exceed the critical value, H0 (i.e. the null hypothesis stipulating that measurements of the fingerprint property show no significant differences between the source categories) is rejected.
b) Using a multivariate Discriminant Function Analysis (DFA) to select from the properties which pass the Kruskal-Wallis H-test, the optimum combination of properties (composite fingerprint) for discriminating between the source groupings. The DFA estimates discriminant function coefficients indicative of the explanatory power of individual fingerprint properties.

Source apportionment on the other hand encompasses the application of a multivariate mixing model, to provide quantitative estimates of the relative contributions of the individual tributaries to the sampled sediment load at the outlet station.

The first application of the fingerprinting approach within the framework of this PhD thesis is to provide a quantitative assessment of the relative contributions of the individual tributaries to the observed sediment load at the basin outlet (Aarschot). The methodology of the fingerprinting approach will be explained using the data from the sampling campaigns.

10.4.1 Sediment source discrimination

The samples from the extensive 2007-2008 sampling campaign were prepared for analysis and consequently analysed for LOI, density, and geochemical composition as described in Section 3.2.2. The geochemical data consisted of the concentration present in the sediment samples of Al, Ca, Fe, K and Si (in weight percentage) and P, S, Ti, Ba, Cr, Cu, Pb, Mn, Ni, Sr, V, Zn, Ce, Cs, Rb and Zr (in ppm). The complete data-set is appended in Addendum C.

10.4.1.1 Preparing the data set

Prior to subjecting this data to the statistical testing described above, the data set was scrutinized. Firstly, samples that were incompletely analysed due to various reasons (insufficient material to perform all analyses, sample loss, …) were removed from the data set. Secondly, parameters of which some measurements fell below the detection limit were addressed.

- If only a few values are below detection limit these values were deleted.
- In the case of V, K and Cs, the southern tributaries are characterized by medium to high levels of these parameters, while the northern tributaries have this parameter fall below detection limit. Therefore, it was opted not to allow these parameters to enter into the Kruskal-Wallis H-Test.

Finally, all remaining elements were subjected to a 'violation test', similar to the one mentioned by Navratil et al. (2012).

This test determines if the values of all properties measured at the outlet, fall within the theoretical range of the values obtained from the tributaries. If not, the failing properties are removed from further analysis.

The upper and lower boundary conditions of this polygon space are calculated as stated in respectively Equations 10.1 and 10.2.

$$Upper\ Boundary = S_{is_{\max}} + stdev_{is_{\max}} \quad \text{Eq. 10.1}$$

in which:
- $S_{is_{\max}}$ is the maximum concentration of property (i) (observed in a source (s))
- $stdev_{is_{\max}}$ is the standard deviation of source (s) in which the maximal value for property S_i was observed

$$Lower\ Boundary = S_{is_{\min}} - stdev_{is_{\min}} \quad \text{Eq. 10.2}$$

in which:
- $S_{is_{\min}}$ is the minimum concentration of property (i) (observed in a source (s))
- $stdev_{is_{\min}}$ is the standard deviation of source (s) in which the minimal value for property Si was observed

However, if the lower boundary calculation yielded a value smaller than zero, the corresponding parameter is considered as failing the test. Either because of the fact that the property in question came close to or fell under the analytical detection limit, or because of the fact that the variability in the tributary with the lowest values is too big.

As there might be a possible need for grain size and organic matter content corrections (as will be discussed in detail in Chapter 11), it has been opted to exclude the proxies to these properties (i.e. LOI, particle size and density) from the statistical analyses.

The remaining properties of the spatial source data set were subjected to the violation test as described above, which Si, S, Cr, Pb and Zr failed while Al, Ca, Fe, P, Ti, Ba, Cu, Mn, Ni, Sr, Zn, Ce and Rb could be allowed into the Kruskal-Wallis H-testing. Furthermore, after elimination of one erroneous S-concentration value in a Hulpe sample, S could be allowed to enter as well.

10.4.1.2 Kruskal-Wallis H-test

The reduced data set (containing only the 14 properties that passed the prior screening and violation testing) was entered into the SPSS software package where the individual properties were submitted to a Kruskal-Wallis H-Test (KW-test).

It is important to recognise that this sort of testing confirms only the presence of general differences between the group means, and not if there are statistically significant differences between all possible source category pairs.

All 14 properties passed the test, by generating test statistics higher than the critical value at 95% confidence. The test results are presented in Table 10.1.

Therefore, all 14 properties were allowed to enter the Discriminant Function Analysis (DFA) in order to obtain a high-performance composite fingerprint.

Table 10.1: Results of the KW-test for the spatial sources sediment samples.
* = properties passing the test @ 95% confidence

Fingerprint property	H-value	P-value
Al	76.642	<0.001*
Ca	64.084	<0.001*
Fe	78.849	<0.001*
Si	74.492	<0.001*
P	75.306	<0.001*
S	69.747	<0.001*
Ti	76.845	<0.001*
Ba	74.958	<0.001*
Cu	65.099	<0.001*
Mn	57.903	<0.001*
Ni	65.784	<0.001*
Sr	65.018	<0.001*
Zn	77.212	<0.001*
Ce	77.679	<0.001*

10.4.1.3 Discriminant Function Analysis

The 14 elements which passed the KW-test were consequently put into a multivariate stepwise DFA based on the minimisation of Wilks' lambda to identify the optimum (i.e. the smallest) combination of properties, or composite fingerprint, for discriminating sediment sources. Therefore, at each step, the variable that minimizes the overall Wilks' lambda is allowed to entered. The minimal partial F-value to allow a parameter to enter was set at 3.84, while the maximal F-value for removal from the composite fingerprint was 2.71. These are the standard settings of the SPSS software.

Prior to testing the different parameters, the classification coefficients are adjusted to take the observed group sizes into account. Separate-groups covariance matrices are used for classification.

The stepwise selection will end when all source material samples are classified correctly, or when none of the remaining properties avaiable for inclusion in the composite fingerprint, improve the discrimination significantly.

In case of the 14 properties that passed the KW-test, the stepwise DFA selected 11 elements (Ti, Zn, Ba, Ce, Fe, Rb, Sr, P, Ca, Mn and Ni) to create a composite fingerprint with a predictive power (PP) of 98.8%. Figure 10.4 visualizes the discriminative power of this fingerprint, and shows the close relation between two of the northern sources (Mangelbeek (source nr 6) and Zwartebeek (source nr 5)) on the one hand, and most of the southern sources (Velpe (source nr 3), Gete (source nr 4), Herk (source nr 7) and Demer-upstream (source nr 8)) on the other hand. Only the Motte (source nr 1) and the Hulpe (source nr 2) are clearly separated from the other tributaries on the graph.

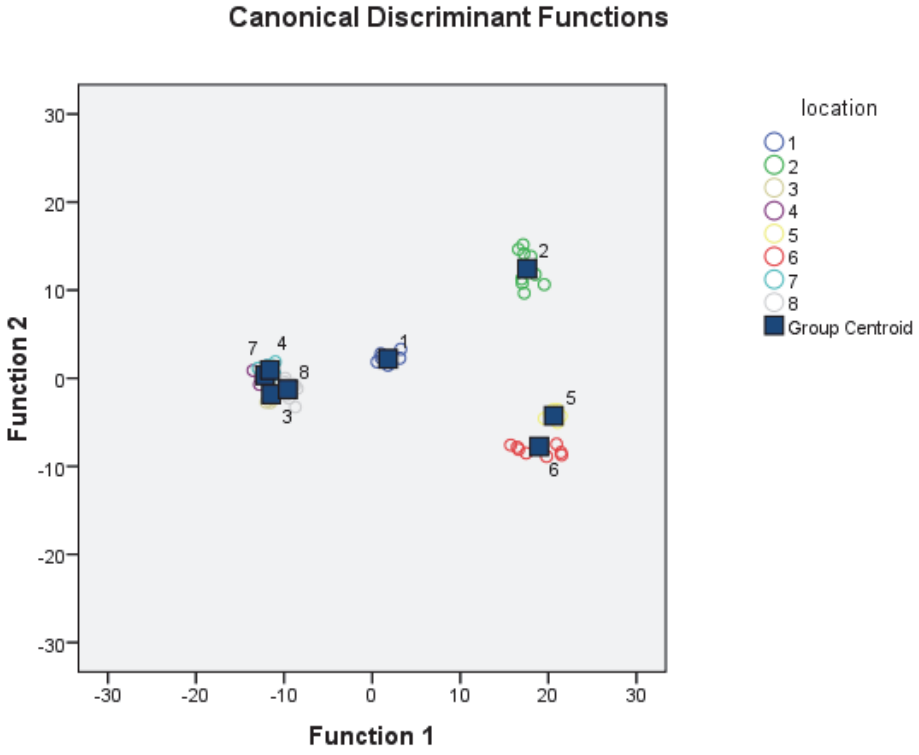

Figure 10.4: Canonical discriminant functions showing the discriminative power of the composite fingerprint which incorporates Ti, Zn, Ba, Ce, Fe, Rb, Sr, P, Ca, Mn and Ni. Sample locations: 1 = Motte; 2 = Hulpe; 3 = Velpe; 4 = Gete; 5 = Zwartebeek; 6 = Mangelbeek; 7 = Herk; 8 = Demer upstream

Table 10.2 shows the selected properties within the composite fingerprint as well as their cumulative predictive power and the Wilks' Lambda values.

Table 10.2: Stepwise DFA output, using the 14 elements passing the KW-test

Step	Fingerprint property	Cumulative predictive power (%)	Wilks' Lambda
1	Ti	60.5	0.019
2	Zn	84.9	0.003
3	Ba	90.7	0.001
4	Ce	93	<0.001
5	Fe	98.8	<0.001
6	Rb	98.8	<0.001
7	Sr	100	<0.001
8	P	100	<0.001
9	Ca	100	<0.001
10	Mn	100	<0.001
11	Ni	98.8	<0.001

However, ideally, a composite fingerprint for discriminating 8 different sources should consist of only 9 properties (one more than there are tributaries, to fulfil the mathematical demands of the model). Therefore, the following methodology was developed and applied in an attempt to decrease the number of properties in the composite fingerprint, without decreasing its predictive power.

To start all properties were entered into a DFA individually and their individual predictive powers were tabulated (see Table 10.3). Additionally, each property's capability to correctly discriminate between individual sources was represented in Table 10.4. Elements Fe, Ce, P, Rb and Zn have good classification power for discriminating between sources 2 and 5 and sources 3-4-7-8, where, Sr helps to discriminate between sources 2 and 5 and S, Ba, Ni and Al can help to discriminate between sources 3-4-7 and 8.

Table 10.3: Discriminatory powers of individual parameters

	Individual predictive power (%)
Fe	75.3
Ce	64.7
Zn	62.4
Sr	62.4
Al	60.5
Ti	60.5
P	57.6
Ba	54.1
Ca	50.6
S	50.0
Rb	48.8
Ni	47.1
Cu	44.7
Mn	40.0

Table 10.4: Percentages of correctly predicted group membership for every individual property. 1 = Motte; 2 = Hulpe; 3 = Velpe; 4 = Gete; 5 = Zwartebeek; 6 = Mangelbeek; 7 = Herk; 8 = Demer upstream

	1	2	3	4	5	6	7	8
Al	100	73	0	38	20	90	75	92
Ca	0	91	70	8	10	90	75	58
Fe	100	91	60	54	80	70	67	100
P	25	91	10	100	50	80	92	0
S	13	55	60	31	40	40	75	75
Ti	100	82	60	23	30	90	33	83
Ba	100	64	30	77	0	80	58	25
Cu	25	9	20	69	0	70	58	58
Mn	38	91	10	0	0	80	25	83
Ni	50	91	30	23	0	30	50	100
Sr	75	91	20	69	80	90	50	33
Zn	63	18	50	62	80	80	75	50
Ce	100	82	80	23	50	80	33	100
Rb	50	73	0	23	60	20	75	83

Consequently, out of these 10 elements (Fe, Ce, P, Rb, Zn, Sr, S, Ba, Ni and Al) all combinations of nine elements were tested with a DFA. In this case, the DFA is not a stepwise function, driven by minimisation of Wilks' Lambda, but rather the nine remaining elements are entered together, therefore, the Wilks' Lambda is not reported. All composite fingerprints discriminated between 98.8 and 100% (see Table 10.5). All of these composite fingerprints are acceptable to be used in the consequent source apportionment modelling.

Of the seven composite fingerprints that yielded a predictive power of 100% one was randomly selected. This fingerprint consists of the following properties: Fe, Sr, Ce, Ba, Rb, P, Al, S and Ni, and will be called Composite Fingerprint A in the rest of this thesis. Its cumulative predictive power is presented in Table 10.6

Table 10.5: Predictive powers of tested composite fingerprints from combination of nine properties in search of Composite Fingerprint A. *= Selected fingerprint

Tested fingerprints	Predictive power (%)
CePRbZnSrSBaNiAl	98.8
FePRbZnSrSBaNiAl	100
FeCeRbZnSrSBaNiAl	100
FeCePZnSrSBaNiAl	98.8
FeCePRbSrSBaNiAl*	100
FeCePRbZnSBaNiAl	100
FeCePRbZnSrBaNiAl	100
FeCePRbZnSSrNiAl	98.8
FeCePRbZnSSrBaAl	100
FeCePRbZnSSrBaNi	100

Table 10.6: Cumulative predictive power of Composite Fingerprint A

step	Property added	Cumulative predictive power (%)
1	Fe	75.3
2	Sr	80
3	Ce	83.5
4	Ba	96.5
5	Rb	98.8
6	P	98.8
7	Al	98.8
8	S	98.8
9	Ni	100

10.4.2 Sediment source apportionment

When a composite fingerprint with sufficient discriminating power can be obtained, it is consequently used to compare the signature of potential sources to that of the sediment outlet samples and to calculate the relative contribution of these individual sources to the total suspended load. To calculate this contribution, a multivariate mixing model needs to be constructed, using linear optimisation algorithms.

10.4.2.1 Principles and algorithms

The sediment mixing model used to obtain quantitative source ascription, is in fact a set of optimisation algorithms that is constrained by boundary conditions. These constraints are based on the simple assumption that the fingerprint property concentrations in any given outlet sample are dependent upon the concentrations of these properties in the various source materials and the contributions of these source material to the outlet sample.

Therefore, the first constraint (noted in Equation 10.3) ensures that the relative contribution from each potential source cannot be smaller than zero or larger than 100%, while the second constraint (Equation 10.4) makes sure that the sum of all source contributions equals 1.

$$0 \le P_s \le 1$$ Eq. 10.3

$$\sum_{s=1}^{n} P_s = 1$$ Eq. 10.4

in which:
- P_s is the optimised percentage contribution from source groupings (s)
- n is number of spatial sediment sources (i.e. eight tributaries).

The sediment mixing model itself is comprised of as many linear equations as there are properties selected in the composite fingerprint (i.e. nine equations for the nine properties in composite fingerprint A). These linear equations relate the concentration of each property (i) in the outlet sample to the mixture representing the sum of the contributions from the different sources.

This set of linear equations is overdetermined, as there are more equations (nine) than there are variables (eight tributaries), which means it cannot be solved directly. Therefore, a sediment mixing model algorithm (referred to as the *objective function of Collins (1995)*, in Walling & Collins (2000)) is created, which when minimized, achieves optimisation of the estimates for the relative contributions from the individual sources. This objective function takes the form of Equation 10.5.

$$\sum_{i=1}^{m} \left(\frac{C_i - \left(\sum_{s=1}^{n} P_s S_{si} F_s \right)}{C_i} \right)^2 \cdot W_i$$ Eq. 10.5

in which:
- C_i = concentration of fingerprint property (i) for the outlet sample
- S_{si} = concentration of fingerprint property (i) for source grouping (s);
- F_s = general correction factor for source grouping (s)
- W_i = Discriminatory Weighting Correction Factor
- n = number of spatial sediment sources (i.e. eight tributaries).
- m = number of fingerprint properties comprising the optimum composite fingerprint (i.e. nine properties in Composite Fingerprint A)

The mixing model algorithm involves the finding of a (local) minimum of the relative errors based on the normalisation of the fingerprint property data. This is accomplished by dividing the result of the subtraction of the predicted property concentration of the mixture of sources from the property concentration of the outlet by the latter.

In the objective function (Equation 10.5) two correctional factors are expressed: a weighting correction factor (W_i) and a general correction factor F_s (which combines corrections for grain size and organic matter content). These are addressed in detail in the next sections.

10.4.2.2 Discriminatory Weighting Correction Factor (W_i)

The Discriminatory Weighting Correction Factor (W_i) is introduced to give more weight to the properties with more predictive power, allowing for a better predictive result, as proposed in Collins et al. (2010 a).

This weighting is based on the relative discriminatory efficiency of each individual property (see Table 10.3). As the discrimination of the source samples collected from any subcatchment will vary for each property in the corresponding optimum signature, it is logical to weigh the optimised mixing model solutions on this basis. The correction factor is determined by dividing the individual

discriminatory power of each property by the property in the composite fingerprint that has the lowest individual discriminatory power. The results of these calculations are the W_i's, shown in Table 10.7 and are used in the respective objective functions.

10.4.2.3 Particle size (GS_s) and Organic Matter Content (OM_s) Correction Factors

The general correction factor F_s is expressed in the sediment mixing model algorithm of Collins (1995) (referred to as the *objective function of Collins (1995)*, in Walling & Collins (2000)) as the product of a particle size correction factor and an organic matter content correction factor (Equation 10.6).

$$F_s = GS_s \cdot OM_s \qquad \text{Eq. 10.6}$$

in which: - GS_s is the particle size correction factor for source grouping (s)
- OM_s is the correction factor for organic matter content for source grouping (s)

However, in the objective function of Walling et al. (1993) (as it is referred to in Walling & Collins (2000)) F_s equals 1. In other words, no corrections were applied. It is therefore arguable if one needs to correct for grain size and/or organic matter content or not.

Table 10.7: Discriminatory Weighting Correction Factors (W_is) determined for properties of Composite Fingerprint A

	W_i
Fe	1.60
Ce	1.37
Sr	1.32
Al	1.29
P	1.22
Ba	1.15
S	1.06
Rb	1.04
Ni	1.00

Collins (1995) argues the necessity of a particle size correction factor due to the well-established relationship between particle size and element concentrations in soils and sediments (He & Owens, 1995; He & Walling, 1996; Horowitz, 1991; Horowitz & Elrick, 1987; Thorne & Nickless, 1981). As a result it is only possible to compare fingerprint property concentrations in a sediment sample with those of its potential source areas if both have similar grain sizes. And as both sediment mobilisation, delivery and even transport can result in sorting of sediment, generally, the outlet samples tend to be finer than the potential source material (Morris & Fan, 1998). Therefore, according to Collins et al. (1997 b) a particle-size or specific surface-area normalisation generally is required prior to sediment-source estimation.

One way of addressing this problem is by sieving the samples (isolating the <63µm fraction) prior to analysis, therefore restricting the analysis of fingerprinting properties to the fine fraction. However, a further and more detailed particle size correction factor is incorporated in the objective function of Collins (1995) which uses the ratio of the specific surface area (SSA) of source and outlet samples. It takes the shape of Equation 10.7.

$$GS_S = \frac{SSA_{outlet}}{SSA_{source}} \qquad \text{Eq. 10.7}$$

in which: - SSA_{outlet} = specific surface area of each outlet sample (m²/g)
- SSA_{source} = mean specific surface area of the samples for source grouping (s) (m²/g)

The SSA of the sediment was not measured directly in the laboratory, but it can be calculated based on the grain size and the density of the material, which have been determined as stated in Chapter 3. The conversion algorithm is stated in Equation 10.8.

$$SSA = \frac{6}{D[3,2] \cdot \rho} \qquad \text{Eq. 10.8}$$

in which:
- SSA = specific surface area (m²/g)
- D[3,2]= surface weighted mean diameter of the particle (µm)
- ρ = density (g/cm³)

Therefore, for each outlet sample a set of grain size correction factors was determined (one for each tributary) by dividing the SSA of the outlet sample by the mean SSA of the specific tributary. The results of which are reported in Table 10.8.

Table 10.8: Grain size correction factors for each tributary and for each outlet sample. Sample locations: 1 = Motte; 2 = Hulpe; 3 = Velpe; 4 = Gete; 5 = Zwartebeek; 6 = Mangelbeek; 7 = Herk; 8 = Demer upstream

Outlet sample numbering	Locations							
	1	2	3	4	5	6	7	8
13	0.75	0.60	0.68	0.72	0.47	0.52	0.72	0.80
14	1.43	1.15	1.29	1.37	0.89	1.00	1.37	1.52
15	1.20	0.96	1.08	1.15	0.74	0.84	1.15	1.27
16	1.28	1.03	1.15	1.23	0.79	0.89	1.23	1.36
17	1.32	1.06	1.19	1.27	0.82	0.92	1.27	1.41
18	1.31	1.06	1.19	1.26	0.82	0.92	1.26	1.40
19	1.09	0.88	0.99	1.05	0.68	0.77	1.05	1.16
20	1.37	1.10	1.24	1.32	0.85	0.96	1.32	1.46
21	2.07	1.67	1.87	1.99	1.29	1.45	1.99	2.20
22	2.05	1.65	1.85	1.97	1.27	1.43	1.97	2.18
27	1.18	0.95	1.07	1.14	0.73	0.83	1.14	1.26
28	1.19	0.96	1.08	1.15	0.74	0.83	1.15	1.27
29	1.09	0.88	0.98	1.05	0.68	0.76	1.05	1.16
30	1.06	0.85	0.96	1.02	0.66	0.74	1.02	1.13
31	1.01	0.81	0.91	0.97	0.62	0.70	0.97	1.07
32	0.80	0.65	0.73	0.77	0.50	0.56	0.77	0.86
33	0.98	0.79	0.89	0.95	0.61	0.69	0.95	1.04
34	1.15	0.93	1.04	1.11	0.71	0.80	1.11	1.22
35	1.31	1.06	1.19	1.26	0.82	0.92	1.26	1.40
36	1.11	0.90	1.00	1.07	0.69	0.78	1.07	1.18
37	0.95	0.77	0.86	0.92	0.59	0.66	0.92	1.01
38	1.12	0.90	1.01	1.08	0.69	0.78	1.08	1.19

As stated in Equation 10.6, Collins (1995) introduced in his F_s, besides a particle size correction, also an organic matter content correction factor. This correction factor was introduced because the amount of organic matter present can influence element concentrations (Hirner et al., 1990) and it takes the shape of Equation 10.9.

$$OM_s = \frac{OMC_{outlet}}{OMC_{source}} \qquad \text{Eq. 10.9}$$

in which:
- OMC_{outlet} is the organic matter content of each outlet sample (%)
- OMC_{source} is the mean organic matter content of the samples for source grouping (s) (%)

However, Walling & Collins (2000) remark that entering the OM_s in the objective function is not always beneficial to its apportioning power, as the relationship between organic matter content and element concentration is complex, and may result in an overcorrection of the property concentrations of the coarser material, when it is used in combination with the particle size correction (Collins et al. 1997 a; Walling et al. 1999, 2003). Also Juracek & Ziegler (2009) state similar objections against a combined particle size and organic matter correction.

They state that the relation between organic matter and constituent concentrations is complex and difficult to generalize and quote Walling (2005) in his findings that enrichment in organic matter is closely related to enrichment in fine particles. Furthermore, Russel et al. (2001) conclude that particle-size normalisation likely accounts, in part, for differences in organic matter content.

In the framework of this PhD, OM correction factors have been determined (using LOI as a surrogate for organic matter content) in a fashion similar to the determination of Z_s: for each outlet sample a set OM_s was determined (one for each tributary) by dividing the LOI observed in the outlet sample by the mean LOI of the specific tributary. The results of which are reported in Table 10.9.

Table 10.9: Organic matter content correction factors for each tributary and for each outlet sample. Sample locations: 1 = Motte; 2 = Hulpe; 3 = Velpe; 4 = Gete; 5 = Zwartebeek; 6 = Mangelbeek; 7 = Herk; 8 = Demer upstream

Outlet sample numbering	Locations							
	1	2	3	4	5	6	7	8
13	2.06	1.14	3.85	4.87	1.42	1.32	3.98	1.80
14	0.69	0.38	1.29	1.63	0.48	0.44	1.33	0.60
15	1.02	0.56	1.91	2.42	0.71	0.66	1.98	0.90
16	0.43	0.24	0.80	1.01	0.30	0.28	0.83	0.38
17	0.55	0.30	1.03	1.30	0.38	0.35	1.06	0.48
18	0.59	0.33	1.10	1.39	0.41	0.38	1.14	0.52
19	0.37	0.20	0.68	0.86	0.25	0.23	0.71	0.32
20	0.47	0.26	0.87	1.10	0.32	0.30	0.90	0.41
21	0.64	0.35	1.19	1.51	0.44	0.41	1.24	0.56
22	0.62	0.34	1.15	1.45	0.42	0.39	1.19	0.54
27	0.82	0.45	1.54	1.94	0.57	0.53	1.59	0.72
28	0.65	0.36	1.22	1.55	0.45	0.42	1.27	0.57
29	0.47	0.26	0.88	1.12	0.33	0.30	0.91	0.41
30	0.43	0.24	0.80	1.01	0.30	0.27	0.83	0.38
31	0.43	0.23	0.79	1.00	0.29	0.27	0.82	0.37
32	0.28	0.16	0.53	0.67	0.19	0.18	0.55	0.25
33	0.44	0.24	0.82	1.04	0.30	0.28	0.85	0.39
34	0.52	0.29	0.97	1.23	0.36	0.33	1.00	0.45
35	0.51	0.28	0.96	1.21	0.35	0.33	0.99	0.45
36	0.56	0.31	1.04	1.32	0.39	0.36	1.08	0.49
37	0.40	0.22	0.75	0.95	0.28	0.26	0.78	0.35
38	0.52	0.29	0.97	1.23	0.36	0.33	1.00	0.45

However, the OM correction factors were not used in the multivariate mixing model together with grain size correction factors, due to the warnings in the literature. The model was run multiple times, allowing different combinations of correction factors to enter the objective function, thus being able to test their efficacy. Which combinations were introduced, is visually presented in Table 10.10.

It should be mentioned that when correction factors such as OM or GS correction factors are introduced into the objective function, they will affect the polygon space, as mentioned in Section 10.4.1.1. Therefore, the violation test (as stated in Equations 10.1 and 10.2) needs to be adjusted to incorporate the effect of these correction factors. The modified version of this test, taking GS corrections into account, is presented in Equations 10.10 and 10.11 while Equations 10.12 and 10.13 show the modified violation test taking the OM corrections into account.

Table 10.10: Overview of the different mixing model produced for a composite fingerprint, using combinations of correction factors entered into the objective function

Name model	Correction Factor		
	W_i	GS_S	OM_S
Zero			
PP	x		
GS		x	
GSPP	x	x	
OM			x
OMPP	x		x

$$Upper\ Boundary = (S_{is_{max}} + stdev_{is_{max}}) \cdot GS_{s_{max}} \qquad \text{Eq. 10.10}$$

in which:
- $S_{is_{max}}$ is the highest concentration of property (i) present in the dataset (observed in a source (s))
- $stdev_{is_{max}}$ is the standard deviation of source (s)
- $GS_{s_{max}}$ is the highest grain size correction factor (observed in that source (s))

$$Lower\ Boundary = (S_{is_{min}} - stdev_{is_{min}}) \cdot GS_{s_{min}} \qquad \text{Eq. 10.11}$$

in which:
- $S_{is_{min}}$ is the lowest concentration of property (i) present in the dataset (observed in a source (s))
- $stdev_{is_{min}}$ is the standard deviation of source (s)
- $GS_{s_{min}}$ is the lowest grain size correction factor (observed in that source (s))

$$Upper\ Boundary = (S_{is_{max}} + stdev_{is_{max}}) \cdot OM_{s_{max}} \qquad \text{Eq. 10.12}$$

in which:
- $S_{is_{max}}$ is the highest concentration of property (i) present in the dataset (observed in a source (s))
- $stdev_{is_{max}}$ is the standard deviation of source (s)
- $OM_{s_{max}}$ is the highest organic matter correction factor (observed in that source (s))

$$Lower\ Boundary = (S_{is_{min}} - stdev_{is_{min}}) \cdot OM_{s_{min}} \qquad \text{Eq. 10.13}$$

in which:
- $S_{is_{min}}$ is the lowest concentration of property (i) present in the dataset (observed in a source (s))
- $stdev_{is_{min}}$ is the standard deviation of source (s)
- $OM_{s_{min}}$ is the lowest organic matter correction factor (observed in that source (s))

Once more, the values of the the values of all properties measured at the outlet must fall within these boundary conditions. If not, the failing properties should be removed from further analysis.

The elements which had passed the violation tests without correction factors (Al, Ca, Fe, P, Ti, Ba, Cu, Mn, Ni, Sr, Zn, Ce and Rb) all passed the adjusted violation tests. Therefore, Composite Fingerprint A, obtained and described in the previous section, can also be used in the modelruns which have GS or OM corrections in them.

10.4.2.4 Concentration values of fingerprint properties per source grouping (S_{si})

One of the main parameters in the objective function (Equation 10.5), is the concentration of a specific fingerprint property for each source grouping (S_{si}). In multiple studies (Collins, 1995; Collins et al., 1996; 1997 b; 1998; Walling et al., 2003; Minella et al., 2008 b; Nosrati et al., 2011)

the value used is the mean concentration associated with a specific source as the concentrations of individual samples may vary significantly. As such, the mean concentration value calculated will more effectively represent the mixture that will originate from this specific source.

However, using an optimisation procedure to find a minimum for this objective function to determine the contributions of different sources to the total sediment load may introduce problems of equifinality, in that several different parameter combinations could possibly produce the same goodness of fit. Recognition of this problem and the uncertainties introduced by the natural variability of source material properties has prompted the application of Bayesian statistics, Monte Carlo routines and other uncertainty analysis to the model fitting procedure (e.g., Rowan et al., 2000; Motha et al., 2003; Small et al., 2002; Douglas et al.,2003; Evrard et al., 2011; Mukundan et al., 2011; Navratil et al., 2012; amongst others).

In this thesis, a Monte Carlo framework was used to address the uncertainty caused by the use of the objective function. Probablility density functions (pdfs) of random deviates for the mean concentration of fingerprint properties of the different sources were generated using the mean and the standard deviation of the property measurements as location and scale estimators. This methodology has been widely used in sediment fingerprinting research (Krause et al., 2003; Motha et al., 2004; Collins and Walling, 2007; Martínez-Carreras et al., 2010; Collins et al., 2010 a).

In more recent publications (Collins et al., 2010 b, 2012), robust estimators median and Qn (the latter as an alternative to the median absolute deviation (MAD)) have been used to generate the deviates, as these estimators are less sensitive to outliers, which are often side effects of collecting relatively few source samples.

Also, Collins et al. (2012) investigated whether the method of sampling deviates of fingerprint property from the pdfs has an influence on the outcome of the mass balance modelling. Conventional random sampling (as had been applied in many fingerprint studies up to that point) was compared to a more stratified sampling, such as Latin Hypercube Sampling (LHS). For the latter approach, the pdfs are divided into a number of equal probability intervals, which ensures a more systematic sampling of the entire pdf with fewer repeat iterations.

As the findings of Collins et al. (2012) suggested that for their dataset, no significant differences could be found between the predicted deviate mean or median proportions for any given source generated by the different types of uncertainty analysis, the methodology using conventional statistics was applied in this thesis, to generate the pdfs of the property concentrations obtained for each potential source

The mean and standard deviations for each property in the composite fingerprint were calculated for each tributary separately (using all available samples), and these statistics are presented in Table 10.11 for all properties that passed the KW-test.

Consequently, the objective function was solved 1,000 times, using each permutation of the Monte Carlo uncertainty analysis. This permits estimation of deviate means. Other studies used higher numbers of iterations (for example Collins et al. (2012) used 5,000 iterations, Evrard et al. (2011) and Navratil et al. (2012) used 10,000 iterations). However, the actual number of iterations entered into the mass balance model is only of importance to ensure that the Monte Carlo repeat solutions converge to one solution. Whether or not this convergence takes place, can be estimated by investigating the 95% confidence limits about the overall average mean source proportions.

Therefore, within the framework of this PhD, both methods (using the mean observed property concentrations as well as using 1,000 Monte Carlo (MC) simulated mean property concentrations) were applied.

To conclude, it is noteworthy to address the search tool used to find an optimum (minimum) in the objective function. Most work using mass balance mixing models for sediment source fingerprinting has been based on local optimisation tools. Such search tools, however, can struggle with identifying globally representative solutions, especially if the objective function is characterised by localised extremes. To address this issue, Collins et al. (2010 b) suggested using a modelling framework incorporating both local and global optimisation.

Results from this study, as well as from Collins et al. (2012) suggest that global optimisation does not necessarily yield better results, and whether it does or not is dataset-specific.

This, combined with the fact that the iteration time for global optimisation is significant (up to 10hours for one run), lead to the conclusion to only use local optimisation tools within the framework of this PhD.

10.5 Modelling and data-analysis

10.5.1 Modelling using Composite Fingerprint A and mean property concentrations

The mixing model algorithms (based on Fingerprint A) were applied, using iterative routines available in the Solver function within Microsoft Excel for Windows. For the methodology of how to program this into Excel, the reader is referred to Walling & Collins (2000), which describes this process in detail.

The initial settings (prior to starting the solver function) are:

- Property concentrations S_{Si}: mean concentration for each tributary (as reported in Table 10.11)
- Source contribution P_s: all 8 potential sources start with an equal contribution of 0.125
- As the model is run for various combinations of correction factors, they are implemented or are left to equal 1 if they are excluded. In total six different models were constructed for each outlet sample (see Table 10.10).

Consequently, the solver function of MS Excel was run to minimize the objective function, and the resulting contributions of the various tributaries for each of the model runs have been presented in Table F.1 (in Addendum F). This addendum tabulates all detailed sediment fingerprinting modelling results. Also reported in Table F.1 are the relative mean errors (RME) associated with every model run. This is a means of estimating the goodness-of-fit provided by the mixing model and is calculated by comparing the actual fingerprint property concentrations measured in the sediment samples with the corresponding values predicted by the optimization procedure. The RME-value is the average for all properties included in each composite fingerprint.

Collins & Walling (2007) reported RME-values in between 9 and 14% as acceptable, while Minella et al. (2008 b) suggested relative errors of <17% indicated that the optimised mixing model was able to provide acceptable predictions of the fingerprint property concentrations associated with the outlet samples. Therefore, within the framework of this PhD a cut-off percentage of 15% RME was deemed acceptable.

Table 10.11: Mean values and standard deviations of property concentrations per tributary. Properties indicated with * are present in Composite Fingerprint A; <dl are values below detection limit.

	Motte		Hulpe		Velpe		Gete		Zwartebeek		Mangelbeek		Herk		Demer	
	mean	stdev	mean	stdev	mean	stdev	mean	stdev	mean	stdev	mean	stdev	mean	stdev	mean	stdev
LOI (%)	20.5	1.9	37.2	4.3	11.0	2.2	9.0	2.0	29.7	2.0	32.1	3.1	10.6	1.8	23.4	5.4
density (g/cm³)	3.0	0.0	3.5	0.2	2.7	0.0	2.7	0.0	3.8	0.2	3.5	0.2	2.7	0.0	2.8	0.1
SSA (m²/g)	0.2	0.0	0.2	0.1	0.2	0.0	0.2	0.0	0.3	0.0	0.3	0.0	0.2	0.0	0.2	0.0
Al (%) *	2.3	0.1	1.0	0.2	4.0	0.3	4.1	0.5	1.2	0.2	1.6	0.2	3.9	0.3	3.2	0.3
Ca (%)	1.0	0.3	7.0	2.9	0.8	0.2	1.4	0.3	0.6	0.2	0.5	0.1	2.0	0.5	1.4	0.2
Fe (%) *	12.1	0.4	14.8	3.9	3.5	0.5	2.8	0.6	23.2	1.1	20.6	1.4	3.0	0.3	7.2	1.5
K (%)	2.8	0.3	< dl	< dl	2.4	0.3	2.5	0.5	< dl	< dl	0.2	0.1	2.4	0.3	1.2	0.3
Si (%)	38.7	4.9	4.0	3.6	81.3	11.4	93.7	11.8	2.7	3.4	9.4	4.3	84.0	8.1	49.4	14.9
P (ppm) *	7471.8	1314.9	14102.9	2466.8	3246.2	718.2	1636.0	238.8	9934.6	1346.7	8121.3	1377.7	3232.0	618.2	10417.8	3737.3
S (ppm) *	2385.4	579.8	3136.9	718.3	1374.3	281.6	1493.7	446.6	2582.7	715.2	4662.3	1341.8	1800.7	301.4	8163.0	2738.3
Ti (ppm)	2647.3	50.8	1286.7	147.6	4076.4	130.3	3984.2	158.1	1496.7	169.3	2073.2	289.6	4002.8	129.5	3729.9	113.8
Ba (ppm) *	295.4	6.0	309.6	47.3	452.3	31.1	476.9	12.4	245.5	30.0	242.7	17.3	503.7	22.9	483.3	16.7
Cr (ppm)	65.9	6.8	29.5	16.0	56.2	6.7	73.6	13.0	26.9	24.1	41.1	12.9	68.5	14.4	305.8	113.3
Cu (ppm)	49.4	9.4	274.1	596.5	34.9	6.5	32.3	7.1	53.0	26.9	75.2	16.0	41.2	7.3	98.7	30.7
Pb (ppm)	39.9	7.6	74.1	35.4	12.5	5.4	15.1	6.9	135.1	17.4	131.4	9.3	14.6	4.5	91.2	29.4
Mn (ppm)	433.2	83.9	185.2	94.4	978.8	298.0	649.5	264.0	489.5	214.6	480.6	71.3	1041.7	420.1	753.6	137.6
Ni (ppm) *	26.1	1.9	23.6	0.3	35.7	1.7	37.1	3.6	26.6	7.1	30.9	4.9	35.1	2.0	72.4	16.4
Sr (ppm) *	77.8	7.2	308.1	121.8	88.8	4.8	86.0	4.0	38.4	7.0	44.3	2.5	103.9	14.0	89.7	7.2
V (ppm)	74.6	13.8	17.6	10.8	32.0	15.9	20.0	21.2	5.2	< dl	21.0	6.9	19.9	13.8	30.3	7.5
Zn (ppm)	338.6	55.4	544.1	233.5	207.7	28.8	206.2	36.4	601.3	72.3	1321.5	246.1	263.1	38.5	738.1	209.2
Ce (ppm) *	63.1	1.4	40.7	3.0	71.2	1.6	71.0	3.4	45.4	3.9	51.5	4.0	73.0	3.2	89.6	7.1
Cs (ppm)	0.7	/	< dl	< dl	6.6	1.4	7.2	0.9	< dl	< dl	< dl	< dl	6.5	1.2	3.9	1.6
Rb (ppm) *	66.6	4.2	23.3	6.1	64.2	6.6	62.0	11.1	32.6	2.9	33.5	3.6	61.4	6.5	42.4	5.9
Zr (ppm)	194.3	37.3	35.8	21.4	421.3	107.9	394.9	85.3	103.4	67.1	127.6	33.3	503.4	111.7	313.6	87.7

10.5.1.1 Modelling results and observations

When investigating the results of Sediment Fingerprint A (see Table F.1 in Addendum F), several observations can be made.

- 6 of the 22 outlet samples have model runs (in all its correction factor incarnations) that yield an RME >15%, hence for these six samples the composite fingerprint fails (indicated with a * in Table F.1 in Addendum F).
- For some outlet samples, models with different combinations of correction factors report acceptable RME's (sometimes of similar size), giving no direct insight into which set of correction factors performs the best. For the 16 outlet samples that have multiple models passing, the models omitting OM and GS correction factors always pass, the others do so far less.The modelling results contain a high number of zero% contributions, in other words the modelling does not attribute any contribution of specific tributaries to the total load measured in Aarschot, which is not realistic.
- In the models that have no OM or GS correction factors (i.e. zero and PP), the model seems to allocate the brunt of the sediment as originating from the Velpe (averaging around 85%). This can be seen in Table 10.12, which shows the average contributions of tributaries as calculated by the different model variations. It should be noted that these contributions might be erroneous, due to the fact that they include both models with RME values <15% and >15%. The data can however be used indicatively.
- In cases where the model including the OM correction passed the error assessment, it seems to lower the contributions of the Velpe in favour of the Herk and the Gete. In cases where the model including GS correction passed the error assessment, such a redistributing of contributions did not take place.
- Modelling results of PP-models (which use the W_i correction factor) often resemble closely their counterparts which do not apply the W_i correction factor (i.e. zero versus PP; OM versus OMPP; GS versus GSPP). The average difference between all source contribution predictions of these coupled models is little more than 1%.

Table 10.12: Average contributions of the eight tributaries to the suspended sediment flux sampled at the Aarschot outlet station, using Composite Fingerprint A and the mean property concentrations in the objective function. Data presented are averaged results from models with RME <15%

code model	contr. Motte (%)	contr. Hulpe (%)	contr. Velpe (%)	contr. Gete (%)	contr. Zwartebeek (%)	contr. Mangelbeek (%)	contr. Herk (%)	contr. Demer (%)
A zero	0	4	81	6	6	0	2	0
A PP	0	4	83	6	6	0	0	1
A GS	0	0	85	7	8	0	0	0
A GSPP	0	0	85	7	7	0	1	0
A OM	0	0	55	11	11	0	23	0
A OMPP	0	0	43	20	15	0	22	0

10.5.1.2 Discussion

Even though Composite Fingerprint A had been tested and should be able to fully discriminate between the different tributaries (it had 100% discriminatory power, as reported in Section 10.4.1.3), Fingerprint A seems to have trouble differentiating between different tributaries (attributing most of the southern contributions to just one tributary (i.e. the Velpe) and failing to attribute any sediment to the Mangelbeek of the northern tributaries). These are unrealistic results.

Additionally, the application of the RME as an error estimator showed that the geochemistry of the sources was able to replicate the geochemistry observed in the outlet samples in Aarschot fairly well. However, the modelling results are environmentally unrealistic, which suggests that the RME might not be the best indicator of error assessment. This is due to the fact that the RME test does not provide a measure of the robustness of the predicted source proportions per se, and it is possible to achieve the same RME with different source inputs.

Furthermore, while OM corrections, when not failing the RME testing, seem to be remedying the overestimation of the contribution of the Velpe somewhat, the use of grain size corrections, again when not failing the RME testing, keeps contributing most of the load to the Velpe. This seems to suggest that it would be reasonable to omit grain size correction from the model. This discussion is addressed in detail in Chapter 11.

The fact that the W_i-correction factor does not seem to have a big impact, is most likely due to the placing of the correction factor in the objective function (Eq. 10.5). This correction factor is placed outside of the bracbets, while the other correction factors are placed within the brackets.

10.5.2 Modelling using Composite Fingerprint A; entering MC simulated property concentrations

Next, the same composite fingerprint was used, and the same six correction factor combinations were applied, but the objective function was solved using the 1,000 permutations of the Monte Carlo uncertainty analysis.

To automate this process, a Visual Basic for Excel macro was used (provided by Prof. dr. Adrian Collins), which enters the 1,000 MC simulated property concentrations for the tributaries one by one and uses the MS Excel Solver Function to minimize the objective function for each simulation. When the macro is finished, the result is a set of 1,000 deviate mean outcomes for the contributions of the tributaries.

For each individual outlet sample, and for each source, the average mean contribution values, the complete ranges, 95% confidence intervals and standard deviations, as well as the RME observed on the average result have been calculated.

10.5.2.1 Modelling results and observations

The detailed modelling results, using Composite Fingerprint A and the Monte Carlo simulated mean property concentrations are tabulated in Addendum F (Table F.2), while Table 10.13 and Figure 10.5 show the overall results of samples 13 through 38 combined.

These results closely resemble the results of the previous version (using only the mean property concentrations).

- Seven instead of 6 of the 22 outlet samples have model runs where the model (in all its correction factor incarnations) has an RME >15%, hence for these 7 samples the composite fingerprint fails (indicated in Table F.2 with an *). The extra failing outlet sample in comparison to the previous modelling setup is sample nr 35.
- Again for some outlet samples, models with different combinations of correction factors report acceptable RME's (sometimes of similar size), giving no direct insight into which set of correction factors performs the best.

Table 10.13: Average mean contributions, 95% mean confidence intervals and ranges of the eight tributaries to the SSF observed in the combined samples 13 through 38 at the Aarschot outlet station, using Composite Fingerprint A and the MC simulated property concentrations in the objective function.

		A zero	A PP	A GS	A GSPP	A OM	A OMPP
Motte	Average mean contribution (%)	1	2	2	2	3	3
	95% Confidence Interval (%)	0	0	0	1	1	1
	range (%)	0-41	0-42	0-55	0-58	0-76	0-63
Hulpe	Average mean contribution (%)	4	4	4	5	9	9
	95% Confidence Interval (%)	0	0	0	0	1	1
	range (%)	0-37	0-36	0-31	0-34	0-95	0-95
Velpen	Average mean contribution (%)	62	62	64	64	38	34
	95% Confidence Interval (%)	2	2	2	2	2	2
	range (%)	0-100	0-100	0-100	0-100	0-100	0-100
Gete	Average mean contribution (%)	20	19	16	15	22	24
	95% Confidence Interval (%)	2	2	2	2	2	2
	range (%)	0-100	0-99	0-100	0-100	0-100	0-100
Zwartebeek	Average mean contribution (%)	5	5	8	8	9	10
	95% Confidence Interval (%)	0	0	0	0	1	1
	range (%)	0-25	0-24	0-32	0-31	0-57	0-50
Mangelbeek	Average mean contribution (%)	0	0	1	1	3	3
	95% Confidence Interval (%)	0	0	0	0	1	1
	range (%)	0-21	0-20	0-25	0-23	0-77	0-75
Herk	Average mean contribution (%)	6	7	4	4	16	16
	95% Confidence Interval (%)	1	1	1	1	1	1
	range (%)	0-100	0-100	0-94	0-92	0-100	0-100
Demer (upstream)	Average mean contribution (%)	1	1	1	1	1	1
	95% Confidence Interval (%)	0	0	0	0	0	0
	range (%)	0-31	0-30	0-40	0-41	0-71	0-73

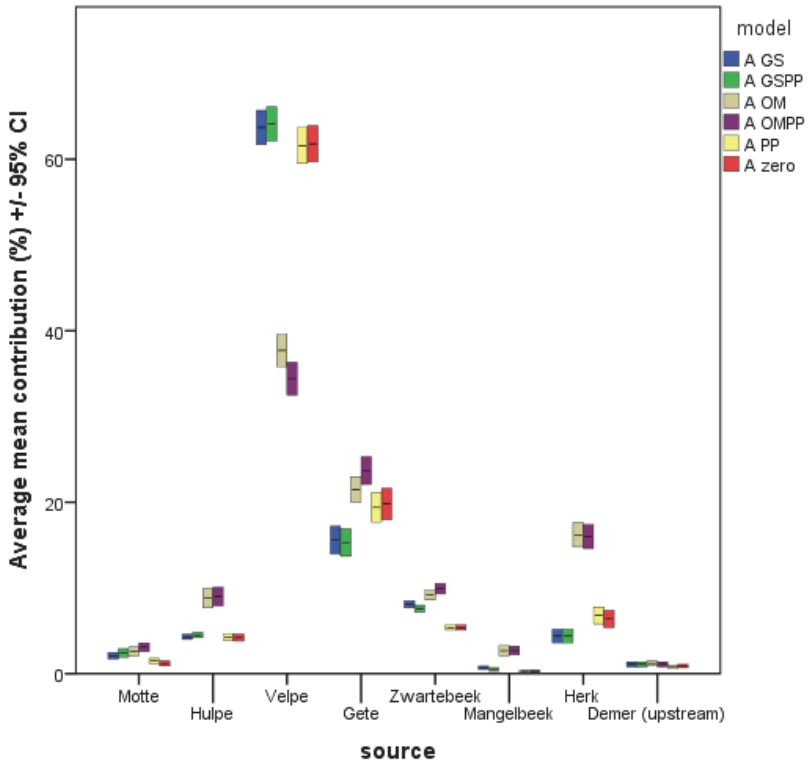

Figure 10.5: The average mean contributions of tributaries (based on all outlet samples), as well as the 95% confidence interval, calculated using Composite Fingerprint A.

- For the 15 outlet samples that have multiple models passing the RME-testing, the models omitting OM and GS correction factors again pass for most outlet samples (most but not all, nr 33 is excluded), the others do so far less.
- When the results for the 22 outlet samples (13 through 38) are combined into one dataset, the average mean contributions of some sources still contain a high number of zero% contributions, or due to the MC simulation approach, extremely low percentages (1-3%) as can be seen in Table 10.13 and Figure 10.5. To rephrase: the MC approach of modelling does not attribute any mean average contributions of specific tributaries to the total load measured in Aarschot either, which remains unrealistic.
- In the models that have no OM or GS correction factors (i.e. zero and PP), the model still seems to allocate most of the sediment to the Velpe, but the average mean contribution already dropped from 85% to 62%. The 20% got allocated to the Gete and the Herk. It should be noted that these contributions might be erroneous, due to the fact that they include both models with RME values <15% and >15%. The data can however be used indicatively.
- In cases where the model including the OM correction passed the RME-error assessment, it seems to lower the average mean contributions of the Velpe even further (down to 46%), again mostly in favour of the Herk and the Gete, but the average mean contributions of the other tributaries also increased, leaving no tributaries without any contribution.
- GS correction models passing the RME-error assessment, like in the mean concentration mode, did not redistribute the contributions from the Velpe to the other tributaries, but rather contributed more to the Velpe.
- Modelling results of PP-models (which use the W_i correction factor) seem to closely resemble their counterparts which do not apply the W_i correction factor (i.e. zero versus PP; OM versus OMPP; GS versus GSPP). The average difference between all average mean source contribution predictions of these coupled models is little more than 1%. This seems to suggest that the model results of W_i-corrected models are not significantly different from models without a W_i-correction. This can be tested by comparing the complete pdfs of the individual sources obtained from models with and without the W_i correction factor using an independent samples Kolmogorov-Smirnov test (K-S test). The results of these tests on the combined deviate set of all outlet samples are presented in Table 10.14 and show that in some of the cases the differences are in effect statistically significant (at a level of 0.05).
- The predicted mean relative contributions of the different tributaries had quite wide ranges, especially the southern tributaries, which all had ranges from 0 up to 100%. Nonetheless, the 95% confidence intervals of the mean contributions remain quite narrow (ranging in between 0 and 3%, depending on the tributary and the correction factor used).

10.5.2.2 Discussion

Using the 1,000 Monte Carlo simulations instead of the mean property concentrations in the Composite Fingerprint A mixing model allows for insight into the uncertainty associated with the modelling results, but the results themselves are similar to those obtained with using the mean concentration values: the contribution of the Velpe is still overpredicted, which seems remedied to a certain extent by applying OM correction factors.

Table 10.14: Asymptotic significances obtained through independent samples Kolmogorov-Smirnov tests between complete pdfs of sources obtained by Composite Fingerprint A models with and without W_i-correction factors, using data from all outlet samples. * significant at a level of 0.05.

Null hypothesis	A zero-A PP	A GS-A GSPP	A OM-A OMPP
The distribution of the contribution of the Motte is the same across the categories of the model	<0.001*	<0.001*	0.001*
The distribution of the contribution of the Hulpe is the same across the categories of the model	0.235	<0.001*	0.003*
The distribution of the contribution of the Velpe is the same across the categories of the model	<0.001*	0.084	<0.001*
The distribution of the contribution of the Gete is the same across the categories of the model	0.512	0.259	<0.001*
The distribution of the contribution of the Zwartebeek is the same across the categories of the model	<0.001*	<0.001*	<0.001*
The distribution of the contribution of the Mangelbeek is the same across the categories of the model	0.979	0.134	0.983
The distribution of the contribution of the Herk is the same across the categories of the model	0.004*	0.054	0.347
The distribution of the contribution of the Demer (upstream) is the same across the categories of the model	0.899	0.398	<0.001*

The uncertainty can be estimated by using the 95% confidence intervals of the tributary contributions modelled, to show whether or not the 1,000 results have a good convergence. In case of the results of Composite Fingerprint A, applying the MC iterations, there is a nice convergence as all 95% confidence intervals are <2%. Also, most of the model runs have RME-values <15%. However, some models produce environmental irrealistic results.

Therefore, another approach was introduced to evaluate the quality of the predictions. Besides calculating the RME based on the differences between the observed and modelled concentrations of properties used in the model, the RME of the properties not entered into the model, but passing the KW-test was calculated. These properties can be considered validational properties. This RME shall be referred to as RME_val in this thesis. The reasoning behind this is that these properties are equally capable of discriminating between the different sources, and if the model apportionment was executed correctly, mixing these elements, using the modelled contributions, should render a result of property concentrations that resemble the concentrations measured in the outlet sample.

The RME_val values were calculated for the tributary contributions averaged from the 1,000 MC simulations obtained from the model run performed with sediment fingerprint A. They are also presented in Table F.2 in Addendum F. Of the 15 outlet samples that reported models with RME values <15%, only two samples reported RME_val values <15%.

This confirms the earlier findings that Composite Fingerprint A is actually not able to apportion the contributions of the different tributaries in a satisfactory way and that perhaps another fingerprint, using different properties, might be more successful. To have a general overview of the effectiveness of a model, the RME was determined on all properties passing the KW-test. It is reported in Table F.2 as RME_avg.

10.5.3 Modelling using Composite Fingerprints B, C and D; entering MC simulated property concentrations

To observe the impact of different properties within the composite fingerprint, three more composite fingerprints were created and tested. Composite Fingerprint B is based on the properties that did not feature in Fingerprint A, but did pass the KW-test. The hypothesis is that these elements might be complementary in their predictive power for certain outlet samples. However, as there were not enough properties left to create a complete non-overlapping fingerprint, the best predictive properties from the previous fingerprints were recycled.

There were three elements always present in the fingerprints with 100% predictive power as presented in Table 10.5, i.e. Fe, Rb and Ba. Hence, these properties were combined with the properties which had passed the KW-test but were not previously entered into Fingerprint A (i.e. Ca, Ti, Cu and Mn). This 7-properties-fingerprint can already discriminate 98.8% but needs at least two more properties to fulfil the data dimensionality of the model.

Testing as described in 10.4.1.3 showed that it was most difficult to discriminate between the Velpe, the Gete and the Herk. Hence, the classification results of individual properties, as reported in Table 10.3 were used again to help select two additional properties that have good discriminative power for these specific tributaries.

Four properties (P, Zn, Ce, S) showed promise and the six combinations possible with the preselected seven properties were entered into a DFA. All six composite fingerprints discriminated between 98.8 and 100% (see Table 10.15). One of the composite fingerprints with a predictive power of 100% was randomly selected (comprised of Ti, Zn, Ba, Ce, Fe, Rb, Ca, Cu and Mn) and will be called Fingerprint B in the rest of this thesis. Its cumulative predictive power is presented in Table 10.16.

Table 10.15: Predictive powers of tested composite fingerprints from combination of 9 properties in search of Composite Fingerprint B. *= Selected fingerprint

Tested fingerprints (for Fingerprint B)	Predictive power (%)
CaTiCuMnFeBaRbCeS	98.8
CaTiCuMnFeBaRbPCe	98.8
CaTiCuMnFeBaRbPS	98.8
CaTiCuMnFeBaRbPZn	98.8
CaTiCuMnFeBaRbZnCe*	100
CaTiCuMnFeBaRbZnS	100

Fingerprint C was constructed during a preliminary phase of the research, at a time when not all samples had been analysed yet. At that time this fingerprint (consisting of Mn, P, Fe, Cu, Zn, Sr, Ba, Ca and Ni) had a predictive power of 100%. After all samples had been analysed, it appeared that this fingerprint was still comprised of properties that both passed the violation and KW-tests. Therefore it still could be admitted as a fingerprint in this study. Its cumulative predictive power, however, as presented in Table 10.16, dropped slightly to 98.7%, which is still a very respectable discriminatory power. Therefore, this fingerprint was also selected for further modelling use.

Finally, a fingerprint was constructed (Fingerprint D) that did not contain the four properties that fingerprint A and B have in common (Fa, Ba, Rb and Ce). This left 10 properties (Al, Ca, P, S, Ni, Sr, Zn, Ti, Cu and Mn) that passed the KW-test, out of which all combinations of nine elements were tested with a DFA. All composite fingerprints discriminated between 98.8 and 100% (see Table 10.17). One of these composite fingerprints with a predictive power of 100% was randomly selected (comprised of Ti, Zn, Ba, Ce, Fe, Rb, Ca, Cu and Mn); its cumulative predictive power is presented in Table 10.16.

Table 10.16: Cumulative predictive power of Composite Fingerprints B, C and D

Fingerprint B			Fingerprint C			Fingerprint D		
Step	Property added	Cumulative predictive power (%)	step	Property added	Cumulative predictive power (%)	step	Property added	Cumulative predictive power (%)
1	Ti	60	1	Fe	75.3	1	Ti	60
2	Zn	78.8	2	Zn	81.2	2	Zn	78.8
3	Ba	81.2	3	Sr	85.9	3	Ni	80
4	Ce	91.8	4	Ba	96.5	4	Ca	97.6
5	Fe	98.8	5	P	98.8	5	Sr	98.8
6	Rb	98.8	6	Ca	98.8	6	Cu	98.8
7	Ca	100	7	Ni	98.8	7	Mn	98.8
8	Cu	98.8	8	Cu	98.8	8	S	98.8
9	Mn	100	9	Mn	98.8	9	P	100

Furthermore, Discriminatory Weighting Correction Factors (W_i) have been determined for Fingerprints B through D, and the values are presented in Table 10.18.

To conclude, composite fingerprints B, C and D should all be capable of discriminating effectively between the different tributaries, and they are based on partially different chemical properties, which should help in discriminating if specific properties are underperforming.

Table 10.17: Predictive powers of tested composite fingerprints from combination of 9 properties in search of Composite Fingerprint D. *= Selected fingerprint

Tested fingerprints	Predictive power (%)
AlCaPSTiCuMnNiSr	98.8
AlCaPSTiCuMnNiZn	98.8
AlCaPSTiCuMnSrZn	98.8
AlCaPSTiCuNiSrZn	98.8
AlCaPSTiMnNiSrZn	100
AlCaPSCuMnNiSrZn	97.6
AlCaPTiCuMnNiSrZn	98.8
AlCaSTiCuMnNiSrZn	100
AlPSTiCuMnNiSrZn	100
CaPSTiCuMnNiSrZn*	100

Table 10.18: Discriminatory Weighting Correction Factors (Wi) determined for properties of Composite Fingerprints B, C and D.

FP B	W_i	FP C	W_i	FP D	W_i
Fe	1.88	Fe	1.88	P	1.44
Ba	1.35	Zn	1.56	S	1.25
Rb	1.22	Sr	1.56	Ni	1.18
Ce	1.62	P	1.44	Sr	1.56
Zn	1.56	Ba	1.35	Zn	1.56
Ca	1.27	Ca	1.27	Ca	1.27
Ti	1.51	Ni	1.18	Ti	1.51
Cu	1.12	Cu	1.12	Cu	1.12
Mn	1.00	Mn	1.00	Mn	1.00

10.5.3.1 Modelling results and observations

The mixing models were run using 1,000 Monte Carlo simulated property concentrations (generated as described in Section 10.4.2.4) and average mean contribution values for the tributaries were calculated for each outlet sample, as well as their ranges and 95% confidence limits. These are presented for Fingerprints B, C and D respectively in Tables F.3, F.4 and F.5 (annexed in Addendum F). Once more the RME, RME_val and RME_avg values have been calculated on the MC simulated results, and are also presented in the respective tables.

Table 10.19 shows the average mean contributions of the eight tributaries to the SSF observed in the combined samples 13 through 38 at the Aarschot outlet station, using Composite Fingerprints B, C and D. It also presents the 95% confidence intervals and the complete range observed for the different sources. Figure 10.6 visualizes the average mean contributions of the tributaries (based

Table 10.19: Average mean contributions, 95% mean confidence intervals and ranges of the eight tributaries to the SSF observed in the combined samples 13 through 38 at the Aarschot outlet station, using Composite Fingerprint A and the MC simulated property concentrations in the objective function.

		B zero	B PP	B GS	B GSPP	B OM	B OMPP	C zero	C PP	C GS	C GSPP	C OM	C OMPP	D zero	D PP	D GS	D GSPP	D OM	D OMPP
Motte	Average mean contribution (%)	7	5	1	1	8	7	13	11.8	4.2	4.3	9.4	9.2	9.4	8.8	1.6	2	8.2	7.6
	95% Confidence Interval (%)	1	1	0	0	1	1	0.7	0.7	0.5	0.5	1	1	0.8	0.8	0.3	0.4	0.9	0.9
	range (%)	0-44	0-39	0-31	0-42	0-61	0-59	0-44	0-42	0-39	0-38	0-100	0-100	0-67	0-59	0-58	0-54	0-91	0-89
Hulpe	Average mean contribution (%)	4	4	4	4	9	9	3.5	3.5	4.3	4.3	7.8	7.6	3.9	4	4.9	5.1	11.7	11.2
	95% Confidence Interval (%)	0	0	1	1	1	1	0.4	0.4	0.4	0.5	0.8	0.8	0.4	0.4	0.4	0.4	0.8	0.8
	range (%)	0-35	0-34	0-42	0-41	0-90	0-90	0-34	0-34	0-41	0-45	0-69	0-79	0-29	0-29	0-41	0-43	0-79	0-79
Velpe	Average mean contribution (%)	17	19	22	25	10	10	20.4	22.9	23.6	27.6	9.6	9.6	30.7	33.4	29.4	32.3	23.5	24.3
	95% Confidence Interval (%)	2	2	2	2	1	1	1.5	1.5	1.7	1.8	0.9	1	1.8	1.9	1.8	1.8	1.3	1.3
	range (%)	0-100	0-100	0-100	0-100	0-86	0-88	0-100	0-100	0-100	0-100	0-81	0-82	0-100	0-100	0-100	0-100	0-95	0-92
Gete	Average mean contribution (%)	55	55	50	49	44	46	48.7	46.8	48.1	45.8	36.6	36.1	43.3	40.8	36.8	35.1	28.4	27.5
	95% Confidence Interval (%)	2	2	2	2	2	2	1.6	1.6	1.7	1.7	1.3	1.3	1.8	1.7	1.7	1.7	1.3	1.3
	range (%)	0-100	0-100	0-100	0-100	0-100	0-100	0-98	0-98	0-100	0-100	0-97	0-97	0-100	0-100	0-100	0-100	0-100	0-100
Zw artebeek	Average mean contribution (%)	4	3	12	10	4	5	2.2	1.8	10.1	7.9	5.5	6.5	7.5	7.7	21.6	19.8	11.1	10.5
	95% Confidence Interval (%)	0	0	1	0	1	1	0.3	0.2	0.5	0.4	0.5	0.5	0.5	0.5	0.8	0.8	1.2	1.2
	range (%)	0-23	0-22	0-36	0-31	0-67	0-58	0-24	0-23	0-35	0-29	0-66	0-55	0-38	0-38	0-60	0-56	0-100	0-87
Mangelbeek	Average mean contribution (%)	3	4	3	3	12	13	1.7	1.8	1.3	1.4	5.6	6	0.5	0.6	0.4	0.5	4.2	4.7
	95% Confidence Interval (%)	0	0	0	0	1	1	0.2	0.2	0.2	0.2	0.5	0.5	0.1	0.1	0.1	0.1	0.4	0.4
	range (%)	0-19	0-20	0-23	0-23	0-43	0-42	0-16	0-15	0-17	0-18	0-51	0-47	0-15	0-16	0-16	0-17	0-45	0-43
Herk	Average mean contribution (%)	8	9	6	5	8	7	6.3	6.5	4.6	4.5	11	12.4	4.3	4.3	4.1	4.1	10.7	12.1
	95% Confidence Interval (%)	1	1	1	1	1	1	0.9	0.9	0.7	0.7	1.1	1.1	0.8	0.8	0.8	0.8	1.1	1.2
	range (%)	0-95	0-95	0-89	0-84	0-90	0-77	0-93	0-93	0-93	0-93	0-99	0-96	0-100	0-99	0-98	0-96	0-100	0-100
Demer (upstream)	Average mean contribution (%)	2	2	2	2	5	5	4.3	4.9	3.8	4.1	14.5	12.6	0.4	0.4	1.1	1.1	2.2	2.1
	95% Confidence Interval (%)	0	0	1	1	1	1	0.4	0.4	0.6	0.6	0.8	0.7	0.1	0.1	0.3	0.3	0.3	0.3
	range (%)	0-39	0-38	0-73	0-77	0-53	0-53	0-39	0-41	0-67	0-69	0-59	0-60	0-24	0-23	0-40	0-41	0-38	0-37

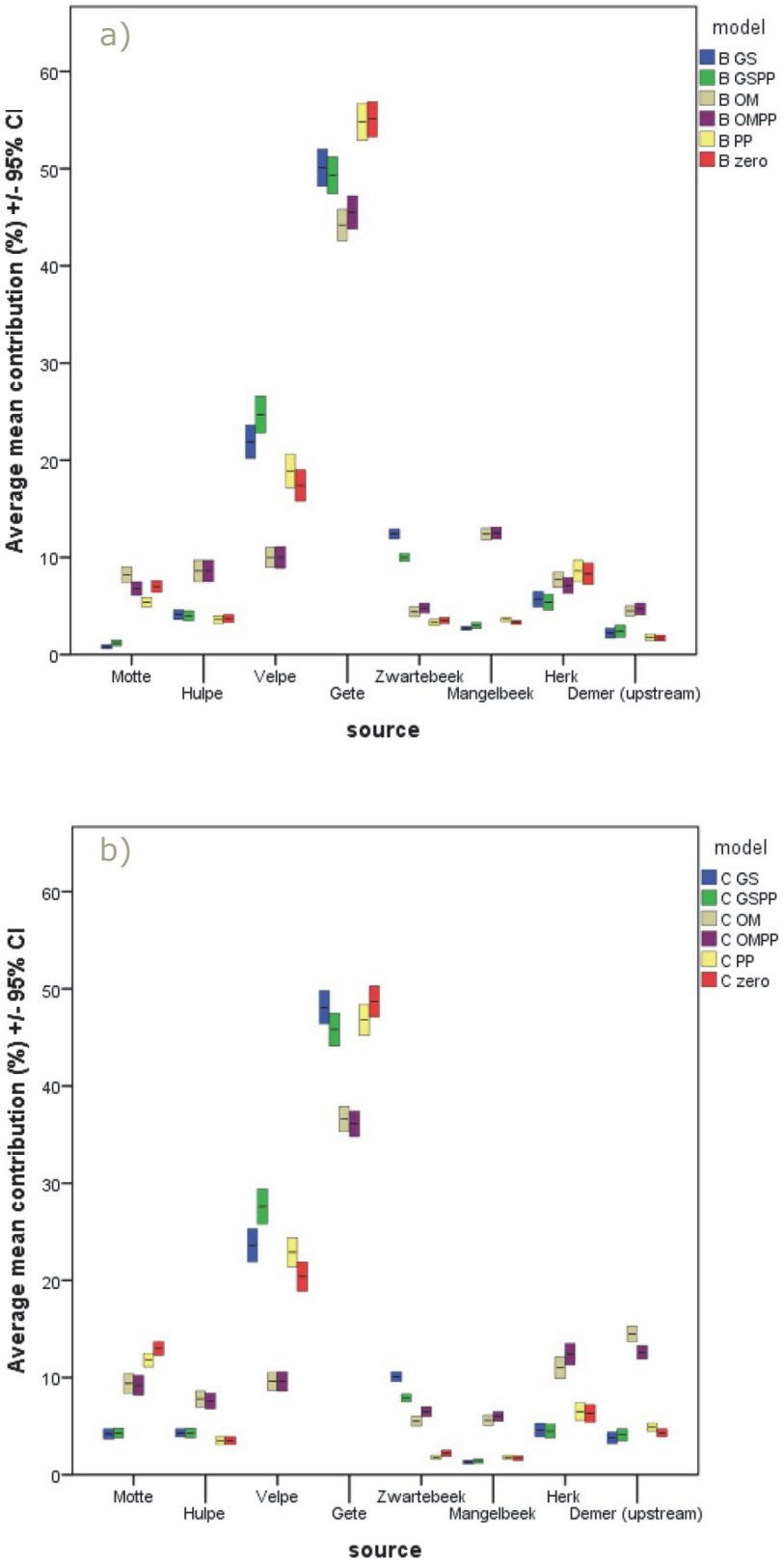

Figure 10.6: The average mean contributions of tributaries (based on all outlet samples), as well as the 95% confidence interval, calculated using (a) Composite Fingerprint B, (b) Composite Fingerprint C and (c) Composite Fingerprint D.

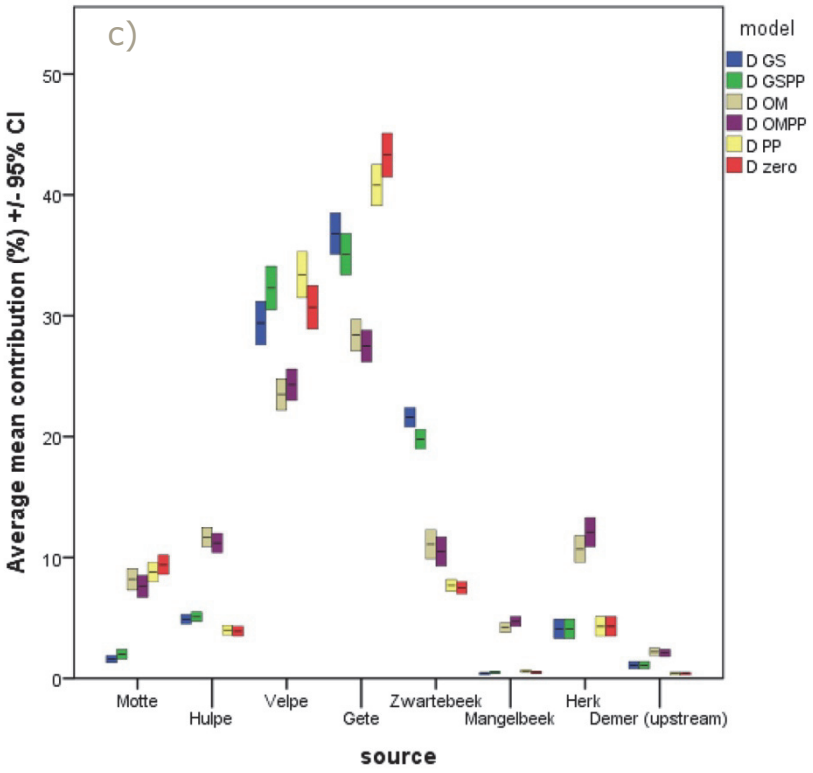

Figure 10.6 (continued): The average mean contributions of tributaries (based on all outlet samples), as well as the 95% confidence interval as calculated (a) by Composite Fingerprint B, (b) by Composite Fingerprint C and (c) by Composite Fingerprint D.

on all outlet samples), as well as the 95% confidence interval as calculated by these different composite fingerprints

The results of these model runs show some similarities but also some distinct differences with the model run from Fingerprint A.

The similarities include:

- Several outlet samples have model runs where the model (in all its correction factor incarnations) has an RME_avg >15%, hence for these samples the respective composite fingerprints fails.
- For some outlet samples, models with different combinations of correction factors report acceptable RME_avg's (sometimes of similar size), giving no direct insight into which set of correction factors performs the best.
- For the outlet samples that have multiple models passing, the models omitting OM and GS correction factors again pass for most outlet samples, the others do so far less.
- The average modelling results still contain a number of zero% contributions, or due to the MC simulation approach, extremely low percentages (1-3%).
- The modelling results of PP-models (which use the W_i correction factor) still resemble their counterparts which do not apply the W_i correction factor (i.e. zero versus PP; OM versus OMPP; GS versus GSPP). The average difference between all average mean source contribution predictions of these coupled models is less than 1%. However, when this was tested using independent samples K-S test, it once more appeared that for more than half of the sources, the differences between the pdfs of W_i-corrected models

are significantly different (at a level of 0.05) from the pdfs of non-W_i-corrected models, as can be seen in Table 10.20.

- Once more the predicted mean relative contributions of the southern tributaries had quite wide ranges, from 0 up to 100%. The northern tributaries are somewhat more narrow in range, however some model incarnations also range from 0-100%. Nonetheless, the 95% confidence intervals of the mean contributions remain quite narrow (ranging in between 0 and 3%, depending on the tributary and the correction factor used, as can be seen in Table 10.19).

Table 10.20: Asymptotic significances obtained through independent samples Kolmogorov Smirnov tests between complete pdfs of sources obtained by Composite Fingerprints B, C and D models with and without W_i-correction factors, using data from all outlet samples. * significant at a level of 0.05.

	B			C			D		
Null hypothesis	**zero-PP**	**GS-GSPP**	**OM-OMPP**	**zero-PP**	**GS-GSPP**	**OM-OMPP**	**zero-PP**	**GS-GSPP**	**OM-OMPP**
The distribution of the contribution of the Motte is the same across the categories of the model	<0.001*	<0.001*	<0.001*	<0.001*	0.004*	0.002*	0.004*	<0.001*	0.008*
The distribution of the contribution of the Hulpe is the same across the categories of the model	0.482	0.425	<0.001*	0.453	0.638	<0.001*	0.006*	0.025*	<0.001*
The distribution of the contribution of the Velpe is the same across the categories of the model	<0.001*	<0.001*	<0.001*	<0.001*	<0.001*	0.104	<0.001*	<0.001*	0.002*
The distribution of the contribution of the Gete is the same across the categories of the model	0.040*	0.001*	<0.001*	<0.001*	<0.001*	<0.001*	<0.001*	<0.001*	<0.001*
The distribution of the contribution of the Zwartebeek is the same across the categories of the model	<0.001*	<0.001*	<0.001*	<0.001*	<0.001*	<0.001*	0.002	<0.001*	0.001*
The distribution of the contribution of the Mangelbeek is the same across the categories of the model	<0.001*	<0.001*	0.574	<0.001*	<0.001*	<0.001*	<0.001*	<0.001*	<0.001*
The distribution of the contribution of the Herk is the same across the categories of the model	0.425	<0.001*	0.003*	0.075	0.024*	<0.001*	1.000	0.52	<0.001*
The distribution of the contribution of the Demer (upstream) is the same across the categories of the model	<0.001*	0.749	0.051	<0.001*	<0.001*	<0.001*	0.993	1.000	0.622

However, Composite Fingerprints B, C and D do not, as Fingerprint A did, attribute most of the sediment to the Velpe. Fingerprints B and C allocate about half of the observed sediment flux in Aarschot to the Gete, while fingerprint D predicts the Velpe and Gete to contribute about the same amounts, i.e. 35%.

Once more it can be observed that when the OM correction is applied, the contributions of the Velpe are reduced in favour of the other tributaries (most clearly the Herk and the Mangelbeek).

To conclude, instead of only looking into the mean relative errors, the relative errors of individual properties were investigated, both as a fingerprint property (see Table 10.21), and as a validation property (Table 10.22). This was possible as all properties had been used in at least one composite fingerprint. For most of the properties the average relative error was smaller when it was used in a composite fingerprint, compared to when it was used as a validation property.

Table 10.21: Descriptive statistics of the relative errors determined per property, when used as a fingerprint property in Composite Fingerprints A through D.

Modelled	Fe	Ba	Rb	Ce	Sr	S	P	Ni	Al	Zn	Ca	Ti	Cu	Mn
Mean	18	13	15	11	12	46	27	15	13	12	19	12	20	35
Standard Error	1	1	1	1	1	2	1	1	1	1	1	1	1	2
Median	11	10	13	7	7	35	23	12	9	7	9	9	16	26
Mode	/	/	/	/	14	18	42	18	/	20	7	18	0	27
Standard Deviation	25	13	11	14	17	39	23	13	13	15	28	11	20	32
Sample Variance	615	170	121	203	301	1542	549	158	167	211	758	120	388	1045
Kurtosis	23	11	0	15	16	9	7	7	4	9	11	2	11	7
Skewness	4	3	1	3	4	3	2	2	2	3	3	1	3	2
Range	199	82	53	89	127	227	154	76	63	92	164	54	141	189
Minimum	0	0	0	0	0	1	0	0	0	0	0	0	0	0
Maximum	199	82	53	89	127	228	154	76	63	92	164	54	141	189
Count	396	396	264	264	396	264	396	396	132	396	396	264	396	396

Table 10.22: Descriptive statistics of the relative errors determined per property, when used as a validation property in Composite Fingerprints A through D.

Validated	Fe	Ba	Rb	Ce	Sr	S	P	Ni	Al	Zn	Ca	Ti	Cu	Mn
Mean	38	15	16	13	13	70	39	13	14	20	25	13	19	62
Standard Error	3	1	1	1	2	3	3	1	1	1	3	1	2	3
Median	31	14	13	10	9	54	39	12	10	16	12	9	15	51
Mode	31	21	4	21	/	/	/	/	9	/	/	/	/	/
Standard Deviation	38	11	14	15	19	54	29	11	11	16	34	13	20	39
Sample Variance	1477	124	206	213	347	2897	827	116	132	263	1183	180	419	1557
Kurtosis	18	5	14	8	18	5	4	8	0	21	10	5	11	2
Skewness	4	2	3	3	4	2	2	2	1	4	3	2	3	1
Range	268	61	114	83	130	281	158	61	54	123	175	72	130	195
Minimum	0	1	0	0	0	8	0	0	0	0	0	0	0	4
Maximum	268	61	114	83	130	288	159	62	54	123	175	72	130	199
Count	132	132	264	264	132	264	132	132	396	132	132	264	132	132

10.5.3.2 Discussion

Composite Fingerprints B, C and D yield theoretically more plausible contributions of the individual tributaries as they no longer contribute most of the material to the Velpe.

The uncertainty visualised by the 95% confidence intervals of the mean tributary contributions modelled, shows that once more the 1,000 results have a good convergence, as the 95% confidence intervals are for all models <2%. Also, most of the model runs have RME-values <15%.

Whether or not the OM corrections are actually beneficial to the modelling result, as could be hypothesised after the results from Fingerprint A, still remains to be answered, as in Fingerprint D, it might actually lead to an underprediction of Velpe contributions. This will be further discussed in Chapter 11.

The investigation into the relative errors of individual properties shows that S, P and Mn are elements that are difficult to predict correctly. Even though they passed the KW-test and therefore have discriminative power, they seem to have difficulty performing within these sediment fingerprints. As at least one of these elements was present in all four of the created sediment fingerprints, it could potentially explain part of the observed high standard deviations. Therefore, another sediment fingerprint should be created that does not contain any of these three properties.

10.5.4 Modelling using Composite Fingerprint E; entering MC simulated property concentrations

As stated above, properties S, P and Mn should be removed from the composite fingerprint. As initially 14 properties passed the KW-test (see Section 10.4.1.2), that leaves 11 properties to use as potential fingerprints, from which 9 were selected using the stepwise DFA based on the minimization of Wilks' Lambda (as described in Section 10.4.1.3). Combined, these 9 properties yielded a predictive power of 100% (as illustrated in Table 10.23). Consequently, W_i's were determined and the values are presented in Table 10.24.

Table 10.23: Cumulative predictive power of Composite Fingerprint E

step	Property added	Cumulative predictive power (%)	Wilks' Lambda
1	Fe	75.3	0.003
2	Sr	89.5	<0.001
3	Ce	93.0	<0.001
4	Zn	96.5	<0.001
5	Ba	97.7	<0.001
6	Rb	100.0	<0.001
7	Al	100.0	<0.001
8	Ca	100.0	<0.001
9	Cu	100.0	<0.001

Table 10.24: Discriminatory Weighting Correction Factors (Wi) determined for properties of Composite Fingerprint E

	W_i
Fe	1.68
Ce	1.45
Sr	1.40
Zn	1.40
Al	1.35
Ba	1.21
Ca	1.13
Rb	1.09
Cu	1.00

10.5.4.1 Modelling results and observations

The mixing model for Composite Fingerprint E was run for all 22 outlet samples, using 1,000 MC-simulated property concentrations (generated as described in Section 10.4.2.4) and mean average contribution values for the tributaries and the associated 95% confidence intervals were once more calculated, as well as their complete ranges. These are presented for each outlet sample separately in Addendum F, in Table F.6, alongside the RME, RME_val and RME_avg values calculated on the average MC simulated result. As S, P and Mn have proven to be poor fingerprints, they have been excluded from the calculations of RME_val and RME_avg.

Table 10.25 shows the complete range of contributions modelled for the eight tributaries for all outlet samples 13 through 38 at the Aarschot outlet station, using Composite Fingerprint E. This table also shows the average mean contributions of the sources and the associated 95% confidence intervals. These latter two are also visualized in Figure 10.7.

The results of these model runs show once more some similarities but also some distinct differences with the model runs from Fingerprints A through D.

The similarities include:

- For some outlet samples, models with different combinations of correction factors report acceptable RME_avg's (sometimes of similar size), giving no direct insight into which set of correction factors performs the best.
- For the outlet samples that have multiple models passing, the models omitting OM and GS correction factors again pass for most outlet samples, the others do so far less.

Table 10.25: Average mean contributions, 95% mean confidence intervals and ranges of the eight tributaries to the SSF observed in the combined samples 13 through 38 at the Aarschot outlet station, using Composite Fingerprint A and the MC simulated property concentrations in the objective function.

		E zero	E PP	E GS	E GSPP	E OM	E OMPP
Motte	Average mean contribution (%)	1	1	0.9	1.2	1.7	1.6
	95% Confidence Interval (%)	0.2	0.2	0.2	0.3	0.3	0.3
	range (%)	0-28	0-31	0-33	0-36	0-50	0-55
Hulpe	Average mean contribution (%)	3.4	3.4	4.0	4.0	7.2	7.3
	95% Confidence Interval (%)	0.4	0.4	0.4	0.4	0.9	0.9
	range (%)	0-34	0-34	0-41	0-40	0-75	0-82
Velpen	Average mean contribution (%)	41.3	41.7	48.1	49.7	20.5	18.8
	95% Confidence Interval (%)	2.1	2.0	2.0	2.0	1.6	1.6
	range (%)	0-100	0-100	0-100	0-100	0-94	0-93
Gete	Average mean contribution (%)	29.5	28.7	21.6	20.6	37.4	39.2
	95% Confidence Interval (%)	1.7	1.7	1.6	1.5	1.8	1.9
	range (%)	0-100	0-100	0-100	0-100	0-100	0-100
Zwartebeek	Average mean contribution (%)	4.4	4.2	8.9	7.7	5.8	6.2
	95% Confidence Interval (%)	0.3	0.3	0.4	0.4	0.6	0.5
	range (%)	0-25	0-22	0-31	0-29	0-70	0-61
Mangelbeek	Average mean contribution (%)	3.5	3.6	2.9	3.0	11.9	11.8
	95% Confidence Interval (%)	0.2	0.2	0.3	0.3	0.6	0.6
	range (%)	0-22	0-21	0-22	0-21	0-41	0-40
Herk	Average mean contribution (%)	15.3	15.8	11.7	11.8	12.6	11.6
	95% Confidence Interval (%)	1.3	1.4	1.1	1.1	1.0	1.0
	range (%)	0-86	0-86	0-81	0-83	0-87	0-91
Demer (upstream)	Average mean contribution (%)	1.6	1.6	2	2.1	2.9	3.4
	95% Confidence Interval (%)	0.2	0.2	0.5	0.5	0.4	0.5
	range (%)	0-32	0-34	0-70	0-75	0-56	0-58

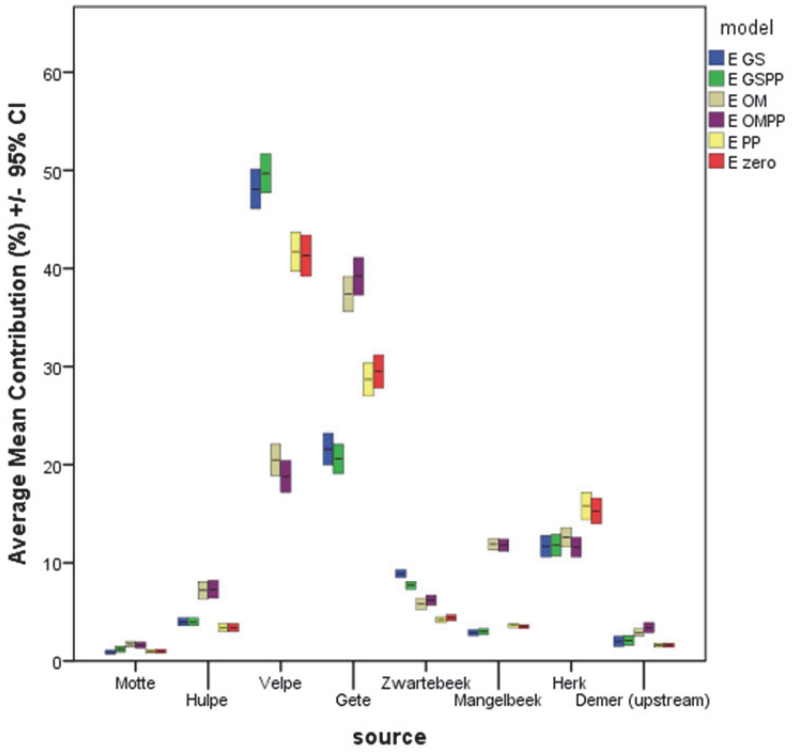

Figure 10.7: The average mean contributions of tributaries (based on all outlet samples), as well as the 95% confidence interval, calculated using Composite Fingerprint E.

- The average modelling results still contain a number of zero% contributions, or due to the MC simulation approach, extremely low percentages (1-2%).
- Composite Fingerprint E attributes on average once more, most of the sediment to the Velpe, as is illustrated in Figure 10.7. Once more does the OM correction reduce the contributions of the Velpe in favour of the other tributaries (most clearly the Gete, Mangelbeek and Hulpe).
- The modelling results of PP-models (which use the W_i correction factor) still resemble their counterparts which do not apply the W_i correction factor (i.e. zero versus PP; OM versus OMPP; GS versus GSPP). The average difference between all average mean source contribution predictions of these coupled models is less than 1%. However, when this was tested using independent samples K-S test, it once more appeared that for more than half of the sources, the differences between the pdfs of W_i-corrected models are significantly different (at a level of 0.05) from the pdfs of non-W_i-corrected models, as can be seen in Table 10.26.
- Once more the predicted mean relative contributions of the southern tributaries had quite wide ranges, from 0 up to 100%. The northern tributaries are somewhat more narrow in range, however some model incarnations also range from 0-86%. Nonetheless, the 95% confidence intervals of the mean contributions remain quite narrow (ranging in between 0 and 3%, depending on the tributary and the correction factor used, as can be seen in Table 10.25).

The biggest difference between Composite Fingerprint E and its predecessors is that Composite Fingerprint E has multiple models yielding RME_avg values <15% for all but one outlet sample (i.e. outlet sample 32). For every sample the zero and PP models pass this test, OM corrected models fail on a mere 5 outlet samples, while GS corrected values still fail on 10 of them. In the cases where multiple models report acceptable RME_avg's, it remains difficult to determine which set of correction factors performs the best.

10.5.4.2 Discussion

Excluding P, S and Mn from the composite fingerprint has had a direct impact on the RME_avg values. Much more models report acceptable relative errors of <15%. However, excluding these properties has not resulted in a decrease in variability observed in the 1,000 MC-simulations.

The 95% confidence intervals of the tributary contributions modelled are once more quite narrow (<2%), which shows that the MC 1,000 results have a good convergence. However, Composite Fingerprint E contributes most of the sediment to the Velpe, which is an environmental irrealistic result.

The OM and GS correction factors have a significant impact on the outcome of the contributions predicted, as is proven by the highly variable outcome of the results. Whether or not the OM or GS corrections are actually beneficial to the modelling result, will be further discussed in Chapter 11.

An important fact, which has not yet been addressed is that the modelling results presented in Figures 10.5, 10.6 and 10.7 and in Tables 10.13, 10.19 10.25 are composite results, which present average mean contributions 95% confidence limits and ranges calculated using all modelling results for all 22 outlet samples. However, the individual outlet samples show very variable modelling results (which have been tabulated in Addendum F). As an illustration, the modelling results of all 22 outlet samples using Composite Fingerprint E without any correction factors (E zero) are presented in Figure 10.8.

Table 10.26: Asymptotic significances obtained through independent samples Kolmogorov-Smirnov tests between complete pdfs of sources obtained by Composite Fingerprint E models with and without W_i-correction factors, using data from all outlet samples. * significant at a level of 0.05.

Null hypothesis	E zero-E PP	E GS-E GSPP	E OM-E OMPP
The distribution of the contribution of the Motte is the same across the categories of the model	0.274	<0.001*	0.78
The distribution of the contribution of the Hulpe is the same across the categories of the model	0.196	0.969	0.64
The distribution of the contribution of the Velpe is the same across the categories of the model	0.021*	<0.001*	<0.001*
The distribution of the contribution of the Gete is the same across the categories of the model	<0.001*	<0.001*	<0.001*
The distribution of the contribution of the Zwartebeek is the same across the categories of the model	<0.001*	<0.001*	<0.001*
The distribution of the contribution of the Mangelbeek is the same across the categories of the model	<0.001*	<0.001*	0.418
The distribution of the contribution of the Herk is the same across the categories of the model	<0.001*	0.011*	<0.001*
The distribution of the contribution of the Demer (upstream) is the same across the categories of the model	0.058	0.482	0.001*

This figure clearly shows that the southern tributaries (Velpe, Gete and Herk) show the highest variability. The same observations can be made for all other model incarnations of Composite Fingerprint E, as well as for all model incarnations of the other composite fingerprints. As an example, Table 10.29 presents the complete range of the pdfs as well as the mean average contributions and associated 95% confidence intervals as well as for all model incarnations of model E for sample 14. Figure 10.9 visualizes this data.

It is self-explanatory that the ranges of the pdfs for the potential sources created for the outlet sample 14 are more narrow than those observed for the compilation of all 22 outlet samples. However, the overall observation that the ranges of the southern tributaries (total observed range equals 0-81%) remain wider than those of the northern tributaries remain (total observed range equals 0-40%). Even though the ranges are still significant, the 95% confidence limits of the mean contributions, are once more very narrow (ranging from 0-1.7%) indicating that the models are converging nicely towards a central tendency.

Like in the compilation of all outlet samples, in sample 14, the modelling results of PP-models (which use the W_i correction factor) resemble their counterparts which do not apply the W_i-correction factor (i.e. zero versus PP; OM versus OMPP; GS versus GSPP). The average difference between all average mean source contribution predictions of these coupled models is less than 1%.

However, this time when the different pdfs were tested using independent samples K-S test, most of the tests showed that the differences between the pdfs of W_i-corrected models were not significantly different (at a level of 0.05) from the pdfs of non-W_i-corrected models, as can be seen in Table 10.28. This indicates that in effect applying the W_i-correction does not yield significant different pdfs for most tributaries for sample 14. Whether the significant differences observed in

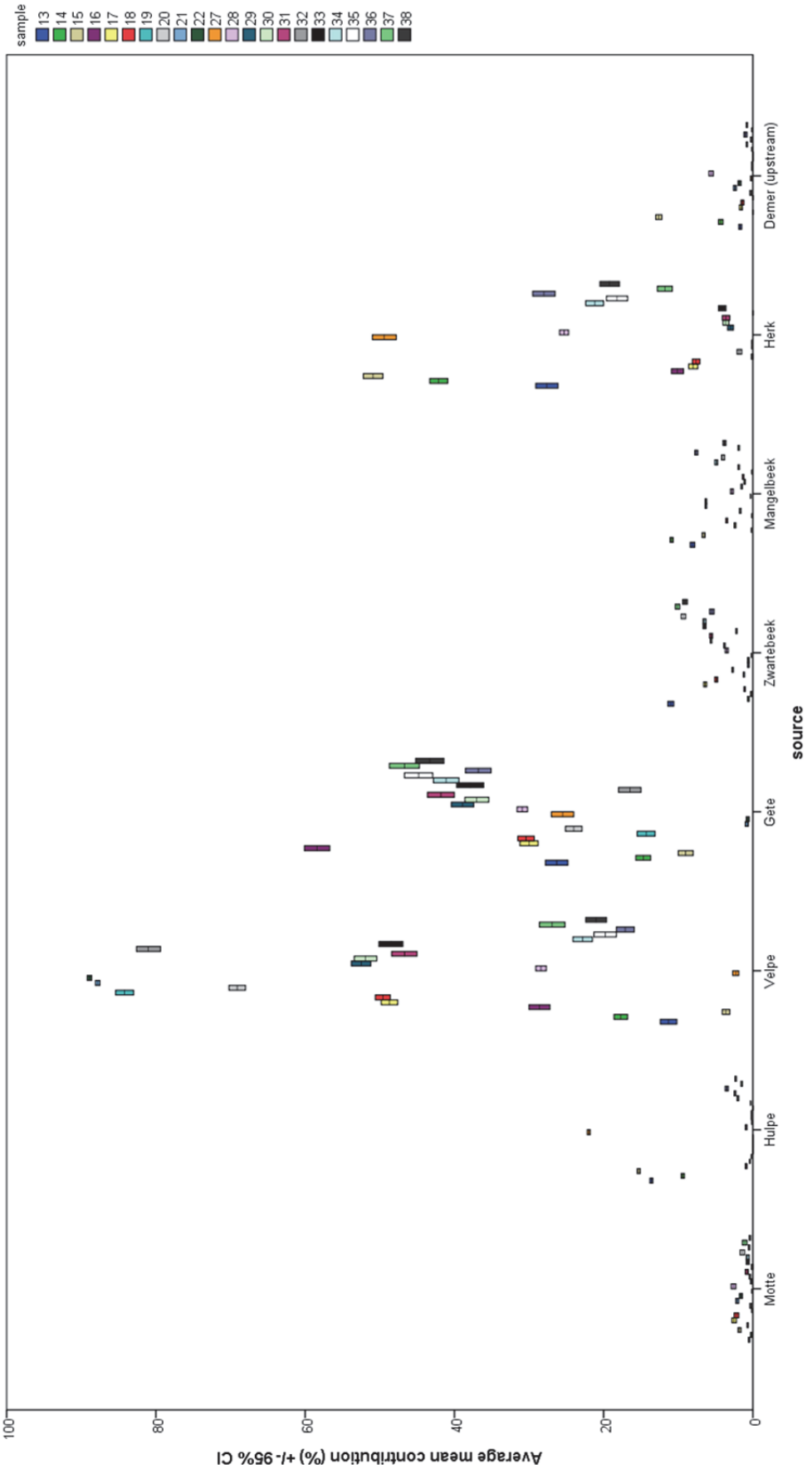

Figure 10.8: The average mean contributions of tributaries and associated 95% confidence interval, calculated using Composite Fingerprint E for the 22 individual outlet samples

Table 10.27: Average mean contributions, 95% mean confidence intervals and ranges of the eight tributaries to the SSF observed in outlet sample 14, using Composite Fingerprint E and the MC simulated property concentrations in the objective function.

		E zero	E PP	E GS	E GSPP	E OM	E OMPP
Motte	Average mean contribution (%)	0.2	0.2	0	0	0.1	0.1
	95% Confidence Interval (%)	0.1	0.1	0	0	0.1	0.1
	range (%)	0-11	0-11	0-0	0-0	0-11	0-12
Hulpe	Average mean contribution (%)	9.4	9.6	8.8	8.8	12.9	12.7
	95% Confidence Interval (%)	0.2	0.2	0.2	0.2	0.4	0.4
	range (%)	0-18	0-19	0-21	0-21	0-33	0-32
Velpe	Average mean contribution (%)	17.7	18.2	44.4	47.6	0.9	0.6
	95% Confidence Interval (%)	0.9	0.9	1.6	1.7	0.2	0.1
	range (%)	0-71	0-71	0-80	0-81	0-30	0-29
Gete	Average mean contribution (%)	14.7	14.3	17.5	16.2	13.8	14.3
	95% Confidence Interval (%)	1	1	1.5	1.5	0.8	0.9
	range (%)	0-73	0-72	0-75	0-77	0-55	0-54
Zwartebeek	Average mean contribution (%)	0.6	0.6	14.9	12.4	1.7	2.3
	95% Confidence Interval (%)	0.1	0.1	0.4	0.4	0.2	0.2
	range (%)	0-8	0-10	0-29	0-27	0-18	0-19
Mangelbeek	Average mean contribution (%)	10.9	10.8	4	4.7	26	26.3
	95% Confidence Interval (%)	0.2	0.2	0.2	0.2	0.3	0.3
	range (%)	0-18	0-18	0-15	0-16	0-40	0-40
Herk	Average mean contribution (%)	42.1	41.7	10.4	10.2	43.8	43.2
	95% Confidence Interval (%)	1.2	1.2	1	1	1	1.1
	range (%)	0-83	0-81	0-74	0-76	0-67	0-67
Demer (upstream)	Average mean contribution (%)	4.3	4.6	0	0	0.8	0.4
	95% Confidence Interval (%)	0.3	0.3	0	0	0.2	0.1
	range (%)	0-25	0-26	0-0	0-0	0-28	0-27

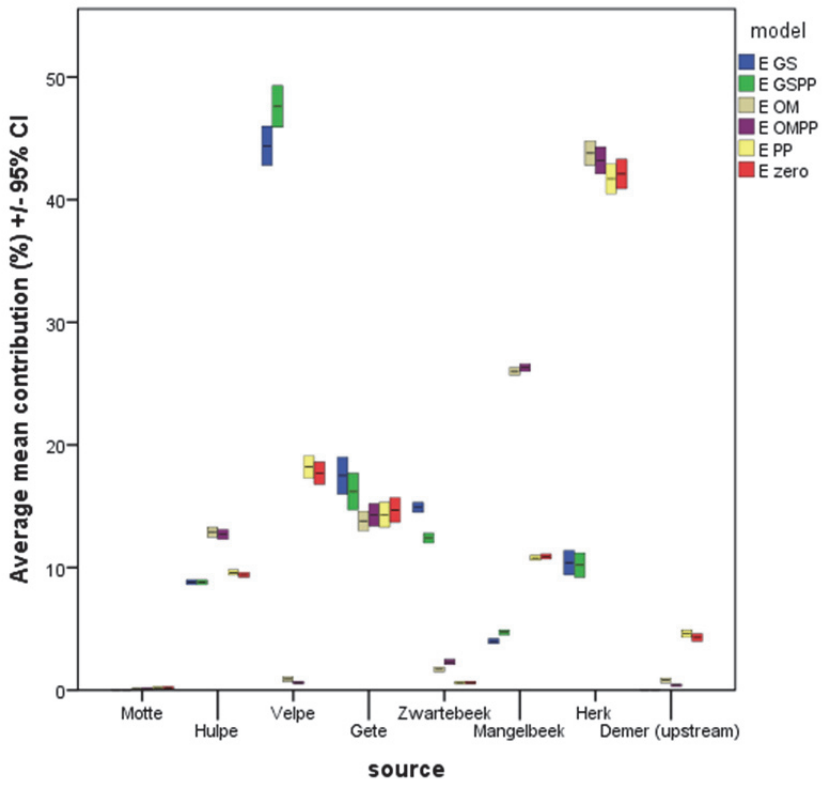

Figure 10.9: The average mean contributions of tributaries and associated 95% confidence interval, calculated using Composite Fingerprint E for outlet sample nr 14

Table 10.28: Asymptotic significances obtained through independent samples Kolmogorov-Smirnov tests between complete pdfs of sources obtained by Composite Fingerprint E models with and without W_i-correction factors, using data from outlet sample 14. * significant at a level of 0.05.

Null hypothesis	E zero-E PP	E GS-E GSPP	E OM-E OMPP
The distribution of the contribution of the Motte is the same across the categories of the model	1,000	1,000	1,000
The distribution of the contribution of the Hulpe is the same across the categories of the model	0.219	0.219	0.685
The distribution of the contribution of the Velpe is the same across the categories of the model	0.723	0.723	0.648
The distribution of the contribution of the Gete is the same across the categories of the model	0.859	0.859	0.536
The distribution of the contribution of the Zwartebeek is the same across the categories of the model	0.980	0.980	0.017*
The distribution of the contribution of the Mangelbeek is the same across the categories of the model	0.610	0.610	0.288
The distribution of the contribution of the Herk is the same across the categories of the model	0.954	0.954	0.859
The distribution of the contribution of the Demer (upstream) is the same across the categories of the model	0.219	0.219	0.013*

the combined dataset are created by the complilation of the 22 samples, or by the fact that some samples do create significant results cannot be determined at this state.

As most of the pdfs of the different sources obtained through modelling with or without the W_i-correction factor are no longer significantly different from one another, this raises the question whether implementing other correction factors (OM and GS) still lead to significantly different pdfs (as found when investigating the compiled dataset), or whether the differences would also turn out to be insignificant when investigated per sample. Therefore, K-S tests were executed, using data from sample 14, and testing the pdfs generated for each source by models E zero, E OM and E GS. The results are presented in Table 10.29, where it can be seen that the pdfs remain significantly different (at a level of 0.05) from one another, except for one exception (Motte contributions modelled by E OM and E GS models).

This suggests that model results of individual outlet samples resemble each other more closely for correction factors which have less influence (such as the W_i-correction factor) but still show significant differences for the more impactfull correction factors (such as OM and PP). Which one of these correction factors yields the best result, cannot be concluded at this stage.

10.5.5 Comparing and evaluating the modelling results of Composite Fingerprints A through E

The five different composite fingerprints (A through E) have each been entered into the objective function, using six different correction factor combinations. All modelling results, using 1,000 MC-simulated input parameters, yielded results with a very narrow 95% confidence interval. This shows that the models were able to produce mean results with a good convergence, indicating that 1,000 simulations were sufficient to find a local minimum for the objective function.

Table 10.29: Asymptotic significances obtained through independent samples Kolmogorov-Smirnov tests between complete pdfs of sources obtained by Composite Fingerprints A through E models, using GS, OM or no correction factors. * significant at a level of 0.05.

		E GS	E OM
The distribution of the contribution of the Motte is the same across the categories of the model	E zero	<0.001*	0.007*
	E GS		0.723
The distribution of the contribution of the Hulpe is the same across the categories of the model	E zero	<0.001*	<0.001*
	E GS		<0.001*
The distribution of the contribution of the Velpe is the same across the categories of the model	E zero	<0.001*	<0.001*
	E GS		<0.001*
The distribution of the contribution of the Gete is the same across the categories of the model	E zero	<0.001*	0.002*
	E GS		<0.001*
The distribution of the contribution of the Zwartebeek is the same across the categories of the model	E zero	<0.001*	<0.001*
	E GS		<0.001*
The distribution of the contribution of the Mangelbeek is the same across the categories of the model	E zero	<0.001*	<0.001*
	E GS		<0.001*
The distribution of the contribution of the Herk is the same across the categories of the model	E zero	<0.001*	<0.001*
	E GS		<0.001*
The distribution of the contribution of the Demer (upstream) is the same across the categories of the model	E zero	<0.001*	<0.001*
	E GS		<0.001*

Therefore, it can be investigated whether the modelling results of different fingerprints with similar correcton factors, yield similar results. This is, once more, tested by comparing the modelled pdfs of the individual sources (of the compiled dataset of all 22 outlet samples) of models using GS, OM and no correction factors, using a K-S test. Table 10.30 shows these test results, which indicate that, save for one, the pdfs of the potential sources generated by the different models, using the same corrections are significantly different (at a level of 0.05). This means that not only do the correction factors have a significant impact on the modelling results, but so do the properties included in the composite fingerprint.

As the results of the five composite fingerprints vary significantly, the question raised is which one of these models provides the best estimate and therefore it is important to have an idea of the actual contributions the tributaries contribute to the Demer.

An indirect way of verifying the correctness of the orders of magnitude of contributions predicted, is to investigate the contributions of discharges the individual tributaries deliver to the outlet station in Aarschot. This data is presented in Table 10.31, which shows the cumulated discharge measured for the May-October 2007 period at the outlet station in Aarschot, as well as the total discharges observed in the tributaries investigated in the sediment fingerprinting research. From this table can be learned that monitoring the eight tributaries, allows for monitoring almost 90% of the total discharge measured in Aarschot, therefore ensuring that no major water (and sediment) source is left unmonitored.

Furthermore, this table shows that the Gete is by far the most contributing tributary (delivering more than 30% of the discharge observed in Aarschot), while the Motte and Velpe contribute the least (3 and 4%). This immediately shows that the models contributing more than half of the observed sediment load in Aarschot to the Velpe must be erroneous, as erosivity in the Velpe and

Gete catchments is of the same order of magnitude. Additionally, Table 10.24 shows that the northern tributaries all contribute about the same amount of water to the Demer, i.e. around 8%.

Table 10.30: Asymptotic significances obtained through independent samples Kolmogorov-Smirnov tests between complete pdfs of sources obtained by Composite Fingerprints A through E models, using GS, OM or no correction factors. * significant at a level of 0.05.

		Zero				GS				OM			
Null hypothesis		**B**	**C**	**D**	**E**	**B**	**C**	**D**	**E**	**B**	**C**	**D**	**E**
The distribution of the contribution of the Motte is the same across the categories of the model	A	<0.001*	<0.001*	<0.001*	<0.001*	<0.001*	<0.001*	<0.001*	<0.001*	<0.001*	<0.001*	<0.001*	<0.001*
	B		<0.001*	<0.001*	<0.001*		<0.001*	<0.001*	<0.001*		<0.001*	<0.001*	0.2
	C			<0.001*	<0.001*			<0.001*	<0.001*			<0.001*	<0.001*
	D				<0.001*				<0.001*				<0.001*
The distribution of the contribution of the Hulpe is the same across the categories of the model	A	<0.001*	<0.001*	<0.001*	<0.001*	<0.001*	<0.001*	<0.001*	<0.001*	<0.001*	<0.001*	<0.001*	<0.001*
	B		<0.001*	<0.001*	<0.001*		<0.001*	<0.001*	<0.001*		<0.001*	<0.001*	<0.001*
	C			<0.001*	<0.001*			<0.001*	<0.001*			<0.001*	<0.001*
	D				<0.001*				<0.001*				<0.001*
The distribution of the contribution of the Velpe is the same across the categories of the model	A	<0.001*	<0.001*	<0.001*	<0.001*	<0.001*	<0.001*	<0.001*	<0.001*	<0.001*	<0.001*	<0.001*	<0.001*
	B		<0.001*	<0.001*	<0.001*		<0.001*	<0.001*	<0.001*		<0.001*	<0.001*	<0.001*
	C			<0.001*	<0.001*			<0.001*	<0.001*			<0.001*	<0.001*
	D				<0.001*				<0.001*				<0.001*
The distribution of the contribution of the Gete is the same across the categories of the model	A	<0.001*	<0.001*	<0.001*	<0.001*	<0.001*	<0.001*	<0.001*	<0.001*	<0.001*	<0.001*	<0.001*	<0.001*
	B		<0.001*	<0.001*	<0.001*		<0.001*	<0.001*	<0.001*		<0.001*	<0.001*	<0.001*
	C			<0.001*	<0.001*			<0.001*	<0.001*			<0.001*	<0.001*
	D				<0.001*				<0.001*				<0.001*
The distribution of the contribution of the Zwartebeek is the same across the categories of the model	A	<0.001*	<0.001*	<0.001*	<0.001*	<0.001*	<0.001*	<0.001*	<0.001*	<0.001*	<0.001*	<0.001*	<0.001*
	B		<0.001*	<0.001*	<0.001*		<0.001*	<0.001*	<0.001*		<0.001*	<0.001*	<0.001*
	C			<0.001*	<0.001*			<0.001*	<0.001*			<0.001*	<0.001*
	D				<0.001*				<0.001*				<0.001*
The distribution of the contribution of the Mangelbeek is the same across the categories of the model	A	<0.001*	<0.001*	<0.001*	<0.001*	<0.001*	<0.001*	<0.001*	<0.001*	<0.001*	<0.001*	<0.001*	<0.001*
	B		<0.001*	<0.001*	<0.001*		<0.001*	<0.001*	<0.001*		<0.001*	<0.001*	0.026*
	C			<0.001*	<0.001*			<0.001*	<0.001*			<0.001*	<0.001*
	D				<0.001*				<0.001*				<0.001*
The distribution of the contribution of the Herk is the same across the categories of the model	A	<0.001*	<0.001*	<0.001*	<0.001*	<0.001*	<0.001*	<0.001*	<0.001*	<0.001*	<0.001*	<0.001*	<0.001*
	B		<0.001*	<0.001*	<0.001*		<0.001*	<0.001*	<0.001*		<0.001*	<0.001*	<0.001*
	C			<0.001*	<0.001*			<0.001*	<0.001*			<0.001*	<0.001*
	D				<0.001*				<0.001*				<0.001*
The distribution of the contribution of the Demer (upstream) is the same across the categories of the model	A	<0.001*	<0.001*	<0.001*	<0.001*	<0.001*	<0.001*	<0.001*	<0.001*	<0.001*	<0.001*	<0.001*	<0.001*
	B		<0.001*	<0.001*	<0.001*		<0.001*	<0.001*	<0.001*		<0.001*	<0.001*	0.075
	C			<0.001*	<0.001*			<0.001*	<0.001*			<0.001*	<0.001*
	D				<0.001*				<0.001*				<0.001*

The most direct way of evaluating the sediment fingerprinting results however, is to compare the modelling results to the actually measured sediment fluxes in the outlet as well as in the different tributaries. Even though there might be a lag-time between sediment peaks passing the outlet stations on the tributaries and the arrival time of the sediment peak in Aarschot, if the period is sufficiently long, this should not pose a problem.

Table 10.31: Cumulated discharge for the May-October 2007 at the sediment fingerprinting sampling locations; raw discharge data obtained from FHR and VMM (*)

	Q (10^6 tonnes)	% of discharge measured at Aarschot
Demer – Aarschot	168	100
Motte-Rillaar*	5	3
Hulpe-Molenstede*	13	8
Gete – Halen	50	30
Velpe – Halen	7	4
Zwartebeek-Lummen*	10	6
Mangelbeek-Lummen*	15	9
Herk – Kermt	17	10
Demer (upstream)-Hasselt*	32	19
sum of all tributaries	148	88

Fully equipping nine locations with sediment sampling equipment and multi-parameter probes and analysing all the necessary samples however, was practically not feasible. Therefore, one southern and one northern tributary were selected to serve as validation catchments. The selected tributaries were the Mangelbeek and the Gete, where the discharge measurement stations of respectively Lummen and Halen were equipped with automatic pumping samplers and YSI multi-parameter probes.

This seems to suggest that the southern tributaries contribute, on average, more than their relative discharges would predict, while the northern tributaries contribute slightly less. This is to be expected as the erosion potential of the southern tributaries is much higher than that of their northern counterparts.

However, if the Gete contributes 65%, several other southern tributaries should contribute somewhat less to reach a complete 100% flux summation at Aarschot. The high contribution of Gete material also clearly indicates that models allocating the brunt of the sediment load in Aarschot to the Velpe are erroneous (models A and E), and those allocating it to the Gete are more correct (model B, C and D).

Also OM corrections, which consistently seem to lower the Velpe contributions, seem to have a positive influence, however, they do not always redistribute this material to the Gete.

The fact that the model results show significant differences between them, even when comparing results from different composite fingerprints, but implementing the same correction factors, seems to indicate that the fingerprints are struggling to perform.

This might be due to a lack of discriminative power of the composite fingerprints, especially when discrimination between the chemically alike southern tributaries such as the Velpe, Gete and Herk catchments is required.

If indeed the problem is situated in the discriminatory power of the composite fingerprints used (even though KW- and DFA-testing described it to have 100% corrective power), then the model should perform better if geochemically alike tributaries are grouped together and are inserted into the model as one source. Therefore, this has been attempted in the following section

10.5.6 Grouping of potential source areas

To test if a gradual reduction of sources would allow the fingerprinting technique to produce more accurate (and environmentally sound) results in the Demer basin, another set of composite fingerprints was constructed. To be able to compare the results with the suspended sediment fluxes obtained in Section 6.2, only the outlet samples obtained in that period (i.e. 14 and 15) were used to test the performance of the new composite fingerprints.

10.5.6.1 Four source groups (Composite Fingerprint F)

The first grouping of sources reduced the amount of sources from eight down to four. On the one hand, the Mangelbeek and the Zwartebeek were grouped together, as they are the two northern tributaries which are most alike, while on the other hand the Gete, Velpe, Herk and Demer (upstream) were combined into one group, leaving the Motte and the Hulpe as separate tributaries.

The entire processes described in Section 10.4 were executed once again (executing violation testing, submitting the remaining properties to a KW-test (which is passed when generating test statistics higher than the critical value at 95% confidence) and consequently entering the properties that passed into a Stepwise DFA (as previously described in Section 10.4.1.3. The statistics are presented in Table G.1 in Addendum G. The results of these procedures is a Composite Fingerprint (F) that is comprised of eight properties (in order of selection: Ca, Rb, Al, Ba, Mn, Ce, Zr and Sr) with a cumulative predictive power of 100%.

It is noteworthy that all properties have very high individual predictive powers, and that cumulatively after step 3 (the addition of Al to the composite fingerprint) the discriminative power of the model already reaches 100%. However, the DFA continues to add properties to the composite fingerprint, in order to reduce the Wilks' Lambda. The canonical functions of the final Composite Fingerprint reveal a complete differentiation between the four different groups (see Figure 10.10).

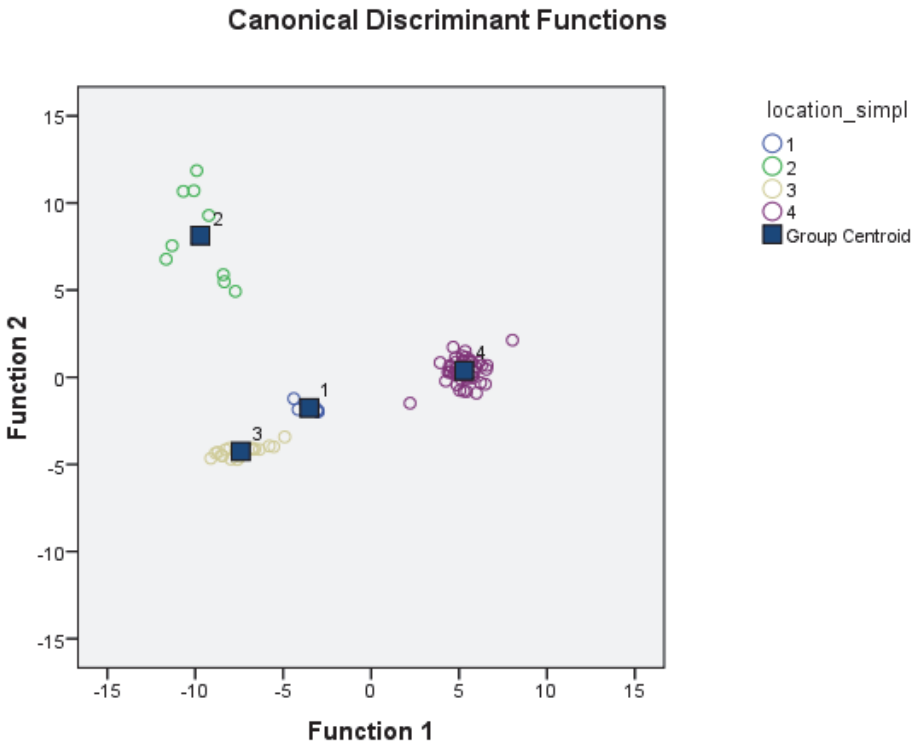

Figure 10.10: Canonical discriminant functions showing the discriminative power of Composite Fingerprint F. Sample groups: 1 = Motte; 2 = Hulpe; 3= Zwartebeek & Mangelbeek; 4 = Velpe, Gete, Herk & Demer (upstream)

Furthermore, OM and GS correction factors for samples 14 and 15 were determined for the new, combined sources and are reported in Table G.2 in Addendum G. Additionally, the W_i was based on the individual predictive powers of the properties and they are also reported in Addendum G (in Table G.1).

A mixing model was programmed into Microsoft Excel, using the same macro as before, adjusted to the dimensional needs of this reduced model, to un-mix the four sources using the eight properties selected. The results of this composite fingerprint for samples 14 and 15 are visually presented in Figures 10.11 and tabulated in Table 10.32.

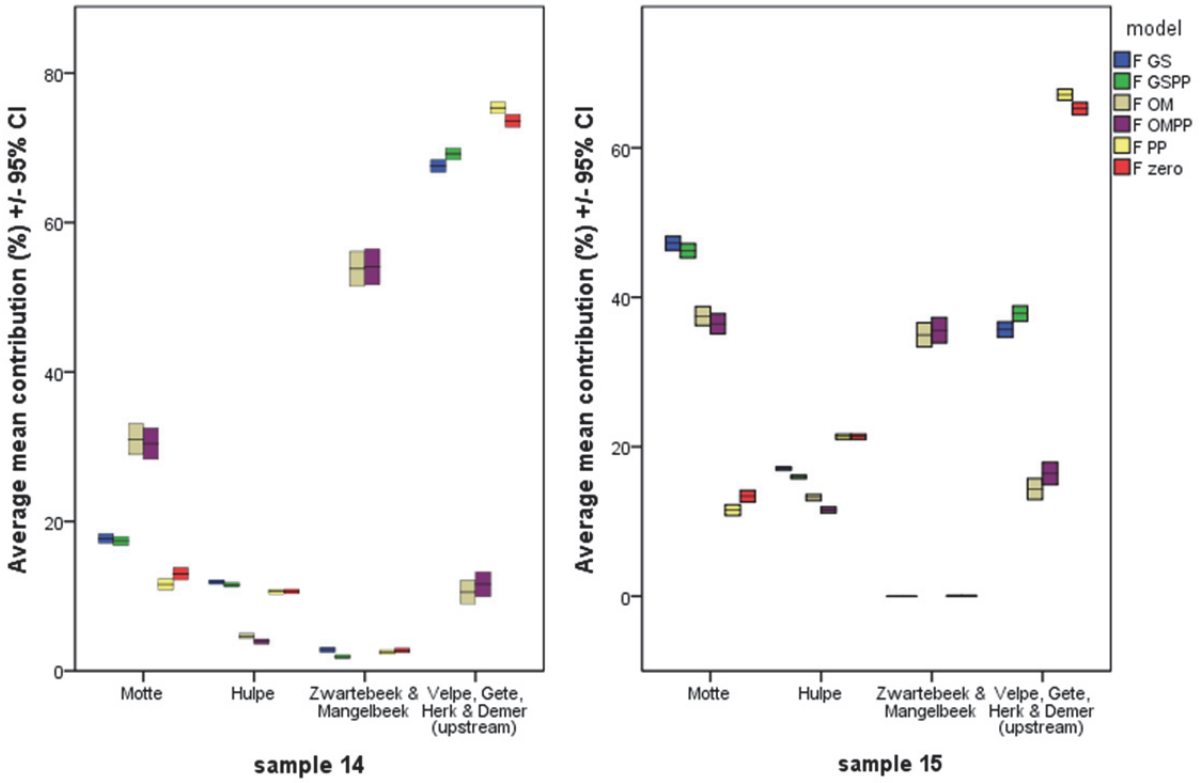

Figure 10.11: The average mean contributions of tributaries and associated 95% confidence interval, calculated using Composite Fingerprint F for outlet samples nr 14 and 15

Once more the results of the paired models with and without the application of a W_i-correction factor seem very similar. Independent samples K-S testing on these coupled pdfs, which revealed that almost all of the combinations are not significantly different from one another (at a level of 0.05), as is presented in Table 10.33. Only the Hulpe showed significantly different pdfs between models using and foregoing the use of W_i-correction factors.

Additionally, the impact of the GS and OM correction factors is once more investigated, using an independent samples K-S test. The results, presented inTable 10.34, show once more that the distributions of the pdfs modelled for the four different source groups are significantly different from one another. Only the combined source of Mangelbeek and Zwartebeek seems to have similar pdfs when GS corrections or no corrections have been applied. This, however, is due to the fact that for these models, their contributions approach zero.

The fact that the source group containing Mangelbeek and Zwartebeek still had zero contributions in the 1,000 MC-simulations, indicates that Composite Fingerprint F is still struggling to correctly apportion the contributions of the different tributaries. As all the southern tributaries are grouped together, now the uncertainty linked to the apportionment of the northern tributaries becomes more apparent. This can be observed in the final modelling results, where GS-corercted and models without correction factors attribute most of the northern contributions to the Hulpe and Motte, and only 0-2%% to the combined Mangelbeek and Zwartebeek source.

Table 10.32: Average mean contributions, 95% mean confidence intervals and ranges of the eight tributaries to the SSF observed in outlet samples 14 and 15, using Composite Fingerprint F and the MC simulated property concentrations in the objective function.

		F zero		F PP		F GS		F GSPP		F OM		F OMPP	
		14	15	14	15	14	15	14	15	14	15	14	15
Motte	Average mean contribution (%)	13.0	13.4	11.6	11.5	17.7	47.2	17.4	46.2	31.0	37.5	30.4	36.5
	95% Confidence Interval (%)	0.8	0.8	0.7	0.7	0.6	0.9	0.6	1.0	2.1	1.3	2.1	1.4
	range (%)	0-50	0-48	0-47	0-45	0-44	0-89	0-44	0-90	0-100	0-96	0-100	0-98
Hulpe	Average mean contribution (%)	10.6	21.3	10.6	21.3	11.9	17.1	11.5	16.0	4.7	13.2	3.9	11.5
	95% Confidence Interval (%)	0.3	0.4	0.3	0.4	0.3	0.2	0.3	0.2	0.3	0.4	0.3	0.4
	range (%)	0-25	9-38	0-25	9-38	0-28	0-28	0-27	0-27	0-21	0-27	0-19	0-27
Zwartebeek & Mangelbeek	Average mean contribution (%)	2.7	0.0	2.5	0.0	2.8	0.0	1.9	0.0	53.8	35.0	54.1	35.6
	95% Confidence Interval (%)	0.3	0.0	0.3	0.0	0.3	0.0	0.3	0.0	2.3	1.6	2.4	1.7
	range (%)	0-23	0-9	0-23	0-9	0-28	0-3	0-25	0-0	0-100	0-98	0-100	0-99
Velpe, Gete, Herk, Demer (upstream)	Average mean contribution (%)	73.6	65.2	75.3	67.1	67.6	35.7	69.2	37.8	10.5	14.3	11.6	16.4
	95% Confidence Interval (%)	0.8	0.8	0.7	0.7	0.8	1.0	0.8	1.0	1.6	1.4	1.7	1.5
	range (%)	45-100	37-91	48-100	40-91	36-100	0-100	41-100	0-100	0-100	0-96	0-100	0-98

Table 10.33: Asymptotic significances obtained through independent samples Kolmogorov-Smirnov tests between complete pdfs of sources obtained by Composite Fingerprint F models with and without W_i-correction factors, using data from outlet samples 14 and 15. * significant at a level of 0.05.

	F zero-F PP		F GS-F GSPP		F OM-F OMPP	
	14	15	14	15	14	15
The distribution of the contribution of the Motte is the same across the categories of the model	0.148	0.008	0.794	0.573	0.432	0.219
The distribution of the contribution of the Hulpe is the same across the categories of the model	1.000	1.000	0.573	<0.001*	0.038*	<0.001*
The distribution of the contribution of the Zwartebeek & Mangelbeek is the same across the categories of the model	0.723	1.000	0.010	1.000	0.500	0.500
The distribution of the contribution of the Velpe, Gete, Herk & Demer (upstream) is the same across the categories of the model	0.200	0.002	0.069	0.069	0.759	0.055

Table 10.34: Asymptotic significances obtained through independent samples Kolmogorov-Smirnov tests between complete pdfs of sources obtained by Composite Fingerprint F models, using GS, OM or no correction factors. * significant at a level of 0.05.

		14		15	
		F GS	F OM	F GS	F OM
The distribution of the contribution of the Motte is the same across the categories of the model	F zero	<0.001*	<0.001*	<0.001*	<0.001*
	F GS		<0.001*		<0.001*
The distribution of the contribution of the Hulpe is the same across the categories of the model	F zero	<0.001*	<0.001*	<0.001*	<0.001*
	F GS		<0.001*		<0.001*
The distribution of the contribution of the Zwartebeek & Mangelbeek is the same across the categories of the model	F zero	0.759	<0.001*	<0.001*	1,000
	F GS		<0.001*		<0.001*
The distribution of the contribution of the Velpe, Gete, Herk & Demer (upstream) is the same across the categories of the model	F zero	<0.001*	<0.001*	<0.001*	<0.001*
	F GS		<0.001*		<0.001*

This is doubtful as the Mangelbeek and Zwartebeek combined contribute around 60% of the northern discharges towards the Demer. Only the OM-corrected modelling results attribute higher contributions to the Mangelbeek and Zwartebeek, but then to such an extent (up to 60% of the total contribution) that the results become, once more, unrealistic. Therefore another reduction in source groupings was executed, in an attempt to reduce the uncertainty on the results and to obtain results that are in line with the environmental realities.

10.5.6.2 Three source groups (Composite Fingerprint G)

The next reduction entailed the combining of the Mangelbeek, Zwartebeek and Motte, in one group, the Velpe, Gete, Herk and Demer (upstream) in another and leaving the Hulpe as a separate tributary. Due to the presence of anthropogenic input, the Hulpe is compositionaly the most different from the other northern tributaries.

Once again, the entire process described in Section 10.4 was executed and the accompanying test statistics can be found in Table G.3 (presented in Addendum G). This time the stepwise DFA, based on minimizing of Wilks' Lambda, suggested allowing only three properties into the composite fingerprint (Ba, Ca and Mn), together yielding a discriminatory power of 100%. However, when un-mixing three sources, to fulfil the dimensional needs of the mixing model, at least four properties are required. Hence, the property with the highest individual predictive power (i.e. Sr) was added to the fingerprint. The total predictive power of this composite fingerprint remained at 100%. Again, it appears possible to completely separate the three groups from one another, as can be seen in their canonical functions (see Figure 10.12). OM and GS correction factors were determined for samples 14 and 15 for the new, combined sources and are reported in Table G.4 in Addendum G. Additionally, the W_i was based on the individual predictive powers of the properties and they are also reported in Addendum G (in Table G.3).

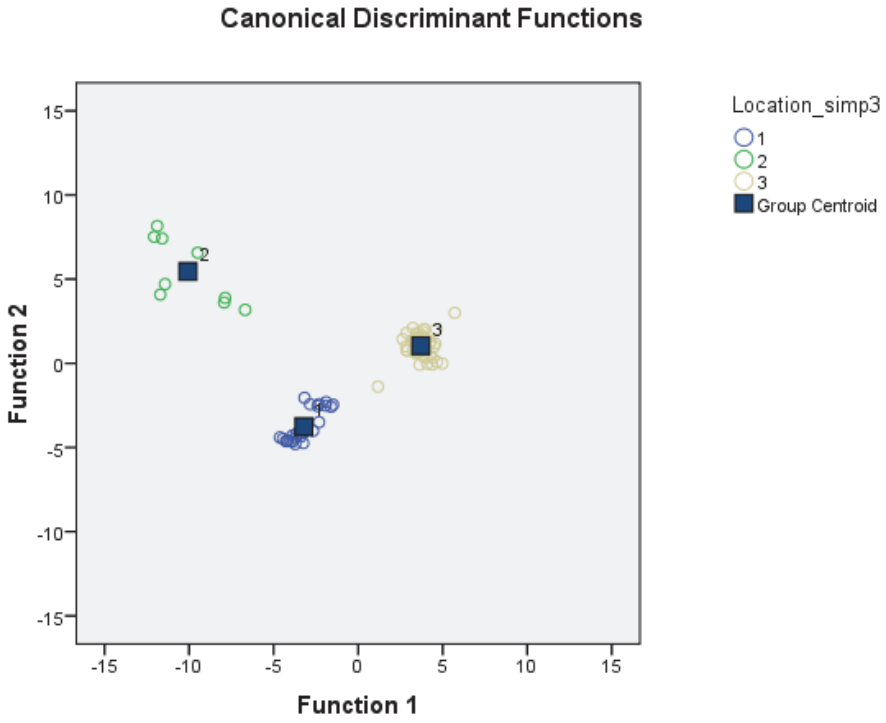

Figure 10.12: Canonical discriminant functions showing the discriminative power of Composite Fingerprint G. Sample groups: 1= Motte, Zwartebeek & Mangelbeek; 2 = Hulpe; 3 = Velpe, Gete, Herk & Demer (upstream)

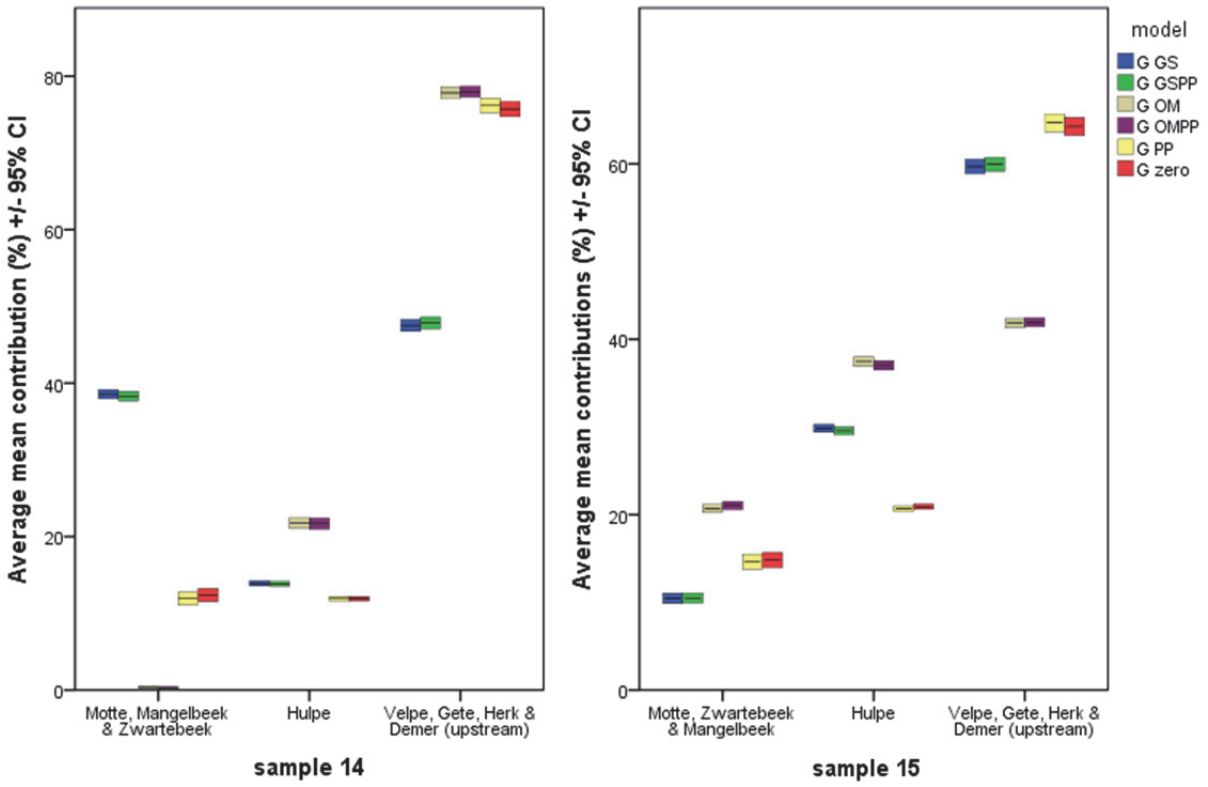

Figure 10.13: The average mean contributions of tributaries and associated 95% confidence interval, calculated using Composite Fingerprint G for outlet samples nr 14 and 15

Once more, a mixing model was programmed into Microsoft Excel to unmix the three sources using the four properties selected. The results for samples 14 and 15 are shown in Figure 10.13 and are tabulated in Table 10.35.

Table 10.35: Average mean contributions, 95% mean confidence intervals and ranges of the eight tributaries to the SSF observed in outlet samples 14 and 15, using Composite Fingerprint F and the MC simulated property concentrations in the objective function.

		G zero		G PP		G GS		G GSPP		G OM		G OMPP	
		14	15	14	15	14	15	14	15	14	15	14	15
Motte, Mangelbeek & Zwartebeek	Average mean contribution (%)	12.4	14.8	11.9	14.6	38.6	10.5	38.3	10.5	0.4	20.7	0.3	21.0
	95% Confidence Interval (%)	0.8	0.9	0.8	0.9	0.6	0.59	0.6	0.6	0.1	0.5	0.1	0.5
	range (%)	0-44	0-48	0-43	0-48	9-61	0-36	9-61	0-36	0-14	0-40	0-14	0-40
Hulpe	Average mean contribution (%)	11.9	20.9	11.9	20.7	13.9	29.8	13.8	29.6	21.8	37.4	21.7	37.0
	95% Confidence Interval (%)	0.3	0.3	0.3	0.3	0.3	0.45	0.3	0.4	0.7	0.5	0.7	0.5
	range (%)	1-25	9-36	1-25	9-35	0-29	9-54	0-29	10-53	0-43	16-67	0-43	16-66
Velpe, Gete, Herk, Demer (upstream)	Average mean contribution (%)	75.7	64.3	76.2	64.7	47.5	59.7	47.9	59.9	77.8	41.8	78.0	41.9
	95% Confidence Interval (%)	1.0	1.0	1.0	1.0	0.8	0.82	0.8	0.8	0.7	0.5	0.7	0.5
	range (%)	38-99	27-91	39-99	28-91	23-80	35-91	24-80	35-90	57-100	27-64	57-100	27-64

The results of the paired models (applying and not applying a W_i-correction factor) seem very similar for both samples, an observation which is confimered by independent samples K-S testing on the coupled pdfs, the results of which are presented in Table 10.36.

Additionally, the impact of the GS and OM correction factors is also investigated using an independent samples K-S test. The results, presented in Table 10.37, show once more that the distributions of the pdfs modelled for the three different source groups are significantly different from one another.

Table 10.36: Asymptotic significances obtained through independent samples Kolmogorov-Smirnov tests between complete pdfs of sources obtained by Composite Fingerprint G models with and without W_i-correction factors, using data from outlet samples 14 and 15. * significant at a level of 0.05.

	G zero-G PP		G GS-G GSPP		G OM-G OMPP	
	14	15	14	15	14	15
The distribution of the contribution of the Motte, Zwartebeek & Mangelbeek is the same across the categories of the model	0.888	1.000	0.913	0.969	1.000	0.794
The distribution of the contribution of the Hulpe is the same across the categories of the model	0.997	0.794	1.000	0.723	0.994	0.794
The distribution of the contribution of the Velpe, Gete, Herk & Demer (upstream) is the same across the categories of the model	0.913	0.980	0.794	0.913	0.936	0.988

Table 10.37: Asymptotic significances obtained through independent samples Kolmogorov-Smirnov tests between complete pdfs of sources obtained by Composite Fingerprint G models, using GS, OM or no correction factors. * significant at a level of 0.05.

		14		15	
		G GS	G OM	G GS	G OM
The distribution of the contribution of the Motte, Zwartebeek & Mangelbeek is the same across the categories of the model	G zero	<0.001*	<0.001*	<0.001*	<0.001*
	G GS		<0.001*		<0.001*
The distribution of the contribution of the Hulpe is the same across the categories of the model	G zero	<0.001*	<0.001*	<0.001*	<0.001*
	G GS		<0.001*		<0.001*
The distribution of the contribution of the Velpe, Gete, Herk & Demer (upstream) is the same across the categories of the model	G zero	<0.001*	<0.001*	<0.001*	<0.001*
	G GS		<0.001*		<0.001*

By grouping the northern tributaries together, leaving only the Hulpe as a separate river, the north-south distribution is reaching environmentally realistic estimations. However, in sample 15 the Hulpe contributions are still overestimated at the expense of the other northern tributaries (see Figure 10.13). In sample 14, the OM-corrected models even reduce the contributions of the Motte, Zwartebeek en Mangelbeek to zero, while the grain size corrected model do seem to increase their contribution.

10.5.6.3 Two source groups (Composite Fingerprints H)

To conlude, the modelling was executed using the northern tributaries and the southern tributaries as end members. The Motte, Hulpe, Mangelbeek and Zwartebeek were grouped into the one (northern) source group, while the southern source group contains the Velpe, Gete, Herk and upstream Demer. The test statistics for this Composite Fingerprint H can once more be found in Addendum G (in Table G.3).

The stepwise DFA suggested to allow four properties into the composite fingerprint (Ba, Ca, Rb and Al), which together yield a discriminatory power of 100%. The distributions of the two groups separate completely when plotted on the one remaining canonical function (see Table 10.38)

Table 10.38: The distributions of the northern and southern tributaries plotted on the one remaining canonical function produced by Composite Fingerprint H

	Northern tributaries	Southern tributaries
	Mangelbeek, Zwartebeek, Hulpe, Motte	Velpe, Gete, Herk and Demer (upstream)
Mean	-6.26	4.66
Stdev	0.994	1.004
N	35	47

For the final time, a mixing model was programmed into Microsoft Excel to unmix the two end members using the four properties selected. The results for samples 14 and 15 are shown in Figure 10.14 and are tabulated in Table 10.39.

The results of the paired models (applying and not applying a W_i-correction factor) seem to deviate slightly more than the two and three source fingerprint (Composite Fingerprints F and G). This is confirmed by independent samples K-S tests on the coupled pdfs, the results of which are presented in Table 10.39.

To conclude, the impact of the GS and OM correction factors is investigated using an independent samples K-S test on more time. The results, presented inTable 10.40, show that like all other incarnations of the composite fingerprints, the distributions of the pdfs modelled for the two different source groups are significantly different from one another. All of the modelling results show realistic distributions of the contributions of the northern and southern tributaries (see Figure 10.14).

The OM-correction once more seems to lower the contributions of the southern tributaries in favour of the northern sources.

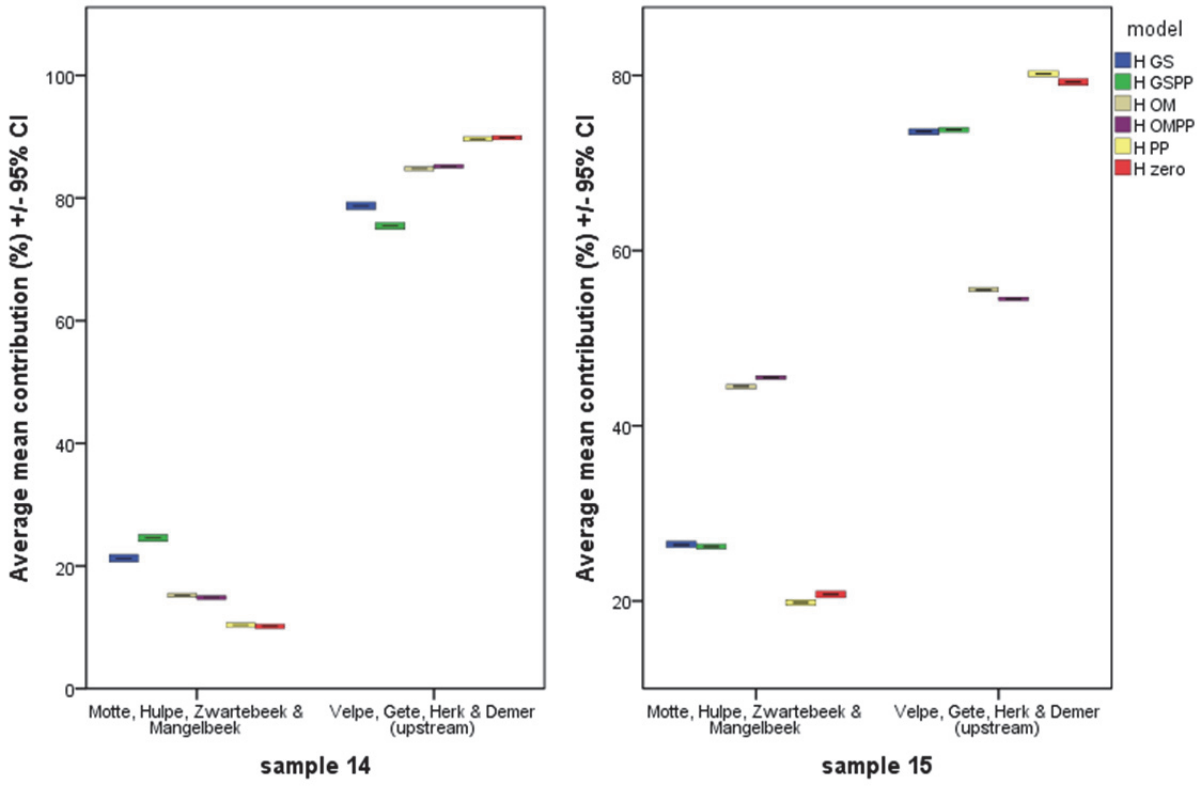

Figure 10.14: The average mean contributions of tributaries and associated 95% confidence interval, calculated using Composite Fingerprint H for outlet samples nr 14 and 15

Table 10.39: Average mean contributions, 95% mean confidence intervals and ranges of the eight tributaries to the SSF observed in outlet samples 14 and 15, using Composite Fingerprint G and the MC simulated property concentrations in the objective function.

		H zero		H PP		H GS		H GSPP		H OM		H OMPP	
		14	15	14	15	14	15	14	15	14	15	14	15
Motte, Hulpe, Mangelbeek & Zwartebeek	Average mean contribution (%)	10.2	20.8	10.4	19.8	21.3	26.4	24.6	26.2	15.2	44.5	14.8	45.5
	95% Confidence Interval (%)	0.4	0.4	0.3	0.3	0.6	0.3	0.6	0.3	0.4	0.3	0.3	0.2
	range (%)	0-29	8-41	0-26	8-35	0-45	12-40	2-46	12-39	0-28	32-54	0-27	33-55
Velpe, Gete, Herk, Demer (upstream)	Average mean contribution (%)	89.8	79.2	89.6	80.2	78.7	73.6	75.4	73.8	84.8	55.5	85.2	54.5
	95% Confidence Interval (%)	0.4	0.4	0.3	0.3	0.6	0.3	0.6	0.3	0.4	0.3	0.3	0.2
	range (%)	71-100	59-92	74-100	65-92	55-100	60-88	54-98	61-88	72-100	46-68	73-100	45-67

Table 10.40: Asymptotic significances obtained through independent samples Kolmogorov-Smirnov tests between complete pdfs of sources obtained by Composite Fingerprint H models with and without W_i-correction factors, using data from outlet samples 14 and 15. * significant at a level of 0.05.

	H zero-H PP		H GS-H GSPP		H OM-H OMPP	
	14	15	14	15	14	15
The distribution of the contribution of the Motte, Hulpe, Zwartebeek & Mangelbeek is the same across the categories of the model	0.121	0.011	<0.001*	0.002*	0.001*	<0.001*
The distribution of the contribution of the Velpe, Gete, Herk & Demer (upstream) is the same across the categories of the model	0.121	0.011	<0.001*	0.002*	0.001*	<0.001*

Table 10.41: Asymptotic significances obtained through independent samples Kolmogorov-Smirnov tests between complete pdfs of sources obtained by Composite Fingerprint G models, using GS, OM or no correction factors. * significant at a level of 0.05.

		14		15	
		H GS	H OM	H GS	H OM
The distribution of the contribution of the Motte, Hulpe, Zwartebeek & Mangelbeek is the same across the categories of the model	H zero	<0.001*	<0.001*	<0.001*	<0.001*
	H GS		<0.001*		<0.001*
The distribution of the contribution of the Velpe, Gete, Herk & Demer (upstream) is the same across the categories of the model	H zero	<0.001*	<0.001*	<0.001*	<0.001*
	H GS		<0.001*		<0.001*

10.5.7 Evaluation of the modelling results of Composite Fingerprints F through H

As already addressed in Section 10.5.5, the Gete and Mangelbeek were used as validation stations to estimate the modelling results. However, as these tributaries are now part of a grouping, their values can only be used indicatively.

The best way to evaluate Composite Fingerprints F through G is to theoretically estimate the total contributions of the northern and southern tributaries (based on the measurements in the Gete and the Mangelbeek) and then compare the modelling results of the Composite Fingerprints with those estimates.

Two approaches are possible to deduce the total contributions of the northern and southern tributaries. The first one is to use the SSFes measured in those tributaries (as calculated in Chapter

6 for the period May-October 2007) and use the ratio between the two as an indicator. In that case the 600 tonnes transported by the Mangelbeek, represents just under 10% of the SSF measured in the Gete, suggesting the northern tributaries contribute 10% of the total transport to the Demer and the southern contribute the remaining 90%.

The second approach makes use of the similarity of the northern tributaries in geological substrate and in sources of sediment (i.e. the formation of authigenic sediment). As this is a continuous, groundwater-driven process, it is reasonable to assume that these tributaries will contribute similar sediment contributions as those observed in the Mangelbeek. The southern tributaries, on the other hand, do not share this kind of continuous process and will therefore have more local differences.

Therefore, based on the calculated SSFes, the contribution of the northern tributaries is estimated to be around 20% of the total SSF observed at Aarschot for that period of record, while the southern tributaries account for the remaining 80%.

Therefore, models giving prediction results for the northern tributaries in the range of 5 to 25% are deemed realistic, while higher estimations indicate a failure in the composite fingerprint (and applied correction factors) to predict the contributions correctly.

Using this rule of thumb, model H seems to make acceptable predictions except for sample 15 using OM corrections. Then the model overpredicts the northern contributions. When GS corrections are implemented, the northern tributaries receive somewhat elevated contributions, bordering on the acceptable limits (around 25%).

Model F and G struggle more to perform. They have problems differentiating between the different northern tributaries, allocating insufficient contributions to the Mangelbeek and Zwartebeek catchments, as already indicated in Section 10.5.6. The combined contribution of all northern tributaries is usually overestimated when OM or GS corrections applied, though not consistently.

10.6 Conclusions

The composite sediment fingerprinting technique is a widely used methodology, applied to identify the relative contributions of various watershed sources to the total suspended sediment load observed at an outlet station. Within the framework of this PhD, the applicability of this approach was tested in the Demer basin, where eight of the Demer tributaries were selected to function as individual sources.

The statistical testing (using KW-testing and Stepwise Discriminant Function Analyses), rendered a composite fingerprint (A), capable of completely differentiating between all eight tributaries. Using this fingerprint, the model was run, entering tributary-averaged values as input parameters. The model results seemed promising as the mean standard error (RME) yielded acceptable low values. However, upon inspection of the modelled contributions of the tributaries, it showed the model to be allocating zero sediment contribution to too many sources, while overestimating the contribution of other sources.

Similar results were obtained when the model was run, using Monte Carlo simulated tributary concentrations, instead of average property concentrations. Most of the RME values ware below 15% and the 95% confidence intervals determined for the average mean contributions are very narrow (less than 2%) showing that the model is capable of converging around a central tendency.

However, environmentally, Composite Fingeprint A tended to allocate too much material to the Velpe. Therefore, an alternative to RME was an estimator of the performance of the model was

introduced: RME-avg. This estimator includes the relative errors of all properties passing the KW-test (so also those excluded from the composite fingerprint). RME-avg values however, showed that Composite Fingerprint A struggled somewhat in apportioning the relative contirbutions of the different tributaries.

Consequently, different combinations of properties were entered into composite fingerprints (Composite Fingerprints B through D, all having discriminative powers of 98.8 up to 100%). This was attempted in order to investigate whether specific properties caused the failure in performance of the models.

The model results were comparable to those of Composite Fingerprint A's, in that way that the confidence intervals show the models are convergent towards a single respons, but still the models struggle to attribute the contributions to the correct tributaries, within the same geographical region.

Using all modelling results of Composite Fingerprints A through D, the individual relative errors of all properties were investigated, to see if any specific properties were continuously distorting the modelling results. Effectively, three properties (Mn, P and S) showed elevated relative errors and consequently, a final attempt was made to create Composite Fingerprint (E) capable of discriminating between all eight tributaries, excluding those three parameters. However, the results of these models did not improve upon the four previous attempts.

Therefore, the amount of sources to be apportioned was reduced, from eight down to four (Composite Fingerprint F), three (Composite Fingerprint G) and finally down to two (Composite Fingerprint H). The latter was a complete separation of the system based on its geological substrate. All of these model runs had besides narrow confidence limits, however, only Composite Fingerprint H generated realistic modelling results, the other models seemed to struggle still to allocate contributions to chemically alike tributaries.

This seems to suggest that even though complete discrimination between the tributaries was statistically possible, the apportionment of the different tributaries could not be performed correctly. This might be caused by anthropogenic impact, or by failing grain size and/or LOI corrections, which will be addressed in Chapter 11.

All models, using Composite Fingerprint A through H, entered only 1,000 MC-simulated input parameters. However, the results showed a very narrow 95% confidence interval (0-2%), which shows that the models were able to produce mean results with a good convergence. This shows using 1,000 simulations was sufficient to find a local minimum for the objective function.

To conclude, when investigating the results of the composite fingerprints, not only were the average contributions and the 95% confidence intervals investigated, the entire distributions were compared, using independent samples Kolmogorov-Sminov tests. The test results for Composite Fingerprints A through E were similar: the predicted distribution functions (compiled from all 22 outlet results) were almost always significantly different from one another when comparing GS, OM or no corrections, while only some distributions were different when comparing the results between models using or foregoing W_i-corrections.

This distinction became even clearer, when the distributions were compared for every individual outlet sample. Then almost none of the W_i versus non-W_i models were significantly different from one another, while virtually all models with GS, OM or no corrections were statistically significantly different.

This indicates the impact of GS and OM corrections on the objective function and the fingerprint modelling results. The necessity of implementing these corrections in the Demer basin is discussed in more detail in Chapter 11.

11. Discussion Chapter: Sediment Fingerprinting

Observations in the previous chapter deserve some detailed investigation and discussion. This will be addressed in this chapter.

First of all, the use of grain size corrections, does not always seem to aid the model in providing better estimates for the contribution of sediment to the total sediment flux measured in the outlet station in Aarschot, while the organic matter corrections do seem to have an overall positive influence.

Therefore, it is useful to open the discussion whether grain size and/or organic matter correction should be applied in all situations in the Demer system, or in other systems in general. This approach is implemented in Sections 11.1 (for grain size correction) and 11.2 (for organic matter corrections).

Secondly, human impact can have both a positive and a negative impact on the potential to discriminate between and to apportion the contributions of different sediment sources. For the Demer basin these impacts are discussed in Section 11.3.

11.1 Grain size correction factors

11.1.1 Use of grain size correction factors in the literature

In the literature grain size correction is never omitted (safe from the initial reference in Walling et al. (1993). The reason most often stated for applying the GS correction is the well-established relationship between particle size and element concentrations in soils and sediments (He & Owens, 1995; He & Walling, 1996; Horowitz, 1991; Horowitz & Elrick, 1987; Thorne & Nickless, 1981) in combination with sediment sorting, ensuring the suspended sediment outlet samples to be enriched in fines compared to the catchment source materials (Morris & Fan, 1998). This is supported by observations in source type sediment fingerprinting research found in the literature, though it should be mentioned that not all authors published their applied correction factors (or reported the observed grain sizes of their source and outlet sediment samples).

Collins et al. (1997 b, 1997 c, 1998, 2001) and Juracek & Ziegler (2009) reported detailed grain size correction factors. In those studies, all sources (such as cultivated land, pastures, woodland, channel bank) reported lower SSA's, than the sampled suspended sediment they contributed to.

Few exceptions to this general rule have been reported. Collins et al. (1997 b) reported channel banks enriched in fines compared to the suspended sediment collected in the Plynlimon catchment (U.K.). Krause et al. (2003) found that the sediment sampled from gully walls in the Wirragulla catchment (Australia) had SSA's three times that of the sink pool they studied as outlet. Krause et al. (2003) reasoned that because of the steepness and limited height of most gully wall faces, there would be only limited potential for the reworking of soil particles on the exposed face of the gully walls, therefore reducing preferential particle sorting.

For spatial source apportionment studies, however, in the few studies where correction coefficients or SSA data were published, the outlet suspended sediment samples were not always enriched in fines compared to the tributary sources. Collins et al. (1997 c) presented data on the Exe and the

Severn basins (U.K.), where the mean particle size correction factors applied, ranged respectively from 0.95 to 1.11 and 0.96 to 1.16.

Such an application of a grain size correction factor implies that certain tributaries became enriched in fines from the place where the original source material was sampled compared to where the outlet material was procured, and that for certain other tributaries, the reverse happened (i.e. they became depleted of fines downstream).

If this was the case, then the grain size correction was rightfully inserted into the mixing model and should aid in obtaining a correct modelling result.

However, if the observed grain size of the suspended sediment obtained at the outlet station is in effect the result of mixing of tributaries with finer sediment and material of tributaries with coarser grain size distributions (each with their inherent chemical composition) where the mixture results in a medium grain sized distribution with a blended geochemistry as well, downstream, then the use of the grain size correction factor will not have the desired effects and its use should be questioned.

11.1.2 Observed grain sizes in sediment in the Demer basin

All the sediment sampled (be it on land, from the riverbed or from the suspended fraction in the river itself) was dried and underwent sieving to procure the fraction <63µm and were consequently subjected to laser diffraction particle size analysis (as described in Section 3.1.5). The results for the source type sampling data as well as the spatial sources are discussed separately below.

11.1.2.1 Source type sampling in the Gete catchment

Grain size analyses on the <63µm fraction of all samples collected in the Gete catchment are presented (per source type) in Figure 11.1.

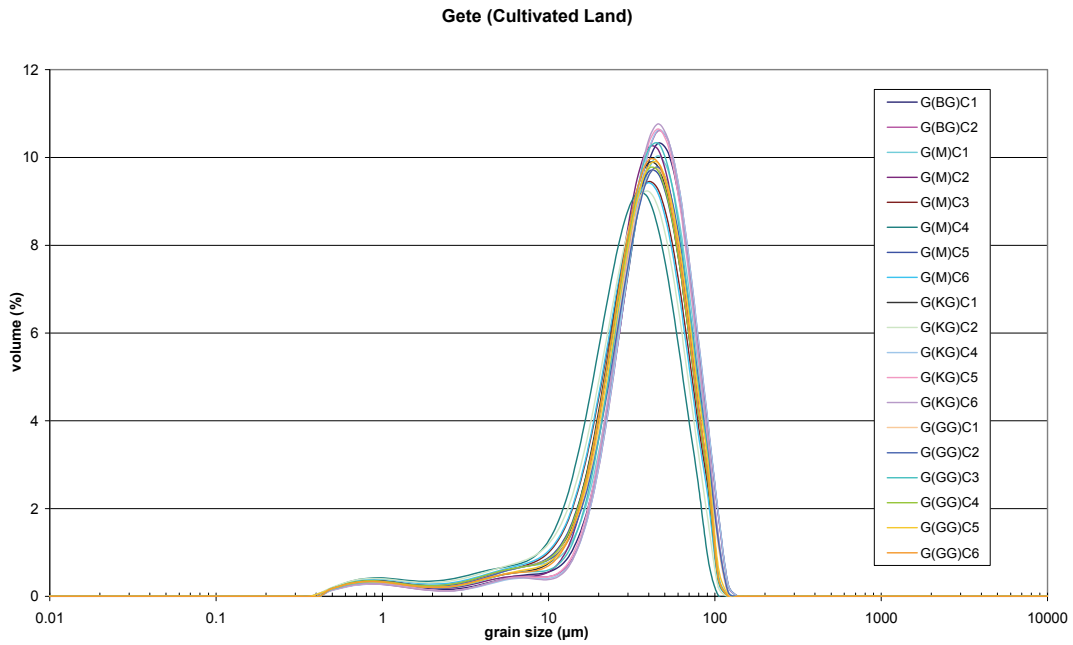

Figure 11.1: Grain size distributions as determined for the <63µm sieved source type samples in the Gete catchment. The sample names reference the names given in Addendum D, for the TIS-sample figure where they represent the timing of sampling (see Figure 10.1)

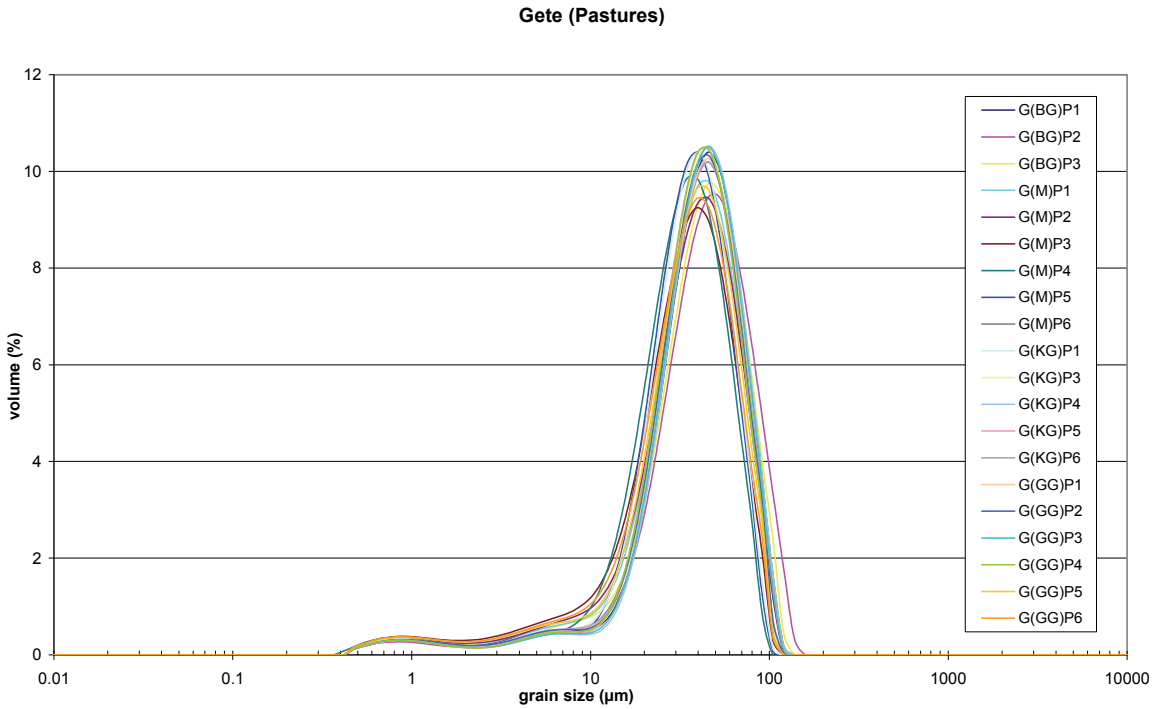

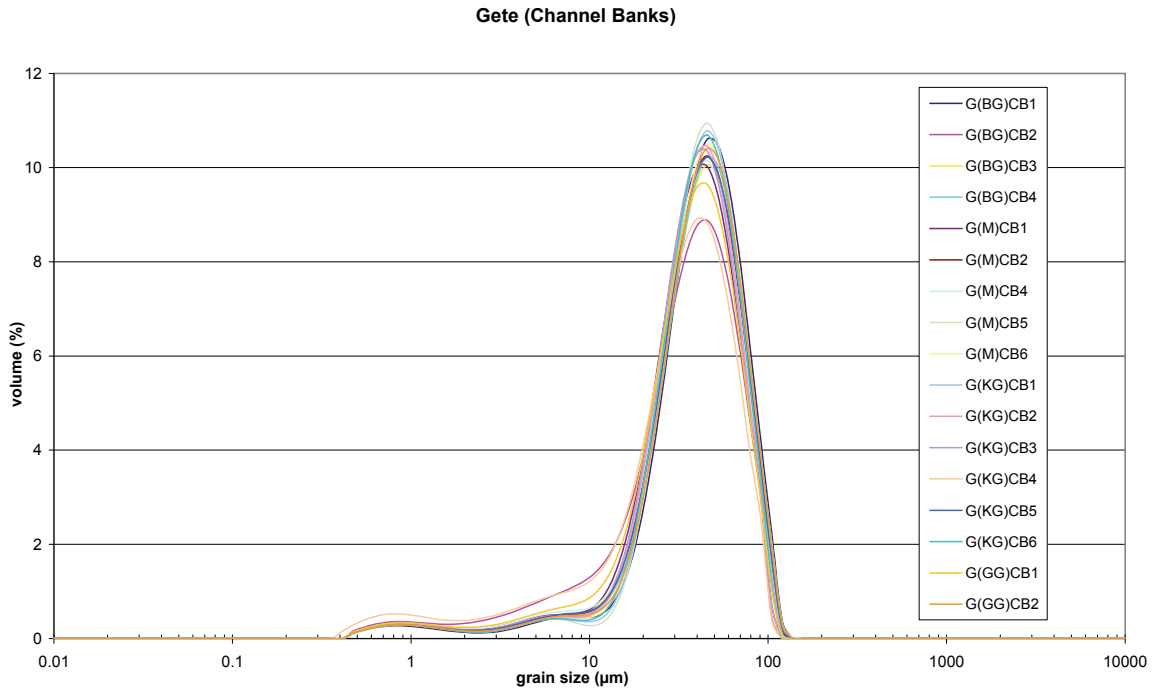

Figure 11.1 (continued)**:** Grain size distributions as determined for the <63µm sieved source type samples in the Gete catchment. The sample names reference the names given in Addendum D, for the TIS-sample figure where they represent the timing of sampling (see Figure 10.1)

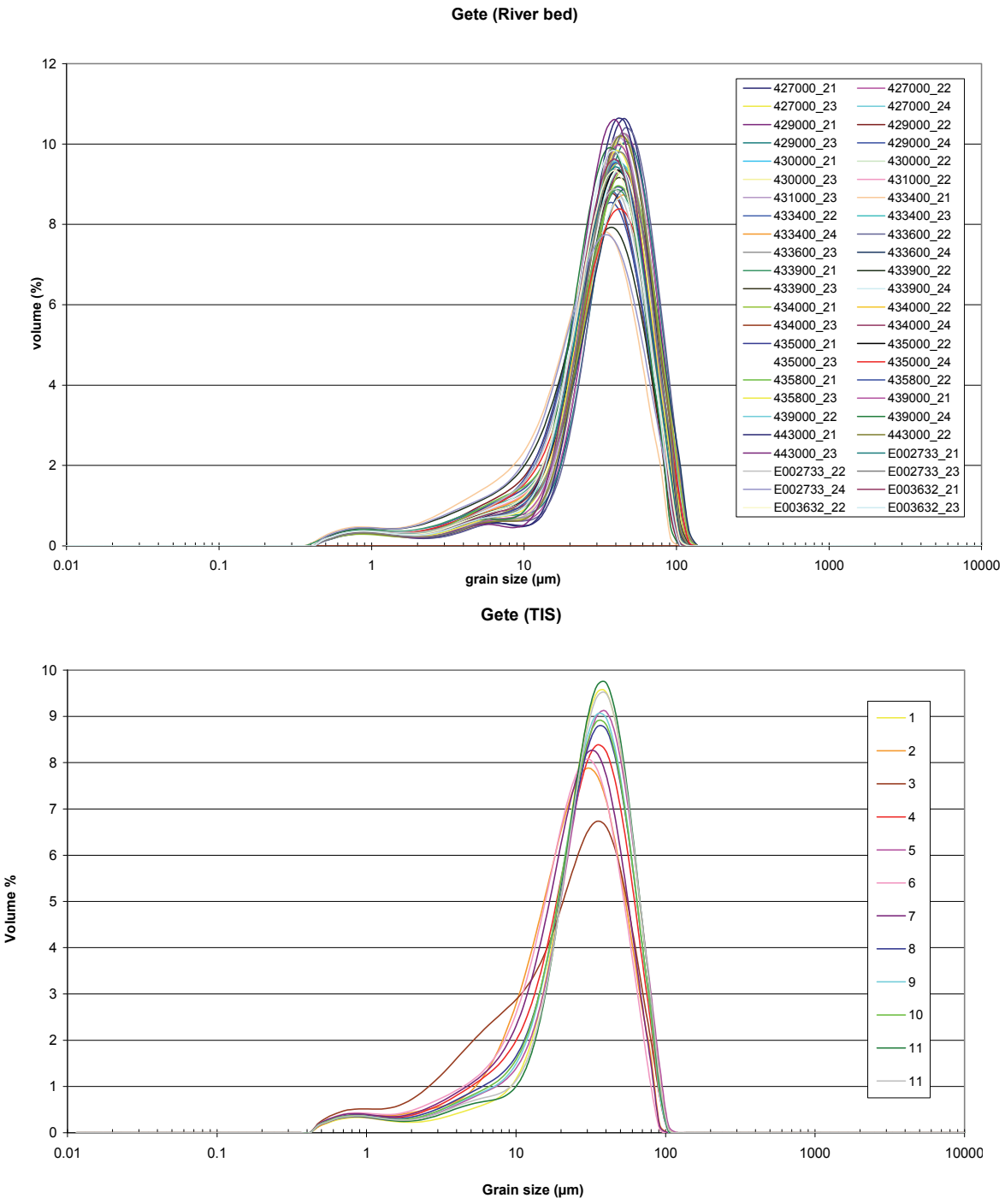

Figure 11.1 (continued)**:** Grain size distributions as determined for the <63µm sieved source type samples in the Gete catchment. The sample names reference the names given in Addendum D, for the TIS-sample figure where they represent the timing of sampling see Figure 10.1)

This figure clearly shows that cultivated land, pastures and channel banks have very similar grain size distributions: they all have a peak around 40-45µm and a tail towards the finer sediments (with a small bump around 0.8-0.9µm). The riverbed samples show a similar trend, but they exhibit a larger variability (peaking around 35-50 µm) and a slightly higher presence in the 2-10 µm range. The outlet (TIS) samples resemble the riverbed samples (higher level of 2-10µm fraction present), but they peak around 30-40µm. This translates fairly well in the specific surface areas that were calculated for the respective source types and TIS samples and are presented in Figure 11.2. The SSA-values for cultivated land, pastures and channel banks (excluding the one outlier present in the latter) all range within 0.13-0.20 m²/g while the TIS-samples range from 0.17 to 0.24 m²/g (excluding the one outlier with a SSA of 0.29 m²/g (sample nr 3)).

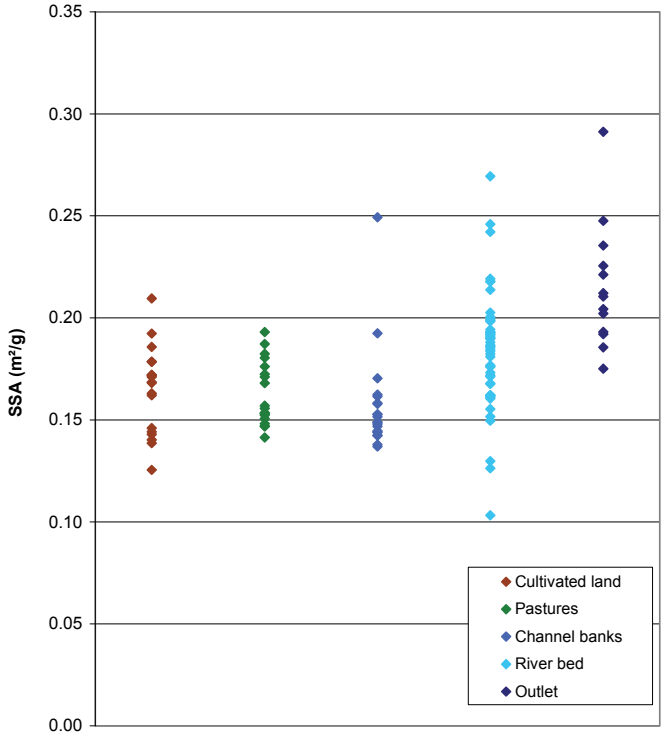

Figure 11.2: SSA-values (m²/g) as determined for sediment samples obtained from cultivated land, pastures, channel banks, riverbed and from outlet TIS-sampling in the Gete catchment.

These observations confirm what has been reported in the literature: the on-land sampled sediments are coarser than the materials sampled in-stream. Therefore, they support the assumption that the sedimentary material becomes enriched in fine material while moving downstream, leading to the conclusion that a grain size correction factor should be implemented.

This is confirmed by the cumulative grain size contributions of the Gete outlet samples, whom do not plot within two distribution curves which represent the envelop of all measured on-land source samples, as shown in Figure 11.3. In this figure, the grain sizes are noted in phi classes. These relate to µm as stated in Equation 11.1.

$$\phi = -\log_2 \frac{D}{D_0} \qquad \text{Eq. 11.1}$$

in which:
- ϕ is the Krombein phi scale
- D is the diameter of the particle
- D_0 is a reference diameter, equal to 1mm.

Therefore, the source samples could not contribute to the outlet samples, without undergoing sorting (a relative enrichment in fines).

However, the range of SSAs of the riverbed material (0.10-0.27 m²/g) covers the entire variability observed in the tributary outlet location (apart from the one outlier). This suggests that the sediment deposited on the riverbed, already underwent some sort of sorting and can be, at least in part, directly linked to the sediment data observed in the TIS samples. Applying one single correction factor on the riverbed data would therefore negatively influence the modelling result.

Consequently, riverbed material cannot be included in a standard type of composite sediment fingerprint (using a standard grain size correction factor based on average SSA of the source and individual SSA of the outlet sample as stated in Equation 10.7). Hence, two options remain: either riverbed material is excluded as a potential (secondary) source of sediment and only the three

primary sources sampled are allowed to drive the model (using a source specific grain size correction factor) or include the riverbed samples, but then another grain size correction factor should be developed.

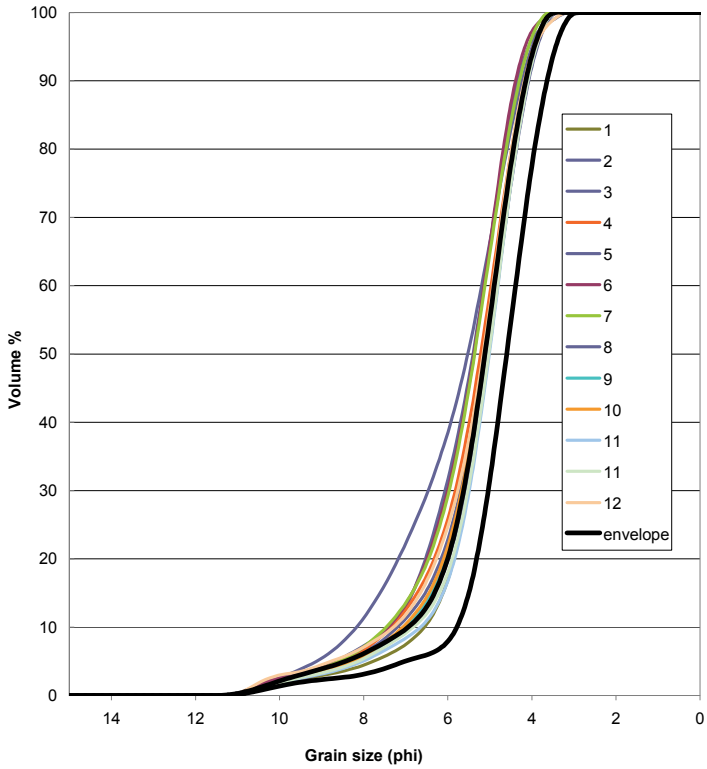

Figure 11.3: Cumulative grain size distributions for the <63µm sieved outlet samples collected in the Gete (Halen) plotted against two distribution curves which represent the envelope of all measured source samples collected on-land in the Gete catchment. The sample names reference the sampling times (shown in Figure 10.1 and given in Addendum D)

11.1.2.2 Source type sampling in the Mangelbeek catchment

Like for the Gete catchment, all available source material from the Mangelbeek catchment was dried, sieved to a fraction <63µm and was consequently subjected to laser diffraction particle size analysis (as discussed in Section 3.2.2). In the Mangelbeek catchment however, one additional source was sampled (compared to the types of samples collected in the Gete catchment), i.e. authigenic sediment. This source, according to the MARS modelling discussed in Part IV, represents around 70% of the total suspended load of the Mangelbeek, and can therefore not be neglected. All the obtained grain size data for the Mangelbeek catchment is graphically presented in Figure 11.4.

As in the Gete catchment, cultivated land, pastures and channel bank samples show a grain size distribution skewed towards the coarser fractions, however their peaks show more variability. Cultivated land and pastures peak around 35-50 µm, while channel banks are slightly coarser (peaking around 40-60µm). Samples from these sources all show a minor secondary peak of very fine material (0.7 – 0.8µm) similar to observations in the Gete catchment.

The biggest differences between Mangelbeek and Gete catchment however is the authigenic sediment and its impact on the riverbed and TIS outlet samples. As described in Section 9.2.2, an attempt was undertaken to sample 'pure' authigenic sediment. However, due to the difficulty of collecting sufficient 'fluffy' authigenic sediment to do a full scope analysis, few samples were

actually analysed with the Mastersizer 2000. Two samples, (MA6_3 and MA 1_2) turned out to be contaminated with non-authigenic sediment, as can be seen in their deviating grain size distributions (see Figure 11.4) as well as in their chemical composition (see Addendum E), which clearly did not contain a sufficiently elevated iron content to be considered authigenic sediment. Therefore, these two samples will be omitted from further analyses.

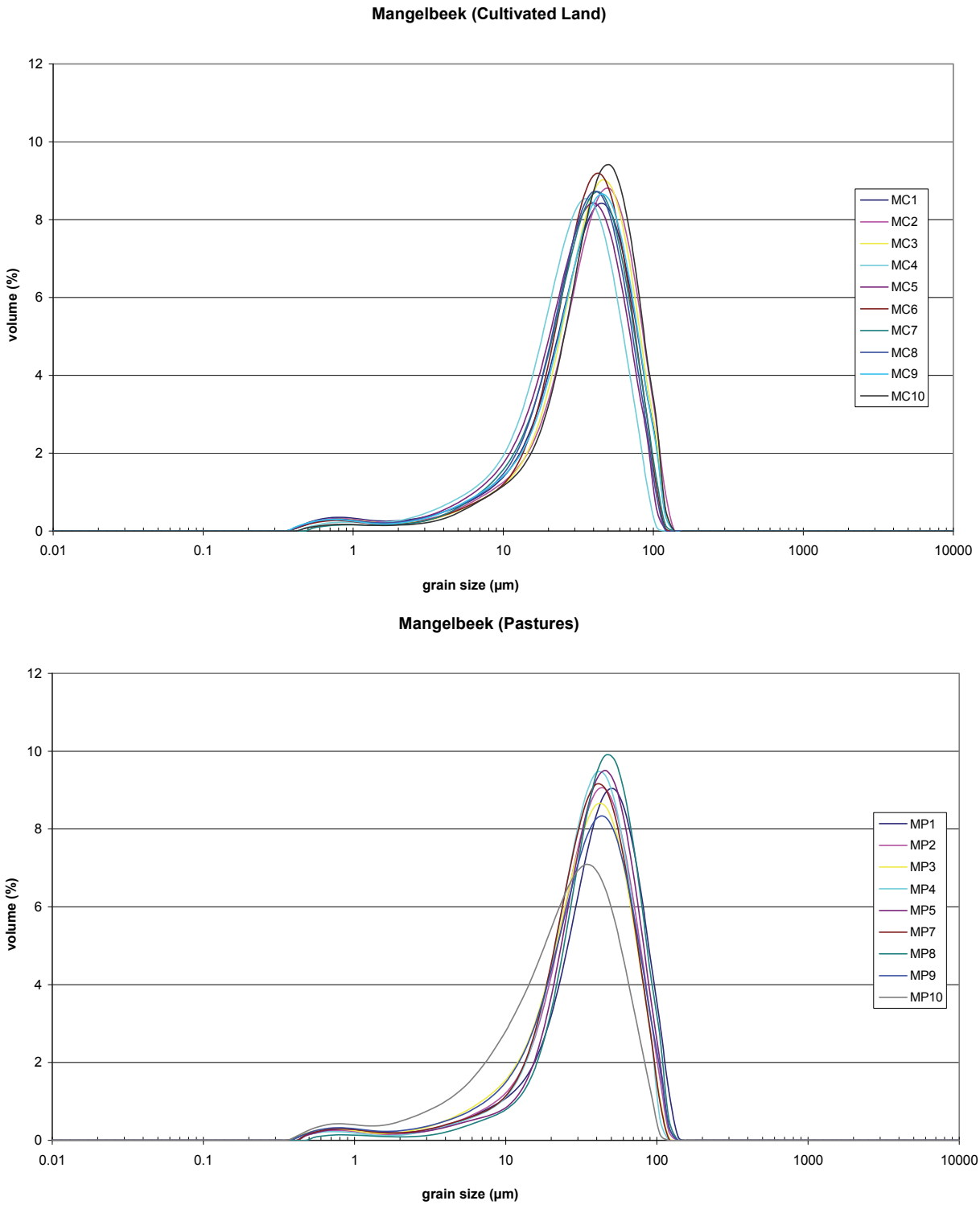

Figure 11.4: Grain size distributions as determined for the <63µm sieved source type samples in the Mangelbeek catchment. The sample names reference the names given in Addendum E, for the TIS-sample figure where they represent the timing of sampling (see Figure 10.1).

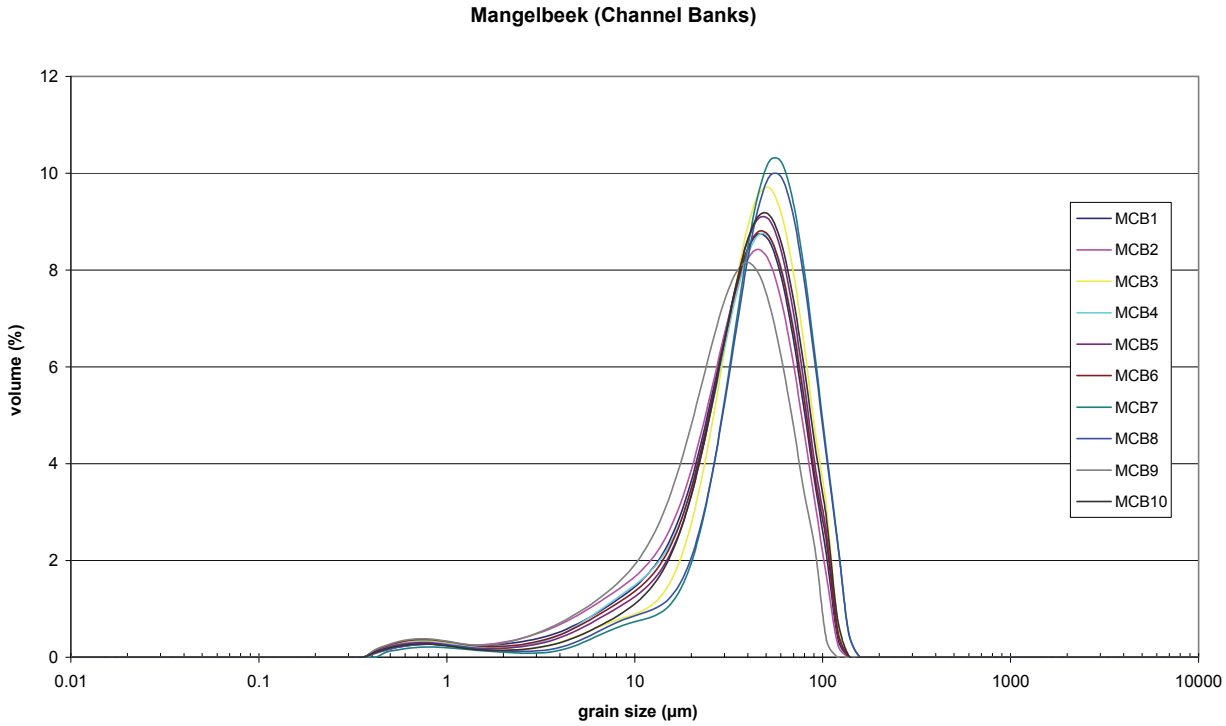

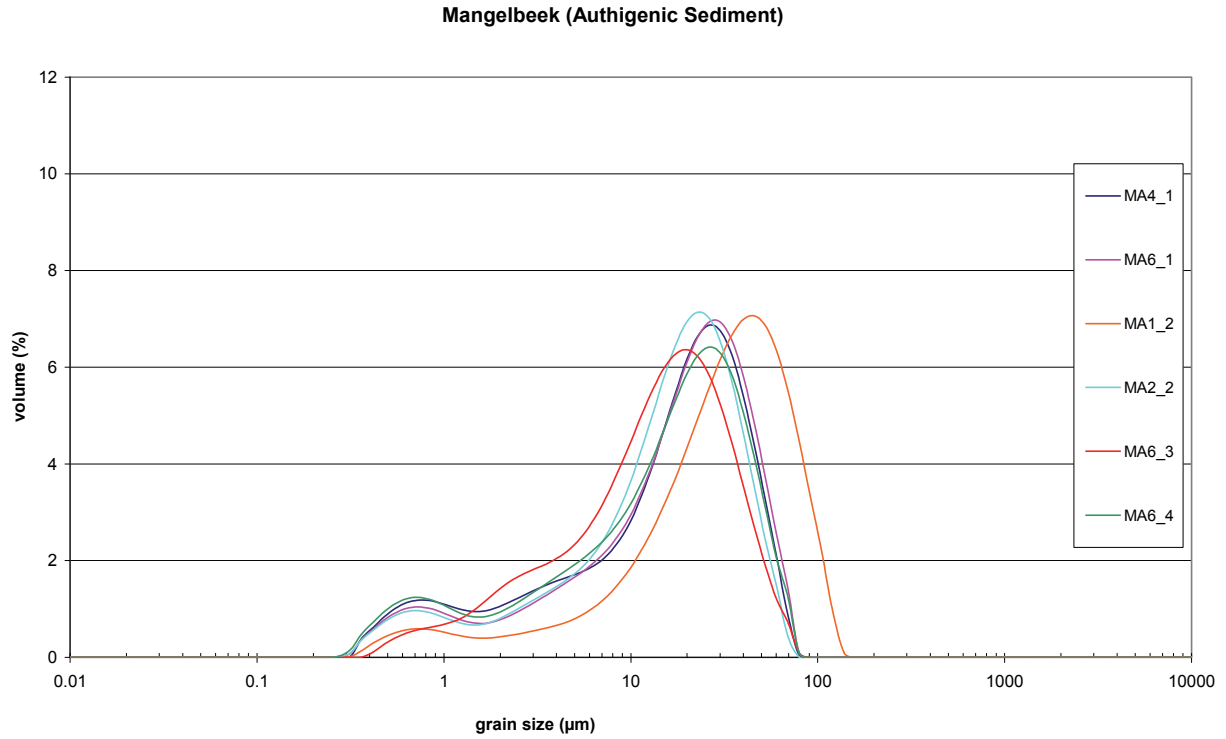

Figure 11.4 (continued): Grain size distributions as determined for the <63µm sieved source type samples in the Mangelbeek catchment. The sample names reference the names given in Addendum E, for the TIS-sample figure where they represent the timing of sampling (see Figure 10.1).

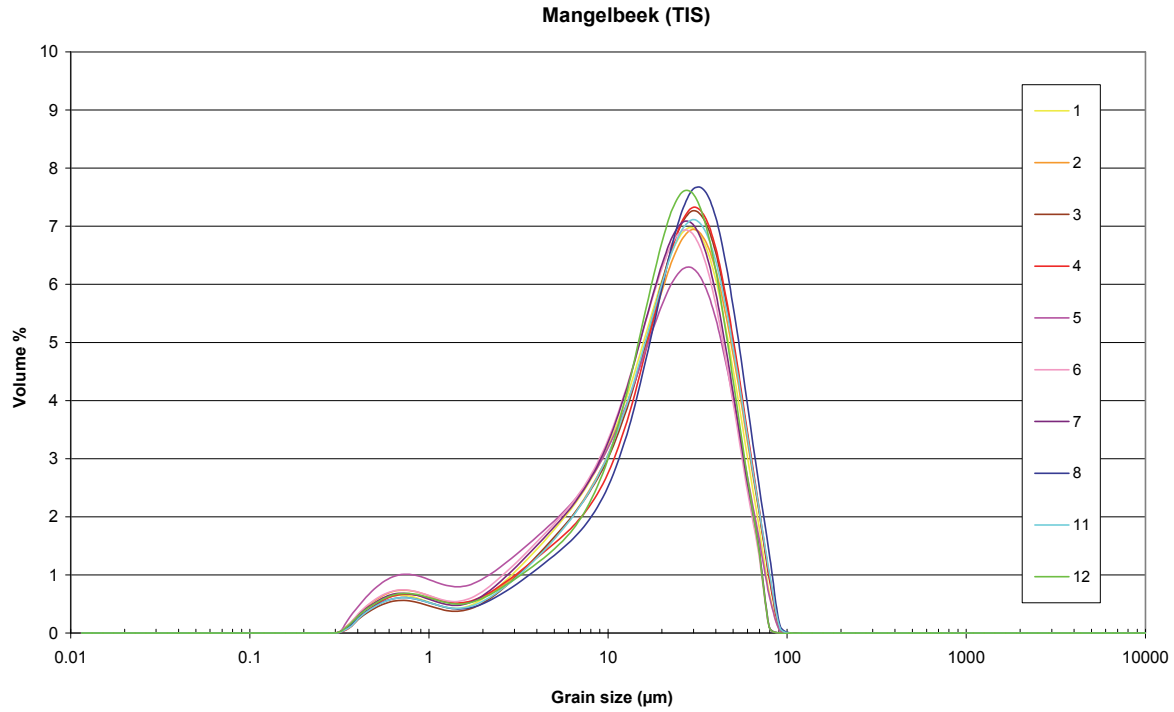

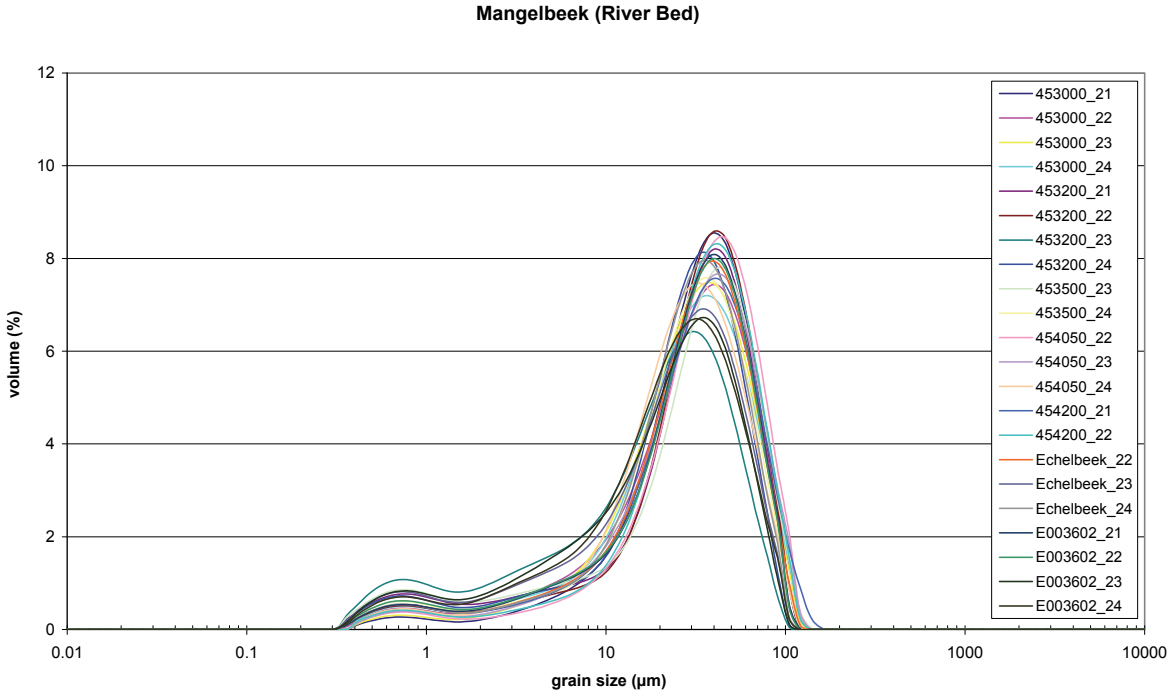

Figure 11.4 (continued): Grain size distributions as determined for the <63µm sieved source type samples in the Mangelbeek catchment. The sample names reference the names given in Addendum E, for the TIS-sample figure where they represent the timing of sampling (see Figure 10.1).

The remaining authigenic sediment samples have a clearly finer grain size distribution, with a more distinct bi-modal course. The distribution is still skewed towards the coarser fraction (with peaks ranging from 25 to 30µm, but with an overall presence of the finer fraction (which peaks around 0.7µm). Consequently, this sediment source influences the riverbed material (peaking around 30-45µm) and the TIS-collected material (peaking around 25-30µm).

These observations are translated in the SSA-values of the respective source types and TIS samples and are presented in Figure 11.5. The SSA-values for cultivated land, pastures (excluding the one outlier) and channel banks all range within 0.10-0.20 m²/g, which are values similar to those observed in the Gete catchment. The authigenic sediment on the other hand has values ranging from 0.30 to 0.36 m²/g, and these values might be an underestimation. The SSA-values of the riverbed samples seem to cover almost the entire variability of SSA-values observed in other samples. Though they tend to not go quite down to 0.10m²/g, they do range from 0.36 to 0.15 m²/g. The TIS samples on the other hand, do not have such a wide range of SSA-values. They range from 0.25 to 0.30 with one possible outlier of 0.38 m²/g.

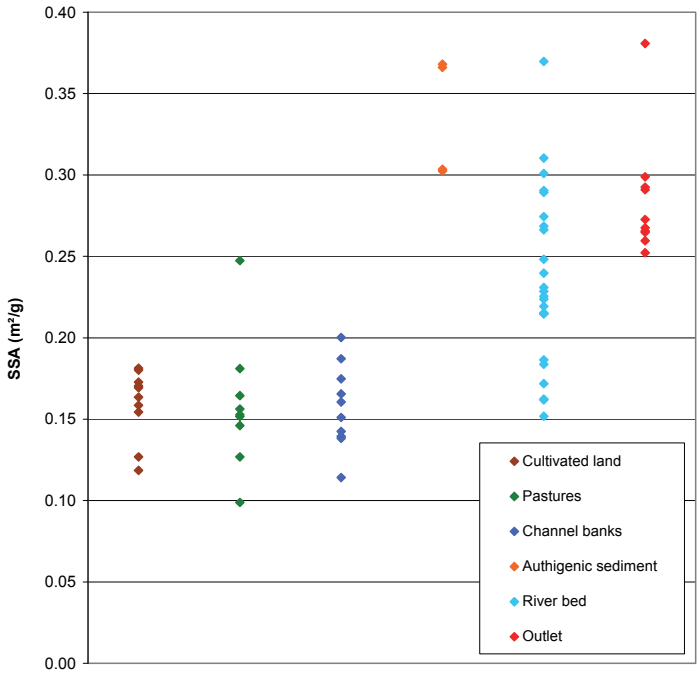

Figure 11.5: SSA-values (m²/g) as determined for sediment samples obtained from cultivated land, pastures, channel banks, authigenic sediment, riverbed and from outlet TIS-sampling in the Mangelbeek catchment

As such, these observations contradict the observations in the literature and the ones made in the Gete catchment where outlet samples are always enriched in fines in comparison to the sources.

In the case of the Mangelbeek catchment, and in extent to all catchments with authigenic sediment as a significant contributor of sediment to the total suspended sediment load, the outlet samples are relatively finer than the on-land sources but coarser than the authigenic sediment, as they are comprised of a mixture of the two.

Therefore, it becomes impossible to apply a simple grain size correction factor (Equation 10.7). Applying such a correction factor would lead to overdecreasing the chemical content of the authigenic sediment and overincreasing the property concentrations of the non-authigenic sources. These overcorrections can be visualized by comparing average grain size correction factors

calculated for the Gete catchment with those calculated for the Mangelbeek catchment. This is illustrated in Table 11.1, where both the observed average SSA-values for the different sediment samples as well as the grain size correction factors per source are reported.

Table 11.1: SSA-values (m²/g) averaged per sample type and the corresponding grain size correction factors calculated for the 'average' outlet sample for both Gete and Mangelbeek catchments. The adjusted GS correction factor for the Mangelbeek is based on the SSA of the Gete outlet.

	Gete		Mangelbeek		
	SSA_avg	GS correction factor	SSA_avg	GS correction factor	Adjusted GS
Cultivated land	0.16	1.31	0.16	1.78	1.35
Pastures	0.16	1.32	0.16	1.8	1.36
Channel banks	0.16	1.37	0.16	1.81	1.37
Authigenic sediment	/	/	0.34	0.85	1
Riverbed	0.18	1.17	0.24	1.21	?
Outlet	0.22	/	0.28	/	/

Both in the Gete and Mangelbeek catchments, cultivated land, pastures, and channel banks have similar SSA-values of 0.16 m²/g. If one assumes that the sorting from land to outlet was similar in both catchments, than similar grain size corrections should be applied. However, due to the significant contribution of authigenic sediment to the sediment load in the Mangelbeek catchment, the average SSA at the outlet (0.28 m²/g) was much higher than the one observed at the Gete outlet (0.22 m²/g), causing the correction factors for the 'on-land' sources to be much higher for the Mangelbeek (+/- 1.8) than for the Gete basin (+/- 1.3). Applying such overestimated correction factors in the Mangelbeek catchment would lead to erroneous results.

Therefore the hypothesis is that the sampled sediment at the Mangelbeek outlet is a mixture of 'on-land' source sediment enriched in fines to a SSA of +/- 0.22 m²/g (similar to the Gete) and very fine authigenic sediment, leading to the average SSA of 0.28 m²/g as observed at the outlet. The adjusted correction factors, based on these assumptions, are also presented in Table 11.1. This hypothesis seems to be confirmed by Figure 11.6, which shows on the phi scale, the cumulative grain size contributions of the Mangelbeek outlet samples, whom all plot within the boundary curves of all measured on-land source samples.

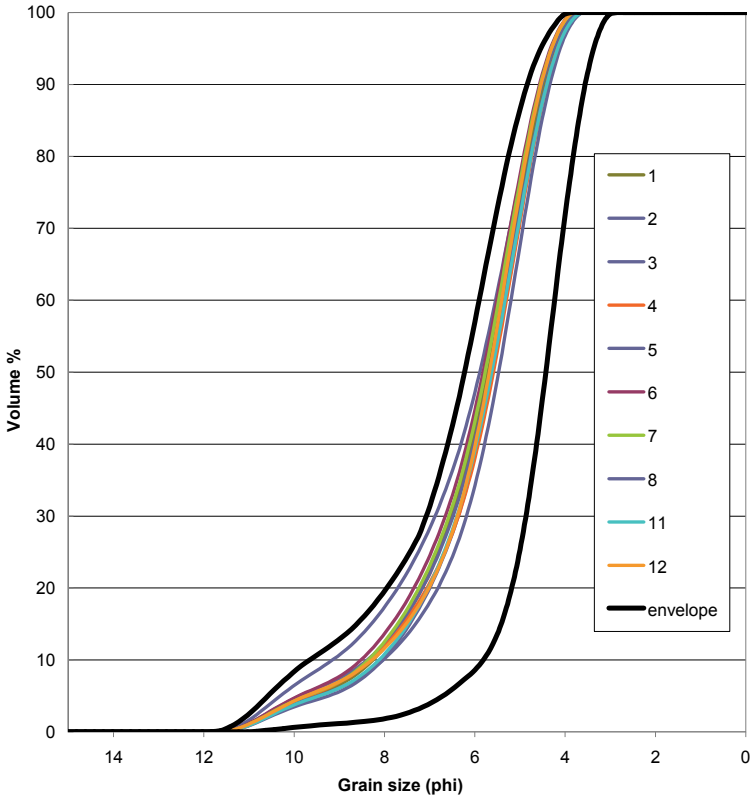

Figure 11.6: Cumulative grain size distributions for the <63µm sieved outlet samples collected in the Mangelbeek (Lummen) plotted against two distribution curves which represent the envelope of all measured source samples collected on-land in the Mangelbeek catchment.

Without the comparison study in the Gete catchment, which fortunately yielded similar results for the 'on-land' sources, it would have been impossible to find applicable grain size correction factors in the Mangelbeek, and this approach cannot be blindly copied in other study areas. Furthermore, this is just one set of 'average' grain size corrections factors. It would be impossible to create correction factors for each outlet sample individually.

Concerning the riverbed material in the Mangelbeek, a similar conclusion as in the Gete catchment can be drawn. As the range of SSAs of the riverbed material (0.15-0.37 m^2/g) again covers the entire variability observed in the tributary outlet location (apart from the one outlier), the application of one single correction factor on the entire riverbed data set would negatively influence the modelling result.

Consequently, either riverbed material is excluded as a potential (secondary) source of sediment in the Mangelbeek catchment as well or the riverbed samples are allowed to be entered, but then another grain size correction factor should be developed.

11.1.2.3 Spatial provenance type sampling in the Demer basin

Grain size distribution data is also available on the <63µm fractions obtained from TIS samples collected on the tributaries of the Demer basin. The data from the Gete and Mangelbeek outlets have already been reported respectively in Figures 11.1 and 11.4. The data from the other tributary locations are presented in Figure 11.7.

These figures indicate that the premise of using a TIS (as described in Section 2.2.2.1) to ensure the collection of time-integrated samples, hence middling out some of the (grain size) variations present in that individual tributary, is valid. The particle size distributions are very similar per tributary and moreover, the similarities seem to be geographically grouped, as can be seen in Figure 11.8. Figure 11.8a shows the grain size distributions averaged per tributary. It is clear that the northern (Mangelbeek, Zwartebeek and Hulpe) as well as southern tributaries (Velpe, Gete and Herk), show a bi-modal distribution skewed towards the coarser fraction, though the bi-modal nature of the distribution is less pronounced in the southern tributaries.

Using the Multiple Mode Analyses tool present in the Mastersizer 2000 software, local modes for the individual peaks of the bi-modal distributions could be tabulated as well as the relative percentages these peaks contributed to the total volume of grains measured in the samples. These data are presented in Table 11.2, showing the northern tributaries have peaks (with local modes around 0.7 and 26 µm) slightly finer than the southern tributaries (with local modes around 0.8 and 34 µm). But more significantly, the contributions of the finest of the two peaks is more elevated for the northern tributaries (6% versus 3% for the southern tributaries). The two tributaries that are more centrally located (the upstream Demer and Motte catchments), show aspects from both geographical origins, but resemble the southern tributaries more. These observations are further illustrated in Figure 11.8b which shows the cumulative grain size distributions averaged per tributary.

These results should be compared to the grain size distributions of the samples obtained at the Aarschot outlet station. The simplest way to do this is to compare the respective SSA-values, which are visually represented in Figure 11.9.

This figure shows that the southern tributaries all have similar SSA-values, ranging from 0.15 to 0.25 m^2/g (excluding the one Gete outlier), while the northern tributaries have higher SSA-values.

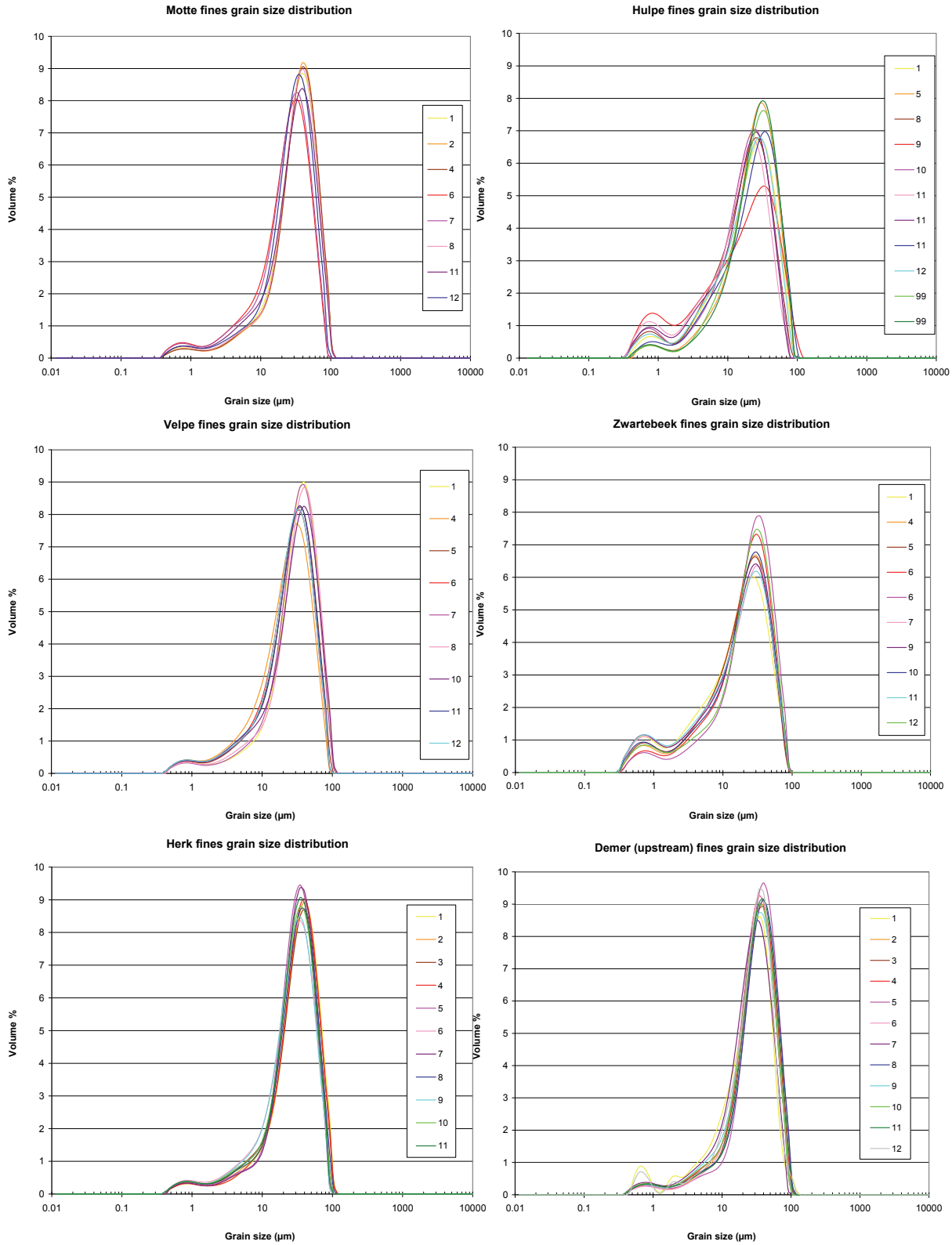

Figure 11.7: Grain size distributions as determined for the <63µm sieved TIS samples obtained in the Motte, Hulpe, Velpe, Zwartebeek, Herk and Demer (upstream) tributaries. The numbering of the samples represents the timing as referenced in Addendum C

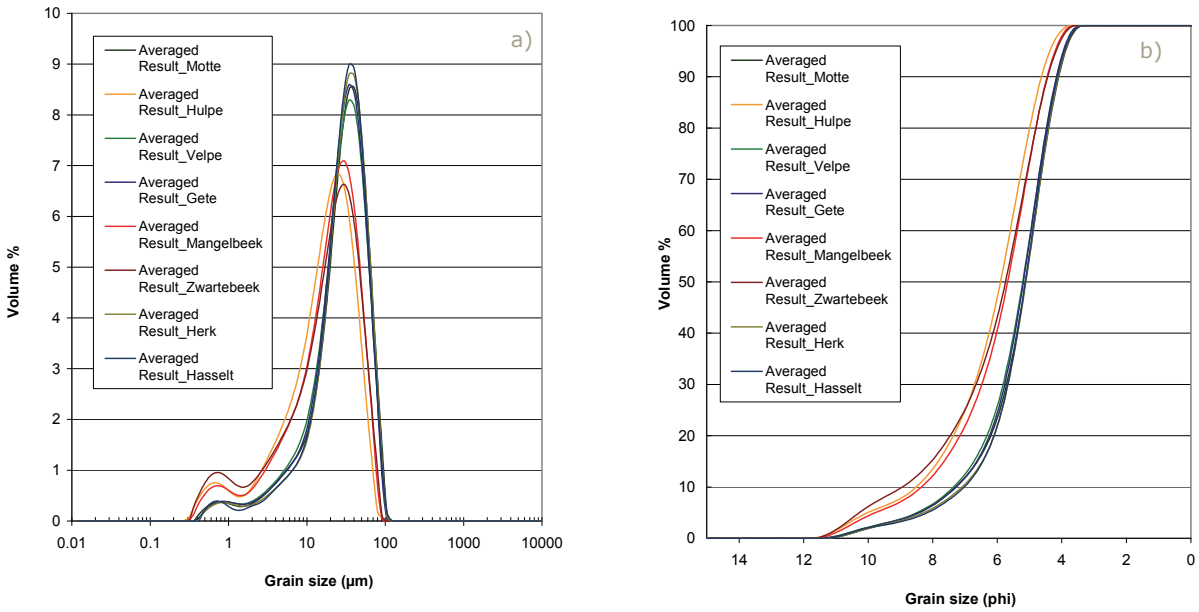

Figure 11.8: Grain size distributions (a) and cumulative distributions (b) for the <63µm sieved samples averaged per tributary

Table 11.2: Local modes for both peaks from the bimodal grain size distributions of the tributaries in the Demer basin, and their respective volume percentages.

	Peak 1 Mode (µm)	Peak 2 Mode (µm)	% Peak 1	% Peak 2
Motte	0.72	35.11	2.9	97.1
Hulpe	0.63	23.26	6.2	93.8
Velpe	0.80	33.59	2.8	97.2
Gete	0.80	33.34	2.7	97.3
Mangelbeek	0.68	27.24	5.6	94.4
Zwartebeek	0.68	27.50	7.9	92.1
Herk	0.79	34.53	2.9	97.1
Demer (upstream)	0.66	34.20	2.5	97.5

It is significant to note that the Hulpe presents quite a large variation of SSA-values, but given the known pollution in the river (both organic and inorganic) and the difficulty preparing the samples for analysis this is not unexpected.

Even though the SSA-values of the Aarschot outlet station all fall within the observed variability of the tributary SSA-values, four samples seem to be outliers and deserve some extra attention. All analyses data from Aarschot outlet samples is available in Addendum C (Table C9).

- Sample 13 is the first outlet sample collected at Aarschot, in this case by the VMM with their AS16-2Y-IJY Alfa Laval flow-through centrifuge. The sample was obtained after a long period of draught. The sample had an unusually high organic matter content (42%) which will have undoubtedly influenced the grain size distribution (the SSA values are quite low as can be seen in Figure 11.9), as well as the chemical composition of the sediment, as it might have scavenged some pollutants. This sample is removed from the data set and excluded from further analyses.
- Samples 21 and 22 were both collected by the Alpha Laval Emmie Centrifuge. The samples are seriously enriched in fine material, but do not exhibit the characteristics of the southern tributaries (nor based on grain size distribution, nor based on chemistry).
- Chemically, these two samples are often singled out from the other outlet samples and they do not resemble chemically the consequent samples. These samples are removed from the data set and excluded from further analyses.

- Sample 32 is a composite ISCO-sample and exhibits a coarser grain size distribution than the other Aarschot outlet samples, possibly due to error in sieving. Chemically, it does not resemble the preceding nor the consequent samples. These samples are removed from the data set and excluded from further analyses.

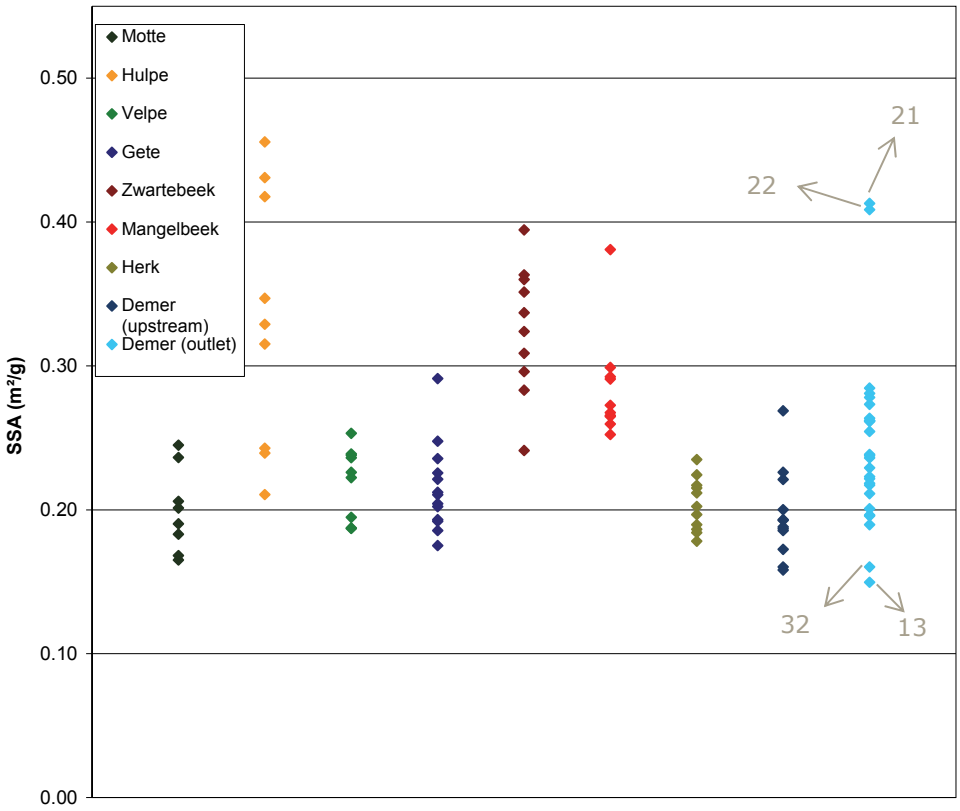

Figure 11.9: SSA-values (m²/g) as determined from outlet TIS-sampling in the tributaries and from Aarschot outlet sampling

For the remaining samples the hypothesis is formulated that the outlet samples consist of a mixture of well-mixed sediment derived from the tributaries, that underwent no further sorting downstream of its sampling location.

To confirm this hypothesis, a more detailed examination of the grain size data, using the cumulative grain size contributions is executed. In Figure 11.10 the cumulative distribution of the Aarschot samples is plotted alongside the two distribution curves which represent the envelope of all measured tributary samples. This figure shows that not all outlet samples fall within the boundaries set by the tributary source material even though their SSA-values predicted they would. This seems to indicate that a grain size correction might be necessary for some if not all the Aarschot outlet samples.

More closely examining which samples fall inside and outside the envelope, the first hypothesis is that the distinction is a result of the sampling device used. The first samples, obtained using the flow-through centrifuge, fall within the boundaries, the later samples, obtained through ISCO-sampling, do not. However, this does not seem to be the case, as the samples 23-26 still fall within the envelope boundaries and are taken with the ISCO-sampler.

Therefore, the reason for the abrupt coarsening should be found elsewhere, such as in the sudden introduction of a source, un-sampled during the 2007-2008 sampling campaign. The samples 27-38 are obtained during the extremely high sediment concentration peaks, sampled in the period

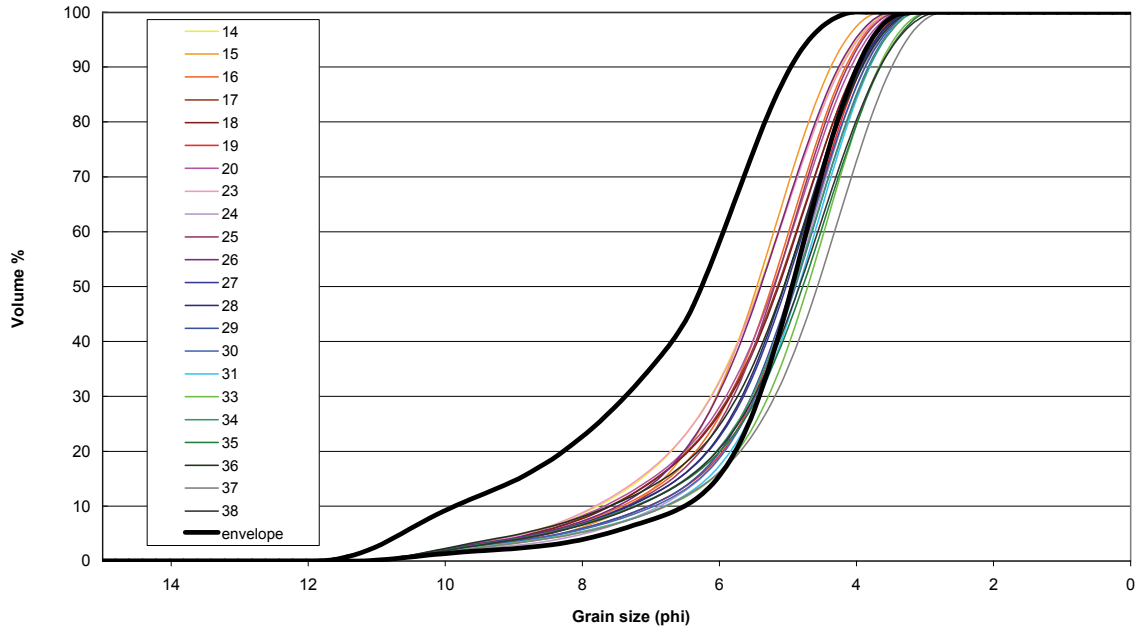

Figure 11.10: Cumulative grain size distributions for the <63µm sieved Aarschot outlet samples plotted against two distribution curves which represent the envelope of all measured TIS tributary samples

January-February 2009, during which river bank maintenance took place in the Demer basin, which proved to be very impactful to the sediment load transported throughout the river system, and whose effects were measurable down to Aarschot (as is mentioned in Chapter 7, Table 7.1).

If the introduction of a new source is the cause of the coarsening of the material sampled at the outlet, these coarser samples should be omitted from further analysis, and they should not influence the discussion whether or not grain size corrections are necessary in the spatial source fingerprinting exercise in the Demer basin.

However, samples 16-20, even though based on grain size fall within acceptable limits, they are also obtained during very impactful events (sample 16 occurs after breaking through of a dam just upstream of the sampling station while samples 17 through 20 take place after structural dike works), introducing once more uncertainties into the nature of the sediment being transported (and sampled) at the time.

To conclude, samples 14 and 15 can be used in sediment fingerprint modelling, preferably without a grain size correction factor, as the mixing of the two types of tributaries (northern and southern) can fully explain the observed grain size distribution in the remaining samples.

11.1.3 Settling tests

The observations in the previous sections show that both in the source type fingerprinting research (in the Mangelbeek catchment), as well as in the spatial sources fingerprinting research executed in the Demer basin, sources of fine sediment mix with more coarse sediment sources. This results in a blended-grain size distribution (and associated geochemistry) at the outlet. Therefore, a simple grain size correction using the SSA-values of both outlet and source sample (such as expressed in Equation 10.7) cannot be applied to correct the geochemical fingerprint.

The only way to obtain a grain size correction that can be applied, is by analysing the geochemistry of different grain size fractions of a bulk sample separately, hence establishing a grain size-property composition relation for each source individually. In other words, if for each source a specific SSA-property concentration relationship can be established, than this relationship can be used to correct the property concentration found in the source samples to comply with the SSA-values obtained in the outlet samples.

One way to obtain different grain size classes of the source samples is to execute natural water settling tests. Therefore, material was collected at the Lummen (Mangelbeek), Halen (Gete) and Aarschot (Demer) outlet stations and settling tests were executed with these samples (the set-up of these tests is addressed in Section 3.2.3 and is described in detail in Cant (2010)).

The purpose of these tests was to establish the relationships between SSA and property concentrations for the Mangelbeek and Gete samples and to consequently use the obtained grain size corrections also for the other, respectively northern and southern tributaries.

Such a fractionation procedure has already been suggested within the framework of sediment fingerprinting, by Small et al. (2005) who used this approach in their FR2K model to obtain a SSA-based grain size enrichment function. This function was created by analysing size-separated subsamples (obtained through settling), and producing functional relationships between the property concentrations and the corresponding SSA-values of the fractionated subsamples. Small et al. (2005) repeated this exercise for every source and for the outlet in their study area. They also made these functional relationships dimensionless by dividing the size-separated property concentrations and SSA-values by the corresponding bulk values.

The functional relationships presented by Small et al. (2005) took the shape of linear or power relationships between the property concentration and SSA and these relationships had positive slopes. To rephrase, their observations confirmed the well-established (inverse) relationship between particle size and element concentrations in soils and sediments as reported in the literature (He & Owens, 1995; He & Walling, 1996; Horowitz, 1991; Horowitz & Elrick, 1987; Thorne & Nickless, 1981). Additionally, Small et al. (2005) tested the impact of their grain size correction using artificially created soil mixtures and found that the model using no grain size corrections fails to apportion the source group contributions with any degree of accuracy (standard deviations ranging from 4-47%, uncertainty envelope ranging from 40 to 90%), while the model using their suggested grain size correction (based on the functional relationships) had less than 3% standard deviations and an uncertainty envelope of 20-35%. As their uncorrected model performs as poor as the results observed in the Demer basin, this suggests that applying an appropriate correction factor might alleviate some of the variance observed in the Demer basin.

However, when investigating the results from the settling tests executed on suspended sediment collected at Lummen (Mangelbeek), Halen (Gete) and Aarschot (Demer), it is clear that they did not deliver the expected fractionation into different grain size classes, due to the flocculation (as reported in Section 9.1.3).

This results in similarly disappointing functional relationships (between SSA-values and the ratio of property subsample concentrations versus average property concentrations). The Mangelbeek settled subsamples all have very similar SSA-values, which lead to very poor functional relationships (as can be seen in Figures 11.11 and 11.12).

The Demer on the other hand does have a wide range of SSA-values in its settled subsamples, however, they have all very similar concentration values (as can also be observed in Figures 11.11 and 11.12).

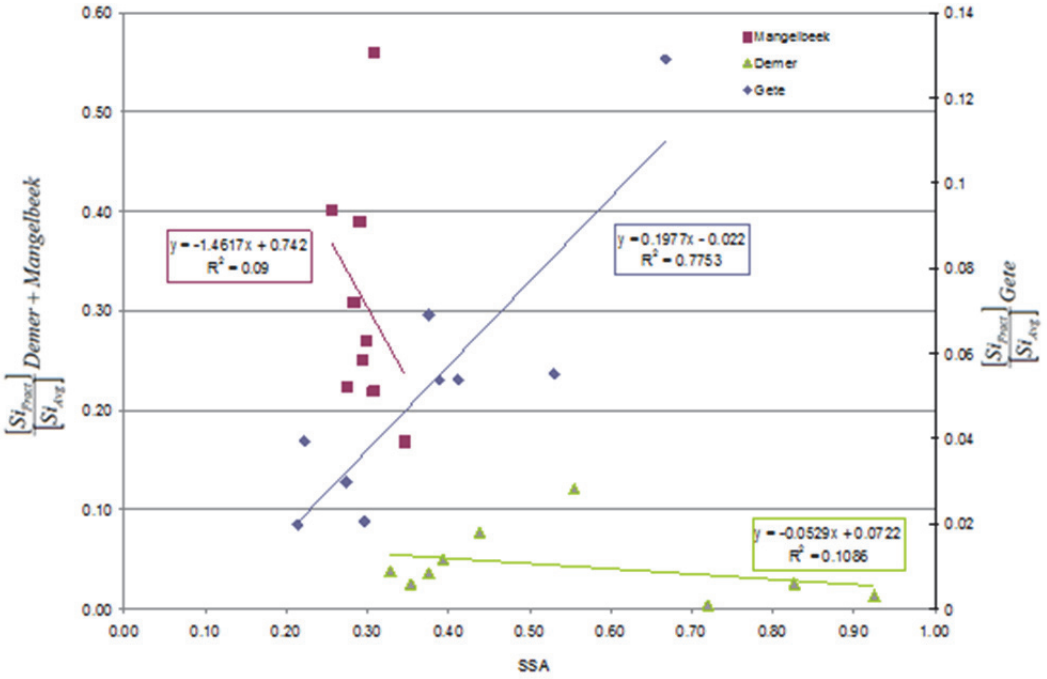

Figure 11.11: Functional relationships for Si for Mangelbeek, Demer and Gete catchments

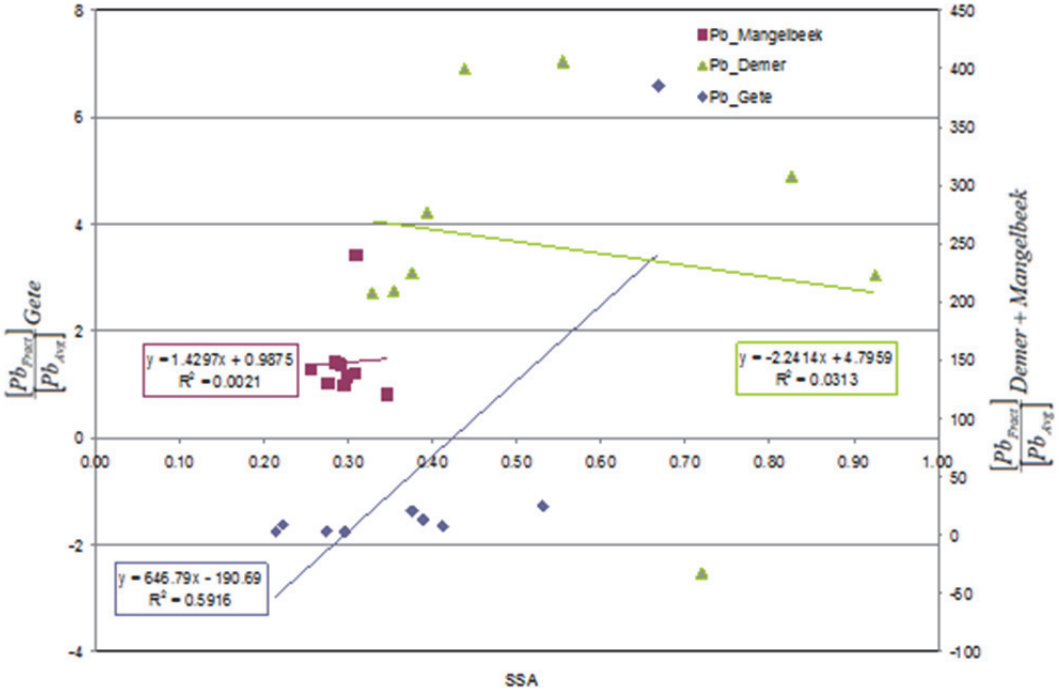

Figure 11.12: Functional relationships for Pb for Mangelbeek, Demer and Gete catchments

Finally, the Gete does show a (positive) linear correlation between the SSA-values and the concentration, but only for the properties associated with detrital erosion (Si, Al, K, Ti) as illustrated in Figure 11.11, which shows the functional relationships for the property Si, for all three rivers tested. For the other properties, the relationship is very scattered. Figure 11.12 shows an example, using the property Pb.

Small et al. (2005) suggested to refrain from using properties that show high degree of scatter and/or unexplainable grain size dependency in the composite fingerprint, therefore, none of these properties seem to be of use within the fingerprinting research within the Demer basin. The fact that the Gete seems to (at least concerning the properties associated with the detrital sediment) follow the conventional rules, is most likely due to the fact this tributary has no authigenic sediment present, reducing the flocculation in the settling column. The assumption that the simple grain size correction factor (as expressed in Equation 10.7) could be used to correct for sorting within the Gete basin seems correct. However, the concentrations of other properties (not associated with detrital sediment sources) show a much more scattered distribution when plotted as function of SSA, leading to the conclusion that the sorting of these elements cannot be readily described by a simple sorting algorithm.

To conclude, it should be mentioned that even though for the Gete and the Demer distinctly different SSA-values were observed in the subsamples obtained through the settling tests, these values do not systematically increase from subsample 1 to subsample 9, as is to be expected from the settling test. This shows once more that the impact of the flocculation is significant with the sediments in the Demer basin, and should also lead to caution when trying to use the obtained relationships to create grain size correction factors from them.

Ideally, another fractionation exercise should be attempted, to effectively separate the different fractions, allowing for the determination of functional relationships between grain size and property concentrations.

For now it can only be concluded that, due to the active flocculation processes, it is very difficult to fractionate samples obtained from tributaries in the Demer basin, and therefore the more complex grain size corrections could not be executed. It is, however, clear that the sediment transport within the Demer basin is a complex process which cannot be reduced to an enrichment or a depletion of fine particles, and therefore also not as an enrichment or depletion of property concentrations.

11.1.4 Conclusions

- When the grain size of the contributing sources significantly differ from one another, the grain size distribution observed in the outlet samples can most likely be attributed to both sorting effects and mixing effects. In that case, simple grain size corrections as suggested by Walling & Collins (2000) should not be executed, as they will not yield correct results.
- In the case that authigenic sediment is present in a catchment, it is assumed that no sorting of this material will take place, as the sediment is created in the river itself and is constructed from highly flocculated material, which will, when submitted to ultrasone dispersion, decompose to its primary (very fine) particles. Therefore, no grain size correction needs to be applied to this source. The other sediment sources (the on-land sources) present in the catchment, however, will be subjected to sorting and need to be grain size corrected.
- As the presence of the authigenic sediment masks the sorting that took place in the distributions of the on-land sources, the grain size corrections for these sources need to be estimated, using correction factors based on similar catchments, devoid of authigenic sediment.

- Comparing SSA-values of sources and outlets as a means of detecting if grain size corrections are necessary is not sufficient. It can create false negatives (as was the case for the Aarschot outlet samples obtained in the period January-February 2009). Therefore, it is useful to investigate the entire grain size distribution, by checking if the outlet observations fall within the envelope of the sources observations when plotted on a cumulative distribution graph.
- Cumulative grain size distribution can help detect if grain size corrections are necessary and can help assess whether a significantly contributing source is left un-sampled.
- Settling tests with material from the Demer, Gete and Mangelbeek rivers revealed the materials to be very difficult to fractionate, suggesting that if sorting takes place in these river systems, the process cannot be simplified to an enrichment or a depletion of fine particles, and therefore the simple GS correction factor (as stated in Equation 10.7) should not be used in this river system.
- The outlet samples from November 2007 onwards (sample numbers 17-38) exhibit a different grain size distribution than the samples obtained before. This is due to the introduction of another (un-sampled) sediment source, originating from human interference. The ramifications of this will be addressed further in Section 11.3.

11.2 Organic matter correction factors

11.2.1 Use of organic matter correction factors in the literature

As already mentioned in Section 10.4.2.3, the amount of organic matter present can influence element concentrations (Hirner et al., 1990). Therefore, the use of an organic matter correction factor might be necessary to compare source material samples with the outlet samples. Walling & Collins (2000), however, remarked that entering the OM_s in the objective function does not always benefit its apportioning power, as the relationship between organic matter content and element concentration is complex, and may result in an overcorrection of the property concentrations of the coarser material when it is used in combination with the particle size correction.

Many of the authors publishing their sediment fingerprinting results have followed their example and have omitted organic matter correction factors from their sediment fingerprint models (Collins et al., 1997 a; Walling et al., 1999; Russel et al., 2001; Minella et al., 2008 b; Juracek & Ziegler, 2009).

However, in some publications (Walling, 2000; Collins et al., 1996, 1997 b, 1997 c, 1998, 2001) organic matter correction factors have been entered, though only after careful investigation to avoid overcorrection. In these publications, the use of both correction factors seemed to assist in the comparison of the fingerprint property concentrations measured in both source and outlet samples.

The OM correction factors used can vary significantly. Collins et al. (1997 b) applied source type fingerprinting in the Dart and Plynlimon catchments and the Exe and Severn basins. They applied correction factors which ranged from 0.43 and 5.17. Collins et al. (1997, 1998) investigated respectively the source type and spatial source contributions in the Exe and Severn basins. For the source types the OM correction factors ranged from 0.77 and 1.98, while for the spatial sources the OM correction factors ranged from 0.47 to 1.47. The OM correction factors determined for the spatial source fingerprinting in the Demer basin (as reported in Table 10.9) ranged from 0.16 to 4.87.

It should also be mentioned that some authors (Nosrati et al., 2011; Navratil et al., 2012 and others) do not mention which correction factors they used within their sediment fingerprinting approach.

Nonetheless, the question remains whether organic matter corrections need to be applied within the Demer basin. As already established in Section 11.1, grain size correction factors should not always be applied, and so the question remains: if grain size correction factors are to be omitted, should organic matter correction factors be rejected as well, or should they be allowed to alter the objective function instead of the grain size correction factors?

11.2.2 Observed LOI in sediment in the Demer basin

LOI is somewhat more straightforward to discuss than grain size, as LOI is reported as a parameter, and not as a distribution. Therefore, in a sense, organic matter is 'just another property', that could just as well be entered into the KW-test, to test its predictive power, were it not for its potential to be used as a correction factor. However, the interactions between organic matter and the different geochemical properties, can be quite complex.

As was done for the grain size data obtained in the Demer basin, the results concerning LOI for the source type sampling data as well as the spatial sources, are discussed below.

11.2.2.1 Source type sampling in the Gete and Mangelbeek catchments

Figure 11.13 shows the results of the observed LOI in all on-land sources as well as in the riverbed and TIS outlet samples collected in the Gete catchment. In this figure it can clearly be seen that the cultivated land has organic matter contents ranging from 3 to 7%, while the pastures (excluding one outlier), the channel banks and even the riverbed material have organic matter contents in the range of 3-11%. The outlet samples have a slightly more elevated LOI, ranging from 5 to 12%. This translates into average correction factors as presented in Table 11.3, which do not closely resemble the earlier obtained grain size correction factors. This seems to indicate the relationship between grain size and organic matter content in the Gete catchment is quite complex.

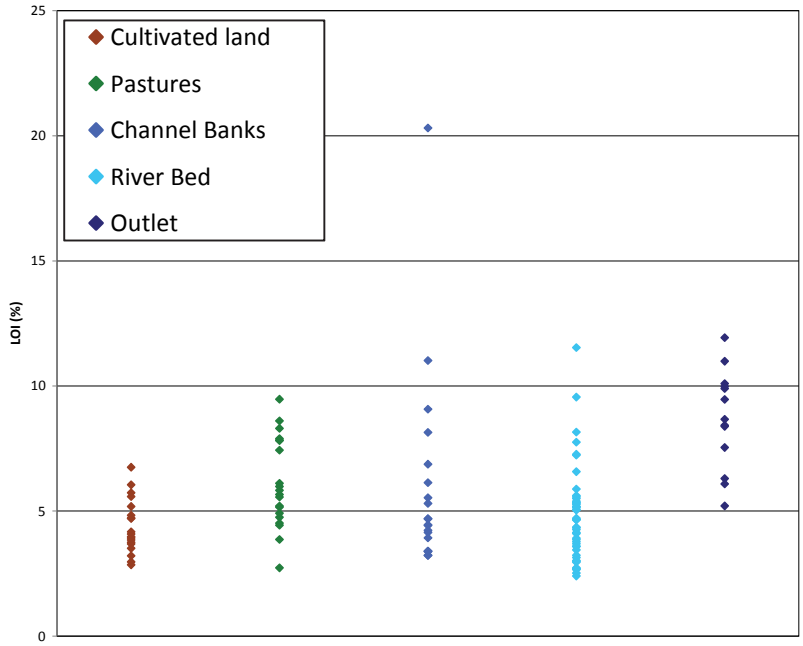

Figure 11.13: LOI (%) as determined for sediment samples obtained from cultivated land, pastures, channel banks, riverbed and from outlet TIS-sampling in the Gete catchment

Table 11.3: LOI (%) averaged per sample type and the corresponding organic matter correction factors calculated for the 'average' outlet sample for both Gete and Mangelbeek catchments.

	Gete		Mangelbeek	
	LOI_avg	OM correction factor	LOI_avg	OM correction factor
Cultivated land	4.40	1.98	24.43	1.28
Pastures	6.10	1.42	27.50	1.14
Channel banks	5.72	1.52	24.83	1.26
Authigenic sediment	/	/	31.45	1.00
Riverbed	4.77	1.82	21.38	1.47
Outlet	8.69	/	31.35	/

Figure 11.14 shows the results of the observed LOI in all on-land sources as well as in the riverbed and TIS outlet samples collected in the Mangelbeek catchment. This shows a somewhat different image. First of all, the observed LOI's are much higher than those observed in the Gete catchment (ranging from 12-37%), although once again the cultivated lands have slightly lower LOI values (14-31%). Secondly, the riverbed samples are much more depleted of organic matter (ranging from 16% (with a possible outlier dipping down to 10%) to 28%). The authigenic sediments are very rich in organic matter and report LOI's ranging from 28 to 35%. The observed Mangelbeek outlet samples fall, just like they did in the grain size, almost entirely within the range observed in the source material.

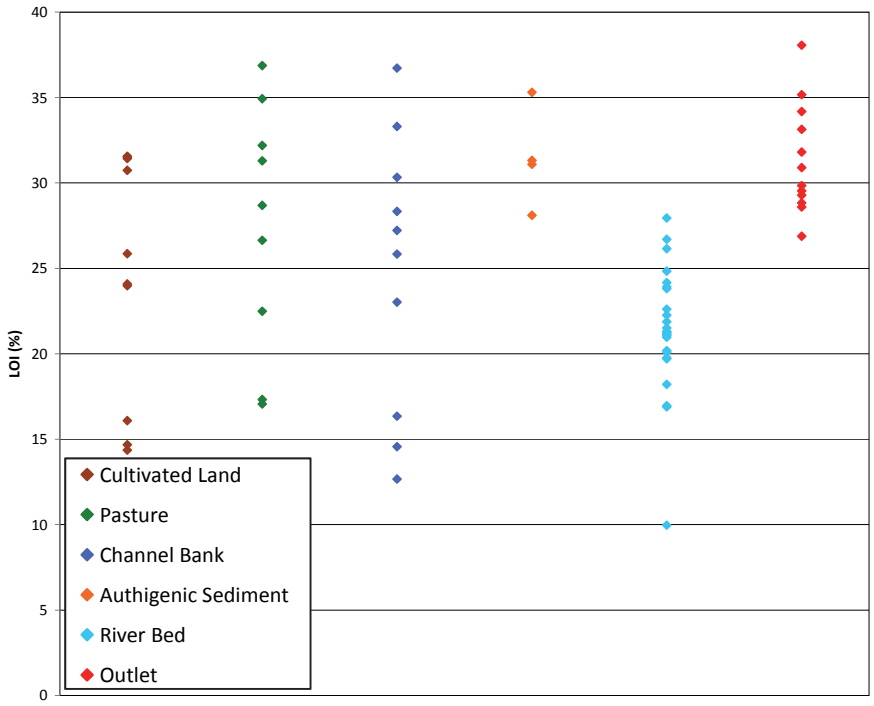

Figure 11.14: LOI (%) as determined for sediment samples obtained from cultivated land, pastures, channel banks, authigenic sediment, riverbed and from outlet TIS-sampling in the Mangelbeek catchment

When these data are transformed into average OM correction factors, as presented in Table 11.3, the values resemble the adjusted grain size correction factors, which were presented in Table 11.1, fairly well. The organic matter correction did not require the authigenic sediment to be corrected. The cultivated land, pastures and channel banks required OM correction factors around 1.14 to 1.28. For comparative measures: the adjusted grain size correction factors had values around 1.35.

This seems to indicate that organic matter content is a better correction factor than the unadjusted grain size to use in catchments where authigenic sediment is present.

11.2.2.2 Spatial provenance type sampling in the Demer basin

The modelling results, as presented in Chapter 10, showed that on average OM corrected models tended to lower the overpredicted Velpe contributions in favour of other models, suggesting the OM corrections might actually aid the performance of the model. However, the decreasing of the Velpe contribution can just as well be a by-product of the failing discriminative power of the composite fingerprint, and therefore may not prove the usefulness of the OM correction factor in spatial source modelling in the Demer basin.

When investigating the spatial provenance data, the LOI-values effectively allow the discrimination between the northern and southern tributaries (see Figure 11.15). The northern tributaries (Hulpe, Zwartebeek and Mangelbeek), all have high LOI-values (ranging from 25 to 42%) while the southern tributaries (Velpe, Gete and Herk) have much lower LOI-levels (5-13%). Interestingly enough, the two more centrally located tributaries (the upstream Demer and Motte catchments), have a mixed signal (the Motte ranging from 18 to 23% and the Demer upstream from 15 to 33%). When looking at grain size only, these tributaries resembled the southern tributaries much more.

Finally, the organic matter data seems to confirm the hypothesis that samples 14-26 could be created by a mixture of the spatial sources, without these sources undergoing some kind of sorting.

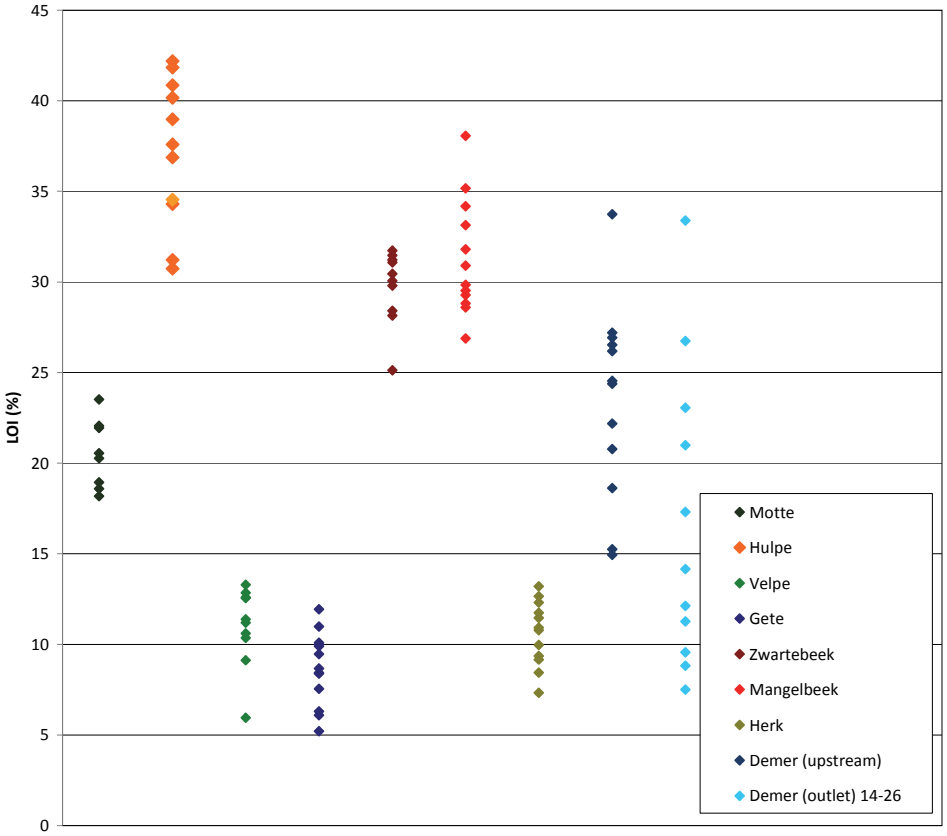

Figure 11.15: LOI (%) as determined from outlet TIS-sampling in the tributaries and from the Aarschot outlet sampling

11.2.3 Conclusions

Organic matter is a very complex correction factor and its signal can get lost during transport, as it seems to be the case in the Gete catchment. However, in the Mangelbeek catchment, organic matter was capable of approximating the adjusted grain size correction factor. Therefore, it could be a good replacement for grain size corrections, where these are complicated through the mixing of upstream sources (which underwent sorting while moving downstream) and very fine authigenic sediment (that did not undergo sorting). However, whether this can be applied to other catchments containing authigenic sediment still needs to be investigated.

Even though, initial observations in the spatial source fingerprinting results seemed to suggest that OM correction might help in the performance of the model, the organic matter data seems to confirm the hypothesis that no correction factors need to be applied when fingerprinting the spatial sources in the Demer basin, as the mixing of the two types of tributaries (northern and southern) can also fully explain the observed LOI-values in the outlet samples under investigation (samples 14-26).

11.3 Human impact on source apportionment

Human impact can have a positive or negative impact on the potential to discriminate between and apportion the contributions of different sediment sources, using the sediment fingerprinting approach. In case of the Demer basin, human interventions yielded both sorts of effects and both are discussed below.

11.3.1 Positive effects of human impact on sediment source apportionment

In the Demer basin, the southern tributaries are very similar to one another, given their similar geological substrates and soil use. Similar reservations can be made about the northern tributaries. However, as addressed in Section 4.3.2.2 the Demer basin is highly subjected to anthropogenic discharges, which could potentially help to discriminate between the different tributaries. However, some of these pollutants are also naturally present in the soil and will enter the river system through physical erosion processes as addressed in Section 4.3.2.1 therefore masking the effects of anthropogenic input. VMM investigated the origins of the top 10 emission properties in all river basins in Flanders (Syncera Water, 2005) and the results for the Demer basin of the relevant properties are presented in Table 11.4. From these results it can clearly be seen that Zn, Ni and Cr are mostly introduced into the basin through sewage treatment discharges, while Pb is dominated by soil erosion.

To investigate if the anthropogenic input indeed helps to discriminate between the sources, the chemical data obtained from the sediment fingerprinting research is compared to the data tabulated in Table 4.5, which summarized the concentrations and loads per tributary introduced into the river system through industrial and sewage treatment discharges.

Cr, Ni and Zn are properties that should show up in tributaries that reported high industrial and sewage treatment discharges in Table 4.5. And indeed, the TIS samples obtained in Hasselt show levels of Ni and Cr that are higher than those of the other tributaries (see Figures 11.16a and b). However, for the element Ni, the Gete also received substantial discharges and no elevated levels of Ni are reported in the TIS samples. Similarly, the elevated concentrations of anthropogenic discharges of Cr reported for the Velpe, do not seem to translate into elevated Cr levels in the TIS samples of that tributary. For Zn however, almost all tributaries received significant contributions,

Table 11.4: Contributions of specific sources to the emission of selected properties in the Demer basin; data from Syncera Water, 2005

Cu	kg/year	%
total	3706	100
wood treatment products	1078	29
soil erosion	684	18
sewage treatment discharges	620	17
households	423	11
corrosion of cu surfaces	226	6

Cr	kg/year	%
total	6423	100
sewage treatment discharges	4616	72
soil erosion	1490	23
households	99	2
chemical industry	96	1
metallurgy	53	1

Zn	kg/year	%
total	15476	100
sewage treatment discharges	4384	28
corrosion of Zn surfaces	2622	17
tire wearing	2519	16
soil erosion	2496	16
households	900	6

Pb	kg/year	%
total	2652	100
soil erosion	1611	61
sewage treatment discharges	522	20
households	181	7

Ni	kg/year	%
total	1650	100
sewage treatment discharges	641	39
soil erosion	362	22
metallurgy	124	8

but the Mangelbeek and Velpe, though receiving similar elevated levels, do not respond in the same fashion. The Mangelbeek TIS samples show a much higher concentration compared to the Velpe's (see Figure 11.16c).

On the other hand, some properties are so abundantly present in the sediment arriving via soil erosion (or through authigenic precipitation in the case of Fe) that no amount of anthropogenic input can disrupt the geochemical signal. Examples of this are Al and Ti of which the southern tributaries contain high levels due to the soil erosion of the loam material present in those catchments, while the northern tributaries lack this sediment input. The anthropogenic input of Al and Ti in the Hulpe cannot be distinguished (as can be seen in Figures 11.16 d and e), nor can the anthropogenic input of Fe in the Hulpe, as it is completely overshadowed by the natural (authigenic) presence of Fe in the northern system (Figure 11.16f).

In some cases, the anthropogenic input can be observed in properties that tend to be geologically oriented. Pb, for instance is mostly associated with the northern tributaries, and therefore the anthropogenic contributions in the Hulpe and Mangelbeek cannot be distinguished as such, however the anthropogenic input through the sewage treatment facilities upstream Hasselt do create a detectable increase in the Pb concentrations observed in the Hasselt TIS samples (Figure 11.16g).

A similar trend, though less pronounced, can be observed for Ba in Figure 11.16h, where the southern tributaries have naturally high levels (due to soil erosion) but the anthropogenic input into the Hulpe, results in a higher value of Ba observed in there than in the TIS samples of the other northern tributaries.

In some cases the anthropogenic input could not be directly linked to the observed property concentrations. The anthropogenic input from V in the Hulpe could not be readily observed (Figure 11.16i), nor could the input of Cu in the Hulpe and Velpe or the input of Mn in the Hulpe and Gete be discriminated (respectively Figures 11.16j and k).

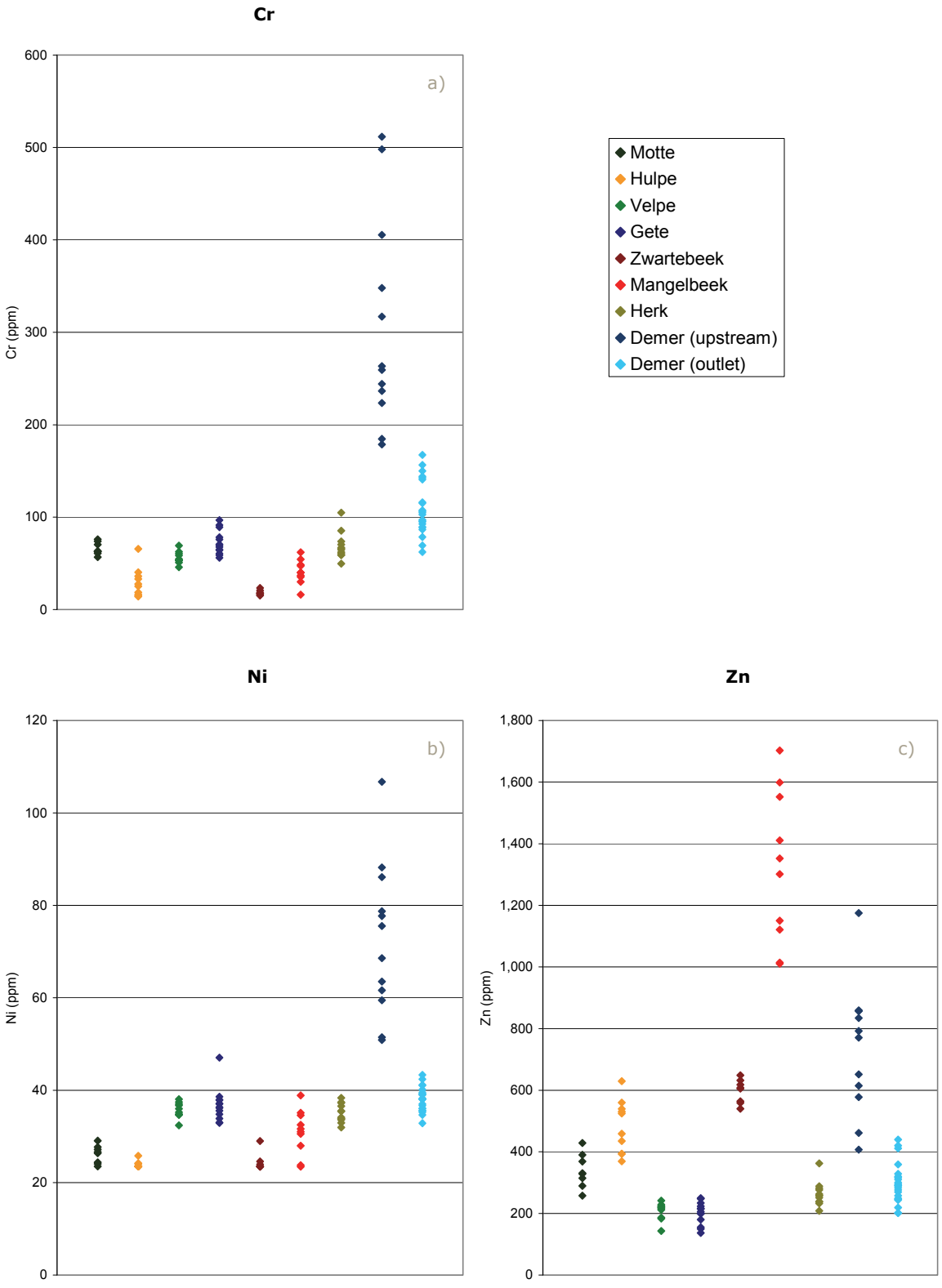

Figure 11.16: Property concentrations as determined from outlet TIS-sampling in the tributaries and from Aarschot outlet sampling

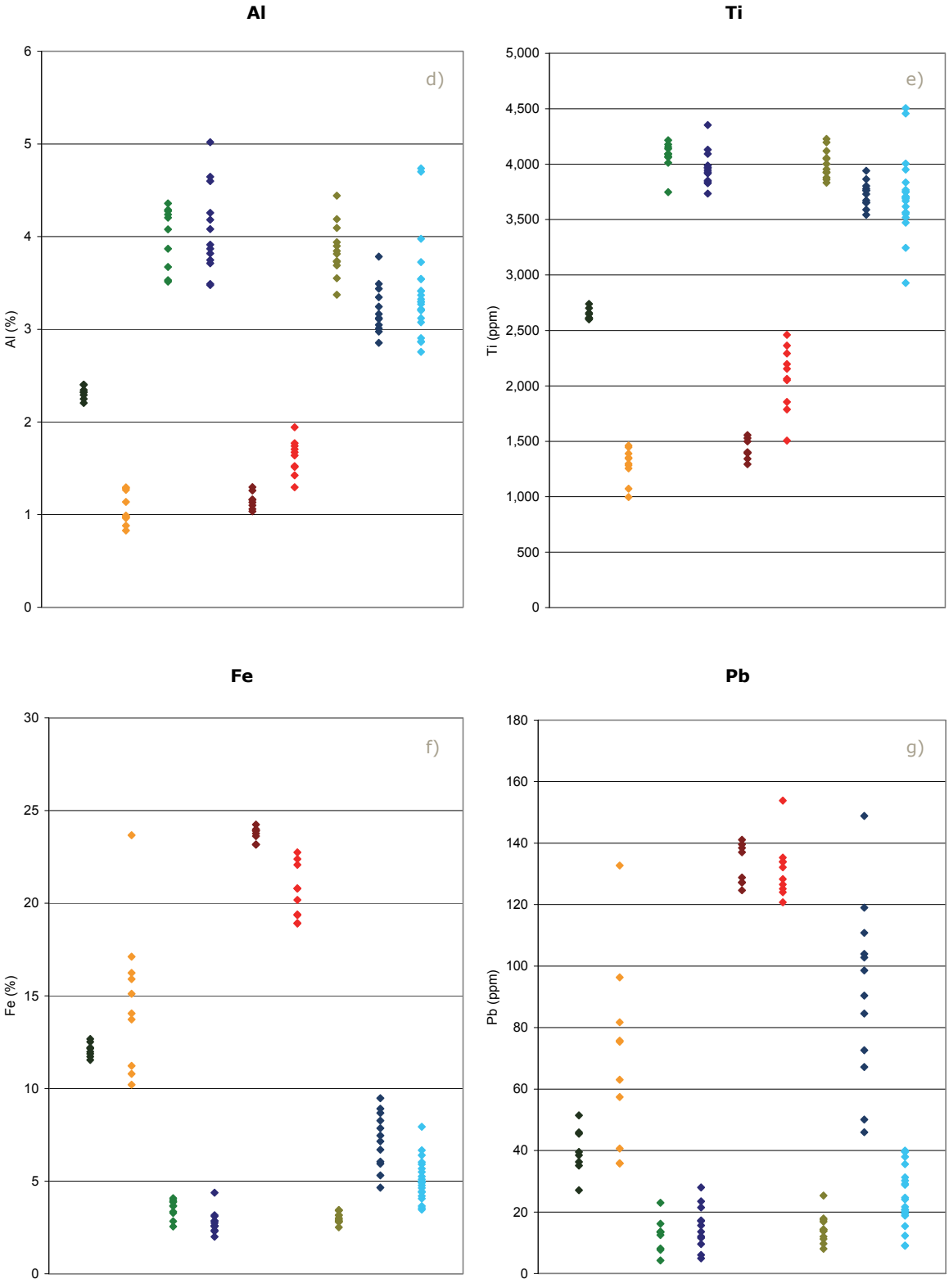

Figure 11.16 (continued): Property concentrations as determined from outlet TIS-sampling in the tributaries and from Aarschot outlet sampling

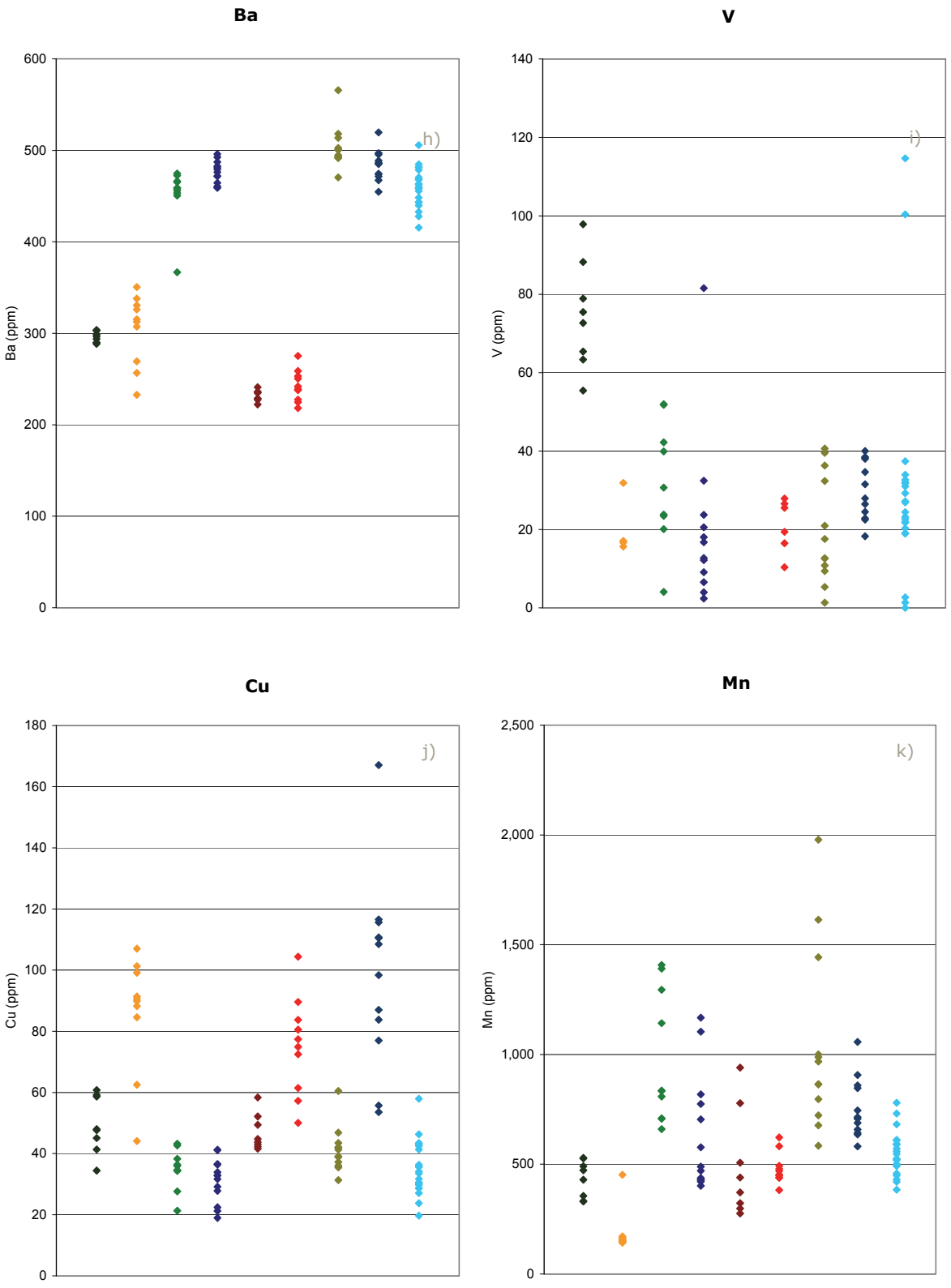

Figure 11.16 (continued): Property concentrations as determined from outlet TIS-sampling in the tributaries and from Aarschot outlet sampling

However, not all of these properties were allowed into the final fingerprints, as some did not pass the violation testing (as described in Section 10.4.1.1). The lower boundaries were often breached for tributaries with low concentrations for a specific property, leading to a negative value when the standard deviation was subtracted from the average observation (see Equation 10.2).

Nonetheless, it can be concluded that the anthropogenic input positively influenced the discriminatory power of the different sediment fingerprints, as most of the properties with a distinguishable anthropogenic signature made it into the final composite fingerprints, allowing their cumulative discriminative power to rise up to 100%.

11.3.2 Negative effects of human impact on sediment source apportionment

Human impact can also hinder the discrimination between sources. It is self-evident that when anthropogenic sources are left un-sampled, they will lead to erroneous modelling results, if those models are composed of properties that are (abundantly) present in those un-sampled sources.

In the case of industrial and sewage treatment facility discharges, this effect will take place when trying to fingerprint on a source type level. Source type fingerprinting exercises, usually include the sampling of topsoil material, as well as sub-surface material, where it is likely this will contribute to the sediment load of the river (such as in gullies or along river banks). However, it can be challenging to retrieve a time-integrated sample of the industrial and/or sewage treatment discharges, and their composition can be subjected to a significant compositional variability, all rendering the fingerprinting exercise more difficult.

If source type fingerprinting is to be executed for the Mangelbeek and Gete catchments, the respective elements that were reported to be introduced into the river system through sewage treatment and industrial discharges (see Table 4.5) should be avoided as fingerprint properties in the composite fingerprint.

The anthropogenic impact can also have a detrimental effect on spatial source apportionment. This became apparent in the Demer basin, when during the sampling period of the sediment fingerprinting research, river maintenance and other public works were executed in the Demer. Some of these works had a significant impact on the sediment load transported to the Aarschot sampling location, whether because they took place relatively closely upstream of the sampling location (the damming of a branch of the river to facilitate the restoration of the mill, the consequent deconstruction of the dam), or because the works themselves introduced large quantities of sediment into the river (river bank maintenance).

These sediment sources are ‘unique’ to the Demer itself, and could therefore not have been registered in the TIS samples obtained in the tributaries. They are in effect ‘un-sampled’ sediment sources, and when a mixing model tries to minimize the objective function, it will fail to do so, as it does not have all the explanatory variables.

These human interventions in the river system, can therefore explain the failure of Composite Fingerprints A through E to produce modelling results with acceptably low standard deviations and realistic contributions of the different tributaries for samples taken after November 2007 (samples 16-38).

The fact that so many of the outlet samples were obtained after November 2007 can also be indirectly traced back to these impactful maintenance works. As explained in Section 2.2.2.1 no TIS could be installed at the Aarschot sampling station and the infrequent sampling with a flow-

through centrifuge proved to be time-consuming, resulting in only a snapshot of the contributions of different tributaries. To create a more time-integrated sample, consecutively sampled ISCO-samples were merged into composite samples. However, these ISCO-samples are usually only 1 litre volume or less, and during normal flow conditions do not contain high concentrations. The amount of samples that would need to be freeze dried (to determine their concentration) and consequently merged would create too much work.

Therefore, ISCO-samples would be compiled during moments of increased transport (during high-flow events) when the sediment concentrations are higher, and less samples needed to be freeze dried and merged. In practice, when a high-flow event was predicted, the sampler would be programmed to sample every hour (instead of every seven hours) and the samples would be collected daily, allowing more material to be collected.

During the high-flow events from November 2007 onwards extremely high quantities of sediment were obtained through the ISCO-samples, which allowed more samples to be prepared for analysis. Sadly enough, these extremely high sediment concentrations originated from partly un-sampled sediment source, introduced into the system by human intervention.

To obtain an overview of all works that took place in the Demer basin prior to and during the monitoring period the river basin managers, responsible for the different sections of the rivers within the Demer basin were contacted. However, this only yielded limited information. The overview of works as presented in Table 7.1 are the most detailed overview that could be obtained. Nonetheless, maintenance works were also executed in some of the tributaries. In the Mangelbeek for instance, elevated sediment concentrations measured in beginning 2009 could be attributed to dredging activities, but no exact dates of dredging could be obtained from the river manager. Other elevated sediment concentrations observed in the Mangelbeek in 2008 and 2009 are most likely to be linked to the construction of the cloverleaf interchange at Lummen.

For other tributaries where incidental higher sediment concentrations were observed (such as in the Gete in October 2010) no river management activities could be obtained.

This indicates that it is difficult to be informed about river basin activities in a highly active managed region such as Flanders, which might render it very difficult to successfully fingerprint basin-sized study areas. Smaller catchments, where river management activities can be more readily monitored might be more successful.

11.3.3 Conclusions about the impact of human interventions on sediment fingerprinting

Anthropogenic input can be both beneficial and detrimental to spatial source fingerprinting. When information about the impactful input is available, sampling strategies can be adjusted to facilitate covering all potential sources. Having data available on the industrial or sewage treatment discharges can help decide which properties to include or exclude from further use in fingerprints.

For instance, the Mangelbeek and Gete catchments could be source type fingerprinted, but the apportionment would prove difficult if this fingerprint included properties such as Zn or Ni, of which is known they are (at least partly) derived from anthropogenic (and therefore un-sampled) sources. On the other hand, including anthropogenic contaminants in spatial source fingerprinting can help increase the predictive power of the composite fingerprint to differentiate between geologically similar sources.

If information is available beforehand on river basin management or public works, which might be potentially hindering to spatial source apportionment, they might be sampled before or during the execution of the works, in order to identify the impact of those works.

However, in a region such as Flanders, this proves to be difficult, as the river basin management is scattered among different administrative services and communication on all levels with the managers proves challenging. Additionally, other types of works (such as road works) can be of influence and information about this might not be readily available.

From a modelling stand point, these influential river management and public works have a hindering effect on the apportionment power of the spatial sources sediment fingerprinting models, if they take place in the main river (as opposed to in a tributary, where the input would be included in the material sampled by the TIS).

Moreover, this hindering effect will remain in play for as long as the sediment has not been transported past the outlet sampling station. The timing of this depends on the residence time of the sediment in the main river channel, which has not been determined for the Demer in the framework of this PhD.

11.4 Overall conclusions

Observations in the grain size distributions of the collected sediment samples (both on-land as well as in the river) clearly show the necessity of grain size corrections, more complex than the ones currently in use in most of the international fingerprinting research.

The fact that in the Demer basin (both for source type fingerprinting as well as for spatial provenance fingerprinting) the sources consist of well-sorted sediment, of which some are particularly finer than others leading to a mixed grain size signal in the outlet samples, makes it impossible to estimate the amount of sorting that might have happened to the initial source material while moving downstream. Therefore, more source-specific grain size corrections need to be applied.

To determine these, it is necessary to obtain insight into the chemical composition of grain size-fractionated sediment samples rather than analysing geochemistry of bulk samples.

However, obtaining these fractionated subsamples has proven to be difficult in the Demer basin, as settling tests have failed to procure subsamples separated by grain size, due to flocculation of the fluvial sediment.

Organic matter correction factors are also very complex, as the signal can be obscured during transport. However, in the Mangelbeek catchment, the results are promising; organic matter was capable of approximating the adjusted grain size correction factor and might therefore be used instead of a grain size correction. Whether this can be applied to other catchments containing authigenic sediment still needs to be investigated.

Human impact can both help and hinder the discrimination and apportionment of sediment sources. Specific elements antropogenically introduced in the river system can help to differentiate between geologically similar spatial sources. For instance Zn helps to differentiate the Mangelbeek from the other northern tributaries. However, this same element can also hinder the source type fingerprinting within this Mangelbeek catchment and should therefore be discarded in this type of fingerprinting research.

As it is not always well-documented which elements enter the river systems via sewage treatment or industrial discharge, or via diffuse sources, this can remain a source of error in the apportionment exercise.

Additionally, humans impact the sediment transport in the river system through maintenance works, and in the Demer basin, these sorts of interventions happened fairly frequent and had sometimes a significant impact on the total suspended sediment flux transported.

These maintenance works could potentially explain the high variability in modelling results as observed in the fingerprint modelling described in Chapter 10. These works, however, do not explain the failure of Composite Fingerprints A through G to correctly attribute the sediment load of Aarschot to the different tributaries for samples 14 and 15, even though all statistical constraints were met. These fingerprints were created according to established methodologies and had extremely high discriminative powers (98.8 up to 100%), and should therefore result in realistic results, with acceptable standard deviations, similar to what has been reported in the literature. Navratil et al. (2012) for instance reported very stable outputs of their mixing model, systematically within a range of +/- 3% to their mean value. The fact that the models in Chapter 10 continue to report unrealistic contributions and average standard deviations around 20%, indicates that there must be something else subverting the apportionment exercise. There are several possible causes:

1) The discriminative power of the composite fingerprints is being overestimated by the statistical testing, and greater variability is present within the tributaries, causing the signal to be lost;
2) Within the Monte Carlo framework, the probablility density functions of random deviates for the mean concentration of fingerprint properties of the different sources were generated using classic statistics (mean and standard deviation). Outliers in the datasets, could have skewed the pdfs created;
3) The conventional random sampling of deviates of fingerprint properties from the pdfs can have an influence on the outcome of the mass balance modelling.
4) The search tool used to find an optimum in the objective function in this thesis was a local search tool. Such search tools, however, can struggle with identifying globally representative solutions, especially if the objective function is characterised by localised extremes;
5) The use or omission of grain size and/or organic matter correction factors has a significant impact on the modelling result. The use of simplified correction factors can lead to incorrect modelling results;
6) One of the unmonitored tributaries has a chemical signature that is capable of disturbing the un-mixing process;
7) There is a not yet identified sediment source in the Demer itself (river bank erosion, riverbed scour, industrial discharges directly into the Demer, …) that has a chemical signature that is capable of hindering the un-mixing process;
8) Previous impactful maintenance works (in the Demer and tributaries) have sediment remnants left in the Demer (due to a prolonged residence time of the sediment), which are being brought into resuspension and are perturbing the modelling results;

The first five causes are linked to the set-up of the mass balancing model, while the last three are linked to environmental aspects.

Of the different causes, the first one is unlikely, as the samples obtained from the tributaries were time-integrated, and would therefore already incorporate the variability present in the tributaries. Furthermore, the Monte Carlo approach used in the mixing model was introduced to bring this variability into account. The Monte Carlo approach, however, can also be the source of some of the modelling problems, as addressed in the second, third and fourth reasons.

To address these issues, more robust location and scale estimators (such as median and Qn) could be used to create the probability density functions of the sources, as suggested by Collins et al. (2010 b). Furthermore, Latin Hypercube sampling could be used as an alternative to conventional random sampling, as introduced by Collins et al. (2012). To conlude, a modelling framework using global optimisation could be implemented, as suggested by Collins et al. (2010 b), to test if globally representative solutions are present.

The fifth cause, the absence of an appropriate correction factor, could potentially be the most impactful. Whether or not the observed variance could drop to acceptable levels, purely by addressing this problem (like was observed in Small et al. (2005)) or if the above mentioned un-sampled sources did contribute to the observed variance) cannot be determined at this time. The only way to answer that question is to determine applicable correction factors and run the model again, after which the variability in the 1,000 MC simulated results will give insight into the acceptability of the results.

Of the environmental causes, the sixth cause is the less realistic, as almost 90% of the total discharge in Aarschot is accounted for, and no major tributaries were un-sampled. The final potential causes (7 and 8) are more likely and deal with un-sampled sources, be it through natural or antropogenic input. If these are in fact of primordial importance, the dataflow from river basin manager to modeller needs to be improved. This has been challenging.

As Flanders is a highly active managed region, finding sampling times with little anthopogenic activity might prove to be difficult. As such, it can be difficult to successfully fingerprint basin-sized study areas in Flanders. Smaller catchments, where river management activities can be more readily monitored, might be more successful.

If the fractionation exercise cannot be completed, or no other method can be found to determine the grain size correction factor, then sediment fingerprinting in the Demer basin (and by extension in Flanders) using the geochemical composition of the sediment cannot be implemented. However, sediment fingerprinting might still be attempted, using a different set of properties. In that case properties should be robust enough not to be influenced by anthropogenic influences and grain size. Properties such as shape parameters of the sediment, heavy minerals or clay minerals present in the sediment might be useful in that respect, taking into account they will remain susceptible to the influence of un-sampled sediment sources contributing to the river system.

Conclusions and Recommendations

The research executed within this PhD research was oriented to answer three questions:

- How much sediment is being transported in selected locations in the Nete and Demer basins?
- Where does this sediment originate from?
- And how much do specific sources contribute to the observed sediment fluxes?

These questions were translated into:

- Determining the total suspended sediment flux at selected (FHR) monitoring stations in rivers in the Nete and Demer basins (discussed in Part III).
- Determining the contribution of authigenic sediment to the total suspended sediment transport in the Kleine Nete basin (discussed in Part IV).
- Investigating the applicability of the sediment fingerprinting approach for source apportionment in the Demer basin (discussed in Part V).

The detailed conclusions which could be drawn from the research in these three fields of interests are already discussed in detail in the respective chapters (6 through 11).

An overview of these conclusions, their implications as well as recommendations for further research are discussed below.

Determining the total suspended sediment flux

At the sediment monitoring locations of FHR, automatic samplers are installed and programmed to sample every seven hours. This sampling frequency is sufficient to calculate annual sediment fluxes. However, when gaps are present in the sediment concentration data, these need to be filled in using linear regression rating curves and/or multivariate rating curves, using a variety of hydrological and/or physical parameters, which should be site-specifically be selected.

For the Grobbendonk measurement location at the Kleine Nete, different rating curves have been constructed and their modelling results have been evaluated. The results show that allowing discharge-derived parameters to enter the model yields a slight improvement of the predictive power compared to only using discharge as a predictive parameter. On the other hand, allowing conductivity and turbidity to enter into the rating curve as well improves the modelling result significantly. However, even then the uncertainty remains quite high (about 50% of the average observed sediment concentration at the sampling station for the period of record).

Nonetheless, if the objective is limited to calculating annual suspended sediment fluxes and more than 75% of the data is available, then most of the models yield very similar results for the remaining 25%, making it unnecessary to determine all the different relationships possible. Hence, it is suggested to use the simple non-logarithmically transformed relationship between Q and SSC (separated for summer and winter data) to estimate sediment concentrations for the data gaps. However, when more detailed estimates are required, such as daily sediment concentrations (as needed for the MARS modelling in Part IV), or event-based studies than the combination of discharge with discharge-derived parameters and physical parameters should still be investigated to procure the relationship with the highest predictive power possible.

These modelling conclusions have been implemented to create rating curves for the Demer, Gete and Mangelbeek sampling locations. However, for Flemish rivers located in completely different geological settings, a preliminary investigation into the additional predictive power of data-transformation and supplementary parameters remains sensible.

The calculated fluxes for locations in the Nete and Demer basin point out the weaknesses in some sediment delivery models based on erosion to predict total sediment export by the rivers. The reported WATEM/SEDEM results show overestimations of the Demer sediment flux by a factor 4, and an underestimation of the Nete flux by at least 100% when compared to the calculated sediment fluxes. These differences in modelling and measurements highlight the need for high-quality sediment concentration monitoring data in the Flemish rivers, so correct sediment fluxes can be calculated and which can be used to calibrate the sediment delivery models, so these can be improved.

The sediment flux calculations at the Aarschot sampling location showed that the river system underwent some significant changes in sediment supply during the period of record. The basin went from an originally slightly sediment-depleted system (from May 2003 to November 2007) to a sediment-enriched system (November 2007 to March 2009) and has been, from April 2009 onwards, gradually returning to its slightly sediment-depleted state. The cause of these changes could be linked to different maintenance works, although not all kind of works have the same impact on the sediment concentrations. Maintenance works involving disturbance of the riverbed or river bank material relatively close to the sampling station in Aarschot caused a significant increase in the sediment concentrations measured at the sampling station, while maintenance works further upstream, and with less perturbation of soil and riverbed seemed to influence the sediment load far less.

During the period that the Demer basin was highly enriched in sediment because of the impactful works, a special phenomenon could be observed: a single discharge peak would generate a double sedimentary response; i.e. one sediment peak arrived +/- simultaneously with the discharge peak while a second sediment peak trailed behind the discharge peak.

In the literature this phenomenon is rarely discussed, and when observed it is usually in isolated occurrences, and the trailing peak is attributed to slow processes such as river bank failure due to saturation of the bank. In the Demer basin however the opposite is true: this phenomenon is not rare at all, as from November 2007 to March 2009, almost half of the high-flow events observed in Aarschot produced such a double sediment peak. Additionally, most of the maintenance works took place close to the monitoring location and generated a sediment influx which was readily available in-stream for further transportation.

Therefore, in this thesis it is hypothesised that bed load transport might be partly responsible for these double sedimentary responses. As bed load material is being transported at a velocity significantly slower than the average stream velocity, the coinciding sediment peak could be the suspension transport of sediment readily available on the riverbed, leading to clockwise hysteresis or single line responses, while the second peak (the trailing peak) could be the bed load arriving at the monitoring location. This hypothesis seems to be further confirmed by the similar shape of the discharge and trailing sediment peaks on the one hand and the fact that no significant increase in SSC_{SW}-values could be observed from Period 2 onwards.

The only way to confirm this theory of bed load transport, is by executing complete cross-sectional sampling campaigns as well as monitoring bed transport during the two sediment peaks generated by a single discharge event. Unfortunately, it proved impossible to launch such a campaign within

the framework of this PhD research. The restraints were the high variability of the lag-times between arrival of discharge and sediment peaks which made it very difficult to pinpoint the arrival time of the trailing sediment peak and the fact that executing a non-stop cross-sectional sampling campaign with a time span of 60+ hours was infrastructurally not possible.

This high variability of lag-times however, did prove to be a good indicator for changes in the river system. Combining this with investigating the secondary sedimentary responses (whether or not a second discharge peak (of similar size as the first) will yield similar sediment concentrations) yields valuable information about the state of sediment depletion (or enrichment) of the basin.

These parameters are as effective and less time-consuming than classifying individual events in different hysteresis classes to help separate periods with different river system dynamics and should therefore be considered as investigative tools for finding periods of changing sediment dynamics in rivers. This could be applicable for all river systems and is not limited to the investigated basin. It goes without saying that when sediment dynamics in a river change, different rating curves need to be established. Therefore, investigating the data set, using lag-time and secondary responses can be of importance. Especially when the secondary responses show a significant increase or decrease compared to the initial sedimentary response. In that case using a set of rating curves (one rating curve to predict the first sedimentary response and another one to predict the secondary) might be necessary.

Investigating whether using the discharge and matching sediment concentration peaks to create rating curves instead of using the entire Q-SSC data set could yield a new method of filling in the data gaps, as part of the variability introduced by hysteresis is reduced by time-shifting the concentration peaks. However, before this is attempted at the FHR measurement locations, the cross-sectional correction factors should be determined (through frequent EWI-method sampling). This would allow to determine the average sediment flux being transported by the river and would eliminate some of the elevated concentration values associated with the bed load transport.

Further, it is highly recommended to investigate the sediment fluxes at the Aarschot sampling location for the period 2010-2013 closely, so it can be determined whether the river system has returned to a sediment-depleted condition or not. Additional information from river basin managers however, will once more be required.

Budgeting authigenic sediment contributions

One sediment source was individually singled out for further investigation within the framework of this PhD research: authigenic sediment. This sediment is formed in the river itself due to interaction between waters with different origin and/or composition, such as groundwater and freshwater. In the Nete and the northern part of the Demer basin, ferric authigenic sediment is generated due to the significant influx of dissolved iron through seepage.

Even though the creation of this sort of material is well-known in the literature, the actual contribution to the total suspended sediment load is usually neglected. Therefore, within the framework of this PhD, both theoretical deductions and modelling (using the Model for Authigenic River Sediment (MARS)) were undertaken to estimate the authigenic contribution to the total sediment load in the Kleine Nete.

The theoretical deductions yielded quite a large range, i.e. in between 43 and 100% contribution, while the MARS model was able to give a more precise estimate. MARS, in its final incarnation

developed during the PhD research, places the average contribution of authigenic sediment to the total sediment flux at Grobbendonk for the decade 1999-2009 at 61%.

This result was obtained by feeding MARS with a variety of parameters, some of which were estimates:

- Groundwater seepage was obtained through WETSPRO numerical filtering. On average the groundwater contributed 85% for the decade 1999-2009
- Fe(II) concentration present in the groundwater was estimated using groundwater data obtained from various sources. Because of the large variability in the data and the uncertainty associated with the quality of the iron data, the median value of the Formation of Diest [0252] was entered into the modelling, i.e. 15.7 mg/l
- Correction factors were applied to convert the amount of Fe(II) entering the river system into amount of authigenic sediment formed. The stoichiometric factor was determined based on the mineralogical composition of the ferric material, i.e. ferrihydrite, while assumptions were made about the sorption factor.
- Erosion, resuspension and accumulation algorithms were adjusted and calibrated by comparing the modelled authigenic fluxes with the total suspended sediment fluxes observed at the Grobbendonk measurement location.

Of these input parameters, the Fe(II) concentration in groundwater is associated with the largest uncertainties and will be the main source of uncertainty in the final modelled contribution of authigenic sediment to the total sediment load.

The modelling results show that authigenic sediment contributes significantly to the total suspended sediment flux this sediment source should not be omitted from sediment transport modelling as this will lead to serious underestimations of the total sediment load of a river system (as was illustrated by comparing WATEM/SEDEM results with the total fluxes observed in the Kleine Nete).

Additionally the research shows that the material is highly flocculated and does not settle like singular particles, hence when authigenic sediment transport is modelled, some adapted cohesive sediment approach should be used.

The continuation of the MARS research in this thesis is already ongoing, since FHR found the results sufficiently interesting to invest in a three-year follow-up research program (divided in three different tiers) which is being executed by a consortium of VITO, KUL and IMDC. In tier 1 (of which the final report has been published in December 2012) the emphasis was placed on reviewing the literature, data collection (in the Nete basin) and laboratory experiments to gain insight into the processes involved in the creation of ferric and Ca-rich authigenic sediment in Flanders. With this information 'MARS 3.0 speciation' could be developed, which calculates the potential for the formation of authigenic sediment resulting from Fe- and Ca-bearing groundwater. With this version of MARS, the potential for authigenic sediment formation was assessed at a spatial level yielding a potency map of (ferric) authigenic sediment creation in Flanders. However, this model does not take into account the authigenic sediment being transported downstream. This will be investigated in the second tier, where a 1D river water quality model (MARS 3.0–river) will be developed that takes into account the formation of authigenic sediment in a specific section of a river as well as the transport to the next part of the river. To develop this model, the fysical interactions in the surface water system such as sorption and desorption as well as sedimentation

and erosion processes will be investigated. In the final tier, the insights and models created will be adapted to be used in an existing sediment transport model.

The results obtained in tier 1 confirm most of the observations made in Chapters 8 and 9 of this thesis. The authigenic sediment does indeed consist of ferrihydrite. Additionally, the research confirmed that the material collected in the upstream reaches of the Nete and northern part of the Demer basin is very high in authigenic sediment content, but is not 100% pure. The laboratory experiments proved that the Fe-content of artificially created authigenic sediment was surprisingly constant and amounted to 44 ± 6%, while the upstream samples had average iron content levels of 35% with maximum values up to 38%.

The lab experiments also showed that the freshly formed Fe-rich particulates are an important sink of P (adsorbing more than 90% of all dissolved P initially added) but did not sorb many other elements. However, as sorption factors have not yet been determined in this research, no comparisons with the sorption correction factors applied in this PhD could be made.

Composite sediment fingerprinting

In the final part of this PhD thesis, the internationally applied composite fingerprinting approach was assessed for its applicability in the Demer basin, and potentially the rest of Flanders. Initially the intent was to determine the contributions of tributaries to the total sediment flux measured in Aarschot (and as such providing FHR with another way to determine sediment budgets) as well as determining the contributions of specific source types in the Mangelbeek and Gete basins. As in the Mangelbeek basin, authigenic sediment is a major contributor, sediment fingerprinting could potentially confirm the modelling results obtained by MARS. However, in the course of the research, the primary focus became the fingerprinting of the spatial sources (i.e. to discriminate and apportion the different tributaries of the Demer basin) and the problems encountered. Therefore the source type fingerprinting was only addressed in the discussion chapter (Chapter 11).

In the attempt to fingerprint the spatial sources in the Demer basin, several composite fingerprints were created, comprised of different combinations of properties. The models (objective functions) were also run using different combinations of correction factors (grain size, LOI and discriminatory weighting correction factor or omitting all correction factors).

From this research several conclusions could be drawn:

- The eight investigated tributaries could statistically be completely differentiated from one another.
- Disappointingly, the models struggled to attribute the contributions to the correct tributaries, within the same geographical region.
- The Relative Mean Error (RME) can be used as a robust test of the ability of the modelling work to predict the measured concntrations in the outlet samples collected at the Aarschot sampling site. But, it cannot be taken as a metric of the predicted proportions themselves. Furthermore, in the case of the Demer basin the RME failed to indicate the poor modelling results. A better estimator can be created when determining a RME_val which includes properties which were excluded from the composite fingerprint, but did pass the Kruskall-Wallis H-test. Otherwise, the descriptive statistics obtained from the 1,000 Monte Carlo simulations (average modelled contributions per

source, the associated standard deviations, minimum and maximal contributions modelled,…) can be used to estimate the quality of the modelling results.

- In an attempt to obtain realistic modelling results the spatial source set-up was simplified, by reducing the amount of sources. Contributions became environmentally realistic in comparisson to the total sediment fluxes at the Halen, Lummen and Aarschot sampling locations as determined in Chapter 6, when the sources were grouped per geological setting (i.e. the northern tributaries were grouped and the southern tributaries were grouped).

Further investigation showed the impact of the grain size and organic matter correction on the modelling results. In specific settings where the sources consist of well-sorted sediment, of which some are particularly finer than others, this will lead to a mixed grain size signal in the outlet samples, which makes it impossible to estimate the amount of sorting that might have happened to the initial source material while moving downstream. Therefore, the simple grain size correction, frequently used in the literature, does not suffice, explaining the equally poor modelling results when grain size correction was applied.

Therefore, to improve modelling results more complex source-specific grain size corrections need to be applied and to determine these, it is necessary to obtain insight into the chemical composition of grain size-fractionated sediment samples rather than analysing geochemistry of bulk samples.

However, obtaining these fractionated subsamples has proven to be difficult in the Demer basin, as settling tests using suspended sediment of Demer, Gete and Mangelbeek have failed to procure subsamples separated by grain size, due to flocculation of the fluvial sediment.

Therefore, if sediment fingerprinting is to be used successfully in the Demer basin (and by extension in Flanders) an approach of fractionation of flocculated material needs to be established so grain size corrections can be determined and implemented. Additionally, further investigation into the applicability of these grain size correction factors in larger geological regions is suggested, as having to establish such correction factors through fractionation tests and separate geochemical analyses for every individual source and sink will be time-consuming. Once the geochemical data on the fractionated samples are available, properties which show too much variation in concentration per grain size class, can be omitted from further use in the composite fingerprint. The consequent fingerprinting results should yield more realistic modelling results.

Concerning the use of organic matter correction factors, the research done within the framework of this PhD shows that LOI is also a complex parameter and the signal can be obscured during transport. However, in the framework of source type fingerprinting in the Mangelbeek catchment, the results are promising, as organic matter content was capable of approximating the adjusted grain size correction factor and might therefore be used instead of a grain size correction. Whether this can be applied to other catchments containing authigenic sediment still needs to be investigated.

Additionally, it is the suggestion of the author to revist the Demer basin and collect more time-integrated samples (both in the tributaries, to investigate whether or not the established fingerprints are still applicable, and at the outlet) at a time when little to no anthropogenic activity is planned. Also, it is recommended to test the efficacy of specific alterations to the model set-up, such as using robust estimators (Qn and median) to generate the probablility density functions of random deviates, and using a Latin Hypercubes stratified sampling technique to sample from them. Furthermore, it is suggested to use a modelling framework incorporating both local and global

optimisation tools. Implementing these changes in the model built-up, can potentially (but not necessarily) have a positive effect on the modelling results.

To conclude, in actively-managed river basins, where human interventions have a significant impact on the sediment load and sediment quality, sediment fingerprinting can prove challenging. Some of the human impact (such as the industrial and sewage discharges) can contribute to the discriminatory power of specific properties in spatial source apportionment. As such, human impact in a river basin should not be considered per definition detrimental to the sediment fingerprinting exercise. Nonetheless, this impact should be investigated prior to allowing specific properties to be entered in the composite fingerprint.

However, in this research some effects of human intervention (the influx of material through river bank, riverbed and other maintenance works, as well as sewage treatment and industrial discharges) obscured the signals of the mixing of sources from distinct different grain size populations. In effect, the human interventions caused an un-sampled source to disrupt the fingerprinting exercise.

Therefore, it can be concluded that sediment fingerprinting in the Demer basin (and by extension in Flanders), using only the geochemical composition of the sediment, cannot be implemented as long as no applicable grain size correction factor is determined and its impact on the sediment fingerprinting results can be determined, allowing for the discrimination of uncertainty caused by the human impact and uncertainty caused by faulty correction factors.

Some of that uncertainty can potentially also be reduced by changing the modelling set-up (using more robust estimators in the creation of the probability density functions, introducing stratified sampling from these distributions and using global search tools to find a global minimum for the objective function).

This still needs to be investigated.

References

Alvarez-Guerra, M.; Viguri, J.R.; Voulvoulis, N. (2009). A multicriteria-based methodology for site prioritisation in sediment management. *Environ. Int.* 35(6): 920-930

AMINAL — Afdeling Water (2003). Bekkenbeheerplan van de Nete: Samenvatting omgevingsanalyse [Report-Draft] (MS Word document). p.53. Online available at: https://circa.vlaanderen.be/Public/irc/mmis/bekken/library?l=/netebekken/bekkenbeheerplan/omgevingsanalyse&vm=detailed&sb=Title [accessed 15 August 2006].

Arnborg, L.; Walker, H.; Peippo, J. (1967). Suspended load in the Colville River, Alaska, 1962. *Geografiska Annaler.Series A.Physical Geography* 49 (2/4): 131-144

Asselman, N. (2000). Fitting and interpretation of sediment rating curves. *Journal of Hydrology* 234(3): 228-248

Bagnold, R. (1966). An approach to the sediment transport problem from general physics. *US Geol.Surv.Prof.Paper (*422) 231-291

Balci, N.; Mayer, B.; Shanks III, W.C.; Mandernack, K.W. (2012). Oxygen and sulfur isotope systematics of sulfate produced during abiotic and bacterial oxidation of sphalerite and elemental sulfur. *Geochim. Cosmochim. Acta 77*: 335-351.

Batelaan, H. (2006). Phreatology, Characterizing groundwater recharge and discharge using remote sensing, GIS, ecology, hydrochemistry and groundwater modelling, Ph.D. Thesis, Vrije Universiteit Brussel, Belgium. 332 p.

Belien, H. (2006). Studie van geflocculeerd ijzerhoudend sediment in de Kleine Nete, Unpublished MSc dissertation, Universiteit Gent: Gent. 103 p.

Belien, H.; Vanlierde, E.; Mostaert, F.; Jacobs, P. (2006). A preliminary study of the flocculation of iron-bound sediment in a Belgian river *Geophys. Res. Abstr. 8 (04521)*

Berckmans, J. (2005). Suspensietransport in het Demerbekken: een verband met de geologische ingesteldheid?. Unpublished MSc dissertation. Universiteit Gent, Belgium. 202 p.

Bettess, R. (1994). Sediment transport and channel stability. In: Calow, P.; Petts, G.E. (eds.). The Rivers Handbook: Hydrological and Ecological Principles, Volume Two. Blackwell Science Ltd: Oxford. p. 227-253

Bicknell, B.; Imhoff, J.; Kittle Jr, J.; Donigian Jr, A.; Johanson, R. (1993). Hydrologic Simulation Program-FORTRAN (HSPF): User's Manual for Release 10. *Rep.no.EPA/600/R-93/174.* US EPA Environmental Research Lab: Athens, Ga. 660 p.

Biedenharn, D.S.; Hubbard, L.C.; Thorne, C.R.; Watson, C.C. (2006). Understanding Sediment Sources, Pathways and Sinks in Regional Sediment Management: Wash Load and Bed-Material Load Concept SWWRP [Technical Note] (pdf document). ERDC TN-SWWRP-06-3. U.S. Army Engineer Research and Development Center: Vicksburg, MS. p.8. Online available at: https://swwrp.usace.army.mil/_swwrp/swwrp/4-Pubs/TechNotes/swwrp-tn-06-3.pdf [accessed 15 August 2012].

Blommaert, W.; de Marmol, P.; Patyn, J. (1988). Hydrochemical Research within the Hades Project (Disposal of high radioactive waste into the Boom clay) 1982-1986. Studiecentrum Voor Kernenergie – Centre d'Etude de l'Energie Nucléaire: Mol. 125 p.

Brasington, J.; Richards, K. (2000). Turbidity and suspended sediment dynamics in small catchments in the Nepal Middle Hills. *Hydrol. Process.* 14(14): 2559-2574

Brown, A. (1985). The potential use of pollen in the identification of suspended sediment sources. *Earth Surf. Process. Landforms* 10(1): 27-32

Caitcheon, G. (1993). Sediment source tracing using environmental magnetism: a new approach with examples from Australia. *Hydrol. Process.* 7(4): 349-358

Cant, P. (2010). Onderzoek naar fysische sedimentkarakteristieken van de Demer en haar bijrivieren: sedimentatieproeven in natuurlijk rivierwater. Unpublished MSc dissertation, Universiteit Gent: Gent. 150 p.

Carter, J.; Owens, P.N.; Walling, D.E.; Leeks, G. (2003). Fingerprinting suspended sediment sources in a large urban river system. *Sci. Total Environ.* 314-316: 513-534

Chen, M.S.; Wartel, S.; Eck, B.V.; Maldegem, D.V. (2005). Suspended matter in the Scheldt estuary. *Hydrobiologia* 540(1): 79-104

Christensen, V.G.; Jian, X.; Ziegler, A.C. (2000). Regression analysis and real-time water-quality monitoring to estimate constituent concentrations, loads, and yields in the Little Arkansas River, south-central Kansas, 1995-99. Report 00-4126. US Department of the Interior, US Geological Survey, Lawrence, Ks. 22 p.

Christensen, V.G.; Ziegler, A.C.; Jian, X. (2001). Continuous turbidity monitoring and regression analysis to estimate total suspended solids and fecal coliform bacteria loads in real time. In: Proceedings of the Seventh Federal Interagency Sedimentation Conference, March 25-29, 2001, Reno, Nevada: Subcommittee on Sedimentation, volume 1. p.III-94 to III-101

Clarck, I. (2009). Groundwater Geochemistry. University of Ottawa: Ottawa, Canada. Online available at: http://mysite.science.uottawa.ca/idclark/GEO4342/2009/Ch%208%20Ion%20Exchange%20Reactions%202008.pdf [accessed 6 May 2012].

Collins, A.L. (1995). The Use of Composite Fingerprints for Tracing the Source of Suspended Sediment in River Basins. Unpublished Ph.D. thesis. University of Exeter: Exeter. 548 p.

Collins, A.L.; Strőmqvist, J.; Davison, P.S.; Lord, E.I (2007). Appraisal of phosphorus and sediment transfer in three pilot areas identified for the catchment sensitive farming initiative in England: application of the prototype PSYCHIC model. *Soil use Manage* 23: 117-132

Collins, A.L.; Walling, D.E. (2002). Selecting fingerprint properties for discriminating potential suspended sediment sources in river basins. *Journal of Hydrology* 261(1): 218-244

Collins, A.L.; Walling, D.E. (2004). Documenting catchment suspended sediment sources: problems, approaches and prospects. *Prog. Phys. Geogr.* 28(2): 159-196

Collins, A.L.; Walling, D.E. (2006). Investigating the remobilization of fine sediment stored on the channel bed of lowland permeable catchments in the UK. *In:* Rowan, J. et al. (eds.) Sediment Dynamics and the Hydromorphology of Fluvial Systems. *IAHS Publ.* 306. IAHS Press: Wallingford. pp. 471-479

Collins, A.L.; Walling, D.E. (2007). Sources of fine sediment recovered from the channel bed of lowland groundwater-fed catchments in the UK. *Geomorphology* 88(1): 120-138

Collins, A.L.; Walling, D.E.; Leeks, G.J.L. (1996). Composite fingerprinting of the spatial source of fluvial suspended sediment: a case study of the Exe and Severn River basins, United Kingdom. *Géomorphologie: Relief, Processus, Environnement* 2(2): 41-53

Collins, A.L.; Walling, D.E.; Leeks, G.J.L. (1997 a). Use of the geochemical record preserved in floodplain deposits to reconstruct recent changes in river basin sediment sources. *Geomorphology* 19(1): 151-167

Collins, A.L.; Walling, D.E.; Leeks, G.J.L. (1997 b). Source type ascription for fluvial suspended sediment based on a quantitative composite fingerprinting technique. *Catena* 29(1): 1-27

Collins, A.L., Walling, D.E.; Leeks, G.J.L. (1997 c). Fingerprinting the origin of fluvial suspended sediment in larger river basins: combining assessment of spatial provenance and source type. *Geografiska Annaler* 79A, 239-254.

Collins, A.L.; Walling, D.E.; Leeks, G.J.L. (1998). Use of composite fingerprints to determine the provenance of the contemporary suspended sediment load transported by rivers. *Earth Surf. Process. Landforms* 23(1): 31-52

Collins, A.L.; Walling, D.E.; Leeks, G.J.L. (2003). Fingerprinting the origin of fluvial suspended sediment in larger river basins: combining assessment of spatial provenance and source type. *Geografiska Annaler: Series A, Physical Geography* 79(4): 239-254

Collins, A.L.; Walling, D.E.; Sichingabula, H.M.; Leeks, G.J.L. (2001). Suspended sediment source fingerprinting in a small tropical catchment and some management implications. *Appl. Geogr.* 21(4): 387-412

Collins, A.L.; Walling, D.E.; Webb, L.; King, P. (2010 a). Apportioning catchment scale sediment sources using a modified composite fingerprinting technique incorporating property weightings and prior information. *Geoderma* 155(3): 249-261.

Collins, A.L.; Zhang, Y.; Walling, D.E.; Grenfell, S.E.; Smith, P. (2010 b). Tracing sediment loss from eroding farm tracks using a geochemical fingerprinting procedure combining local and genetic algorithm optimisation. *Sci. Total Environ.* 408(22): 5461-5471.

Collins, A. L.; Zhang, Y.; Walling, D.E.; Grenfell, S.E.; Smith, P.; Grischeff, J.; Locke, A.; Sweetapple, A.; Brogden, D. (2012). Quantifying fine-grained sediment sources in the River Axe catchment, southwest England: application of a Monte Carlo numerical modelling framework incorporating local and genetic algorithm optimisation. *Hydrol. Process. 26*(13): 1962-1983.

Coynel, A.; Schäfer, J.; Hurtrez, J.E.; Dumas, J.; Etcheber, H.; Blanc, G. (2004). Sampling frequency and accuracy of SPM flux estimates in two contrasted drainage basins. *Sci. Total Environ.* 330(1): 233-247

Crawford, C.G. (1991). Estimation of suspended-sediment rating curves and mean suspended-sediment loads. *Journal of Hydrology* 129(1): 331-348

Darchuk, L.; Tsybrii, Z.; Worobiec, A.; Vazquez, C.; Palacios, O.M.; Stefaniak, E.A.; Rotondo, G.G.; Sizov, F.; Van Grieken, R. (2010). Argentinean prehistoric pigments' study by combined SEM/EDX and molecular spectroscopy. *Spectrochim. Acta. A* 75(5): 1398-1402

De Maeyer-Worobiec, A.; Dekov, V.M.; Laane, R.W.P.M.; Van Grieken, R. (2009). EPXMA survey of shelf sediments (Southern Bight, North Sea): A glance beyond the XRD-invisible. *Microchem. Journal* 91(1): 21-31.

DOV (2011). DOV|HCOV kartering [ONLINE] online available at: https://dov.vlaanderen.be/dovweb/html/3hcov.html#codering [accessed 10-8-2011]

Davide, V.; Pardos, M.; Diserens, J.; Ugazio, G.; Thomas, R.; Dominik, J. (2003). Characterisation of bed sediments and suspension of the river Po (Italy) during normal and high flow conditions. *Water Res.* 37(12): 2847-2864

Davis, B.E. (2005). A guide to the proper selection and use of federally approved sediment and water-quality samplers. Open File Report 2005-1087. US Department of the Interior, US Geological Survey. 20 p.

De Ignacio, C.; Munoz, M.; Sagredo, J.; Fernandez-Santin, S.; Johansson, Å. (2006). Isotope geochemistry and FOZO mantle component of the alkaline-carbonatitic association of Fuerteventura, Canary Islands, Spain. *Chem. Geol.* 232: 99-113.

De Meuter, F.J.; Laga, P. (1976). Lithostratigraphy and biostratigraphy based on benthonic foraminifera of the Neogene deposits of northern Belgium. Bulletin de la Societé belge de Géologie, 85(4): 133-152.

De Schutter, J.; Mostaert, F. (2009 a). Instructie: Bepalen van droogrest. I-WL-PP31-5 Versie 01. Waterbouwkundig Laboratorium: Antwerpen. 6 p.

De Schutter, J.; Mostaert, F. (2009 b). Instructie: Vriesdrogen. I-WL-PP31-3 Versie 01. Waterbouwkundig Laboratorium: Antwerpen. 18 p.

De Schutter, J.; Mostaert, F. (2009 c). Instructie: Bepalen van as- (gloei-)rest en gloeiverlies. I-WL-PP31-6 Versie 01. Waterbouwkundig Laboratorium: Antwerpen. 3 p.

De Schutter, J.; Mostaert, F. (2009 d). Instructie: Bepalen van korrelgrootte. I-WL-PP31-4 Versie 01. Waterbouwkundig Laboratorium: Antwerpen. 16 p.

De Schutter, J.; Mostaert, F. (2009 e). Instructie: Mengen. I-WL-PP31-8 Versie 01. Waterbouwkundig Laboratorium: Antwerpen. 3 p.

De Schutter, J.; Mostaert, F. (2009 f). Instructie: Persen. I-WL-PP31-9 Versie 01. Waterbouwkundig Laboratorium: Antwerpen. 2 p.

De Schutter, J.; Mostaert, F. (2009 g). Instructie: Bepalen van de dichtheid volgens gaspycnometrie I-WL-PP31-10 Versie 01. Waterbouwkundig Laboratorium: Antwerpen. 9 p.

De Schutter, J.; Mostaert, F. (2010). Instructie: IJken en programmeren van YSI. I-WL-PP31-12 Versie 02. Waterbouwkundig Laboratorium: Antwerpen. 15 p.

De Smedt, F.; Muls, J.; Sas, M.; Smits, J. (1989). Een computermodel voor de berekening van de consolidatie van slib. *Water* 47: 140-143.

De Sutter, R. (2000). Integrated river management of a small Flemish river catchment. In: The Role of Erosion and Sediment Transport in Nutrient and Contaminant Transfer: Proceedings of a Symposium Held at Waterloo, Ontario, Canada in July 2000. Volume 263. 191 p.

De Vries, A.; Klavers H.C. (1994). Riverine fluxes of pollutants: monitoring strategy first, calculation methods second. *European Journal of Water Pollution Control* 4: 12–17.

Dearing, J.A. (2000). Natural magnetic tracers in fluvial geomorphology. In: Foster I.D.L. (ed.) Tracers in Geomorphology. John Wiley and Sons: Chichester. 57–82.

Dekov, V.M.; Hålenius, U.; Billström, K.; Kamenov, G.D.; Munnik, F.; Eriksson, L.; Dyer, A; Schmidt, M.; Botz, R. (2009). Native Sn–Pb droplets in a zeolitic amygdale (Isle of Mull, Inner Hebrides). *Geochim. Cosmochim. Acta* 73(10): 2907-2919.

Dekov, V.M.; Vanlierde, E.; Billström, K.; Garbe-Schönberg, C.-D.; Weiss, D.J.; Gatto Rotondo, G.; Van Meel, K.; Kuzmann, E.; Fortin, D.; Darchuk, L.; Shanks, W.C.; Van Grieken, R. (in preperation). Ferrihydrite precipitation in groundwater-fed river systems (Nete and Demer river basins, Belgium): Insights from a combined O-Fe-Zn-Sr-Nd-Pb-isotopes study. In prep.

Desmet, P.J.J.; Govers, G. (1996). A GIS procedure for automatically calculating the USLE LS factor on topographically complex landscape units*. J. Soil Water Conserv.* 51(5): 427-433

DHI (2000). A Modelling System for Rivers and Channels, Reference Manual. DHI Water & Environment: Hørsholm, Danmark. 514 p.

Douglas, G.; Gray, C.; Hart, B.; Beckett, R. (1995). A strontium isotopic investigation of the origin of suspended particulate matter (SPM) in the Murray-Darling River system, Australia. *Geochim. Cosmochim. Acta* 59(18): 3799-3815

Douglas, G.; Palmer, M.; Caitcheon, G. (2003). The provenance of sediments in Moreton Bay, Australia: a synthesis of major, trace element and Sr–Nd–Pb isotopic geochemistry, modelling and landscape analysis. *Hydrobiologia* 494:145–152.

Droppo, I.G.; Leppard, G.G.; Flannigan, D.T.; Liss, S.N. (1997). The freshwater floc: a functional relationship of water and organic and inorganic floc constituents affecting suspended sediment properties. *Water, Air, & Soil Pollution* 99(1): 43-53

Droppo, I.G.; Leppard, G.G.; Liss, S.N.; Milligan, T.G. (eds) (2005). Flocculation in natural and engineered environmental systems. CRC Press: Boca Raton, USA. 188 p.

Droppo, I.G.; Walling, D.E.; Ongley, E.D. (2000). Influence of floc size, density and porosity on sediment and contaminant transport. *IAHS Publ.* 263. IAHS Press: Wallingford. pp. 141-147

Duan, N. (1983). Smearing estimate: a nonparametric retransformation method. *Journal of the American Statistical Association* 78(383): 605-610

Eder, A.; Strauss, P.; Krueger, T.; Quinton, J. (2010). Comparative calculation of suspended sediment loads with respect to hysteresis effects (in the Petzenkirchen catchment, Austria). *Journal of Hydrology* 389(1): 168-176

Edwards, T.K.; Glysson, G.D. (1999). Chapter C2: Field methods for measurement of fluvial sediment. In: Techniques of Water-Resources Investigations. Book 3: Applications of Hydraulics. US Geological Survey: Reston, VA. 98 p. Available at http://pubs.usgs.gov/twri/twri3-c2/pdf/TWRI_3-C2.pdf [accessed 19/04/2003]

Eijkelkamp (2012). Water sampler 'Watertrap' [ONLINE]. Eikelkamp. Available at http://en.eijkelkamp.com/products/soil/soil-and-sediment-sampling/samplers-for-suspended-sediment/water-sampler-watertrap-/water-sampler-watertrap-.htm [accessed 27-12-2012]

Einstein, H.A. (1950). The bed-load function for sediment transportation in open channel flows. Technical Bulletin No. 1026. US Department of Agriculture, Soil Conservation Service: Washington D.C. 71 p.

Eisma, D., Skei, J., Westerlund, S., Kalf, J., Magnusson, B., Naes, K., Sörensen, K. (1984). Distribution and composition of suspended particulate matter and trace metals in the Skagerrak. ICES papers. Rostock Meeting, February 1984. 1-13.

Evans, D.; Gibson, C.; Rossell, R. (2006). Sediment loads and sources in heavily modified Irish catchments: A move towards informed management strategies. *Geomorphology* 79(1): 93-113

Evrard, O.; Navratil, O.; Ayrault, S.; Ahmadi, M.; Némery, J.; Legout, C.; Lefèvre, I.; Poirel, A.; Bonté, P.; Esteves, M. (2011). Combining suspended sediment monitoring and fingerprinting to determine the spatial origin of fine sediment in a mountainous river catchment. *Earth Surf. Process. Landforms* 36(8): 1072-1089

Fang, H.; Cai, Q.; Chen, H.; Li, Q. (2008). Temporal changes in suspended sediment transport in a gullied loess basin: the lower Chabagou Creek on the Loess Plateau in China. *Earth Surf. Process. Landforms* 33(13): 1977-1992

Federal Inter-Agency Sedimentation Project (1963). Determination of fluvial sediment discharge. Inter-Agency Report 14. FISP: Minneapolis, Minnesota. 151 p.

Federal Interagency Sedimentation Project (2011). Churn Sample Splitter, Polyethylene, 8-L [ONLINE]. Available at http://water.usgs.gov/fisp/products/4111001.html [accessed 1/12/2011]

Fenn, C.; Gurnell, A.; Beecroft, I. (1985). An evaluation of the use of suspended sediment rating curves for the prediction of suspended sediment concentration in a proglacial stream. *Geografiska Annaler* 67A: 71-82

Foster, I.D.L.; Millington, R.; Grew, R.G. (1992). The impact of particle size controls on stream turbidity measurement; some implications for suspended sediment yield estimation. In: Bogen, J.; Walling, D.E.; Day, T.J. (eds) Erosion and Sediment Transport Monitoring Programmes in River Basins. *IAHS Publ*. 210. IAHS Press: Wallingford. pp. 51-62

Fox, J.F.; Papanicolaou, A.N. (2007). The Use of Carbon and Nitrogen Isotopes to Study Watershed Erosion Processes1. *JAWRA Journal of the American Water Resources Association* 43(4): 1047-1064

Garbe-Schönberg, C.D. (1993). Simultaneous determination of thirty seven trace elements in twenty eight international rock standards by ICP-MS. *Geostandard Newslett. 175(1)*: 81-97.

Gippel, C.J. (1995). Potential of turbidity monitoring for measuring the transport of suspended solids in streams. *Hydrol. Process.* 9(1): 83-97

Golterman, H.L. (2004). The chemistry of phosphate and nitrogen compounds in sediments. Springer: Dordrecht. 284 p.

Govoreanu, R. (2004). Activated sludge flocculation dynamics: on-line measurement methodology and modelling. Unpublished PhD Thesis. Faculty of Bioscience Engineering. Ghent University: Ghent. pp. 290

Goodwin, T.H.; Young, A.R.; Holmes, M.G.R.; Old, G.H.; Hewitt, N.; Leeks, G.J.L.; Packman, J.C.; Smith, B.P.G. (2003). The temporal and spatial variability of sediment transport and yields within the Bradford Beck catchment, West Yorkshire. *Sci. Total Environ.* 314: 475-494

Govers, G.; Vandaele, K.; Desmet, P.; Poesen, J.; Bunte, K. (1994). The role of tillage in soil redistribution on hillslopes. *Eur. J. Soil Sci.* 45(4): 469-478

Graf, W.L. (1984). A probabilistic approach to the spatial assessment of river channel instability. *Water Resour. Res.* 20(7): 953-962

Grimshaw, D.; Lewin, J. (1980). Source identification for suspended sediments. *Journal of Hydrology* 47(1): 151-162

Grimshaw H.M.; Parkinson J.A.; Allen S.E. (1974). Chemical analysis of ecological materials. Blackwell Scientific Publications: Oxford. 565 p.

Gruszowski, K.; Foster, I.D.L.; Lees, J.; Charlesworth, S. (2003). Sediment sources and transport pathways in a rural catchment, Herefordshire, UK. *Hydrol. Process.* 17(13): 2665-2681

Guy, H. (1970). Chapter C1: Fluvial sediment concepts. In: Techniques of Water-Resources Investigations. Book 3: Applications of Hydraulics. US Geological Survey: Arlington, VA. 55 p. Available at http://pubs.usgs.gov/twri/twri3-c1/pdf/TWRI_3-C1.pdf [accessed 24/6/2009]

Hatfield, R.G.; Maher, B.A. (2008). Suspended sediment characterization and tracing using a magnetic fingerprinting technique: Bassenthwaite Lake, Cumbria, UK. *The Holocene* (18): 105-115.

He, Q.; Owens, P. (1995). Determination of suspended sediment provenance using caesium-137, unsupported lead-210 and radium-226: A numerical mixing model approach. In: Foster, I.D.L.; Gurnell, A.M.; Webb, B.W. (Eds). Sediment and Water Quality in River Catchments. Wiley: Chichester. 207-227

He, Q.; Walling, D. (1996). Interpreting particle size effects in the adsorption of Cs-137 and unsupported Pb-210 by mineral soils and sediments. *J. Environ. Radioact.* 30(2): 117-137

Heidel, S. (1956). The progressive lag of sediment concentration with flood waves. *Trans.Am.Geophys.Union* 37(1): 56-66

Helsel, D.R.; Hirsch, R.M. (2002). Chapter A3: Statistical methods in water resources. In: Techniques of Water-Resources Investigations Book 4: Hydrologic Analysis and Interpretation. US Geological survey: Reston, Va. 522 p. Available at http://pubs.usgs.gov/twri/twri4a3/pdf/twri4a3-new.pdf [accessed 15/4/2005]

Hinrichs, J.; Dellwig, O.; Brumsack, H.J. (2002). Lead in sediments and suspended particulate matter of the German Bight: natural versus anthropogenic origin. *Appl. Geochem.* 17(5): 621-632

Hirner, A.; Kritsotakis, K.; Tobschall, H. (1990). Metal-organic associations in sediments—I. Comparison of unpolluted recent and ancient sediments and sediments affected by anthropogenic pollution. *Appl. Geochem.* 5(4): 491-505

Horowitz, A.J. (1991). A Primer on Sediment Trace Element Chemistry (second edn). Lewis Publishers Inc.: Chelsea, Michigan, USA., 136 p.

Horowitz, A.J. (1995). The Use of Suspended Sediment and Associated Trace Elements in Water Quality Studies. *IAHS Spec. Publ.* 4. IAHS Press: Wallingford. 58 p.

Horowitz, A.J. (2003). An evaluation of sediment rating curves for estimating suspended sediment concentrations for subsequent flux calculations. *Hydrol. Process.* 17(17): 3387-3409

Horowitz, A.J. (2006). The effect of the "Great Flood of 1993" on subsequent suspended sediment concentrations and fluxes in the Mississippi River Basin, USA. In: Rowan, J.S.: Duck, R.W.; Werritty, A. (eds) Sediment Dynamics and the Hydromophology of Fluvial Systems. *IAHS Publ.* 306. IAHS Press: Wallingford. pp.110-119

Horowitz, A.J.; Elrick, K.A. (1987). The relation of stream sediment surface area, grain size and composition to trace element chemistry. *Appl. Geochem.* 2(4): 437-451

Horowitz, A.J.; Elrick, K.A.; Smith, J.J. (2001). Estimating suspended sediment and trace element fluxes in large river basins: methodological considerations as applied to the NASQAN programme. *Hydrol. Process.* 15(7): 1107-1132

Horowitz, A.J.; Rinella, F.A.; Lamothe, P.; Miller, T.L.; Edwards, T.K.; Roche, R.L.; Rickert, D.A. (1989). Cross-sectional variability in suspended sediment and associated trace element concentrations in selected rivers in the US. In: Hadley, R.F.; Ongley, E.D. (eds) Sediment and the Environment. *IAHS Publ.* 184. IAHS Press: Wallingford. pp. 57-66

Horowitz, A.J.; Rinella, F.A.; Lamothe, P.; Miller, T.L.; Edwards, T.K.; Roche, R.L.; Rickert, D.A. (1990). Variations in suspended sediment and associated trace element concentrations in selected riverine cross sections. *Environ. Sci. Technol.* 24(9): 1313-1320

Hudson, P.F. (2003). Event sequence and sediment exhaustion in the lower Panuco Basin, Mexico. *Catena* 52(1): 57-76

Huygens, M.; Verhoeven, R.; De Sutter, R.; Van Poucke, L.; Parzonka, W.; Glowski, R.; Kasperek, R. (2001). Identification of sediment transport in a small river catchment, leading to integral management. *Water and Land Development* (4): 113–122.

International Marine and Dredging Consultants; Belgroma; Soresma; HAECON; Resource Analysis; Technum (2003). Actualisatie van het Sigmaplan. Integrale verkenning Scheldebekken. Integrale verkenning Rupelbekken. Planstudie rivierherstelproject Durme: deelopdracht 3. Hydrologische en hydraulische modellen: volume 1b. Statistiek/ hydrologie Rupelbekken. Versie 2.1. Ministerie van de Vlaamse Gemeenschap. Afdeling Zeeschelde: Antwerpen. 296 p. + appendices (1 file)

Janssens, R. (2007). Het modelleren van de input van autigeen sediment in het Nete-bekken aan de hand van ijzerconcentraties in suspensie: het MARS-model. Unpublished bachelor internship report. Faculty of Sciences. Ghent University: Ghent. pp. 52

Jansson, M.B. (2002). Determining sediment source areas in a tropical river basin, Costa Rica. *Catena* 47(1): 63-84

Juracek, K.; Ziegler, A. (2009). Estimation of sediment sources using selected chemical tracers in the Perry lake basin, Kansas, USA. *International Journal of Sediment Research* 24(1): 108-125

Kamnev, A.A.; Tugarova, A.V.; Kovacs, K.; Kuzmann, E.; Biro, B.; Tarantilis, P.A.; Homonnay, Z. (2013). Emission (Co-57) Mössbauer spectroscopy as a tool for probing speciation and metabolic transformations of cobalt(II) in bacterial cells. *Anal. Bioanal. Chem. 405 (6)*: 1921-1927

Kimoto, A.; Nearing. M.; Shipitalo, M.J.; Polyakov, V.O. (2006). Multi-year tracking of sediment sources in a small agricultural watershed using rare earth elements. *Earth Surf. Process. Landforms* 31: 1763–1774.

Klein, M. (1984). Anti clockwise hysteresis in suspended sediment concentration during individual storms: Holbeck Catchment; Yorkshire, England. *Catena* 11(1): 251-257

Kleinhans, M.G., (2005). Dune-Phase Fluvial Transport and Deposition Model of Gravelly Sand. In: Blum, M.D., et al. (Eds.). Fluvial Sedimentology VII Special Publication 35 of the International Association of Sedimentologists. Blackwell publishing Ltd.: Oxford. p. 75-97.

Kleinhans, M.G.; Wilbers, A.; Brinke, W.B.M. (2007). Opposite hysteresis of sand and gravel transport upstream and downstream of a bifurcation during a flood in the River Rhine, the Netherlands. *Netherlands Journal of Geosciences* 86(3): 273

Knighton, A. (1998). Fluvial form and processes: A new perspective. Arnold: London. 383 p.

Koch, R.W.; Smillie, G.M. (1986). Bias in hydrologic prediction using log-transformed regression models. *JAWRA Journal of the American Water Resources Association* 22(5): 717-723

Krause, A.; Franks, S.; Kalma, J.; Loughran, R.; Rowan, J. (2003). Multi-parameter fingerprinting of sediment deposition in a small gullied catchment in SE Australia. *Catena* 53(4): 327-348

Kung, S.Y.; Chiang, T.C. (1977). Soil erosion and its control in small gully watersheds in the rolling loess area on the middle reaches of the Yellow River. [S.n.]: Peking. 21 p.

Lane, S.; Flanagan, S.; Wilde, F. (2003). Chapter A2: Selection of Equipment for Water Sampling (Ver.2.0). In: Techniques of Water-Resources Investigations. Book 9: National Field Manual for the Collection of Water-Quality Data. US Geological Survey: Reston, Va. 123 p. Available at http://water.usgs.gov/owq/FieldManual/Chapter2/Chapter2_V2uncompressed.pdf [accessed 15/12/2004]

Langley, S.; Gault, A.G.; Ibrahim, A.; Takahashi, Y; Renaud, R.; Fortin, D; Clark, I.D.; Ferris, F.G. (2009). Sorption of strontium onto bacteriogenic iron oxides. *Environ. Sc. & Techn.* 43(4): 1008-1014.

Lebbe, L.C. (1999). Hydraulic parameter identification: generalized interpretation method for single and multiple pumping tests. Springer: Berlin, p. 359.

Lefrançois, J.; Grimaldi, C.; Gascuel-Odoux, C.; Gilliet, N. (2007). Suspended sediment and discharge relationships to identify bank degradation as a main sediment source on small agricultural catchments. *Hydrol. Process.* 21(21): 2923-2933

Lenzi, M.A.; Mao, L.; Comiti, F. (2003). Interannual variation of suspended sediment load and sediment yield in an alpine catchment. *Hydrological Sciences Journal* 48(6): 899-915

Lenzi, M.A.; Marchi, L. (2000). Suspended sediment load during floods in a small stream of the Dolomites (northeastern Italy). *Catena* 39(4): 267-282

Lewin, J.; Wolfenden, P.J. (1978). The assessment of sediment sources: a field experiment. *Earth Surface Processes* 3(2): 171-178

Lewis, J. (1996). Turbidity-controlled suspended sediment sampling for runoff-event load estimation. *Water Resour. Res.* 32(7): 2299-2310

Li, D.H.; Ganczarczyk, J.J. (1987). Stroboscopic determination of settling velocity, size and porosity of activated sludge flocs. *Water Res.* 21(3): 257-262

Lietz, A.C; Debiak, E.A. (2005). Development of Rating Curve Estimators for Suspended-Sediment Concentration and Transport in the C-51 Canal Based on Surrogate Technology, Palm Beach County, Florida, 2004-05. *Open-File Report 2005-1394*. U.S. Geological Survey: Ft. Lauderdale, FL. 19 p. Available at http://pubs.usgs.gov/of/2005/1394/ [accessed July 9, 2009].

Lijklema, L. (1979). Binding van o-fosfaat door ijzer (III)-en aluminiumhydroxiden; theorie en praktische betekenis. H2O 12 (23), 511–513.

Luyendyk, B.P. (2012) Authigenic sediment (geology) [ONLINE]. Encyclopædia Britannica, Inc. Available at http://www.britannica.com/EBchecked/topic/44632/authigenic-sediment [Accessed 28-12-2012]

Malvern Instruments (2007). Mastersizer 2000 User Manual – Mano384 Issue 1.0. Malvern Instruments Ltd.: Worcestershire. P. 152.

Maréchal, R.; Laga, P. (1988). Voorstel lithostratigrafische indeling van het Paleogeen. Belgisch Geologische Dienst: Brussel. 52-58.

Martin, G.R.; Smoot, J.L.; White, K.D. (1992). A comparison of surface-grab and cross sectionally integrated stream-water-quality sampling methods. *Water Environ. Res.*: 866-876

Martínez-Carreras, N.; Krein, A.; Udelhoven, T.; Gallart, F.; Iffly, J.F.; Hoffmann, L.; Pfister, L.; Walling, D.E. (2010). A rapid spectral-reflectance-based fingerprinting approach for documenting suspended sediment sources during storm runoff events. *Journal of Soils and Sediments* 10(3): 400-413

McDowell, R.; Wilcock, R. (2004). Particulate phosphorus transport within stream flow of an agricultural catchment. *J. Environ. Qual.* 33(6): 2111-2121

McGraw-Hill (2003). McGraw-Hill Dictionary of Scientific & Technical Terms, 6E. The McGraw-Hill Companies, Inc.: New York. p. 2380.

Meade, R.H.; Dunne, T.; Richey, J.E.; Santos, U.M.; Salati, E. (1985). Storage and remobilization of suspended sediment in the lower Amazon River of Brazil. *Science* 228(4698): 488-490

Mikes, D.; Verney, R.; Lafite, R.; Belorgey, M. (2004). Controlling factors in estuarine flocculation processes: experimental results with material from the Seine estuary, northwestern France. *J. Coast. Res.* 82-89

Miller, C.R. (1951). Analysis of Flow-duration: Sediment-rating Curve Method of Computing Sediment Yield. United States Department of Interior, Bureau of Reclamation: Denver. 15p.

Minella, J.P.G.; Merten, G.H.; Reichert, J.M.; Clarke, R.T. (2008 a). Estimating suspended sediment concentrations from turbidity measurements and the calibration problem*. Hydrol. Process.* 22(12): 1819-1830

Minella, J.P.G.; Walling, D.E.; Merten, G.H. (2008 b). Combining sediment source tracing techniques with traditional monitoring to assess the impact of improved land management on catchment sediment yields*. Journal of Hydrology* 348(3): 546-563

Morgan, R.; Quinton, J.; Smith, R.; Govers, G.; Poesen, J.; Auerswald, K.; Chisci, G.; Torri, D.; Styczen, M. (1998). The European Soil Erosion Model (EUROSEM): a dynamic approach for predicting sediment transport from fields and small catchments*. Earth Surf. Process. Landforms* 23(6): 527-544

Morris, G.L.; Fan, J. (1998). Reservoir sedimentation handbook: Design and management of dams, reservoirs, and watersheds for sustainable use. McGraw-Hill: New York. p. 848

Motha, J.A.; Wallbrink, P.J.; Hairsine, P.B.; Grayson, R.B. (2003). Determining the sources of suspended sediment in a forested catchment in southeastern Australia. *Water Resour Res*.39 (3):1056.

Mukundan, R.; Radcliffe, D.E.; Ritchie, J.C. (2011). Channel stability and sediment source assessment in streams draining a Piedmont watershed in Georgia, USA*. Hydrol. Process.* 25: 1243-1253

Nathan, R.J.; McMahon, T.A. (1992). Estimating low flow characteristics in ungauged catchments*. Water Resour. Manage.* 6(2): 85-100

Navratil, O.; Evrard, O.; Esteves, M.; Legout, C.; Ayrault, S.; Némery, J.; Mate-Marin, A.; Ahmadi, M.; Lefèvre, I.; Poirel, A. (2012). Temporal variability of suspended sediment sources in an alpine catchment combining river/rainfall monitoring and sediment fingerprinting*. Earth Surf. Process. Landforms.* John Wiley & Sons: New York. 19p.

Neitsch, S.L.; Arnold, J.G.; Kiniry, J.R.; Srinivasan, R.; Williams, J.R. (2005). Soil and Water Assessment Tool Theoretical Documentation, version 2005. Grassland, Soil and Water Research Laboratory, Agricultural Research Service: Temple, TX. 494 p. Available at http://swat.tamu.edu/media/1292/swat2005theory.pdf [accessed 10/01/2013].

Nopens, I. (2005). Modelling the activated sludge flocculation process: a population balance approach. Doctoral Thesis. Faculty of Bioscience Engineering. Ghent University: Ghent. 293 p.

Nosrati, K.; Govers, G.; Ahmadi, H.; Sharifi, F.; Amoozegar, M.A.; Merckx, R.; Vanmaercke, M. (2011). An exploratory study on the use of enzyme activities as sediment tracers: biochemical fingerprints?*. International Journal of Sediment Research* 26(2): 136-151

Olive, L.; Rieger, W. (1992). Stream suspended sediment transport monitoring-why, how and what is being measured. In: Bogen, J.; Walling, D.E.; Day, T.J. (eds) Erosion and Sediment Transport Monitoring Programmes in River Basins. *IAHS Publ.* 210. IAHS Press: Wallingford. pp. 245-254

Olley, J.; Murray, A.; Mackenzie, D.; Edwards, K. (1993). Identifying sediment sources in a gullied catchment using natural and anthropogenic radioactivity*. Water Resour. Res.* 29(4): 1037-1043

Ongley, E.D. (1992). Environmental quality: changing times for sediment programs*.* In: Bogen, J.; Walling, D.E.; Day, T.J. (eds) Erosion and Sediment Transport Monitoring Programmes in River Basins. *IAHS Publ.* 210. IAHS Press: Wallingford. pp. 379-389

Ongley, E.D.; Blachford, D.P. (1982). Application of continuous flow centrifugation to contaminant analysis of suspended sediment in fluvial systems*. Environ. Technol.* 3(1-11): 219-228

Ongley, E.D.; Thomas, R.L. (1989). Dewatering suspended solids by continuous-flow centrifugation: Practical considerations. *Hydrol. Process.* 3(3): 255-260

Orwin, J.F.; Smart, C.C. (2004). The evidence for paraglacial sedimentation and its temporal scale in the deglacierizing basin of Small River Glacier, Canada. *Geomorphology* 58(1): 175-202

Osán, J.; Török, S.; Alföldy, B.; Alsecz, A.; Falkenberg, G.; Baik, S.Y.; Van Grieken, R. (2007). Comparison of sediment pollution in the rivers of the Hungarian Upper Tisza Region using non-destructive analytical techniques. *Spectrochimica Acta Part B: Atomic Spectroscopy* 62(2): 123-136

Ott, R. (1993). An introduction to statistical methods and data analysis. Duxbury Prress: Belmont, CA. 1051 p.

Overloop S., Tits M., Elsen A., Bries J., Govers G., Verstraeten G., Van Rompaey A., Poesen J., Notebaert B., Ruysschaert G., De Meyer A., Tirry D., Gulinck H., Van Orshoven J., Cardon M., D'Haene K., Oorts K., Maene S. (2011). Milieurapport Vlaanderen, Achtergronddocument 2010, Bodem. Vlaamse Milieumaatschappij: Erembodegem. pp.140. available at http://www.milieurapport.be/Upload/main/miradata/MIRA-T/02_themas/02_15/AG_bodem.pdf [accessed 25-8-2012]

Peart, M.R. (1984). Sediment sources in two Devon catchments. Unpublished Ph.D. thesis. University of Exeter, UK.

Peart, M.R.; Walling, D. (1986). Fingerprinting sediment source: the example of a drainage basin in Devon, UK. In: Hadley, F. (ed) Drainage Basin Sediment Delivery. *IAHS Publ.* 159. IAHS Press: Wallingford. pp. 41-51

Peart, M.R.; Walling, D. (1988). Techniques for establishing suspended sediment sources in two drainage basins in Devon, UK: a comparative assessment. In: Bordas, M.P.; Walling, E.D. (eds) Sediment Budgets. *IAHS Publ.* 174. IAHS Press: Wallingford. pp. 269-279

Pfannkuche, J.; Schmidt, A. (2003). Determination of suspended particulate matter concentration from turbidity measurements: particle size effects and calibration procedures. *Hydrol. Process.* 17(10): 1951-1963

Phillips, J.; Russell, M.; Walling, D. (2000). Time-integrated sampling of fluvial suspended sediment: a simple methodology for small catchments. *Hydrol. Process.* 14(14): 2589-2602

Poesen, J.W.A.; Verstraeten, G.; Soenens, R.; Seynaeve, L. (2001). Soil losses due to harvesting of chicory roots and sugar beet: an underrated geomorphic process?. *Catena* 43(1): 35-47

Rasmussen, P.P.; Gray, J.R.; Glysson, G.D.; Ziegler, A.C. (2009). Chapter C4: Guidelines and procedures for computing time-series suspended-sediment concentrations and loads from in-stream turbidity-sensor and stream flow data. In: Techniques and Methods. Book 3: Application of Hydraulics. U.S. Geological Survey: Reston, VA. 53 p. Available at http://pubs.usgs.gov/tm/tm3c4/pdf/TM3C4.pdf [accessed 12/12/2012]

Rasmussen, P.P.; Ziegler, A.C.; Garner, B.D.; Jian, X. (2010). Methods for Computing Water Quality Using Regression Analysis, NRTWQ - Kansas Real-Time Water Quality program of the USGS [ONLINE], Department of the Interior, US Geological Survey. Available at http://nrtwq.usgs.gov/ks/methods/ [accessed 02-04-2010]

Rasmussen, T.J.; Lee, C.J.; Ziegler, A.C. (2008). Estimation of constituent concentrations, loads, and yields in streams of Johnson County, northeast Kansas, using continuous water-quality monitoring and regression models, October 2002 through December 2006. Scientific Investigations Report 2008–5014. U.S. Geological Survey: Reston, Va. 103 p. Available at http://pubs.usgs.gov/sir/2008/5014/pdf/SIR2008-5014.pdf [accessed 2-04-2010]

Rees, T.F.; Leenheer, J.A.; Ranville, J.F. (1991). Use of a single-bowl continuous-flow centrifuge for dewatering suspended sediments: Effect on sediment physical and chemical characteristics. *Hydrol. Process.* 5(2): 201-214

Richards, K.S. (1982). Rivers: Form and process in alluvial channels. Methuen: London. 361 p.

Riley, S. (1998). The sediment concentration-turbidity relation: its value in monitoring at Ranger Uranium Mine, Northern Territory, Australia. *Catena* 32(1): 1-14

Rodríguez-Blanco, M.; Taboada-Castro, M.; Taboada-Castro, M. (2010). Factors controlling hydro-sedimentary response during runoff events in a rural catchment in the humid Spanish zone. *Catena* 82(3): 206-217

Rowan, J.S.; Goodwill, P.; Franks, S.W. (2000). Uncertainty estimation in fingerprinting suspended sediment sources. In: Foster, I.D.L. (ed) Tracers in Geomorphology. Chichester7 Wiley. pp. 279-90.

Russell, M.A.; Walling, D.E.; Hodgkinson, R.A. (2001). Suspended sediment sources in two small lowland agricultural catchments in the UK. *Journal of Hydrology* 252(1): 1-24

Salant, N.L.; Hassan, M.A.; Alonso, C.V. (2008). Suspended sediment dynamics at high and low storm flows in two small watersheds. *Hydrol. Process.* 22(11): 1573-1587

Sharp, Z.D. (1990). A laser-based microanalytical method for the in situ determination of oxygen isotope ratios of silicates and oxides. Geochim. Cosmochim. Acta 54, 1353-1357.

Simons, D.B.; Sentürk, F. (1977). Sediment transport technology. Water Resources Publications: Fort Collins, CO.

Sloto, R.A.; Crouse, M.Y. (1996). HYSEP: A computer program for stream flow hydrograph separation and analysis. Water-Resources Investigations report 96-4040. US Geological Survey: Lemoyne, PA. 46 p.

Small, I.F.; Rowan, J.S.; Franks, S.W. (2002). Quantitative sediment fingerprinting using a Bayesian uncertainty estimation framework. The Structure, Function and Management Implications of Fluvial Sedimentary Systems. (Proceedings Alice Springs Symposium, 2002). *IAHS Publ.* 276. IAHS Press: Wallingford. pp. 443-450.

Small, I.F.; Rowan, J.S.; Duck, R.W.; Dyer, T.D.; Franks, S.W.; Wyatt, A. (2005). Can reservoir bottom sediments in the estimation of long-term catchment sediment budgets? In: Walling, D.E.; Horowitz, A.J. (eds) Sediment Budgets (Vol. 2). *IAHS Publ.* 292. IAHS Press: Wallingford. pp. 231-238

Spicuzza, M.J.; Valley, J.W.; Kohn, M.J.; Girard, J.P.; Fouillac, A.M. (1998). The rapid heating, defocused beam technique: a CO2-laser-based method for highly precise and accurate determination of δ18O values of quartz. *Chem. Geol.* 144: 195-203.

Spronk, G.; Bakker, I. (2012). Afstemming deeltjesgroottebepaling tbv MONEOS. VNSC - werkgroep O&M - projectgroep Monitoring en Data: Bergen-op-Zoom. 51 p.

Steegen, A.; Govers, G.; Nachtergaele, J.; Takken, I.; Beuselinck, L.; Poesen, J. (2000). Sediment export by water from an agricultural catchment in the Loam Belt of central Belgium. *Geomorphology* 33(1): 25-36

Strömqvist, J.; Collins, A.; Davison, P.; Lord, E. (2008). PSYCHIC–A process-based model of phosphorus and sediment transfers within agricultural catchments. Part 2. A preliminary evaluation. *Journal of Hydrology* 350(3): 303-316

Stumm, W.; Morgan, J.J. (1970). Aquatic Chemistry; An Introduction Emphasizing Chemical Equilibria in Natural Waters. Wiley-Interscience: New York. 583 p.

Stumm, W.; Morgan, J.J. (1996). Aquatic chemistry: chemical equilibrium and rates in natural waters. John Wiley: New York. 1022 p.

Stutter, M.; Langan, S.; Lumsdon, D.; Clark, L. (2009). Multi-element signatures of stream sediments and sources under moderate to low flow conditions*. Appl. Geochem.* 24(5): 800-809

Syncera Water N.V. (2005). Emissie-inventaris water: metalen, Eindrapport project W03A0067 [Report] (pdf document) Vlaamse Milieumaatschappij. 40p. Available at http://www.vmm.be/publicaties/w03a0067_eindrapport.pdf [Accessed 26/08/2011]

Taylor, H.; Garbarino, J.; Brinton, T. (1990). The occurrence and distribution of trace metals in the Mississippi River and its tributaries*. Sci. Total Environ.* 97: 369-384

Teledyne Technologies Incorporated (2012). Teledyne Isco – Products - 6712FR Fiberglass Refrigerated Sampler [ONLINE] Teledyne Technologies Incorporated. Available at http://www.isco.com/products/products3.asp?PL=201202010 [accessed 12/12/2012]

Tessier, A. (1992). Sorption of trace elements on natural particles in oxic environments. In: Buffle, J.; van Leeuwen, H.P. (eds) Environmental Particles vol. 1. Lewis Publishers Inc: Chelsea, Michigan: 425-453

Thornbury, W.D. (1954). Principles of geomorphology. John Wiley & Sons, Inc.: New York. 618 p.

Thorne, L.T.; Nickless, G. (1981). The relation between heavy metals and particle size fractions within the Severn estuary (UK) inter-tidal sediments*. Sci. Total Environ.* 19(3): 207-213

Truhlar, J. (1978). Determining suspended sediment loads from turbidity records/La détermination des charges en suspension des rapports sur la turbidité*. Hydrological Sciences Journal* 23(4): 409-417

Uhrich, M.A.; Bragg H.M. (2003). Monitoring in-stream turbidity to estimate continuous suspended-sediment sediment loads and clay-water volumes in the upper North Santiam River Basin, Oregon, 1998–2000. Water-Resources Investigations Report 03-4098. US Geological Survey: Portland, Oregon. 43 p. Available at http://pubs.usgs.gov/wri/WRI03-4098/pdf/wri034098.pdf [accessed 14-06-2010]

USEPA (1999). Protocol for Developing Sediment TMDLs. EPA 841-B-99-004. United States Environmental Protection Agency. Office of Water(4503F): Washington, DC. 132 p. Available at http://www.epa.gov/owowwtr1/tmdl/sediment/pdf/sediment.pdf [accessed 1/10/2012].

Van Den Eeckhaut M.; Poesen J.; Verstraeten G. (2007). Opstellen van een gevoeligheidskaart met betrekking tot massabewegingen (massatransport) voor de Vlaamse Ardennen. Rapport in opdracht van Vlaamse Overheid, Departement Leefmilieu, Natuur en Energie, Afdeling Land en Bodembescherming, Ondergrond, Natuurlijke Rijkdommen. K.U.Leuven. Onderzoeksgroep Fysische en Regionale Geografie: Leuven. 97 p.

Van Der Beken, A.; Huybrechts, W. (1990). De Waterbalans van het Vlaams Gewest, Een rationeel Waterbeheer via kennis van de Waterbalans*. Water (*50): 88-92

Van Eetvelt, B. (2007). Studie van geflocculeerd ijzerhoudend sediment in het Netebekken. Unpublished bachelor internship report. Faculty of Sciences, Ghent University: Ghent. pp. 65.

Van Hoestenberghe, T.; Eylenbosch, J.; Voet, M. (2006). Sedimenttransport meten in onbevaarbare waterlopen in Vlaanderen. *Water,* 26(1): 9-17

Van Hoestenberghe, T. (2008). Sedimenttransport meten in onbevaarbare waterlopen in Vlaanderen. Vlaamse Milieumaatschappij: Erembodegem. 126 p.

Van Kerckhoven, S.; Riksen, M.; Cornelis, W.M. (2009). Afbakening van gebieden gevoelig aan winderosie in Vlaanderen. Eindrapport. Universiteit Gent, Vakgroep Bodembeheer: Gent 79p.

Van Leussen, W. (1994). Estuarine macroflocs and their role in fine-grained sediment dynamics. Unpublished Ph.D. Thesis, Universiteit Utrecht, Netherlands. 488 p.

Van Meel, K. (2009). Application of high-energy polarized-beam energy-dispersive X-ray fluorescence for industrial and environmental purposes. Unpublished Ph.D. thesis, University of Antwerp: Antwerp. 249 p.

Van Meel, K.; Vanlierde, E.; Collins, A.L.; De Cooman, W.; Makarovska, Y.; Mostaert, F.; Jacobs, P.; Van Grieken, R. (2008). EDXRF for fingerprinting fine-grained sediment sources in the Demer basin, Belgium. In: Fazinic, S. et al. (Eds.). EXRS 2008. European Conference on X-Ray Spectrometry, 16th - 20th June 2008, Cavtat, Dubrovnik, Croatia: book of abstracts. 77 p.

Van Meel, K.; Vanlierde, E.; Collins, A.L.; Margui, E.; Queralt, I.; De Schutter, J.; Jacobs, P.; Van Grieken, R.; Mostaert, F. (2010). Discriminating tributaries in the River Demer drainage basin, Belgium, using chemical, physical and mineralogical properties. In: Caracciolo, L. et al. (eds.). 60 p.

Van Muysen, W.; Govers, G.; Van Oost, K.; Van Rompaey, A. (2000). The effect of tillage depth, tillage speed, and soil condition on chisel tillage erosivity. *J. Soil Water Conserv.* 55(3): 355-364

Van Oost, K.; Govers, G.; Desmet, P. (2000). Evaluating the effects of changes in landscape structure on soil erosion by water and tillage. *Landscape Ecol.* 15(6): 577-589

Van Rompaey, A.; Krasa, J.; Dostal, T.; Govers, G. (2003). Modelling sediment supply to rivers and reservoirs in Eastern Europe during and after the collectivisation period. *Hydrobiologia* 494(1): 169-176

Vance, D.B. (1994). Iron — The environmental impact of a universal element. *National Environmental Journal* 4(3): 24-25

Vanhoof, C.; Corthouts, V.; Tirez, K. (2004). Energy-dispersive X-ray fluorescence systems as analytical tool for assessment of contaminated soils. *J. Environ. Monit.* 6(4): 344-350

Vanlierde, E. (2003). Sedimenttransport in het Scheldebekken: een bijdrage tot de optimalisatie van het meetnet en tot de voorbereiding van de modellering van het transport. MSc Thesis. Universiteit Gent: Gent. 250 pp.

Vanlierde, E.; De Schutter, J.; Jacobs, P.; Mostaert, F. (2006). Authigeen sediment: een belangrijke bijdrage tot de totale sedimentlading van de Kleine Nete, *Water* 26(2): pp. 71-74

Vanlierde, E.; De Schutter, J.; Jacobs, P.; Mostaert, F. (2007 a). Estimating and modeling the annual contribution of authigenic sediment to the total suspended sediment load in the Kleine Nete Basin, Belgium. *Sediment. Geol.* 202(1): 317-332

Vanlierde, E.; De Schutter, J.; Meys, J.F.A.; Mostaert, F.; Jacobs, P. (2005 a). Contributions of authigenic iron compounds to fluvial suspended sediment concentrations and fluxes in the Nete sub-basin, Belgium. In: Walling, D.E.; Horowitz, A.J. (eds) Sediment Budgets (Vol. 1). *IAHS Publ.* 291. IAHS Press: Wallingford. pp. 54-63

Vanlierde, E.; De Schutter, J.; Meys, J.F.A.; Mostaert, F.; Jacobs, P. (2005 b). The composition of authigenic iron compounds and its contribution to fluvial suspended sediment concentrations and fluxes in the Nete Basin, Belgium. In: Faganeli, J.; Ogrinc, N.; Horvat, M. (eds) RMZ - Materials and Geoenvironment: periodical for mining, metallurgy and geology 52(1): 360

Vanlierde, E.; De Schutter, J.; Van Eetvelt, B.; Janssens, R.; Mostaert, F.; Jacobs, P. (2007 b). Modeling the contribution of autigenic fluvial sediment to the total suspended sediment load in the Kleine Nete: the MARS-model, version 2.0 River. In: Proceedings of the tenth International Symposium on River Sedimentation, Effects of River Sediments and Channel Processes on Social, Economic and Environmental Safety, p 301-310

Vanlierde, E.; Van Meel, K.; De Cooman, W.; Mostaert, F. (2008) Sediment fingerprinting in the Demer basin: procedural notes, Versie 2.0. WL Rapporten, 613b_07. ADAS/Flanders Hydraulics Research/UA/UGent/VMM: Antwerpen. 5 p. +1 cd-rom.

VanSickle, J.; Beschta, R.L. (1983). Supply-based models of suspended sediment transport in streams*. Water Resour. Res.* 19(3): 768-778

Vereecken, H.; Mostaert, F. (2012). Instructie: EWI's. I-WL-PP33-5 Versie 01. Waterbouwkundig Laboratorium: Antwerpen. 10 p.

Vereecken, H.; Mostaert, F. (2013 a). Instructie: Nemen van schepstalen met verzwaarde fles. I-WL-PP33-8 Versie 01. Waterbouwkundig Laboratorium: Antwerpen. 3 p.

Vereecken, H.; Mostaert, F. (2013 b). Instructie: Onderhoud & Gebruik van de Automatische pompsamplers. I-WL-PP34-1 Versie 01. Waterbouwkundig Laboratorium: Antwerpen. 8 p.

Vereecken, H.; Mostaert, F. (2013 c). Instructie: Onderhoud & Gebruik van de Emmie Alfa Laval doorstroomcentrifuge. I-WL-PP33-9 Versie 01. Waterbouwkundig Laboratorium: Antwerpen. 16 p.

Verstraeten, G.; Oost, K.; Rompaey, A.; Poesen, J.; Govers, G. (2002). Evaluating an integrated approach to catchment management to reduce soil loss and sediment pollution through modelling*. Soil use Manage.* 18(4): 386-394

VITO (2012) Compendium voor Monsterneming en Analyse (CMA) | EMIS energie-en milieu-informatiesysteem voor het Vlaams Gewest [ONLINE] VITO. Available at http://www.emis.vito.be/referentielabo-ovam [accessed 08/01/2013]

VLM (1997). Fosfaatverzadiging van zandige bodems in Vlaanderen. VLM: Brussel. 143 p.

VMM (2008 a). Grondwater in Vlaanderen: het Centraal Kempisch Systeem. Vlaamse Milieumaatschappij: Erembodegem. 110 p.

VMM (2008 b). Grondwater in Vlaanderen: het Brulandkrijtsysteem. Vlaamse Milieumaatschappij: Erembodegem. 125 p.

VMM (2012). Procedure voor de monsterneming en verdeling van oppervlaktewater t.b.v. fysisch-chemisch onderzoek d.m.v. een schepmonster. VMM/WAT/GP/3.105.

Walden, J.; Slattery, M.C.; Burt, T.P. (1997). Use of mineral magnetic measurements to fingerprint suspended sediment sources: approaches and techniques for data analysis*. Journal of Hydrology* 202(1-4): 353-372

Walling, D.E. (1974). Suspended sediment and solute yields from a small catchment prior to urbanization. In: Gregory, K.J.; Walling, D.E. (Eds.) Fluvial Processes in Instrumented Watersheds. *Spec. Pub*. 6. Inst. Bri. Geogr. Spec.: London. pp. 169-192.

Walling, D.E. (1977 a). Assessing the accuracy of suspended sediment rating curves for a small basin*. Water Resour. Res.* 13(3): 531-538

Walling, D.E. (1977 b). Limitations of the rating curve technique for estimating suspended sediment loads, with particular reference to British rivers. In: Erosion and Solid Matter Transport in Inland Waters. *IAHS Publ.* 122. IAHS Press: Wallingford. pp.34-48

Walling, D.E. (2000). Tracing suspended sediment sources in river basins: progress, problems and prospects. in: Australia Proceedings of Advisory group meeting on Sediment tracing (fingerprinting) by nuclear techniques and their application to the assessment of the effectiveness of erosion and sedimentation remediation strategies with emphasis on dam sustainability (AG-1090) Isotope Hydrology Section (IAEA), 10-12 October 2000, Vienna, Australia. pp. 25

Walling, D.E. (2003). Using environmental radionuclides as tracers in sediment budget investigations. In: Bogen, J.; Fergus, T.; Walling, D.E. (eds.) Erosion and Sediment Transport Measurement in Rivers: Technological and Methodological Advances. *IAHS Publ.* 283. IAHS Press: Wallingford. pp. 57-78

Walling, D.E. (2005). Tracing suspended sediment sources in catchments and river systems*. Sci. Total Environ.* 344(1-3): 159-184

Walling, D.E.; Collins, A.L. (2000). Integrated Assessment of Catchment Sediment Budgets: A Technical Manuel. Department for International Development. University of Exeter: Exeter. 168 p.

Walling, D.E.; Collins, A.L.; McMellin, G. (2003). A reconnaissance survey of the source of interstitial fine sediment recovered from salmonid spawning gravels in England and Wales*. Hydrobiologia* 497(1): 91-108

Walling, D.E.; Owens, P.N.; Leeks, G.J.L. (1999). Fingerprinting suspended sediment sources in the catchment of the River Ouse, Yorkshire, UK*. Hydrol. Process.* 13(7): 955-975

Walling, D.E.; Webb, B.W. (1981). Reliability of suspended sediment load data. In: Erosion and Sediment Transport Measurement. IAHS Publ. 133. IAHS Press: Wallingford. pp. 279-288

Walling, D.E.; Webb, B.W. (1983). Dissolved Loads of Rivers: A Global Overview. In: Webb, B.W. (ed) Dissolved Loads of Rivers and surface water quantity/quality relationships. *IAHS Publ.* 141. IAHS Press: Wallingford. pp. 3-20

Walling, D.E.; Webb, B.W. (1985). Estimating the discharge of contaminants to coastal waters by rivers: some cautionary comments*. Mar. Pollut. Bull.* 16(12): 488-492

Walling, D.; Webb, B. (1988). The reliability of rating curve estimates of suspended sediment yield: some further comments*.* In: Bordas, M.P.; Walling, E.D. (eds) Sediment Budgets. *IAHS Publ.* 174. IAHS Press: Wallingford. pp. 337-350

Walling, D.; Webb, B.; Woodward, J. (1992). Some sampling considerations in the design of effective strategies for monitoring sediment-associated transport*.* In: Bogen, J.; Walling, D.E.; Day, T.J. (eds) Erosion and Sediment Transport Monitoring Programmes in River Basins. *IAHS Publ.* 210. IAHS Press: Wallingford. pp. 279-288

Walling, D.E.. Woodward, J.C.. Nicholas, A.P. (1993). A multi-parameter approach to fingerprinting suspended sediment sources. In: Peters, N.E. et al. (eds.) Tracers in Hydrology. *IAHS Publ.* 215. IAHS: Wallingford. pp. 329– 337

Wilde, F.D. (2006). Chapter A4: Collection of water samples (ver. 2.0). In: Techniques of Water-Resources Investigations. Book 9: U.S. Geological Survey: Reston, Va. Available at http://pubs.water.usgs.gov/twri9A4/ [accessed 11-08-2011]

Wilkinson, S.N.; Hancock, G.J.; Bartley, R.; Hawdon, A.A.; Keen, R. (2012). Using sediment tracing to assess processes and spatial patterns of erosion in grazed rangelands, Burdekin River basin, Queensland, Australia. Agriculture, Ecosystems and Environment, DOI: 10.1016/j.agee.2012.02.002

Wilkinson, S.N; Wallbrink, P.J.; Hancock, G.J.; Blake, W.H.; Shakesby, R.A.; Doerr, S.H. (2009). Fallout radionuclide tracers identify a switch in sediment sources and transport-limited sediment yield following wildfire in a eucalypt forrest*. Geomorphology* 110(3): 140-151

Willems, P. (2000). Probabilistic Modeling of the Emission Receiving Surface Waters. Unpublished Ph.D. thesis, Katholieke Universiteit Leuven: Leuven

Williams, G.P. (1989). Sediment concentration versus water discharge during single hydrologic events in rivers*. Journal of Hydrology* 111(1): 89-106

Wittenberg, H. (1999). Baseflow recession and recharge as nonlinear storage processes*. Hydrol. Process.* 13(5): 715-726

Wood, P. (1977). Controls of variation in suspended sediment concentration in the River Rother, West Sussex, England*. Sedimentology* 24(3): 437-445

Yang, C.T.; Simões, F.J. (2005). Wash load and bed-material load transport in the Yellow River*. J. Hydraul. Eng.* 131(5): 413-418

Young, R.A.; Onstad, C.A.; Bosch, D.D.; Anderson, W.P. (1989). AGNPS: A nonpoint-source pollution model for evaluating agricultural watersheds*. J. Soil Water Conserv.* 44(2): 168-173

YSI (2012 a). YSI 6920 V2 – Water Quality Sonde for Unattended Monitoring of Dissolved Oxygen and More [ONLINE]. Available at http://www.ysi.com/productsdetail.php?6920-V2-3 [accessed 20/12/2012]

YSI (2012 b). Water Quality Sonde for CTD, Dissolved Oxygen, Chlorophyll; and More - YSI 6600 V2 Sonde [ONLINE]. Available at http://www.ysi.com/productsdetail.php?6600V2-1 on 20/12/2012.

Addenda

Addendum A: Aquifer and Aquitard systems as defined in the HCOV system

Table A.1: Aquifer and Aquitard systems as defined in the HCOV system of the VLAREM I regulations (Order of the Flemish Government of 6 February 1991 concerning Environmental Licences).

HOOFDEENHEID		SUB-EENHEID		BASISEENHEID	
0000	ONBEPAALD				
0100	QUARTAIRE AQUIFERSYSTEMEN	0110	Ophogingen		
		0120	Duinen		
		0130	Polderafzettingen	0131	Kleiige polderafzettingen van de kustvlakte
				0132	Kleiige polderafzettingen van het Meetjesland
				0133	Kleiige polderafzettingen van Waasland-Antwerpen
				0134	Zandige kreekruggen
				0135	Veen-kleiige poelgronden
		0140	Alluviale deklagen		
		0150	Deklagen	0151	Zandige deklagen
				0152	Zand-lemige deklagen
				0153	Lemige deklagen
				0154	Kleiige deklagen
		0160	Pleistocene afzettingen	0161	Pleistoceen van de Kustvlakte
				0162	Pleistoceen van de Vlaamse Vallei
				0163	Pleistoceen van de riviervalleien
		0170	Maas- en Rijnafzettingen	0171	Afzettingen Hoofdterras
				0172	Afzettingen Tussenterrassen
				0173	Afzettingen Maasvlakte
0200	KEMPENS AQUIFERSYSTEEM	0210	Kiezeloölietformatie ten noorden van Feldbiss	0211	Zandige eenheid boven de Brunssum I-klei
				0212	Brunssum I-klei
				0213	Zand van Pey
				0214	Brunssum II-klei
				0215	Zand van Waubach
		0220	Klei-zand-complex van de Kempen	0221	Klei van Turnhout
				0222	Zand van Beerse
				0223	Klei van Rijkevorsel
		0230	Pleistoceen en Plioceen Aquifer	0231	Zanden van Brasschaat en/of Merksplas
				0232	Zand van Mol
				0233	Zandige top van Lillo
				0234	Zand van Poederlee en/of zandige top van Kasterlee
		0240	Pliocene kleiige laag	0241	Kleiig deel van Lillo en/of van de overgang Lillo-Kattendijk
				0242	Kleiige overgang tussen de zanden van Kasterlee en Diest
		0250	Mioceen Aquifersysteem	0251	Zand van Kattendijk en/of onderste zandlaag van Lillo
				0252	Zand van Diest
				0253	Zand van Bolderberg
				0254	Zanden van Berchem en/of Voort
				0255	Klei van Veldhoven
				0256	Zand van Eigenbilzen

0300	**BOOM AQUITARD**			0301	Kleiig deel van Eigenbilzen
				0302	Klei van Putte
				0303	Klei van Terhagen
				0304	Klei van Belsele-Waas
0400	**OLIGOCEEN AQUIFERSYSTEEM**	0410	Zand van Kerniel	Zand van Kerniel	
		0420	Klei van Kleine-Spouwen	Klei van Kleine-Spouwen	
		0430	Ruisbroek-Berg Aquifer	0431	Zand van Berg
				0432	Zand van Kerkom
				0433	Kleiig zand van Oude Biezen
				0434	Zand van Boutersem
				0435	Zand van Ruisbroek
				0436	Zand van Wintham
		0440	Tongeren Aquitard	0441	Klei van Henis
				0442	Klei van Watervliet
		0450	Onder-Oligoceen Aquifersysteem	0451	Zand van Neerrepen
				0452	Zand-klei van Grimmertingen
				0453	Kleiig zand van Bassevelde
0500	**BARTOON AQUITARDSYSTEEM**			0501	Klei van Onderdijke
				0502	Zand van Buisputten
				0503	Klei van Zomergem
				0504	Zand van Onderdaele
				0505	Kleien van Ursel en/of Asse
0600	**LEDO PANISELIAAN BRUSSELIAAN AQUIFERSYSTEEM**	0610	Wemmel-Lede Aquifer	0611	Zand van Wemmel
				0612	Zand van Lede
		0620	Zand van Brussel	Zand van Brussel	
		0630	Afzettingen van het Boven-Paniseliaan	0631	Zanden van Aalter en/of Oedelem
				0632	Zandige klei van Beernem
		0640	Zandige afzettingen van het Onder-Paniseliaan	Zand van Vlierzele en/of Aalterbrugge	
0700	**PANISELIAAN AQUITARD**			0701	Klei van Pittem
				0702	Klei van Merelbeke
0800	**IEPERIAAN AQUIFER**			Zand van Egem en/of Mont-Panisel	
0900	**IEPERIAAN AQUITARDSYSTEEM**	0910	Silt van Kortemark	Silt van Kortemark	
		0920	Afzettingen van Kortrijk	0921	Klei van Aalbeke
				0922	Klei van Moen
				0923	Zand van Mons-en-Pévèle
				0924	Klei van Saint-Maur
				0925	Klei van Mont-Héribu
1,000	**PALEOCEEN AQUIFERSYSTEEM**	1010	Landeniaan Aquifersysteem	1011	Zand van Knokke
				1012	Zandige afzettingen van Loksbergen en/of Dormaal
				1013	Zand van Grandglise
				1014	Kleiig deel van Lincent
				1015	Versteend deel van Lincent
		1020	Landeniaan en Heersiaan Aquitard	1021	Kleiige afzetting van Halen
				1022	Klei van Waterschei
				1023	Slecht doorlatend deel van de Mergels van Gelinden
		1030	Heersiaan en Opglabeek Aquifersysteem	1031	Doorlatend deel van de Mergels van Gelinden
				1032	Zand van Orp
				1033	Zand van Eisden
				1034	Klei van Opoeteren
				1035	Zand van Maasmechelen

1100	**KRIJT AQUIFERSYSTEEM**	1110	Krijt Aquifer	1111	Kalksteen van Houthem
				1112	Tufkrijt van Maastricht
				1113	Krijt van Gulpen
		1120	Afzettingen van Vaals	Smectiet van Herve	
		1130	Zand van Aken	Zand van Aken	
		1140	Turoonmergels op Massief van Brabant		
		1150	Wealdiaan		
1200	**JURA - TRIAS - PERM**	1210	Jura		
		1220	Trias		
		1230	Perm		
1300	**SOKKEL**	1310	Boven-Carboon "Steenkool-terrein en -lagen"		
		1320	Kolenkalk		
		1330	Devoon		
		1340	Cambro-Siluur Massief van Brabant		

Addendum B: Statistical testing using Grobbendonk measurement data 1999-2009

1. Regression model nr 2: SSC = f(Q)
   a. Test statistics for regression model

Model Summary(b)

Model	R	R Square	Adjusted R Square	Std. Error of the Estimate
2	.701(a)	.491	.491	18.8428

a Predictors: (Constant), Q
b Dependent Variable: SSC

ANOVA(b)

Model		Sum of Squares	df	Mean Square	F	Sig.
2	Regression	910071.728	1	910071.728	2563.210	.000(a)
	Residual	943371.943	2657	355.052		
	Total	1853443.671	2658			

a Predictors: (Constant), Q
b Dependent Variable: SSC

Coefficients(a)

Model		Unstandardized Coefficients		Standardized Coefficients	t	Sig.
		B	Std. Error	Beta	B	Std. Error
2	(Constant)	.761	.605		1.257	.209
	Q	4.027	.080	.701	50.628	.000

a Dependent Variable: SSC

   b. Residuals plotted in function of predicted values

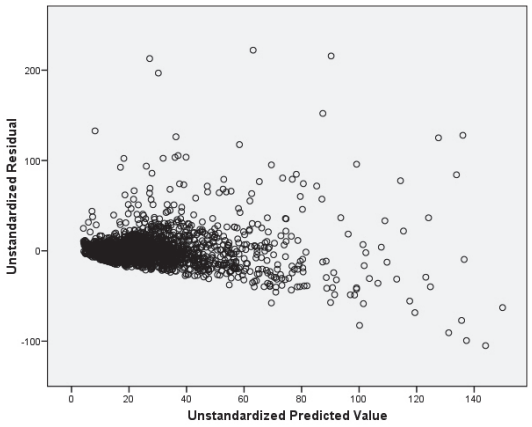

   c. Histogram of the residuals

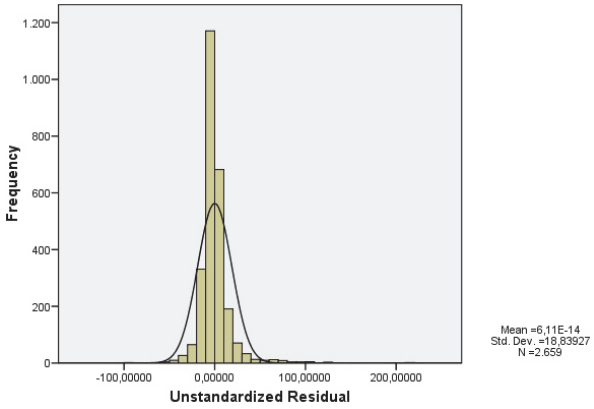

2. Regression model nr 3: SSC_{Winter} = f(Q) & SSC_{Summer} = f(Q)
   a. Test statistics for regression model Summer data

Model Summary(b)

Model	R	R Square	Adjusted R Square	Std. Error of the Estimate
3	.551(a)	.303	.303	8.7382

a Predictors: (Constant), Q
b Dependent Variable: SSC

ANOVA(b)

Model		Sum of Squares	df	Mean Square	F	Sig.
3	Regression	45887.012	1	45887.012	600.965	.000(a)
	Residual	105523.359	1382	76.356		
	Total	151410.371	1383			

a Predictors: (Constant), Q
b Dependent Variable: SSC

Coefficients(a)

Model		Unstandardized Coefficients		Standardized Coefficients	t	Sig.
		B	Std. Error	Beta	B	Std. Error
3	(Constant)	3.318	.498		6.667	.000
	Q	2.643	.108	.551	24.515	.000

a Dependent Variable: SSC

b. Residuals plotted in function of predicted values Summer data

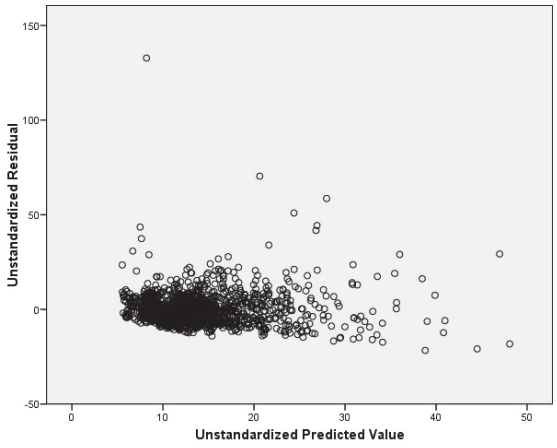

c. Histogram of the residuals Summer data

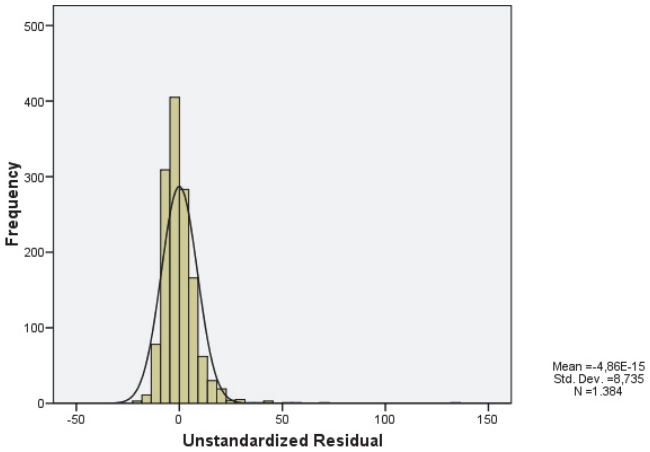

d. Test statistics for regression model Winter data

Model Summary(b)

Model	R	R Square	Adjusted R Square	Std. Error of the Estimate
3	.639(a)	.409	.408	25.0055

a Predictors: (Constant), Q
b Dependent Variable: SSC

ANOVA(b)

Model		Sum of Squares	df	Mean Square	F	Sig.
3	Regression	549827.847	1	549827.847	879.337	.000(a)
	Residual	795975.832	1273	625.276		
	Total	1345803.679	1274			

a Predictors: (Constant), Q
b Dependent Variable: SSC

Coefficients(a)

Model		Unstandardized Coefficients		Standardized Coefficients	t	Sig.
		B	Std. Error	Beta	B	Std. Error
3	(Constant)	5.964	1.266		4.711	.000
	Q	3.800	.128	.639	29.654	.000

a Dependent Variable: SSC

e. Residuals plotted in function of predicted values (Winter data)

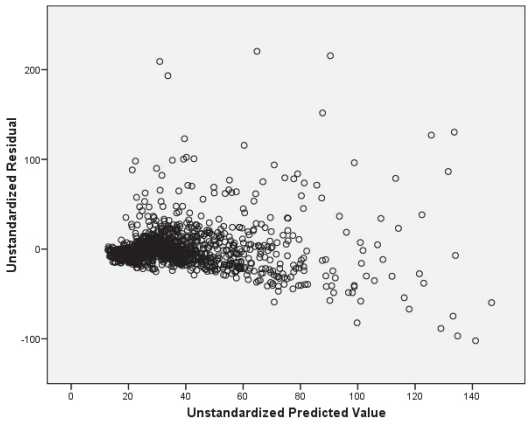

f. Histogram of the residuals Winter data

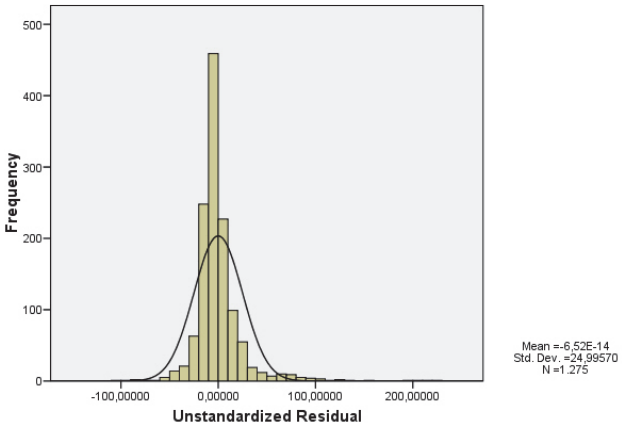

3. Regression models nr 4 & 5: log SSC = f(log Q)
   a. Test statistics for regression model

Model Summary(b)

Model	R	R Square	Adjusted R Square	Std. Error of the Estimate
4&5	.738(a)	.544	.544	.264833454871335

a Predictors: (Constant), logQ
b Dependent Variable: logSSC

ANOVA(b)

Model		Sum of Squares	df	Mean Square	F	Sig.
4&5	Regression	222.242	1	222.242	3168.694	.000(a)
	Residual	186.353	2657	.070		
	Total	408.595	2658			

a Predictors: (Constant), logQ
b Dependent Variable: logSSC

Coefficients(a)

Model		Unstandardized Coefficients		Standardized Coefficients	t	Sig.
		B	Std. Error	Beta	B	Std. Error
4&5	(Constant)	.509	.014		36.785	.000
	logQ	1.049	.019	.738	56.291	.000

a Dependent Variable: logSSC

b. Residuals plotted in function of predicted values

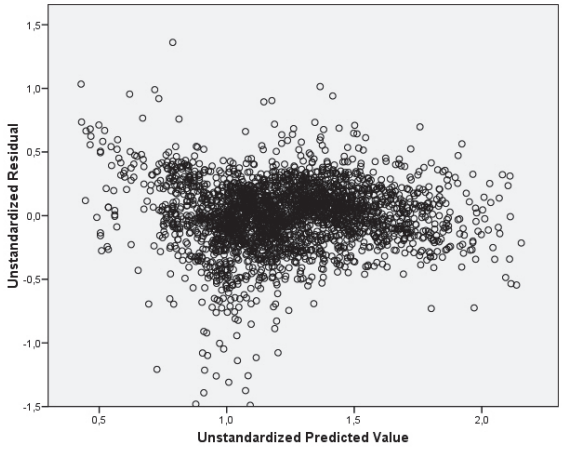

c. Histogram of the residuals

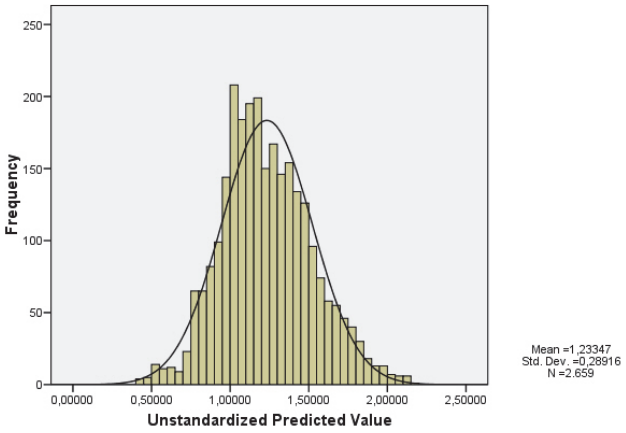

4. Regression models nr 6 & 7: log SSC_{Winter} = f(log Q) & log SSC_{Summer} = f(log Q)
   a. Test statistics for regression model log SSC_{Winter} = f(log Q)

Model Summary(b)

Model	R	R Square	Adjusted R Square	Std. Error of the Estimate
6&7	.763(a)	.582	.582	.228790992912688

a Predictors: (Constant), logQ
b Dependent Variable: logSSC

ANOVA(b)

Model		Sum of Squares	df	Mean Square	F	Sig.
6&7	Regression	92.824	1	92.824	1773.292	.000(a)
	Residual	66.636	1273	.052		
	Total	159.459	1274			

a Predictors: (Constant), logQ
b Dependent Variable: logSSC

Coefficients(a)

Model		Unstandardized Coefficients		Standardized Coefficients	t	Sig.
		B	Std. Error	Beta	B	Std. Error
6&7	(Constant)	.559	.022		25.543	.000
	logQ	1.053	.025	.763	42.110	.000

a Dependent Variable: logSSC

b. Residuals plotted in function of predicted values (winter data)

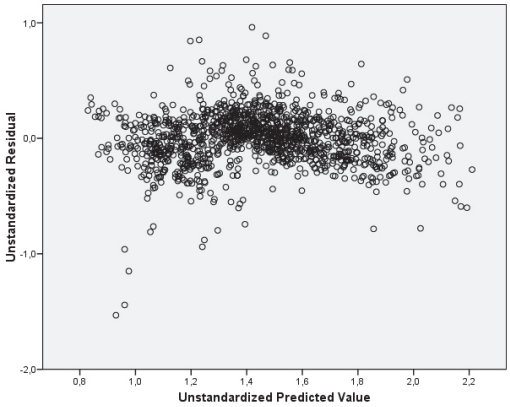

c. Histogram of the residuals (winter data)

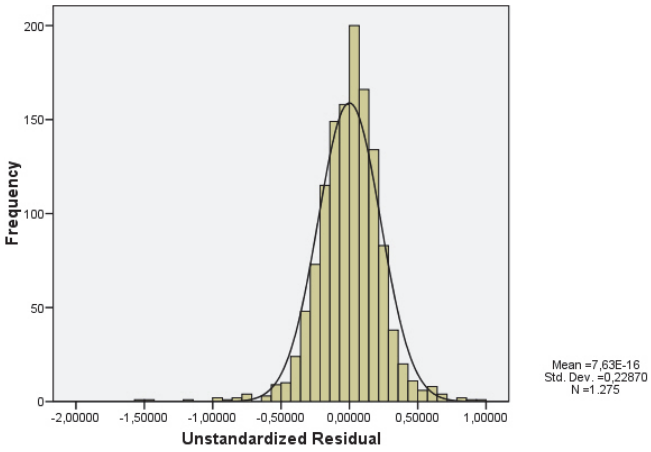

d. Test statistics for regression model log SSC_{Summer} = f(log Q)

Model Summary(b)

Model	R	R Square	Adjusted R Square	Std. Error of the Estimate
6&7	.508(a)	.258	.257	.278514448839065

a Predictors: (Constant), logQ
b Dependent Variable: logSSC

ANOVA(b)

Model		Sum of Squares	df	Mean Square	F	Sig.
6&7	Regression	37.279	1	37.279	480.581	.000(a)
	Residual	107.202	1382	.078		
	Total	144.481	1383			

a Predictors: (Constant), logQ
b Dependent Variable: logSSC

Coefficients(a)

Model		Unstandardized Coefficients		Standardized Coefficients	t	Sig.
		B	Std. Error	Beta	B	Std. Error
6&7	(Constant)	.624	.021		30.434	.000
	logQ	.754	.034	.508	21.922	.000

a Dependent Variable: logSSC

e. Residuals plotted in function of predicted values (summer data)

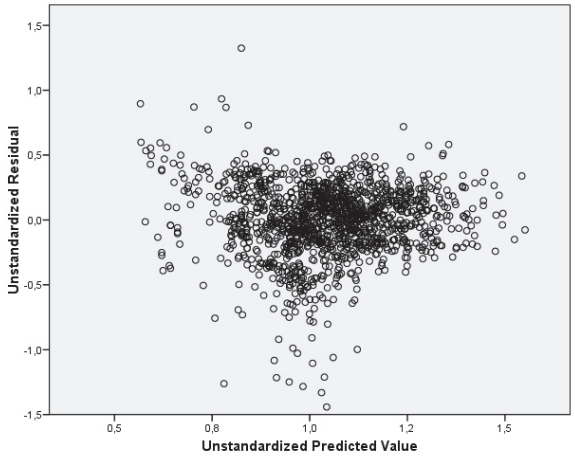

f. Histogram of the residuals (summer data)

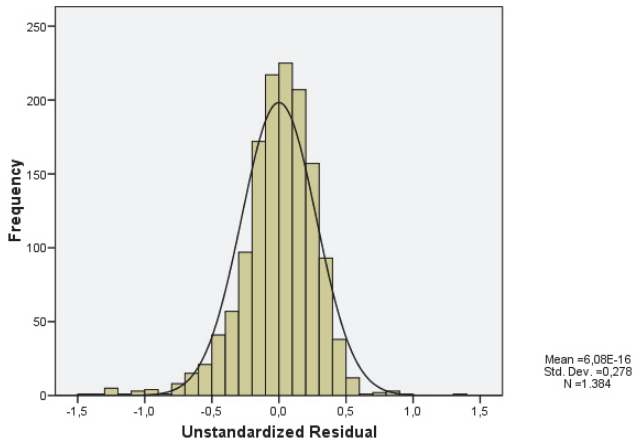

5. Model nr 8 Regression model SSC = f(Q, IFp, OFn, OF, BFn, Qn, Qp)
   a. Pearson's correlation coefficients

Correlations

		SSC	Q	QBF	QIF	QOF	Qp	QBFp	QIFp	QOFp	Qn	QBFn	QIFn	QOFn
SSC	Pearson Correlation	1	.701(**)	.577(**)	.571(**)	.618(**)	.571(**)	.562(**)	.436(**)	.406(**)	.694(**)	.589(**)	.643(**)	.516(**)
	Sig. (2-tailed)		0,000	0,000	0,000	0,000	0,000	0,000	0,000	0,000	0,000	0,000	0,000	0,000
	N	2.659	2.659	2.659	2.659	2.659	2.659	2.659	2.659	2.659	2.659	2.659	2.659	2.659
Q	Pearson Correlation	.701(**)	1	.802(**)	.897(**)	.826(**)	.904(**)	.781(**)	.771(**)	.703(**)	.904(**)	.814(**)	.886(**)	.560(**)
	Sig. (2-tailed)	0,000		0,000	0,000	0,000	0,000	0,000	0,000	0,000	0,000	0,000	0,000	0,000
	N	2.659	2.659	2.659	2.659	2.659	2.659	2.659	2.659	2.659	2.659	2.659	2.659	2.659
QBF	Pearson Correlation	.577(**)	.802(**)	1	.534(**)	.380(**)	.811(**)	.998(**)	.544(**)	.388(**)	.782(**)	.998(**)	.514(**)	.352(**)
	Sig. (2-tailed)	0,000	0,000		0,000	0,000	0,000	0,000	0,000	0,000	0,000	0,000	0,000	0,000
	N	2.659	2.659	2.659	2.659	2.659	2.659	2.659	2.659	2.659	2.659	2.659	2.659	2.659
QIF	Pearson Correlation	.571(**)	.897(**)	.534(**)	1	.790(**)	.886(**)	.508(**)	.917(**)	.866(**)	.774(**)	.550(**)	.918(**)	.515(**)
	Sig. (2-tailed)	0,000	0,000	0,000		0,000	0,000	0,000	0,000	0,000	0,000	0,000	0,000	0,000
	N	2.659	2.659	2.659	2.659	2.659	2.659	2.659	2.659	2.659	2.659	2.659	2.659	2.659
QOF	Pearson Correlation	.618(**)	.826(**)	.380(**)	.790(**)	1	.561(**)	.350(**)	.513(**)	.578(**)	.708(**)	.399(**)	.868(**)	.577(**)
	Sig. (2-tailed)	0,000	0,000	0,000	0,000		0,000	0,000	0,000	0,000	0,000	0,000	0,000	0,000
	N	2.659	2.659	2.659	2.659	2.659	2.659	2.659	2.659	2.659	2.659	2.659	2.659	2.659
Qp	Pearson Correlation	.571(**)	.904(**)	.811(**)	.886(**)	.561(**)	1	.800(**)	.895(**)	.821(**)	.794(**)	.817(**)	.756(**)	.382(**)
	Sig. (2-tailed)	0,000	0,000	0,000	0,000	0,000		0,000	0,000	0,000	0,000	0,000	0,000	0,000
	N	2.659	2.659	2.659	2.659	2.659	2.659	2.659	2.659	2.659	2.659	2.659	2.659	2.659
QBFp	Pearson Correlation	.562(**)	.781(**)	.998(**)	.508(**)	.350(**)	.800(**)	1	.527(**)	.370(**)	.762(**)	.994(**)	.485(**)	.331(**)
	Sig. (2-tailed)	0,000	0,000	0,000	0,000	0,000	0,000		0,000	0,000	0,000	0,000	0,000	0,000
	N	2.659	2.659	2.659	2.659	2.659	2.659	2.659	2.659	2.659	2.659	2.659	2.659	2.659
QIFp	Pearson Correlation	.436(**)	.771(**)	.544(**)	.917(**)	.513(**)	.895(**)	.527(**)	1	.786(**)	.649(**)	.554(**)	.745(**)	.334(**)
	Sig. (2-tailed)	0,000	0,000	0,000	0,000	0,000	0,000	0,000		0,000	0,000	0,000	0,000	0,000
	N	2.659	2.659	2.659	2.659	2.659	2.659	2.659	2.659	2.659	2.659	2.659	2.659	2.659
QOFp	Pearson Correlation	.406(**)	.703(**)	.388(**)	.866(**)	.578(**)	.821(**)	.370(**)	.786(**)	1	.545(**)	.398(**)	.710(**)	.285(**)
	Sig. (2-tailed)	0,000	0,000	0,000	0,000	0,000	0,000	0,000	0,000		0,000	0,000	0,000	0,000
	N	2.659	2.659	2.659	2.659	2.659	2.659	2.659	2.659	2.659	2.659	2.659	2.659	2.659
Qn	Pearson Correlation	.694(**)	.904(**)	.782(**)	.774(**)	.708(**)	.794(**)	.762(**)	.649(**)	.545(**)	1	.803(**)	.899(**)	.826(**)
	Sig. (2-tailed)	0,000	0,000	0,000	0,000	0,000	0,000	0,000	0,000	0,000		0,000	0,000	0,000
	N	2.659	2.659	2.659	2.659	2.659	2.659	2.659	2.659	2.659	2.659	2.659	2.659	2.659
QBFn	Pearson Correlation	.589(**)	.814(**)	.998(**)	.550(**)	.399(**)	.817(**)	.994(**)	.554(**)	.398(**)	.803(**)	1	.539(**)	.383(**)
	Sig. (2-tailed)	0,000	0,000	0,000	0,000	0,000	0,000	0,000	0,000	0,000	0,000		0,000	0,000
	N	2.659	2.659	2.659	2.659	2.659	2.659	2.659	2.659	2.659	2.659	2.659	2.659	2.659
QIFn	Pearson Correlation	.643(**)	.886(**)	.514(**)	.918(**)	.868(**)	.756(**)	.485(**)	.745(**)	.710(**)	.899(**)	.539(**)	1	.790(**)
	Sig. (2-tailed)	0,000	0,000	0,000	0,000	0,000	0,000	0,000	0,000	0,000	0,000	0,000		0,000
	N	2.659	2.659	2.659	2.659	2.659	2.659	2.659	2.659	2.659	2.659	2.659	2.659	2.659
QOFn	Pearson Correlation	.516(**)	.560(**)	.352(**)	.515(**)	.577(**)	.382(**)	.331(**)	.334(**)	.285(**)	.826(**)	.383(**)	.790(**)	1
	Sig. (2-tailed)	0,000	0,000	0,000	0,000	0,000	0,000	0,000	0,000	0,000	0,000	0,000	0,000	
	N	2.659	2.659	2.659	2.659	2.659	2.659	2.659	2.659	2.659	2.659	2.659	2.659	2.659

**. Correlation is significant at the 0.01 level (2-tailed).

b. Test statistics for regression model

Model Summary(l)

Model	R	R Square	Adjusted R Square	Std. Error of the Estimate
8	.737(k)	.543	.542	17.8739

k Predictors: (Constant), Q, QOFn, QOF, QBFn, Qn, Qp, QIFp
l Dependent Variable: SSC

ANOVA(l)

Model		Sum of Squares	df	Mean Square	F	Sig.
8	Regression	1006512.454	7	143787.493	450.073	.000(k)
	Residual	846931.217	2651	319.476		
	Total	1853443.671	2658			

k Predictors: (Constant), Q, QOFn, QOF, QBFn, Qn, Qp, QIFp
l Dependent Variable: SSC

Coefficients(a)

Model		Unstandardized Coefficients		Standardized Coefficients	t	Sig.
		B	Std. Error	Beta	B	Std. Error
8	(Constant)	-1.444	.735		-1.966	.049
	Q	-8.986	2.539	-1.564	-3.538	.000
	QIFp	3.441	1.052	.210	3.271	.001
	QOFn	14.737	3.242	.938	4.546	.000
	QOF	21.447	3.306	1.357	6.488	.000
	QBFn	18.844	2.484	1.557	7.586	.000
	Qn	-8.370	2.289	-1.466	-3.657	.000
	Qp	3.296	.679	.569	4.857	.000

a Dependent Variable: SSC

c. Residuals plotted in function of predicted values

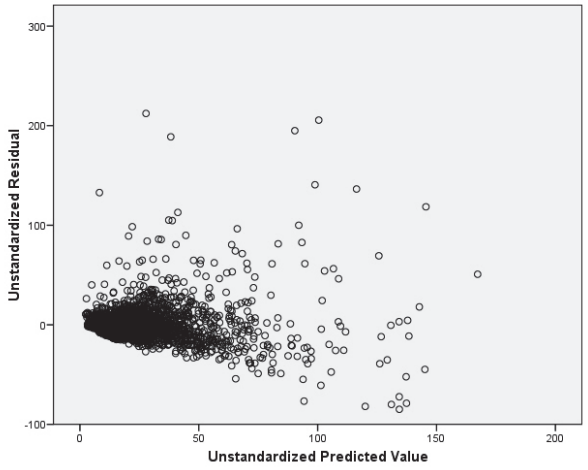

d. Histogram of the residuals

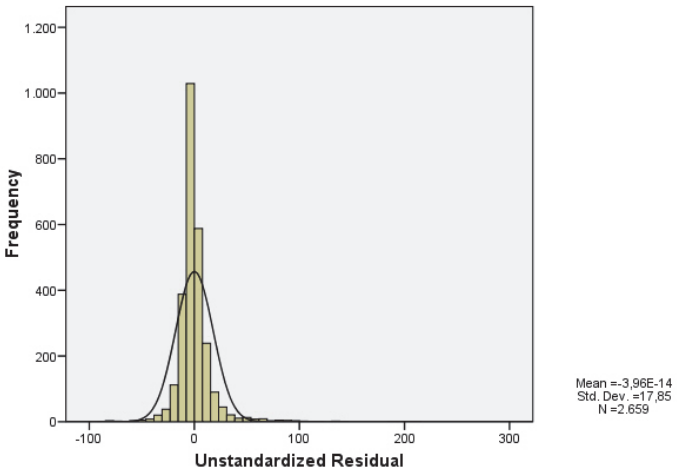

6. Model nr 9: Regression model SSC_{Winter} = f(Q, Qp, QOFn, QIFp) & SSC_{Summer} = f(Q, QIFp)
   a. Pearson's correlation coefficients (winter data)

Correlations

		SSC	Q	QBF	QIF	QOF	Qp	QBFp	QIFp	QOFp	Qn	QBFn	QIFn	QOFn
SSC	Pearson Correlation	1	.639(**)	.456(**)	.526(**)	.610(**)	.471(**)	.438(**)	.365(**)	.358(**)	.635(**)	.472(**)	.615(**)	.500(**)
	Sig. (2-tailed)		0,000	0,000	0,000	0,000	0,000	0,000	0,000	0,000	0,000	0,000	0,000	0,000
	N	1.275	1.275	1.275	1.275	1.275	1.275	1.275	1.275	1.275	1.275	1.275	1.275	1.275
Q	Pearson Correlation	.639(**)	1	.747(**)	.901(**)	.841(**)	.878(**)	.719(**)	.753(**)	.698(**)	.877(**)	.762(**)	.888(**)	.533(**)
	Sig. (2-tailed)	0,000		0,000	0,000	0,000	0,000	0,000	0,000	0,000	0,000	0,000	0,000	0,000
	N	1.275	1.275	1.275	1.275	1.275	1.275	1.275	1.275	1.275	1.275	1.275	1.275	1.275
QBF	Pearson Correlation	.456(**)	.747(**)	1	.484(**)	.335(**)	.761(**)	.997(**)	.498(**)	.349(**)	.718(**)	.997(**)	.457(**)	.300(**)
	Sig. (2-tailed)	0,000	0,000		0,000	0,000	0,000	0,000	0,000	0,000	0,000	0,000	0,000	0,000
	N	1.275	1.275	1.275	1.275	1.275	1.275	1.275	1.275	1.275	1.275	1.275	1.275	1.275

QIF	Pearson Correlation	.526(**)	.901(**)	.484(**)	1	.779(**)	.887(**)	.454(**)	.908(**)	.859(**)	.756(**)	.504(**)	.910(**)	.483(**)
	Sig. (2-tailed)	0,000	0,000	0,000		0,000	0,000	0,000	0,000	0,000	0,000	0,000	0,000	0,000
	N	1.275	1.275	1.275	1.275	1.275	1.275	1.275	1.275	1.275	1.275	1.275	1.275	1.275
QOF	Pearson Correlation	.610(**)	.841(**)	.335(**)	.779(**)	1	.534(**)	.299(**)	.482(**)	.552(**)	.702(**)	.357(**)	.861(**)	.550(**)
	Sig. (2-tailed)	0,000	0,000	0,000	0,000		0,000	0,000	0,000	0,000	0,000	0,000	0,000	0,000
	N	1.275	1.275	1.275	1.275	1.275	1.275	1.275	1.275	1.275	1.275	1.275	1.275	1.275
Qp	Pearson Correlation	.471(**)	.878(**)	.761(**)	.887(**)	.534(**)	1	.746(**)	.898(**)	.837(**)	.739(**)	.768(**)	.734(**)	.330(**)
	Sig. (2-tailed)	0,000	0,000	0,000	0,000	0,000		0,000	0,000	0,000	0,000	0,000	0,000	0,000
	N	1.275	1.275	1.275	1.275	1.275	1.275	1.275	1.275	1.275	1.275	1.275	1.275	1.275
QBFp	Pearson Correlation	.438(**)	.719(**)	.997(**)	.454(**)	.299(**)	.746(**)	1	.479(**)	.327(**)	.692(**)	.992(**)	.422(**)	.274(**)
	Sig. (2-tailed)	0,000	0,000	0,000	0,000	0,000	0,000		0,000	0,000	0,000	0,000	0,000	0,000
	N	1.275	1.275	1.275	1.275	1.275	1.275	1.275	1.275	1.275	1.275	1.275	1.275	1.275
QIFp	Pearson Correlation	.365(**)	.753(**)	.498(**)	.908(**)	.482(**)	.898(**)	.479(**)	1	.774(**)	.609(**)	.511(**)	.719(**)	.292(**)
	Sig. (2-tailed)	0,000	0,000	0,000	0,000	0,000	0,000	0,000		0,000	0,000	0,000	0,000	0,000
	N	1.275	1.275	1.275	1.275	1.275	1.275	1.275	1.275	1.275	1.275	1.275	1.275	1.275
QOFp	Pearson Correlation	.358(**)	.698(**)	.349(**)	.859(**)	.552(**)	.837(**)	.327(**)	.774(**)	1	.517(**)	.361(**)	.690(**)	.248(**)
	Sig. (2-tailed)	0,000	0,000	0,000	0,000	0,000	0,000	0,000	0,000		0,000	0,000	0,000	0,000
	N	1.275	1.275	1.275	1.275	1.275	1.275	1.275	1.275	1.275	1.275	1.275	1.275	1.275
Qn	Pearson Correlation	.635(**)	.877(**)	.718(**)	.756(**)	.702(**)	.739(**)	.692(**)	.609(**)	.517(**)	1	.746(**)	.903(**)	.842(**)
	Sig. (2-tailed)	0,000	0,000	0,000	0,000	0,000	0,000	0,000	0,000	0,000		0,000	0,000	0,000
	N	1.275	1.275	1.275	1.275	1.275	1.275	1.275	1.275	1.275	1.275	1.275	1.275	1.275
QBFn	Pearson Correlation	.472(**)	.762(**)	.997(**)	.504(**)	.357(**)	.768(**)	.992(**)	.511(**)	.361(**)	.746(**)	1	.488(**)	.336(**)
	Sig. (2-tailed)	0,000	0,000	0,000	0,000	0,000	0,000	0,000	0,000	0,000	0,000		0,000	0,000
	N	1.275	1.275	1.275	1.275	1.275	1.275	1.275	1.275	1.275	1.275	1.275	1.275	1.275
QIFn	Pearson Correlation	.615(**)	.888(**)	.457(**)	.910(**)	.861(**)	.734(**)	.422(**)	.719(**)	.690(**)	.903(**)	.488(**)	1	.779(**)
	Sig. (2-tailed)	0,000	0,000	0,000	0,000	0,000	0,000	0,000	0,000	0,000	0,000	0,000		0,000
	N	1.275	1.275	1.275	1.275	1.275	1.275	1.275	1.275	1.275	1.275	1.275	1.275	1.275
QOFn	Pearson Correlation	.500(**)	.533(**)	.300(**)	.483(**)	.550(**)	.330(**)	.274(**)	.292(**)	.248(**)	.842(**)	.336(**)	.779(**)	1
	Sig. (2-tailed)	0,000	0,000	0,000	0,000	0,000	0,000	0,000	0,000	0,000	0,000	0,000	0,000	
	N	1.275	1.275	1.275	1.275	1.275	1.275	1.275	1.275	1.275	1.275	1.275	1.275	1.275

**. Correlation is significant at the 0.01 level (2-tailed).

b. Test statistics for regression model (winter data)

Model Summary(e)

Model	R	R Square	Adjusted R Square	Std. Error of the Estimate
9	.683(d)	.466	.464	23.7911

d Predictors: (Constant), Q, Qp, QOFn, QIFp
e Dependent Variable: SSC

ANOVA(e)

Model		Sum of Squares	df	Mean Square	F	Sig.
9	Regression	626965.795	4	156741.449	276.921	.000(d)
	Residual	718837.884	1270	566.014		
	Total	1345803.679	1274			

d Predictors: (Constant), Q, Qp, QOFn, QIFp
e Dependent Variable: SSC

Coefficients(a)

Model		Unstandardized Coefficients		Standardized Coefficients	t	Sig.
		B	Std. Error	Beta		
4	(Constant)	6.282	1.454		4.321	.000
	Q	4.613	.308	.776	14.967	.000
	Qp	-.777	.409	-.129	-1.899	.058
	QOFn	2.563	.382	.174	6.718	.000
	QIFp	-2.448	.755	-.154	-3.242	.001

a. Dependent Variable: SSC

c. Residuals versus predicted (winter data)

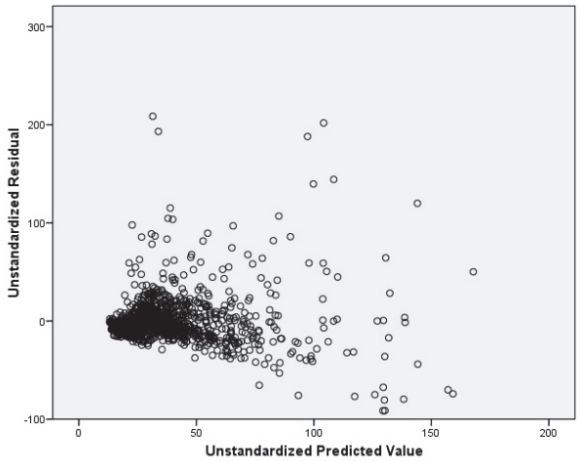

d. Histogram residuals (winter data)

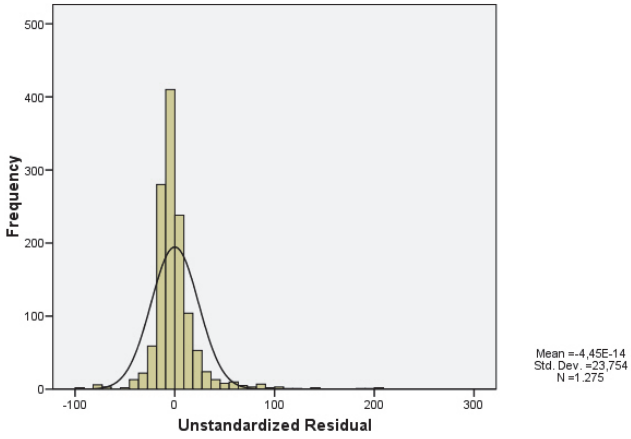

e. Pearson's correlation coefficients (summer data)

Correlations

		SSC	Q	QBF	QIF	QOF	Qp	QBFp	QIFp	QOFp	Qn	QBFn	QIFn	QOFn
SSC	Pearson Correlation	1	.551(**)	.440(**)	.405(**)	.438(**)	.460(**)	.428(**)	.302(**)	.328(**)	.496(**)	.445(**)	.422(**)	.264(**)
	Sig. (2-tailed)		0,000	0,000	0,000	0,000	0,000	0,000	0,000	0,000	0,000	0,000	0,000	0,000
	N	1.384	1.384	1.384	1.384	1.384	1.384	1.384	1.384	1.384	1.384	1.384	1.384	1.384
Q	Pearson Correlation	.551(**)	1	.742(**)	.846(**)	.766(**)	.893(**)	.715(**)	.718(**)	.666(**)	.889(**)	.756(**)	.826(**)	.466(**)
	Sig. (2-tailed)	0,000		0,000	0,000	0,000	0,000	0,000	0,000	0,000	0,000	0,000	0,000	0,000
	N	1.384	1.384	1.384	1.384	1.384	1.384	1.384	1.384	1.384	1.384	1.384	1.384	1.384
QBF	Pearson Correlation	.440(**)	.742(**)	1	.350(**)	.203(**)	.754(**)	.997(**)	.382(**)	.238(**)	.712(**)	.996(**)	.310(**)	.163(**)
	Sig. (2-tailed)	0,000	0,000		0,000	0,000	0,000	0,000	0,000	0,000	0,000	0,000	0,000	0,000
	N	1.384	1.384	1.384	1.384	1.384	1.384	1.384	1.384	1.384	1.384	1.384	1.384	1.384
QIF	Pearson Correlation	.405(**)	.846(**)	.350(**)	1	.762(**)	.835(**)	.319(**)	.912(**)	.869(**)	.706(**)	.371(**)	.907(**)	.450(**)
	Sig. (2-tailed)	0,000	0,000	0,000		0,000	0,000	0,000	0,000	0,000	0,000	0,000	0,000	0,000
	N	1.384	1.384	1.384	1.384	1.384	1.384	1.384	1.384	1.384	1.384	1.384	1.384	1.384
QOF	Pearson Correlation	.438(**)	.766(**)	.203(**)	.762(**)	1	.474(**)	.166(**)	.460(**)	.572(**)	.652(**)	.223(**)	.860(**)	.564(**)
	Sig. (2-tailed)	0,000	0,000	0,000	0,000		0,000	0,000	0,000	0,000	0,000	0,000	0,000	0,000
	N	1.384	1.384	1.384	1.384	1.384	1.384	1.384	1.384	1.384	1.384	1.384	1.384	1.384
Qp	Pearson Correlation	.460(**)	.893(**)	.754(**)	.835(**)	.474(**)	1	.740(**)	.854(**)	.780(**)	.756(**)	.762(**)	.676(**)	.251(**)
	Sig. (2-tailed)	0,000	0,000	0,000	0,000	0,000		0,000	0,000	0,000	0,000	0,000	0,000	0,000
	N	1.384	1.384	1.384	1.384	1.384	1.384	1.384	1.384	1.384	1.384	1.384	1.384	1.384
QBFp	Pearson Correlation	.428(**)	.715(**)	.997(**)	.319(**)	.166(**)	.740(**)	1	.361(**)	.217(**)	.687(**)	.992(**)	.274(**)	.138(**)
	Sig. (2-tailed)	0,000	0,000	0,000	0,000	0,000	0,000		0,000	0,000	0,000	0,000	0,000	0,000
	N	1.384	1.384	1.384	1.384	1.384	1.384	1.384	1.384	1.384	1.384	1.384	1.384	1.384
QIFp	Pearson Correlation	.302(**)	.718(**)	.382(**)	.912(**)	.460(**)	.854(**)	.361(**)	1	.776(**)	.571(**)	.398(**)	.714(**)	.243(**)
	Sig. (2-tailed)	0,000	0,000	0,000	0,000	0,000	0,000	0,000		0,000	0,000	0,000	0,000	0,000
	N	1.384	1.384	1.384	1.384	1.384	1.384	1.384	1.384	1.384	1.384	1.384	1.384	1.384
QOFp	Pearson Correlation	.328(**)	.666(**)	.238(**)	.869(**)	.572(**)	.780(**)	.217(**)	.776(**)	1	.485(**)	.251(**)	.705(**)	.234(**)
	Sig. (2-tailed)	0,000	0,000	0,000	0,000	0,000	0,000	0,000	0,000		0,000	0,000	0,000	0,000
	N	1.384	1.384	1.384	1.384	1.384	1.384	1.384	1.384	1.384	1.384	1.384	1.384	1.384
Qn	Pearson Correlation	.496(**)	.889(**)	.712(**)	.706(**)	.652(**)	.756(**)	.687(**)	.571(**)	.485(**)	1	.740(**)	.842(**)	.768(**)
	Sig. (2-tailed)	0,000	0,000	0,000	0,000	0,000	0,000	0,000	0,000	0,000		0,000	0,000	0,000
	N	1.384	1.384	1.384	1.384	1.384	1.384	1.384	1.384	1.384	1.384	1.384	1.384	1.384
QBFn	Pearson Correlation	.445(**)	.756(**)	.996(**)	.371(**)	.223(**)	.762(**)	.992(**)	.398(**)	.251(**)	.740(**)	1	.341(**)	.200(**)
	Sig. (2-tailed)	0,000	0,000	0,000	0,000	0,000	0,000	0,000	0,000	0,000	0,000		0,000	0,000
	N	1.384	1.384	1.384	1.384	1.384	1.384	1.384	1.384	1.384	1.384	1.384	1.384	1.384
QIFn	Pearson Correlation	.422(**)	.826(**)	.310(**)	.907(**)	.860(**)	.676(**)	.274(**)	.714(**)	.705(**)	.842(**)	.341(**)	1	.761(**)
	Sig. (2-tailed)	0,000	0,000	0,000	0,000	0,000	0,000	0,000	0,000	0,000	0,000	0,000		0,000
	N	1.384	1.384	1.384	1.384	1.384	1.384	1.384	1.384	1.384	1.384	1.384	1.384	1.384
QOFn	Pearson Correlation	.264(**)	.466(**)	.163(**)	.450(**)	.564(**)	.251(**)	.138(**)	.243(**)	.234(**)	.768(**)	.200(**)	.761(**)	1
	Sig. (2-tailed)	0,000	0,000	0,000	0,000	0,000	0,000	0,000	0,000	0,000	0,000	0,000	0,000	
	N	1.384	1.384	1.384	1.384	1.384	1.384	1.384	1.384	1.384	1.384	1.384	1.384	1.384

**. Correlation is significant at the 0.01 level (2-tailed).

f. Test statistics for regression model (summer data)

Model Summary(c)

Model	R	R Square	Adjusted R Square	Std. Error of the Estimate
9	.566(b)	.321	.320	8.6293

b Predictors: (Constant), Q, QIFp
c Dependent Variable: SSC

ANOVA(c)

Model		Sum of Squares	df	Mean Square	F	Sig.
9	Regression	48575.537	2	24287.769	326.168	.000(b)
	Residual	102834.834	1381	74.464		
	Total	151410.371	1383			

b Predictors: (Constant), Q, QIFp
c Dependent Variable: SSC

Coefficients(a)

Model		Unstandardized Coefficients		Standardized Coefficients	t	Sig.
		B	Std. Error	Beta	B	Std. Error
9	(Constant)	2.318	.519		4.468	.000
	Q	3.302	.153	.688	21.595	.000
	QIFp	-2.374	.395	-.191	-6.009	.000

a Dependent Variable: SSC

g. Residuals versus predicted (summer data)

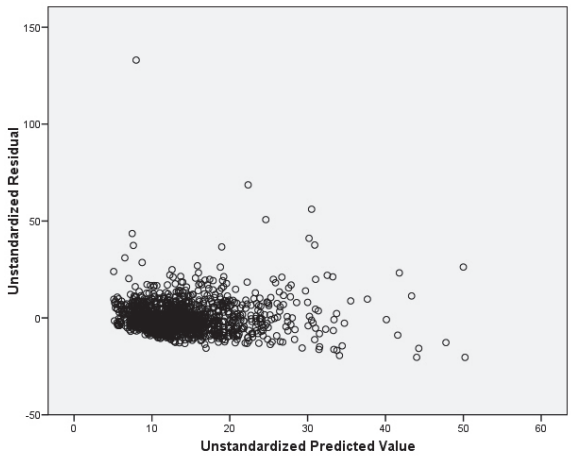

h. Histogram residuals (summer data)

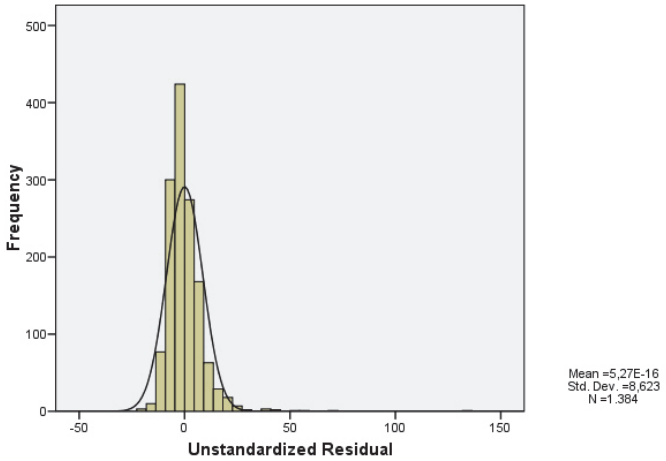

7. Regression model nrs 10&11: log SSC = f(log Q, log IFp, log OFn, logBFn, logIF)

a. Pearson's correlation coefficients

Correlations

		log SSC	log Q	log BF1	log QIF1	log QOF1	log Qp	log QBF1p	log QIF1p	log QOF1p	log Qn	log QBF1n	log QIF1n	log QOF1n
logSSC	Pearson Correlation	1	.738(**)	.686(**)	.557(**)	.518(**)	.685(**)	.675(**)	.486(**)	.420(**)	.728(**)	.693(**)	.578(**)	.454(**)
	Sig. (2-tailed)		0,000	0,000	0,000	0,000	0,000	0,000	0,000	0,000	0,000	0,000	0,000	0,000
	N	2.659	2.659	2.659	2.659	2.659	2.659	2.659	2.659	2.659	2.659	2.659	2.659	2.659
logQ	Pearson Correlation	.738(**)	1	.884(**)	.811(**)	.719(**)	.952(**)	.869(**)	.742(**)	.648(**)	.951(**)	.890(**)	.793(**)	.554(**)
	Sig. (2-tailed)	0,000		0,000	0,000	0,000	0,000	0,000	0,000	0,000	0,000	0,000	0,000	0,000
	N	2.659	2.659	2.659	2.659	2.659	2.659	2.659	2.659	2.659	2.659	2.659	2.659	2.659
logQBF1	Pearson Correlation	.686(**)	.884(**)	1	.515(**)	.376(**)	.890(**)	.998(**)	.523(**)	.382(**)	.869(**)	.998(**)	.496(**)	.348(**)
	Sig. (2-tailed)	0,000	0,000		0,000	0,000	0,000	0,000	0,000	0,000	0,000	0,000	0,000	0,000
	N	2.659	2.659	2.659	2.659	2.659	2.659	2.659	2.659	2.659	2.659	2.659	2.659	2.659
logQIF1	Pearson Correlation	.557(**)	.811(**)	.515(**)	1	.829(**)	.792(**)	.493(**)	.938(**)	.870(**)	.744(**)	.528(**)	.937(**)	.608(**)
	Sig. (2-tailed)	0,000	0,000	0,000		0,000	0,000	0,000	0,000	0,000	0,000	0,000	0,000	0,000
	N	2.659	2.659	2.659	2.659	2.659	2.659	2.659	2.659	2.659	2.659	2.659	2.659	2.659
log QOF1	Pearson Correlation	.518(**)	.719(**)	.376(**)	.829(**)	1	.557(**)	.347(**)	.613(**)	.671(**)	.651(**)	.391(**)	.872(**)	.666(**)
	Sig. (2-tailed)	0,000	0,000	0,000	0,000		0,000	0,000	0,000	0,000	0,000	0,000	0,000	0,000
	N	2.659	2.659	2.659	2.659	2.659	2.659	2.659	2.659	2.659	2.659	2.659	2.659	2.659
logQp	Pearson Correlation	.685(**)	.952(**)	.890(**)	.792(**)	.557(**)	1	.884(**)	.808(**)	.714(**)	.890(**)	.892(**)	.709(**)	.420(**)
	Sig. (2-tailed)	0,000	0,000	0,000	0,000	0,000		0,000	0,000	0,000	0,000	0,000	0,000	0,000
	N	2.659	2.659	2.659	2.659	2.659	2.659	2.659	2.659	2.659	2.659	2.659	2.659	2.659

logQBF1p	Pearson Correlation	.675(**)	.869(**)	.998(**)	.493(**)	.347(**)	.884(**)	1	.510(**)	.367(**)	.854(**)	.995(**)	.470(**)	.326(**)
	Sig. (2-tailed)	0,000	0,000	0,000	0,000	0,000	0,000		0,000	0,000	0,000	0,000	0,000	0,000
	N	2.659	2.659	2.659	2.659	2.659	2.659	2.659	2.659	2.659	2.659	2.659	2.659	2.659
logQIF1p	Pearson Correlation	.486(**)	.742(**)	.523(**)	.938(**)	.613(**)	.808(**)	.510(**)	1	.825(**)	.659(**)	.532(**)	.798(**)	.424(**)
	Sig. (2-tailed)	0,000	0,000	0,000	0,000	0,000	0,000	0,000		0,000	0,000	0,000	0,000	0,000
	N	2.659	2.659	2.659	2.659	2.659	2.659	2.659	2.659	2.659	2.659	2.659	2.659	2.659
logQOF1p	Pearson Correlation	.420(**)	.648(**)	.382(**)	.870(**)	.671(**)	.714(**)	.367(**)	.825(**)	1	.547(**)	.390(**)	.751(**)	.387(**)
	Sig. (2-tailed)	0,000	0,000	0,000	0,000	0,000	0,000	0,000	0,000		0,000	0,000	0,000	0,000
	N	2.659	2.659	2.659	2.659	2.659	2.659	2.659	2.659	2.659	2.659	2.659	2.659	2.659
logQn	Pearson Correlation	.728(**)	.951(**)	.869(**)	.744(**)	.651(**)	.890(**)	.854(**)	.659(**)	.547(**)	1	.885(**)	.813(**)	.718(**)
	Sig. (2-tailed)	0,000	0,000	0,000	0,000	0,000	0,000	0,000	0,000	0,000		0,000	0,000	0,000
	N	2.659	2.659	2.659	2.659	2.659	2.659	2.659	2.659	2.659	2.659	2.659	2.659	2.659
logQBF1n	Pearson Correlation	.693(**)	.890(**)	.998(**)	.528(**)	.391(**)	.892(**)	.995(**)	.532(**)	.390(**)	.885(**)	1	.518(**)	.376(**)
	Sig. (2-tailed)	0,000	0,000	0,000	0,000	0,000	0,000	0,000	0,000	0,000	0,000		0,000	0,000
	N	2.659	2.659	2.659	2.659	2.659	2.659	2.659	2.659	2.659	2.659	2.659	2.659	2.659
logQIF1n	Pearson Correlation	.578(**)	.793(**)	.496(**)	.937(**)	.872(**)	.709(**)	.470(**)	.798(**)	.751(**)	.813(**)	.518(**)	1	.826(**)
	Sig. (2-tailed)	0,000	0,000	0,000	0,000	0,000	0,000	0,000	0,000	0,000	0,000	0,000		0,000
	N	2.659	2.659	2.659	2.659	2.659	2.659	2.659	2.659	2.659	2.659	2.659	2.659	2.659
logQOF1n	Pearson Correlation	.454(**)	.554(**)	.348(**)	.608(**)	.666(**)	.420(**)	.326(**)	.424(**)	.387(**)	.718(**)	.376(**)	.826(**)	1
	Sig. (2-tailed)	0,000	0,000	0,000	0,000	0,000	0,000	0,000	0,000	0,000	0,000	0,000	0,000	
	N	2.659	2.659	2.659	2.659	2.659	2.659	2.659	2.659	2.659	2.659	2.659	2.659	2.659

**. Correlation is significant at the 0.01 level (2-tailed).

b. Test statistics for regression model

Model Summary

Model	R	R Square	Adjusted R Square	Std. Error of the Estimate
10&11	.750(e)	.563	.562	.259543766345681

e Predictors: (Constant), logQ, logQIFp, logQOFn, logQBFn, logQIF

ANOVA(f)

Model		Sum of Squares	df	Mean Square	F	Sig.
10&11	Regression	229.881	5	45.976	682.515	.000(e)
	Residual	178.714	2653	.067		
	Total	408.595	2658			

e Predictors: (Constant), logQ, logQIFp, logQOFn, logQBFn, logQIF

f Dependent Variable: logSSC

Coefficients(a)

Model		Unstandardized Coefficients		Standardized Coefficients	t	Sig.
		B	Std. Error	Beta	B	Std. Error
10&11	(Constant)	.361	.024		15.130	.000
	logQ	.520	.106	.366	4.899	.000
	logQIFp	-.489	.094	-.283	-5.184	.000
	logQOFn	.096	.036	.053	2.680	.007
	logQBFn	.723	.115	.329	6.306	.000
	logQIF	.551	.144	.320	3.840	.000

a Dependent Variable: logSSC

c. Residuals plotted in function of predicted values

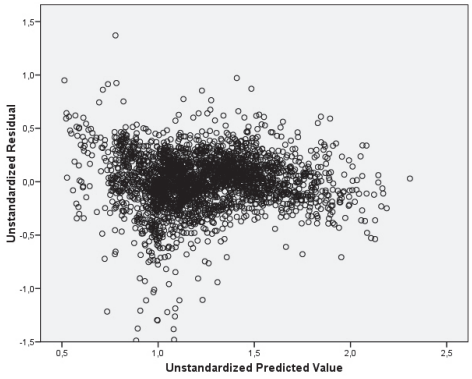

d. Histogram of the residuals

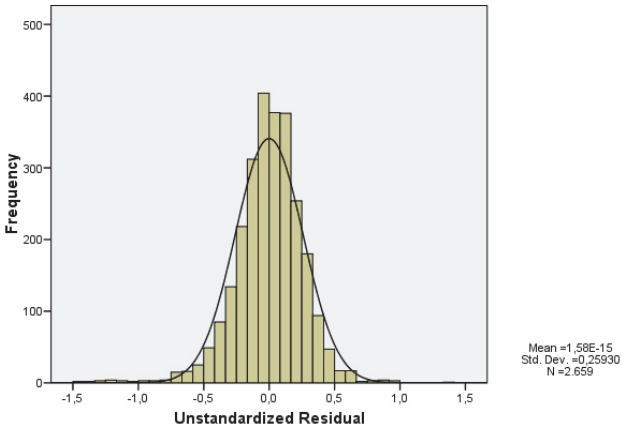

8. Regression model nr 12&13: log SSC_{winter} = f(log Q, log IFp, log OFn, logBF, logIF)

a. Pearson's r correlation coefficients (winter data)

		log SSC	logQ	logBF'	log QIF'	log QOF'	log Qp	Log QBFp'	log QIFp'	log QOFp'	log Qn	log QBFn'	log QIFn'	log QOFn'
log SSC	Pearson Correlation	1	.763(**)	.677(**)	.532(**)	.516(**)	.684(**)	.665(**)	.438(**)	.380(**)	.758(**)	.686(**)	.566(**)	.455(**)
	Sig. (2-tailed)		0,000	0,000	0,000	0,000	0,000	0,000	0,000	0,000	0,000	0,000	0,000	0,000
	N	1.275	1.275	1.275	1.275	1.275	1.275	1.275	1.275	1.275	1.275	1.275	1.275	1.275
logQ	Pearson Correlation	.763(**)	1	.853(**)	.804(**)	.730(**)	.936(**)	.835(**)	.719(**)	.641(**)	.934(**)	.862(**)	.781(**)	.533(**)
	Sig. (2-tailed)	0,000		0,000	0,000	0,000	0,000	0,000	0,000	0,000	0,000	0,000	0,000	0,000
	N	1.275	1.275	1.275	1.275	1.275	1.275	1.275	1.275	1.275	1.275	1.275	1.275	1.275
logQBF'	Pearson Correlation	.677(**)	.853(**)	1	.444(**)	.318(**)	.864(**)	.998(**)	.456(**)	.330(**)	.833(**)	.998(**)	.419(**)	.286(**)
	Sig. (2-tailed)	0,000	0,000		0,000	0,000	0,000	0,000	0,000	0,000	0,000	0,000	0,000	0,000
	N	1.275	1.275	1.275	1.275	1.275	1.275	1.275	1.275	1.275	1.275	1.275	1.275	1.275
logQIF'	Pearson Correlation	.532(**)	.804(**)	.444(**)	1	.820(**)	.778(**)	.419(**)	.930(**)	.860(**)	.721(**)	.459(**)	.930(**)	.582(**)
	Sig. (2-tailed)	0,000	0,000	0,000		0,000	0,000	0,000	0,000	0,000	0,000	0,000	0,000	0,000
	N	1.275	1.275	1.275	1.275	1.275	1.275	1.275	1.275	1.275	1.275	1.275	1.275	1.275
logQOF'	Pearson Correlation	.516(**)	.730(**)	.318(**)	.820(**)	1	.534(**)	.287(**)	.587(**)	.648(**)	.645(**)	.335(**)	.862(**)	.642(**)
	Sig. (2-tailed)	0,000	0,000	0,000	0,000		0,000	0,000	0,000	0,000	0,000	0,000	0,000	0,000
	N	1.275	1.275	1.275	1.275	1.275	1.275	1.275	1.275	1.275	1.275	1.275	1.275	1.275
logQp	Pearson Correlation	.684(**)	.936(**)	.864(**)	.778(**)	.534(**)	1	.856(**)	.799(**)	.723(**)	.855(**)	.867(**)	.677(**)	.373(**)
	Sig. (2-tailed)	0,000	0,000	0,000	0,000	0,000		0,000	0,000	0,000	0,000	0,000	0,000	0,000
	N	1.275	1.275	1.275	1.275	1.275	1.275	1.275	1.275	1.275	1.275	1.275	1.275	1.275
LogQBFp'	Pearson Correlation	.665(**)	.835(**)	.998(**)	.419(**)	.287(**)	.856(**)	1	.442(**)	.313(**)	.815(**)	.995(**)	.390(**)	.263(**)
	Sig. (2-tailed)	0,000	0,000	0,000	0,000	0,000	0,000		0,000	0,000	0,000	0,000	0,000	0,000
	N	1.275	1.275	1.275	1.275	1.275	1.275	1.275	1.275	1.275	1.275	1.275	1.275	1.275
logQIFp'	Pearson Correlation	.438(**)	.719(**)	.456(**)	.930(**)	.587(**)	.799(**)	.442(**)	1	.814(**)	.616(**)	.465(**)	.774(**)	.383(**)
	Sig. (2-tailed)	0,000	0,000	0,000	0,000	0,000	0,000	0,000		0,000	0,000	0,000	0,000	0,000
	N	1.275	1.275	1.275	1.275	1.275	1.275	1.275	1.275	1.275	1.275	1.275	1.275	1.275
logQOFp'	Pearson Correlation	.380(**)	.641(**)	.330(**)	.860(**)	.648(**)	.723(**)	.313(**)	.814(**)	1	.517(**)	.338(**)	.728(**)	.345(**)
	Sig. (2-tailed)	0,000	0,000	0,000	0,000	0,000	0,000	0,000	0,000		0,000	0,000	0,000	0,000
	N	1.275	1.275	1.275	1.275	1.275	1.275	1.275	1.275	1.275	1.275	1.275	1.275	1.275
logQn	Pearson Correlation	.758(**)	.934(**)	.833(**)	.721(**)	.645(**)	.855(**)	.815(**)	.616(**)	.517(**)	1	.851(**)	.806(**)	.732(**)
	Sig. (2-tailed)	0,000	0,000	0,000	0,000	0,000	0,000	0,000	0,000	0,000		0,000	0,000	0,000
	N	1.275	1.275	1.275	1.275	1.275	1.275	1.275	1.275	1.275	1.275	1.275	1.275	1.275
logQBFn'	Pearson Correlation	.686(**)	.862(**)	.998(**)	.459(**)	.335(**)	.867(**)	.995(**)	.465(**)	.338(**)	.851(**)	1	.445(**)	.318(**)
	Sig. (2-tailed)	0,000	0,000	0,000	0,000	0,000	0,000	0,000	0,000	0,000	0,000		0,000	0,000
	N	1.275	1.275	1.275	1.275	1.275	1.275	1.275	1.275	1.275	1.275	1.275	1.275	1.275
logQIFn'	Pearson Correlation	.566(**)	.781(**)	.419(**)	.930(**)	.862(**)	.677(**)	.390(**)	.774(**)	.728(**)	.806(**)	.445(**)	1	.817(**)
	Sig. (2-tailed)	0,000	0,000	0,000	0,000	0,000	0,000	0,000	0,000	0,000	0,000	0,000		0,000
	N	1.275	1.275	1.275	1.275	1.275	1.275	1.275	1.275	1.275	1.275	1.275	1.275	1.275
logQOFn'	Pearson Correlation	.455(**)	.533(**)	.286(**)	.582(**)	.642(**)	.373(**)	.263(**)	.383(**)	.345(**)	.732(**)	.318(**)	.817(**)	1
	Sig. (2-tailed)	0,000	0,000	0,000	0,000	0,000	0,000	0,000	0,000	0,000	0,000	0,000	0,000	
	N	1.275	1.275	1.275	1.275	1.275	1.275	1.275	1.275	1.275	1.275	1.275	1.275	1.275

**. Correlation is significant at the 0.01 level (2-tailed).

b. Test statistics for regression model (winter data)

Model Summary

Model	R	R Square	Adjusted R Square	Std. Error of the Estimate
12&13	.785(c)	.616	.615	.219521475791349

c Predictors: (Constant), logQ, logQIFp', logQn

ANOVA(d)

Model		Sum of Squares	df	Mean Square	F	Sig.
12&13	Regression	98.210	3	32.737	679.330	.000(c)
	Residual	61.249	1271	.048		
	Total	159.459	1274			

c Predictors: (Constant), logQ, logQIFp', logQn

d Dependent Variable: log SSC

Coefficients(a)

Model		Unstandardized Coefficients	Standardized Coefficients	t	Sig.

		B	Std. Error	Beta	B	Std. Error
12&13	(Constant)	.465	.023		20.284	.000
	logQ	.908	.078	.658	11.595	.000
	logQIFp'	-.274	.035	-.198	-7.715	.000
	logQn	.367	.069	.265	5.299	.000

a Dependent Variable: log SSC

c. Residuals plotted in function of predicted values (winter data)

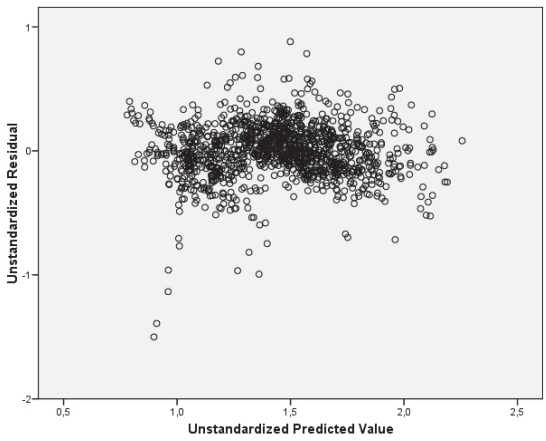

d. Histogram residuals (winter data)

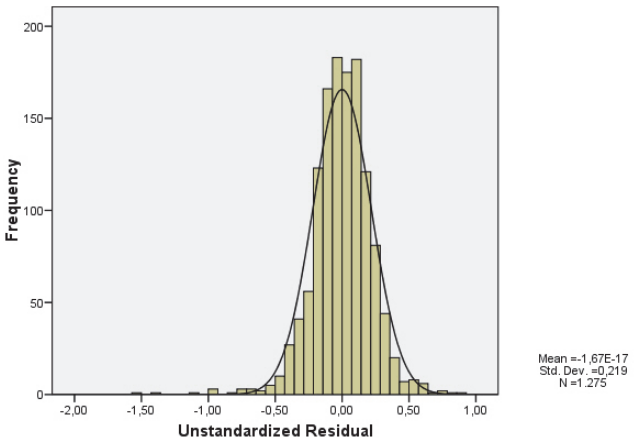

e. Pearson's r correlation coefficients (summer data)

Correlations

		log SSC	log Q	log BF'	log IF'	log OF'	log Qp	log QBFp'	log QIFp'	log QOFp'	log Qn	log QBFn'	log QIFn'	log QOFn'
logSSC	Pearson Correlation	1	.508(**)	.421(**)	.414(**)	.407(**)	.455(**)	.409(**)	.346(**)	.335(**)	.480(**)	.426(**)	.417(**)	.298(**)
	Sig. (2-tailed)		0,000	0,000	0,000	0,000	0,000	0,000	0,000	0,000	0,000	0,000	0,000	0,000
	N	1.384	1.384	1.384	1.384	1.384	1.384	1.384	1.384	1.384	1.384	1.384	1.384	1.384
logQ	Pearson Correlation	.508(**)	1	.827(**)	.790(**)	.694(**)	.935(**)	.802(**)	.711(**)	.626(**)	.932(**)	.835(**)	.763(**)	.484(**)
	Sig. (2-tailed)	0,000		0,000	0,000	0,000	0,000	0,000	0,000	0,000	0,000	0,000	0,000	0,000
	N	1.384	1.384	1.384	1.384	1.384	1.384	1.384	1.384	1.384	1.384	1.384	1.384	1.384
logQBF'	Pearson Correlation	.421(**)	.827(**)	1	.384(**)	.239(**)	.836(**)	.996(**)	.409(**)	.267(**)	.800(**)	.995(**)	.347(**)	.194(**)
	Sig. (2-tailed)	0,000	0,000		0,000	0,000	0,000	0,000	0,000	0,000	0,000	0,000	0,000	0,000
	N	1.384	1.384	1.384	1.384	1.384	1.384	1.384	1.384	1.384	1.384	1.384	1.384	1.384
logQIF'	Pearson Correlation	.414(**)	.790(**)	.384(**)	1	.808(**)	.768(**)	.353(**)	.931(**)	.870(**)	.707(**)	.402(**)	.928(**)	.554(**)
	Sig. (2-tailed)	0,000	0,000	0,000		0,000	0,000	0,000	0,000	0,000	0,000	0,000	0,000	0,000
	N	1.384	1.384	1.384	1.384	1.384	1.384	1.384	1.384	1.384	1.384	1.384	1.384	1.384
logQOF'	Pearson Correlation	.407(**)	.694(**)	.239(**)	.808(**)	1	.494(**)	.199(**)	.564(**)	.652(**)	.618(**)	.257(**)	.865(**)	.642(**)
	Sig. (2-tailed)	0,000	0,000	0,000	0,000		0,000	0,000	0,000	0,000	0,000	0,000	0,000	0,000
	N	1.384	1.384	1.384	1.384	1.384	1.384	1.384	1.384	1.384	1.384	1.384	1.384	1.384
logQp	Pearson Correlation	.455(**)	.935(**)	.836(**)	.768(**)	.494(**)	1	.828(**)	.793(**)	.700(**)	.849(**)	.840(**)	.657(**)	.319(**)
	Sig. (2-tailed)	0,000	0,000	0,000	0,000	0,000		0,000	0,000	0,000	0,000	0,000	0,000	0,000
	N	1.384	1.384	1.384	1.384	1.384	1.384	1.384	1.384	1.384	1.384	1.384	1.384	1.384
logQBFp'	Pearson Correlation	.409(**)	.802(**)	.996(**)	.353(**)	.199(**)	.828(**)	1	.390(**)	.248(**)	.775(**)	.991(**)	.310(**)	.164(**)
	Sig. (2-tailed)	0,000	0,000	0,000	0,000	0,000	0,000		0,000	0,000	0,000	0,000	0,000	0,000
	N	1.384	1.384	1.384	1.384	1.384	1.384	1.384	1.384	1.384	1.384	1.384	1.384	1.384
logQIFp'	Pearson Correlation	.346(**)	.711(**)	.409(**)	.931(**)	.564(**)	.793(**)	.390(**)	1	.813(**)	.610(**)	.422(**)	.773(**)	.352(**)
	Sig. (2-tailed)	0,000	0,000	0,000	0,000	0,000	0,000	0,000		0,000	0,000	0,000	0,000	0,000
	N	1.384	1.384	1.384	1.384	1.384	1.384	1.384	1.384	1.384	1.384	1.384	1.384	1.384
logQOFp'	Pearson Correlation	.335(**)	.626(**)	.267(**)	.870(**)	.652(**)	.700(**)	.248(**)	.813(**)	1	.510(**)	.278(**)	.744(**)	.349(**)
	Sig. (2-tailed)	0,000	0,000	0,000	0,000	0,000	0,000	0,000	0,000		0,000	0,000	0,000	0,000
	N	1.384	1.384	1.384	1.384	1.384	1.384	1.384	1.384	1.384	1.384	1.384	1.384	1.384

logQn	Pearson Correlation	.480(**)	.932(**)	.800(**)	.707(**)	.618(**)	.849(**)	.775(**)	.610(**)	.510(**)	1	.826(**)	.788(**)	.692(**)
	Sig. (2-tailed)	0,000	0,000	0,000	0,000	0,000	0,000	0,000	0,000	0,000		0,000	0,000	0,000
	N	1.384	1.384	1.384	1.384	1.384	1.384	1.384	1.384	1.384	1.384	1.384	1.384	1.384
logQBFn'	Pearson Correlation	.426(**)	.835(**)	.995(**)	.402(**)	.257(**)	.840(**)	.991(**)	.422(**)	.278(**)	.826(**)	1	.378(**)	.234(**)
	Sig. (2-tailed)	0,000	0,000	0,000	0,000	0,000	0,000	0,000	0,000	0,000	0,000		0,000	0,000
	N	1.384	1.384	1.384	1.384	1.384	1.384	1.384	1.384	1.384	1.384	1.384	1.384	1.384
logQlFn'	Pearson Correlation	.417(**)	.763(**)	.347(**)	.928(**)	.865(**)	.657(**)	.310(**)	.773(**)	.744(**)	.788(**)	.378(**)	1	.804(**)
	Sig. (2-tailed)	0,000	0,000	0,000	0,000	0,000	0,000	0,000	0,000	0,000	0,000	0,000		0,000
	N	1.384	1.384	1.384	1.384	1.384	1.384	1.384	1.384	1.384	1.384	1.384	1.384	1.384
logQOFn'	Pearson Correlation	.298(**)	.484(**)	.194(**)	.554(**)	.642(**)	.319(**)	.164(**)	.352(**)	.349(**)	.692(**)	.234(**)	.804(**)	1
	Sig. (2-tailed)	0,000	0,000	0,000	0,000	0,000	0,000	0,000	0,000	0,000	0,000	0,000	0,000	
	N	1.384	1.384	1.384	1.384	1.384	1.384	1.384	1.384	1.384	1.384	1.384	1.384	1.384

**. Correlation is significant at the 0.01 level (2-tailed).

f. Test statistics for regression model (summer data)

Model Summary

Model	R	R Square	Adjusted R Square	Std. Error of the Estimate
12&13	.526(d)	0,277	0,276	0,275095021168394

d. Predictors: (Constant), logQOF', logQBFn'

ANOVA(e)

Model		Sum of Squares	df	Mean Square	F	Sig.
12&13	Regression	39,971	2	19,985	264,086	.000(d)
	Residual	104,510	1.381	0,076		
	Total	144,481	1.383			

d. Predictors: (Constant), logOF', logQBFn'
e. Dependent Variable: log SSC

Coefficients(a)

Model		Unstandardized Coefficients		Standardized Coefficients	t	Sig.
		B	Std. Error	Beta		
12&13	(Constant)	0,435	0,034		12,629	0,000
	logQOF'	0,663	0,049	0,319	13,457	0,000
	logQBFn'	0,899	0,062	0,345	14,548	0,000

a. Dependent Variable: log SSC

g. Residuals plotted in function of predicted values (summer data)

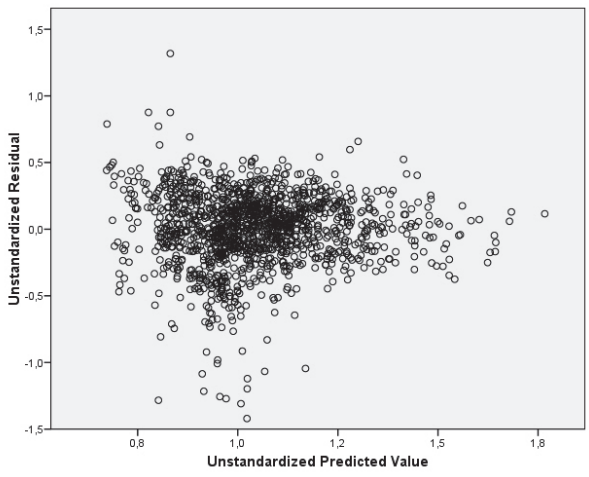

h. Histogram residuals (summer data)

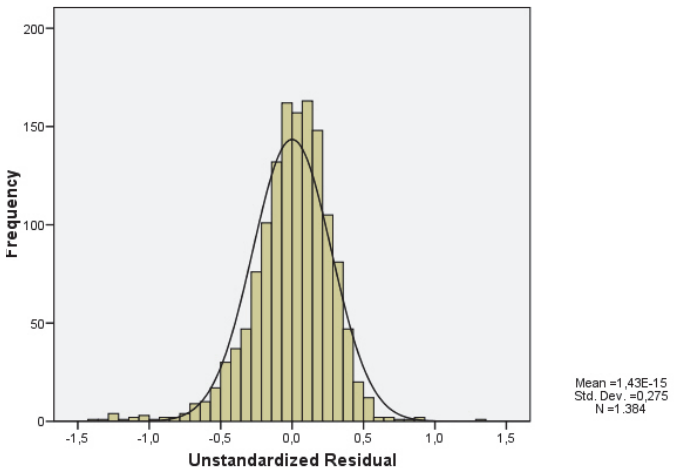

9. Regression model nr 14: SSC = f(Qn, QIF, Cond, QIFn, Turb)

a. Pearson's r correlation coefficients

Correlations

		SSC	Turb	Cond	Q	QBF	QIF	QOF	Qp	QBFp	QIFp	QOFp	Qn	QBFn	QIFn	QOFn
SSC	Pearson Correlation	1	.611(**)	-.641(**)	.663(**)	.628(**)	.477(**)	.460(**)	.548(**)	.621(**)	.395(**)	.212(**)	.786(**)	.650(**)	.626(**)	.628(**)
	Sig. (2-tailed)		0.000	0.000	0.000	0.000	0.000	0.000	0.000	0.000	0.000	0.000	0.000	0.000	0.000	0.000
	N	327	327	327	327	327	327	327	327	327	327	327	327	327	327	327
Turb	Pearson Correlation	.611(**)	1	-.630(**)	.840(**)	.671(**)	.663(**)	.719(**)	.678(**)	.651(**)	.497(**)	.453(**)	.731(**)	.691(**)	.670(**)	.402(**)
	Sig. (2-tailed)	0.000		0.000	0.000	0.000	0.000	0.000	0.000	0.000	0.000	0.000	0.000	0.000	0.000	0.000
	N	327	327	327	327	327	327	327	327	327	327	327	327	327	327	327
Cond	Pearson Correlation	-.641(**)	-.630(**)	1	-.763(**)	-.831(**)	-.558(**)	-.362(**)	-.794(**)	-.824(**)	-.581(**)	-.428(**)	-.701(**)	-.835(**)	-.488(**)	-.290(**)
	Sig. (2-tailed)	0.000	0.000		0.000	0.000	0.000	0.000	0.000	0.000	0.000	0.000	0.000	0.000	0.000	0.000
	N	327	327	327	327	327	327	327	327	327	327	327	327	327	327	327
Q	Pearson Correlation	.663(**)	.840(**)	-.763(**)	1	.811(**)	.866(**)	.775(**)	.895(**)	.791(**)	.761(**)	.625(**)	.884(**)	.831(**)	.818(**)	.484(**)
	Sig. (2-tailed)	0.000	0.000	0.000		0.000	0.000	0.000	0.000	0.000	0.000	0.000	0.000	0.000	0.000	0.000
	N	327	327	327	327	327	327	327	327	327	327	327	327	327	327	327
QBF	Pearson Correlation	.628(**)	.671(**)	-.831(**)	.811(**)	1	.488(**)	.298(**)	.860(**)	.998(**)	.541(**)	.359(**)	.743(**)	.998(**)	.414(**)	.246(**)
	Sig. (2-tailed)	0.000	0.000	0.000	0.000		0.000	0.000	0.000	0.000	0.000	0.000	0.000	0.000	0.000	0.000
	N	327	327	327	327	327	327	327	327	327	327	327	327	327	327	327
QIF	Pearson Correlation	.477(**)	.663(**)	-.558(**)	.866(**)	.488(**)	1	.781(**)	.814(**)	.460(**)	.909(**)	.822(**)	.760(**)	.513(**)	.899(**)	.513(**)
	Sig. (2-tailed)	0.000	0.000	0.000	0.000	0.000		0.000	0.000	0.000	0.000	0.000	0.000	0.000	0.000	0.000
	N	327	327	327	327	327	327	327	327	327	327	327	327	327	327	327
QOF	Pearson Correlation	.460(**)	.719(**)	-.362(**)	.775(**)	.298(**)	.781(**)	1	.462(**)	.271(**)	.495(**)	.470(**)	.651(**)	.332(**)	.846(**)	.516(**)
	Sig. (2-tailed)	0.000	0.000	0.000	0.000	0.000	0.000		0.000	0.000	0.000	0.000	0.000	0.000	0.000	0.000
	N	327	327	327	327	327	327	327	327	327	327	327	327	327	327	327
Qp	Pearson Correlation	.548(**)	.678(**)	-.794(**)	.895(**)	.860(**)	.814(**)	.462(**)	1	.846(**)	.856(**)	.758(**)	.769(**)	.865(**)	.637(**)	.301(**)
	Sig. (2-tailed)	0.000	0.000	0.000	0.000	0.000	0.000	0.000		0.000	0.000	0.000	0.000	0.000	0.000	0.000
	N	327	327	327	327	327	327	327	327	327	327	327	327	327	327	327
QBFp	Pearson Correlation	.621(**)	.651(**)	-.824(**)	.791(**)	.998(**)	.460(**)	.271(**)	.846(**)	1	.522(**)	.333(**)	.729(**)	.995(**)	.389(**)	.235(**)
	Sig. (2-tailed)	0.000	0.000	0.000	0.000	0.000	0.000	0.000	0.000		0.000	0.000	0.000	0.000	0.000	0.000
	N	327	327	327	327	327	327	327	327	327	327	327	327	327	327	327
QIFp	Pearson Correlation	.395(**)	.497(**)	-.581(**)	.761(**)	.541(**)	.909(**)	.495(**)	.856(**)	.522(**)	1	.763(**)	.662(**)	.555(**)	.720(**)	.360(**)
	Sig. (2-tailed)	0.000	0.000	0.000	0.000	0.000	0.000	0.000	0.000	0.000		0.000	0.000	0.000	0.000	0.000
	N	327	327	327	327	327	327	327	327	327	327	327	327	327	327	327
QOFp	Pearson Correlation	.212(**)	.453(**)	-.428(**)	.625(**)	.359(**)	.822(**)	.470(**)	.758(**)	.333(**)	.763(**)	1	.448(**)	.369(**)	.587(**)	.172(**)
	Sig. (2-tailed)	0.000	0.000	0.000	0.000	0.000	0.000	0.000	0.000	0.000	0.000		0.000	0.000	0.000	0.002
	N	327	327	327	327	327	327	327	327	327	327	327	327	327	327	327
Qn	Pearson Correlation	.786(**)	.731(**)	-.701(**)	.884(**)	.743(**)	.760(**)	.651(**)	.769(**)	.729(**)	.662(**)	.448(**)	1	.771(**)	.878(**)	.805(**)
	Sig. (2-tailed)	0.000	0.000	0.000	0.000	0.000	0.000	0.000	0.000	0.000	0.000	0.000		0.000	0.000	0.000
	N	327	327	327	327	327	327	327	327	327	327	327	327	327	327	327
QBFn	Pearson Correlation	.650(**)	.691(**)	-.835(**)	.831(**)	.998(**)	.513(**)	.332(**)	.865(**)	.995(**)	.555(**)	.369(**)	.771(**)	1	.452(**)	.283(**)
	Sig. (2-tailed)	0.000	0.000	0.000	0.000	0.000	0.000	0.000	0.000	0.000	0.000	0.000	0.000		0.000	0.000
	N	327	327	327	327	327	327	327	327	327	327	327	327	327	327	327
QIFn	Pearson Correlation	.626(**)	.670(**)	-.488(**)	.818(**)	.414(**)	.899(**)	.846(**)	.637(**)	.389(**)	.720(**)	.587(**)	.878(**)	.452(**)	1	.808(**)
	Sig. (2-tailed)	0.000	0.000	0.000	0.000	0.000	0.000	0.000	0.000	0.000	0.000	0.000	0.000	0.000		0.000
	N	327	327	327	327	327	327	327	327	327	327	327	327	327	327	327
QOFn	Pearson Correlation	.628(**)	.402(**)	-.290(**)	.484(**)	.246(**)	.513(**)	.516(**)	.301(**)	.235(**)	.360(**)	.172(**)	.805(**)	.283(**)	.808(**)	1
	Sig. (2-tailed)	0.000	0.000	0.000	0.000	0.000	0.000	0.000	0.000	0.000	0.000	0.002	0.000	0.000	0.000	
	N	327	327	327	327	327	327	327	327	327	327	327	327	327	327	327

**. Correlation is significant at the 0.01 level (2-tailed).

b. Test statistics for regression model

Model Summary

Model	R	R Square	Adjusted R Square	Std. Error of the Estimate
14	.830(e)	.688	.683	13.074077234557690

e Predictors: (Constant), Qn, QIF, Cond, QIFn, Turb

ANOVA(f)

Model		Sum of Squares	df	Mean Square	F	Sig.
14	Regression	121122.883	5	24224.577	141.721	.000(e)
	Residual	54869.010	321	170.931		
	Total	175991.893	326			

e Predictors: (Constant), Qn, QIF, Cond, QIFn, Turb
f Dependent Variable: SSC

Coefficients(a)

Model		Unstandardized Coefficients		Standardized Coefficients	t	Sig.
		B	Std. Error	Beta	B	Std. Error
14	(Constant)	27.223	6.435		4.230	.000
	Qn	3.436	.646	.532	5.315	.000
	QIF	-13.155	1.948	-.584	-6.753	.000
	Cond	-54.047	10.365	-.298	-5.214	.000
	QIFn	9.166	2.476	.464	3.701	.000
	Turb	.093	.041	.110	2.269	.024

a Dependent Variable: SSC

c. Residuals versus predicted

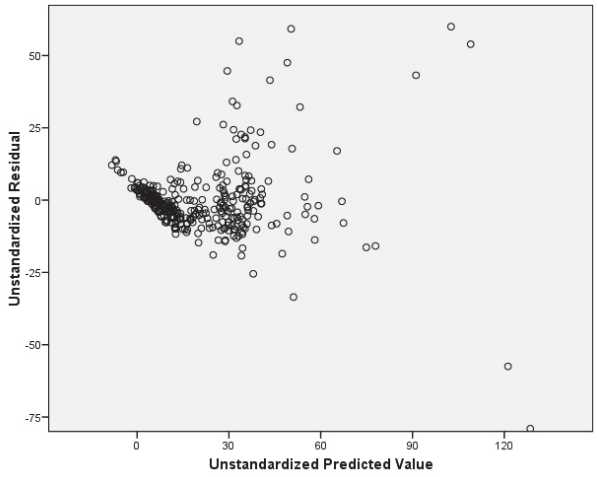

d. Histogram Residuals

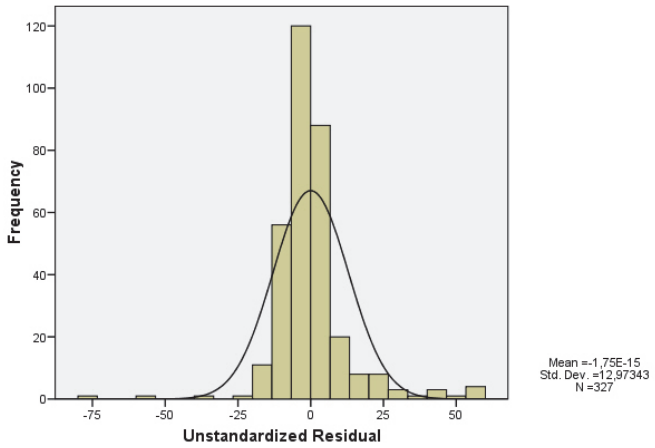

10. Model 15 SSC_{winter} = f(QIF, Cond, QIFp) and SSC_{summer} = f(Qn, Turb, QIFp, QOFp)

a. Pearson's r correlation coefficients (winter data)

Correlations

		SSC	Turb	Cond	Q	QBF	QIF	QOF	Qp	QBFp	QIFp	QOFp	Qn	QBFn	QIFn	QOFn
SSC	Pearson Correlation	1	.402(**)	-.481(**)	.467(**)	.424(**)	.335(**)	.379(**)	.288(**)	.425(**)	.234(**)	0.051	.668(**)	.454(**)	.542(**)	.606(**)
	Sig. (2-tailed)		0.000	0.000	0.000	0.000	0.000	0.000	0.001	0.000	0.006	0.556	0.000	0.000	0.000	0.000
	N	136	136	136	136	136	136	136	136	136	136	136	136	136	136	136
Turb	Pearson Correlation	.402(**)	1	-.523(**)	.815(**)	.524(**)	.666(**)	.785(**)	.548(**)	.493(**)	.430(**)	.427(**)	.625(**)	.559(**)	.669(**)	.338(**)
	Sig. (2-tailed)	0.000		0.000	0.000	0.000	0.000	0.000	0.000	0.000	0.000	0.000	0.000	0.000	0.000	0.000
	N	136	136	136	136	136	136	136	136	136	136	136	136	136	136	136
Cond	Pearson Correlation	-.481(**)	-.523(**)	1	-.662(**)	-.856(**)	-.495(**)	-.295(**)	-.727(**)	-.854(**)	-.530(**)	-.396(**)	-.551(**)	-.854(**)	-.390(**)	-.175(*)
	Sig. (2-tailed)	0.000	0.000		0.000	0.000	0.000	0.001	0.000	0.000	0.000	0.000	0.000	0.000	0.000	0.042
	N	136	136	136	136	136	136	136	136	136	136	136	136	136	136	136
Q	Pearson Correlation	.467(**)	.815(**)	-.662(**)	1	.702(**)	.909(**)	.842(**)	.822(**)	.670(**)	.756(**)	.623(**)	.808(**)	.737(**)	.847(**)	.439(**)
	Sig. (2-tailed)	0.000	0.000	0.000		0.000	0.000	0.000	0.000	0.000	0.000	0.000	0.000	0.000	0.000	0.000
	N	136	136	136	136	136	136	136	136	136	136	136	136	136	136	136
QBF	Pearson Correlation	.424(**)	.524(**)	-.856(**)	.702(**)	1	.485(**)	.261(**)	.786(**)	.997(**)	.561(**)	.362(**)	.583(**)	.996(**)	.363(**)	0.153
	Sig. (2-tailed)	0.000	0.000	0.000	0.000		0.000	0.002	0.000	0.000	0.000	0.000	0.000	0.000	0.000	0.075
	N	136	136	136	136	136	136	136	136	136	136	136	136	136	136	136
QIF	Pearson Correlation	.335(**)	.666(**)	-.495(**)	.909(**)	.485(**)	1	.766(**)	.848(**)	.447(**)	.895(**)	.801(**)	.750(**)	.521(**)	.882(**)	.459(**)
	Sig. (2-tailed)	0.000	0.000	0.000	0.000	0.000		0.000	0.000	0.000	0.000	0.000	0.000	0.000	0.000	0.000
	N	136	136	136	136	136	136	136	136	136	136	136	136	136	136	136
QOF	Pearson Correlation	.379(**)	.785(**)	-.295(**)	.842(**)	.261(**)	.766(**)	1	.430(**)	.224(**)	.450(**)	.411(**)	.654(**)	.314(**)	.831(**)	.460(**)
	Sig. (2-tailed)	0.000	0.000	0.001	0.000	0.002	0.000		0.000	0.009	0.000	0.000	0.000	0.000	0.000	0.000
	N	136	136	136	136	136	136	136	136	136	136	136	136	136	136	136
Qp	Pearson Correlation	.288(**)	.548(**)	-.727(**)	.822(**)	.786(**)	.848(**)	.430(**)	1	.763(**)	.899(**)	.828(**)	.625(**)	.793(**)	.606(**)	.207(*)
	Sig. (2-tailed)	0.001	0.000	0.000	0.000	0.000	0.000	0.000		0.000	0.000	0.000	0.000	0.000	0.000	0.015
	N	136	136	136	136	136	136	136	136	136	136	136	136	136	136	136
QBFp	Pearson Correlation	.425(**)	.493(**)	-.854(**)	.670(**)	.997(**)	.447(**)	.224(**)	.763(**)	1	.537(**)	.324(**)	.565(**)	.992(**)	.332(**)	0.144
	Sig. (2-tailed)	0.000	0.000	0.000	0.000	0.000	0.000	0.009	0.000		0.000	0.000	0.000	0.000	0.000	0.094
	N	136	136	136	136	136	136	136	136	136	136	136	136	136	136	136
QIFp	Pearson Correlation	.234(**)	.430(**)	-.530(**)	.756(**)	.561(**)	.895(**)	.450(**)	.899(**)	.537(**)	1	.744(**)	.619(**)	.576(**)	.681(**)	.302(**)
	Sig. (2 tailed)	0.006	0.000	0.000	0.000	0.000	0.000	0.000	0.000	0.000		0.000	0.000	0.000	0.000	0.000
	N	136	136	136	136	136	136	136	136	136	136	136	136	136	136	136
QOFp	Pearson Correlation	0.051	.427(**)	-.396(**)	.623(**)	.362(**)	.801(**)	.411(**)	.828(**)	.324(**)	.744(**)	1	.383(**)	.371(**)	.527(**)	0.093
	Sig. (2-tailed)	0.556	0.000	0.000	0.000	0.000	0.000	0.000	0.000	0.000	0.000		0.000	0.000	0.000	0.279
	N	136	136	136	136	136	136	136	136	136	136	136	136	136	136	136
Qn	Pearson Correlation	.668(**)	.625(**)	-.551(**)	.808(**)	.583(**)	.750(**)	.654(**)	.625(**)	.565(**)	.619(**)	.383(**)	1	.632(**)	.917(**)	.861(**)
	Sig. (2-tailed)	0.000	0.000	0.000	0.000	0.000	0.000	0.000	0.000	0.000	0.000	0.000		0.000	0.000	0.000
	N	136	136	136	136	136	136	136	136	136	136	136	136	136	136	136

QBFn	Pearson Correlation	.454(**)	.559(**)	-.854(**)	.737(**)	.996(**)	.521(**)	.314(**)	.793(**)	.992(**)	.576(**)	.371(**)	.632(**)	1	.419(**)	.207(*)
	Sig. (2-tailed)	0.000	0.000	0.000	0.000	0.000	0.000	0.000	0.000	0.000	0.000	0.000	0.000		0.000	0.016
	N	136	136	136	136	136	136	136	136	136	136	136	136	136	136	136
QIFn	Pearson Correlation	.542(**)	.669(**)	-.390(**)	.847(**)	.363(**)	.882(**)	.831(**)	.606(**)	.332(**)	.681(**)	.527(**)	.917(**)	.419(**)	1	.790(**)
	Sig. (2-tailed)	0.000	0.000	0.000	0.000	0.000	0.000	0.000	0.000	0.000	0.000	0.000	0.000	0.000		0.000
	N	136	136	136	136	136	136	136	136	136	136	136	136	136	136	136
QOFn	Pearson Correlation	.606(**)	.338(**)	-.175(*)	.439(**)	0.153	.459(**)	.460(**)	.207(*)	0.144	.302(**)	0.093	.861(**)	.207(*)	.790(**)	1
	Sig. (2-tailed)	0.000	0.000	0.042	0.000	0.075	0.000	0.000	0.015	0.094	0.000	0.279	0.000	0.016	0.000	
	N	136	136	136	136	136	136	136	136	136	136	136	136	136	136	136

**. Correlation is significant at the 0.01 level (2-tailed).
*. Correlation is significant at the 0.05 level (2-tailed).

a. Test statistics for regression model (winter data)

Model Summary

Model	R	R Square	Adjusted R Square	Std. Error of the Estimate
15	.754(e)	.569	.559	18.375328542801340

e Predictors: (Constant), QIF, Cond, QIFn

ANOVA(f)

Model		Sum of Squares	df	Mean Square	F	Sig.
15	Regression	58728.398	3	19576.133	57.977	.000(e)
	Residual	44570.156	132	337.653		
	Total	103298.554	135			

e Predictors: (Constant), QIF, Cond, QIFn
f Dependent Variable: SSC

Coefficients(a)

Model		Unstandardized Coefficients		Standardized Coefficients	t	Sig.
		B	Std. Error	Beta	B	Std. Error
15	(Constant)	75.783	6.904		10.977	.000
	QIF	-19.962	2.626	-.986	-7.603	.000
	Cond	-130.542	17.525	-.493	-7.449	.000
	QIFn	21.306	2.137	1.220	9.971	.000

a Dependent Variable: SSC

b. Residuals versus predicted (winter data)

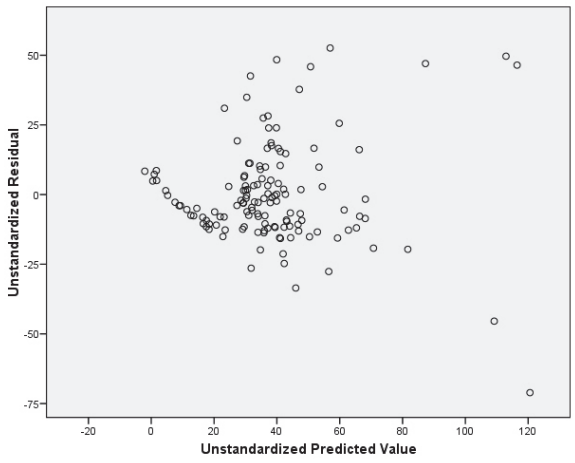

c. Histogram residuals (winter data)

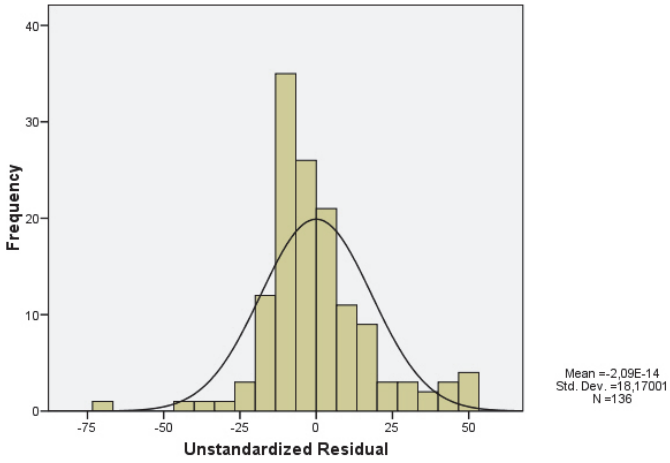

d. Pearson's r correlation coefficients (summer data)

Correlations

		SSC	Turb	Cond	Q	QBF	QIF	QOF	Qp	QBFp	QIFp	QOFp	Qn	QBFn	QIFn	QOFn
SSC	Pearson Correlation	1	.770(**)	-.634(**)	.851(**)	.848(**)	.348(**)	.352(**)	.791(**)	.843(**)	.311(**)	.274(**)	.867(**)	.853(**)	.367(**)	.314(**)
	Sig. (2-tailed)		0.000	0.000	0.000	0.000	0.000	0.000	0.000	0.000	0.000	0.000	0.000	0.000	0.000	0.000
	N	191	191	191	191	191	191	191	191	191	191	191	191	191	191	191
Turb	Pearson Correlation	.770(**)	1	-.530(**)	.705(**)	.766(**)	.206(**)	.148(*)	.689(**)	.762(**)	.237(**)	.174(*)	.676(**)	.764(**)	0.140	0.049
	Sig. (2-tailed)	0.000		0.000	0.000	0.000	0.004	0.041	0.000	0.000	0.001	0.016	0.000	0.000	0.053	0.497
	N	191	191	191	191	191	191	191	191	191	191	191	191	191	191	191
Cond	Pearson Correlation	-.634(**)	-.530(**)	1	-.760(**)	-.703(**)	-.506(**)	-.307(**)	-.765(**)	-.699(**)	-.531(**)	-.421(**)	-.712(**)	-.703(**)	-.403(**)	-.151(*)
	Sig. (2-tailed)	0.000	0.000		0.000	0.000	0.000	0.000	0.000	0.000	0.000	0.000	0.000	0.000	0.000	0.037
	N	191	191	191	191	191	191	191	191	191	191	191	191	191	191	191
Q	Pearson Correlation	.851(**)	.705(**)	-.760(**)	1	.908(**)	.634(**)	.497(**)	.960(**)	.898(**)	.608(**)	.517(**)	.951(**)	.912(**)	.556(**)	.274(**)
	Sig. (2-tailed)	0.000	0.000	0.000		0.000	0.000	0.000	0.000	0.000	0.000	0.000	0.000	0.000	0.000	0.000
	N	191	191	191	191	191	191	191	191	191	191	191	191	191	191	191
QBF	Pearson Correlation	.848(**)	.766(**)	-.703(**)	.908(**)	1	.286(**)	0.122	.914(**)	.999(**)	.371(**)	.218(**)	.887(**)	.999(**)	.190(**)	0.070
	Sig. (2-tailed)	0.000	0.000	0.000	0.000		0.000	0.093	0.000	0.000	0.000	0.002	0.000	0.000	0.008	0.336
	N	191	191	191	191	191	191	191	191	191	191	191	191	191	191	191
QIF	Pearson Correlation	.348(**)	.206(**)	-.506(**)	.634(**)	.286(**)	1	.736(**)	.622(**)	.267(**)	.907(**)	.878(**)	.541(**)	.295(**)	.884(**)	.375(**)
	Sig. (2-tailed)	0.000	0.004	0.000	0.000	0.000		0.000	0.000	0.000	0.000	0.000	0.000	0.000	0.000	0.000
	N	191	191	191	191	191	191	191	191	191	191	191	191	191	191	191
QOF	Pearson Correlation	.352(**)	.148(*)	-.307(**)	.497(**)	0.122	.736(**)	1	.307(**)	0.100	.410(**)	.586(**)	.452(**)	0.135	.862(**)	.572(**)
	Sig. (2-tailed)	0.000	0.041	0.000	0.000	0.093	0.000		0.000	0.169	0.000	0.000	0.000	0.063	0.000	0.000
	N	191	191	191	191	191	191	191	191	191	191	191	191	191	191	191
Qp	Pearson Correlation	.791(**)	.689(**)	-.765(**)	.960(**)	.914(**)	.622(**)	.307(**)	1	.909(**)	.692(**)	.566(**)	.891(**)	.915(**)	.449(**)	0.120
	Sig. (2-tailed)	0.000	0.000	0.000	0.000	0.000	0.000	0.000		0.000	0.000	0.000	0.000	0.000	0.000	0.098
	N	191	191	191	191	191	191	191	191	191	191	191	191	191	191	191
QBFp	Pearson Correlation	.843(**)	.762(**)	-.699(**)	.898(**)	.999(**)	.267(**)	0.100	.909(**)	1	.359(**)	.204(**)	.879(**)	.997(**)	.171(*)	0.061
	Sig. (2-tailed)	0.000	0.000	0.000	0.000	0.000	0.000	0.169	0.000		0.000	0.005	0.000	0.000	0.018	0.405
	N	191	191	191	191	191	191	191	191	191	191	191	191	191	191	191
QIFp	Pearson Correlation	.311(**)	.237(**)	-.531(**)	.608(**)	.371(**)	.907(**)	.410(**)	.692(**)	.359(**)	1	.769(**)	.506(**)	.376(**)	.672(**)	.158(*)
	Sig. (2-tailed)	0.000	0.001	0.000	0.000	0.000	0.000	0.000	0.000	0.000		0.000	0.000	0.000	0.000	0.029
	N	191	191	191	191	191	191	191	191	191	191	191	191	191	191	191
QOFp	Pearson Correlation	.274(**)	.174(*)	-.421(**)	.517(**)	.218(**)	.878(**)	.586(**)	.566(**)	.204(**)	.769(**)	1	.382(**)	.220(**)	.693(**)	.157(*)
	Sig. (2-tailed)	0.000	0.016	0.000	0.000	0.002	0.000	0.000	0.000	0.005	0.000		0.000	0.002	0.000	0.030
	N	191	191	191	191	191	191	191	191	191	191	191	191	191	191	191
Qn	Pearson Correlation	.867(**)	.676(**)	-.712(**)	.951(**)	.887(**)	.541(**)	.452(**)	.891(**)	.879(**)	.506(**)	.382(**)	1	.899(**)	.587(**)	.495(**)
	Sig. (2-tailed)	0.000	0.000	0.000	0.000	0.000	0.000	0.000	0.000	0.000	0.000	0.000		0.000	0.000	0.000
	N	191	191	191	191	191	191	191	191	191	191	191	191	191	191	191
QBFn	Pearson Correlation	.853(**)	.764(**)	-.703(**)	.912(**)	.999(**)	.295(**)	0.135	.915(**)	.997(**)	.376(**)	.220(**)	.899(**)	1	.209(**)	0.095
	Sig. (2-tailed)	0.000	0.000	0.000	0.000	0.000	0.000	0.063	0.000	0.000	0.000	0.002	0.000		0.004	0.192
	N	191	191	191	191	191	191	191	191	191	191	191	191	191	191	191
QIFn	Pearson Correlation	.367(**)	0.140	-.403(**)	.556(**)	.190(**)	.884(**)	.862(**)	.449(**)	.171(*)	.672(**)	.693(**)	.587(**)	.209(**)	1	.745(**)
	Sig. (2-tailed)	0.000	0.053	0.000	0.000	0.008	0.000	0.000	0.000	0.018	0.000	0.000	0.000	0.004		0.000
	N	191	191	191	191	191	191	191	191	191	191	191	191	191	191	191
QOFn	Pearson Correlation	.314(**)	0.049	-.151(*)	.274(**)	0.070	.375(**)	.572(**)	0.120	0.061	.158(*)	.157(*)	.495(**)	0.095	.745(**)	1
	Sig. (2-tailed)	0.000	0.497	0.037	0.000	0.336	0.000	0.000	0.098	0.405	0.029	0.030	0.000	0.192	0.000	
	N	191	191	191	191	191	191	191	191	191	191	191	191	191	191	191

**. Correlation is significant at the 0.01 level (2-tailed).
*. Correlation is significant at the 0.05 level (2-tailed).

e. Test statistics regression model (summer data)

Model Summary(h)

Model	R	R Square	Adjusted R Square	Std. Error of the Estimate
15	.925(g)	.856	.852	3.304875116616437

g Predictors: (Constant), QOF, Turb, QOFn, QIFn, Qp
h Dependent Variable: SSC

ANOVA(h)

Model		Sum of Squares	df	Mean Square	F	Sig.
15	Regression	12011.516	5	2402.303	219.947	.000(g)
	Residual	2020.607	185	10.922		
	Total	14032.123	190			

g Predictors: (Constant), QOF, Turb, QOFn, QIFn, Qp
h Dependent Variable: SSC

Coefficients(a)

Model		Unstandardized Coefficients		Standardized Coefficients	t	Sig.
		B	Std. Error	Beta	B	Std. Error
15	(Constant)	-2.313	.508		-4.557	.000
	QOF	10.358	1.217	.536	8.511	.000
	Turb	.141	.027	.228	5.149	.000
	QOFn	11.183	.941	.599	11.886	.000
	QIFn	-18.226	1.822	-.942	-10.004	.000
	Qp	3.288	.219	.821	15.045	.000

a Dependent Variable: SSC

f. Residuals versus predicted (summer data)

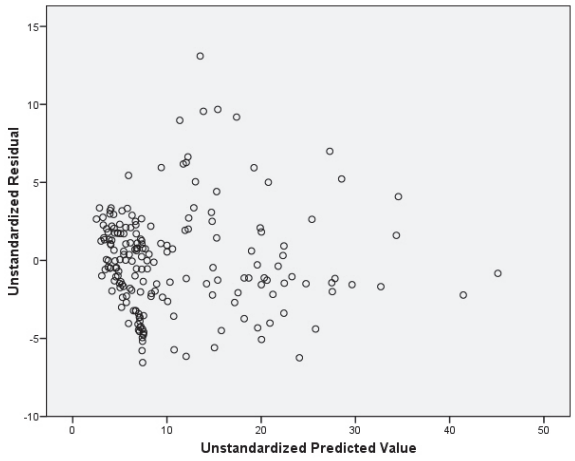

g. Histogram residuals (summer data)

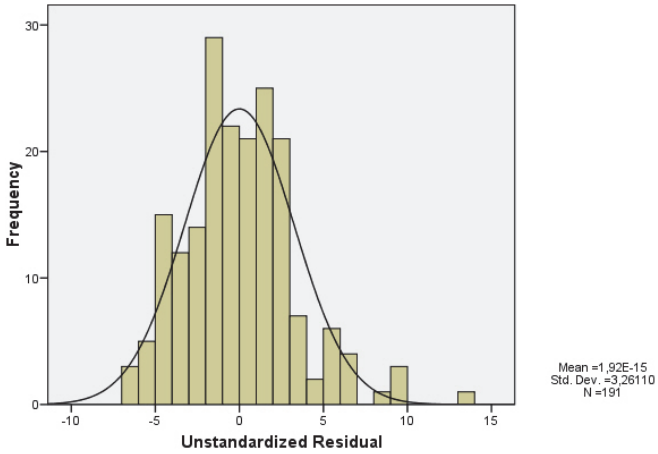

11. Model 16&17: LogSSC = (f(logQn, logTurb, logQIF', logCond, logQBFn')

a. Pearson's r correlation coefficients

Correlations

		logTurb	logCond	log SSC	logQ	logQBF'	logQIF'	logQOF'	logQp	LogQBFp'	logQIFp'	logQOFp'	logQn	logQBFn'	logQIFn'	logQOFn'
logTurb	Pearson Correlation	1	-.816(**)	.851(**)	.882(**)	.883(**)	.523(**)	.481(**)	.838(**)	.876(**)	.472(**)	.368(**)	.853(**)	.890(**)	.521(**)	.377(**)
	Sig. (2-tailed)		0.000	0.000	0.000	0.000	0.000	0.000	0.000	0.000	0.000	0.000	0.000	0.000	0.000	0.000
	N	327	327	327	327	327	327	327	327	327	327	327	327	327	327	327
logCond	Pearson Correlation	-.816(**)	1	-.781(**)	-.884(**)	-.847(**)	-.645(**)	-.474(**)	-.901(**)	-.840(**)	-.659(**)	-.550(**)	-.837(**)	-.851(**)	-.578(**)	-.372(**)
	Sig. (2-tailed)	0.000		0.000	0.000	0.000	0.000	0.000	0.000	0.000	0.000	0.000	0.000	0.000	0.000	0.000
	N	327	327	327	327	327	327	327	327	327	327	327	327	327	327	327
log SSC	Pearson Correlation	.851(**)	-.781(**)	1	.831(**)	.813(**)	.495(**)	.441(**)	.780(**)	.808(**)	.432(**)	.325(**)	.859(**)	.823(**)	.547(**)	.491(**)
	Sig. (2-tailed)	0.000	0.000		0.000	0.000	0.000	0.000	0.000	0.000	0.000	0.000	0.000	0.000	0.000	0.000
	N	327	327	327	327	327	327	327	327	327	327	327	327	327	327	327
logQ	Pearson Correlation	.882(**)	-.884(**)	.831(**)	1	.903(**)	.744(**)	.651(**)	.955(**)	.892(**)	.691(**)	.567(**)	.951(**)	.912(**)	.708(**)	.486(**)
	Sig. (2-tailed)	0.000	0.000	0.000		0.000	0.000	0.000	0.000	0.000	0.000	0.000	0.000	0.000	0.000	0.000
	N	327	327	327	327	327	327	327	327	327	327	327	327	327	327	327
logQBF'	Pearson Correlation	.883(**)	-.847(**)	.813(**)	.903(**)	1	.447(**)	.305(**)	.923(**)	.999(**)	.479(**)	.347(**)	.867(**)	.999(**)	.402(**)	.260(**)
	Sig. (2-tailed)	0.000	0.000	0.000	0.000		0.000	0.000	0.000	0.000	0.000	0.000	0.000	0.000	0.000	0.000
	N	327	327	327	327	327	327	327	327	327	327	327	327	327	327	327

logQIF'	Pearson Correlation	.523(**)	-.645(**)	.495(**)	.744(**)	.447(**)	1	.818(**)	.703(**)	.426(**)	.934(**)	.827(**)	.703(**)	.466(**)	.931(**)	.621(**)
	Sig. (2-tailed)	0.000	0.000	0.000	0.000	0.000		0.000	0.000	0.000	0.000	0.000	0.000	0.000	0.000	0.000
	N	327	327	327	327	327	327	327	327	327	327	327	327	327	327	327
logQOF'	Pearson Correlation	.481(**)	-.474(**)	.441(**)	.651(**)	.305(**)	.818(**)	1	.473(**)	.283(**)	.596(**)	.570(**)	.587(**)	.331(**)	.839(**)	.600(**)
	Sig. (2-tailed)	0.000	0.000	0.000	0.000	0.000	0.000		0.000	0.000	0.000	0.000	0.000	0.000	0.000	0.000
	N	327	327	327	327	327	327	327	327	327	327	327	327	327	327	327
logQp	Pearson Correlation	.838(**)	-.901(**)	.780(**)	.955(**)	.923(**)	.703(**)	.473(**)	1	.917(**)	.736(**)	.642(**)	.897(**)	.926(**)	.605(**)	.358(**)
	Sig. (2-tailed)	0.000	0.000	0.000	0.000	0.000	0.000	0.000		0.000	0.000	0.000	0.000	0.000	0.000	0.000
	N	327	327	327	327	327	327	327	327	327	327	327	327	327	327	327
LogQBFp'	Pearson Correlation	.876(**)	-.840(**)	.808(**)	.892(**)	.999(**)	.426(**)	.283(**)	.917(**)	1	.464(**)	.328(**)	.857(**)	.997(**)	.381(**)	.247(**)
	Sig. (2-tailed)	0.000	0.000	0.000	0.000	0.000	0.000	0.000	0.000		0.000	0.000	0.000	0.000	0.000	0.000
	N	327	327	327	327	327	327	327	327	327	327	327	327	327	327	327
logQIFp'	Pearson Correlation	.472(**)	-.659(**)	.432(**)	.691(**)	.479(**)	.934(**)	.596(**)	.736(**)	.464(**)	1	.811(**)	.632(**)	.489(**)	.787(**)	.447(**)
	Sig. (2-tailed)	0.000	0.000	0.000	0.000	0.000	0.000	0.000	0.000	0.000		0.000	0.000	0.000	0.000	0.000
	N	327	327	327	327	327	327	327	327	327	327	327	327	327	327	327
logQOFp'	Pearson Correlation	.368(**)	-.550(**)	.325(**)	.567(**)	.347(**)	.827(**)	.570(**)	.642(**)	.328(**)	.811(**)	1	.479(**)	.352(**)	.662(**)	.302(**)
	Sig. (2-tailed)	0.000	0.000	0.000	0.000	0.000	0.000	0.000	0.000	0.000	0.000		0.000	0.000	0.000	0.000
	N	327	327	327	327	327	327	327	327	327	327	327	327	327	327	327
logQn	Pearson Correlation	.853(**)	-.837(**)	.859(**)	.951(**)	.867(**)	.703(**)	.587(**)	.897(**)	.857(**)	.632(**)	.479(**)	1	.882(**)	.760(**)	.675(**)
	Sig. (2-tailed)	0.000	0.000	0.000	0.000	0.000	0.000	0.000	0.000	0.000	0.000	0.000		0.000	0.000	0.000
	N	327	327	327	327	327	327	327	327	327	327	327	327	327	327	327
logQBFn'	Pearson Correlation	.890(**)	-.851(**)	.823(**)	.912(**)	.999(**)	.466(**)	.331(**)	.926(**)	.997(**)	.489(**)	.352(**)	.882(**)	1	.429(**)	.289(**)
	Sig. (2-tailed)	0.000	0.000	0.000	0.000	0.000	0.000	0.000	0.000	0.000	0.000	0.000	0.000		0.000	0.000
	N	327	327	327	327	327	327	327	327	327	327	327	327	327	327	327
logQIFn'	Pearson Correlation	.521(**)	.578(**)	.547(**)	.708(**)	.402(**)	.931(**)	.839(**)	.605(**)	.381(**)	.787(**)	.662(**)	.760(**)	.429(**)	1	.842(**)
	Sig. (2-tailed)	0.000	0.000	0.000	0.000	0.000	0.000	0.000	0.000	0.000	0.000	0.000	0.000	0.000		0.000
	N	327	327	327	327	327	327	327	327	327	327	327	327	327	327	327
logQOFn'	Pearson Correlation	.377(**)	-.372(**)	.491(**)	.486(**)	.260(**)	.621(**)	.600(**)	.358(**)	.247(**)	.447(**)	.302(**)	.675(**)	.289(**)	.842(**)	1
	Sig. (2-tailed)	0.000	0.000	0.000	0.000	0.000	0.000	0.000	0.000	0.000	0.000	0.000	0.000	0.000	0.000	
	N	327	327	327	327	327	327	327	327	327	327	327	327	327	327	327

**. Correlation is significant at the 0.01 level (2-tailed).

b. Test statistics regression model

Model Summary

Model	R	R Square	Adjusted R Square	Std. Error of the Estimate
16&17	.900(e)	.811	.808	.192180044615667

e Predictors: (Constant), logQn, logTurb, logQIF', logCond, logQBFn'

ANOVA(f)

Model		Sum of Squares	df	Mean Square	F	Sig.
16&17	Regression	50.818	5	10.164	275.191	.000(e)
	Residual	11.856	321	.037		
	Total	62.674	326			

e Predictors: (Constant), logQn, logTurb, logQIF', logCond, logQBFn'

f Dependent Variable: log SSC

Coefficients(a)

Model		Unstandardized Coefficients		Standardized Coefficients	t	Sig.
		B	Std. Error	Beta	B	Std. Error
16&17		.080	.044		1.812	.071
	logQn	1.241	.125	.731	9.898	.000
	logTurb	.437	.061	.405	7.139	.000
	logQIF'	-.615	.105	-.251	-5.870	.000
	logCond	-.625	.170	-.204	-3.679	.000
	logQBFn'	-.605	.197	-.239	-3.071	.002

a Dependent Variable: log SSC

c. Residuals versus predicted

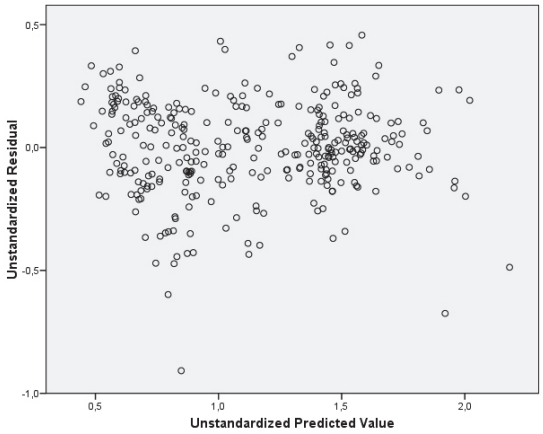

d. Histogram residuals

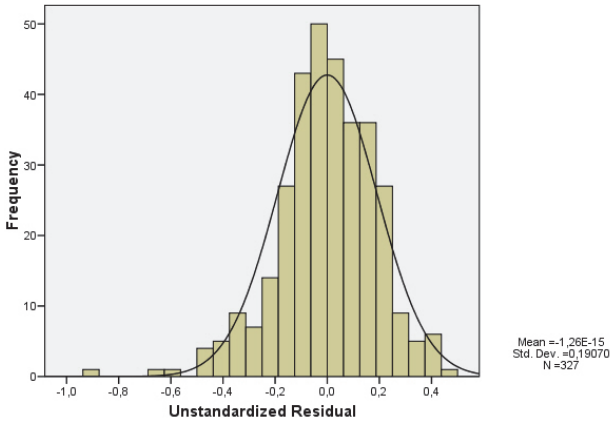

12. Models 18&19: Regression model log SSC_{winter} = f(log Qn, QIFn, Turb, QBFn) and SSC_{summer} = f(Turb, Qn)

a. Pearson's r correlation coefficients (winter data)

Correlations

		logTurb	logCond	log SSC	logQ	logQBF'	logQIF'	logQOF'	logQp	LogQBFp'	logQIFp'	logQOFp'	logQn	logQBFn'	logQIFn'	logQOFn'
logTurb	Pearson Correlation	1	-.744(**)	.725(**)	.872(**)	.775(**)	.588(**)	.593(**)	.754(**)	.762(**)	.496(**)	.370(**)	.764(**)	.794(**)	.557(**)	.335(**)
	Sig. (2-tailed)		0.000	0.000	0.000	0.000	0.000	0.000	0.000	0.000	0.000	0.000	0.000	0.000	0.000	0.000
	N	136	136	136	136	136	136	136	136	136	136	136	136	136	136	136
logCond	Pearson Correlation	-.744(**)	1	-.678(**)	-.818(**)	-.841(**)	-.567(**)	-.388(**)	-.868(**)	-.836(**)	-.602(**)	-.515(**)	-.714(**)	-.841(**)	-.456(**)	-.239(**)
	Sig. (2-tailed)	0.000		0.000	0.000	0.000	0.000	0.000	0.000	0.000	0.000	0.000	0.000	0.000	0.000	0.005
	N	136	136	136	136	136	136	136	136	136	136	136	136	136	136	136
log SSC	Pearson Correlation	.725(**)	-.678(**)	1	.718(**)	.697(**)	.406(**)	.365(**)	.620(**)	.695(**)	.334(**)	.183(*)	.781(**)	.714(**)	.478(**)	.459(**)
	Sig. (2-tailed)	0.000	0.000		0.000	0.000	0.000	0.000	0.000	0.000	0.000	0.033	0.000	0.000	0.000	0.000
	N	136	136	136	136	136	136	136	136	136	136	136	136	136	136	136
logQ	Pearson Correlation	.872(**)	-.818(**)	.718(**)	1	.807(**)	.812(**)	.730(**)	.897(**)	.790(**)	.736(**)	.575(**)	.887(**)	.830(**)	.744(**)	.454(**)
	Sig. (2-tailed)	0.000	0.000	0.000		0.000	0.000	0.000	0.000	0.000	0.000	0.000	0.000	0.000	0.000	0.000
	N	136	136	136	136	136	136	136	136	136	136	136	136	136	136	136
logQBF'	Pearson Correlation	.775(**)	-.841(**)	.697(**)	.807(**)	1	.406(**)	.235(**)	.869(**)	.998(**)	.476(**)	.328(**)	.711(**)	.997(**)	.309(**)	0.132
	Sig. (2-tailed)	0.000	0.000	0.000	0.000		0.000	0.006	0.000	0.000	0.000	0.000	0.000	0.000	0.000	0.125
	N	136	136	136	136	136	136	136	136	136	136	136	136	136	136	136
logQIF'	Pearson Correlation	.588(**)	-.567(**)	.406(**)	.812(**)	.406(**)	1	.796(**)	.738(**)	.380(**)	.925(**)	.781(**)	.753(**)	.435(**)	.922(**)	.591(**)
	Sig. (2-tailed)	0.000	0.000	0.000	0.000	0.000		0.000	0.000	0.000	0.000	0.000	0.000	0.000	0.000	0.000
	N	136	136	136	136	136	136	136	136	136	136	136	136	136	136	136
logQOF'	Pearson Correlation	.593(**)	-.388(**)	.365(**)	.730(**)	.235(**)	.796(**)	1	.438(**)	.210(*)	.554(**)	.480(**)	.601(**)	.277(**)	.801(**)	.522(**)
	Sig. (2-tailed)	0.000	0.000	0.000	0.000	0.006	0.000		0.000	0.014	0.000	0.000	0.000	0.001	0.000	0.000
	N	136	136	136	136	136	136	136	136	136	136	136	136	136	136	136
logQp	Pearson Correlation	.754(**)	-.868(**)	.620(**)	.897(**)	.869(**)	.738(**)	.438(**)	1	.857(**)	.801(**)	.718(**)	.782(**)	.872(**)	.577(**)	.271(**)
	Sig. (2-tailed)	0.000	0.000	0.000	0.000	0.000	0.000	0.000		0.000	0.000	0.000	0.000	0.000	0.000	0.001
	N	136	136	136	136	136	136	136	136	136	136	136	136	136	136	136
LogQBFp'	Pearson Correlation	.762(**)	-.836(**)	.695(**)	.790(**)	.998(**)	.380(**)	.210(*)	.857(**)	1	.458(**)	.302(**)	.699(**)	.995(**)	.286(**)	0.122
	Sig. (2-tailed)	0.000	0.000	0.000	0.000	0.000	0.000	0.014	0.000		0.000	0.000	0.000	0.000	0.001	0.158
	N	136	136	136	136	136	136	136	136	136	136	136	136	136	136	136
logQIFp'	Pearson Correlation	.496(**)	-.602(**)	.334(**)	.736(**)	.476(**)	.925(**)	.554(**)	.801(**)	.458(**)	1	.789(**)	.654(**)	.489(**)	.760(**)	.408(**)
	Sig. (2-tailed)	0.000	0.000	0.000	0.000	0.000	0.000	0.000	0.000	0.000		0.000	0.000	0.000	0.000	0.000
	N	136	136	136	136	136	136	136	136	136	136	136	136	136	136	136
logQOFp'	Pearson Correlation	.370(**)	-.515(**)	.183(*)	.575(**)	.328(**)	.781(**)	.480(**)	.718(**)	.302(**)	.789(**)	1	.443(**)	.331(**)	.583(**)	.215(*)
	Sig. (2-tailed)	0.000	0.000	0.033	0.000	0.000	0.000	0.000	0.000	0.000	0.000		0.000	0.000	0.000	0.012
	N	136	136	136	136	136	136	136	136	136	136	136	136	136	136	136
logQn	Pearson Correlation	.764(**)	-.714(**)	.781(**)	.887(**)	.711(**)	.753(**)	.601(**)	.782(**)	.699(**)	.654(**)	.443(**)	1	.742(**)	.834(**)	.758(**)
	Sig. (2-tailed)	0.000	0.000	0.000	0.000	0.000	0.000	0.000	0.000	0.000	0.000	0.000		0.000	0.000	0.000
	N	136	136	136	136	136	136	136	136	136	136	136	136	136	136	136

logQBFn'	Pearson Correlation	.794(**)	-.841(**)	.714(**)	.830(**)	.997(**)	.435(**)	.277(**)	.872(**)	.995(**)	.489(**)	.331(**)	.742(**)	1	.350(**)	.173(*)
	Sig. (2-tailed)	0.000	0.000	0.000	0.000	0.000	0.000	0.001	0.000	0.000	0.000	0.000	0.000		0.000	0.044
	N	136	136	136	136	136	136	136	136	136	136	136	136	136	136	136
logQIFn'	Pearson Correlation	.557(**)	-.456(**)	.478(**)	.744(**)	.309(**)	.922(**)	.801(**)	.577(**)	.286(**)	.760(**)	.583(**)	.834(**)	.350(**)	1	.829(**)
	Sig. (2-tailed)	0.000	0.000	0.000	0.000	0.000	0.000	0.000	0.000	0.001	0.000	0.000	0.000	0.000		0.000
	N	136	136	136	136	136	136	136	136	136	136	136	136	136	136	136
logQOFn'	Pearson Correlation	.335(**)	-.239(**)	.459(**)	.454(**)	0.132	.591(**)	.522(**)	.271(**)	0.122	.408(**)	.215(*)	.758(**)	.173(*)	.829(**)	1
	Sig. (2-tailed)	0.000	0.005	0.000	0.000	0.125	0.000	0.000	0.001	0.158	0.000	0.012	0.000	0.044	0.000	
	N	136	136	136	136	136	136	136	136	136	136	136	136	136	136	136

**. Correlation is significant at the 0.01 level (2-tailed).

*. Correlation is significant at the 0.05 level (2-tailed).

b. Statistical tests regression model (winter data)

Model Summary(f)

Model	R	R Square	Adjusted R Square	Std. Error of the Estimate
18&19	.866(e)	.749	.740	.181742602505004

e Predictors: (Constant), logQn, logQIFn', logTurb, logQBFn', logQOFn'

f Dependent Variable: log SSC

ANOVA(f)

Model		Sum of Squares	df	Mean Square	F	Sig.
18&19	Regression	12.834	5	2.567	77.711	.000(e)
	Residual	4.294	130	.033		
	Total	17.128	135			

e Predictors: (Constant), logQn, logQIFn', logTurb, logQBFn', logQOFn'

f Dependent Variable: log SSC

Coefficients(a)

Model		Unstandardized Coefficients		Standardized Coefficients	t	Sig.
		B	Std. Error	Beta	B	Std. Error
18&19	(Constant)	.087	.098		.889	.376
	logQn	3.229	.511	1.980	6.321	.000
	logQIFn'	-1.308	.195	-.831	-6.721	.000
	logTurb	.352	.102	.296	3.472	.001
	logQBFn'	-1.687	.486	-.639	-3.474	.001
	logQOFn'	-.481	.223	-.341	-2.154	.033

a Dependent Variable: log SSC

c. Residuals versus Predicted (winter data)

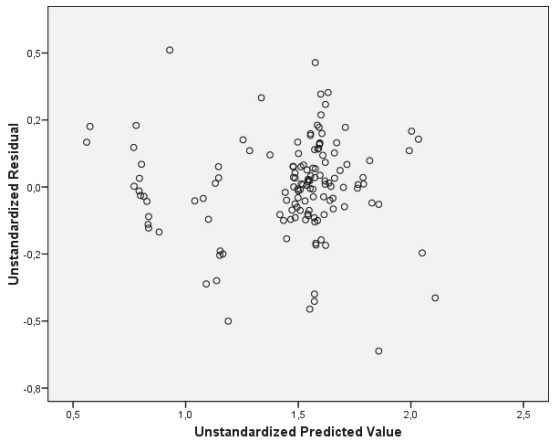

d. Histogram residuals (winter data)

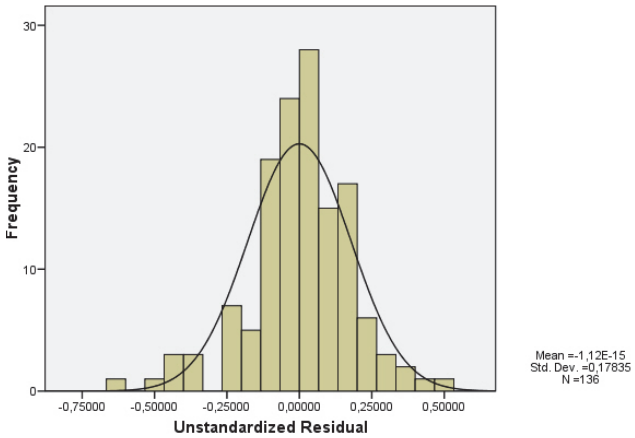

e. Pearson's r correlation coefficients (summer data)

Correlations

		log SSC	logQ	logQBF'	logQIF'	logQOF'	logQp	LogQBFp'	logQIFp'	logQOFp'	logQn	logQBFn'	logQIFn'	logQOFn'	logTurb	logCond
log SSC	Pearson Correlation	1	.760(**)	.754(**)	.249(**)	.273(**)	.717(**)	.752(**)	.200(**)	.204(**)	.775(**)	.756(**)	.280(**)	.261(**)	.777(**)	-.632(**)
	Sig. (2-tailed)		0.000	0.000	0.001	0.000	0.000	0.000	0.006	0.005	0.000	0.000	0.000	0.000	0.000	0.000
	N	191	191	191	191	191	191	191	191	191	191	191	191	191	191	191
logQ	Pearson Correlation	.760(**)	1	.903(**)	.549(**)	.461(**)	.967(**)	.894(**)	.517(**)	.456(**)	.960(**)	.907(**)	.496(**)	.278(**)	.786(**)	-.846(**)
	Sig. (2-tailed)	0.000		0.000	0.000	0.000	0.000	0.000	0.000	0.000	0.000	0.000	0.000	0.000	0.000	0.000
	N	191	191	191	191	191	191	191	191	191	191	191	191	191	191	191
logQBF'	Pearson Correlation	.754(**)	.903(**)	1	.199(**)	0.083	.913(**)	.999(**)	.258(**)	.153(*)	.883(**)	.999(**)	0.132	0.035	.867(**)	-.762(**)
	Sig. (2-tailed)	0.000	0.000		0.006	0.255	0.000	0.000	0.000	0.035	0.000	0.000	0.068	0.631	0.000	0.000
	N	191	191	191	191	191	191	191	191	191	191	191	191	191	191	191
logQIF'	Pearson Correlation	.249(**)	.549(**)	.199(**)	1	.783(**)	.528(**)	.181(*)	.920(**)	.877(**)	.481(**)	.209(**)	.904(**)	.456(**)	.144(*)	-.510(**)
	Sig. (2-tailed)	0.001	0.000	0.006		0.000	0.000	0.012	0.000	0.000	0.000	0.004	0.000	0.000	0.047	0.000
	N	191	191	191	191	191	191	191	191	191	191	191	191	191	191	191
logQOF'	Pearson Correlation	.273(**)	.461(**)	0.083	.783(**)	1	.309(**)	0.061	.500(**)	.643(**)	.423(**)	0.097	.866(**)	.618(**)	0.119	-.316(**)
	Sig. (2-tailed)	0.000	0.000	0.255	0.000		0.000	0.400	0.000	0.000	0.000	0.184	0.000	0.000	0.102	0.000
	N	191	191	191	191	191	191	191	191	191	191	191	191	191	191	191
logQp	Pearson Correlation	.717(**)	.967(**)	.913(**)	.528(**)	.309(**)	1	.908(**)	.577(**)	.495(**)	.907(**)	.914(**)	.403(**)	0.136	.770(**)	-.865(**)
	Sig. (2-tailed)	0.000	0.000	0.000	0.000	0.000		0.000	0.000	0.000	0.000	0.000	0.000	0.060	0.000	0.000
	N	191	191	191	191	191	191	191	191	191	191	191	191	191	191	191
LogQBFp'	Pearson Correlation	.752(**)	.894(**)	.999(**)	.181(*)	0.061	.908(**)	1	.247(**)	0.139	.875(**)	.998(**)	0.113	0.024	.866(**)	-.757(**)
	Sig. (2-tailed)	0.000	0.000	0.000	0.012	0.400	0.000		0.001	0.055	0.000	0.000	0.119	0.744	0.000	0.000
	N	191	191	191	191	191	191	191	191	191	191	191	191	191	191	191
logQIFp'	Pearson Correlation	.200(**)	.517(**)	.258(**)	.920(**)	.500(**)	.577(**)	.247(**)	1	.799(**)	.429(**)	.263(**)	.720(**)	.235(**)	.158(*)	-.552(**)
	Sig. (2-tailed)	0.006	0.000	0.000	0.000	0.000	0.000	0.001		0.000	0.000	0.000	0.000	0.001	0.029	0.000
	N	191	191	191	191	191	191	191	191	191	191	191	191	191	191	191
logQOFp'	Pearson Correlation	.204(**)	.456(**)	.153(*)	.877(**)	.643(**)	.495(**)	0.139	.799(**)	1	.351(**)	.156(*)	.714(**)	.222(**)	0.111	-.444(**)
	Sig. (2-tailed)	0.005	0.000	0.035	0.000	0.000	0.000	0.055	0.000		0.000	0.031	0.000	0.002	0.125	0.000
	N	191	191	191	191	191	191	191	191	191	191	191	191	191	191	191
logQn	Pearson Correlation	.775(**)	.960(**)	.883(**)	.481(**)	.423(**)	.907(**)	.875(**)	.429(**)	.351(**)	1	.894(**)	.529(**)	.458(**)	.769(**)	-.789(**)
	Sig. (2-tailed)	0.000	0.000	0.000	0.000	0.000	0.000	0.000	0.000	0.000		0.000	0.000	0.000	0.000	0.000
	N	191	191	191	191	191	191	191	191	191	191	191	191	191	191	191
logQBFn'	Pearson Correlation	.756(**)	.907(**)	.999(**)	.209(**)	0.097	.914(**)	.998(**)	.263(**)	.156(*)	.894(**)	1	.151(*)	0.060	.866(**)	-.763(**)
	Sig. (2-tailed)	0.000	0.000	0.000	0.004	0.184	0.000	0.000	0.000	0.031	0.000		0.037	0.409	0.000	0.000
	N	191	191	191	191	191	191	191	191	191	191	191	191	191	191	191
logQIFn'	Pearson Correlation	.280(**)	.496(**)	0.132	.904(**)	.866(**)	.403(**)	0.113	.720(**)	.714(**)	.529(**)	.151(*)	1	.777(**)	0.110	-.395(**)
	Sig. (2-tailed)	0.000	0.000	0.068	0.000	0.000	0.000	0.119	0.000	0.000	0.000	0.037		0.000	0.131	0.000
	N	191	191	191	191	191	191	191	191	191	191	191	191	191	191	191
logQOFn'	Pearson Correlation	.261(**)	.278(**)	0.035	.456(**)	.618(**)	0.136	0.024	.235(**)	.222(**)	.458(**)	0.060	.777(**)	1	0.054	-.147(*)
	Sig. (2-tailed)	0.000	0.000	0.631	0.000	0.000	0.060	0.744	0.001	0.002	0.000	0.409	0.000		0.459	0.042
	N	191	191	191	191	191	191	191	191	191	191	191	191	191	191	191
logTurb	Pearson Correlation	.777(**)	.786(**)	.867(**)	.144(*)	0.119	.770(**)	.866(**)	.158(*)	0.111	.769(**)	.866(**)	0.110	0.054	1	-.693(**)
	Sig. (2-tailed)	0.000	0.000	0.000	0.047	0.102	0.000	0.000	0.029	0.125	0.000	0.000	0.131	0.459		0.000
	N	191	191	191	191	191	191	191	191	191	191	191	191	191	191	191
logCond	Pearson Correlation	-.632(**)	-.846(**)	-.762(**)	-.510(**)	-.316(**)	-.865(**)	-.757(**)	-.552(**)	-.444(**)	-.789(**)	-.763(**)	-.395(**)	-.147(*)	-.693(**)	1
	Sig. (2-tailed)	0.000	0.000	0.000	0.000	0.000	0.000	0.000	0.000	0.000	0.000	0.000	0.000	0.042	0.000	
	N	191	191	191	191	191	191	191	191	191	191	191	191	191	191	191

**. Correlation is significant at the 0.01 level (2-tailed).

*. Correlation is significant at the 0.05 level (2-tailed).

f. Statistical tests regression model (summer data)

Model Summary(c)

Model	R	R Square	Adjusted R Square	Std. Error of the Estimate
18&19	.825(b)	.681	.677	.190859197733223

b Predictors: (Constant), logTurb, logQn

c Dependent Variable: log SSC

ANOVA(c)

Model		Sum of Squares	df	Mean Square	F	Sig.
18&19	Regression	14.604	2	7.302	200.460	.000(b)
	Residual	6.848	188	.036		
	Total	21.453	190			

b Predictors: (Constant), logTurb, logQn

c Dependent Variable: log SSC

Coefficients(a)

Model		Unstandardized Coefficients		Standardized Coefficients	t	Sig.
		B	Std. Error	Beta	B	Std. Error
18&19	(Constant)	.086	.045		1.927	.056
	logTurb	.459	.067	.443	6.871	.000
	logQn	.731	.109	.434	6.726	.000

a Dependent Variable: log SSC

g. Residuals versus Predicted (summer data)

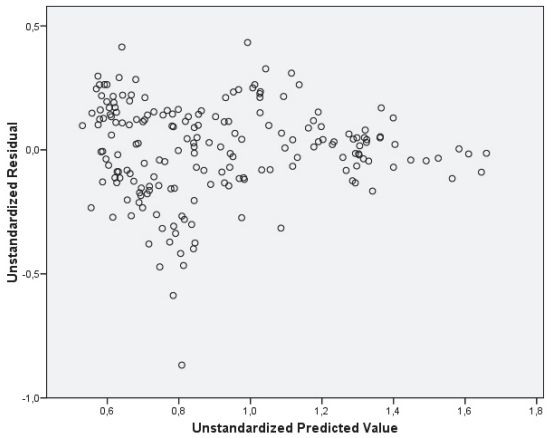

h. Histogram residuals (summer data)

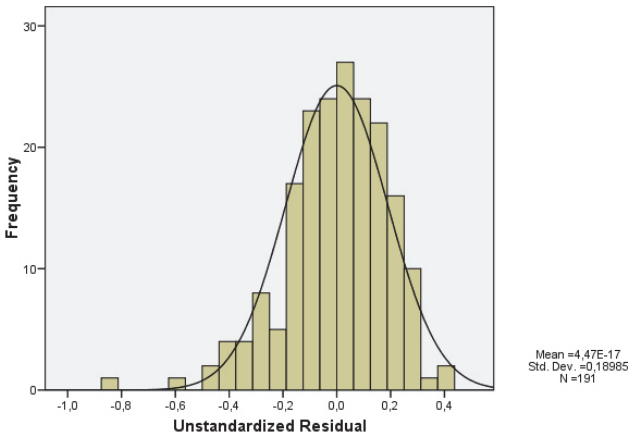

Addendum C: Dataset of spatial sources

Key

Locations

Motte-Rillaar	TIS
Hulpe-Molenstede	TIS
Velpe-Halen	TIS
Gete-Halen	TIS
Zwartebeek Lummen	TIS
Mangelbeek Lummen	TIS
Herk Kermt	TIS
Demer Hasselt	TIS
Demer Aarschot	OUTLET

Timing

1	20/04/2007	TIS
2	24/05/2007	TIS
3	21/06/2007	TIS
4	06/08/2007	TIS
5	29/08/2007	TIS
6	27/09/2007	TIS
7	06/11/2007	TIS
8	18/12/2007	TIS
9	28/01/2008	TIS
10	28/02/2008	TIS
11	10/04/2008	TIS
12	22/05/2008	TIS
13	13/04/2007	OUTLET - centrifuge VMM
14	14/09/2007	OUTLET - centrifuge VMM
15	24/10/2007	OUTLET - centrifuge FHR
16	04/12/2007	OUTLET - centrifuge FHR
17	21/03/2008 10:20h-11:20h	OUTLET - centrifuge FHR
18	21/03/2008 11:40h-12:40h	OUTLET - centrifuge FHR
19	21/03/2008 12:55h-13:45h	OUTLET - centrifuge FHR
20	21/03/2008 14h-14:30h	OUTLET - centrifuge FHR
21	03/06/2008 16:45h-17:00h	OUTLET - centrifuge FHR
22	03/06/2008 17:35h-18:05h	OUTLET - centrifuge FHR
23	03/06/2008 to 04/06/2008	OUTLET - ISCO compilation sample
24	04/08/2008 to 11/08/2008	OUTLET - ISCO compilation sample
25	07/10/2008 to 13/10/2008	OUTLET - ISCO compilation sample
26	28/10/2008 to 03/11/2008	OUTLET - ISCO compilation sample
27	20/01/2009 to 27/01/2009	OUTLET - ISCO compilation sample
28	10/02/2009 14:27h - 11/02/2009 6:27h	OUTLET - ISCO compilation sample
29	11/02/2009 7:27h - 19:39h	OUTLET - ISCO compilation sample
30	11/02/09 20:39h - 12/02/09 14:39h	OUTLET - ISCO compilation sample
31	12/02/2009 15:39h - 13/02/2009 12:39h	OUTLET - ISCO compilation sample
32	13/02/2009 13:06h - 17/02/2009 09:06h	OUTLET - ISCO compilation sample
33	17/02/2009 12:59h - 18/02/2009 4:59h	OUTLET - ISCO compilation sample
34	18/02/2009 5:59h - 20:30h	OUTLET - ISCO compilation sample
35	18/02/2009 21:30h - 19/02/2009 9:30h	OUTLET - ISCO compilation sample
36	19/02/2009 12:30h - 20/02/2009 4:06h	OUTLET - ISCO compilation sample
37	20/02/2009 9:06h - 22/02/2009 6:06h	OUTLET - ISCO compilation sample
38	22/02/2009 16:06h - 24/02/2009 8:06h	OUTLET - ISCO compilation sample
99	unspecified timing	

<dl = values below detection limit

d.u. = data unavailable.

		Timing											
		1	2	3	4	5	6	7	8	9	10	11	12
L.O.I.	**(%)**	18.6	20.6	d.u.	18.9	d.u.	23.5	22.1	18.2	d.u.	d.u.	21.9	20.3
Density	**(g/cm³)**	3.0168	2.9973	d.u.	2.9707	d.u.	3.0392	3.0346	2.9644	d.u.	d.u.	2.9697	2.9714
D [3, 2]	**(µm)**	10.9	12.1	d.u.	12.0	d.u.	8.1	8.4	10.6	d.u.	d.u.	9.8	10.0
SSA	**(m²/g)**	0.1829	0.1652	d.u.	0.1681	d.u.	0.2450	0.2363	0.1903	d.u.	d.u.	0.2060	0.2013
Al	**(%)**	2.40	2.40	d.u.	2.32	d.u.	2.29	2.32	2.20	d.u.	d.u.	2.35	2.25
Ca	**(%)**	0.90	0.76	d.u.	0.90	d.u.	1.66	1.34	0.98	d.u.	d.u.	0.96	0.74
Fe	**(%)**	11.54	12.21	d.u.	11.72	d.u.	12.52	12.68	12.16	d.u.	d.u.	11.98	11.88
K	**(%)**	2.91	2.75	d.u.	2.81	d.u.	2.92	2.72	2.34	d.u.	d.u.	3.25	2.68
Si	**(%)**	45.15	42.73	d.u.	41.50	d.u.	29.89	34.87	38.16	d.u.	d.u.	36.36	41.20
P	**(ppm)**	5534.8	7369.0	d.u.	9115.3	d.u.	8718.4	8534.2	7310.7	d.u.	d.u.	5760.2	7431.4
S	**(ppm)**	1464.4	2174.7	d.u.	2046.9	d.u.	2003.5	3046.2	2715.3	d.u.	d.u.	3192.8	2439.1
Ti	**(ppm)**	2599.9	2658.4	d.u.	2739.7	d.u.	2647.9	2606.2	2613.7	d.u.	d.u.	2702.0	2610.7
Ba	**(ppm)**	296.7	298.7	d.u.	302.8	d.u.	289.8	288.4	293.9	d.u.	d.u.	289.6	303.7
Cr	**(ppm)**	70.4	62.7	d.u.	74.0	d.u.	63.3	61.0	56.7	d.u.	d.u.	76.0	62.9
Cu	**(ppm)**	34.5	47.6	d.u.	59.1	d.u.	60.8	58.7	41.3	d.u.	d.u.	48.0	45.1
Pb	**(ppm)**	27.1	36.4	d.u.	39.6	d.u.	51.4	45.9	35.1	d.u.	d.u.	45.5	38.5
Mn	**(ppm)**	472.2	490.7	d.u.	331.0	d.u.	528.5	526.4	332.3	d.u.	d.u.	355.3	429.6
Ni	**(ppm)**	27.2	26.4	d.u.	27.7	d.u.	23.5	24.4	26.6	d.u.	d.u.	29.1	24.1
Sr	**(ppm)**	76.6	76.2	d.u.	72.8	d.u.	94.3	81.3	73.5	d.u.	d.u.	73.4	74.1
V	**(ppm)**	88.2	63.3	d.u.	75.4	d.u.	78.9	72.7	55.4	d.u.	d.u.	97.9	65.4
Zn	**(ppm)**	257.5	330.8	d.u.	368.6	d.u.	428.9	390.4	289.7	d.u.	d.u.	328.8	314.4
Ce	**(ppm)**	64.6	63.2	d.u.	61.9	d.u.	64.3	62.3	61.4	d.u.	d.u.	65.1	62.1
Cs	**(ppm)**	<dl	<dl	d.u.	<dl	d.u.	<dl	<dl	<dl	d.u.	d.u.	<dl	0.7
Rb	**(ppm)**	67.3	66.5	d.u.	66.3	d.u.	69.8	64.3	60.6	d.u.	d.u.	74.5	63.2
Zr	**(ppm)**	222.5	177.3	d.u.	202.2	d.u.	141.9	186.4	266.7	d.u.	d.u.	173.5	183.9
Remarks				not enough material present for analysis		not enough material present for analysis				not enough material present for analysis			

Table C.1: Data Motte-Rillaar

		Timing																
		1	2	3	4	5	5	6	7	8	9	10	11	11	11	12	99	99
L.O.I.	(%)	34.3	d.u.	d.u.	d.u.	d.u.	31.2	d.u.	d.u.	40.9	30.7	41.8	36.9	34.5	37.6	39.0	42.2	40.2
Density	(g/cm³)	3.3802	d.u.	d.u.	d.u.	d.u.	3.4533	d.u.	d.u.	3.6070	3.7898	3.1430	3.6121	3.7014	d.u.	3.5780	3.1155	d.u.
D [3, 2]	(µm)	5.6	d.u.	d.u.	d.u.	d.u.	8.3	d.u.	d.u.	4.8	3.5	4.6	6.8	3.8	4.3	5.1	8.0	8.3
SSA	(m²/g)	0.3152	d.u.	d.u.	d.u.	d.u.	0.2106	d.u.	d.u.	0.3470	0.4556	0.4175	0.2428	0.4309	d.u.	0.3290	0.2394	d.u.
Al	(%)	0.83	d.u.	d.u.	d.u.	d.u.	1.14	d.u.	d.u.	0.88	1.14	0.98	1.29	1.27	1.29	0.96	0.98	0.99
Ca	(%)	8.31	d.u.	d.u.	d.u.	d.u.	4.89	d.u.	d.u.	7.85	0.31	9.83	6.17	6.30	5.51	7.62	9.39	9.66
Fe	(%)	13.73	d.u.	d.u.	d.u.	d.u.	16.61	d.u.	d.u.	14.05	23.68	10.21	16.24	15.90	17.11	15.12	11.23	10.79
K	(%)		d.u.	d.u.	d.u.	d.u.	<dl	d.u.	d.u.	<dl	<dl	<dl	<dl	<dl	<dl	<dl	<dl	<dl
Si	(%)	4.28	d.u.	d.u.	d.u.	d.u.	12.08	d.u.	d.u.	1.61	1.65	<dl	5.64	5.14	4.37	4.35	0.82	0.18
P	(ppm)	18210.0	d.u.	d.u.	d.u.	d.u.	13585.5	d.u.	d.u.	12371.5	9555.2	13044.2	16277.3	16121.8	16530.3	12348.2	14967.8	14547.9
S	(ppm)	66.9	d.u.	d.u.	d.u.	d.u.	2046.2	d.u.	d.u.	2267.1	2753.7	3257.8	4164.5	4074.1	3664.9	3424.9	3157.1	3086.6
Ti	(ppm)	1297.8	d.u.	d.u.	d.u.	d.u.	1413.5	d.u.	d.u.	996.7	1460.7	1255.0	1390.1	1351.9	1447.3	1071.8	1345.1	1284.7
Ba	(ppm)	350.6	d.u.	d.u.	d.u.	d.u.	395.5	d.u.	d.u.	269.2	232.7	307.3	325.9	330.6	338.0	256.6	312.7	315.2
Cr	(ppm)	65.6	d.u.	d.u.	d.u.	d.u.	43.1	d.u.	d.u.	27.5	18.7	16.4	36.1	33.1	40.3	14.9	25.3	14.2
Cu	(ppm)	107.0	d.u.	d.u.	d.u.	d.u.	1971.0	d.u.	d.u.	84.6	44.1	99.1	91.4	90.6	88.2	62.5	101.3	89.9
Pb	(ppm)	96.3	d.u.	d.u.	d.u.	d.u.	128.0	d.u.	d.u.	63.0	132.7	35.8	75.8	75.4	81.8	57.4	40.6	35.9
Mn	(ppm)	143.5	d.u.	d.u.	d.u.	d.u.	175.6	d.u.	d.u.	143.1	452.3	158.3	163.8	162.1	171.1	151.3	148.0	153.6
Ni	(ppm)	24.1	d.u.	d.u.	d.u.	d.u.	23.5	d.u.	d.u.	23.5	24.2	23.5	23.5	23.5	25.8	23.5	23.5	23.5
Sr	(ppm)	345.1	d.u.	d.u.	d.u.	d.u.	251.2	d.u.	d.u.	339.3	30.5	459.9	249.8	258.6	228.6	321.1	415.9	409.6
V	(ppm)	31.9	d.u.	d.u.	d.u.	d.u.	5.7	d.u.	d.u.	<dl	<dl	<dl	15.6	17.1	16.7	<dl	<dl	<dl
Zn	(ppm)	524.7	d.u.	d.u.	d.u.	d.u.	1166.8	d.u.	d.u.	434.9	629.5	393.4	539.3	530.5	559.8	458.8	394.2	369.3
Ce	(ppm)	41.6	d.u.	d.u.	d.u.	d.u.	42.0	d.u.	d.u.	37.6	43.8	37.5	45.9	43.0	44.0	38.6	40.0	37.2
Cs	(ppm)	<dl	d.u.	d.u.	d.u.	d.u.	<dl	d.u.	d.u.	<dl	<dl	<dl	<dl	<dl	<dl	<dl	<dl	<dl
Rb	(ppm)	22.9	d.u.	d.u.	d.u.	d.u.	28.6	d.u.	d.u.	22.1	33.0	16.6	27.2	27.9	29.0	23.0	17.5	13.8
Zr	(ppm)	25.1	d.u.	d.u.	d.u.	d.u.	75.9	d.u.	d.u.	23.3	73.2	21.7	39.8	34.8	31.5	26.7	19.7	18.4
Remarks			not enough material present due to weeds covering the inlet				Resuspended river bed material collected by centrifugation	not enough material present for analysis					different subsamples					not enough material for density analysis

		Timing											
		1	2	3	4	5	6	7	8	9	10	11	12
L.O.I.	**(%)**	6.0	d.u.	12.9	10.4	11.2	10.6	11.4	9.1	d.u.	12.6	13.3	12.6
Density	**(g/cm³)**	2.7214	d.u.	d.u.	2.6833	2.6588	2.6908	2.7142	2.7039	d.u.	2.7194	2.7238	2.7268
D [3, 2]	**(µm)**	11.8	d.u.	d.u.	8.8	10.0	9.4	11.8	11.4	d.u.	9.9	9.3	9.2
SSA	**(m²/g)**	0.1874	d.u.	d.u.	0.2532	0.2260	0.2363	0.1871	0.1947	d.u.	0.2224	0.2380	0.2387
Al	**(%)**	4.21	d.u.	4.28	4.29	3.51	4.08	3.53	4.36	d.u.	3.67	4.24	3.87
Ca	**(%)**	0.78	d.u.	0.87	0.84	0.62	0.68	0.35	0.79	d.u.	0.98	1.14	0.83
Fe	**(%)**	3.35	d.u.	3.90	3.67	2.84	3.66	2.55	3.28	d.u.	4.08	3.87	3.98
K	**(%)**	2.49	d.u.	2.65	2.60	1.99	2.58	1.94	2.23	d.u.	2.35	2.67	2.40
Si	**(%)**	87.25	d.u.	75.93	81.26	83.03	74.48	96.40	102.22	d.u.	67.52	68.37	76.44
P	**(ppm)**	2488.8	d.u.	3229.3	3166.2	2147.2	3173.8	2682.5	3541.3	d.u.	4688.8	3654.3	3689.9
S	**(ppm)**	1561.6	d.u.	1201.2	1039.6	1513.0	1515.0	858.5	1504.4	d.u.	1387.5	1835.2	1327.5
Ti	**(ppm)**	4070.5	d.u.	4154.7	4215.8	3747.4	4139.6	4012.0	4062.5	d.u.	4093.2	4177.4	4091.1
Ba	**(ppm)**	466.2	d.u.	455.9	459.1	366.6	465.4	453.3	458.2	d.u.	472.6	450.6	474.7
Cr	**(ppm)**	62.5	d.u.	53.3	60.5	50.8	53.3	52.9	69.2	d.u.	45.8	54.6	58.7
Cu	**(ppm)**	36.0	d.u.	34.6	34.5	27.6	36.4	21.3	34.3	d.u.	42.6	43.2	38.3
Pb	**(ppm)**	8.1	d.u.	23.0	13.6	4.3	12.5		7.7	d.u.	13.5	16.2	13.4
Mn	**(ppm)**	808.5	d.u.	1142.2	833.7	659.5	835.0	708.7	707.3	d.u.	1391.2	1294.6	1407.0
Ni	**(ppm)**	34.8	d.u.	36.7	36.0	34.7	35.2	32.4	34.7	d.u.	37.4	38.1	37.0
Sr	**(ppm)**	88.3	d.u.	91.2	93.4	87.8	86.7	78.4	85.8	d.u.	91.6	95.7	88.9
V	**(ppm)**	23.5	d.u.	51.8	52.0	4.1	30.7		20.1	d.u.	23.8	39.9	42.2
Zn	**(ppm)**	216.1	d.u.	211.8	220.3	183.5	220.1	143.4	186.6	d.u.	224.3	241.8	228.8
Ce	**(ppm)**	71.4	d.u.	68.0	70.0	70.8	70.8	71.2	72.7	d.u.	72.5	73.7	70.5
Cs	**(ppm)**	7.5	d.u.	6.7	8.8	3.8	7.6	5.3	5.6	d.u.	7.1	6.8	6.9
Rb	**(ppm)**	64.9	d.u.	72.4	70.3	62.2	68.4	49.9	58.8	d.u.	62.0	68.8	64.5
Zr	**(ppm)**	392.6	d.u.	308.3	333.8	402.5	349.0	634.6	572.7	d.u.	478.9	393.4	347.2
Remarks			not enough material present for analysis	not enough material for grain size and density analysis						not enough material present for analysis			

Table C.3: Data Velpe – Halen

Table C.4: Data Gete – Halen

		Timing												
		1	2	3	4	5	6	7	8	9	10	11	11	12
L.O.I.	**(%)**	5.2	9.5	11.9	9.9	8.4	11.0	10.0	8.7	8.4	10.1	6.1	6.3	7.5
Density	**(g/cm³)**	2.7104	2.7191	2.7699	2.6732	2.6664	2.7051	2.7000	2.6876	2.6654	2.7146	2.6867	2.6841	2.6965
D [3, 2]	**(µm)**	12.6	9.8	7.4	10.1	11.7	9.0	9.4	10.6	11.0	10.9	12.0	11.6	10.5
SSA	**(m²/g)**	0.1751	0.2255	0.2912	0.2212	0.1931	0.2476	0.2355	0.2104	0.2043	0.2021	0.1856	0.1920	0.2122
Al	**(%)**	3.48	3.75	5.02	4.08	3.91	4.18	4.26	4.64	3.82	4.60	3.71	3.49	3.87
Ca	**(%)**	1.00	1.85	1.35	1.54	1.31	1.52	1.61	1.42	1.37	1.45	0.86	0.88	1.07
Fe	**(%)**	2.00	2.56	4.38	2.86	2.59	3.10	3.16	2.84	2.58	2.74	2.30	2.35	2.58
K	**(%)**	1.93	2.12	3.90	2.44	2.47	2.72	2.76	2.61	2.39	2.43	2.19	2.18	2.38
Si	**(%)**	115.83	99.76	75.33	87.66	93.89	87.54	82.19	109.33	96.82	112.02	89.50	92.23	97.95
P	**(ppm)**	1312.5	1821.2	1832.5	1952.6	1538.2	1806.8	1804.7	1495.0	1861.1	1418.9	1368.2	1286.6	1446.5
S	**(ppm)**	859.5	1330.9	1044.9	1153.6	1283.7	1487.9	1892.3	2069.2	1893.0	2251.4	1056.1	1029.4	1431.5
Ti	**(ppm)**	3734.1	3917.3	4354.0	3965.1	3927.7	4092.4	4131.1	3945.0	3851.4	3987.1	3827.8	3841.0	3969.9
Ba	**(ppm)**	459.4	471.7	495.9	487.3	459.1	492.6	482.7	476.1	479.3	481.2	464.5	460.7	471.8
Cr	**(ppm)**	60.5	70.6	91.5	89.2	75.8	96.7	78.3	64.3	65.0	69.5	58.8	55.9	67.6
Cu	**(ppm)**	18.9	29.2	36.6	36.4	32.8	41.2	41.1	32.9	31.6	33.9	21.2	22.4	27.8
Pb	**(ppm)**	<dl	12.1	28.0	17.3	11.6	21.5	23.5	17.1	13.6	15.6	5.0	6.1	9.6
Mn	**(ppm)**	429.9	1167.3	1103.5	818.3	577.1	774.8	704.7	437.6	401.3	489.3	428.1	421.6	470.3
Ni	**(ppm)**	33.0	37.1	47.0	37.9	35.5	37.8	38.6	37.0	36.2	36.3	32.9	33.9	34.8
Sr	**(ppm)**	83.4	90.3	88.3	88.7	85.2	89.5	90.5	86.0	86.9	87.2	78.9	78.9	81.5
V	**(ppm)**	<dl	4.0	81.6	16.7	2.4	20.6	23.7	32.4	9.1	12.2	6.6	12.7	18.0
Zn	**(ppm)**	137.0	200.0	233.9	223.1	205.3	248.2	249.6	216.0	198.9	215.0	150.0	155.0	180.1
Ce	**(ppm)**	73.4	72.1	80.6	70.6	70.1	70.9	72.2	70.7	68.6	69.9	67.0	67.7	71.7
Cs	**(ppm)**	5.2	7.5	8.6	6.0	7.6	8.3	7.2	7.4	6.5	6.9	6.4	6.4	7.8
Rb	**(ppm)**	48.0	54.7	93.5	61.7	58.6	66.6	65.9	62.9	58.0	58.2	52.9	53.6	57.4
Zr	**(ppm)**	623.3	476.9	248.4	395.6	429.7	336.2	372.9	388.4	396.2	385.5	422.7	432.6	453.4
Remarks												different subsamples		

Table C.5: Data Zwartebeek – Lummen; there was no sample collected at timing 3; Sample 4 is two months' worth of sediment collecting

		Timing												
		1	2	3	4	5	6	6	7	8	9	10	11	12
L.O.I.	(%)	31.1	d.u.	d.u.	30.1	30.5	29.8	25.1	28.4	d.u.	31.5	28.1	31.7	31.2
Density	(g/cm³)	4.0976	d.u.	d.u.	3.8506	3.8978	3.6241	3.5477	3.8334	d.u.	3.9284	3.7864	3.7082	3.8838
D [3, 2]	(µm)	4.2	d.u.	d.u.	5.3	5.0	4.9	7.0	4.3	d.u.	4.2	4.9	4.1	5.5
SSA	(m²/g)	0.3513	d.u.	d.u.	0.2960	0.3087	0.3371	0.2413	0.3600	d.u.	0.3632	0.3239	0.3945	0.2832
Al	(%)	1.26	d.u.	d.u.	1.30	1.16	1.61	1.44	1.04	d.u.	1.10	1.13	1.16	1.06
Ca	(%)	0.75	d.u.	d.u.	0.42	0.98	0.90	0.49	0.43	d.u.	0.64	0.34	0.46	0.32
Fe	(%)	23.90	d.u.	d.u.	23.99	23.93	20.84	21.48	24.24	d.u.	23.76	23.17	23.16	23.62
K	(%)	<dl	d.u.	d.u.	<dl	<dl	<dl	<dl	<dl	d.u.	<dl	<dl	<dl	<dl
Si	(%)	0.65	d.u.	d.u.	2.59	0.15	8.60	8.62	1.04	d.u.	<dl	1.86	0.72	0.19
P	(ppm)	10438.1	d.u.	d.u.	9439.9	7913.0	12136.5	12057.7	8759.6	d.u.	8975.6	9701.9	10071.9	9851.3
S	(ppm)	2440.4	d.u.	d.u.	1767.9	2164.8	2533.7	2730.5	1667.9	d.u.	2591.6	2737.2	2962.3	4230.5
Ti	(ppm)	1392.0	d.u.	d.u.	1401.0	1292.7	1770.7	1784.9	1341.9	d.u.	1398.9	1529.1	1557.1	1499.0
Ba	(ppm)	227.3	d.u.	d.u.	241.0	234.9	312.9	288.1	228.6	d.u.	222.2	236.3	235.2	228.7
Cr	(ppm)	15.7	d.u.	d.u.	17.0	17.5	94.5	29.2	15.3	d.u.	18.4	23.4	20.7	17.4
Cu	(ppm)	58.4	d.u.	d.u.	42.3	49.4	126.3	28.8	44.7	d.u.	43.0	41.6	43.8	52.1
Pb	(ppm)	139.6	d.u.	d.u.	138.4	137.0	176.8	110.1	141.1	d.u.	127.2	124.6	127.2	128.8
Mn	(ppm)	507.2	d.u.	d.u.	777.9	940.0	455.8	505.7	439.9	d.u.	275.7	322.6	298.1	371.8
Ni	(ppm)	23.4	d.u.	d.u.	23.4	24.6	46.1	24.7	23.5	d.u.	23.9	29.0	23.5	23.5
Sr	(ppm)	38.4	d.u.	d.u.	34.8	42.0	54.2	44.3	33.0	d.u.	37.4	33.3	36.2	30.3
V	(ppm)	<dl	d.u.	d.u.	<dl	<dl	5.2	<dl	<dl	d.u.	<dl	<dl	<dl	<dl
Zn	(ppm)	648.4	d.u.	d.u.	617.6	558.8	753.5	485.6	539.9	d.u.	607.8	604.9	563.9	632.1
Ce	(ppm)	45.2	d.u.	d.u.	43.4	41.5	45.7	47.3	40.9	d.u.	54.8	46.2	45.6	43.3
Cs	(ppm)	<dl	d.u.	d.u.	<dl	<dl	<dl	<dl	<dl	d.u.	<dl	<dl	<dl	<dl
Rb	(ppm)	32.4	d.u.	d.u.	37.0	34.4	34.9	35.2	33.2	d.u.	31.7	29.4	29.7	27.9
Zr	(ppm)	60.9	d.u.	d.u.	83.4	78.3	95.3	282.5	70.2	d.u.	68.4	142.6	86.2	66.6
Remarks				no sample collected			centrifuge sample	riverbed sample						

Table C.6: Data Mangelbeek – Lummen

		Timing											
		1	2	3	4	5	6	7	8	9	10	11	12
L.O.I.	**(%)**	35.2	29.8	30.9	28.6	29.3	33.1	38.1	29.5	d.u.	d.u.	34.2	31.8
Density	**(g/cm³)**	3.7298	3.7855	3.4861	3.2859	3.4903	3.7256	3.4181	3.4012	d.u.	d.u.	3.4236	3.7105
D [3, 2]	**(µm)**	6.1	5.8	6.8	6.3	4.5	5.5	5.9	6.8	d.u.	d.u.	6.6	6.1
SSA	**(m²/g)**	0.2648	0.2727	0.2523	0.2909	0.3808	0.2925	0.2989	0.2596	d.u.	d.u.	0.2675	0.2656
Al	**(%)**	1.42	1.30	1.71	1.94	1.64	1.52	1.74	1.77	d.u.	d.u.	1.67	1.52
Ca	**(%)**	0.53	0.69	0.50	0.43	0.35	0.34	0.51	0.31	d.u.	d.u.	0.51	0.55
Fe	**(%)**	22.38	22.74	20.80	18.92	20.18	22.07	19.39	18.92	d.u.	d.u.	19.36	20.80
K	**(%)**	<dl	<dl	<dl	0.33	0.08	<dl	<dl	0.30	d.u.	d.u.	0.10	<dl
Si	**(%)**	3.90	3.42	9.08	14.57	10.03	6.51	13.69	15.50	d.u.	d.u.	10.56	7.12
P	**(ppm)**	7846.9	11856.7	7901.8	7311.1	6947.1	8130.6	8261.5	7545.2	d.u.	d.u.	7335.6	8077.0
S	**(ppm)**	2706.3	3871.2	3584.2	6406.4	5559.9	3228.4	5183.4	6711.0	d.u.	d.u.	5014.9	4357.1
Ti	**(ppm)**	1788.1	1506.8	2063.0	2460.9	2197.2	1855.5	2154.7	2291.6	d.u.	d.u.	2363.8	2050.5
Ba	**(ppm)**	218.3	227.5	242.0	275.3	237.8	224.7	250.4	258.7	d.u.	d.u.	253.2	239.0
Cr	**(ppm)**	30.0	16.2	40.1	61.9	54.5	35.5	39.9	48.5	d.u.	d.u.	47.2	36.9
Cu	**(ppm)**	50.1	57.2	72.5	104.4	80.5	61.5	74.9	83.8	d.u.	d.u.	89.6	77.4
Pb	**(ppm)**	126.5	133.9	125.1	135.3	153.8	134.0	120.8	124.0	d.u.	d.u.	132.1	128.3
Mn	**(ppm)**	478.3	622.7	469.1	382.9	447.4	582.4	493.1	438.1	d.u.	d.u.	452.6	439.2
Ni	**(ppm)**	28.0	23.4	23.8	34.6	32.5	31.0	38.9	35.1	d.u.	d.u.	30.6	31.6
Sr	**(ppm)**	46.4	41.4	46.9	46.6	44.5	40.5	43.4	41.2	d.u.	d.u.	45.9	46.7
V	**(ppm)**	<dl	<dl	10.4	26.6	25.5	<dl	19.4	27.9	d.u.	d.u.	16.5	<dl
Zn	**(ppm)**	1010.8	1014.4	1552.0	1598.7	1702.8	1410.9	1352.2	1301.5	d.u.	d.u.	1121.4	1150.4
Ce	**(ppm)**	50.4	43.8	49.9	54.6	52.1	46.9	51.7	54.7	d.u.	d.u.	57.8	52.6
Cs	**(ppm)**	<dl	<dl	<dl	<dl	<dl	<dl	<dl	<dl	d.u.	d.u.	<dl	<dl
Rb	**(ppm)**	30.8	31.2	32.4	37.7	39.7	32.1	29.3	36.7	d.u.	d.u.	35.1	30.1
Zr	**(ppm)**	185.2	101.5	80.8	139.2	121.5	91.3	102.9	148.5	d.u.	d.u.	153.3	151.5
Remarks										not enough material present for analysis			

Table C.7: Data Herk – Kermt

		Timing											
		1	2	3	4	5	6	7	8	9	10	11	12
L.O.I.	**(%)**	10.9	12.7	13.2	10.0	7.3	8.4	9.4	10.8	12.3	11.5	9.2	11.7
Density	**(g/cm³)**	2.7099	2.6677	2.7398	2.6616	2.6887	2.6969	2.7274	2.7115	2.7303	2.7005	2.6904	2.7151
D [3, 2]	**(µm)**	12.4	11.9	11.1	12.2	11.0	9.5	11.8	10.4	9.8	10.2	10.4	d.u.
SSA	**(m²/g)**	0.1782	0.1895	0.1968	0.1841	0.2023	0.2350	0.1864	0.2118	0.2242	0.2170	0.2151	d.u.
Al	**(%)**	4.09	3.37	4.44	3.74	3.55	3.94	3.73	3.85	3.90	3.82	3.69	4.19
Ca	**(%)**	2.91	2.74	2.55	1.80	1.44	1.82	1.79	2.11	2.07	1.93	1.62	1.37
Fe	**(%)**	2.82	3.01	3.41	2.80	2.51	2.95	2.82	3.17	3.44	3.16	2.89	3.44
K	**(%)**	2.37	2.04	2.82	2.10	2.08	2.27	2.15	2.51	2.51	2.32	2.22	2.84
Si	**(%)**	91.82	67.41	93.65	94.19	88.60	83.57	91.10	79.79	77.11	81.37	79.96	78.99
P	**(ppm)**	3848.4	4407.2	4022.2	3097.7	2704.0	3317.5	2898.9	3161.0	3450.2	2960.5	2655.9	2260.0
S	**(ppm)**	2285.3	2220.7	1782.6	1644.3	1331.3	1589.4	1775.5	2078.9	1945.1	1939.2	1572.8	1443.1
Ti	**(ppm)**	3879.0	3861.6	4227.2	3925.5	3956.1	4197.2	3929.7	4001.8	4049.6	4055.1	3832.0	4119.2
Ba	**(ppm)**	518.1	500.7	565.7	494.6	492.3	491.6	500.7	502.6	513.7	500.5	492.9	470.4
Cr	**(ppm)**	85.4	66.0	104.8	64.7	62.1	73.7	70.4	59.1	60.9	59.0	49.6	66.9
Cu	**(ppm)**	42.1	42.0	60.5	41.3	31.3	39.1	36.0	43.5	46.9	38.9	35.5	37.2
Pb	**(ppm)**	13.8	14.4	25.4	11.3	8.1	13.9	9.7	16.9	17.9	14.3	12.0	17.5
Mn	**(ppm)**	1978.2	1443.2	1613.2	677.3	584.7	864.6	1,000.6	722.7	967.5	863.5	796.2	988.2
Ni	**(ppm)**	35.4	32.9	38.3	33.8	32.0	33.8	33.6	36.6	37.3	35.5	34.1	37.4
Sr	**(ppm)**	130.5	113.6	131.0	97.3	93.7	98.3	96.9	101.2	102.7	100.3	91.9	89.4
V	**(ppm)**	20.9	12.6	39.5	10.8	5.3	9.4	1.3	32.4	36.3	17.6	12.6	40.6
Zn	**(ppm)**	276.6	262.7	362.4	258.3	208.7	251.2	232.9	281.4	288.2	257.7	238.2	238.7
Ce	**(ppm)**	78.7	70.3	77.5	71.1	71.2	77.5	73.7	69.6	72.0	72.3	69.2	72.7
Cs	**(ppm)**	4.6	5.7	7.1	6.9	5.8	6.1	4.8	7.9	7.6	6.3	7.4	8.5
Rb	**(ppm)**	63.8	55.0	75.3	56.5	54.4	59.7	56.3	62.3	65.2	59.5	57.6	71.0
Zr	**(ppm)**	715.2	523.7	491.5	481.4	537.6	651.0	604.6	376.7	401.8	491.6	417.8	347.3
Remarks													not enough material for grain size analysis

Table C.8: Data Demer (upstream reaches) – Hasselt

		Timing											
		1	2	3	4	5	6	7	8	9	10	11	12
L.O.I.	(%)	24.5	33.7	22.2	24.4	18.6	26.2	20.8	14.9	26.9	26.5	15.2	27.2
Density	(g/cm³)	2.8750	2.8595	2.7741	2.8761	2.8238	2.8742	2.8257	2.7461	2.8371	2.7783	2.7371	2.7903
D [3, 2]	(µm)	7.8	12.2	11.2	11.2	13.4	13.0	9.6	11.7	11.0	10.8	11.7	9.5
SSA	(m²/g)	0.2703	0.1779	0.1862	0.1890	0.1554	0.1630	0.2275	0.1809	0.1967	0.2031	0.1845	0.2170
Al	(%)	2.98	2.86	3.11	3.35	3.44	3.01	3.17	3.79	3.05	3.24	3.49	3.12
Ca	(%)	1.85	1.59	1.37	1.20	1.17	1.37	1.42	1.02	1.52	1.51	1.07	1.59
Fe	(%)	8.68	9.48	7.15	7.46	6.05	8.91	7.85	5.31	8.27	6.70	4.66	5.94
K	(%)	0.96	0.44	1.30	1.34	1.48	0.86	1.16	1.48	1.21	1.48	1.63	1.48
Si	(%)	38.37	29.43	46.85	45.18	61.31	41.29	45.32	84.09	36.94	44.42	66.53	52.54
P	(ppm)	11260.8	18877.5	10730.0	10336.5	8264.7	14167.9	12808.5	6998.2	10906.4	8585.2	4771.8	7306.6
S	(ppm)	9183.8	11211.0	7891.0	8073.8	5014.8	8010.5	8459.8	4628.4	13811.3	6662.7	4809.0	10199.4
Ti	(ppm)	3589.2	3542.6	3730.7	3865.1	3764.1	3673.8	3764.0	3940.7	3654.3	3777.9	3803.1	3653.1
Ba	(ppm)	474.2	519.6	486.2	454.6	488.8	496.9	495.5	471.6	467.3	485.8	474.3	485.0
Cr	(ppm)	405.3	511.4	498.0	263.3	259.2	347.9	244.2	184.6	317.0	223.5	178.6	236.5
Cu	(ppm)	110.7	167.1	108.5	115.7	83.8	116.6	98.4	55.7	110.5	87.0	53.5	77.0
Pb	(ppm)	103.9	148.8	98.6	102.8	72.6	110.8	90.4	50.1	119.0	84.6	45.9	67.2
Mn	(ppm)	643.0	745.6	847.0	859.5	714.8	1056.7	906.5	658.0	635.3	707.6	581.3	688.2
Ni	(ppm)	86.1	106.7	78.7	75.5	61.6	88.2	68.6	51.5	77.7	63.5	50.9	59.5
Sr	(ppm)	96.1	93.4	88.8	103.0	87.5	96.3	94.7	79.3	86.3	81.9	80.4	88.9
V	(ppm)	27.9	22.5	26.5	38.0	31.6	24.5	38.5	22.8	40.0	34.7	18.3	38.3
Zn	(ppm)	857.6	1175.1	792.1	858.9	614.7	856.6	770.3	461.5	834.4	651.7	407.2	577.5
Ce	(ppm)	96.3	98.0	81.1	93.2	84.7	96.5	93.6	82.4	97.2	89.7	79.3	82.8
Cs	(ppm)	2.1	1.7	4.6	2.6	5.4	2.2	2.6	4.4	4.9	5.9	5.0	6.0
Rb	(ppm)	38.1	27.5	41.5	45.9	46.3	36.6	42.6	46.4	44.5	45.4	48.0	45.9
Zr	(ppm)	295.7	246.8	311.6	248.6	355.4	233.4	320.2	528.5	209.9	281.3	410.2	321.3

Table C.9: Demer (outlet) – Aarschot

		Timing													
		13	14	15	16	17	18	19	20	21	22	23	24	25	26
L.O.I.	(%)	42.3	14.2	21.0	8.8	11.3	12.1	7.5	9.6	13.1	12.6	17.3	23.1	33.4	26.7
Density	(g/cm³)	2.9056	2.7800	2.8195	2.7157	2.7419	2.7193	2.7105	2.7151	2.7288	2.7351	2.7706	2.7766	2.5478	2.6821
D [3, 2]	(µm)	13.8	7.6	8.9	8.7	8.3	8.4	10.1	8.1	5.3	5.4	7.7	11.0	9.0	8.0
SSA	(m²/g)	0.1496	0.2846	0.2384	0.2545	0.2636	0.2619	0.2183	0.2734	0.4130	0.4086	0.2808	0.1965	0.2614	0.2781
Al	(%)	2.76	3.27	3.30	3.73	3.20	3.37	3.30	3.54	4.70	4.74	d.u.	d.u.	d.u.	d.u.
Ca	(%)	2.13	1.91	2.69	1.33	1.04	1.03	0.72	0.89	0.69	0.67	d.u.	d.u.	d.u.	d.u.
Fe	(%)	7.93	6.40	6.67	3.47	4.97	4.93	3.55	4.07	5.10	5.00	d.u.	d.u.	d.u.	d.u.
K	(%)	1.64	1.97	2.20	2.55	2.29	2.31	2.06	2.23	3.43	3.45	d.u.	d.u.	d.u.	d.u.
Si	(%)	52.91	62.77	53.98	88.34	71.64	71.70	90.16	86.05	73.95	79.94	d.u.	d.u.	d.u.	d.u.
P	(ppm)	8260.7	7559.1	6266.4	2366.9	4081.5	3664.8	2919.2	3128.9	2708.0	2787.6	d.u.	d.u.	d.u.	d.u.
S	(ppm)	2087.0	1501.0	919.5	1037.8	1337.0	1326.0	1039.8	1236.8	868.9	863.3	d.u.	d.u.	d.u.	d.u.
Ti	(ppm)	3245.9	3565.1	3563.8	4004.6	3617.0	3689.1	3668.8	3951.5	4457.6	4505.9	d.u.	d.u.	d.u.	d.u.
Ba	(ppm)	427.9	505.7	468.2	468.0	432.7	443.4	448.4	455.7	481.3	478.7	d.u.	d.u.	d.u.	d.u.
Cr	(ppm)	78.4	92.6	116.0	62.3	89.2	86.6	69.4	89.1	104.9	95.7	d.u.	d.u.	d.u.	d.u.
Cu	(ppm)	43.4	46.3	57.9	28.7	36.3	35.8	23.8	31.7	43.1	42.5	d.u.	d.u.	d.u.	d.u.
Pb	(ppm)	31.3	35.6	39.7	12.3	19.4	20.8	9.1	15.4	39.6	38.0	d.u.	d.u.	d.u.	d.u.
Mn	(ppm)	779.6	681.9	608.4	497.0	449.1	458.2	383.7	419.5	546.1	592.4	d.u.	d.u.	d.u.	d.u.
Ni	(ppm)	38.1	41.0	42.4	35.6	35.6	36.1	32.9	36.1	39.0	39.3	d.u.	d.u.	d.u.	d.u.
Sr	(ppm)	112.7	120.7	126.2	89.9	84.5	84.8	81.3	83.8	85.3	84.5	d.u.	d.u.	d.u.	d.u.
V	(ppm)	19.1	29.3	37.4	32.6	31.0	33.9	1.4	20.3	114.6	100.4	d.u.	d.u.	d.u.	d.u.
Zn	(ppm)	411.3	420.4	439.9	218.9	276.4	283.3	201.6	243.6	294.5	290.9	d.u.	d.u.	d.u.	d.u.
Ce	(ppm)	62.9	65.9	65.6	66.9	67.1	68.7	65.2	70.6	72.3	70.4	d.u.	d.u.	d.u.	d.u.
Cs	(ppm)	2.2	3.8	5.0	6.4	4.1	5.1	5.7	5.5	7.7	8.6	d.u.	d.u.	d.u.	d.u.
Rb	(ppm)	44.8	54.8	59.1	58.1	53.6	55.9	50.4	54.9	92.2	90.9	d.u.	d.u.	d.u.	d.u.
Zr	(ppm)	299.8	262.9	201.3	329.5	383.0	355.4	415.7	420.1	198.9	211.7	d.u.	d.u.	d.u.	d.u.
Remarks												not enough material present for chemical analysis			

Table C.9: Demer (outlet) – Aarschot (continued)

		Timing											
		27	28	29	30	31	32	33	34	35	36	37	38
L.O.I.	**(%)**	16.9	13.4	9.7	8.8	8.7	5.8	9.1	10.6	10.5	11.5	8.3	10.7
Density	**(g/cm³)**	2.8276	2.7548	2.7405	2.7390	2.7641	2.7415	2.7478	2.7654	2.7786	2.7763	2.7423	2.7715
D [3, 2]	**(µm)**	9.0	9.2	10.1	10.4	10.8	13.7	11.2	9.5	9.7	8.2	11.5	9.7
SSA	**(m²/g)**	0.2361	0.2377	0.2173	0.2113	0.2007	0.1603	0.1958	0.2291	0.2216	0.2621	0.1896	0.2230
Al	**(%)**	2.86	3.54	3.98	3.33	3.22	2.91	3.08	3.41	3.12	3.42	2.87	3.21
Ca	**(%)**	3.66	1.34	0.99	0.98	1.00	0.65	0.98	1.37	1.38	1.53	1.23	1.37
Fe	**(%)**	4.93	4.78	4.21	4.41	4.44	3.66	4.64	5.50	5.92	6.03	5.26	5.68
K	**(%)**	1.73	2.21	2.07	1.88	1.88	1.40	1.76	1.92	1.87	1.92	1.66	1.77
Si	**(%)**	57.74	65.92	101.98	78.46	74.06	80.69	77.51	70.01	71.68	67.62	74.38	72.55
P	**(ppm)**	3071.8	3785.8	3355.6	4240.7	4249.2	3975.5	4802.6	5548.0	6181.8	6322.5	5350.1	5859.7
S	**(ppm)**	5478.6	1674.4	1081.6	1206.7	1099.0	732.2	1068.6	1225.2	1141.0	1324.0	1062.5	1315.8
Ti	**(ppm)**	2929.1	3701.9	3747.7	3708.0	3768.0	3707.6	3835.5	3752.7	3473.3	3696.2	3517.7	3550.7
Ba	**(ppm)**	415.6	459.3	462.4	459.4	458.5	439.7	458.6	470.5	482.1	484.6	443.0	463.5
Cr	**(ppm)**	102.9	95.1	107.4	106.2	115.2	97.1	156.4	142.6	149.8	167.3	140.7	144.0
Cu	**(ppm)**	43.0	41.3	30.2	30.2	27.1	19.7	28.6	34.1	30.6	35.6	29.7	33.5
Pb	**(ppm)**	21.7	24.7	20.3	18.9	19.7	9.0	20.8	30.2	29.2	40.0	24.1	28.8
Mn	**(ppm)**	730.4	519.8	499.2	499.4	524.8	430.8	492.4	588.9	558.2	610.9	520.1	570.9
Ni	**(ppm)**	38.2	39.5	36.7	35.3	37.0	34.7	38.1	41.2	39.0	43.3	38.0	40.1
Sr	**(ppm)**	138.2	88.9	83.8	83.3	85.9	77.5	85.8	91.8	93.4	98.4	87.4	90.6
V	**(ppm)**	22.0	27.2	18.9	26.9	2.7	<dl	22.7	24.4	31.8	32.0	21.8	23.2
Zn	**(ppm)**	310.2	300.3	245.8	248.6	257.7	201.3	269.4	319.4	328.7	359.0	289.8	316.4
Ce	**(ppm)**	61.1	68.7	68.6	70.3	69.4	67.6	68.9	71.0	69.4	72.4	68.0	69.4
Cs	**(ppm)**	3.7	5.6	5.0	6.0	5.7	4.8	4.9	4.4	4.5	3.6	3.6	4.3
Rb	**(ppm)**	47.4	56.9	52.5	49.9	49.3	41.3	48.3	51.9	50.3	52.5	45.6	47.6
Zr	**(ppm)**	299.8	345.9	443.4	516.9	548.1	743.8	621.8	455.6	471.0	440.0	564.1	525.7

Addendum D: Dataset of source types collected in the Gete catchment

Key

Location Riverbed Samples

	VMM location code
17	427000
18	429000
19	430000
20	431,000
21	433400
22	433600
23	433900
24	434000
25	435000
26	435800
27	439000
28	443000
29	E002733
30	E003632

Sub-catchments (as referred to in sample code)

BG	Beneden-Gete
M	Melsterbeek
KG	Kleine Gete
GG	Grote Gete

Timing

1	20/04/2007	TIS
2	24/05/2007	TIS
3	21/06/2007	TIS
4	06/08/2007	TIS
5	29/08/2007	TIS
6	27/09/2007	TIS
7	06/11/2007	TIS
8	18/12/2007	TIS
9	28/01/2008	TIS
10	28/02/2008	TIS
11	10/04/2008	TIS
12	22/05/2008	TIS
21	from 21/5/07 - 4/6/07	Campaign 1
22	from 11/9/07 - 20/9/07	Campaign 2
23	from 15/2/08 - 28/2/08	Campaign 3
24	from 29/5/08 - 14/7/08	Campaign 4

<dl = values below detection limit

d.u. = data unavailable.

Table D.1: Data Gete – Halen (outlet) samples

		Timing												
		1	2	3	4	5	6	7	8	9	10	11	11	12
L.O.I.	(%)	5.2	9.5	11.9	9.9	8.4	11.0	10.0	8.7	8.4	10.1	6.1	6.3	7.5
Density	(g/cm³)	2.7104	2.7191	2.7699	2.6732	2.6664	2.7051	2.7000	2.6876	2.6654	2.7146	2.6867	2.6841	2.6965
D [3, 2]	(µm)	12.6	9.8	7.4	10.1	11.7	9.0	9.4	10.6	11.0	10.9	12.0	11.6	10.5
SSA	(m²/g)	0.1751	0.2255	0.2912	0.2212	0.1931	0.2476	0.2355	0.2104	0.2043	0.2021	0.1856	0.1920	0.2122
Al	(%)	3.48	3.75	5.02	4.08	3.91	4.18	4.26	4.64	3.82	4.60	3.71	3.49	3.87
Ca	(%)	1.00	1.85	1.35	1.54	1.31	1.52	1.61	1.42	1.37	1.45	0.86	0.88	1.07
Fe	(%)	2.00	2.56	4.38	2.86	2.59	3.10	3.16	2.84	2.58	2.74	2.30	2.35	2.58
K	(%)	1.93	2.12	3.90	2.44	2.47	2.72	2.76	2.61	2.39	2.43	2.19	2.18	2.38
Si	(%)	115.83	99.76	75.33	87.66	93.89	87.54	82.19	109.33	96.82	112.02	89.50	92.23	97.95
P	(ppm)	1312.5	1821.2	1832.5	1952.6	1538.2	1806.8	1804.7	1495.0	1861.1	1418.9	1368.2	1286.6	1446.5
S	(ppm)	859.5	1330.9	1044.9	1153.6	1283.7	1487.9	1892.3	2069.2	1893.0	2251.4	1056.1	1029.4	1431.5
Ti	(ppm)	3734.1	3917.3	4354.0	3965.1	3927.7	4092.4	4131.1	3945.0	3851.4	3987.1	3827.8	3841.0	3969.9
Ba	(ppm)	459.4	471.7	495.9	487.3	459.1	492.6	482.7	476.1	479.3	481.2	464.5	460.7	471.8
Cr	(ppm)	60.5	70.6	91.5	89.2	75.8	96.7	78.3	64.3	65.0	69.5	58.8	55.9	67.6
Cu	(ppm)	18.9	29.2	36.6	36.4	32.8	41.2	41.1	32.9	31.6	33.9	21.2	22.4	27.8
Pb	(ppm)	<dl	12.1	28.0	17.3	11.6	21.5	23.5	17.1	13.6	15.6	5.0	6.1	9.6
Mn	(ppm)	429.9	1167.3	1103.5	818.3	577.1	774.8	704.7	437.6	401.3	489.3	428.1	421.6	470.3
Ni	(ppm)	33.0	37.1	47.0	37.9	35.5	37.8	38.6	37.0	36.2	36.3	32.9	33.9	34.8
Sr	(ppm)	83.4	90.3	88.3	88.7	85.2	89.5	90.5	86.0	86.9	87.2	78.9	78.9	81.5
V	(ppm)	<dl	4.0	81.6	16.7	2.4	20.6	23.7	32.4	9.1	12.2	6.6	12.7	18.0
Zn	(ppm)	137.0	200.0	233.9	223.1	205.3	248.2	249.6	216.0	198.9	215.0	150.0	155.0	180.1
Ce	(ppm)	73.4	72.1	80.6	70.6	70.1	70.9	72.2	70.7	68.6	69.9	67.0	67.7	71.7
Cs	(ppm)	5.2	7.5	8.6	6.0	7.6	8.3	7.2	7.4	6.5	6.9	6.4	6.4	7.8
Rb	(ppm)	48.0	54.7	93.5	61.7	58.6	66.6	65.9	62.9	58.0	58.2	52.9	53.6	57.4
Zr	(ppm)	623.3	476.9	248.4	395.6	429.7	336.2	372.9	388.4	396.2	385.5	422.7	432.6	453.4
Remarks												different subsamples		

Table D.2: Data samples collected in the Beneden-Gete catchment

		Sample code									
		G(BG)C1	G(BG)C2	G(BG)C3	G(BG)P1	G(BG)P2	G(BG)P3	G(BG)CB1	G(BG)CB2	G(BG)CB3	G(BG)CB4
L.O.I.	(%)	5.7	6.0	3.6	5.8	7.4	9.5	3.2	11.0	4.4	5.3
Density	(g/cm³)	2.6653	2.6899	1.9649	2.6744	2.6680	2.6701	2.6764	2.6759	2.6689	2.6733
D [3, 2]	(µm)	15.4	15.9	6.0	15.3	15.9	14.4	16.4	11.7	14.7	15.1
SSA	(m²/g)	0.1460	0.1402	0.5077	0.1468	0.1414	0.1557	0.1369	0.1925	0.1527	0.1486
Al	(%)	3.33	3.28	3.31	2.81	3.46	3.07	3.41	3.73	3.43	3.51
Ca	(%)	0.41	<dl	<dl	0.35	2.29	3.43	0.18	2.23	<dl	0.77
Fe	(%)	2.00	1.90	1.70	1.59	2.09	1.80	1.88	2.63	2.00	2.02
K	(%)	2.19	2.37	1.98	1.66	2.10	1.87	1.90	2.46	2.20	2.11
Si	(%)	105.34	107.36	111.85	96.12	94.37	92.46	116.35	83.25	113.89	111.13
P	(ppm)	1062.2	1017.8	715.9	1274.9	1036.2	1468.4	528.2	2708.3	558.9	1576.1
S	(ppm)	516.8	323.3	205.6	498.1	906.8	847.4	136.0	1602.6	271.1	318.8
Ti	(ppm)	3697.2	3870.5	4028.8	3185.2	3496.4	3452.8	3630.6	3765.4	3917.2	3685.7
Ba	(ppm)	465.0	434.8	467.4	342.8	481.8	425.4	451.4	496.1	473.1	464.6
Cr	(ppm)	57.7	55.8	82.8	34.6	60.6	51.2	36.8	128.3	83.4	54.8
Cu	(ppm)	24.7	12.5	13.5	16.5	20.0	16.5	6.2	50.8	15.0	24.0
Pb	(ppm)	32.3	0.1	<dl	17.2	34.8	13.2	<dl	32.4	3.4	20.2
Mn	(ppm)	349.9	337.4	372.9	290.3	343.9	357.4	357.6	431.0	321.6	382.8
Ni	(ppm)	32.5	31.2	29.7	30.6	33.7	31.7	30.5	34.9	31.0	32.0
Sr	(ppm)	71.3	68.8	62.6	73.9	108.8	75.6	70.1	99.9	65.0	75.1
V	(ppm)	<dl	<dl	<dl	<dl	1.5	<dl	<dl	11.9	<dl	<dl
Zn	(ppm)	166.9	95.8	80.4	133.7	151.1	142.9	63.3	282.1	84.0	153.3
Ce	(ppm)	68.4	71.3	70.4	67.9	70.1	66.2	66.6	69.1	66.3	69.0
Cs	(ppm)	5.6	4.3	6.1	2.9	6.4	4.8	6.4	7.0	5.7	6.3
Rb	(ppm)	49.6	53.2	47.9	45.2	50.8	44.0	50.9	56.0	54.7	51.1
Zr	(ppm)	515.6	571.1	666.9	563.9	419.0	479.6	459.3	426.6	525.4	489.6

		Sample Code																	
		G(M)C1	G(M)C2	G(M)C3	G(M)C4	G(M)C5	G(M)C6	G(M)P1	G(M)P2	G(M)P3	G(M)P4	G(M)P5	G(M)P6	G(M)CB1	G(M)CB2	G(M)CB3	G(M)CB4	G(M)CB5	G(M)CB6
L.O.I.	(%)	4.1	3.8	6.8	3.7	3.5	3.2	4.9	7.8	4.4	6.0	5.6	4.7	4.7	6.9	2.6	3.9	4.2	4.4
Density	(g/cm³)	2.6656	2.6773	2.6909	2.6751	2.6824	2.6703	2.6702	2.6718	2.6846	2.6778	2.6703	2.6743	2.6703	2.6873	2.6753	2.6849	2.6801	2.6852
D [3, 2]	(µm)	13.2	13.7	12.0	10.7	12.5	11.7	13.0	12.8	11.6	12.3	13.1	14.6	13.8	14.7	16.9	13.8	15.7	15.5
SSA	(m²/g)	0.1711	0.1630	0.1857	0.2095	0.1785	0.1923	0.1725	0.1761	0.1930	0.1824	0.1711	0.1532	0.1624	0.1515	0.1326	0.1614	0.1423	0.1440
Al	(%)	3.51	3.27	3.57	3.78	3.26	3.34	3.71	3.24	3.89	3.81	3.32	3.58	3.33	3.16	3.47	3.50	3.17	3.15
Ca	(%)	2.79	<dl	<dl	<dl	<dl	<dl	0.20	0.34	<dl	0.01	<dl	<dl	1.12	<dl	<dl	0.86	0.34	0.63
Fe	(%)	2.22	1.71	2.00	2.08	1.68	1.69	2.12	1.68	2.39	2.23	1.96	2.18	1.70	1.66	1.63	1.91	1.56	1.63
K	(%)	2.14	2.05	2.24	2.34	2.16	2.28	2.26	1.76	2.87	2.86	2.33	2.49	1.89	1.64	1.75	2.14	1.72	1.88
Si	(%)	94.85	119.76	109.42	115.75	119.99	116.32	103.47	111.06	103.31	103.25	104.67	106.49	102.61	107.60	115.48	103.75	115.63	106.03
P	(ppm)	836.4	542.4	824.8	509.2	561.1	541.5	514.6	827.2	560.0	1018.0	731.4	722.0	869.1	436.3	461.0	579.6	824.5	920.2
S	(ppm)	387.4	199.7	311.7	217.7	163.7	176.0	286.8	458.5	264.3	274.7	320.7	187.0	487.3	500.4	355.4	289.0	423.9	458.1
Ti	(ppm)	3750.8	3903.6	3987.2	3886.9	3983.5	4101.2	3924.3	3743.1	4076.8	4069.1	3728.6	3903.8	3504.6	3858.2	3934.6	3993.6	3915.5	3802.1
Ba	(ppm)	434.0	450.7	474.4	457.0	476.9	470.8	444.9	470.4	457.4	455.5	394.6	408.0	464.6	369.1	455.6	462.5	440.1	451.9
Cr	(ppm)	49.6	32.3	51.5	40.7	39.1	35.7	46.3	46.9	46.7	56.8	51.0	40.4	32.8	36.3	41.7	51.2	49.3	56.1
Cu	(ppm)	7.7	7.0	37.6	9.6	7.1	6.2	8.4	15.3	12.3	12.8	13.9	13.1	22.0	7.2	5.8	15.7	11.7	17.1
Pb	(ppm)	<dl	<dl	9.5	<dl	<dl	<dl	<dl	5.5	<dl	0.7	<dl	<dl	<dl	<dl	<dl	5.9	<dl	4.3
Mn	(ppm)	363.2	351.5	407.0	362.1	414.4	412.6	329.5	294.6	352.3	290.2	353.8	376.1	263.4	345.8	352.4	324.8	290.3	308.1
Ni	(ppm)	33.0	29.4	31.3	33.3	29.1	29.3	31.5	33.8	34.0	33.2	31.3	33.0	30.4	29.9	28.8	32.1	29.4	29.7
Sr	(ppm)	71.9	66.1	70.3	68.6	64.6	65.3	70.2	73.6	70.1	70.1	66.1	65.9	81.0	74.8	71.8	79.4	74.6	76.0
V	(ppm)	<dl	<dl	6.5	<dl	<dl	<dl	<dl	<dl	14.7	8.0	<dl	8.1	<dl	<dl	<dl	<dl	<dl	<dl
Zn	(ppm)	70.4	74.7	173.9	83.8	71.7	72.7	79.6	133.5	89.4	103.4	76.9	77.4	143.0	75.8	66.7	147.5	130.6	153.4
Ce	(ppm)	70.3	68.9	70.3	68.1	69.1	70.0	70.1	67.3	72.2	72.2	69.9	71.7	64.4	76.4	71.4	73.7	74.3	70.4
Cs	(ppm)	5.6	6.9	6.6	6.8	5.7	5.9	5.6	4.8	7.8	8.0	4.9	6.1	6.3	3.7	6.9	6.0	6.0	4.7
Rb	(ppm)	54.7	48.2	50.7	54.7	50.9	50.2	54.8	44.4	59.3	63.3	51.4	54.9	46.0	50.8	47.1	50.3	42.0	42.1
Zr	(ppm)	458.5	536.9	479.8	373.6	523.2	546.7	505.1	582.4	449.5	470.0	493.4	473.2	465.7	651.6	609.1	568.2	747.9	654.8

Table D.3: Data samples collected in the Melsterbeek catchment

Table D.4: Data samples collected in the Kleine Gete catchment

		Sample Code																	
		G(KG) C1	G(KG) C2	G(KG) C3	G(KG) C4	G(KG) C5	G(KG) C6	G(KG) P1	G(KG) P2	G(KG) P3	G(KG) P4	G(KG) P5	G(KG) P6	G(KG) CB1	G(KG) CB2	G(KG) CB3	G(KG) CB4	G(KG) CB5	G(KG) CB6
L.O.I.	(%)	2.9	4.2	2.6	5.2	4.8	4.7	7.9	3.0	2.7	5.2	4.5	7.8	8.1	3.2	3.4	6.1	9.1	4.7
Density	(g/cm^3)	2.6686	2.6753	2.6748	2.6787	2.6728	2.6701	2.6758	2.5331	2.6788	2.6690	2.6704	2.6675	2.6776	2.6706	2.6866	2.6632	2.6885	2.4550
D [3, 2]	(µm)	13.1	10.9	17.9	16.2	15.6	15.7	13.3	8.0	14.6	15.3	14.8	14.7	15.7	14.7	14.1	9.0	15.0	15.5
SSA	(m^2/g)	0.1720	0.2067	0.1255	0.1386	0.1441	0.1429	0.1681	0.2961	0.1535	0.1470	0.1523	0.1529	0.1424	0.1528	0.1582	0.2494	0.1490	0.1579
Al	(%)	3.43	3.85	3.11	3.10	3.10	3.13	3.37	3.06	3.22	3.25	3.34	3.08	3.45	3.32	3.12	2.91	4.08	3.25
Ca	(%)	<dl	<dl	<dl	1.83	0.75	0.57	0.47	<dl	<dl	<dl	<dl	0.32	0.38	<dl	0.88	0.53	0.85	0.87
Fe	(%)	1.72	2.15	1.61	1.57	1.80	1.73	1.98	1.49	1.60	1.75	1.70	1.85	1.64	1.89	1.59	1.60	2.82	1.83
K	(%)	2.02	2.61	1.86	1.64	1.90	1.87	2.47	1.76	1.84	1.97	2.04	2.00	1.75	2.42	1.59	1.75	2.89	1.91
Si	(%)	123.37	110.82	113.54	107.39	106.16	109.91	101.01	114.23	123.33	107.50	121.89	108.19	122.22	97.63	114.06	113.80	94.92	110.08
P	(ppm)	485.9	742.2	683.9	1023.8	820.2	1179.0	1334.9	473.7	461.9	630.2	534.8	1136.6	758.1	855.5	629.7	599.4	1199.9	836.3
S	(ppm)	170.4	191.7	182.7	517.7	321.1	395.8	366.9	197.0	196.5	377.5	278.3	537.1	395.7	489.6	565.1	396.0	533.4	433.4
Ti	(ppm)	3994.8	3919.2	3953.5	3422.7	3607.2	3624.8	3887.8	3703.6	3605.5	3732.1	3752.2	3650.8	3672.2	4002.6	5137.4	3642.2	4030.3	3683.2
Ba	(ppm)	455.0	462.3	447.9	435.4	442.4	458.5	475.4	445.6	458.6	442.6	441.4	449.0	467.9	451.0	446.2	436.6	468.7	445.8
Cr	(ppm)	47.1	48.0	49.9	45.8	35.7	44.8	39.0	39.2	42.6	35.4	37.0	38.8	53.2	62.0	102.2	39.7	49.2	45.4
Cu	(ppm)	7.9	11.3	9.7	11.2	12.3	15.4	17.5	10.2	7.2	6.1	5.7	18.3	16.3	9.7	11.7	6.6	19.2	12.8
Pb	(ppm)	<dl	<dl	<dl	5.7	6.7	9.1	8.4	<dl	<dl	<dl	<dl	9.1	6.4	<dl	<dl	16.1	7.1	6.2
Mn	(ppm)	373.0	395.2	336.1	349.9	338.1	331.9	365.3	329.0	338.6	364.7	361.1	381.5	297.7	355.7	339.4	340.7	444.3	355.5
Ni	(ppm)	29.9	32.6	29.3	29.5	30.8	30.3	33.3	29.0	29.1	29.2	29.6	31.1	33.7	30.3	34.0	29.2	36.7	30.6
Sr	(ppm)	65.9	70.0	67.3	78.2	78.1	76.2	78.9	70.5	68.0	64.0	64.4	69.2	74.9	65.2	83.8	68.3	75.6	77.7
V	(ppm)	<dl	2.2	<dl	<dl	<dl	<dl	0.3	<dl	<dl	<dl	<dl	<dl	<dl	<dl	<dl	<dl	31.5	<dl
Zn	(ppm)	69.3	85.0	78.4	111.2	112.0	139.3	147.8	75.5	76.0	72.1	70.1	130.3	149.1	149.4	91.4	131.4	144.9	115.0
Ce	(ppm)	72.6	69.3	72.6	68.1	67.5	67.1	70.5	68.0	66.1	69.7	70.3	66.1	69.7	68.6	114.0	66.5	72.0	69.6
Cs	(ppm)	4.6	6.8	6.0	4.8	5.1	5.3	7.6	5.3	5.6	6.1	6.7	6.1	5.1	6.7	0.9	6.4	8.7	6.6
Rb	(ppm)	48.6	57.7	46.0	42.3	46.1	46.2	54.5	43.0	47.8	46.0	45.3	47.9	44.1	48.8	40.1	44.1	66.1	46.7
Zr	(ppm)	620.2	434.6	683.5	575.9	544.3	546.0	511.4	570.5	487.4	554.4	570.3	527.4	618.4	479.7	1558.3	528.0	338.9	570.0

		Sample Code																	
		G(GG) C1	G(GG) C2	G(GG) C3	G(GG) C4	G(GG) C5	G(GG) C6	G(GG) P1	G(GG) P2	G(GG) P3	G(GG) P4	G(GG) P5	G(GG) P6	G(GG) CB1	G(GG) CB2	G(GG) CB3	G(GG) CB4	G(GG) CB5	G(GG) CB6
L.O.I.	(%)	5.6	3.9	4.7	4.0	3.8	3.0	8.3	5.2	6.1	8.6	5.7	3.9	5.5	20.3	4.1	4.2	3.4	3.4
Density	(g/cm³)	2.6855	2.6700	2.6794	2.6809	2.6741	2.6840	2.6734	2.6794	2.6717	<dl	2.6719	2.6833	2.6783	2.6778	2.6811	2.6842	2.6806	2.6782
D [3, 2]	(µm)	13.3	13.1	13.8	12.5	13.1	13.3	14.9	14.3	15.2	14.8	12.4	11.9	13.1	15.5	15.2	16.2	15.6	15.1
SSA	(m²/g)	0.1681	0.1720	0.1621	0.1785	0.1717	0.1685	0.1506	0.1570	0.1481	<dl	0.1804	0.1871	0.1704	0.1445	0.1468	0.1379	0.1439	0.1479
Al	(%)	3.49	3.64	3.32	3.92	3.46	3.57	3.19	3.30	3.12	3.31	3.39	3.68	3.47	3.08	3.48	3.34	3.31	3.24
Ca	(%)	0.81	<dl	<dl	0.66	1.01	<dl	0.67	0.45	0.47	0.55	2.27	0.11	0.43	0.78	0.33	0.95	0.36	0.17
Fe	(%)	2.00	1.73	1.97	2.15	2.03	1.91	1.83	1.85	1.94	1.95	2.15	2.09	2.05	1.95	1.91	1.89	1.83	1.75
K	(%)	2.07	2.50	1.98	2.45	2.21	2.28	2.02	2.04	2.37	2.05	2.50	2.49	2.20	2.17	1.98	1.66	1.77	1.60
Si	(%)	100.14	138.25	110.03	101.36	103.48	109.09	104.34	111.20	102.65	97.51	92.35	111.39	102.28	107.52	110.59	102.43	103.07	119.26
P	(ppm)	1068.3	1037.0	1261.6	913.4	786.6	705.8	1310.0	1152.4	1255.9	1444.6	986.2	825.8	920.1	1145.4	875.1	1003.6	858.1	921.1
S	(ppm)	554.6	222.7	431.0	238.4	358.7	141.6	687.1	392.9	511.6	803.9	435.9	224.1	487.2	531.8	439.7	382.8	326.1	324.4
Ti	(ppm)	3838.4	4188.5	3790.5	3950.3	3805.6	4107.9	3546.0	3756.0	3532.0	3693.2	3783.1	3985.6	3920.5	3473.6	3728.4	3639.8	3744.6	3822.6
Ba	(ppm)	438.7	493.0	499.1	447.5	479.5	441.3	440.7	455.6	445.4	463.5	460.0	456.0	461.1	458.3	454.2	469.2	439.7	437.8
Cr	(ppm)	57.6	53.4	366.3	42.3	48.7	44.1	36.5	62.4	42.1	59.5	49.9	53.4	41.6	38.3	49.6	51.5	43.3	53.8
Cu	(ppm)	23.6	13.3	31.0	44.9	12.5	7.2	17.2	19.2	11.1	29.0	9.9	8.4	27.1	26.2	11.8	25.8	10.0	8.9
Pb	(ppm)	9.3	0.3	25.1	<dl	13.9	<dl	12.3	23.2	<dl	34.5	12.7	<dl	24.4	25.8	9.2	29.6	<dl	<dl
Mn	(ppm)	382.6	680.1	316.6	376.4	405.9	347.2	333.3	354.7	358.7	344.5	367.2	461.1	376.5	335.7	377.9	313.5	369.4	378.0
Ni	(ppm)	31.5	28.5	32.3	34.2	32.1	31.5	31.1	31.9	29.7	33.0	31.9	32.1	31.3	32.8	31.1	32.3	30.2	30.4
Sr	(ppm)	75.7	72.1	66.1	78.3	79.9	67.4	68.3	71.5	67.1	80.5	91.5	69.5	72.8	72.4	75.4	76.7	71.9	69.9
V	(ppm)	<dl	8.6	5.0	0.7	<dl	<dl	<dl	<dl	<dl	<dl	<dl	0.1	6.2	<dl	<dl	<dl	<dl	<dl
Zn	(ppm)	130.4	93.4	161.5	89.1	140.3	68.4	130.3	147.7	91.1	167.6	118.1	82.7	141.0	157.2	105.9	147.0	140.1	99.5
Ce	(ppm)	68.4	75.1	68.3	72.6	68.2	74.7	66.2	70.2	64.4	66.5	69.6	70.7	71.3	65.4	70.1	68.6	68.7	70.4
Cs	(ppm)	5.8	5.3	6.2	6.2	6.2	6.0	7.2	7.2	6.2	6.7	4.7	5.6	7.5	6.0	5.2	5.6	5.8	6.3
Rb	(ppm)	49.1	64.4	49.7	57.7	51.1	49.7	46.3	47.8	47.5	48.6	55.2	51.8	51.3	51.0	49.2	46.1	44.8	43.1
Zr	(ppm)	528.9	700.4	547.0	494.1	458.8	579.4	501.7	532.4	474.1	497.1	460.6	493.6	554.3	445.1	508.8	540.9	543.7	630.7

Table D.5: Data samples collected in the Grote Gete catchment

		Sample Code																			
		17	17	17	17	18	18	18	18	19	19	19	19	20	20	20	20	21	21	21	21
L.O.I.	(%)	2.7	4.1	3.1	3.5	4.4	4.7	2.7	5.2	3.6	3.9	2.7	d.u.	2.3	3.8	2.4	d.u.	11.5	9.6	6.6	7.3
Density	(g/cm³)	2.6804	2.6919	2.6787	2.7011	2.6970	2.6906	2.6716	2.6922	2.6676	2.6727	2.6686	d.u.	2.7303	2.6920	2.6752	d.u.	2.7161	2.6976	2.6795	2.7098
D [3, 2]	(µm)	14.8	14.3	13.9	13.0	11.6	10.2	14.0	10.2	11.7	12.1	12.8	d.u.	17.4	11.6	13.0	d.u.	8.2	10.4	12.2	11.6
SSA	(m²/g)	0.1517	0.1554	0.1617	0.1712	0.1912	0.2179	0.1605	0.2179	0.1921	0.1857	0.1763	d.u.	0.1263	0.1929	0.1732	d.u.	0.2695	0.2138	0.1836	0.1902
Al	(%)	3.17	3.32	3.14	0.60	3.44	3.78	0.60	3.70	3.31	3.52	3.14	d.u.	3.16	3.57	3.10	d.u.	3.83	3.63	3.70	3.24
Ca	(%)	0.78	1.00	0.68	0.57	1.26	0.93	0.77	0.69	0.87	0.86	0.55	d.u.	0.58	0.89	0.48	d.u.	0.51	0.50	0.16	0.17
Fe	(%)	1.71	1.89	1.71	1.79	2.22	2.21	1.61	2.32	1.70	1.88	1.51	d.u.	1.42	1.95	1.54	d.u.	4.49	3.78	3.41	3.13
K	(%)	1.51	1.59	1.60	1.51	1.84	2.18	1.44	2.36	1.74	1.85	1.48	d.u.	1.27	1.93	1.43	d.u.	2.14	2.07	2.17	1.64
Si	(%)	113.10	102.52	102.57	105.87	95.60	98.59	100.62	97.16	109.67	103.09	117.47	d.u.	122.03	107.79	116.73	d.u.	69.03	78.05	87.29	90.27
P	(ppm)	1502.1	1438.1	901.1	922.8	1905.8	1043.5	929.2	1163.1	990.9	986.4	753.6	d.u.	764.6	1140.2	646.6	d.u.	7303.3	4864.1	1784.0	4117.7
S	(ppm)	486.8	731.2	744.8	507.6	704.8	955.3	1325.0	793.0	696.8	814.1	445.8	d.u.	496.8	741.0	687.8	d.u.	2653.5	3233.6	2723.3	1669.7
Ti	(ppm)	3849.9	4174.7	3879.9	3935.8	4236.3	4353.8	4361.2	4170.7	3891.4	3900.7	3630.0	d.u.	3966.7	4378.5	4166.1	d.u.	4050.1	3882.7	3946.9	3677.5
Ba	(ppm)	437.9	441.0	442.3	443.8	460.9	440.2	426.1	461.3	446.1	452.1	450.4	d.u.	430.7	453.9	440.0	d.u.	494.1	459.6	434.5	442.1
Cr	(ppm)	58.5	106.8	59.3	93.9	70.4	58.6	73.7	57.1	55.1	62.4	52.0	d.u.	64.1	85.7	70.2	d.u.	70.1	65.8	51.1	64.3
Cu	(ppm)	10.5	15.8	23.5	16.2	13.4	16.6	11.3	16.4	11.5	13.5	10.1	d.u.	10.9	14.6	9.7	d.u.	46.1	39.0	20.0	24.5
Pb	(ppm)	<dl	5.2	<dl	5.6	9.0	3.7	2.1	1.9	<dl	<dl	<dl	d.u.	<dl	0.2	<dl	d.u.	27.9	19.8	9.9	8.2
Mn	(ppm)	407.5	466.3	349.7	370.9	530.9	389.0	328.7	397.0	293.8	299.9	273.4	d.u.	266.1	359.6	276.7	d.u.	839.6	639.7	343.6	390.9
Ni	(ppm)	29.9	30.8	30.2	31.1	32.7	32.6	30.0	32.5	31.7	32.1	29.5	d.u.	27.8	30.5	29.2	d.u.	36.6	33.1	32.2	32.5
Sr	(ppm)	78.4	78.5	76.3	74.0	83.2	80.4	78.3	76.8	78.5	77.9	77.2	d.u.	78.2	81.5	80.6	d.u.	102.1	108.5	94.1	76.7
V	(ppm)	<dl	<dl	<dl	<dl	<dl	4.8	<dl	13.7	<dl	<dl	<dl	d.u.	<dl	<dl	<dl	d.u.	38.8	20.3	20.2	6.5
Zn	(ppm)	93.7	127.8	112.1	117.8	132.6	128.4	97.7	125.9	109.5	115.7	96.4	d.u.	90.0	115.6	95.5	d.u.	320.1	267.9	184.6	202.3
Ce	(ppm)	78.3	83.1	72.5	76.0	79.8	84.9	93.6	77.8	77.2	73.9	71.6	d.u.	79.9	85.0	84.6	d.u.	74.8	73.5	76.1	69.9
Cs	(ppm)	4.7	4.3	4.3	5.5	5.8	5.6	6.6	7.0	5.5	6.2	5.9	d.u.	5.0	7.0	3.8	d.u.	6.5	6.1	4.9	6.7
Rb	(ppm)	41.3	43.3	42.5	44.4	47.0	52.5	39.3	53.9	44.0	47.2	42.1	d.u.	38.2	47.6	40.4	d.u.	63.2	58.6	58.3	48.1
Zr	(ppm)	956.3	1101.2	701.5	900.3	865.9	862.5	1517.1	684.9	831.1	734.8	711.0	d.u.	1066.6	946.2	996.9	d.u.	479.2	504.5	676.0	626.8
Remarks													sample lost				sample lost				

Table D.6: Data riverbed samples Gete

		Sample Code																			
		22	22	22	22	23	23	23	23	24	24	24	24	25	25	25	25	26	26	26	26
L.O.I.	(%)	1.8	3.0	3.9	5.6	5.2	5.6	5.9	5.5	5.1	4.6	d.u.	4.3	5.2	5.3	5.3	5.3	8.2	7.2	5.4	d.u.
Density	(g/cm³)	2.6706	2.6807	2.6814	2.6879	2.6958	2.6857	2.6802	2.6934	2.6731	2.6936	d.u.	2.7010	2.6857	2.6753	2.6795	2.7031	2.6823	2.6746	2.6795	d.u.
D [3, 2]	(µm)	17.3	15.0	13.8	12.2	10.2	9.2	12.0	11.2	13.9	11.9	d.u.	12.6	11.0	11.7	12.1	11.2	11.3	12.4	12.7	d.u.
SSA	(m²/g)	0.1298	0.1496	0.1620	0.1823	0.2192	0.2421	0.1866	0.1993	0.1611	0.1880	d.u.	0.1767	0.2026	0.1920	0.1846	0.1983	0.1986	0.1810	0.1760	d.u.
Al	(%)	2.68	3.01	2.98	3.23	3.54	4.28	4.24	3.46	3.43	3.48	d.u.	3.25	3.17	1.91	3.39	3.25	3.46	3.49	3.29	d.u.
Ca	(%)	<dl	<dl	<dl	<dl	1.26	0.76	1.22	1.19	1.30	1.13	d.u.	0.99	2.00	0.38	1.38	1.23	2.03	1.84	1.65	d.u.
Fe	(%)	1.24	1.36	1.50	1.81	2.74	3.09	2.57	2.47	2.08	1.96	d.u.	1.93	2.25	16.37	2.34	2.27	2.02	2.07	1.93	d.u.
K	(%)	1.07	1.24	1.41	1.65	2.05	2.97	2.10	1.86	1.81	1.80	d.u.	1.67	1.67	0.09	1.78	1.84	1.73	1.88	1.73	d.u.
Si	(%)	118.52	116.75	120.75	96.71	83.98	89.59	116.13	88.50	97.49	101.30	d.u.	104.92	92.35	19.98	91.15	91.32	91.15	91.27	97.24	d.u.
P	(ppm)	1086.7	1090.9	893.1	1063.8	3615.2	1311.5	2140.1	1803.8	1718.5	1369.1	d.u.	1325.2	2916.6	8458.8	1632.6	1600.9	1790.0	879.3	1184.9	d.u.
S	(ppm)	754.9	638.5	1240.3	2830.2	1421.2	937.6	1010.4	1662.1	1119.6	967.6	d.u.	864.9	2007.2	8318.5	1467.0	1466.8	2191.7	2761.3	2050.8	d.u.
Ti	(ppm)	4231.6	3786.4	4313.6	3884.5	4131.5	4320.4	4147.1	4042.1	4133.6	4319.3	d.u.	3879.2	4002.7	3023.8	4074.9	4005.5	3935.4	3837.3	4101.9	d.u.
Ba	(ppm)	425.5	444.7	446.7	452.0	576.2	515.6	509.2	466.7	469.2	471.7	d.u.	459.2	530.3	272.6	470.0	460.0	487.4	486.2	459.6	d.u.
Cr	(ppm)	72.1	58.6	44.4	58.2	226.7	136.3	262.6	148.8	130.2	131.0	d.u.	141.8	153.7	108.1	186.1	125.7	110.9	106.3	118.0	d.u.
Cu	(ppm)	8.1	12.0	13.8	20.5	28.8	22.3	28.8	25.3	28.8	30.3	d.u.	23.9	38.3	45.1	35.1	32.6	46.7	46.0	32.1	d.u.
Pb	(ppm)	<dl	<dl	<dl	<dl	26.9	8.5	22.0	6.6	8.4	11.3	d.u.	8.3	25.9	106.5	20.5	16.1	24.2	23.8	12.5	d.u.
Mn	(ppm)	210.1	216.6	223.7	230.3	552.3	536.3	487.4	449.2	335.8	325.2	d.u.	352.8	360.1	409.4	338.2	348.5	295.5	272.7	283.2	d.u.
Ni	(ppm)	26.2	27.5	28.5	29.6	33.0	36.8	33.3	33.2	32.8	30.2	d.u.	33.0	30.9	31.7	32.9	32.2	32.4	32.5	31.9	d.u.
Sr	(ppm)	64.7	68.5	68.5	66.7	100.0	86.0	89.7	82.8	87.7	87.7	d.u.	80.1	99.1	44.3	87.5	81.6	95.3	90.5	91.3	d.u.
V	(ppm)	<dl	<dl	<dl	<dl	<dl	28.7	<dl	<dl	<dl	<dl	d.u.	<dl	<dl	23.0	3.7	<dl	<dl	<dl	<dl	d.u.
Zn	(ppm)	81.4	97.4	109.7	145.2	280.8	153.5	199.0	160.6	175.2	179.8	d.u.	169.5	265.6	1363.8	197.0	190.1	220.0	245.6	187.0	d.u.
Ce	(ppm)	87.7	76.6	78.3	70.8	78.8	78.7	83.3	77.3	83.8	79.7	d.u.	77.7	82.2	80.9	80.2	74.3	75.1	72.9	81.8	d.u.
Cs	(ppm)	5.6	5.9	6.0	5.5	6.5	8.0	7.1	5.5	6.0	6.5	d.u.	5.8	5.2		5.4	6.2	5.3	7.1	4.5	d.u.
Rb	(ppm)	33.2	39.0	40.0	43.4	52.8	70.7	54.6	49.4	46.9	46.6	d.u.	44.5	43.7	29.5	48.3	46.7	44.4	46.9	44.6	d.u.
Zr	(ppm)	1637.3	1039.2	1044.9	807.4	870.0	561.8	928.9	831.7	1199.1	895.5	d.u.	939.9	1004.2	1987.4	867.7	788.3	781.4	649.3	931.2	d.u.
Remarks												sample lost									sample lost

Table D.6: Data riverbed samples Gete (continued)

		Sample Code														
		27	27	27	27	28	28	28	28	29	29	29	29	30	30	30
L.O.I.	(%)	4.3	4.7	1.6	3.0	2.7	4.7	3.0	d.u.	2.5	4.1	3.7	7.8	3.2	5.0	3.6
Density	(g/cm³)	2.7057	2.6945	2.6892	2.6899	2.6804	2.6787	2.6706	d.u.	2.6572	2.6965	2.6823	2.7126	2.6751	2.6878	2.6668
D [3, 2]	(µm)	13.2	12.0	21.6	11.5	13.8	13.8	13.1	d.u.	11.7	11.1	13.3	9.0	11.8	11.6	11.9
SSA	(m²/g)	0.1676	0.1860	0.1033	0.1943	0.1617	0.1622	0.1719	d.u.	0.1932	0.2005	0.1679	0.2459	0.1904	0.1929	0.1897
Al	(%)	3.39	3.38	2.65	3.25	3.37	3.11	3.13	d.u.	3.46	3.30	3.15	4.16	3.24	3.57	3.13
Ca	(%)	1.05	1.08	0.48	0.29	2.36	0.95	0.76	d.u.	0.98	0.88	0.68	0.90	1.36	1.46	1.03
Fe	(%)	1.90	2.03	1.31	1.73	1.98	1.48	1.57	d.u.	1.98	1.98	1.74	2.87	1.62	1.87	1.55
K	(%)	1.76	1.98	1.00	1.89	1.77	1.50	1.61	d.u.	1.91	1.78	1.58	2.81	1.87	2.01	1.76
Si	(%)	107.47	98.71	111.27	107.38	102.84	108.19	108.86	d.u.	103.62	104.87	105.00	91.68	101.27	106.89	109.33
P	(ppm)	1534.2	1248.3	638.4	846.7	647.3	684.3	646.6	d.u.	1333.7	941.1	985.7	1469.1	753.0	939.4	797.7
S	(ppm)	1318.2	1581.6	788.0	480.8	891.4	669.6	578.8	d.u.	967.0	1026.1	914.5	875.4	995.4	1027.7	815.6
Ti	(ppm)	4346.3	4552.0	4521.0	3829.6	3989.9	3972.4	4451.6	d.u.	4084.6	4283.8	4835.9	4076.9	3972.9	3885.7	3900.5
Ba	(ppm)	444.3	444.2	408.5	442.2	472.4	453.4	460.2	d.u.	446.3	443.2	425.1	466.6	468.3	474.7	463.4
Cr	(ppm)	74.8	62.7	80.4	42.6	62.5	62.9	58.0	d.u.	56.0	61.2	77.6	67.4	51.7	55.0	43.4
Cu	(ppm)	23.3	22.9	7.5	9.4	13.5	10.0	10.5	d.u.	15.9	15.3	16.0	23.4	21.3	29.7	20.3
Pb	(ppm)	5.2	5.8	<dl	<dl	0.3	<dl	<dl	d.u.	1.6	4.0	1.3	14.3	<dl	3.6	<dl
Mn	(ppm)	323.2	367.1	253.9	293.6	347.3	275.0	314.6	d.u.	363.1	368.1	333.9	571.5	248.7	305.9	270.5
Ni	(ppm)	32.9	32.1	26.9	29.7	41.1	37.5	33.1	d.u.	31.0	30.8	30.0	36.5	29.9	32.0	30.1
Sr	(ppm)	84.1	82.3	72.6	73.7	86.5	80.3	81.0	d.u.	81.0	80.5	78.7	77.7	85.2	85.0	81.9
V	(ppm)	<dl	<dl	<dl	<dl	<dl	<dl	<dl	d.u.	<dl	<dl	<dl	33.0	<dl	<dl	<dl
Zn	(ppm)	167.3	152.7	74.0	89.4	118.9	98.0	102.0	d.u.	123.2	120.0	112.2	152.9	124.1	163.8	126.4
Ce	(ppm)	86.1	89.1	92.1	65.9	74.7	76.3	80.4	d.u.	79.8	84.6	97.4	73.4	72.5	71.5	73.1
Cs	(ppm)	4.9	5.6	2.7	6.5	6.4	5.4	4.0	d.u.	5.5	5.3	5.1	8.7	6.2	5.7	5.1
Rb	(ppm)	43.1	45.9	32.9	44.8	47.8	40.4	42.5	d.u.	46.6	44.9	41.7	62.6	45.7	48.3	43.7
Zr	(ppm)	1065.7	1141.2	1780.4	452.0	693.1	799.0	853.2	d.u.	909.1	976.9	1421.6	450.7	596.0	551.2	677.3
Remarks									sample lost							

Table D.6: Data riverbed samples Gete (continued)

Addendum E: Dataset of source types collected in the Mangelbeek catchment

Key

Location Riverbed Samples

	VMM location code
31	453000
32	453200
33	453500
34	454050
35	454200
36	454600
37	E003602

Timing

1	20/04/2007	TIS
2	24/05/2007	TIS
3	21/06/2007	TIS
4	06/08/2007	TIS
5	29/08/2007	TIS
6	27/09/2007	TIS
7	06/11/2007	TIS
8	18/12/2007	TIS
9	28/01/2008	TIS
10	28/02/2008	TIS
11	10/04/2008	TIS
12	22/05/2008	TIS
21	from 21/5/07 - 4/6/07	Campaign 1
22	from 11/9/07 - 20/9/07	Campaign 2
23	from 15/2/08 - 28/2/08	Campaign 3
24	from 29/5/08 - 14/7/08	Campaign 4

<dl = values below detection limit

d.u. = data unavailable.

Table E.1: Data Mangelbeek – Lummen (outlet) samples

		Timing											
		1	2	3	4	5	6	7	8	9	10	11	12
L.O.I.	**(%)**	35.2	29.8	30.9	28.6	29.3	33.1	38.1	29.5	d.u.	d.u.	34.2	31.8
Density	**(g/cm³)**	3.7298	3.7855	3.4861	3.2859	3.4903	3.7256	3.4181	3.4012	d.u.	d.u.	3.4236	3.7105
D [3, 2]	**(µm)**	6.1	5.8	6.8	6.3	4.5	5.5	5.9	6.8	d.u.	d.u.	6.6	6.1
SSA	**(m²/g)**	0.2648	0.2727	0.2523	0.2909	0.3808	0.2925	0.2989	0.2596	d.u.	d.u.	0.2675	0.2656
Al	**(%)**	1.42	1.30	1.71	1.94	1.64	1.52	1.74	1.77	d.u.	d.u.	1.67	1.52
Ca	**(%)**	0.53	0.69	0.50	0.43	0.35	0.34	0.51	0.31	d.u.	d.u.	0.51	0.55
Fe	**(%)**	22.38	22.74	20.80	18.92	20.18	22.07	19.39	18.92	d.u.	d.u.	19.36	20.80
K	**(%)**	<dl	<dl	<dl	0.33	0.08	<dl	<dl	0.30	d.u.	d.u.	0.10	<dl
Si	**(%)**	3.90	3.42	9.08	14.57	10.03	6.51	13.69	15.50	d.u.	d.u.	10.56	7.12
P	**(ppm)**	7846.9	11856.7	7901.8	7311.1	6947.1	8130.6	8261.5	7545.2	d.u.	d.u.	7335.6	8077.0
S	**(ppm)**	2706.3	3871.2	3584.2	6406.4	5559.9	3228.4	5183.4	6711.0	d.u.	d.u.	5014.9	4357.1
Ti	**(ppm)**	1788.1	1506.8	2063.0	2460.9	2197.2	1855.5	2154.7	2291.6	d.u.	d.u.	2363.8	2050.5
Ba	**(ppm)**	218.3	227.5	242.0	275.3	237.8	224.7	250.4	258.7	d.u.	d.u.	253.2	239.0
Cr	**(ppm)**	30.0	16.2	40.1	61.9	54.5	35.5	39.9	48.5	d.u.	d.u.	47.2	36.9
Cu	**(ppm)**	50.1	57.2	72.5	104.4	80.5	61.5	74.9	83.8	d.u.	d.u.	89.6	77.4
Pb	**(ppm)**	126.5	133.9	125.1	135.3	153.8	134.0	120.8	124.0	d.u.	d.u.	132.1	128.3
Mn	**(ppm)**	478.3	622.7	469.1	382.9	447.4	582.4	493.1	438.1	d.u.	d.u.	452.6	439.2
Ni	**(ppm)**	28.0	23.4	23.8	34.6	32.5	31.0	38.9	35.1	d.u.	d.u.	30.6	31.6
Sr	**(ppm)**	46.4	41.4	46.9	46.6	44.5	40.5	43.4	41.2	d.u.	d.u.	45.9	46.7
V	**(ppm)**	<dl	<dl	10.4	26.6	25.5	<dl	19.4	27.9	d.u.	d.u.	16.5	<dl
Zn	**(ppm)**	1010.8	1014.4	1552.0	1598.7	1702.8	1410.9	1352.2	1301.5	d.u.	d.u.	1121.4	1150.4
Ce	**(ppm)**	50.4	43.8	49.9	54.6	52.1	46.9	51.7	54.7	d.u.	d.u.	57.8	52.6
Cs	**(ppm)**	<dl	<dl	<dl	<dl	<dl	<dl	<dl	<dl	d.u.	d.u.	<dl	<dl
Rb	**(ppm)**	30.8	31.2	32.4	37.7	39.7	32.1	29.3	36.7	d.u.	d.u.	35.1	30.1
Zr	**(ppm)**	185.2	101.5	80.8	139.2	121.5	91.3	102.9	148.5	d.u.	d.u.	153.3	151.5
Remarks										not enough material present for analysis			

		Cultivated Land										Pastures									
Sample code		MC1	MC2	MC3	MC4	MC5	MC6	MC7	MC8	MC9	MC10	MP1	MP2	MP3	MP4	MP5	MP6	MP7	MP8	MP9	MP10
L.O.I.	(%)	14.4	16.1	14.7	30.7	31.4	31.5	31.6	24.1	24.0	25.9	17.3	36.9	32.2	28.7	22.5	d.u.	34.9	31.3	17.1	26.6
Density	(g/cm³)	2.8319	2.7573	2.7547	2.7753	2.7547	2.7694	2.8460	2.8479	3.0877	2.8590	2.7281	2.8039	3.2123	3.1951	2.6909	d.u.	2.7083	2.8998	2.7643	2.8362
D [3, 2]	(µm)	11.7	12.8	13.3	12.8	12.1	13.7	16.6	12.2	12.6	17.7	14.1	14.6	12.3	14.8	14.6	d.u.	13.5	20.9	12.0	8.6
SSA	(m²/g)	0.1813	0.1704	0.1635	0.1694	0.1802	0.1586	0.1268	0.1727	0.1544	0.1186	0.1563	0.1461	0.1516	0.1269	0.1527	d.u.	0.1645	0.0989	0.1810	0.2474
Al	(%)	2.77	2.76	2.90	2.62	2.60	2.68	2.47	2.44	2.24	2.68	2.66	2.16	3.18	2.15	2.53	2.03	2.65	2.61	3.15	2.50
Ca	(%)	0.19	<dl	<dl	<dl	0.19	<dl	0.32	0.61	0.10	0.21	<dl	0.06	1.54	<dl	<dl	0.58	0.48	0.48	1.54	1.28
Fe	(%)	6.14	5.83	5.39	7.93	6.39	8.07	8.60	9.48	15.57	9.66	3.98	6.73	5.18	16.71	1.82	2.62	2.60	9.91	5.20	10.38
K	(%)	2.20	2.18	1.82	1.11	1.80	0.52	1.12	1.15	1.14	1.18	1.86	1.14	2.24	1.51	1.10	0.43	1.72	1.30	2.14	2.16
Si	(%)	73.77	72.24	86.42	63.91	67.49	61.51	54.59	55.90	31.91	56.57	71.09	53.15	75.14	29.05	86.40	39.12	64.96	51.00	71.84	42.69
P	(ppm)	4247.5	4009.5	4565.9	7422.9	6792.3	5117.2	7309.9	8036.6	4855.5	7281.4	4543.4	3466.4	2075.9	4061.0	1106.3	2666.1	4058.8	3799.4	2078.4	5431.4
S	(ppm)	954.0	1126.6	877.6	1463.4	1753.1	1427.7	1458.4	1128.3	995.3	1098.0	1538.2	3568.0	1042.6	1240.7	1649.5	6216.9	2258.0	1483.7	1092.4	1701.7
Ti	(ppm)	3707.8	3723.1	3769.4	4079.0	3695.7	3966.5	3817.8	3468.5	2938.6	3591.6	3862.7	3013.5	3760.8	2600.8	3704.9	3045.6	4000.6	3627.4	3782.0	3227.4
Ba	(ppm)	364.0	374.2	367.1	303.2	325.6	330.3	317.8	306.3	256.2	308.3	394.9	308.5	407.7	271.3	353.6	297.9	399.3	307.6	405.8	328.4
Cr	(ppm)	80.0	80.5	76.4	75.1	52.6	85.1	72.6	85.2	66.1	84.7	80.7	56.9	90.2	93.3	45.6	31.9	74.7	100.4	91.1	108.2
Cu	(ppm)	25.2	26.0	29.1	51.4	42.1	47.0	61.2	60.4	44.8	49.5	15.6	17.9	34.4	24.2	13.4	31.0	26.6	30.8	34.4	60.9
Pb	(ppm)	43.8	37.6	43.0	87.7	66.4	100.2	83.7	83.5	70.5	81.3	14.0	63.6	33.2	87.8	32.4	81.1	85.2	81.8	33.3	98.2
Mn	(ppm)	552.9	365.4	459.7	437.6	308.1	590.8	431.6	667.8	811.3	690.0	499.3	272.2	377.9	406.4	194.2	211.6	574.1	873.5	376.4	527.4
Ni	(ppm)	27.8	26.7	27.9	27.2	28.2	29.8	28.6	27.5	23.4	25.4	25.7	26.6	32.5	25.9	27.2	32.0	32.5	27.5	32.8	32.0
Sr	(ppm)	52.5	51.9	54.5	31.4	40.0	38.0	46.0	46.8	38.4	43.6	53.1	37.0	68.9	34.4	41.1	34.7	46.0	47.1	69.2	55.9
V	(ppm)	152.7	105.1	127.8	149.0	61.7	126.2	146.6	166.9	142.4	176.2	67.8	124.0	66.6	226.9			67.1	263.3	70.1	169.4
Zn	(ppm)	172.7	135.1	136.1	105.4	148.9	170.0	192.2	206.3	230.5	187.7	157.2	173.7	266.6	196.7	78.8	216.3	198.8	426.5	269.5	401.0
Ce	(ppm)	73.6	65.1	64.5	72.4	68.4	74.9	75.3	69.5	59.8	70.7	72.1	56.7	76.6	56.7	68.3	54.5	70.7	69.6	76.1	75.2
Cs	(ppm)	1.7	3.6	2.6	2.6	3.2	2.5	2.0	1.4	<dl	0.8	4.2	2.6	4.0	<dl	4.7	6.3	5.9	1.6	4.7	0.8
Rb	(ppm)	51.9	40.9	42.5	47.5	36.0	31.3	33.4	38.6	34.7	37.2	37.9	29.1	50.3	51.3	31.1	20.7	41.5	38.1	50.9	52.1
Zr	(ppm)	1013.5	895.9	829.2	750.6	785.6	807.1	1041.7	767.5	596.3	829.8	1445.6	639.2	1077.1	387.1	1194.7	605.8	933.3	1038.6	1056.6	861.9

Table E.2: Data Cultivated Land and Pastures Mangelbeek samples

		Channel Banks										Authigenic Sediment									
Sample code		MCB1	MCB2	MCB3	MCB4	MCB5	MCB6	MCB7	MCB8	MCB9	MCB10	MA1_1	MA2_1	MA3_1	MA4_1	MA5_1	MA6_1	MA1_2	MA2_2	MA6_3	MA6_4
L.O.I.	(%)	33.3	30.3	16.3	27.2	25.8	23.0	14.6	12.7	36.7	28.3	d.u.	d.u.	d.u.	28.1	d.u.	31.3	17.0	35.3	d.u.	31.1
Density	(g/cm³)	3.3990	2.6850	2.7961	3.0694	3.0774	2.9995	2.7736	2.7736	2.9994	2.9791	d.u.	d.u.	d.u.	4.0220	d.u.	4.4214	3.0613	4.3939	3.5769	4.3115
D [3, 2]	(µm)	12.7	11.9	13.0	12.2	12.9	11.4	19.0	15.6	10.0	14.1	d.u.	d.u.	d.u.	4.1	d.u.	4.5	7.7	d.u.	5.4	3.8
SSA	(m²/g)	0.1395	0.1871	0.1655	0.1605	0.1511	0.1748	0.1141	0.1383	0.2001	0.1425	d.u.	d.u.	d.u.	0.3681	d.u.	0.3035	0.2552	d.u.	0.3095	0.3660
Al	(%)	1.51	2.91	2.41	2.09	2.02	2.25	2.58	2.64	2.38	1.98	d.u.	d.u.	d.u.	0.71	d.u.	1.06	1.62	0.75	2.93	0.72
Ca	(%)	0.29	<dl	0.26	0.95	3.88	0.97	0.59	0.44	0.29	0.74	d.u.	d.u.	d.u.	0.14	d.u.	<dl	0.42	0.55	1.83	0.25
Fe	(%)	19.27	15.28	7.39	13.58	13.41	12.16	5.26	5.18	13.37	11.83	d.u.	d.u.	d.u.	26.75	d.u.	25.82	14.02	25.68	12.39	26.73
K	(%)	<dl	1.65	0.88	0.32	0.22	0.68	1.14	1.07	0.25	0.30	d.u.	d.u.	d.u.	<dl	d.u.	<dl	0.42	<dl	3.20	<dl
Si	(%)	13.10	27.48	59.72	30.33	28.21	40.96	71.93	70.32	26.97	34.27	d.u.	d.u.	d.u.	<dl	d.u.	<dl	33.38	<dl	31.68	<dl
P	(ppm)	5128.6	3511.7	3689.4	4528.2	5137.9	3505.2	2990.0	3126.0	12911.7	6412.1	d.u.	d.u.	d.u.	3453.5	d.u.	10054.1	3897.5	3903.8	1549.4	3465.2
S	(ppm)	2338.9	4144.4	1913.2	2050.1	1660.8	1567.7	1930.8	1845.7	7903.3	3002.4	d.u.	d.u.	d.u.	2527.7	d.u.	4287.6	1541.8	2982.6	5189.8	4493.1
Ti	(ppm)	2205.5	3319.3	3596.5	3074.6	2535.8	3069.1	4235.0	4586.4	3051.5	3760.2	d.u.	d.u.	d.u.	842.7	d.u.	1272.3	3810.2	978.3	3117.6	864.2
Ba	(ppm)	224.8	320.2	363.5	305.9	283.7	310.0	387.7	386.5	346.3	323.8	d.u.	d.u.	d.u.	156.2	d.u.	138.1	287.3	179.1	281.0	173.5
Cr	(ppm)	38.4	70.1	85.5	83.6	96.1	56.8	147.1	155.0	61.6	73.2	d.u.	d.u.	d.u.	1.3	d.u.	12.6	71.4	0.3	85.1	<dl
Cu	(ppm)	48.3	46.7	33.4	40.2	41.8	34.3	38.1	35.7	72.1	56.8	d.u.	d.u.	d.u.	26.7	d.u.	70.8	32.8	40.0	29.1	24.8
Pb	(ppm)	90.9	74.7	23.8	59.7	71.3	46.0	29.5	22.7	156.2	74.0	d.u.	d.u.	d.u.	149.0	d.u.	148.2	46.4	132.2	20.8	154.3
Mn	(ppm)	305.6	315.8	394.1	527.4	474.9	493.2	316.6	310.1	229.3	520.6	d.u.	d.u.	d.u.	192.6	d.u.	162.5	590.0	272.9	655.1	181.8
Ni	(ppm)	23.4	28.4	32.4	32.8	30.0	27.2	32.0	32.5	39.1	34.0	d.u.	d.u.	d.u.	23.5	d.u.	23.5	28.9	23.5	37.5	23.5
Sr	(ppm)	42.4	41.3	58.3	55.4	84.2	58.1	65.3	63.0	50.3	59.6	d.u.	d.u.	d.u.	19.2	d.u.	3.4	58.4	26.1	80.0	21.0
V	(ppm)	1.9	77.7	46.4	54.8	62.3	29.5	47.3	43.5	53.6	30.3	d.u.	d.u.	d.u.	<dl	d.u.	<dl	7.0	<dl	153.2	<dl
Zn	(ppm)	465.8	180.5	339.7	689.1	922.3	465.4	387.2	326.2	737.2	533.8	d.u.	d.u.	d.u.	165.9	d.u.	268.2	348.7	244.7	257.2	195.5
Ce	(ppm)	55.1	79.9	87.2	74.9	66.2	62.3	108.4	117.3	73.4	93.7	d.u.	d.u.	d.u.	33.2	d.u.	100.1	100.8	34.7	79.6	33.6
Cs	(ppm)	<dl	<dl	1.8	<dl	<dl	<dl	1.7	3.2	0.0	<dl	d.u.	d.u.	d.u.	<dl	d.u.	<dl	<dl	<dl	0.8	<dl
Rb	(ppm)	31.0	54.8	33.8	31.4	30.8	33.5	36.1	35.7	26.9	26.8	d.u.	d.u.	d.u.	19.1	d.u.	16.3	32.0	18.3	71.7	20.0
Zr	(ppm)	478.8	785.4	1487.6	1142.8	624.1	491.8	2848.0	3519.8	681.8	2664.3	d.u.	d.u.	d.u.	15.9	d.u.	82.8	3495.9	34.9	498.8	18.0
Remarks												not enough material present for analysis				not enough material present for analysis		riverbed sediment	not enough material present for grain size analysis		

Table E.3: Data Channel Banks and Authigenic sediment Mangelbeek samples

location code		31	31	31	31	32	32	32	32	33	33	33	33	34	34	34	34
timing		21	22	23	24	21	22	23	24	21	22	23	24	21	22	23	24
L.O.I.	(%)	22.6	21.0	24.8	17.0	23.8	20.1	26.2	21.9	21.2	d.u.	21.2	21.1	16.9	18.2	19.8	21.5
Density	(g/cm³)	3.1628	3.1602	3.2103	2.9592	3.5152	3.2657	3.6139	3.4642	3.3072	d.u.	3.5500	3.2671	3.1298	3.3032	d.u.	3.0899
D [3, 2]	(µm)	12.5	8.7	10.9	8.5	6.4	8.5	4.5	6.5	6.6	d.u.	5.8	7.4	10.4	11.2	10.1	9.0
SSA	(m²/g)	0.1517	0.2192	0.1718	0.2397	0.2685	0.2152	0.3698	0.2662	0.2744	d.u.	0.2893	0.2482	0.1836	0.1623	d.u.	0.2148
Al	(%)	1.82	3.42	1.66	2.40	1.63	2.39	1.57	1.87	1.65	d.u.	1.28	1.67	1.83	1.91	2.42	2.34
Ca	(%)	0.48	1.33	0.72	0.24	<dl	<dl	<dl	<dl	<dl	d.u.	<dl	0.04	0.29	0.39	0.46	0.31
Fe	(%)	16.10	2.18	15.69	10.90	22.33	18.36	22.30	20.91	19.36	d.u.	22.56	17.59	17.33	16.61	14.30	13.68
K	(%)	0.07	1.80	0.00	1.28	<dl	1.50	<dl	0.17	0.17	d.u.	<dl	0.65	<dl	0.20	0.63	0.85
Si	(%)	21.06	97.58	17.33	43.61	10.52	17.79	7.98	13.13	16.73	d.u.	8.52	22.76	20.48	21.66	29.74	33.83
P	(ppm)	7594.4	1588.5	6617.6	4285.1	7362.0	5881.7	5976.9	6878.2	4970.0	d.u.	5815.3	4957.8	9336.7	10010.3	7912.3	7461.9
S	(ppm)	2982.7	2238.4	6629.1	2278.4	1633.2	1692.2	2947.3	1767.4	1612.5	d.u.	1425.0	2261.1	1985.0	2490.6	2454.9	2691.5
Ti	(ppm)	3152.6	4080.8	3035.3	3917.1	2034.2	2615.7	1892.4	2222.1	2341.2	d.u.	1864.2	2886.5	2878.7	3792.7	3708.8	3587.6
Ba	(ppm)	280.2	495.5	262.9	319.7	278.6	278.7	435.5	274.8	257.9	d.u.	231.3	281.1	260.5	270.8	287.3	290.0
Cr	(ppm)	82.3	130.0	107.3	99.1	52.3	72.4	41.7	96.2	73.9	d.u.	42.9	113.3	71.2	88.0	83.0	147.7
Cu	(ppm)	50.9	34.1	44.4	37.5	51.3	39.9	49.3	44.5	23.3	d.u.	18.1	29.1	42.8	46.1	32.9	63.0
Pb	(ppm)	80.0	14.2	84.6	59.7	118.7	79.1	139.4	106.5	86.2	d.u.	138.5	94.9	82.3	126.7	79.4	398.0
Mn	(ppm)	343.2	321.8	606.9	549.9	196.3	225.2	191.8	211.7	323.6	d.u.	264.2	360.4	278.9	332.2	292.4	295.3
Ni	(ppm)	34.7	31.1	37.3	33.2	26.9	29.1	35.6	30.3	30.1	d.u.	23.5	32.6	37.8	37.0	39.5	51.1
Sr	(ppm)	51.9	88.6	48.2	53.6	23.3	33.6	27.5	29.5	27.4	d.u.	22.9	36.7	51.3	65.2	69.5	58.8
V	(ppm)	2.1	<dl	2.8	58.9	18.9	112.3	29.4	50.4	61.0	d.u.	30.7	99.2	14.7	40.0	48.5	50.9
Zn	(ppm)	1195.8	188.7	1219.9	593.4	347.1	316.0	365.5	450.0	451.5	d.u.	453.0	503.1	1455.5	1906.9	1255.9	4248.8
Ce	(ppm)	72.0	81.0	74.8	83.8	51.7	64.0	49.5	58.6	62.2	d.u.	61.6	78.5	72.9	104.2	101.6	86.3
Cs	(ppm)	<dl	6.5	<dl	<dl	<dl	<dl	<dl	<dl	<dl	d.u.	<dl	<dl	<dl	<dl	<dl	<dl
Rb	(ppm)	30.0	47.0	25.4	40.8	42.7	62.2	41.2	42.6	29.7	d.u.	31.2	39.8	22.8	32.3	38.1	39.2
Zr	(ppm)	1528.3	888.8	1755.9	2136.2	483.8	570.3	292.8	806.4	724.7	d.u.	611.0	1713.0	1880.5	4066.2	3125.2	2204.8
Remarks											not enough material present for analysis						

Table E.4: Data Riverbed Mangelbeek samples

location code		35	35	35	35	36	36	36	36	37	37	37	37
timing		21	22	23	24	21	22	23	24	21	22	23	24
L.O.I.	**(%)**	21.3	20.2	d.u.	d.u.	10.0	19.7	23.9	21.1	22.3	24.2	26.7	27.9
Density	**(g/cm³)**	3.1700	3.1308	d.u.	d.u.	2.9237	3.2683	3.4936	3.3622	3.4930	3.5634	3.5115	3.3390
D [3, 2]	**(µm)**	8.3	10.3	d.u.	d.u.	12.7	8.1	5.7	8.0	8.0	7.3	5.5	6.2
SSA	**(m²/g)**	0.2286	0.1864	d.u.	d.u.	0.1618	0.2255	0.3009	0.2237	0.2147	0.2309	0.3104	0.2905
Al	**(%)**	2.14	2.22	d.u.	2.02	2.10	1.68	1.37	1.78	1.70	1.53	1.60	2.24
Ca	**(%)**	<dl	0.21	d.u.	0.19	0.11	0.49	0.29	0.19	0.01	0.28	0.08	0.52
Fe	**(%)**	16.07	14.79	d.u.	12.21	9.97	16.34	20.99	19.51	21.69	21.38	21.47	18.55
K	**(%)**	0.37	0.63	d.u.	0.43	1.06	0.24	<dl	0.75	0.10	<dl	<dl	0.66
Si	**(%)**	24.18	26.57	d.u.	33.02	51.05	17.20	12.04	16.53	12.91	12.27	9.26	16.70
P	**(ppm)**	11939.5	10317.5	d.u.	9377.0	2538.2	2802.0	3246.0	2731.4	4258.1	4760.9	4916.4	4296.9
S	**(ppm)**	2506.7	2689.9	d.u.	2437.9	1720.9	4187.1	7856.8	4961.3	2765.2	2258.3	2940.1	5754.0
Ti	**(ppm)**	3731.1	3997.1	d.u.	5357.7	5413.2	3697.4	2243.5	2467.8	2066.5	2015.6	2015.8	2434.2
Ba	**(ppm)**	271.4	292.8	d.u.	293.0	577.9	274.1	220.8	226.1	213.3	222.2	225.9	251.8
Cr	**(ppm)**	99.7	95.0	d.u.	177.5	142.4	75.2	43.5	67.8	59.9	95.7	42.9	75.6
Cu	**(ppm)**	46.0	42.2	d.u.	32.8	61.5	51.3	48.1	49.7	46.6	43.9	51.5	59.4
Pb	**(ppm)**	75.2	89.9	d.u.	59.7	48.0	79.2	113.7	96.4	120.3	115.2	117.6	87.8
Mn	**(ppm)**	317.3	348.3	d.u.	315.4	378.8	518.1	335.2	325.8	246.7	277.5	247.5	302.5
Ni	**(ppm)**	58.1	67.4	d.u.	60.2	32.2	29.7	34.5	40.8	26.9	23.5	24.4	29.4
Sr	**(ppm)**	42.6	54.3	d.u.	51.1	66.5	52.3	33.8	35.0	32.1	39.2	33.3	53.2
V	**(ppm)**	21.9	37.4	d.u.	33.0	24.3	31.4	18.1	50.6	14.2	11.8	15.7	37.0
Zn	**(ppm)**	758.4	990.9	d.u.	758.7	293.6	472.3	595.9	537.4	521.2	609.2	516.7	639.3
Ce	**(ppm)**	102.9	129.1	d.u.	133.2	111.4	110.8	74.4	83.4	53.8	52.1	50.6	55.3
Cs	**(ppm)**	<dl	<dl	d.u.	<dl	<dl	<dl	<dl	<dl	<dl	<dl	<dl	<dl
Rb	**(ppm)**	34.0	36.5	d.u.	30.4	37.6	32.6	33.9	42.8	43.7	38.2	42.4	44.0
Zr	**(ppm)**	3398.9	4404.3	d.u.	7294.0	4432.6	3283.8	1074.7	1329.1	612.6	447.1	372.3	285.6
Remarks				lost sample	not enough material present for grain size and density analysis								

Table E.4: Data Riverbed samples Mangelbeek (continued)

Addendum F: Modelling results of composite Fingerprints A, B, C, D and E

Table F.1: Modeled contributions of the eight tributaries to the suspended sediment flux sampled at the Aarschot outlet station, using composite fingerprint A and the mean property concentrations in the objective function; * = failing the RME test.

Nr outlet sample	code model	contr. Motte (%)	contr. Hulpe (%)	contr. Velpe (%)	contr. Gete (%)	contr. Zwarte-beek (%)	contr. Mangel-beek (%)	contr. Herk (%)	contr. Demer (%)	RME (%)
13	A zero	0	18	61	0	15	0	0	6	10
13	A PP	0	18	61	0	14	0	0	6	10
13	A GS	31	16	0	0	0	0	32	20	163*
13	A GSPP	35	17	0	0	0	0	28	20	155*
13	A OM	0	57	7	0	2	34	0	0	39*
13	A OMPP	0	58	7	0	0	35	0	0	39*
14	A zero	0	18	77	0	5	0	0	0	10
14	A PP	0	18	77	0	5	0	0	0	10
14	A GS	0	9	75	0	16	0	0	0	17*
14	A GSPP	0	9	76	0	15	0	0	0	17*
14	A OM	0	23	49	0	12	0	16	0	21*
14	A OMPP	0	22	43	0	15	0	21	0	21*
15	A zero	0	6	88	0	6	0	0	0	20*
15	A PP	0	8	86	0	7	0	0	0	19*
15	A GS	0	3	83	0	14	0	0	0	63*
15	A GSPP	0	5	81	0	14	0	0	0	61*
15	A OM	0	56	34	0	10	0	0	0	54*
15	A OMPP	0	58	35	0	8	0	0	0	55*
16	A zero	0	0	58	42	0	0	0	0	9
16	A PP	0	0	57	43	0	0	0	0	9
16	A GS	0	0	68	32	0	0	0	0	11
16	A GSPP	0	0	64	36	0	0	0	0	11
16	A OM	0	0	60	40	0	0	0	0	26*
16	A OMPP	0	0	53	45	2	0	0	0	27*
17	A zero	0	1	91	0	8	0	0	0	7
17	A PP	0	1	91	0	8	0	0	0	7
17	A GS	0	0	85	0	15	0	0	0	8
17	A GSPP	0	0	87	0	13	0	0	0	8
17	A OM	0	0	60	0	19	0	20	0	22*
17	A OMPP	0	0	57	0	20	0	23	0	23*
18	A zero	0	0	91	2	7	0	0	0	5
18	A PP	0	0	90	2	7	0	0	0	5
18	A GS	0	0	88	0	12	0	0	0	7
18	A GSPP	0	0	89	0	11	0	0	0	8
18	A OM	0	3	79	0	17	0	0	0	21*
18	A OMPP	0	4	79	0	17	0	0	0	21*
19	A zero	0	0	91	9	0	0	0	0	13
19	A PP	0	0	88	12	1	0	0	0	13
19	A GS	0	0	98	0	2	0	0	0	23*
19	A GSPP	0	0	98	0	2	0	0	0	23*
19	A OM	0	0	37	53	0	0	9	0	19*
19	A OMPP	0	0	22	63	5	0	10	0	17*

Nr outlet sample	code model	contr. Motte (%)	contr. Hulpe (%)	contr. Velpe (%)	contr. Gete (%)	contr. Zwarte-beek (%)	contr. Mangel-beek (%)	contr. Herk (%)	contr. Demer (%)	RME (%)
20	A zero	0	0	80	16	3	0	0	0	6
20	A PP	0	0	79	17	3	0	0	0	6
20	A GS	0	0	95	1	4	0	0	0	11
20	A GSPP	0	0	97	0	3	0	0	0	11
20	A OM	0	0	58	30	7	0	5	0	30*
20	A OMPP	0	0	49	35	10	0	6	0	31*
21	A zero	0	0	100	0	0	0	0	0	19*
21	A PP	0	0	95	4	1	0	0	0	19*
21	A GS	0	0	100	0	0	0	0	0	26*
21	A GSPP	0	0	97	3	0	0	0	0	26*
21	A OM	0	0	82	0	18	0	0	0	88*
21	A OMPP	0	0	83	0	17	0	0	0	88*
22	A zero	0	0	100	0	0	0	0	0	19*
22	A PP	0	0	99	0	1	0	0	0	19*
22	A GS	0	0	100	0	0	0	0	0	23*
22	A GSPP	0	0	100	0	0	0	0	0	23*
22	A OM	0	0	84	0	16	0	0	0	86*
22	A OMPP	0	0	84	0	16	0	0	0	86*
27	A zero	0	8	0	77	0	5	0	10	20*
27	A PP	0	10	0	78	0	4	0	8	19*
27	A GS	0	11	0	77	0	12	0	0	60*
27	A GSPP	0	12	0	78	0	10	0	0	61*
27	A OM	0	33	0	34	0	21	0	12	38*
27	A OMPP	0	40	0	35	0	15	0	10	40*
28	A zero	0	2	31	30	8	0	28	1	4
28	A PP	0	2	67	22	6	0	0	3	4
28	A GS	0	0	80	8	10	0	0	1	13
28	A GSPP	0	0	79	7	10	0	3	1	13
28	A OM	0	9	70	2	0	17	0	2	17*
28	A OMPP	0	9	72	0	0	16	0	2	17*
29	A zero	0	0	98	0	2	0	0	0	8
29	A PP	0	0	97	0	3	0	0	0	8
29	A GS	0	0	95	0	5	0	0	0	13
29	A GSPP	0	0	95	0	5	0	0	0	13
29	A OM	0	0	84	12	4	0	0	0	8
29	A OMPP	0	0	73	20	7	0	0	0	8
30	A zero	0	1	94	0	5	0	0	0	10
30	A PP	0	1	94	0	5	0	0	0	10
30	A GS	0	3	89	0	8	0	0	0	22*
30	A GSPP	0	3	89	0	7	0	0	0	22*
30	A OM	0	0	29	31	8	0	32	0	12
30	A OMPP	0	0	14	42	13	0	31	0	12

Nr outlet sample	code model	contr. Motte (%)	contr. Hulpe (%)	contr. Velpe (%)	contr. Gete (%)	contr. Zwarte-beek (%)	contr. Mangel-beek (%)	contr. Herk (%)	contr. Deme r (%)	RME (%)
31	A zero	0	1	94	0	5	0	0	0	12
31	A PP	0	1	94	0	5	0	0	0	12
31	A GS	0	6	89	0	6	0	0	0	22*
31	A GSPP	0	6	88	0	6	0	0	0	22*
31	A OM	0	0	54	26	6	0	14	0	15*
31	A OMPP	0	0	37	38	11	0	14	0	14
32	A zero	0	0	100	0	0	0	0	0	25*
32	A PP	0	0	100	0	0	0	0	0	25*
32	A GS	0	6	92	0	2	0	0	0	39*
32	A GSPP	0	7	91	0	2	0	0	0	39*
32	A OM	0	0	0	100	0	0	0	0	29*
32	A OMPP	0	0	0	100	0	0	0	0	29*
33	A zero	0	2	92	0	6	0	0	0	15
33	A PP	0	2	92	0	6	0	0	0	15
33	A GS	0	7	86	0	6	0	0	0	21*
33	A GSPP	0	8	86	0	7	0	0	0	21*
33	A OM	0	0	69	12	7	0	11	0	17*
33	A OMPP	0	0	53	24	12	0	10	0	16*
34	A zero	0	5	87	0	8	0	0	0	12
34	A PP	0	5	87	0	8	0	0	0	12
34	A GS	0	5	83	0	12	0	0	0	17*
34	A GSPP	0	5	83	0	12	0	0	0	17*
34	A OM	0	0	71	0	12	0	16	0	13
34	A OMPP	0	0	58	11	16	0	15	0	13
35	A zero	0	5	85	0	10	0	0	0	14
35	A PP	0	6	85	0	10	0	0	0	15
35	A GS	0	0	79	0	21	0	0	0	20*
35	A GSPP	0	0	80	0	19	0	0	0	20*
35	A OM	0	0	75	0	15	0	11	0	21*
35	A OMPP	0	0	64	4	18	0	14	0	21*
36	A zero	0	8	83	0	9	0	0	0	12
36	A PP	0	8	83	0	9	0	0	0	12
36	A GS	1	11	79	0	9	0	0	0	17*
36	A GSPP	3	10	78	0	8	0	0	0	17*
36	A OM	0	0	57	0	17	0	26	0	15*
36	A OMPP	0	0	49	1	19	0	31	0	15
37	A zero	0	3	88	0	9	0	0	0	17*
37	A PP	0	3	88	0	9	0	0	0	17*
37	A GS	0	11	81	0	9	0	0	0	30*
37	A GSPP	2	11	79	0	8	0	0	0	30*
37	A OM	0	0	31	35	10	0	24	0	21*
37	A OMPP	0	0	7	55	18	0	20	0	20*
38	A zero	0	6	84	0	10	0	0	0	13
38	A PP	0	6	85	0	9	0	0	0	13
38	A GS	0	8	79	0	14	0	0	0	19*
38	A GSPP	0	10	77	0	13	0	0	0	19*
38	A OM	0	0	37	0	18	0	45	0	13
38	A OMPP	0	0	24	9	22	0	44	0	14

Table F.2: Modeled contributions of the eight tributaries to the suspended sediment flux sampled at the Aarschot outlet station, using composite fingerprint A and the Monte Carlo simulated property concentrations in the objective function; * = failing the RME test.

Nr outlet sample	code model	Motte			Hulpe			Velpe			Gete			Zwartebeek			Mangelbeek			Herk			Demer (upstream)			relative mean error	
		contribution	95% CI	range	contribution	95% CI	range	contribution	95% CI	range	contribution	95% CI	range	contribution	95% CI	range	contribution	95% CI	range	contribution	95% CI	range	contribution	95% CI	range	RME (%)	RME_val (%)	RME_avg (%)
13	Azero	0.8	0.2	0-32	18.6	0.4	7-37	36.6	1.5	0-68	5.6	0.7	0-57	14.8	0.3	0-25	0.2	0.1	0-21	18.0	1.4	0-68	5.4	0.2	0-16	10	9	10
13	A PP	1.4	0.3	0-33	18.4	0.4	8-36	36.6	1.5	0-67	4.9	0.7	0-57	14.0	0.3	0-24	0.2	0.1	0-20	18.9	1.4	0-68	5.6	0.2	0-16	10	9	10
13	A GS	31.4	0.5	0-55	15.5	0.3	0-31	1.1	0.3	0-43	4.8	0.7	0-45	0.0	0.0	0-0	0.0	0.0	0-0	25.7	0.8	0-48	21.4	0.4	9-40	24*	25*	25*
13	A GSPP	34.7	0.5	0-58	16.4	0.3	0-34	0.7	0.3	0-39	4.1	0.6	0-42	0.0	0.0	0-0	0.0	0.0	0-0	22.4	0.7	0-43	21.7	0.4	9-41	24*	26*	25*
13	A OM	1.9	0.4	0-32	56.3	1.1	17-95	5.9	0.2	0-11	0.3	0.1	0-7	10.2	0.9	0-57	25.1	1.3	0-77	0.1	0.0	0-8	0.1	0.1	0-16	55*	84*	66*
13	A OMPP	1.8	0.4	0-34	58.7	1.1	18-95	6.4	0.2	0-12	0.3	0.1	0-8	4.0	0.6	0-50	28.3	1.2	0-75	0.1	0.0	0-8	0.5	0.1	0-24	56*	87*	67*
14	Azero	2.0	0.3	0-32	17.2	0.3	5-33	62.0	1.5	0-83	4.0	0.8	0-73	4.7	0.2	0-15	0.0	0.0	0-4	9.7	1.3	0-82	0.4	0.1	0-6	11	12	11
14	A PP	2.3	0.3	0-32	17.3	0.3	6-33	61.3	1.5	0-83	3.5	0.7	0-72	4.6	0.2	0-14	0.0	0.0	0-4	10.5	1.3	0-82	0.4	0.1	0-7	11	13	11
14	A GS	0.0	0.0	0-0	9.6	0.2	0-26	67.8	1.1	0-81	5.1	1.0	0-74	16.6	0.2	3-28	0.0	0.0	0-0	0.9	0.4	0-71	0.0	0.0	0-0	18*	21*	19*
14	A GSPP	0.0	0.0	0-0	9.9	0.2	0-26	70.3	1.0	0-82	4.2	0.9	0-74	14.7	0.2	2-27	0.0	0.0	0-0	0.9	0.4	0-73	0.0	0.0	0-0	19*	22*	20*
14	A OM	3.6	0.5	0-46	22.6	0.4	1-50	33.2	1.5	0-70	5.9	0.7	0-53	11.9	0.5	0-35	0.0	0.0	0-0	22.1	1.3	0-66	0.6	0.1	0-11	14	15*	14
14	A OMPP	4.6	0.6	0-48	21.5	0.4	1-49	30.0	1.5	0-70	6.0	0.7	0-52	13.1	0.5	0-34	0.0	0.0	0-0	24.4	1.4	0-65	0.4	0.1	0-10	14	15*	14
15	Azero	2.3	0.4	0-41	7.1	0.3	0-22	67.1	2.1	0-96	15.4	1.9	0-89	5.8	0.3	0-20	0.0	0.0	0-0	2.3	0.8	0-91	0.0	0.0	0-0	20*	33*	25*
15	A PP	2.7	0.5	0-42	8.2	0.3	0-24	65.3	2.1	0-93	15.0	1.8	0-86	6.3	0.3	0-19	0.0	0.0	0-0	2.4	0.8	0-89	0.0	0.0	0-0	20*	31*	24*
15	A GS	0.1	0.1	0-21	5.1	0.3	0-21	68.5	1.8	0-91	12.0	1.6	0-82	13.7	0.4	0-31	0.0	0.0	0-0	0.6	0.3	0-72	0.0	0.0	0-0	21*	35*	26*
15	A GSPP	0.2	0.1	0-24	6.5	0.3	0-22	67.2	1.8	0-88	11.6	1.6	0-81	13.7	0.4	0-31	0.0	0.0	0-0	0.8	0.4	0-79	0.0	0.0	0-0	20*	34*	25*
15	A OM	4.1	0.8	0-76	50.6	0.9	14-80	28.2	0.8	0-44	4.0	0.6	0-30	12.9	0.8	0-53	0.1	0.1	0-38	0.3	0.2	0-31	0.0	0.0	0-0	28*	12	22*
15	A OMPP	3.6	0.7	0-63	52.8	0.7	21-79	29.3	0.8	0-44	3.6	0.5	0-30	10.3	0.7	0-45	0.2	0.1	0-38	0.3	0.2	0-32	0.0	0.0	0-0	28*	13	22*
16	Azero	0.2	0.1	0-12	0.4	0.1	0-6	52.0	1.9	0-100	45.4	1.8	0-97	0.6	0.1	0-6	0.0	0.0	0-0	1.5	0.5	0-100	0.0	0.0	0-0	9	21*	13
16	A PP	0.2	0.1	0-12	0.4	0.1	0-6	50.4	1.9	0-100	46.7	1.7	0-97	0.7	0.1	0-6	0.0	0.0	0-1	1.5	0.5	0-100	0.0	0.0	0-0	9	21*	13
16	A GS	0.0	0.0	0-0	0.0	0.0	0-0	61.2	2.0	0-100	37.6	1.9	0-100	1.1	0.1	0-9	0.0	0.0	0-0	0.1	0.1	0-68	0.0	0.0	0-0	27*	36*	30*
16	A GSPP	0.0	0.0	0-0	0.0	0.0	0-1	59.9	1.9	0-100	39.1	1.9	0-100	0.9	0.1	0-8	0.0	0.0	0-0	0.1	0.1	0-52	0.0	0.0	0-0	26*	36*	30*
16	A OM	0.8	0.2	0-21	0.9	0.2	0-19	45.7	1.6	0-97	44.9	1.2	0-93	1.6	0.2	0-15	0.0	0.0	0-0	6.2	0.9	0-95	0.0	0.0	0-1	11	19*	14
16	A OMPP	1.0	0.2	0-22	0.9	0.2	0-22	41.8	1.6	0-95	47.4	1.2	0-93	2.5	0.2	0-16	0.0	0.0	0-0	6.5	0.9	0-100	0.0	0.0	0-2	11	19*	14
17	Azero	2.7	0.4	0-29	1.8	0.1	0-12	65.3	1.6	0-94	14.7	1.3	0-83	7.4	0.2	0-13	0.0	0.0	0-9	8.0	0.9	0-91	0.1	0.0	0-3	8	23*	13
17	A PP	3.4	0.4	0-28	1.6	0.1	0-12	65.1	1.6	0-94	13.9	1.2	0-83	7.0	0.2	0-13	0.0	0.0	0-9	8.9	0.9	0-91	0.1	0.0	0-3	8	23*	13
17	A GS	0.0	0.0	0-0	0.0	0.0	0-4	76.3	1.1	0-90	8.2	1.0	0-79	15.4	0.1	10-25	0.0	0.0	0-0	0.0	0.0	0-22	0.0	0.0	0-0	20*	35*	25*
17	A GSPP	0.0	0.0	0-0	0.0	0.0	0-4	79.0	1.1	0-91	7.1	1.0	0-81	13.8	0.1	9-23	0.0	0.0	0-0	0.0	0.0	0-18	0.0	0.0	0-0	20*	36*	26*
17	A OM	5.8	0.7	0-47	1.9	0.2	0-25	44.7	1.5	0-86	8.8	0.7	0-60	16.3	0.5	0-31	0.0	0.0	0-0	22.0	1.2	0-81	0.7	0.1	0-13	8	22*	13
17	A OMPP	6.6	0.7	0-49	1.6	0.2	0-26	41.5	1.4	0-85	9.4	0.7	0-58	16.7	0.5	0-31	0.0	0.0	0-0	23.7	1.2	0-80	0.5	0.1	0-13	8	22*	13
18	Azero	2.0	0.3	0-27	1.0	0.1	0-10	63.6	1.5	0-95	20.0	1.3	0-85	7.1	0.1	0-12	0.1	0.0	0-10	6.2	0.7	0-92	0.0	0.0	0-3	5	22*	11
18	A PP	2.4	0.3	0-27	0.9	0.1	0-10	63.1	1.5	0-95	19.8	1.2	0-85	6.9	0.2	0-12	0.1	0.0	0-10	6.8	0.8	0-92	0.0	0.0	0-3	5	22*	11
18	A GS	0.0	0.0	0-0	0.0	0.0	0-3	69.7	1.5	0-93	16.7	1.4	0-83	13.5	0.2	7-23	0.0	0.0	0-0	0.1	0.1	0-31	0.0	0.0	0-0	19*	31*	24*
18	A GSPP	0.0	0.0	0-0	0.0	0.0	0-3	71.9	1.4	0-94	15.8	1.3	0-85	12.2	0.1	6-21	0.0	0.0	0-0	0.1	0.1	0-25	0.0	0.0	0-0	20*	33*	24*
18	A OM	3.2	0.5	0-42	5.4	0.3	0-28	55.1	1.1	0-84	10.8	0.8	0-54	17.0	0.4	0-30	0.5	0.1	0-20	7.8	0.7	0-75	0.3	0.1	0-8	5	20*	10
18	A OMPP	3.6	0.5	0-43	5.3	0.3	0-26	54.7	1.1	0-84	10.4	0.7	0-53	16.6	0.4	0-29	0.6	0.1	0-20	8.6	0.7	0-75	0.3	0.1	0-8	5	20*	10
19	Azero	0.5	0.1	0-16	0.4	0.1	0-9	67.0	2.0	0-100	28.3	1.8	0-96	1.4	0.1	0-8	0.0	0.0	0-2	2.5	0.6	0-100	0.0	0.0	0-0	13	46*	25*
19	A PP	0.5	0.1	0-15	0.4	0.1	0-9	67.1	2.0	0-100	28.2	1.7	0-96	1.3	0.1	0-7	0.0	0.0	0-2	2.5	0.6	0-99	0.0	0.0	0-0	13	46*	25*
19	A GS	0.0	0.0	0-0	0.1	0.0	0-7	78.4	1.6	0-100	17.3	1.4	0-92	3.9	0.2	0-14	0.0	0.0	0-0	0.3	0.2	0-61	0.0	0.0	0-0	13	43*	24*
19	A GSPP	0.0	0.0	0-0	0.1	0.0	0-7	79.5	1.5	0-100	16.7	1.4	0-91	3.4	0.1	0-13	0.0	0.0	0-0	0.3	0.2	0-56	0.0	0.0	0-0	13	43*	24*
19	A OM	1.0	0.2	0-19	0.1	0.0	0-9	24.8	1.4	0-74	49.0	1.1	0-96	0.8	0.1	0-12	0.0	0.0	0-0	24.0	1.5	0-100	0.3	0.1	0-10	18*	31*	22*
19	A OMPP	1.6	0.2	0-21	0.1	0.0	0-11	22.1	1.4	0-79	52.5	1.1	0-96	2.2	0.2	0-14	0.0	0.0	0-0	21.2	1.4	0-100	0.3	0.1	0-10	18*	29*	22*
20	Azero	0.8	0.2	0-19	0.4	0.1	0-9	64.6	1.6	0-100	26.6	1.4	0-91	3.4	0.1	0-9	0.0	0.0	0-5	4.2	0.7	0-96	0.0	0.0	0-2	6	28*	14
20	A PP	0.9	0.2	0-19	0.4	0.1	0-9	64.6	1.6	0-100	26.2	1.3	0-90	3.4	0.1	0-8	0.0	0.0	0-6	4.4	0.7	0-96	0.0	0.0	0-3	6	28*	14
20	A GS	0.0	0.0	0-0	0.0	0.0	0-0	71.1	1.8	0-100	22.6	1.7	0-91	6.2	0.2	0-16	0.0	0.0	0-1	0.0	0.1	0-26	0.0	0.0	0-0	29*	52*	37*
20	A GSPP	0.0	0.0	0-0	0.0	0.0	0-0	73.2	1.7	0-100	21.9	1.6	0-92	4.9	0.2	0-14	0.0	0.0	0-2	0.0	0.0	0-16	0.0	0.0	0-0	29*	52*	38*
20	A OM	2.8	0.4	0-29	0.3	0.1	0-18	41.2	1.6	0-100	31.2	0.9	0-80	6.6	0.3	0-21	0.0	0.0	0-0	17.6	1.1	0-89	0.3	0.1	0-10	9	26*	15*
20	A OMPP	3.5	0.5	0-30	0.2	0.1	0-17	36.0	1.6	0-100	34.5	0.9	0-80	8.0	0.3	0-21	0.0	0.0	0-0	17.6	1.1	0-81	0.3	0.1	0-11	9	26*	15*
21	Azero	0.8	0.2	0-19	0.0	0.0	0-3	66.4	2.5	0-100	29.9	2.2	0-97	2.0	0.2	0-11	0.0	0.0	0-0	0.8	0.5	0-100	0.0	0.0	0-0	18*	31*	23*
21	A PP	1.0	0.2	0-22	0.0	0.0	0-3	63.1	2.5	0-100	32.1	2.2	0-96	3.1	0.2	0-12	0.0	0.0	0-1	0.7	0.4	0-97	0.0	0.0	0-0	19*	31*	23*
21	A GS	0.0	0.0	0-0	0.0	0.0	0-0	65.2	2.7	0-100	33.1	2.5	0-100	1.7	0.2	0-15	0.0	0.0	0-0	0.0	0.0	0-0	0.0	0.0	0-0	85*	106*	93*
21	A GSPP	0.0	0.0	0-0	0.0	0.0	0-0	63.8	2.6	0-100	34.8	2.5	0-100	1.4	0.2	0-13	0.0	0.0	0-0	0.0	0.0	0-0	0.0	0.0	0-0	85*	106*	93*
21	A OM	4.0	0.7	0-58	4.0	0.5	0-42	57.7	2.1	0-93	16.5	1.5	0-68	16.2	0.6	0-43	0.7	0.2	0-34	0.9	0.5	0-73	0.0	0.0	0-0	22*	30*	25*
21	A OMPP	3.8	0.7	0-56	3.8	0.4	0-41	57.8	2.1	0-93	16.8	1.5	0-69	15.9	0.6	0-41	0.9	0.2	0-37	1.0	0.5	0-72	0.0	0.0	0-0	22*	30*	25*
22	Azero	0.8	0.2	0-18	0.0	0.0	0-3	68.4	2.4	0-100	28.1	2.2	0-97	2.0	0.2	0-11	0.0	0.0	0-0	0.8	0.5	0-100	0.0	0.0	0-0	18*	29*	22*
22	A PP	1.0	0.2	0-21	0.0	0.0	0-3	65.5	2.4	0-100	29.8	2.2	0-96	3.0	0.2	0-11	0.0	0.0	0-1	0.7	0.4	0-97	0.0	0.0	0-0	18*	29*	22*
22	A GS	0.0	0.0	0-0	0.0	0.0	0-0	67.1	2.6	0-100	31.0	2.5	0-100	1.9	0.2	0-16	0.0	0.0	0-0	0.0	0.0	0-0	0.0	0.0	0-0	84*	100*	90*
22	A GSPP	0.0	0.0	0-0	0.0	0.0	0-0	65.9	2.6	0-100	32.5	2.5	0-100	1.6	0.2	0-13	0.0	0.0	0-0	0.0	0.0	0-0	0.0	0.0	0-0	84*	100*	90*
22	A OM	3.8	0.6	0-56	3.4	0.4	0-39	60.9	2.1	0-95	15.8	1.5	0-70	14.8	0.6	0-42	0.4	0.1	0-25	0.9	0.4	0-73	0.0	0.0	0-0	21*	28*	23*
22	A OMPP	3.7	0.6	0-54	3.1	0.4	0-36	60.8	2.1	0-94	16.2	1.5	0-70	14.8	0.5	0-40	0.5	0.2	0-25	0.9	0.5	0-74	0.0	0.0	0-0	20*	28*	23*
27	Azero	0.0	0.0	0-4	6.4	0.3	0-20	0.7	0.4	0-84	59.0	1.7	0-84	0.0	0.0	0-7	6.0	0.2	0-16	17.7	1.8	0-90	10.1	0.4	0-31	21*	21*	21*
27	A PP	0.0	0.0	0-4	7.8	0.3	0-21	0.8	0.4	0-85	60.1	1.7	0-85	0.0	0.0	0-6	5.3	0.2	0-14	17.8	1.8	0-90	8.2	0.4	0-30	20*	19*	20*
27	A GS	0.0	0.0	0-0	6.9	0.3	0-20	9.0	1.3	0-86	52.2	1.8	0-81	1.1	0.2	0-21	13.1	0.4	0-25	16.2	1.7	0-83	1.5	0.1	0-16	26*	24*	25*

		Motte			Hulpe			Velpe			Gete			Zwartebeek			Mangelbeek			Herk			Demer (upstream)			relative mean error		
Nr outlet sample	code model	contribution	95% CI	range	contribution	95% CI	range	contribution	95% CI	range	contribution	95% CI	range	contribution	95% CI	range	contribution	95% CI	range	contribution	95% CI	range	contribution	95% CI	range	RME (%)	RME_val (%)	RME_avg (%)
27	A OM	0.0	0.0	0-0	26.6	0.9	0-63	1.9	0.5	0-52	24.6	0.8	0-42	0.0	0.0	0-0	21.4	0.7	0-54	8.4	1.0	0-51	17.2	1.1	0-71	24*	27*	25*
27	A OMPP	0.0	0.0	0-0	31.0	0.9	0-64	2.7	0.6	0-54	24.4	0.9	0-43	0.0	0.0	0-0	16.7	0.7	0-53	8.5	1.0	0-52	16.7	1.1	0-73	23*	25*	24*
28	A zero	1.0	0.2	0-20	1.5	0.1	0-9	44.5	1.2	0-92	22.9	0.9	0-81	6.2	0.1	0-11	0.3	0.1	0-10	21.2	1.0	0-80	2.5	0.1	0-11	4	18*	9
28	A PP	1.3	0.2	0-20	1.4	0.1	0-8	43.9	1.1	0-93	22.6	0.9	0-81	6.1	0.1	0-10	0.3	0.1	0-10	21.9	1.0	0-73	2.4	0.1	0-10	4	18*	9
28	A GS	0.0	0.0	0-1	0.7	0.1	0-9	64.4	1.1	0-93	15.5	0.9	0-79	9.9	0.2	0-17	1.3	0.2	0-14	7.6	0.7	0-68	0.5	0.1	0-5	6	25*	13
28	A GSPP	0.0	0.0	0-0	0.7	0.1	0-9	66.9	1.1	0-93	14.2	0.9	0-79	9.2	0.2	0-16	1.4	0.2	0-14	7.2	0.6	0-50	0.5	0.1	0-5	6	26*	13
28	A OM	0.6	0.2	0-29	10.9	0.4	0-33	51.9	1.0	0-78	10.2	0.7	0-53	4.3	0.4	0-24	12.2	0.5	0-33	6.1	0.7	0-71	3.7	0.3	0-21	6	16*	10
28	A OMPP	0.6	0.2	0-28	11.1	0.4	0-34	52.6	1.0	0-78	9.1	0.7	0-52	3.2	0.3	0-23	12.9	0.5	0-32	6.7	0.7	0-71	3.8	0.3	0-22	6	16*	10
29	A zero	0.6	0.2	0-20	0.5	0.1	0-10	73.1	1.9	0-100	20.7	1.7	0-93	3.3	0.1	0-10	0.0	0.0	0-4	1.8	0.6	0-97	0.0	0.0	0-0	8	23*	13
29	A PP	0.6	0.2	0-20	0.5	0.1	0-10	73.4	1.8	0-100	20.2	1.6	0-92	3.4	0.1	0-9	0.0	0.0	0-4	1.8	0.6	0-96	0.0	0.0	0-0	8	23*	13
29	A GS	0.0	0.0	0-6	0.5	0.1	0-10	78.7	1.5	0-100	14.1	1.3	0-89	6.1	0.2	0-15	0.0	0.0	0-3	0.6	0.3	0-58	0.0	0.0	0-0	8	23*	13
29	A GSPP	0.1	0.0	0-7	0.5	0.1	0-10	78.9	1.4	0-99	13.8	1.3	0-88	6.1	0.1	0-14	0.0	0.0	0-5	0.7	0.3	0-56	0.0	0.0	0-0	8	23*	13
29	A OM	1.7	0.3	0-33	0.6	0.2	0-26	60.2	1.9	0-100	22.8	1.3	0-82	6.0	0.3	0-25	0.0	0.0	0-0	8.6	1.0	0-93	0.0	0.0	0-7	13	18*	15
29	A OMPP	2.0	0.4	0-34	0.5	0.1	0-26	54.8	1.8	0-100	26.2	1.2	0-82	7.6	0.3	0-25	0.0	0.0	0-0	8.9	1.0	0-92	0.0	0.0	0-8	13	17*	14
30	A zero	1.3	0.2	0-24	1.9	0.1	0-14	72.4	1.8	0-97	12.3	1.4	0-88	5.1	0.1	0-11	0.0	0.0	0-4	7.0	1.0	0-94	0.0	0.0	0-2	11	24*	16*
30	A PP	1.6	0.3	0-21	1.7	0.1	0-14	73.3	1.7	0-97	10.9	1.3	0-87	4.8	0.1	0-10	0.0	0.0	0-4	7.7	1.0	0-93	0.0	0.0	0-2	11	24*	16*
30	A GS	0.2	0.1	0-10	3.2	0.1	0-16	76.2	1.2	0-95	5.9	0.9	0-80	8.3	0.2	0-18	0.0	0.0	0-0	6.0	0.8	0-88	0.1	0.0	0-3	10	21*	14
30	A GSPP	0.3	0.1	0-10	3.1	0.1	0-16	77.1	1.2	0-95	4.8	0.8	0-80	7.9	0.2	0-17	0.0	0.0	0-6	6.7	0.8	0-88	0.2	0.0	0-3	10	21*	14
30	A OM	2.8	0.4	0-29	0.2	0.1	0-13	30.1	1.8	0-98	28.7	1.2	0-82	5.3	0.3	0-18	0.0	0.0	0-0	32.1	1.7	0-100	0.7	0.1	0-15	16*	19*	17*
30	A OMPP	3.9	0.5	0-33	0.1	0.1	0-11	24.4	1.7	0-100	34.6	1.2	0-82	7.6	0.4	0-21	0.0	0.0	0-0	28.7	1.6	0-97	0.5	0.1	0-14	16*	18*	17*
31	A zero	1.0	0.2	0-24	2.3	0.1	0-15	73.0	2.0	0-98	14.7	1.6	0-90	4.8	0.1	0-12	0.0	0.0	0-1	4.3	0.9	0-94	0.0	0.0	0-0	13	24*	17*
31	A PP	1.3	0.2	0-24	2.2	0.1	0-15	73.8	1.9	0-98	13.4	1.5	0-89	4.5	0.1	0-11	0.0	0.0	0-0	4.8	0.9	0-94	0.0	0.0	0-0	13	25*	17*
31	A GS	1.2	0.2	0-15	5.4	0.2	0-19	72.9	1.6	0-94	8.8	1.2	0-85	6.0	0.2	0-17	0.0	0.0	0-4	5.5	0.9	0-88	0.1	0.0	0-2	11	23*	15*
31	A GSPP	1.6	0.2	0-16	5.4	0.2	0-19	72.7	1.5	0-94	8.0	1.1	0-84	5.8	0.2	0-17	0.0	0.0	0-4	6.4	0.9	0-88	0.1	0.0	0-2	11	23*	16*
31	A OM	2.3	0.4	0-29	0.5	0.1	0-16	38.3	2.0	0-100	26.6	1.3	0-83	4.9	0.3	0-20	0.0	0.0	0-0	27.2	1.7	0-100	0.3	0.1	0-12	18*	19*	18*
31	A OMPP	3.3	0.5	0-32	0.4	0.1	0-13	31.3	1.9	0-100	32.2	1.3	0-83	7.4	0.4	0-22	0.0	0.0	0-0	25.2	1.6	0-97	0.2	0.1	0-9	18*	18*	18*
32	A zero	0.3	0.1	0-17	0.3	0.1	0-8	72.4	2.5	0-100	23.4	2.3	0-100	1.6	0.1	0-11	0.0	0.0	0-0	1.9	0.8	0-100	0.0	0.0	0-0	26*	49*	34*
32	A PP	0.4	0.1	0-17	0.3	0.1	0-9	73.5	2.5	0-100	22.2	2.3	0-99	1.7	0.1	0-10	0.0	0.0	0-0	1.9	0.7	0-99	0.0	0.0	0-0	26*	49*	34*
32	A GS	1.6	0.2	0-21	5.8	0.2	0-18	73.0	2.1	0-98	13.3	1.7	0-90	2.6	0.2	0-16	0.0	0.0	0-0	3.7	0.9	0-94	0.0	0.0	0-0	22*	34*	26*
32	A GSPP	2.3	0.2	0-21	6.3	0.2	0-19	71.6	2.0	0-96	12.8	1.7	0-88	2.7	0.2	0-16	0.0	0.0	0-0	4.3	1.0	0-92	0.0	0.0	0-0	21*	34*	26*
32	A OM	0.0	0.0	0-10	0.0	0.0	0-8	18.2	1.4	0-76	70.3	1.6	0-100	0.1	0.0	0-12	0.0	0.0	0-0	11.3	1.4	0-100	0.0	0.0	0-4	32*	22*	29*
32	A OMPP	0.2	0.1	0-13	0.0	0.0	0-6	16.5	1.3	0-75	72.4	1.6	0-100	0.3	0.1	0-14	0.0	0.0	0-0	10.5	1.4	0-100	0.0	0.0	0-1	32*	22*	29*
33	A zero	1.3	0.3	0-27	2.8	0.2	0-16	72.2	2.0	0-96	13.9	1.7	0-89	5.7	0.2	0-13	0.0	0.0	0-0	4.2	0.9	0-93	0.0	0.0	0-0	16*	26*	19*
33	A PP	1.6	0.3	0-25	2.8	0.2	0-16	73.1	1.9	0-96	12.5	1.6	0-88	5.3	0.2	0-12	0.0	0.0	0-0	4.6	1.0	0-93	0.0	0.0	0-0	16*	27*	20*
33	A GS	2.3	0.2	0-20	7.0	0.2	0-22	70.7	1.6	0-92	8.2	1.2	0-83	6.1	0.3	0-20	0.0	0.0	0-4	5.7	1.0	0-87	0.1	0.0	0-2	14	26*	18*
33	A GSPP	3.0	0.3	0-21	7.0	0.2	0-22	70.3	1.6	0-91	7.3	1.1	0-81	5.9	0.3	0-20	0.0	0.0	0-2	6.5	1.0	0-87	0.1	0.0	0-2	14	26*	18*
33	A OM	2.6	0.4	0-32	0.9	0.2	0-18	44.5	2.1	0-100	19.8	1.3	0-79	7.3	0.4	0-25	0.0	0.0	0-0	24.7	1.7	0-95	0.2	0.1	0-10	20*	21*	20*
33	A OMPP	3.5	0.5	0-36	0.7	0.1	0-17	37.0	2.0	0-100	24.4	1.4	0-79	9.8	0.4	0-26	0.0	0.0	0-0	24.5	1.6	0-93	0.1	0.0	0-9	20*	20*	20*
34	A zero	1.6	0.3	0-30	5.2	0.2	0-19	71.9	1.7	0-92	8.6	1.2	0-84	7.7	0.2	0-16	0.0	0.0	0-3	5.1	1.0	0-89	0.0	0.0	0-2	13	19*	15
34	A PP	2.1	0.4	0-31	5.2	0.2	0-19	72.3	1.6	0-92	7.4	1.1	0-83	7.4	0.2	0-15	0.0	0.0	0-3	5.7	1.0	0-88	0.0	0.0	0-2	13	19*	15
34	A GS	0.2	0.1	0-14	5.3	0.2	0-17	73.1	1.3	0-89	6.4	1.0	0-80	12.4	0.2	0-24	0.0	0.0	0-0	2.5	0.6	0-82	0.0	0.0	0-1	12	20*	15*
34	A GSPP	0.3	0.1	0-15	5.4	0.2	0-18	74.2	1.2	0-88	5.2	0.9	0-77	12.0	0.2	0-23	0.0	0.0	0-0	2.8	0.7	0-80	0.0	0.0	0-2	12	20*	15*
34	A OM	3.5	0.5	0-41	1.3	0.2	0-20	44.9	2.0	0-95	14.4	1.2	0-72	12.8	0.4	0-31	0.0	0.0	0-0	22.6	1.5	0-87	0.4	0.1	0-12	17*	18*	18*
34	A OMPP	4.3	0.6	0-43	1.0	0.2	0-19	38.7	1.9	0-94	17.6	1.2	0-71	14.8	0.4	0-31	0.0	0.0	0-0	23.4	1.5	0-86	0.2	0.1	0-10	17*	18*	17*
35	A zero	2.1	0.4	0-36	5.9	0.2	0-21	67.6	1.8	0-90	11.1	1.5	0-82	9.2	0.2	0-18	0.0	0.0	0-0	4.2	0.9	0-88	0.0	0.0	0-0	15*	23*	18*
35	A PP	2.5	0.4	0-35	6.1	0.2	0-21	67.9	1.8	0-90	9.9	1.4	0-82	8.9	0.2	0-18	0.0	0.0	0-0	4.7	1.0	0-87	0.0	0.0	0-0	15*	23*	18*
35	A GS	0.0	0.0	0-0	1.4	0.1	0-14	68.8	1.5	0-86	8.5	1.3	0-77	20.7	0.2	10-32	0.0	0.0	0-0	0.6	0.3	0-77	0.0	0.0	0-0	19*	33*	24*
35	A GSPP	0.0	0.0	0-0	1.5	0.1	0-14	71.4	1.4	0-86	7.3	1.2	0-78	19.2	0.2	9-29	0.0	0.0	0-0	0.7	0.3	0-67	0.0	0.0	0-0	19*	34*	24*
35	A OM	3.6	0.6	0-45	2.4	0.3	0-28	43.9	2.0	0-93	13.9	1.2	0-71	14.8	0.5	0-34	0.0	0.0	0-0	21.1	1.6	0-84	0.2	0.0	0-8	20*	21*	21*
35	A OMPP	4.4	0.7	0-46	1.8	0.3	0-23	37.6	1.9	0-90	16.7	1.3	0-70	17.1	0.5	0-35	0.0	0.0	0-0	22.4	1.6	0-83	0.1	0.0	0-7	20*	20*	20*
36	A zero	1.6	0.3	0-34	8.2	0.2	0-23	68.4	1.6	0-88	6.4	1.0	0-80	8.3	0.2	0-17	0.0	0.0	0-9	6.9	1.1	0-87	0.1	0.0	0-4	13	18*	15
36	A PP	2.1	0.4	0-35	8.2	0.2	0-23	68.4	1.6	0-88	5.4	0.9	0-80	8.0	0.2	0-17	0.0	0.0	0-9	7.6	1.2	0-87	0.2	0.0	0-4	13	18*	15
36	A GS	4.2	0.3	0-26	9.7	0.2	0-26	61.8	1.6	0-84	7.3	1.1	0-76	8.5	0.3	0-24	0.0	0.0	0-8	8.2	1.1	0-81	0.2	0.0	0-4	13	17*	14
36	A GSPP	5.2	0.4	0-28	9.6	0.2	0-25	61.4	1.5	0-83	6.2	1.0	0-75	8.3	0.3	0-24	0.0	0.0	0-6	9.1	1.2	0-81	0.2	0.0	0-4	13	17*	14
36	A OM	3.6	0.6	0-43	2.5	0.3	0-22	38.8	1.9	0-90	12.3	1.1	0-67	15.9	0.5	0-33	0.0	0.0	0-0	26.3	1.6	0-83	0.7	0.1	0-13	18*	19*	18*
36	A OMPP	4.4	0.7	0-47	2.0	0.3	0-21	33.5	1.8	0-89	14.4	1.1	0-67	17.7	0.5	0-34	0.0	0.0	0-0	27.8	1.6	0-82	0.4	0.1	0-12	18*	18*	18*
37	A zero	1.5	0.3	0-35	4.1	0.2	0-18	66.1	2.0	0-92	15.6	1.7	0-87	8.6	0.2	0-17	0.0	0.0	0-0	4.2	0.9	0-90	0.0	0.0	0-0	18*	23*	19*
37	A PP	1.8	0.4	0-34	4.2	0.2	0-18	67.1	2.0	0-92	14.2	1.7	0-86	8.1	0.2	0-16	0.0	0.0	0-0	4.5	1.0	0-90	0.0	0.0	0-0	18*	23*	19*
37	A GS	4.2	0.4	0-28	9.9	0.3	0-26	61.8	1.7	0-86	9.4	1.3	0-77	7.6	0.3	0-24	0.0	0.0	0-4	7.0	1.1	0-83	0.0	0.0	0-3	16*	19*	17*
37	A GSPP	5.6	0.4	0-29	9.8	0.3	0-26	60.6	1.7	0-85	8.6	1.2	0-76	7.4	0.3	0-24	0.0	0.0	0-2	7.9	1.2	0-82	0.0	0.0	0-3	16*	19*	17*
37	A OM	2.3	0.4	0-31	0.7	0.2	0-18	29.0	1.9	0-100	29.4	1.5	0-86	6.4	0.4	0-23	0.0	0.0	0-0	31.9	1.9	0-100	0.4	0.1	0-12	24*	19*	22*
37	A OMPP	3.2	0.5	0-34	0.4	0.1	0-18	21.8	1.7	0-100	36.8	1.5	0-84	10.0	0.4	0-27	0.0	0.0	0-0	27.6	1.7	0-97	0.2	0.1	0-10	24*	18*	22*
38	A zero	1.0	0.3	0-32	6.4	0.2	0-20	64.3	1.8	0-89	9.9	1.3	0-81	9.6	0.2	0-18	0.0	0.0	0-3	8.7	1.3	0-87	0.1	0.0	0-4	14	17*	15*
38	A PP	1.4	0.3	0-32	6.3	0.2	0-20	65.1	1.7	0-89	8.3	1.2	0-81	9.1	0.2	0-17	0.0	0.0	0-0	9.6	1.3	0-87	0.2	0.0	0-4	14	18*	15*
38	A GS	0.2	0.1	0-11	7.7	0.2	0-21	65.4	1.4	0-85	6.1	1.0	0-75	14.1	0.2	0-27	0.0	0.0	0-1	6.3	0.9	0-78	0.2	0.0	0-3	13	17*	15
38	A GSPP	0.7	0.1	0-16	8.8	0.2	0-22	62.6	1.2	0-86	7.7	0.9	0-76	14.6	0.3	0-28	0.0	0.0	0-1	5.3	0.7	0-72	0.2	0.0	0-3	14	16*	15
38	A OM	2.9	0.5	0-47	1.7	0.2	0-20	30.6	1.8	0-91	13.2	1.1	0-68	16.7	0.4	0-31	0.0	0.0	0-0	33.6	1.7	0-84	1.3	0.2	0-18	18*	17*	17*
38	A OMPP	3.7	0.6	0-48	1.2	0.2	0-20	25.4	1.7	0-90	16.0	1.1	0-67	18.7	0.5	0-33	0.0	0.0	0-0	34.2	1.6	0-83	0.8	0.1	0-14	17*	16*	17*

Table F.3: Modeled contributions of the eight tributaries to the suspended sediment flux sampled at the Aarschot outlet station, using Composite Fingerprint B and the Monte Carlo simulated property concentrations in the objective function; * = failing the RME test.

		Motte			Hulpe			Velpe			Gete			Zwartebeek			Mangelbeek			Herk			Demer (upstream)			relative mean error		
Nr outlet sample	code model	contribution	95% CI	range	contribution	95% CI	range	contribution	95% CI	range	contribution	95% CI	range	contribution	95% CI	range	contribution	95% CI	range	contribution	95% CI	range	contribution	95% CI	range	RME (%)	RME_val (%)	RME_avg (%)
13	B zero	0.0	0.0	0-0	13.7	0.3	2-30	16.9	1.3	0-72	20.9	1.2	0-72	9.0	0.4	0-23	8.5	0.2	0-19	29.7	1.3	0-75	1.4	0.2	0-18	5	14	8
13	B PP	0.0	0.0	0-10	13.8	0.3	2-30	16.3	1.3	0-72	21.6	1.2	0-72	8.5	0.3	0-22	9.0	0.2	0-19	29.5	1.3	0-75	1.3	0.2	0-19	5	14	8
13	B GS	9.4	0.4	0-31	11.0	0.2	0-21	0.9	0.3	0-39	1.0	0.4	0-49	0.0	0.0	0-0	0.5	0.1	0-14	37.7	0.7	0-59	39.5	0.6	20-73	21*	28*	24*
13	B GSPP	17.3	0.5	0-42	11.2	0.2	0-21	0.4	0.2	0-33	0.7	0.3	0-41	0.0	0.0	0-0	0.4	0.1	0-16	28.3	0.6	0-48	41.7	0.6	23-77	22*	30*	24*
13	B OM	11.0	0.9	0-54	48.0	1.0	21-90	5.1	0.3	0-14	0.0	0.0	0-0	27.3	1.0	0-67	2.4	0.4	0-43	0.0	0.0	0-0	6.2	0.6	0-41	65*	66*	66*
13	B OMPP	11.6	0.9	0-59	55.1	1.1	24-90	5.0	0.3	0-15	0.0	0.0	0-0	15.7	0.9	0-58	2.1	0.3	0-35	0.0	0.0	0-0	10.6	0.8	0-47	68*	79*	72*
14	B zero	0.6	0.1	0-19	8.2	0.2	0-20	5.2	0.6	0-66	37.2	1.2	0-76	1.1	0.1	0-11	11.1	0.2	0-19	30.9	1.3	0-81	5.7	0.3	0-27	4	26*	12
14	B PP	0.5	0.1	0-20	7.8	0.2	0-20	3.3	0.6	0-68	36.4	1.3	0-76	1.3	0.1	0-11	11.5	0.2	0-20	34.0	1.3	0-82	5.2	0.3	0-27	4	26*	12
14	B GS	0.0	0.0	0-0	9.3	0.3	0-30	22.3	1.6	0-77	45.7	1.6	0-75	15.9	0.4	0-30	4.0	0.2	0-14	2.8	0.6	0-72	0.0	0.0	0-2	17*	23*	19*
14	B GSPP	0.0	0.0	0-0	9.5	0.3	0-29	25.6	1.7	0-79	45.2	1.7	0-78	12.7	0.4	0-28	4.7	0.2	0-15	2.3	0.6	0-72	0.0	0.0	0-2	17*	25*	20*
14	B OM	0.2	0.1	0-16	13.4	0.4	0-31	0.3	0.1	0-20	27.4	0.9	0-53	2.0	0.2	0-20	27.6	0.3	6-42	26.4	1.1	0-65	2.6	0.3	0-31	6	27*	13
14	B OMPP	0.1	0.1	0-13	12.3	0.4	0-28	0.2	0.1	0-19	26.9	0.9	0-51	2.5	0.3	0-23	28.9	0.3	0-42	27.3	1.1	0-65	1.8	0.2	0-24	6	27*	13
15	B zero	2.5	0.3	0-22	18.7	0.3	8-33	3.3	0.6	0-59	28.1	1.2	0-65	0.0	0.0	0-6	4.3	0.2	0-14	26.6	1.4	0-76	16.4	0.4	0-39	6	51*	22*
15	B PP	2.0	0.3	0-21	18.3	0.2	7-33	2.9	0.6	0-59	27.6	1.2	0-65	0.1	0.0	0-6	4.6	0.2	0-15	28.0	1.4	0-77	16.6	0.4	0-38	6	51*	22*
15	B GS	0.7	0.1	0-15	21.6	0.3	9-38	6.9	0.8	0-65	39.3	1.2	0-70	0.3	0.1	0-13	8.5	0.3	0-20	16.8	1.2	0-74	5.9	0.2	0-19	6	46*	20*
15	B GSPP	0.3	0.1	0-11	21.1	0.3	9-38	6.6	0.8	0-66	39.1	1.3	0-71	0.2	0.1	0-12	8.9	0.3	0-19	18.4	1.3	0-74	5.4	0.2	0-19	6	45*	20*
15	B OM	4.7	0.4	0-28	44.7	0.5	25-67	10.7	0.6	0-39	11.8	0.5	0-31	0.0	0.0	0-9	3.6	0.3	0-19	4.4	0.5	0-36	20.1	0.6	0-51	8	61*	27*
15	B OMPP	2.9	0.3	0-23	44.8	0.4	26-66	11.4	0.6	0-39	10.7	0.5	0-30	0.0	0.0	0-6	2.8	0.2	0-17	4.7	0.5	0-39	22.7	0.6	0-53	8	63*	28*
16	B zero	4.1	0.3	0-18	1.2	0.1	0-9	8.7	1.2	0-97	82.0	1.3	0-100	0.8	0.1	0-7	0.3	0.0	0-4	3.0	0.7	0-95	0.1	0.0	0-7	9	13	10
16	B PP	3.3	0.2	0-15	1.1	0.1	0-8	8.7	1.1	0-97	82.8	1.2	0-100	0.7	0.1	0-6	0.4	0.0	0-4	2.9	0.6	0-95	0.1	0.0	0-6	9	13	10
16	B GS	0.0	0.0	0-0	0.8	0.1	0-12	19.4	1.9	0-100	73.7	2.0	0-100	5.1	0.2	0-15	0.0	0.0	0-0	1.0	0.4	0-89	0.0	0.0	0-0	28*	31*	29*
16	B GSPP	0.0	0.0	0-0	0.6	0.1	0-9	22.6	1.9	0-100	72.7	2.0	0-100	3.3	0.2	0-11	0.0	0.0	0-0	0.8	0.3	0-82	0.0	0.0	0-0	28*	31*	29*
16	B OM	5.6	0.5	0-32	2.9	0.3	0-23	2.4	0.4	0-43	73.2	1.0	0-95	2.6	0.3	0-17	3.2	0.3	0-19	9.4	1.0	0-90	0.7	0.2	0-24	9	16*	12
16	B OMPP	4.5	0.4	0-29	2.0	0.2	0-19	1.9	0.3	0-36	75.6	0.9	0-96	3.6	0.3	0-18	3.5	0.3	0-20	8.5	0.9	0-77	0.5	0.1	0-23	9	16*	12
17	B zero	18.4	0.8	0-43	0.4	0.1	0-12	10.1	1.2	0-90	64.1	1.4	0-90	2.7	0.3	0-16	2.2	0.1	0-12	1.4	0.4	0-67	0.7	0.1	0-11	11	14	12
17	B PP	15.4	0.7	0-38	0.4	0.1	0-11	11.9	1.3	0-91	64.9	1.4	0-91	2.6	0.2	0-15	2.5	0.1	0-12	1.4	0.4	0-72	0.9	0.1	0-11	11	14	12
17	B GS	0.0	0.0	0-11	0.6	0.1	0-13	17.8	1.7	0-85	57.7	1.7	0-84	22.8	0.3	8-34	0.0	0.0	0-4	1.0	0.3	0-69	0.0	0.0	0-0	28*	20*	25*
17	B GSPP	0.0	0.0	0-3	0.6	0.1	0-14	22.5	1.8	0-88	57.3	1.8	0-86	18.8	0.2	5-28	0.1	0.0	0-4	0.7	0.3	0-65	0.0	0.0	0-0	28*	23*	26*
17	B OM	24.1	0.9	0-50	1.0	0.1	0-17	5.2	0.6	0-75	43.2	0.8	0-64	4.6	0.5	0-34	9.3	0.4	0-34	2.9	0.6	0-62	9.6	0.5	0-46	8	17*	11
17	B OMPP	22.1	0.8	0-47	0.7	0.1	0-14	5.7	0.6	0-63	44.8	0.8	0-65	5.2	0.5	0-32	9.9	0.4	0-33	2.6	0.6	0-64	9.0	0.5	0-42	8	17*	11
18	B zero	17.3	0.8	0-42	0.3	0.1	0-11	11.2	1.2	0-90	64.2	1.4	0-91	2.1	0.2	0-15	2.9	0.2	0-12	1.4	0.4	0-68	0.7	0.1	0-11	10	12	11
18	B PP	13.9	0.7	0-39	0.3	0.1	0-10	13.6	1.4	0-91	64.1	1.5	0-91	2.2	0.2	0-14	3.2	0.2	0-11	1.8	0.5	0-73	0.9	0.1	0-12	10	12	11
18	B GS	0.0	0.0	0-12	0.5	0.1	0-11	17.4	1.6	0-86	59.7	1.6	0-86	21.4	0.3	7-33	0.1	0.0	0-6	1.0	0.3	0-70	0.0	0.0	0-0	26*	18*	23*
18	B GSPP	0.0	0.0	0-4	0.5	0.1	0-12	21.9	1.8	0-89	59.1	1.7	0-87	17.6	0.2	4-27	0.2	0.0	0-6	0.7	0.3	0-65	0.0	0.0	0-0	26*	20*	24*
18	B OM	31.3	0.8	0-56	1.3	0.2	0-18	8.2	0.8	0-71	35.5	0.8	0-56	2.3	0.4	0-32	6.4	0.4	0-32	2.4	0.5	0-56	12.5	0.5	0-47	10	16*	12
18	B OMPP	28.9	0.7	0-52	1.2	0.2	0-17	9.5	0.8	0-73	35.9	0.8	0-57	2.2	0.4	0-30	6.2	0.4	0-29	2.2	0.5	0-56	13.9	0.5	0-45	10	15*	12
19	B zero	8.2	0.5	0-31	0.0	0.0	0-3	24.3	1.8	0-100	65.1	1.8	0-99	2.0	0.2	0-11	0.0	0.0	0-4	0.3	0.2	0-59	0.0	0.0	0-0	29*	18*	25*
19	B PP	6.0	0.4	0-25	0.0	0.0	0-3	30.1	1.9	0-100	61.9	1.9	0-99	1.7	0.1	0-10	0.1	0.0	0-5	0.3	0.2	0-55	0.0	0.0	0-0	28*	18*	25*
19	B GS	0.0	0.0	0-3	0.1	0.0	0-4	30.5	1.9	0-97	55.5	1.9	0-94	13.6	0.3	2-26	0.0	0.0	0-2	0.3	0.2	0-56	0.0	0.0	0-0	29*	14	24*
19	B GSPP	0.0	0.0	0-0	0.1	0.0	0-3	37.1	2.0	0-99	52.7	1.9	0-95	10.0	0.2	0-20	0.0	0.0	0-2	0.2	0.1	0-50	0.0	0.0	0-0	29*	15*	24*
19	B OM	6.6	0.6	0-42	0.0	0.0	0-2	14.4	1.0	0-79	62.7	0.9	0-90	3.7	0.4	0-28	11.3	0.4	0-33	1.0	0.4	0-65	0.2	0.1	0-20	19*	24*	21*
19	B OMPP	3.9	0.5	0-38	0.0	0.0	0-0	13.8	0.9	0-72	65.4	0.8	0-90	5.2	0.4	0-30	11.1	0.4	0-31	0.6	0.3	0-60	0.1	0.0	0-10	19*	23*	20*
20	B zero	13.3	0.6	0-35	0.1	0.0	0-8	15.8	1.5	0-97	67.2	1.6	0-96	1.7	0.2	0-13	1.0	0.1	0-8	0.8	0.3	0-76	0.0	0.0	0-5	16*	10	14
20	B PP	10.4	0.5	0-29	0.1	0.0	0-7	18.6	1.6	0-97	67.3	1.6	0-96	1.5	0.2	0-11	1.2	0.1	0-7	0.8	0.3	0-81	0.1	0.0	0-6	16*	11	14
20	B GS	0.0	0.0	0-0	0.2	0.0	0-7	25.1	2.0	0-94	58.4	1.9	0-93	15.9	0.3	3-29	0.0	0.0	0-0	0.5	0.2	0-65	0.0	0.0	0-0	41*	29*	37*
20	B GSPP	0.0	0.0	0-0	0.1	0.0	0-10	31.9	2.1	0-98	56.3	2.0	0-94	11.3	0.2	0-21	0.0	0.0	0-1	0.3	0.2	0-59	0.0	0.0	0-0	42*	30*	37*
20	B OM	16.3	0.8	0-46	0.1	0.0	0-11	10.0	0.9	0-80	53.6	1.0	0-80	2.6	0.3	0-28	10.9	0.5	0-33	2.1	0.5	0-71	4.5	0.4	0-42	14	18*	15*
20	B OMPP	12.9	0.7	0-41	0.0	0.0	0-6	11.2	0.9	0-75	55.7	0.9	0-80	3.2	0.4	0-27	11.6	0.4	0-32	1.8	0.5	0-66	3.5	0.4	0-36	13	17*	15
21	B zero	16.5	0.7	0-44	0.0	0.0	0-0	54.7	1.4	0-93	22.2	1.4	0-88	0.8	0.1	0-14	4.6	0.2	0-14	0.1	0.1	0-14	1.1	0.1	0-12	19*	38*	26*
21	B PP	12.2	0.6	0-36	0.0	0.0	0-0	59.7	1.4	0-94	20.7	1.3	0-88	0.8	0.1	0-15	5.0	0.2	0-13	0.1	0.1	0-15	1.4	0.2	0-14	18*	36*	25*
21	B GS	0.0	0.0	0-0	0.0	0.0	0-0	59.0	1.6	0-92	19.2	1.4	0-80	21.8	0.4	8-36	0.0	0.0	0-0	0.0	0.0	0-8	0.0	0.0	0-0	79*	108*	89*
21	B GSPP	0.0	0.0	0-0	0.0	0.0	0-0	70.6	1.5	0-100	15.0	1.3	0-84	14.3	0.3	0-26	0.0	0.0	0-0	0.0	0.0	0-2	0.0	0.0	0-0	80*	108*	90*
21	B OM	25.6	0.8	0-61	0.0	0.0	0-0	44.2	1.1	0-79	9.9	0.6	0-43	1.1	0.3	0-34	10.5	0.5	0-41	0.1	0.1	0-13	8.7	0.5	0-44	19*	45*	28*
21	B OMPP	21.6	0.7	0-58	0.0	0.0	0-0	48.7	1.1	0-82	9.0	0.6	0-44	1.0	0.2	0-33	10.8	0.5	0-39	0.1	0.1	0-12	8.9	0.5	0-39	18*	44*	27*
22	B zero	12.9	0.7	0-40	0.0	0.0	0-0	63.3	1.3	0-94	17.0	1.2	0-87	0.7	0.1	0-13	4.9	0.2	0-13	0.1	0.0	0-10	1.1	0.1	0-12	17*	36*	24*
22	B PP	9.2	0.5	0-32	0.0	0.0	0-0	67.8	1.2	0-94	15.5	1.2	0-88	0.7	0.1	0-12	5.3	0.2	0-13	0.1	0.0	0-11	1.3	0.2	0-13	17*	34*	23*
22	B GS	0.0	0.0	0-0	0.0	0.0	0-0	66.8	1.4	0-93	13.7	1.2	0-79	19.6	0.3	7-32	0.0	0.0	0-0	0.0	0.0	0-1	0.0	0.0	0-0	76*	105*	86*
22	B GSPP	0.0	0.0	0-0	0.0	0.0	0-0	77.3	1.2	0-100	10.1	1.1	0-82	12.6	0.3	0-24	0.0	0.0	0-0	0.0	0.0	0-0	0.0	0.0	0-0	77*	105*	87*
22	B OM	17.5	0.7	0-55	0.0	0.0	0-0	53.0	1.1	0-86	9.3	0.6	0-47	1.0	0.2	0-34	13.3	0.5	0-37	0.1	0.1	0-13	5.8	0.5	0-35	17*	39*	25*
22	B OMPP	14.2	0.7	0-50	0.0	0.0	0-0	56.9	1.0	0-88	8.6	0.6	0-48	1.1	0.2	0-32	13.9	0.4	0-36	0.1	0.1	0-13	5.2	0.4	0-29	17*	37*	24*
27	B zero	0.0	0.0	0-0	23.7	0.2	15-35	4.2	0.6	0-64	30.3	1.2	0-78	0.0	0.0	0-3	0.1	0.0	0-3	41.6	1.3	0-84	0.1	0.0	0-6	10	34*	19*
27	B PP	0.0	0.0	0-0	22.9	0.2	14-34	3.0	0.5	0-54	30.4	1.2	0-78	0.0	0.0	0-3	0.1	0.0	0-3	43.4	1.3	0-84	0.2	0.0	0-6	10	34*	19*
27	B GS	0.0	0.0	0-0	28.0	0.3	7-42	22.6	1.3	0-77	33.5	1.4	0-78	0.3	0.1	0-14	0.0	0.0	0-5	15.6	1.0	0-79	0.0	0.0	0-0	15	39*	23*

		Motte			Hulpe			Velpe			Gete			Zwartebeek			Mangelbeek			Herk			Demer (upstream)			relative mean error		
Nr outlet sample	code model	contribution	95% CI	range	contribution	95% CI	range	contribution	95% CI	range	contribution	95% CI	range	contribution	95% CI	range	contribution	95% CI	range	contribution	95% CI	range	contribution	95% CI	range	RME (%)	RME_val (%)	RME_avg (%)
27	B OM	0.0	0.0	0-0	57.1	0.2	43-65	5.0	0.5	0-35	6.2	0.5	0-38	0.0	0.0	0-4	0.2	0.0	0-7	29.7	0.7	0-47	1.9	0.2	0-24	7	36*	18*
27	B OMPP	0.0	0.0	0-0	56.2	0.2	41-65	4.2	0.4	0-35	5.3	0.5	0-37	0.0	0.0	0-3	0.1	0.0	0-6	31.1	0.6	0-47	3.0	0.3	0-24	7	36*	17*
28	B zero	10.6	0.5	0-31	2.4	0.2	0-16	8.7	1.2	0-89	63.4	1.4	0-90	1.1	0.1	0-11	2.6	0.2	0-13	5.3	0.9	0-84	6.0	0.3	0-24	6	9	7
28	B PP	8.3	0.5	0-27	2.3	0.2	0-18	8.7	1.2	0-89	65.5	1.4	0-92	1.2	0.1	0-10	2.9	0.2	0-12	4.8	0.8	0-82	6.3	0.3	0-24	5	9	7
28	B GS	0.2	0.1	0-19	3.1	0.2	0-19	15.8	1.6	0-88	63.1	1.8	0-90	11.0	0.4	0-26	3.5	0.2	0-15	3.0	0.7	0-83	0.2	0.0	0-6	11	9	11
28	B GSPP	0.1	0.0	0-12	3.0	0.2	0-18	17.8	1.7	0-90	63.3	1.8	0-90	9.0	0.3	0-22	3.9	0.2	0-15	2.8	0.7	0-84	0.1	0.0	0-6	12	10	11
28	B OM	20.4	0.7	0-43	10.5	0.4	0-31	9.9	0.8	0-66	30.4	0.8	0-53	0.8	0.2	0-29	2.3	0.2	0-21	4.1	0.7	0-54	21.6	0.5	0-53	8	14	10
28	B OMPP	17.8	0.6	0-39	10.9	0.4	0-30	11.5	0.8	0-67	30.0	0.8	0-54	0.6	0.1	0-25	2.1	0.2	0-21	4.1	0.7	0-54	23.1	0.5	0-53	8	15	10
29	B zero	8.2	0.6	0-30	0.2	0.1	0-9	18.5	1.4	0-96	68.2	1.5	0-95	3.1	0.2	0-13	1.1	0.1	0-7	0.7	0.3	0-64	0.0	0.0	0-5	12	15*	13
29	B PP	6.3	0.5	0-26	0.2	0.1	0-9	20.7	1.5	0-97	67.6	1.5	0-95	3.0	0.2	0-11	1.3	0.1	0-7	0.7	0.3	0-61	0.1	0.0	0-6	12	15	13
29	B GS	0.0	0.0	0-14	0.6	0.1	0-11	24.5	1.6	0-94	60.7	1.6	0-91	12.2	0.3	0-23	1.0	0.1	0-10	1.0	0.3	0-64	0.0	0.0	0-1	12	15	13
29	B GSPP	0.0	0.0	0-10	0.5	0.1	0-10	27.3	1.6	0-95	59.7	1.6	0-92	10.3	0.2	0-19	1.3	0.1	0-10	0.9	0.3	0-60	0.0	0.0	0-1	12	14	12
29	B OM	9.3	0.7	0-41	0.3	0.1	0-9	12.4	0.8	0-57	56.6	0.8	0-78	6.0	0.5	0-29	11.0	0.4	0-30	2.4	0.5	0-64	2.0	0.3	0-35	9	23*	14
29	B OMPP	7.1	0.6	0-40	0.1	0.0	0-8	12.5	0.8	0-54	58.6	0.7	3-79	7.1	0.5	0-31	11.2	0.4	0-31	2.0	0.4	0-62	1.4	0.2	0-30	9	22*	14
30	B zero	8.0	0.6	0-33	0.2	0.1	0-9	18.9	1.4	0-95	66.8	1.5	0-94	4.2	0.2	0-14	1.1	0.1	0-8	0.7	0.3	0-60	0.1	0.0	0-7	13	17*	14
30	B PP	6.4	0.5	0-28	0.2	0.1	0-9	20.8	1.4	0-96	66.4	1.5	0-94	4.0	0.2	0-12	1.3	0.1	0-8	0.8	0.3	0-61	0.1	0.0	0-5	13	17*	14
30	B GS	0.1	0.1	0-16	0.5	0.1	0-11	22.6	1.5	0-92	60.6	1.5	0-89	13.4	0.3	0-25	1.6	0.1	0-10	1.2	0.4	0-64	0.1	0.0	0-5	12	16*	13
30	B GSPP	0.1	0.0	0-12	0.5	0.1	0-11	24.7	1.5	0-93	60.0	1.5	0-90	11.5	0.3	0-21	2.0	0.1	0-10	1.1	0.3	0-60	0.0	0.0	0-0	12	16*	13
30	B OM	2.1	0.3	0-30	0.1	0.0	0-6	8.0	0.6	0-45	67.1	0.6	14-87	4.7	0.4	0-25	14.8	0.4	0-33	2.7	0.4	0-63	0.7	0.2	0-29	11	21*	15
30	B OMPP	0.8	0.2	0-27	0.0	0.0	0-4	6.1	0.5	0-39	70.0	0.5	24-86	6.8	0.4	0-28	14.2	0.5	0-32	1.9	0.3	0-57	0.2	0.1	0-13	11	20*	14
31	B zero	4.9	0.5	0-31	0.2	0.1	0-8	19.6	1.4	0-95	68.3	1.4	0-95	5.1	0.2	0-14	1.3	0.1	0-9	0.6	0.3	0-59	0.0	0.0	0-2	13	21*	16*
31	B PP	3.5	0.4	0-26	0.2	0.1	0-8	21.2	1.4	0-96	68.0	1.5	0-96	4.9	0.2	0-13	1.6	0.1	0-9	0.6	0.3	0-56	0.0	0.0	0-4	13	21*	16*
31	B GS	0.3	0.1	0-13	0.5	0.1	0-11	21.1	1.3	0-91	61.7	1.4	0-90	10.8	0.3	0-23	3.6	0.2	0-14	1.9	0.4	0-62	0.1	0.0	0-7	11	21*	15
31	B GSPP	0.4	0.1	0-12	0.4	0.1	0-9	21.9	1.3	0-90	61.6	1.4	0-90	9.3	0.3	0-21	4.3	0.2	0-14	2.0	0.4	0-60	0.2	0.0	0-8	11	22*	15
31	B OM	0.8	0.2	0-26	0.1	0.0	0-6	8.0	0.6	0-39	67.6	0.6	12-88	4.8	0.4	0-29	15.4	0.4	0-34	3.4	0.4	0-52	0.1	0.1	0-16	12	24*	16*
31	B OMPP	0.3	0.1	0-23	0.0	0.0	0-3	5.6	0.5	0-34	70.6	0.5	23-87	6.2	0.4	0-29	14.9	0.5	0-33	2.4	0.3	0-46	0.0	0.0	0-5	12	24*	16*
32	B zero	3.3	0.4	0-29	0.0	0.0	0-1	39.2	2.0	0-100	53.9	1.9	0-100	3.4	0.2	0-13	0.1	0.0	0-4	0.1	0.1	0-39	0.0	0.0	0-0	34*	37*	35*
32	B PP	2.3	0.3	0-24	0.0	0.0	0-1	47.1	2.1	0-100	47.8	2.0	0-100	2.7	0.2	0-10	0.1	0.0	0-4	0.1	0.1	0-34	0.0	0.0	0-0	34*	37*	35*
32	B GS	0.8	0.2	0-18	0.1	0.0	0-5	36.4	1.4	0-94	49.3	1.4	0-90	10.0	0.3	0-25	3.0	0.2	0-15	0.5	0.2	0-44	0.0	0.0	0-5	19*	32*	23*
32	B GSPP	1.4	0.2	0-18	0.0	0.0	0-5	38.5	1.4	0-93	47.7	1.4	0-90	8.0	0.3	0-21	3.7	0.2	0-14	0.6	0.2	0-41	0.1	0.0	0-8	19*	32*	24*
32	B OM	0.0	0.0	0-0	0.0	0.0	0-0	14.1	0.9	0-52	78.8	0.8	33-100	0.4	0.1	0-16	5.9	0.3	0-25	0.8	0.2	0-35	0.0	0.0	0-0	24*	36*	28*
32	B OMPP	0.0	0.0	0-0	0.0	0.0	0-0	8.9	0.7	0-49	82.4	0.7	36-100	0.9	0.2	0-18	7.2	0.3	0-25	0.6	0.2	0-38	0.0	0.0	0-0	24*	36*	29*
33	B zero	6.7	0.6	0-36	0.2	0.1	0-9	17.2	1.4	0-95	67.9	1.5	0-94	5.2	0.3	0-16	2.0	0.1	0-11	0.7	0.3	0-59	0.0	0.0	0-2	14	25*	18*
33	B PP	5.1	0.5	0-30	0.2	0.1	0-9	18.6	1.4	0-95	68.1	1.5	0-94	4.9	0.2	0-14	2.4	0.1	0-10	0.7	0.3	0-56	0.0	0.0	0-5	14	26*	18*
33	B GS	1.1	0.2	0-18	0.5	0.1	0-12	18.0	1.3	0-89	62.1	1.4	0-88	9.5	0.3	0-25	6.2	0.2	0-19	2.2	0.5	0-66	0.4	0.1	0-11	12	26*	17*
33	B GSPP	1.5	0.2	0-18	0.4	0.1	0-10	18.7	1.3	0-90	62.1	1.3	0-88	7.9	0.3	0-23	6.7	0.2	0-18	2.2	0.5	0-63	0.6	0.1	0-11	11	26*	17*
33	B OM	1.6	0.3	0-29	0.1	0.0	0-7	7.2	0.6	0-44	64.2	0.6	7-83	4.3	0.4	0-29	19.6	0.4	0-38	2.7	0.4	0-63	0.3	0.1	0-26	12	28*	18*
33	B OMPP	0.6	0.2	0-26	0.0	0.0	0-4	5.5	0.5	0-37	67.0	0.5	20-82	5.9	0.4	0-30	19.0	0.4	0-37	1.9	0.3	0-58	0.1	0.0	0-15	12	28*	18*
34	B zero	3.7	0.4	0-29	2.2	0.2	0-14	10.0	1.1	0-86	64.3	1.3	0-90	5.1	0.3	0-16	5.4	0.2	0-14	8.3	0.8	0-86	1.0	0.1	0-18	7	24*	13
34	B PP	3.0	0.4	0-26	2.1	0.2	0-14	9.3	1.1	0-86	65.1	1.3	0-90	5.0	0.2	0-15	5.7	0.2	0-14	8.5	0.8	0-86	1.3	0.2	0-15	7	24*	13
34	B GS	0.1	0.0	0-9	2.7	0.2	0-18	14.6	1.4	0-85	58.6	1.5	0-84	13.2	0.3	0-26	5.0	0.2	0-15	5.8	0.7	0-78	0.1	0.0	0-5	8	22*	13
34	B GSPP	0.0	0.0	0-6	2.6	0.2	0-17	15.0	1.4	0-84	59.2	1.4	0-85	11.5	0.3	0-24	5.8	0.2	0-15	5.7	0.7	0-79	0.1	0.0	0-5	8	23*	13
34	B OM	0.9	0.2	0-27	1.5	0.2	0-16	1.0	0.2	0-23	55.1	0.7	0-76	6.0	0.4	0-27	21.3	0.4	0-38	13.9	0.8	0-78	0.5	0.1	0-30	9	26*	15
34	B OMPP	0.3	0.1	0-22	0.8	0.1	0-13	0.5	0.1	0-16	57.3	0.7	10-76	7.9	0.4	0-29	20.8	0.4	0-38	12.1	0.8	0-65	0.2	0.1	0-20	9	26*	15
35	B zero	4.2	0.5	0-37	2.3	0.2	0-17	7.3	1.0	0-87	66.8	1.2	0-89	8.1	0.3	0-20	4.5	0.2	0-15	6.7	0.8	0-86	0.1	0.1	0-10	9	28*	16*
35	B PP	3.4	0.4	0-33	2.2	0.2	0-16	6.9	1.0	0-85	67.5	1.2	0-87	7.8	0.3	0-19	5.2	0.2	0-15	6.9	0.8	0-86	0.2	0.1	0-12	9	28*	16*
35	B GS	0.0	0.0	0-0	1.4	0.2	0-17	12.5	1.4	0-82	59.8	1.4	0-82	24.5	0.3	7-34	0.2	0.1	0-10	1.5	0.4	0-68	0.0	0.0	0-0	18*	27*	21*
35	B GSPP	0.0	0.0	0-0	1.5	0.2	0-18	14.5	1.5	0-83	60.3	1.5	0-83	22.0	0.2	6-31	0.4	0.1	0-9	1.4	0.4	0-63	0.0	0.0	0-0	19*	29*	22*
35	B OM	0.8	0.2	0-28	2.0	0.2	0-18	0.5	0.1	0-17	53.4	0.8	0-75	8.4	0.5	0-35	21.6	0.5	0-42	13.3	0.9	0-78	0.1	0.0	0-17	12	30*	18*
35	B OMPP	0.2	0.1	0-22	1.0	0.1	0-14	0.2	0.1	0-13	55.3	0.7	0-74	10.3	0.5	0-36	21.2	0.5	0-41	11.7	0.8	0-75	0.0	0.0	0-11	11	30*	18*
36	B zero	2.3	0.3	0-32	3.7	0.2	0-16	7.2	1.0	0-82	58.4	1.3	0-87	4.6	0.3	0-17	8.1	0.2	0-17	14.5	1.1	0-85	1.2	0.2	0-17	7	25*	13
36	B PP	1.9	0.3	0-31	3.6	0.2	0-15	6.6	1.0	0-83	58.5	1.3	0-87	4.5	0.2	0-15	8.4	0.2	0-16	15.0	1.1	0-85	1.5	0.2	0-19	7	25*	13
36	B GS	0.9	0.1	0-18	4.2	0.2	0-18	7.6	1.0	0-79	54.5	1.3	0-82	7.7	0.4	0-26	10.4	0.3	0-23	13.8	1.1	0-80	0.8	0.1	0-14	7	25*	13
36	B GSPP	1.1	0.2	0-17	3.9	0.2	0-17	6.7	0.8	0-78	54.8	1.2	0-82	7.1	0.3	0-22	10.8	0.3	0-23	14.5	1.0	0-78	1.0	0.1	0-14	7	25*	13
36	B OM	0.5	0.1	0-25	3.0	0.3	0-19	0.3	0.1	0-17	48.2	0.8	0-69	5.1	0.4	0-30	25.1	0.4	0-41	17.6	1.0	0-74	0.3	0.1	0-26	10	27*	16*
36	B OMPP	0.2	0.1	0-19	1.7	0.2	0-16	0.1	0.1	0-10	49.9	0.8	0-72	6.8	0.4	0-30	25.0	0.4	0-41	16.1	0.9	0-74	0.1	0.1	0-20	9	27*	16*
37	B zero	4.7	0.5	0-37	1.4	0.1	0-15	9.8	1.2	0-89	70.5	1.4	0-91	8.1	0.3	0-18	2.4	0.2	0-13	2.9	0.6	0-86	0.1	0.0	0-10	11	29*	17*
37	B PP	3.6	0.5	0-32	1.4	0.1	0-15	9.7	1.2	0-88	71.7	1.3	0-91	7.8	0.3	0-17	2.8	0.2	0-12	2.9	0.6	0-79	0.2	0.1	0-11	11	29*	17*
37	B GS	2.9	0.3	0-25	2.3	0.2	0-16	7.1	0.9	0-80	58.0	1.2	0-85	8.8	0.4	0-26	7.7	0.3	0-21	11.5	1.0	0-81	1.7	0.2	0-16	10	29*	17*
37	B GSPP	4.0	0.3	0-26	2.0	0.2	0-15	6.3	0.8	0-79	57.8	1.2	0-83	8.2	0.4	0-23	7.5	0.3	0-20	11.8	0.9	0-81	2.3	0.2	0-19	10	30*	17*
37	B OM	0.0	0.0	0-4	0.2	0.1	0-10	0.4	0.1	0-14	67.9	0.8	14-90	0.9	0.2	0-21	16.7	0.3	0-29	13.7	0.9	0-74	0.2	0.1	0-19	15	30*	20*
37	B OMPP	0.0	0.0	0-0	0.0	0.0	0-6	0.1	0.1	0-12	70.8	0.7	19-91	2.0	0.3	0-24	17.0	0.4	0-29	10.1	0.8	0-67	0.0	0.0	0-5	15	30*	20*
38	B zero	3.0	0.4	0-33	2.8	0.2	0-17	9.7	1.2	0-85	65.0	1.3	0-89	7.5	0.3	0-18	4.5	0.2	0-14	6.6	0.8	0-87	0.9	0.1	0-17	8	22*	13
38	B PP	2.3	0.3	0-36	2.8	0.2	0-17	10.0	1.2	0-85	65.1	1.4	0-89	7.1	0.3	0-17	4.8	0.2	0-14	6.8	0.8	0-87	1.0	0.1	0-17	8	22*	13
38	B GS	0.0	0.0	0-7	3.4	0.2	0-19	13.3	1.3	0-81	55.5	1.4	0-81	15.7	0.4	0-29	4.7	0.2	0-16	7.1	0.8	0-78	0.3	0.1	0-7	9	21*	13
38	B GSPP	0.0	0.0	0-5	3.3	0.2	0-19	13.8	1.4	0-82	56.0	1.4	0-82	13.9	0.4	0-27	5.5	0.2	0-16	7.1	0.8	0-77	0.3	0.1	0-8	8	21*	13
38	B OM	0.6	0.2	0-26	2.3	0.2	0-18	0.6	0.1	0-21	50.0	0.8	0-73	8.5	0.4	0-30	21.5	0.4	0-41	16.0	0.9	0-74	0.5	0.1	0-33	10	25*	15*
38	B OMPP	0.2	0.1	0-12	1.3	0.2	0-14	0.3	0.1	0-14	52.2	0.7	0-73	10.7	0.4	0-31	20.8	0.5	0-40	14.4	0.8	0-74	0.2	0.1	0-24	10	25*	15*

Table F.4: Modeled contributions of the eight tributaries to the suspended sediment flux sampled at the Aarschot outlet station, using Composite Fingerprint C and the Monte Carlo simulated property concentrations in the objective function; * = failing the RME test.

Nr outlet sample	code model	Motte			Hulpe			Velpe			Gete			Zwartebeek			Mangelbeek			Herk			Demer (upstream)			relative mean error	
		contribution	95% CI	range	contribution	95% CI	range	contribution	95% CI	range	contribution	95% CI	range	contribution	95% CI	range	contribution	95% CI	range	contribution	95% CI	range	contribution	95% CI	range	RME (%)	RME_val (%)	RME_avg (%)
C zero	13	8.1	0.7	0-43	13.7	0.2	6-30	25.1	1.3	0-68	5.6	0.6	0-57	9.3	0.4	0-24	2.7	0.2	0-16	25.1	1.1	0-69	10.4	0.3	0-27	8	12	10
C PP	13	9.2	0.8	0-42	13.7	0.2	6-30	24.9	1.3	0-67	4.7	0.5	0-51	8.4	0.4	0-23	2.6	0.2	0-15	24.9	1.1	0-68	11.6	0.3	0-29	8	13	10
C GS	13	3.6	0.4	0-29	26.3	0.3	17-41	4.7	0.6	0-38	0.5	0.2	0-31	0.7	0.1	0-16	1.1	0.2	0-15	22.3	0.8	0-44	40.7	0.5	23-67	19*	35*	25*
C GSPP	13	7.8	0.5	0-38	28.3	0.3	19-45	3.1	0.4	0-32	0.4	0.2	0-30	1.2	0.2	0-22	1.5	0.2	0-18	16.3	0.6	0-37	41.4	0.5	25-69	18*	37*	25*
C OM	13	50.4	2.2	0-100	24.8	0.8	0-69	3.3	0.3	0-20	0.0	0.0	0-3	17.7	1.3	0-66	2.1	0.3	0-39	0.0	0.0	0-0	1.8	0.3	0-32	74*	71*	73*
C OMPP	13	51.1	2.0	0-100	28.0	0.9	0-79	3.7	0.3	0-21	0.0	0.0	0-1	10.2	1.0	0-55	2.2	0.3	0-40	0.0	0.0	0-0	4.8	0.5	0-45	79*	78*	79*
C zero	14	5.7	0.5	0-31	12.4	0.2	2-24	24.8	1.2	0-71	17.7	1.0	0-61	2.1	0.2	0-15	2.6	0.2	0-13	16.2	1.1	0-71	18.5	0.4	3-38	9	24*	14
C PP	14	5.3	0.4	0-27	12.5	0.2	2-25	25.6	1.2	0-71	16.2	0.9	0-57	1.8	0.2	0-14	2.5	0.2	0-12	16.5	1.1	0-70	19.7	0.4	4-41	9	25*	15
C GS	14	4.5	0.5	0-33	8.2	0.2	0-19	27.0	1.5	0-85	40.2	1.5	0-75	8.5	0.4	0-29	4.3	0.2	0-16	6.1	1.0	0-79	1.1	0.1	0-12	15*	37*	23*
C GSPP	14	3.8	0.4	0-28	8.0	0.2	0-20	31.1	1.6	0-86	37.5	1.5	0-76	6.3	0.4	0-26	4.8	0.2	0-15	6.9	1.0	0-81	1.7	0.1	0-13	16*	40*	24*
C OM	14	5.2	0.5	0-40	13.3	0.5	0-32	1.1	0.2	0-36	20.4	0.9	0-51	4.7	0.4	0-29	5.3	0.4	0-26	28.9	1.2	0-75	21.2	0.7	0-46	14	19*	16*
C OMPP	14	5.4	0.6	0-41	11.8	0.5	0-31	1.0	0.2	0-36	19.6	0.9	0-53	6.0	0.4	0-30	6.5	0.4	0-27	31.0	1.2	0-74	18.8	0.7	0-45	14	19*	16*
C zero	15	1.1	0.2	0-20	18.2	0.2	9-34	1.7	0.3	0-44	34.0	1.0	0-61	0.6	0.1	0-10	4.0	0.2	0-11	20.5	1.1	0-67	19.8	0.3	7-39	4	58*	24*
C PP	15	1.0	0.2	0-20	17.9	0.2	9-34	1.7	0.3	0-41	33.0	1.0	0-62	0.6	0.1	0-9	4.1	0.2	0-12	21.8	1.2	0-67	20.0	0.3	7-41	4	58*	24*
C GS	15	1.2	0.2	0-22	18.7	0.2	6-36	4.1	0.5	0-59	43.7	1.1	0-68	1.7	0.2	0-17	6.7	0.2	0-17	13.4	1.1	0-72	10.5	0.2	2-21	5	53*	22*
C GSPP	15	1.0	0.2	0-21	18.1	0.2	6-36	4.4	0.5	0-56	43.2	1.1	0-68	1.6	0.2	0-17	6.5	0.2	0-16	14.4	1.1	0-72	10.9	0.2	3-21	5	54*	23*
C OM	15	4.9	0.4	0-34	39.6	0.4	18-59	7.1	0.5	0-37	15.0	0.5	0-31	0.7	0.1	0-17	8.4	0.4	0-26	3.4	0.4	0-37	20.9	0.6	0-59	9	60*	27*
C OMPP	15	3.8	0.4	0-30	39.7	0.4	18-59	8.2	0.6	0-41	13.7	0.5	0-31	0.5	0.1	0-15	7.2	0.4	0-23	3.5	0.4	0-37	23.4	0.6	0-60	9	62*	28*
C zero	16	5.8	0.3	0-19	1.0	0.1	0-6	6.7	0.7	0-80	83.2	0.7	0-98	0.5	0.1	0-7	0.2	0.0	0-3	2.5	0.5	0-72	0.1	0.0	0-6	8	15	10
C PP	16	5.0	0.2	0-15	1.0	0.1	0-6	7.4	0.7	0-69	82.9	0.7	7-98	0.4	0.1	0-6	0.2	0.0	0-3	2.8	0.4	0-63	0.3	0.0	0-8	8	15	10
C GS	16	0.0	0.0	0-4	0.0	0.0	0-2	12.1	1.2	0-100	83.6	1.2	0-100	4.1	0.2	0-14	0.0	0.0	0-1	0.2	0.1	0-30	0.0	0.0	0-0	25*	35*	28*
C GSPP	16	0.0	0.0	0-3	0.0	0.0	0-2	14.2	1.2	0-100	83.0	1.1	0-100	2.5	0.1	0-10	0.0	0.0	0-1	0.2	0.1	0-19	0.0	0.0	0-0	24*	36*	28*
C OM	16	2.4	0.3	0-26	8.6	0.5	0-31	2.3	0.3	0-34	64.6	0.8	1-87	3.2	0.3	0-19	1.7	0.2	0-16	12.5	1.0	0-86	4.9	0.3	0-28	11	19*	14
C OMPP	16	2.4	0.3	0-26	7.5	0.4	0-30	2.0	0.3	0-35	64.4	0.8	4-85	4.0	0.3	0-19	1.9	0.2	0-16	13.9	1.0	0-84	3.9	0.3	0-24	11	19*	14
C zero	17	28.0	0.5	0-44	0.2	0.0	0-7	10.2	1.1	0-87	57.1	1.0	0-82	0.5	0.1	0-15	0.6	0.1	0-6	1.1	0.3	0-56	2.3	0.1	0-12	11	15	12
C PP	17	25.0	0.4	0-39	0.2	0.0	0-7	12.5	1.1	0-87	56.8	1.1	0-79	0.4	0.1	0-13	0.6	0.1	0-6	1.2	0.3	0-52	3.3	0.2	0-14	11	16*	12
C GS	17	0.2	0.1	0-20	0.2	0.0	0-5	17.3	1.6	0-92	59.8	1.5	0-84	21.6	0.3	6-35	0.1	0.0	0-5	0.8	0.3	0-51	0.0	0.0	0-1	25*	26*	25*
C GSPP	17	0.2	0.1	0-12	0.1	0.0	0-5	22.6	1.7	0-94	58.6	1.6	0-86	17.8	0.2	3-29	0.1	0.0	0-5	0.6	0.2	0-44	0.0	0.0	0-1	25*	29*	27*
C OM	17	20.0	0.9	0-49	4.4	0.3	0-22	5.4	0.5	0-61	35.4	0.7	0-56	5.7	0.5	0-31	2.2	0.2	0-21	3.5	0.6	0-63	23.4	0.5	0-51	11	22*	15
C OMPP	17	19.8	0.9	0-49	4.0	0.3	0-21	5.8	0.5	0-66	36.0	0.7	0-56	6.4	0.5	0-30	2.4	0.2	0-21	4.0	0.6	0-63	21.6	0.5	0-46	11	21*	14
C zero	18	23.6	0.5	0-42	0.1	0.0	0-7	10.4	1.1	0-91	60.8	1.0	0-85	0.8	0.1	0-14	1.6	0.1	0-9	0.9	0.3	0-50	1.8	0.1	0-11	11	12	11
C PP	18	21.1	0.4	0-37	0.1	0.0	0-6	12.4	1.1	0-91	60.5	1.0	0-83	0.6	0.1	0-12	1.7	0.1	0-8	1.0	0.3	0-46	2.6	0.2	0-13	10	13	11
C GS	18	0.1	0.1	0-15	0.1	0.0	0-4	15.9	1.5	0-90	62.9	1.4	0-85	20.2	0.3	3-34	0.2	0.0	0-5	0.6	0.2	0-47	0.0	0.0	0-1	23*	24*	23*
C GSPP	18	0.1	0.0	0-9	0.1	0.0	0-3	20.7	1.5	0-93	61.8	1.4	0-87	16.7	0.2	0-28	0.3	0.1	0-6	0.4	0.2	0-39	0.0	0.0	0-1	23*	26*	24*
C OM	18	24.7	0.8	0-52	4.8	0.3	0-25	8.2	0.7	0-61	33.5	0.7	0-53	3.7	0.4	0-32	6.1	0.3	0-28	1.6	0.4	0-52	17.4	0.5	0-46	9	21*	14
C OMPP	18	24.2	0.8	0-51	4.7	0.3	0-25	9.5	0.8	0-62	33.7	0.7	0-53	3.1	0.4	0-29	6.1	0.3	0-28	1.7	0.4	0-51	17.1	0.5	0-45	9	20*	13
C zero	19	10.9	0.5	0-31	0.0	0.0	0-2	24.0	1.7	0-100	63.7	1.6	0-96	1.3	0.2	0-12	0.0	0.0	0-2	0.1	0.1	0-25	0.0	0.0	0-0	27*	21*	25*
C PP	19	8.7	0.4	0-25	0.0	0.0	0-1	29.8	1.8	0-100	60.4	1.6	0-95	1.0	0.1	0-9	0.0	0.0	0-2	0.1	0.1	0-27	0.0	0.0	0-2	27*	21*	25*
C GS	19	0.0	0.0	0-13	0.0	0.0	0-2	29.2	1.8	0-100	57.2	1.7	0-92	13.3	0.3	0-30	0.0	0.0	0-3	0.1	0.1	0-36	0.0	0.0	0-0	28*	17*	24*
C GSPP	19	0.0	0.0	0-8	0.0	0.0	0-2	36.5	1.8	0-100	53.5	1.7	0-93	9.8	0.2	0-22	0.0	0.0	0-3	0.1	0.1	0-31	0.0	0.0	0-0	27*	18*	24*
C OM	19	7.1	0.6	0-43	0.7	0.1	0-18	14.7	0.9	0-78	48.5	0.9	0-79	6.3	0.4	0-30	2.0	0.2	0-21	3.5	0.7	0-77	17.1	0.7	0-57	21*	28*	24*
C OMPP	19	6.7	0.6	0-43	0.6	0.1	0-17	14.7	0.9	0-75	49.3	0.9	0-81	8.0	0.4	0-28	2.5	0.3	0-22	4.5	0.7	0-75	13.6	0.6	0-49	21*	27*	23*
C zero	20	17.3	0.5	0-36	0.0	0.0	0-4	15.0	1.3	0-98	65.6	1.2	0-92	0.9	0.1	0-12	0.5	0.1	0-7	0.4	0.2	0-35	0.2	0.0	0-8	15*	12	14
C PP	20	14.8	0.4	0-30	0.0	0.0	0-4	18.6	1.4	0-98	64.3	1.3	0-92	0.7	0.1	0-10	0.6	0.1	0-7	0.4	0.2	0-35	0.5	0.1	0-11	15*	12	14
C GS	20	0.0	0.0	0-1	0.0	0.0	0-2	21.8	1.8	0-100	63.9	1.7	0-92	14.3	0.3	0-30	0.0	0.0	0-2	0.1	0.1	0-33	0.0	0.0	0-0	40*	32*	37*
C GSPP	20	0.0	0.0	0-0	0.0	0.0	0-1	28.3	1.9	0-100	61.5	1.7	0-94	10.1	0.2	0-23	0.0	0.0	0-2	0.1	0.1	0-23	0.0	0.0	0-0	39*	35*	37*
C OM	20	11.9	0.7	0-45	2.2	0.2	0-22	8.3	0.7	0-70	44.8	0.8	0-69	5.3	0.4	0-28	3.1	0.3	0-21	2.5	0.6	0-69	21.9	0.5	0-51	14	27*	19*
C OMPP	20	11.7	0.7	0-43	1.8	0.2	0-19	9.3	0.7	0-77	45.7	0.8	0-70	5.9	0.4	0-27	3.5	0.3	0-23	2.8	0.6	0-69	19.3	0.5	0-45	14	25*	18*
C zero	21	3.3	0.4	0-36	0.0	0.0	0-0	46.2	1.4	0-95	40.7	1.3	0-87	1.5	0.2	0-17	8.3	0.2	0-16	0.0	0.0	0-10	0.1	0.0	0-5	16*	35*	23*
C PP	21	2.2	0.3	0-32	0.0	0.0	0-0	49.4	1.4	0-95	38.8	1.2	0-87	1.3	0.1	0-13	8.2	0.1	0-15	0.0	0.0	0-8	0.0	0.0	0-5	16*	35*	23*
C GS	21	0.0	0.0	0-0	0.0	0.0	0-0	51.0	2.0	0-100	35.7	1.7	0-89	13.3	0.4	0-35	0.0	0.0	0-6	0.0	0.0	0-0	0.0	0.0	0-0	95*	85*	91*
C GSPP	21	0.0	0.0	0-0	0.0	0.0	0-0	60.8	1.9	0-100	31.7	1.7	0-92	7.5	0.3	0-26	0.0	0.0	0-4	0.0	0.0	0-0	0.0	0.0	0-0	94*	88*	92*
C OM	21	7.5	0.6	0-46	0.2	0.1	0-11	35.3	1.1	0-77	18.6	0.7	0-49	4.5	0.5	0-39	28.2	0.6	0-51	0.0	0.0	0-11	5.7	0.6	0-56	20*	47*	30*
C OMPP	21	6.9	0.6	0-43	0.2	0.1	0-13	39.5	1.1	0-79	17.6	0.7	0-49	3.7	0.4	0-36	27.1	0.5	0-47	0.0	0.0	0-9	5.0	0.6	0-56	20*	45*	29*
C zero	22	2.5	0.3	0-33	0.0	0.0	0-0	55.6	1.3	0-95	32.7	1.2	0-86	1.2	0.1	0-14	7.9	0.1	0-15	0.0	0.0	0-4	0.1	0.0	0-6	15	34*	22*
C PP	22	1.6	0.2	0-27	0.0	0.0	0-0	58.4	1.3	0-95	31.0	1.1	0-87	1.1	0.1	0-12	7.8	0.1	1-14	0.0	0.0	0-3	0.1	0.0	0-5	14	33*	21*
C GS	22	0.0	0.0	0-0	0.0	0.0	0-0	60.3	1.9	0-100	28.0	1.6	0-88	11.6	0.4	0-33	0.0	0.0	0-5	0.0	0.0	0-0	0.0	0.0	0-0	91*	84*	88*
C GSPP	22	0.0	0.0	0-0	0.0	0.0	0-0	69.6	1.7	0-100	24.1	1.5	0-90	6.3	0.3	0-23	0.0	0.0	0-3	0.0	0.0	0-0	0.0	0.0	0-0	90*	87*	89*
C OM	22	4.8	0.5	0-37	0.0	0.0	0-4	43.8	1.0	0-81	15.7	0.6	0-50	3.5	0.4	0-31	26.1	0.5	0-46	0.0	0.0	0-9	6.0	0.6	0-52	17*	45*	27*
C OMPP	22	4.5	0.5	0-34	0.0	0.0	0-8	47.3	1.0	1-82	14.9	0.6	0-50	3.0	0.3	0-29	25.3	0.5	0-43	0.0	0.0	0-8	4.8	0.5	0-50	17*	43*	26*
C zero	27	0.0	0.0	0-0	12.7	0.2	2-21	0.5	0.2	0-36	55.6	1.3	0-87	0.0	0.0	0-4	1.7	0.1	0-8	29.2	1.4	0-93	0.1	0.0	0-7	13	29*	18*
C PP	27	0.0	0.0	0-0	12.6	0.2	2-21	0.4	0.2	0-33	57.3	1.2	0-87	0.0	0.0	0-5	2.1	0.1	0-9	27.5	1.4	0-93	0.1	0.0	0-7	13	29*	18*
C GS	27	0.0	0.0	0-3	12.9	0.2	0-21	0.6	0.2	0-36	68.6	1.0	0-88	0.2	0.1	0-8	1.5	0.1	0-9	16.2	1.1	0-93	0.0	0.0	0-2	12	41*	22*

		Motte			Hulpe			Velpe			Gete			Zwartebeek			Mangelbeek			Herk			Demer (upstream)			relative mean error		
Nr outlet sample	code model	contribution	95% CI	range	contribution	95% CI	range	contribution	95% CI	range	contribution	95% CI	range	contribution	95% CI	range	contribution	95% CI	range	contribution	95% CI	range	contribution	95% CI	range	RME (%)	RME_val (%)	RME_avg (%)
C OM	27	0.2	0.1	0-24	44.7	0.4	22-60	4.0	0.5	0-65	41.4	0.5	0-56	0.2	0.1	0-14	5.2	0.3	0-18	4.1	0.5	0-64	0.3	0.1	0-36	19*	40*	27*
C OMPP	27	0.2	0.1	0-19	44.7	0.4	22-59	4.1	0.5	0-68	42.5	0.6	0-57	0.1	0.0	0-11	4.2	0.2	0-17	3.8	0.5	0-66	0.5	0.2	0-36	19*	41*	27*
C zero	28	14.5	0.4	0-30	1.7	0.1	0-11	5.9	0.8	0-84	63.2	0.9	0-82	0.5	0.1	0-11	1.2	0.1	0-7	4.5	0.7	0-82	8.5	0.2	0-22	6	9	7
C PP	28	13.1	0.4	0-26	1.6	0.1	0-9	6.4	0.8	0-87	63.3	0.9	0-82	0.4	0.1	0-10	1.2	0.1	0-7	4.7	0.7	0-76	9.2	0.2	0-22	5	10	7
C GS	28	4.0	0.4	0-31	1.8	0.1	0-10	12.6	1.3	0-90	64.8	1.3	0-85	9.4	0.4	0-24	2.4	0.2	0-14	3.3	0.7	0-74	1.8	0.1	0-10	10	13	11
C GSPP	28	3.4	0.3	0-27	1.5	0.1	0-9	14.7	1.2	0-91	64.3	1.3	0-86	8.0	0.3	0-21	2.4	0.2	0-12	3.5	0.7	0-67	2.2	0.1	0-10	10	15	12
C OM	28	16.3	0.7	0-42	12.0	0.4	0-35	7.7	0.7	0-52	34.5	0.6	0-52	1.7	0.3	0-22	5.6	0.3	0-23	1.6	0.4	0-59	20.6	0.5	0-56	8	13	10
C OMPP	28	14.8	0.7	0-41	12.3	0.4	0-35	9.4	0.7	0-54	34.0	0.6	0-52	1.3	0.2	0-20	5.4	0.3	0-22	1.5	0.4	0-56	21.3	0.5	1-58	8	13	10
C zero	29	15.4	0.5	0-31	0.1	0.0	0-5	19.7	1.3	0-97	62.1	1.1	0-89	1.2	0.2	0-12	0.4	0.0	0-6	0.6	0.2	0-35	0.6	0.1	0-11	12	16*	14
C PP	29	13.8	0.4	0-27	0.1	0.0	0-4	23.0	1.3	0-95	60.1	1.1	0-89	0.9	0.1	0-10	0.5	0.1	0-6	0.6	0.2	0-33	1.0	0.1	0-12	12	16*	14
C GS	29	2.1	0.3	0-20	0.4	0.1	0-7	26.1	1.4	0-94	57.7	1.4	0-88	11.5	0.3	0-26	0.7	0.1	0-8	1.1	0.3	0-45	0.3	0.0	0-5	13	14	13
C GSPP	29	2.3	0.3	0-20	0.4	0.1	0-6	30.4	1.4	0-95	55.1	1.3	0-89	9.2	0.3	0-21	0.9	0.1	0-8	1.2	0.3	0-40	0.5	0.1	0-6	12	14	13
C OM	29	9.7	0.7	0-43	1.6	0.2	0-17	12.5	0.8	0-72	46.5	0.8	0-70	7.1	0.5	0-29	1.9	0.2	0-22	5.1	0.7	0-71	15.6	0.5	0-47	13	24*	17*
C OMPP	29	9.3	0.7	0-42	1.3	0.2	0-15	12.5	0.8	0-69	46.5	0.8	0-70	8.1	0.5	0-28	2.2	0.2	0-22	6.2	0.7	0-68	13.8	0.5	0-41	13	23*	17*
C zero	30	20.2	0.5	0-35	0.1	0.0	0-5	23.3	1.4	0-93	53.6	1.2	0-87	1.0	0.2	0-13	0.1	0.0	0-5	0.8	0.3	0-42	0.8	0.1	0-13	14	16*	15
C PP	30	18.1	0.4	0-32	0.2	0.0	0-5	27.5	1.4	0-93	51.0	1.3	0-85	0.7	0.1	0-12	0.2	0.0	0-4	1.0	0.3	0-43	1.4	0.1	0-14	14	17*	15
C GS	30	6.3	0.5	0-28	1.0	0.1	0-8	29.7	1.5	0-93	49.0	1.5	0-84	10.8	0.4	0-27	0.6	0.1	0-7	1.8	0.4	0-51	0.9	0.1	0-8	14	14	14
C GSPP	30	6.6	0.5	0-28	1.0	0.1	0-9	34.7	1.5	0-94	45.5	1.5	0-83	8.3	0.4	0-22	0.7	0.1	0-8	1.9	0.4	0-54	1.3	0.1	0-9	14	14	14
C OM	30	4.7	0.5	0-38	0.8	0.1	0-15	9.3	0.7	0-67	44.7	1.0	0-75	6.5	0.4	0-28	1.6	0.2	0-21	13.1	1.0	0-85	19.4	0.7	0-55	18*	22*	19*
C OMPP	30	4.6	0.5	0-37	0.6	0.1	0-14	7.8	0.7	0-64	44.0	1.0	0-75	9.5	0.4	0-30	2.2	0.3	0-22	15.7	1.1	0-84	15.5	0.7	0-46	18*	21*	19*
C zero	31	16.0	0.6	0-33	0.2	0.0	0-5	25.8	1.4	0-94	54.0	1.3	0-88	2.3	0.2	0-15	0.3	0.0	0-4	0.9	0.3	0-42	0.5	0.1	0-11	15*	19*	17*
C PP	31	14.8	0.5	0-30	0.3	0.0	0-5	30.0	1.4	0-94	50.6	1.3	0-87	1.8	0.2	0-12	0.3	0.0	0-5	1.2	0.3	0-44	1.0	0.1	0-13	15*	20*	17*
C GS	31	7.6	0.6	0-32	1.6	0.1	0-12	31.8	1.5	0-93	44.9	1.4	0-80	8.4	0.4	0-26	1.2	0.1	0-11	2.8	0.5	0-63	1.7	0.1	0-11	16*	17*	16*
C GSPP	31	7.7	0.5	0-30	1.7	0.1	0-11	35.9	1.4	0-92	41.6	1.4	0-81	6.5	0.4	0-21	1.4	0.1	0-10	3.1	0.6	0-61	2.2	0.2	0-12	15*	18*	16*
C OM	31	3.6	0.5	0-38	0.7	0.1	0-14	11.0	0.8	0-68	45.5	1.0	0-79	7.4	0.4	0-30	2.6	0.3	0-21	15.0	1.0	0-87	14.1	0.7	0-51	20*	20*	20*
C OMPP	31	3.4	0.5	0-37	0.6	0.1	0-14	8.8	0.7	0-65	44.4	1.1	0-80	10.2	0.5	0-33	3.2	0.3	0-22	18.0	1.1	0-86	11.4	0.7	0-45	20*	20*	20*
C zero	32	7.6	0.5	0-31	0.0	0.0	0-1	42.9	1.9	0-100	47.0	1.7	0-96	2.4	0.2	0-15	0.0	0.0	0-3	0.1	0.1	0-21	0.0	0.0	0-0	32*	40*	35*
C PP	32	6.4	0.4	0-24	0.0	0.0	0-1	50.2	1.8	0-100	41.6	1.7	0-95	1.8	0.2	0-12	0.0	0.0	0-2	0.1	0.1	0-24	0.0	0.0	0-2	32*	40*	35*
C GS	32	7.4	0.6	0-33	0.8	0.1	0-10	45.9	1.5	0-92	33.0	1.4	0-80	9.5	0.5	0-27	0.9	0.1	0-11	1.0	0.3	0-48	1.5	0.1	0-11	23*	28*	25*
C GSPP	32	8.5	0.5	0-29	1.0	0.1	0-10	51.1	1.4	0-90	28.3	1.3	0-81	6.9	0.4	0-22	1.0	0.1	0-10	1.2	0.3	0-47	2.0	0.2	0-13	23*	29*	25*
C OM	32	0.2	0.1	0-18	0.0	0.0	0-0	18.5	1.0	0-66	54.4	1.3	0-97	1.7	0.2	0-24	2.4	0.3	0-22	12.6	1.1	0-87	10.2	0.7	0-42	31*	32*	31*
C OMPP	32	0.2	0.1	0-27	0.0	0.0	0-0	13.5	0.9	0-71	53.7	1.5	0-97	4.4	0.4	0-27	4.5	0.4	0-23	15.7	1.3	0-90	7.9	0.6	0-39	31*	33*	32*
C zero	33	20.5	0.6	0-38	0.2	0.0	0-6	22.5	1.4	0-92	52.4	1.3	0-85	2.0	0.2	0-16	0.3	0.1	0-6	0.9	0.3	0-52	1.2	0.1	0-14	17*	23*	20*
C PP	33	18.5	0.5	0-35	0.3	0.0	0-5	26.8	1.4	0-92	49.4	1.3	0-84	1.5	0.2	0-13	0.4	0.1	0-6	1.1	0.3	0-52	2.1	0.2	0-16	17*	24*	20*
C GS	33	11.3	0.7	0-38	1.7	0.1	0-12	27.8	1.5	0-88	43.7	1.4	0-75	7.8	0.5	0-26	1.4	0.1	0-13	2.6	0.6	0-73	3.8	0.2	0-16	17*	22*	19*
C GSPP	33	10.8	0.6	0-34	1.8	0.1	0-12	32.0	1.5	0-87	40.4	1.4	0-77	6.2	0.4	0-23	1.4	0.1	0-13	2.7	0.6	0-70	4.7	0.2	0-17	17*	23*	19*
C OM	33	4.6	0.5	0-40	0.9	0.1	0-15	9.2	0.7	0-63	45.0	1.0	0-79	7.5	0.4	0-31	2.8	0.3	0-26	10.7	1.0	0-82	19.3	0.8	0-59	21*	24*	22*
C OMPP	33	4.4	0.5	0-40	0.7	0.1	0-15	7.8	0.7	0-62	44.4	1.0	0-76	10.1	0.5	0-32	3.6	0.4	0-27	13.3	1.0	0-82	15.7	0.7	0-51	21*	23*	21*
C zero	34	15.5	0.7	0-36	3.1	0.1	0-14	18.7	1.3	0-89	43.8	1.2	0-77	3.3	0.3	0-16	0.9	0.1	0-9	7.3	0.9	0-80	7.3	0.3	0-24	11	21*	15
C PP	34	14.9	0.6	0-34	3.1	0.1	0-14	20.6	1.3	0-88	41.4	1.2	0-77	2.7	0.3	0-15	0.9	0.1	0-8	7.8	0.9	0-81	8.5	0.3	0-26	11	22*	15*
C GS	34	8.6	0.7	0-36	3.4	0.2	0-16	22.5	1.3	0-87	45.6	1.3	0-75	10.1	0.5	0-28	1.5	0.2	0-13	5.1	0.8	0-80	3.2	0.2	0-14	13	20*	15*
C GSPP	34	8.0	0.6	0-33	3.3	0.2	0-16	25.8	1.4	0-88	43.0	1.3	0-75	8.7	0.4	0-25	1.7	0.2	0-13	5.6	0.8	0-81	4.0	0.2	0-15	12	21*	16*
C OM	34	4.4	0.5	0-38	2.7	0.3	0-20	2.5	0.4	0-42	37.5	1.0	0-71	8.8	0.5	0-32	2.9	0.3	0-25	22.9	1.2	0-86	18.4	0.7	0-50	18*	19*	18*
C OMPP	34	4.1	0.5	0-40	2.0	0.2	0-19	1.9	0.3	0-39	36.0	1.1	0-72	11.7	0.5	0-34	3.7	0.3	0-26	25.7	1.2	0-84	14.9	0.7	0-48	18*	18*	18*
C zero	35	17.2	0.9	0-44	3.7	0.2	0-15	17.4	1.3	0-84	44.3	1.3	0-79	5.4	0.4	0-21	1.3	0.1	0-12	7.2	0.9	0-83	3.4	0.2	0-20	15*	22*	17*
C PP	35	16.8	0.8	0-41	3.9	0.2	0-15	19.8	1.4	0-85	41.1	1.3	0-78	4.5	0.4	0-19	1.4	0.1	0-11	8.0	1.0	0-83	4.5	0.3	0-21	15	23*	18*
C GS	35	2.6	0.4	0-36	1.8	0.1	0-11	17.7	1.4	0-89	54.8	1.4	0-81	20.3	0.4	0-33	0.4	0.1	0-8	2.4	0.5	0-71	0.1	0.0	0-4	17*	33*	23*
C GSPP	35	2.9	0.4	0-32	1.8	0.1	0-10	22.0	1.5	0-89	52.3	1.5	0-81	17.4	0.4	0-29	0.6	0.1	0-8	2.7	0.5	0-67	0.2	0.0	0-6	18*	35*	24*
C OM	35	4.8	0.6	0-42	4.1	0.3	0-25	2.0	0.3	0-52	39.2	1.1	0-75	11.0	0.6	0-40	4.6	0.4	0-28	21.9	1.3	0-85	12.3	0.7	0-48	21*	17*	20*
C OMPP	35	4.4	0.6	0-43	3.1	0.3	0-23	1.4	0.3	0-37	37.7	1.1	0-73	13.8	0.6	0-40	5.4	0.4	0-30	24.7	1.3	0-83	9.6	0.6	0-46	21*	16*	19*
C zero	36	11.5	0.7	0-40	5.6	0.2	0-19	19.0	1.3	0-80	37.7	1.2	0-74	4.7	0.3	0-18	1.8	0.2	0-13	9.8	1.1	0-83	10.0	0.4	0-28	12	21*	15*
C PP	36	11.3	0.7	0-37	5.6	0.2	0-18	20.7	1.3	0-80	34.9	1.2	0-72	4.0	0.3	0-17	1.8	0.2	0-12	10.5	1.1	0-82	11.2	0.4	0-30	12	22*	16*
C GS	36	10.1	0.7	0-37	6.0	0.2	0-20	19.5	1.3	0-79	38.2	1.2	0-70	8.0	0.5	0-28	2.3	0.2	0-15	8.7	1.0	0-75	7.2	0.3	0-21	12	20*	15*
C GSPP	36	9.5	0.7	0-35	6.0	0.2	0-20	21.7	1.3	0-77	35.9	1.3	0-70	7.1	0.5	0-27	2.4	0.2	0-16	9.2	1.0	0-75	8.2	0.3	0-22	12	21*	15*
C OM	36	12.4	0.7	0-44	1.8	0.2	0-20	0.6	0.2	0-27	37.4	1.1	0-78	2.1	0.3	0-24	2.6	0.3	0-25	28.3	1.3	0-90	14.9	0.8	0-49	19*	17*	18*
C OMPP	36	15.5	0.7	0-45	1.1	0.2	0-18	0.3	0.1	0-25	35.3	1.2	0-76	3.2	0.4	0-27	3.7	0.4	0-28	30.4	1.3	0-87	10.5	0.7	0-46	19*	15*	18*
C zero	37	22.1	0.8	0-42	1.5	0.1	0-9	15.3	1.2	0-87	52.0	1.2	0-82	3.0	0.3	0-19	0.5	0.1	0-6	3.6	0.6	0-74	2.1	0.2	0-16	14	28*	19*
C PP	37	20.8	0.7	0-39	1.6	0.1	0-9	18.0	1.3	0-88	49.3	1.2	0-82	2.4	0.3	0-17	0.5	0.1	0-7	4.3	0.7	0-72	3.1	0.2	0-18	14	29*	19*
C GS	37	13.1	0.8	0-38	5.1	0.2	0-19	21.2	1.3	0-78	38.4	1.2	0-71	7.5	0.5	0-28	1.4	0.2	0-14	7.0	0.9	0-77	6.3	0.3	0-20	14	26*	18*
C GSPP	37	12.8	0.7	0-36	5.3	0.2	0-19	23.7	1.3	0-77	35.8	1.2	0-70	6.5	0.5	0-26	1.4	0.2	0-13	7.4	0.9	0-74	7.2	0.3	0-21	14	27*	18*
C OM	37	0.8	0.2	0-28	1.2	0.2	0-20	1.3	0.3	0-44	46.2	1.3	0-89	3.1	0.3	0-28	3.4	0.3	0-25	29.0	1.4	0-99	15.1	0.8	0-45	24*	18*	22*
C OMPP	37	0.7	0.2	0-30	0.9	0.2	0-18	0.7	0.2	0-34	44.5	1.4	0-87	6.4	0.4	0-29	5.3	0.4	0-30	31.3	1.5	0-96	10.2	0.7	0-43	24*	17*	21*
C zero	38	18.7	0.8	0-40	3.1	0.1	0-14	17.3	1.2	0-86	43.6	1.2	0-77	3.6	0.3	0-18	0.8	0.1	0-9	6.8	0.9	0-79	6.1	0.3	0-22	12	20*	15
C PP	38	17.9	0.7	0-37	3.2	0.1	0-14	19.4	1.3	0-84	40.9	1.2	0-76	3.0	0.3	0-16	0.8	0.1	0-9	7.5	0.9	0-79	7.4	0.3	0-24	12	21*	15*
C GS	38	10.6	0.8	0-39	4.0	0.2	0-18	21.4	1.3	0-85	43.1	1.3	0-73	10.6	0.5	0-30	1.3	0.1	0-13	5.5	0.8	0-78	3.5	0.2	0-15	13	19*	15*
C GSPP	38	10.0	0.7	0-36	4.0	0.2	0-18	24.6	1.3	0-84	40.5	1.3	0-72	9.3	0.5	0-27	1.4	0.1	0-13	5.9	0.9	0-78	4.3	0.2	0-16	13	21*	16*
C OM	38	5.1	0.6	0-40	3.3	0.3	0-22	2.1	0.3	0-41	36.8	1.0	0-70	9.9	0.5	0-34	2.9	0.3	0-25	22.4	1.2	0-83	17.6	0.8	0-50	18*	15*	17*
C OMPP	38	4.7	0.6	0-43	2.5	0.3	0-20	1.5	0.3	0-36	35.4	1.1	0-72	13.1	0.5	0-36	3.6	0.3	0-26	25.1	1.2	0-83	14.1	0.7	0-48	18*	15	17*

Table F.5: Modeled contributions of the eight tributaries to the suspended sediment flux sampled at the Aarschot outlet station, using Composite Fingerprint D and the Monte Carlo simulated property concentrations in the objective function; * = failing the RME test.

Nr outlet sample	code model	Motte			Hulpe			Velpe			Gete			Zwartebeek			Mangelbeek			Herk			Demer (upstream)			relative mean error	
		contribution	95% CI	range	contribution	95% CI	range	contribution	95% CI	range	contribution	95% CI	range	contribution	95% CI	range	contribution	95% CI	range	contribution	95% CI	range	contribution	95% CI	range	RME (%)	RME_val (%)	RME_avg (%)
D zero	13	4.3	0.6	0-51	15.1	0.2	5-28	31.0	1.2	0-70	3.7	0.5	0-53	18.1	0.6	0-38	3.0	0.2	0-15	22.2	1.1	0-73	2.6	0.2	0-12	10	9	10
D PP	13	4.7	0.6	0-52	15.2	0.2	5-28	31.1	1.2	0-67	3.0	0.4	0-51	18.6	0.6	0-38	3.1	0.2	0-15	21.6	1.1	0-69	2.7	0.2	0-12	10	10	10
D GS	13	0.2	0.1	0-21	23.2	0.3	11-41	8.1	1.0	0-55	0.4	0.3	0-50	0.0	0.0	0-0	1.0	0.1	0-10	44.3	1.2	0-67	23.4	0.4	11-40	21*	26*	23*
D GSPP	13	0.4	0.1	0-26	24.5	0.3	13-43	7.4	0.9	0-53	0.4	0.2	0-48	0.0	0.0	0-0	1.0	0.1	0-13	42.3	1.1	0-64	24.0	0.4	11-41	21*	26*	23*
D OM	13	7.6	0.9	0-86	16.3	0.3	0-40	2.4	0.1	0-9	0.2	0.0	0-6	73.6	0.8	11-100	0.0	0.0	0-0	0.0	0.0	0-3	0.0	0.0	0-0	42*	66*	51*
D OMPP	13	9.0	0.9	0-81	16.4	0.3	0-39	2.5	0.1	0-9	0.2	0.0	0-6	71.9	0.8	15-87	0.0	0.0	0-0	0.0	0.0	0-3	0.0	0.0	0-0	43*	66*	51*
D zero	14	4.7	0.6	0-51	15.3	0.2	3-28	43.8	1.2	0-79	11.3	0.9	0-67	13.6	0.6	0-34	2.9	0.2	0-15	8.5	0.9	0-71	0.1	0.0	0-7	13	15	14
D PP	14	4.5	0.6	0-53	15.5	0.2	4-28	44.7	1.2	0-78	9.7	0.8	0-66	13.7	0.6	0-34	3.4	0.2	0-16	8.3	0.9	0-70	0.0	0.0	0-6	13	16*	14
D GS	14	0.5	0.2	0-58	10.2	0.2	0-19	30.5	1.3	0-73	23.2	1.2	0-62	33.1	0.4	0-49	0.0	0.0	0-4	2.4	0.5	0-60	0.0	0.0	0-0	13	21*	16*
D GSPP	14	0.6	0.2	0-54	10.5	0.2	0-19	32.1	1.3	0-71	21.2	1.2	0-60	33.1	0.3	3-47	0.1	0.0	0-5	2.4	0.5	0-60	0.0	0.0	0-0	13	21*	16*
D OM	14	4.1	0.6	0-53	26.0	0.5	0-49	19.8	1.0	0-65	15.3	0.9	0-54	4.0	0.5	0-42	7.6	0.4	0-26	21.6	1.1	0-70	1.7	0.2	0-21	16*	7	13
D OMPP	14	3.7	0.6	0-52	25.3	0.5	0-49	18.9	1.0	0-63	13.7	0.9	0-52	3.5	0.5	0-39	9.2	0.4	0-28	24.1	1.1	0-69	1.7	0.2	0-23	16*	7	13
D zero	15	2.1	0.4	0-67	15.5	0.3	0-29	39.6	2.1	0-89	31.3	2.0	0-89	2.5	0.3	0-25	0.0	0.0	0-5	9.0	1.4	0-100	0.0	0.0	0-0	28*	7	20*
D PP	15	2.0	0.4	0-57	15.8	0.3	0-29	40.8	2.1	0-88	28.9	2.0	0-87	3.2	0.3	0-25	0.1	0.0	0-6	9.1	1.4	0-99	0.0	0.0	0-0	28*	6	20*
D GS	15	0.3	0.2	0-29	15.0	0.3	0-34	39.9	2.0	0-89	28.0	1.9	0-88	12.0	0.7	0-52	0.0	0.0	0-6	4.7	0.9	0-98	0.0	0.0	0-0	28*	4	19*
D GSPP	15	0.4	0.2	0-30	15.3	0.3	0-32	41.1	2.0	0-89	26.0	1.9	0-87	12.1	0.7	0-49	0.1	0.0	0-7	4.9	1.0	0-96	0.0	0.0	0-0	28*	4	19*
D OM	15	5.7	1.0	0-91	41.6	0.9	2-79	18.7	0.7	0-43	4.3	0.5	0-31	28.2	1.1	0-70	0.5	0.2	0-30	1.0	0.2	0-26	0.0	0.0	0-0	27*	27*	27*
D OMPP	15	5.8	1.0	0-89	40.6	0.8	4-79	18.9	0.7	0-42	4.6	0.5	0-30	28.6	1.1	0-68	0.5	0.2	0-31	1.0	0.2	0-27	0.0	0.0	0-0	27*	27*	27*
D zero	16	3.1	0.3	0-22	0.8	0.1	0-5	16.2	1.2	0-100	77.1	1.2	0-100	1.1	0.1	0-10	0.0	0.0	0-1	1.7	0.4	0-83	0.0	0.0	0-0	13	4	10
D PP	16	2.6	0.3	0-20	0.8	0.1	0-5	18.0	1.2	0-100	75.7	1.2	0-100	1.1	0.1	0-10	0.0	0.0	0-2	1.8	0.4	0-73	0.0	0.0	0-0	13	4	10
D GS	16	0.0	0.0	0-0	0.0	0.0	0-0	18.6	1.6	0-100	70.8	1.4	0-100	10.4	0.4	0-31	0.0	0.0	0-0	0.2	0.1	0-52	0.0	0.0	0-0	30*	25*	28*
D GSPP	16	0.0	0.0	0-0	0.0	0.0	0-0	21.1	1.6	0-100	70.5	1.4	0-100	8.4	0.4	0-27	0.0	0.0	0-0	0.1	0.1	0-38	0.0	0.0	0-0	30*	25*	28*
D OM	16	1.5	0.3	0-26	15.0	0.4	0-34	16.9	0.9	0-65	54.3	1.1	0-88	0.9	0.2	0-18	1.0	0.1	0-14	10.1	1.0	0-92	0.3	0.1	0-10	13	15*	14
D OMPP	16	1.3	0.2	0-24	13.5	0.4	0-32	17.3	0.9	0-67	54.5	1.1	0-88	0.7	0.1	0-17	1.0	0.1	0-13	11.5	1.0	0-91	0.2	0.1	0-9	14	14	14
D zero	17	25.2	1.0	0-61	0.3	0.0	0-6	13.1	1.2	0-84	52.9	1.2	0-84	7.9	0.5	0-34	0.1	0.0	0-4	0.5	0.2	0-61	0.0	0.0	0-0	12	13	12
D PP	17	23.8	1.0	0-57	0.4	0.0	0-6	15.3	1.2	0-86	51.8	1.1	0-81	8.0	0.5	0-32	0.1	0.0	0-4	0.6	0.2	0-58	0.0	0.0	0-0	12	13	12
D GS	17	0.0	0.0	0-12	0.2	0.0	0-4	12.3	1.2	0-81	48.4	1.1	0-75	38.8	0.4	19-57	0.0	0.0	0-0	0.3	0.2	0-53	0.0	0.0	0-0	20*	23*	21*
D GSPP	17	0.0	0.0	0-6	0.1	0.0	0-3	15.0	1.3	0-83	48.4	1.1	0-75	36.2	0.4	16-52	0.0	0.0	0-0	0.2	0.1	0-49	0.0	0.0	0-0	20*	24*	21*
D OM	17	24.0	1.2	0-68	7.5	0.5	0-33	17.6	1.2	0-73	30.6	1.0	0-63	6.8	0.7	0-46	5.8	0.3	0-26	4.5	0.7	0-62	3.2	0.3	0-26	16*	9	13
D OMPP	17	22.4	1.2	0-66	7.4	0.4	0-34	19.9	1.3	0-75	29.8	1.0	0-64	5.9	0.7	0-44	6.6	0.4	0-24	5.1	0.7	0-64	3.0	0.3	0-25	16*	8	13
D zero	18	19.8	0.9	0-55	0.3	0.0	0-6	13.4	1.2	0-94	57.5	1.1	0-85	8.2	0.5	0-32	0.3	0.1	0-5	0.5	0.2	0-60	0.0	0.0	0-0	13	10	12
D PP	18	18.1	0.9	0-51	0.3	0.0	0-5	15.5	1.2	0-94	56.7	1.1	0-83	8.5	0.5	0-29	0.4	0.1	0-6	0.5	0.2	0-58	0.0	0.0	0-0	12	10	12
D GS	18	0.0	0.0	0-3	0.1	0.0	0-3	11.5	1.2	0-86	52.8	1.1	0-78	35.4	0.4	13-53	0.0	0.0	0-0	0.2	0.1	0-50	0.0	0.0	0-0	20*	21*	21*
D GSPP	18	0.0	0.0	0-0	0.0	0.0	0-2	13.8	1.2	0-88	53.0	1.1	0-78	33.0	0.4	12-50	0.0	0.0	0-0	0.1	0.1	0-40	0.0	0.0	0-0	20*	21*	21*
D OM	18	23.3	1.2	0-65	6.5	0.4	0-30	16.0	1.1	0-70	31.3	0.9	0-58	13.7	0.9	0-53	6.8	0.4	0-28	2.0	0.4	0-54	0.5	0.1	0-15	13	13	13
D OMPP	18	22.1	1.2	0-64	6.3	0.4	0-28	18.0	1.2	0-72	31.0	0.9	0-58	12.7	0.9	0-51	7.4	0.4	0-28	2.2	0.4	0-55	0.4	0.1	0-13	13	11	12
D zero	19	9.3	0.7	0-46	0.0	0.0	0-1	27.4	1.9	0-100	58.7	1.6	0-95	4.6	0.4	0-25	0.0	0.0	0-0	0.0	0.1	0-41	0.0	0.0	0-0	31*	16*	26*
D PP	19	7.9	0.6	0-40	0.0	0.0	0-1	32.8	1.9	0-100	55.3	1.7	0-94	3.9	0.3	0-22	0.0	0.0	0-0	0.0	0.1	0-39	0.0	0.0	0-0	31*	15*	25*
D GS	19	0.0	0.0	0-0	0.0	0.0	0-1	24.2	1.6	0-100	47.1	1.4	0-85	28.6	0.6	0-53	0.0	0.0	0-1	0.1	0.1	0-40	0.0	0.0	0-0	31*	23*	28*
D GSPP	19	0.0	0.0	0-0	0.0	0.0	0-1	29.9	1.7	0-100	45.4	1.4	0-86	24.6	0.5	0-46	0.0	0.0	0-1	0.0	0.1	0-36	0.0	0.0	0-0	30*	20*	27*
D OM	19	10.1	0.8	0-50	3.2	0.3	0-24	30.7	1.3	0-95	39.5	1.2	0-81	1.7	0.3	0-31	2.9	0.2	0-21	5.0	0.8	0-67	6.9	0.4	0-32	22*	24*	23*
D OMPP	19	8.0	0.7	0-47	2.6	0.3	0-22	33.8	1.3	0-92	38.9	1.2	0-83	1.1	0.2	0-28	2.9	0.2	0-18	6.0	0.8	0-68	6.7	0.4	0-32	22*	24*	23*
D zero	20	15.8	0.8	0-49	0.0	0.0	0-3	16.7	1.4	0-98	61.4	1.3	0-90	5.8	0.4	0-28	0.0	0.0	0-3	0.1	0.1	0-58	0.0	0.0	0-0	18*	12	16*
D PP	20	14.1	0.7	0-45	0.0	0.0	0-3	19.9	1.5	0-99	60.1	1.3	0-89	5.6	0.4	0-25	0.1	0.0	0-4	0.1	0.1	0-56	0.0	0.0	0-0	18*	11	15*
D GS	20	0.0	0.0	0-0	0.0	0.0	0-1	15.1	1.4	0-100	52.1	1.3	0-83	32.8	0.5	0-55	0.0	0.0	0-0	0.0	0.0	0-18	0.0	0.0	0-0	36*	32*	35*
D GSPP	20	0.0	0.0	0-0	0.0	0.0	0-1	19.1	1.6	0-97	51.9	1.3	0-84	29.0	0.5	3-50	0.0	0.0	0-0	0.0	0.0	0-8	0.0	0.0	0-0	36*	32*	35*
D OM	20	18.4	1.0	0-56	4.3	0.4	0-26	20.2	1.3	0-81	39.7	1.1	0-75	3.9	0.5	0-40	5.7	0.3	0-22	3.4	0.6	0-65	4.4	0.3	0-29	18*	16*	17*
D OMPP	20	16.3	0.9	0-54	3.9	0.3	0-26	23.1	1.3	0-85	39.4	1.1	0-75	3.1	0.4	0-39	6.2	0.3	0-21	3.9	0.7	0-69	4.1	0.3	0-27	18*	15	17*
D zero	21	2.0	0.3	0-29	0.0	0.0	0-1	62.4	1.7	0-100	32.2	1.5	0-96	3.1	0.3	0-23	0.3	0.1	0-7	0.1	0.1	0-22	0.0	0.0	0-0	27*	16*	23*
D PP	21	1.3	0.2	0-24	0.0	0.0	0-1	66.0	1.6	0-100	29.5	1.5	0-95	2.7	0.2	0-19	0.4	0.1	0-8	0.1	0.1	0-20	0.0	0.0	0-0	27*	16*	23*
D GS	21	0.0	0.0	0-0	0.0	0.0	0-0	51.5	2.1	0-100	25.9	1.6	0-90	22.6	0.8	0-59	0.0	0.0	0-0	0.0	0.0	0-0	0.0	0.0	0-0	107*	59*	90*
D GSPP	21	0.0	0.0	0-0	0.0	0.0	0-0	57.9	2.1	0-100	24.2	1.6	0-91	17.9	0.8	0-54	0.0	0.0	0-0	0.0	0.0	0-0	0.0	0.0	0-0	108*	58*	90*
D OM	21	6.7	1.0	0-71	1.8	0.2	0-24	37.8	1.2	0-79	12.5	0.8	0-51	37.0	1.2	0-67	4.1	0.5	0-45	0.2	0.1	0-17	0.0	0.0	0-0	30*	33*	31*
D OMPP	21	5.9	1.0	0-71	1.5	0.2	0-23	40.1	1.2	0-83	12.8	0.8	0-52	35.2	1.1	0-64	4.4	0.5	0-43	0.1	0.1	0-13	0.0	0.0	0-0	30*	31*	30*
D zero	22	1.4	0.2	0-26	0.0	0.0	0-0	70.5	1.6	0-100	25.2	1.4	0-93	2.5	0.2	0-20	0.2	0.0	0-7	0.1	0.1	0-19	0.0	0.0	0-0	26*	15	22*
D PP	22	0.9	0.2	0-21	0.0	0.0	0-1	73.5	1.5	0-100	22.9	1.3	0-95	2.3	0.2	0-17	0.4	0.1	0-7	0.1	0.1	0-19	0.0	0.0	0-0	25*	15	22*
D GS	22	0.0	0.0	0-0	0.0	0.0	0-0	58.3	2.0	0-100	20.5	1.5	0-89	21.2	0.8	0-60	0.0	0.0	0-0	0.0	0.0	0-0	0.0	0.0	0-0	102*	59*	87*
D GSPP	22	0.0	0.0	0-0	0.0	0.0	0-0	64.2	2.0	0-100	18.9	1.5	0-90	16.9	0.8	0-56	0.0	0.0	0-0	0.0	0.0	0-0	0.0	0.0	0-0	103*	58*	87*
D OM	22	5.8	0.9	0-65	1.5	0.2	0-22	46.2	1.1	0-85	10.1	0.8	0-53	32.4	1.0	0-61	3.7	0.5	0-40	0.2	0.1	0-17	0.0	0.0	0-0	27*	30*	28*
D OMPP	22	5.1	0.8	0-65	1.2	0.2	0-21	48.4	1.2	0-86	10.3	0.8	0-54	30.7	1.0	0-59	4.1	0.5	0-38	0.2	0.1	0-15	0.0	0.0	0-0	27*	28*	27*
D zero	27	0.0	0.0	0-0	11.4	0.2	0-23	0.1	0.1	0-27	53.2	1.5	0-83	0.0	0.0	0-0	1.2	0.1	0-9	28.5	1.7	0-95	5.6	0.3	0-24	21*	15	19*
D PP	27	0.0	0.0	0-0	11.7	0.2	0-22	0.1	0.1	0-19	55.2	1.4	0-84	0.0	0.0	0-0	1.6	0.1	0-9	26.6	1.7	0-96	4.8	0.3	0-23	21*	14	18*
D GS	27	0.0	0.0	0-0	13.6	0.2	0-23	0.3	0.1	0-46	65.4	1.1	0-85	0.3	0.1	0-13	3.2	0.2	0-11	16.2	1.3	0-93	1.1	0.1	0-12	20*	24*	22*

		Motte			Hulpe			Velpe			Gete			Zwartebeek			Mangelbeek			Herk			Demer (upstream)			relative mean error		
Nr outlet sample	code model	contribution	95% CI	range	contribution	95% CI	range	contribution	95% CI	range	contribution	95% CI	range	contribution	95% CI	range	contribution	95% CI	range	contribution	95% CI	range	contribution	95% CI	range	RME (%)	RME_val (%)	RME_avg (%)
D OM	27	1.0	0.3	0-49	39.0	0.5	0-58	1.2	0.3	0-37	36.5	0.6	0-50	3.0	0.4	0-41	11.0	0.4	0-30	5.7	0.6	0-56	2.6	0.4	0-38	25*	24*	25*
D OMPP	27	1.2	0.3	0-50	39.6	0.5	0-58	1.0	0.2	0-35	37.2	0.5	0-49	3.3	0.4	0-41	10.9	0.4	0-31	4.4	0.6	0-56	2.3	0.4	0-37	25*	24*	24*
D zero	28	17.3	0.8	0-52	2.6	0.1	0-9	8.5	0.8	0-84	58.8	0.9	0-82	5.6	0.4	0-27	2.3	0.1	0-9	4.1	0.6	0-76	0.8	0.1	0-8	7	10	8
D PP	28	16.2	0.8	0-49	2.6	0.1	0-9	9.4	0.9	0-86	58.5	0.9	0-82	5.5	0.4	0-26	2.5	0.1	0-9	4.4	0.6	0-77	0.8	0.1	0-8	7	10	8
D GS	28	3.9	0.4	0-38	2.6	0.1	0-9	7.7	0.8	0-87	58.5	0.8	0-76	23.9	0.4	0-41	0.8	0.1	0-10	2.4	0.5	0-77	0.1	0.0	0-4	7	13	9
D GSPP	28	4.0	0.4	0-34	2.5	0.1	0-9	8.1	0.8	0-88	59.0	0.8	0-75	22.9	0.4	0-38	0.9	0.1	0-10	2.5	0.5	0-71	0.1	0.0	0-4	7	13	9
D OM	28	22.2	1.1	0-60	8.8	0.4	0-31	7.7	0.7	0-66	37.4	0.7	0-56	12.1	0.8	0-48	6.8	0.3	0-27	2.9	0.5	0-56	2.0	0.2	0-19	7	10	8
D OMPP	28	21.9	1.0	0-58	8.4	0.4	0-29	8.2	0.7	0-65	37.7	0.7	0-56	12.0	0.8	0-47	7.0	0.3	0-26	3.0	0.5	0-56	1.7	0.2	0-18	7	9	8
D zero	29	9.2	0.6	0-39	0.1	0.0	0-4	28.3	1.6	0-100	56.2	1.4	0-90	5.8	0.4	0-22	0.0	0.0	0-3	0.4	0.2	0-59	0.0	0.0	0-0	15*	10	13
D PP	29	8.4	0.6	0-37	0.1	0.0	0-4	31.6	1.6	0-100	53.6	1.4	0-89	5.8	0.4	0-21	0.0	0.0	0-4	0.4	0.2	0-56	0.0	0.0	0-0	15*	9	13
D GS	29	0.2	0.1	0-23	0.6	0.1	0-6	29.6	1.6	0-98	47.7	1.4	0-86	21.4	0.5	0-40	0.0	0.0	0-6	0.5	0.2	0-52	0.0	0.0	0-0	15	16*	15*
D GSPP	29	0.2	0.1	0-20	0.6	0.1	0-6	33.2	1.6	0-99	45.7	1.3	0-85	19.7	0.4	0-36	0.0	0.0	0-6	0.5	0.2	0-49	0.0	0.0	0-0	15	14	15
D OM	29	10.4	0.9	0-55	7.6	0.4	0-29	33.2	1.4	0-91	32.7	1.2	0-74	5.7	0.6	0-38	3.7	0.3	0-20	5.9	0.7	0-68	0.8	0.1	0-16	16*	16*	16*
D OMPP	29	9.3	0.8	0-52	7.1	0.4	0-27	35.4	1.4	0-89	31.5	1.2	0-74	4.6	0.5	0-34	4.4	0.3	0-21	6.9	0.8	0-68	0.8	0.1	0-15	16*	15	16*
D zero	30	16.7	0.9	0-51	0.2	0.0	0-5	27.3	1.5	0-94	48.1	1.4	0-85	7.3	0.5	0-28	0.0	0.0	0-2	0.3	0.2	0-46	0.0	0.0	0-0	16*	16*	16*
D PP	30	16.4	0.8	0-47	0.2	0.0	0-5	31.1	1.5	0-94	44.9	1.3	0-83	7.1	0.4	0-25	0.0	0.0	0-2	0.3	0.2	0-44	0.0	0.0	0-0	15*	16*	15*
D GS	30	2.8	0.3	0-39	2.0	0.1	0-9	31.7	1.5	0-90	38.5	1.3	0-77	24.3	0.4	0-42	0.0	0.0	0-4	0.7	0.3	0-56	0.0	0.0	0-0	15	18*	16*
D GSPP	30	3.5	0.4	0-36	2.2	0.1	0-9	35.9	1.5	0-90	35.6	1.3	0-76	22.1	0.4	0-39	0.0	0.0	0-4	0.7	0.2	0-54	0.0	0.0	0-0	15	17*	16*
D OM	30	5.4	0.5	0-45	3.9	0.3	0-21	31.1	1.2	0-81	31.4	1.3	0-78	0.8	0.2	0-26	2.9	0.2	0-19	17.0	1.2	0-80	7.5	0.4	0-32	18*	17*	18*
D OMPP	30	5.4	0.5	0-45	3.9	0.3	0-21	31.1	1.2	0-81	31.4	1.3	0-78	0.8	0.2	0-26	2.9	0.2	0-19	17.0	1.2	0-80	7.5	0.4	0-32	18*	17*	18*
D zero	31	9.9	0.7	0-45	0.3	0.0	0-5	33.5	1.7	0-100	48.3	1.5	0-86	7.6	0.4	0-27	0.0	0.0	0-3	0.5	0.2	0-47	0.0	0.0	0-0	18*	14	17*
D PP	31	9.7	0.7	0-43	0.4	0.0	0-5	37.3	1.7	0-100	44.4	1.5	0-85	7.6	0.4	0-26	0.0	0.0	0-3	0.6	0.2	0-44	0.0	0.0	0-0	18*	14	17*
D GS	31	2.6	0.4	0-36	3.1	0.1	0-11	40.5	1.6	0-94	33.3	1.4	0-79	19.0	0.5	0-39	0.2	0.1	0-9	1.4	0.4	0-56	0.0	0.0	0-2	17*	14	16*
D GSPP	31	3.4	0.4	0-35	3.4	0.1	0-10	44.4	1.5	0-94	29.8	1.3	0-78	17.2	0.5	0-36	0.3	0.1	0-9	1.6	0.4	0-55	0.0	0.0	0-2	18*	14	16*
D OM	31	4.9	0.5	0-45	5.2	0.4	0-28	34.5	1.2	0-85	32.8	1.3	0-79	1.6	0.3	0-24	2.9	0.3	0-19	15.3	1.2	0-84	2.9	0.3	0-25	20*	16*	19*
D OMPP	31	4.0	0.5	0-42	4.3	0.3	0-27	35.3	1.2	0-84	30.8	1.3	0-79	1.2	0.2	0-23	3.3	0.3	0-20	18.2	1.2	0-86	3.0	0.3	0-24	20*	16*	19*
D zero	32	2.5	0.4	0-32	0.0	0.0	0-0	53.4	2.1	0-100	41.6	2.0	0-100	2.5	0.3	0-26	0.0	0.0	0-0	0.0	0.0	0-18	0.0	0.0	0-0	42*	20*	35*
D PP	32	2.1	0.3	0-30	0.0	0.0	0-0	59.7	2.0	0-100	35.9	1.9	0-100	2.2	0.2	0-23	0.0	0.0	0-0	0.0	0.0	0-15	0.0	0.0	0-0	42*	20*	34*
D GS	32	1.0	0.2	0-32	1.3	0.1	0-8	55.8	1.7	0-100	24.7	1.4	0-87	16.6	0.6	0-45	0.1	0.0	0-7	0.5	0.2	0-36	0.0	0.0	0-0	28*	17*	24*
D GSPP	32	1.6	0.3	0-31	1.7	0.1	0-8	60.9	1.6	0-100	20.7	1.4	0-84	14.4	0.6	0-42	0.1	0.0	0-7	0.6	0.2	0-35	0.0	0.0	0-0	28*	17*	24*
D OM	32	0.4	0.1	0-21	0.4	0.1	0-16	41.3	1.0	0-78	39.9	1.5	0-100	0.1	0.0	0-14	0.5	0.1	0-15	16.2	1.2	0-95	1.3	0.2	0-21	28*	32*	30*
D OMPP	32	0.1	0.1	0-16	0.2	0.1	0-14	40.1	1.0	0-78	39.1	1.6	0-100	0.0	0.0	0-6	0.4	0.1	0-14	18.8	1.3	0-99	1.2	0.2	0-22	29*	32*	30*
D zero	33	12.6	0.9	0-56	0.3	0.0	0-6	31.2	1.7	0-100	46.4	1.6	0-89	8.9	0.5	0-31	0.0	0.0	0-4	0.4	0.2	0-45	0.0	0.0	0-0	21*	16*	19*
D PP	33	12.4	0.9	0-53	0.4	0.1	0-6	35.5	1.7	0-100	42.2	1.6	0-85	9.0	0.5	0-30	0.0	0.0	0-3	0.5	0.2	0-45	0.0	0.0	0-0	21*	17*	19*
D GS	33	5.5	0.6	0-46	3.9	0.2	0-11	39.7	1.6	0-92	29.4	1.4	0-75	19.7	0.6	0-42	0.3	0.1	0-11	1.5	0.4	0-56	0.0	0.0	0-2	20*	15*	18*
D GSPP	33	6.8	0.6	0-46	4.1	0.2	0-11	43.6	1.6	0-92	26.0	1.3	0-73	17.4	0.6	0-39	0.5	0.1	0-12	1.5	0.4	0-55	0.0	0.0	0-3	20*	15*	18*
D OM	33	7.4	0.7	0-52	6.5	0.4	0-28	33.6	1.4	0-90	32.5	1.3	0-80	2.8	0.4	0-31	4.0	0.3	0-23	10.8	1.0	0-79	2.3	0.3	0-24	22*	15	19*
D OMPP	33	6.2	0.6	0-49	5.6	0.4	0-28	35.0	1.3	0-90	30.9	1.3	0-80	2.2	0.3	0-27	4.7	0.3	0-23	13.1	1.1	0-81	2.4	0.3	0-23	22*	14	19*
D zero	34	9.6	0.9	0-55	4.5	0.1	0-12	34.0	1.6	0-93	36.1	1.5	0-77	11.6	0.5	0-31	0.2	0.1	0-7	3.9	0.7	0-82	0.0	0.0	0-0	16*	11	14
D PP	34	9.1	0.9	0-52	4.8	0.1	0-12	36.6	1.6	0-91	32.8	1.4	0-76	12.4	0.5	0-30	0.3	0.1	0-7	4.1	0.7	0-82	0.0	0.0	0-0	16*	12	15
D GS	34	2.1	0.4	0-42	5.9	0.2	0-14	35.2	1.5	0-89	30.1	1.4	0-73	23.8	0.5	0-43	0.2	0.0	0-9	2.8	0.6	0-64	0.0	0.0	0-1	16*	13	15*
D GSPP	34	2.6	0.4	0-43	6.1	0.2	0-13	37.5	1.5	0-88	27.4	1.3	0-71	23.1	0.4	0-41	0.3	0.1	0-9	3.0	0.6	0-62	0.0	0.0	0-1	16*	14	15*
D OM	34	5.6	0.6	0-48	11.9	0.5	0-37	25.1	1.2	0-76	27.3	1.2	0-70	3.6	0.4	0-31	4.5	0.3	0-23	20.1	1.3	0-84	1.9	0.2	0-23	18*	12	16*
D OMPP	34	5.1	0.6	0-45	10.7	0.4	0-33	24.9	1.2	0-74	24.9	1.2	0-70	3.1	0.4	0-31	5.6	0.3	0-22	23.5	1.3	0-85	2.0	0.3	0-24	18*	12	16*
D zero	35	9.8	0.9	0-61	4.3	0.1	0-12	31.1	1.7	0-92	39.5	1.6	0-87	11.9	0.6	0-33	0.1	0.0	0-7	3.3	0.7	0-78	0.0	0.0	0-0	20*	12	17*
D PP	35	9.5	0.9	0-57	4.7	0.1	0-12	34.0	1.7	0-92	35.2	1.6	0-85	12.9	0.6	0-32	0.2	0.1	0-7	3.5	0.7	0-78	0.0	0.0	0-0	20*	13	17*
D GS	35	0.1	0.1	0-46	2.3	0.1	0-10	25.8	1.6	0-84	36.3	1.6	0-78	34.3	0.5	0-59	0.0	0.0	0-0	1.0	0.3	0-50	0.0	0.0	0-0	22*	19*	21*
D GSPP	35	0.2	0.1	0-44	2.7	0.1	0-10	29.0	1.6	0-83	33.5	1.5	0-76	33.6	0.4	1-54	0.0	0.0	0-0	1.0	0.3	0-48	0.0	0.0	0-0	22*	19*	21*
D OM	35	4.3	0.6	0-49	17.3	0.5	0-41	25.8	1.2	0-75	25.5	1.2	0-67	4.2	0.5	0-33	5.0	0.3	0-24	17.1	1.2	0-79	0.9	0.2	0-19	20*	15*	19*
D OMPP	35	3.8	0.6	0-48	16.2	0.5	0-40	25.3	1.2	0-77	23.5	1.2	0-67	3.6	0.5	0-32	6.3	0.4	0-23	20.2	1.2	0-79	1.0	0.2	0-21	21*	15*	19*
D zero	36	7.6	0.8	0-57	7.4	0.2	0-16	35.0	1.5	0-87	29.8	1.4	0-75	14.2	0.6	0-33	0.6	0.1	0-11	5.4	0.9	0-83	0.0	0.0	0-2	17*	13	15*
D PP	36	7.3	0.8	0-55	7.6	0.2	0-17	37.1	1.5	0-87	26.4	1.3	0-71	14.9	0.6	0-33	0.8	0.1	0-11	5.7	0.9	0-76	0.0	0.0	0-2	17*	14	16*
D GS	36	6.5	0.7	0-51	9.3	0.2	0-20	36.7	1.5	0-85	23.3	1.2	0-66	17.0	0.6	0-38	1.6	0.2	0-16	5.6	0.8	0-70	0.1	0.0	0-4	17*	13	15*
D GSPP	36	7.5	0.7	0-52	9.4	0.2	0-20	38.1	1.5	0-84	20.5	1.2	0-65	16.1	0.6	0-37	2.2	0.2	0-17	6.2	0.8	0-68	0.1	0.0	0-4	17*	13	15*
D OM	36	4.8	0.6	0-45	15.1	0.5	0-39	20.7	1.1	0-71	25.8	1.2	0-66	3.7	0.4	0-32	6.1	0.4	0-25	21.7	1.3	0-80	2.2	0.3	0-25	19*	12	16*
D OMPP	36	4.4	0.6	0-44	14.0	0.5	0-34	20.2	1.1	0-69	23.3	1.2	0-66	3.1	0.4	0-31	7.5	0.4	0-24	25.2	1.3	0-82	2.3	0.3	0-26	19*	12	16*
D zero	37	11.3	0.9	0-58	1.9	0.1	0-9	29.0	1.7	0-97	46.2	1.7	0-92	9.6	0.5	0-31	0.0	0.0	0-5	1.9	0.5	0-80	0.0	0.0	0-0	20*	16*	18*
D PP	37	11.2	0.9	0-56	2.2	0.1	0-8	32.4	1.8	0-96	42.0	1.7	0-90	10.1	0.5	0-29	0.1	0.0	0-5	2.1	0.5	0-76	0.0	0.0	0-0	20*	16*	18*
D GS	37	5.8	0.6	0-47	8.4	0.2	0-18	41.8	1.6	0-89	24.3	1.3	0-72	15.1	0.6	0-38	0.9	0.1	0-12	3.7	0.7	0-70	0.0	0.0	0-3	19*	12	16*
D GSPP	37	6.9	0.7	0-48	8.6	0.2	0-18	44.0	1.5	0-88	21.2	1.3	0-70	13.9	0.6	0-36	1.3	0.1	0-13	4.1	0.7	0-71	0.0	0.0	0-3	19*	12	16*
D OM	37	1.3	0.3	0-34	6.9	0.4	0-30	15.9	1.0	0-61	37.6	1.6	0-87	0.4	0.1	0-17	2.0	0.2	0-22	33.1	1.6	0-100	2.8	0.3	0-29	22*	19*	21*
D OMPP	37	1.0	0.2	0-29	5.6	0.4	0-27	15.6	0.9	0-63	34.4	1.6	0-87	0.3	0.1	0-16	2.5	0.2	0-19	37.7	1.7	0-100	2.8	0.3	0-30	22*	19*	21*
D zero	38	12.5	1.0	0-61	4.6	0.1	0-12	29.3	1.5	0-90	36.8	1.4	0-75	13.3	0.6	0-31	0.2	0.1	0-7	3.3	0.6	0-78	0.0	0.0	0-1	15	15	15
D PP	38	12.2	1.0	0-59	4.8	0.1	0-11	31.9	1.5	0-88	33.4	1.4	0-72	13.9	0.6	0-32	0.2	0.1	0-7	3.5	0.6	0-79	0.0	0.0	0-0	15	15*	15
D GS	38	4.5	0.5	0-49	7.0	0.2	0-15	32.9	1.4	0-85	28.3	1.2	0-67	24.1	0.5	0-43	0.3	0.1	0-9	3.0	0.6	0-70	0.0	0.0	0-3	15	15*	15
D GSPP	38	5.4	0.6	0-51	7.1	0.2	0-15	35.0	1.4	0-84	25.5	1.2	0-65	23.3	0.5	0-42	0.4	0.1	0-10	3.3	0.6	0-64	0.0	0.0	0-3	15	15*	15
D OM	38	6.4	0.7	0-46	12.1	0.5	0-31	20.8	1.1	0-71	26.6	1.2	0-68	3.1	0.4	0-31	5.4	0.4	0-23	21.5	1.3	0-83	4.0	0.4	0-28	17*	13	16*
D OMPP	38	5.9	0.7	0-46	11.2	0.4	0-29	20.8	1.1	0-70	24.1	1.2	0-67	2.7	0.4	0-31	6.4	0.4	0-22	24.7	1.3	0-84	4.1	0.4	0-30	18*	14	16*

Table F.6: Modeled contributions of the eight tributaries to the suspended sediment flux sampled at the Aarschot outlet station, using composite fingerprint E and the Monte Carlo simulated property concentrations in the objective function; * = failing the RME test; RME_val and RME_avg exclude P, S and Mn.

		Motte			Hulpe			Velpe			Gete			Zwartebeek			Mangelbeek			Herk			Demer (upstream)			relative mean error		
Nr outlet sample	code model	contribution	95% CI	range	contribution	95% CI	range	contribution	95% CI	range	contribution	95% CI	range	contribution	95% CI	range	contribution	95% CI	range	contribution	95% CI	range	contribution	95% CI	range	RME (%)	RME_val (%)	RME_avg (%)
E zero	13	0.5	0.1	0-20	13.6	0.2	4-30	11.3	1.1	0-71	26.3	1.5	0-71	11.0	0.4	0-25	8.1	0.3	0-22	27.6	1.5	0-73	1.7	0.2	0-20	6	6	6
E PP	13	0.5	0.1	0-21	13.6	0.2	4-29	11.9	1.1	0-71	25.1	1.5	0-70	10.3	0.3	0-22	8.4	0.3	0-21	28.4	1.5	0-73	1.8	0.2	0-22	6	6	6
E GS	13	13.8	0.4	0-33	19.7	0.2	13-33	0.0	0.0	0-6	4.9	0.7	0-42	0.0	0.0	0-0	0.1	0.0	0-8	25.8	0.8	0-49	35.7	0.6	14-70	20*	7	47*
E GSPP	13	17.4	0.5	0-36	20.2	0.2	13-34	0.0	0.0	0-0	4.2	0.5	0-34	0.0	0.0	0-0	0.1	0.0	0-8	19.6	0.7	0-42	38.5	0.6	17-75	20*	7	44*
E OM	13	13.4	0.8	0-50	35.0	0.7	14-75	1.9	0.2	0-11	0.0	0.0	0-4	37.9	0.9	0-70	2.8	0.4	0-41	0.0	0.0	0-0	9.0	0.7	0-47	70*	13	68*
E OMPP	13	13.7	0.9	0-55	38.2	0.8	15-82	1.2	0.2	0-11	0.0	0.0	0-4	27.9	0.8	0-61	2.9	0.4	0-39	0.0	0.0	0-0	16.1	0.8	0-53	75*	14	70*
E zero	14	0.2	0.1	0-11	9.4	0.2	0-18	17.7	0.9	0-71	14.7	1.0	0-73	0.6	0.1	0-8	10.9	0.2	0-18	42.1	1.2	0-83	4.3	0.3	0-25	5	5	5
E PP	14	0.2	0.1	0-11	9.6	0.2	0-19	18.2	0.9	0-71	14.3	1.0	0-72	0.6	0.1	0-10	10.8	0.2	0-18	41.7	1.2	0-81	4.6	0.3	0-26	5	5	5
E GS	14	0.0	0.0	0-0	8.8	0.2	0-21	44.4	1.6	0-80	17.5	1.5	0-75	14.9	0.4	0-29	4.0	0.2	0-15	10.4	1.0	0-74	0.0	0.0	0-0	15	5	14
E GSPP	14	0.0	0.0	0-0	8.8	0.2	0-21	47.6	1.7	0-81	16.2	1.5	0-77	12.4	0.4	0-27	4.7	0.2	0-16	10.2	1.0	0-76	0.0	0.0	0-0	15*	5	15
E OM	14	0.1	0.1	0-11	12.9	0.4	0-33	0.9	0.2	0-30	13.8	0.8	0-55	1.7	0.2	0-18	26.0	0.3	0-40	43.8	1.0	0-67	0.8	0.2	0-28	6	6	6
E OMPP	14	0.1	0.1	0-12	12.7	0.4	0-32	0.6	0.1	0-29	14.3	0.9	0-54	2.3	0.2	0-19	26.3	0.3	0-40	43.2	1.1	0-67	0.4	0.1	0-27	6	6	6
E zero	15	1.8	0.2	0-22	15.3	0.2	8-30	3.6	0.5	0-51	9.0	1.0	0-67	0.2	0.1	0-8	6.6	0.2	0-14	50.9	1.3	0-79	12.6	0.4	0-32	4	6	5
E PP	15	1.4	0.2	0-22	15.2	0.2	8-30	3.6	0.5	0-51	9.5	0.9	0-62	0.2	0.1	0-9	6.9	0.2	0-15	50.7	1.2	0-78	12.4	0.4	0-34	4	6	5
E GS	15	0.3	0.1	0-10	15.8	0.2	6-31	9.4	0.8	0-65	11.4	1.0	0-67	1.4	0.2	0-15	11.8	0.2	0-20	46.8	1.2	0-75	3.1	0.2	0-15	5	5	13
E GSPP	15	0.1	0.0	0-7	15.5	0.2	6-31	9.5	0.8	0-66	11.2	1.0	0-67	1.3	0.2	0-15	12.2	0.2	0-20	47.6	1.2	0-75	2.6	0.2	0-15	5	5	13
E OM	15	5.9	0.4	0-29	37.0	0.4	21-60	17.1	0.7	0-41	2.6	0.3	0-28	0.5	0.1	0-16	4.7	0.3	0-24	8.6	0.6	0-37	23.7	0.6	0-56	8	8	8
E OMPP	15	4.7	0.4	0-26	37.0	0.4	21-59	17.2	0.7	0-40	2.4	0.3	0-28	0.3	0.1	0-12	3.4	0.3	0-21	7.8	0.5	0-37	27.1	0.6	0-58	8	8	8
E zero	16	0.7	0.1	0-11	0.9	0.1	0-5	28.6	1.4	0-96	58.4	1.7	0-100	1.1	0.1	0-6	0.2	0.0	0-4	10.1	0.8	0-62	0.0	0.0	0-1	5	5	4
E PP	16	0.8	0.1	0-11	0.9	0.1	0-5	29.6	1.3	0-95	56.8	1.6	0-100	1.0	0.1	0-6	0.2	0.0	0-4	10.7	0.8	0-60	0.0	0.0	0-1	5	5	4
E GS	16	0.0	0.0	0-0	0.3	0.1	0-5	61.7	1.7	0-100	34.6	1.7	0-100	1.8	0.1	0-9	0.0	0.0	0-1	1.6	0.3	0-29	0.0	0.0	0-0	21*	5	20*
E GSPP	16	0.0	0.0	0-0	0.3	0.0	0-5	63.9	1.6	0-100	33.1	1.6	0-100	1.2	0.1	0-8	0.0	0.0	0-1	1.6	0.3	0-28	0.0	0.0	0-0	21*	5	20*
E OM	16	0.5	0.1	0-18	1.0	0.2	0-16	5.1	0.5	0-42	71.9	0.8	22-97	3.8	0.2	0-17	2.4	0.2	0-17	15.2	0.9	0-60	0.0	0.0	0-8	6	6	8
E OMPP	16	0.4	0.1	0-16	0.9	0.1	0-14	3.5	0.4	0-36	74.3	0.7	35-98	4.7	0.3	0-17	2.6	0.2	0-16	13.6	0.8	0-62	0.0	0.0	0-6	6	6	8
E zero	17	2.5	0.3	0-25	0.4	0.0	0-5	48.7	1.1	0-92	30.0	1.2	0-89	6.4	0.2	0-12	2.4	0.1	0-10	8.0	0.6	0-48	1.6	0.2	0-14	6	6	5
E PP	17	3.1	0.3	0-25	0.4	0.0	0-5	48.4	1.1	0-92	30.0	1.2	0-89	5.8	0.2	0-12	2.5	0.1	0-10	8.2	0.6	0-48	1.7	0.2	0-13	6	6	5
E GS	17	0.0	0.0	0-0	0.4	0.1	0-5	69.6	1.0	0-90	12.7	1.0	0-78	15.9	0.1	9-22	0.0	0.0	0-3	1.3	0.2	0-25	0.0	0.0	0-0	18*	5	15*
E GSPP	17	0.0	0.0	0-0	0.3	0.0	0-5	72.4	1.0	0-91	11.8	1.0	0-82	14.2	0.1	6-20	0.1	0.0	0-3	1.3	0.2	0-23	0.0	0.0	0-0	18*	5	15*
E OM	17	3.2	0.4	0-33	0.6	0.1	0-12	29.7	0.7	0-60	27.1	0.8	0-63	11.0	0.4	0-30	12.2	0.4	0-29	13.3	0.6	0-53	2.9	0.3	0-26	5	7	6
E OMPP	17	3.4	0.4	0-35	0.7	0.1	0-11	28.4	0.7	0-60	28.4	0.8	0-63	11.5	0.4	0-31	12.3	0.4	0-29	13.0	0.6	0-54	2.3	0.3	0-24	5	7	6
E zero	18	2.2	0.3	0-23	0.2	0.0	0-5	49.6	1.0	0-89	30.4	1.1	0-89	4.9	0.2	0-12	3.5	0.1	0-10	7.6	0.5	0-46	1.4	0.2	0-14	4	6	4
E PP	18	2.5	0.3	0-23	0.2	0.0	0-4	49.6	0.9	0-89	30.4	1.1	0-88	4.5	0.2	0-12	3.7	0.1	0-10	7.6	0.5	0-46	1.5	0.2	0-14	4	6	4
E GS	18	0.0	0.0	0-0	0.3	0.0	0-4	70.2	1.0	0-91	13.6	1.0	0-80	14.3	0.1	5-20	0.1	0.0	0-5	1.5	0.2	0-25	0.0	0.0	0-0	15*	5	14
E GSPP	18	0.0	0.0	0-0	0.2	0.0	0-4	72.6	1.0	0-92	12.6	0.9	0-81	12.7	0.1	3-19	0.3	0.0	0-6	1.5	0.2	0-23	0.0	0.0	0-0	15*	5	14
E OM	18	4.8	0.5	0-31	1.7	0.1	0-13	41.6	0.6	0-73	17.1	0.6	0-49	9.2	0.4	0-26	10.5	0.4	0-27	10.2	0.6	0-41	5.0	0.3	0-30	3	8	5
E OMPP	18	4.9	0.5	0-30	1.6	0.1	0-11	41.3	0.6	0-71	17.2	0.6	0-46	9.0	0.4	0-25	10.5	0.4	0-27	10.4	0.6	0-40	5.2	0.3	0-30	3	8	5
E zero	19	0.1	0.0	0-7	0.0	0.0	0-1	84.2	1.2	0-100	14.3	1.2	0-99	1.2	0.1	0-6	0.1	0.0	0-3	0.1	0.1	0-16	0.0	0.0	0-0	16*	5	14
E PP	19	0.2	0.0	0-7	0.0	0.0	0-1	84.9	1.2	0-100	13.6	1.1	0-99	1.1	0.1	0-6	0.1	0.0	0-3	0.1	0.1	0-16	0.0	0.0	0-0	15*	5	14
E GS	19	0.0	0.0	0-0	0.0	0.0	0-2	88.3	0.8	0-100	7.2	0.7	0-89	4.3	0.1	0-11	0.0	0.0	0-3	0.1	0.0	0-12	0.0	0.0	0-0	14	5	16*
E GSPP	19	0.0	0.0	0-0	0.0	0.0	0-2	89.9	0.7	4-100	6.4	0.7	0-86	3.5	0.1	0-10	0.0	0.0	0-2	0.1	0.0	0-11	0.0	0.0	0-0	14	5	16*
E OM	19	0.0	0.0	0-15	0.0	0.0	0-0	37.9	1.2	0-78	55.8	1.1	8-93	1.7	0.2	0-17	4.4	0.2	0-18	0.3	0.2	0-43	0.0	0.0	0-0	16*	5	15
E OMPP	19	0.0	0.0	0-16	0.0	0.0	0-0	30.6	1.2	0-74	60.8	1.1	11-94	3.0	0.3	0-18	5.3	0.3	0-19	0.2	0.1	0-41	0.0	0.0	0-0	16*	5	15
E zero	20	0.3	0.1	0-12	0.0	0.0	0-2	69.1	1.1	5-99	24.0	1.1	0-89	2.7	0.1	0-8	1.7	0.1	0-7	1.8	0.3	0-32	0.3	0.1	0-8	6	5	5
E PP	20	0.3	0.1	0-12	0.0	0.0	0-2	69.2	1.1	6-99	24.0	1.1	0-87	2.5	0.1	0-7	1.8	0.1	0-7	1.8	0.3	0-31	0.4	0.1	0-9	6	5	5
E GS	20	0.0	0.0	0-0	0.0	0.0	0-1	88.7	0.6	0-100	4.6	0.6	0-86	6.7	0.1	0-14	0.0	0.0	0-0	0.1	0.0	0-8	0.0	0.0	0-0	25*	5	23*
E GSPP	20	0.0	0.0	0-0	0.0	0.0	0-1	91.0	0.6	8-100	3.9	0.5	0-81	5.0	0.1	0-11	0.0	0.0	0-1	0.1	0.0	0-5	0.0	0.0	0-0	25*	5	23*
E OM	20	0.2	0.1	0-21	0.0	0.0	0-2	40.0	0.9	0-78	45.1	0.8	0-81	2.8	0.3	0-20	10.7	0.3	0-26	0.8	0.2	0-39	0.3	0.1	0-15	7	5	9
E OMPP	20	0.2	0.1	0-20	0.0	0.0	0-2	36.2	1.0	0-73	48.1	0.8	0-82	3.9	0.3	0-21	10.9	0.3	0-26	0.5	0.2	0-31	0.2	0.1	0-12	7	5	9
E zero	21	2.1	0.2	0-17	0.0	0.0	0-1	87.8	0.3	64-95	0.8	0.2	0-25	0.6	0.1	0-8	6.3	0.1	0-12	0.1	0.0	0-9	2.4	0.2	0-15	10	6	10
E PP	21	1.8	0.2	0-17	0.0	0.0	0-0	87.8	0.3	63-95	0.9	0.2	0-26	0.8	0.1	0-8	6.3	0.1	0-12	0.1	0.0	0-9	2.2	0.2	0-14	10	6	10
E GS	21	0.0	0.0	0-0	0.0	0.0	0-0	88.1	0.2	79-100	0.0	0.0	0-0	11.9	0.2	0-21	0.0	0.0	0-0	0.0	0.0	0-0	0.0	0.0	0-0	62*	5	51*
E GSPP	21	0.0	0.0	0-0	0.0	0.0	0-0	91.4	0.2	84-100	0.0	0.0	0-0	8.6	0.2	0-16	0.0	0.0	0-0	0.0	0.0	0-0	0.0	0.0	0-0	63*	5	52*
E OM	21	1.1	0.2	0-21	0.0	0.0	0-0	81.0	0.2	67-92	0.9	0.1	0-14	2.2	0.2	0-18	14.4	0.3	0-27	0.0	0.0	0-2	0.4	0.1	0-12	10	5	18*
E OMPP	21	0.9	0.2	0-20	0.0	0.0	0-0	80.6	0.2	66-91	1.1	0.1	0-14	2.6	0.2	0-17	14.5	0.3	0-26	0.0	0.0	0-2	0.3	0.1	0-12	10	5	18*
E zero	22	1.6	0.2	0-17	0.0	0.0	0-1	88.9	0.3	67-95	0.7	0.2	0-23	0.6	0.1	0-8	6.3	0.1	0-11	0.1	0.0	0-8	1.8	0.2	0-13	10	5	10
E PP	22	1.4	0.2	0-17	0.0	0.0	0-0	89.0	0.3	66-95	0.9	0.2	0-24	0.8	0.1	0-8	6.3	0.1	0-11	0.1	0.0	0-9	1.6	0.2	0-12	10	5	10
E GS	22	0.0	0.0	0-0	0.0	0.0	0-0	88.5	0.2	79-100	0.0	0.0	0-0	11.5	0.2	0-21	0.0	0.0	0-0	0.0	0.0	0-0	0.0	0.0	0-0	63*	5	52*
E GSPP	22	0.0	0.0	0-0	0.0	0.0	0-0	91.7	0.2	84-100	0.0	0.0	0-0	8.3	0.2	0-16	0.0	0.0	0-0	0.0	0.0	0-0	0.0	0.0	0-0	63*	5	52*
E OM	22	0.5	0.1	0-16	0.0	0.0	0-0	82.2	0.3	65-94	1.3	0.2	0-16	1.4	0.2	0-16	14.4	0.3	0-25	0.0	0.0	0-4	0.3	0.1	0-12	11	5	19*
E OMPP	22	0.4	0.1	0-15	0.0	0.0	0-0	81.5	0.3	64-93	1.7	0.2	0-17	1.8	0.2	0-16	14.6	0.3	0-25	0.0	0.0	0-3	0.2	0.1	0-10	11	5	19*
E zero	27	0.1	0.0	0-11	22.0	0.2	12-34	2.3	0.4	0-58	25.5	1.5	0-79	0.2	0.0	0-5	0.3	0.0	0-5	49.4	1.6	0-85	0.2	0.1	0-9	11	5	11
E PP	27	0.1	0.0	0-9	21.2	0.2	12-34	1.9	0.4	0-54	22.9	1.5	0-79	0.2	0.0	0-5	0.3	0.0	0-5	53.1	1.6	0-85	0.3	0.1	0-10	11	5	11
E GS	27	0.0	0.0	0-0	24.8	0.3	9-41	23.6	1.4	0-79	27.2	1.7	0-80	2.1	0.2	0-14	0.2	0.0	0-5	22.2	1.4	0-81	0.0	0.0	0-1	16*	5	22*

		Motte			Hulpe			Velpe			Gete			Zwartebeek			Mangelbeek			Herk			Demer (upstream)			relative mean error		
Nr outlet sample	code model	contribution	95% CI	range	contribution	95% CI	range	contribution	95% CI	range	contribution	95% CI	range	contribution	95% CI	range	contribution	95% CI	range	contribution	95% CI	range	contribution	95% CI	range	RME (%)	RME_val (%)	RME_avg (%)
E OM	27	0.2	0.1	0-12	55.3	0.3	41-68	3.9	0.4	0-39	5.6	0.6	0-37	0.1	0.0	0-8	0.4	0.1	0-13	30.7	0.8	0-46	3.8	0.3	0-26	7	5	8
E OMPP	27	0.2	0.1	0-10	54.0	0.3	39-68	3.8	0.4	0-40	4.7	0.5	0-36	0.1	0.0	0-7	0.3	0.1	0-10	31.7	0.8	0-47	5.3	0.4	0-29	7	5	8
E zero	28	2.6	0.3	0-20	0.9	0.1	0-6	28.4	0.7	0-73	30.9	0.7	0-81	3.5	0.2	0-10	2.8	0.2	0-10	25.3	0.6	0-68	5.6	0.3	0-19	2	6	3
E PP	28	2.7	0.3	0-19	0.9	0.1	0-5	28.4	0.7	0-69	31.1	0.7	0-82	3.4	0.2	0-9	2.8	0.2	0-10	25.1	0.6	0-70	5.6	0.2	0-18	2	6	2
E GS	28	0.0	0.0	0-0	1.4	0.1	0-9	44.7	1.2	0-90	24.0	1.4	0-88	8.8	0.2	0-17	3.4	0.2	0-12	17.3	0.8	0-59	0.4	0.1	0-7	7	5	9
E GSPP	28	0.0	0.0	0-0	1.3	0.1	0-9	45.9	1.2	0-90	24.2	1.5	0-88	7.7	0.2	0-17	3.8	0.2	0-13	16.8	0.8	0-59	0.2	0.0	0-5	7	5	9
E OM	28	6.1	0.5	0-31	8.0	0.3	0-23	34.8	0.7	0-69	10.6	0.6	0-43	4.8	0.3	0-21	4.3	0.3	0-23	14.4	0.7	0-49	16.9	0.5	0-40	3	8	4
E OMPP	28	6.3	0.5	0-29	8.0	0.3	0-25	34.9	0.6	0-69	10.2	0.6	0-41	4.4	0.3	0-19	3.8	0.3	0-21	14.2	0.6	0-49	18.0	0.4	0-42	3	8	4
E zero	29	0.2	0.1	0-14	0.1	0.0	0-4	52.5	1.3	0-97	38.9	1.5	0-95	3.8	0.1	0-9	1.5	0.1	0-7	3.0	0.4	0-34	0.1	0.0	0-6	6	5	5
E PP	29	0.2	0.1	0-14	0.1	0.0	0-4	52.7	1.3	0-97	38.9	1.4	0-95	3.6	0.1	0-9	1.7	0.1	0-7	2.9	0.4	0-34	0.1	0.0	0-5	6	5	5
E GS	29	0.0	0.0	0-1	0.2	0.0	0-6	55.6	1.2	0-95	31.7	1.3	0-93	6.6	0.2	0-14	1.8	0.1	0-9	4.2	0.4	0-35	0.1	0.0	0-4	5	5	6
E GSPP	29	0.0	0.0	0-1	0.1	0.0	0-5	55.9	1.1	0-94	31.7	1.3	0-94	6.0	0.2	0-13	2.0	0.1	0-9	4.1	0.4	0-34	0.1	0.0	0-5	5	5	6
E OM	29	0.1	0.1	0-22	0.0	0.0	0-6	28.3	1.0	0-63	53.6	0.8	6-84	6.1	0.4	0-23	9.7	0.4	0-25	1.8	0.3	0-35	0.2	0.1	0-21	8	5	7
E OMPP	29	0.1	0.1	0-15	0.0	0.0	0-5	24.8	0.9	0-61	56.9	0.8	11-84	7.3	0.4	0-24	9.5	0.4	0-24	1.2	0.2	0-29	0.1	0.1	0-17	8	5	7
E zero	30	0.4	0.1	0-19	0.2	0.0	0-5	51.9	1.5	0-97	37.0	1.6	0-94	5.6	0.1	0-11	1.1	0.1	0-7	3.6	0.4	0-43	0.1	0.0	0-6	8	5	7
E PP	30	0.5	0.1	0-18	0.1	0.0	0-4	52.2	1.4	0-97	36.5	1.6	0-94	5.3	0.1	0-11	1.3	0.1	0-8	3.9	0.4	0-43	0.2	0.0	0-7	8	5	7
E GS	30	0.0	0.0	0-6	0.4	0.1	0-7	52.9	1.2	0-93	28.0	1.4	0-91	9.3	0.2	0-17	1.9	0.1	0-10	7.3	0.6	0-43	0.2	0.0	0-7	7	5	9
E GSPP	30	0.0	0.0	0-7	0.4	0.1	0-7	54.1	1.2	0-93	26.5	1.4	0-91	8.6	0.2	0-17	2.1	0.1	0-10	8.0	0.6	0-43	0.3	0.1	0-7	7	5	9
E OM	30	0.0	0.0	0-7	0.0	0.0	0-4	11.8	0.8	0-49	67.6	0.7	13-88	4.6	0.4	0-23	13.0	0.4	0-26	2.7	0.4	0-53	0.2	0.1	0-16	10	5	9
E OMPP	30	0.0	0.0	0-13	0.0	0.0	0-4	8.3	0.6	0-45	70.7	0.6	20-88	6.4	0.4	0-25	12.6	0.4	0-27	1.9	0.3	0-53	0.0	0.0	0-10	10	5	9
E zero	31	0.8	0.2	0-24	0.2	0.0	0-6	46.7	1.7	0-96	41.8	1.8	0-95	5.6	0.2	0-12	1.3	0.1	0-9	3.6	0.5	0-48	0.0	0.0	0-4	10	5	9
E PP	31	0.8	0.2	0-24	0.2	0.0	0-5	47.2	1.6	0-96	40.9	1.8	0-94	5.3	0.2	0-11	1.5	0.1	0-8	4.0	0.5	0-48	0.0	0.0	0-5	10	5	9
E GS	31	0.2	0.1	0-12	0.8	0.1	0-9	43.2	1.4	0-92	35.0	1.7	0-91	7.8	0.3	0-19	3.8	0.2	0-13	9.0	0.7	0-53	0.2	0.0	0-6	9	5	11
E GSPP	31	0.4	0.1	0-15	0.9	0.1	0-8	44.6	1.4	0-91	32.6	1.7	0-89	7.1	0.3	0-18	4.1	0.2	0-13	10.1	0.8	0-53	0.2	0.1	0-8	9	5	11
E OM	31	0.0	0.0	0-8	0.1	0.0	0-8	8.8	0.7	0-45	68.0	0.7	10-88	4.8	0.4	0-25	14.1	0.4	0-28	4.1	0.5	0-60	0.0	0.0	0-9	12	5	12
E OMPP	31	0.0	0.0	0-0	0.1	0.0	0-7	5.5	0.5	0-39	71.2	0.6	19-88	6.2	0.4	0-27	13.9	0.4	0-27	3.0	0.4	0-56	0.0	0.0	0-6	12	5	12
E zero	32	0.1	0.1	0-9	0.0	0.0	0-0	81.0	1.6	0-100	16.5	1.5	0-99	2.2	0.1	0-9	0.1	0.0	0-3	0.0	0.0	0-14	0.0	0.0	0-0	26*	5	22*
E PP	32	0.2	0.1	0-9	0.0	0.0	0-0	82.4	1.5	0-100	15.2	1.4	0-98	2.1	0.1	0-8	0.1	0.0	0-3	0.0	0.0	0-13	0.0	0.0	0-0	26*	5	22*
E GS	32	1.0	0.2	0-18	0.3	0.1	0-6	61.0	1.4	0-96	25.9	1.5	0-92	5.0	0.3	0-17	3.5	0.2	0-12	3.2	0.4	0-36	0.2	0.0	0-6	16*	5	21*
E GSPP	32	2.3	0.2	0-19	0.3	0.1	0-6	60.6	1.4	0-95	25.1	1.5	0-90	4.1	0.3	0-16	3.8	0.2	0-12	3.3	0.4	0-36	0.4	0.1	0-8	16*	6	21*
E OM	32	0.0	0.0	0-0	0.0	0.0	0-0	13.5	1.0	0-51	82.3	0.9	5-100	0.3	0.1	0-13	3.6	0.2	0-16	0.4	0.2	0-87	0.0	0.0	0-0	25*	5	24*
E OMPP	32	0.0	0.0	0-0	0.0	0.0	0-0	8.2	0.8	0-50	85.7	0.8	7-100	0.6	0.1	0-14	5.2	0.3	0-18	0.3	0.2	0-91	0.0	0.0	0-0	25*	5	24*
E zero	33	0.7	0.2	0-25	0.3	0.0	0-6	48.5	1.6	0-95	37.9	1.8	0-93	6.5	0.2	0-13	1.9	0.1	0-10	4.1	0.5	0-47	0.1	0.0	0-6	11	5	10
E PP	33	0.7	0.2	0-25	0.3	0.0	0-6	49.3	1.6	0-95	36.9	1.7	0-92	5.9	0.2	0-13	2.2	0.1	0-10	4.5	0.5	0-47	0.1	0.0	0-7	11	5	9
E GS	33	0.7	0.1	0-17	1.1	0.1	0-9	43.3	1.3	0-89	29.8	1.6	0-86	6.6	0.3	0-20	6.1	0.2	0-16	11.6	0.8	0-56	0.8	0.1	0-10	9	5	11
E GSPP	33	1.1	0.2	0-17	1.2	0.1	0-8	44.3	1.2	0-88	28.0	1.5	0-87	6.0	0.3	0-18	6.2	0.2	0-15	12.2	0.8	0-57	1.1	0.1	0-12	9	5	11
E OM	33	0.0	0.0	0-9	0.1	0.0	0-8	10.6	0.7	0-45	61.5	0.8	10-83	4.5	0.4	0-26	18.0	0.4	0-31	5.1	0.5	0-61	0.1	0.1	0-12	12	5	13
E OMPP	33	0.0	0.0	0-9	0.1	0.0	0-8	7.3	0.6	0-41	64.8	0.6	13-83	6.1	0.4	0-26	17.7	0.4	0-31	4.0	0.5	0-66	0.0	0.0	0-10	12	5	13
E zero	34	0.7	0.2	0-19	2.0	0.1	0-10	22.8	1.3	0-88	41.1	1.7	0-89	6.5	0.2	0-16	4.9	0.2	0-14	21.2	1.2	0-86	0.8	0.1	0-14	6	6	6
E PP	34	0.8	0.2	0-18	1.9	0.1	0-9	23.3	1.2	0-87	39.6	1.6	0-88	6.2	0.2	0-14	5.1	0.2	0-13	22.2	1.2	0-83	1.0	0.1	0-14	6	6	6
E GS	34	0.0	0.0	0-3	2.2	0.1	0-11	28.8	1.3	0-85	34.2	1.7	0-84	12.3	0.3	0-23	4.8	0.2	0-16	17.6	1.1	0-72	0.1	0.0	0-7	7	5	7
E GSPP	34	0.0	0.0	0-3	2.1	0.1	0-11	30.0	1.3	0-85	32.6	1.7	0-84	11.3	0.3	0-22	5.2	0.2	0-16	18.6	1.1	0-71	0.1	0.0	0-6	6	5	7
E OM	34	0.1	0.1	0-13	1.0	0.1	0-15	0.5	0.1	0-19	50.0	0.8	4-74	6.8	0.4	0-29	19.6	0.4	0-34	22.0	0.9	0-79	0.1	0.0	0-17	8	5	8
E OMPP	34	0.1	0.0	0-16	0.9	0.1	0-19	0.2	0.1	0-15	52.6	0.8	8-75	8.2	0.4	0-29	19.0	0.4	0-34	19.1	0.9	0-73	0.0	0.0	0-14	9	5	9
E zero	35	1.4	0.3	0-28	2.4	0.1	0-12	19.8	1.5	0-87	44.8	1.9	0-87	9.3	0.3	0-19	4.0	0.2	0-16	18.2	1.4	0-86	0.2	0.1	0-10	9	6	9
E PP	35	1.5	0.3	0-28	2.5	0.1	0-11	20.6	1.4	0-86	42.6	1.9	0-87	8.8	0.3	0-18	4.4	0.2	0-15	19.5	1.4	0-86	0.2	0.1	0-11	9	6	9
E GS	35	0.0	0.0	0-0	1.6	0.1	0-9	36.1	1.7	0-84	33.7	1.9	0-83	22.1	0.3	6-31	0.3	0.1	0-8	6.1	0.7	0-58	0.0	0.0	0-0	16*	5	15*
E GSPP	35	0.0	0.0	0-0	1.7	0.1	0-9	39.5	1.7	0-85	31.3	1.8	0-83	20.4	0.2	6-29	0.4	0.1	0-8	6.8	0.7	0-57	0.0	0.0	0-0	17*	5	15*
E OM	35	0.1	0.1	0-19	2.0	0.2	0-20	0.6	0.2	0-26	45.4	1.0	0-73	8.7	0.5	0-32	18.9	0.5	0-34	24.3	1.2	0-80	0.0	0.0	0-17	12	5	12
E OMPP	35	0.0	0.0	0-13	1.6	0.2	0-21	0.1	0.1	0-16	47.7	1.0	0-73	10.1	0.5	0-31	18.6	0.5	0-34	21.8	1.1	0-79	0.0	0.0	0-12	12	5	12
E zero	36	0.5	0.1	0-17	3.5	0.2	0-13	17.1	1.2	0-83	36.8	1.7	0-86	5.5	0.3	0-16	7.6	0.2	0-17	28.0	1.5	0-86	1.0	0.2	0-17	6	6	7
E PP	36	0.6	0.1	0-18	3.6	0.2	0-12	18.1	1.1	0-81	34.1	1.6	0-85	5.3	0.3	0-16	7.7	0.2	0-17	29.5	1.4	0-86	1.2	0.2	0-18	6	6	7
E GS	36	0.6	0.1	0-15	3.9	0.2	0-14	15.9	1.1	0-78	34.4	1.6	0-82	7.8	0.4	0-23	9.8	0.3	0-22	26.8	1.4	0-81	0.8	0.1	0-13	6	6	7
E GSPP	36	0.8	0.1	0-16	3.9	0.2	0-13	16.2	1.0	0-76	32.9	1.6	0-81	7.3	0.4	0-21	10.1	0.3	0-21	27.8	1.4	0-81	1.0	0.2	0-15	6	6	7
E OM	36	0.0	0.0	0-6	2.4	0.2	0-18	0.2	0.1	0-15	39.5	1.0	0-71	5.4	0.4	0-28	22.5	0.4	0-34	29.9	1.1	0-80	0.0	0.0	0-21	10	5	11
E OMPP	36	0.0	0.0	0-9	2.1	0.2	0-21	0.0	0.0	0-9	41.8	0.9	0-70	6.8	0.4	0-30	22.1	0.4	0-35	27.1	1.1	0-78	0.0	0.0	0-18	10	5	11
E zero	37	1.1	0.3	0-28	1.5	0.1	0-11	26.9	1.7	0-91	46.7	2.0	0-91	10.1	0.3	0-17	1.9	0.1	0-13	11.8	1.0	0-76	0.1	0.0	0-7	11	6	10
E PP	37	1.3	0.3	0-31	1.5	0.1	0-10	27.6	1.6	0-91	44.7	2.0	0-89	9.4	0.2	0-17	2.1	0.1	0-13	13.3	1.1	0-76	0.2	0.1	0-9	11	6	10
E GS	37	2.1	0.2	0-22	3.4	0.2	0-12	19.9	1.2	0-79	32.4	1.7	0-81	8.9	0.4	0-23	6.9	0.3	0-19	24.9	1.4	0-81	1.5	0.2	0-16	9	6	13
E GSPP	37	3.2	0.3	0-23	3.4	0.2	0-12	20.0	1.2	0-78	31.2	1.6	0-80	8.4	0.4	0-23	6.8	0.3	0-18	25.1	1.4	0-81	2.0	0.2	0-17	9	6	13
E OM	37	0.0	0.0	0-0	0.3	0.1	0-11	0.0	0.0	0-7	59.7	1.0	7-88	1.0	0.2	0-21	15.3	0.3	0-26	23.7	1.2	0-83	0.0	0.0	0-11	16*	5	15
E OMPP	37	0.0	0.0	0-1	0.2	0.1	0-13	0.0	0.0	0-0	63.6	1.0	8-90	2.1	0.3	0-23	15.8	0.3	0-27	18.3	1.1	0-81	0.0	0.0	0-1	16*	5	16*
E zero	38	0.4	0.1	0-22	2.3	0.1	0-11	21.0	1.4	0-88	43.3	1.9	0-88	9.1	0.3	0-17	3.8	0.2	0-14	19.2	1.3	0-86	0.8	0.1	0-13	8	6	8
E PP	38	0.5	0.1	0-20	2.3	0.1	0-11	21.6	1.4	0-87	41.9	1.9	0-88	8.6	0.2	0-17	4.0	0.2	0-14	20.2	1.3	0-86	0.9	0.1	0-13	8	6	8
E GS	38	0.0	0.0	0-1	2.9	0.2	0-13	25.3	1.4	0-85	33.1	1.7	0-82	15.1	0.3	0-26	4.3	0.2	0-16	19.0	1.2	0-75	0.3	0.1	0-8	8	5	8
E GSPP	38	0.0	0.0	0-3	2.9	0.2	0-12	26.6	1.4	0-84	31.5	1.7	0-83	14.0	0.3	0-25	4.8	0.2	0-16	19.9	1.2	0-80	0.3	0.1	0-8	8	5	8
E OM	38	0.0	0.0	0-15	1.9	0.2	0-17	0.4	0.1	0-23	42.2	1.0	0-71	9.0	0.4	0-30	19.3	0.4	0-34	27.1	1.1	0-80	0.1	0.0	0-19	10	5	10
E OMPP	38	0.0	0.0	0-17	1.6	0.2	0-20	0.1	0.1	0-16	44.8	0.9	0-71	10.7	0.4	0-31	18.5	0.4	0-35	24.3	1.0	0-79	0.0	0.0	0-15	10	5	10

Addendum G: Results of DFA and Correction Factors for Composite Fingerprints F, G and H

Table G.1: Individual and cumulative predictive power and Discriminatory Weighting Correction Factors (W_i) determined for the properties constituting Composite Fingerprint F, W_i is the weighting factor

step	property added	Individual Predictive power	Cumulative predictive power	W_i	Wilks' Lambda
1	Ca	72.0	72	1.00	0.044
2	Rb	67.5	80.5	0.94	0.005
3	Al	83.1	100	1.15	0.002
4	Ba	91.6	100	1.27	0.001
5	Mn	62.7	100	0.87	<0.001
6	Ce	84.3	100	1.17	<0.001
7	Zr	81.9	100	1.14	<0.001
8	Sr	89.0	100	1.24	<0.001

Table G.2: Grain size and organic matter correction factors for each (grouped) tributary for outlet samples 14 and 15, used in composite Fingerprint F.

Outlet sample numbering	Correction factor	Locations			
		Motte	Hulpe	Zwartebeek & Mangelbeek	Velpe, Gete, Herk & Demer (upstream)
14	OM	0.69	0.37	1.05	0.45
15	OM	1.02	0.56	1.56	0.67
14	GS	1.43	0.82	1.37	0.93
15	GS	1.20	0.69	1.14	0.78

Table G.3: Individual and cumulative predictive power and Discriminatory Weighting Correction Factors (W_i) determined for the properties constituting Composite Fingerprint G

step	property added	Individual Predictive power	Cumulative predictive power	W_i	Wilks' Lambda
1	Ba	85.5	85.5	1.09	0.66
2	Ca	81.7	100	1.04	0.05
3	Mn	78.3	100	1.00	0.05
4	Sr	90.2	100	1.15	undetermined

Table G.4: Grain size and organic matter correction factors for each (grouped) tributary for outlet samples 14 and 15, used in composite Fingerprint G.

Outlet sample numbering	Correction factor	Locations		
		Motte, Zwartebeek & Mangelbeek	Hulpe	Velpe, Gete, Herk & Demer (upstream)
14	OM	0.51	0.37	1.05
15	OM	0.75	0.56	1.56
14	GS	1.04	0.82	1.37
15	GS	0.87	0.69	1.14

Table G.5: Individual and cumulative predictive power and Discriminatory Weighting Correction Factors (W_i) determined for the properties constituting Composite Fingerprint H

step	property added	Individual Predictive power	Cumulative predictive power	W_i	Wilks' Lambda
1	Ba	98.8	98.8	1.59	0.088
2	Ca	62.2	100	1.00	0.056
3	Rb	77.1	98.8	1.24	0.052
4	Al	100	100	1.61	0.032

Table G.6: Grain size and organic matter correction factors for each (grouped) tributary for outlet samples 14 and 15, used in composite Fingerprint H.

Outlet sample numbering	Correction factor	Locations	
		Motte, Hulpe, Zwartebeek & Mangelbeek	Velpe, Gete, Herk & Demer (upstream)
14	OM	0.37	1.05
15	OM	0.56	1.03
14	GS	0.82	1.37
15	GS	0.69	1.14